Università Politecnica delle Marche
Scuola di Dottorato in Scienze dell'Ingegneria
Corso di Dottorato in Ingegneria Industriale: Curriculum in Ingegneria dei Materiali

---

Comparison between commercial and recycled carbon-based fillers and fibers for the development of smart and sustainable multifunctional mortars

Ph.D. Dissertation of:

Eng. Alberto BELLI

Advisor:

Prof. Francesca TITTARELLI

XVII cycle - new series

Università Politecnica delle Marche
Dipartimento di Scienze e Ingegneria della Materia, dell'Ambiente ed Urbanistica
Via Brecce Bianche, 12 — 60131 - Ancona, Italy

Questo mio contributo alla ricerca è dedicato a Paolo Belli. Queste pagine sono state scritte grazie alla sua opera fisica e morale.

Il suo splendido esempio di umanità si è radicato nella mia coscienza grazie a una presenza discreta ma immensa.
Grazie al suo animo buono e gentile, mai sconfitto dalla cattiveria e dall'egoismo, ho compreso i veri valori che innalzano l'individuo.

Più di ogni altro mi ha trasmesso l'amore per i frutti del buon lavoro. Il mezzo posseduto dall'uomo per avvicinarsi a Dio.
La fatica è sacra in quanto strumento di creazione.

Attraverso il suo mestiere, lo stesso di Cristo, ha trasmesso l'amore per un'arte antica, piena della semplicità e dell'umiltà che rende primi gli ultimi.

Il suo lavoro e i suoi sacrifici mi hanno permesso di raggiungere i più alti livelli di istruzione. E mi hanno regalato un illimitato numero di opportunità e possibilità.
Cercherò di utilizzare al meglio il suo regalo, per il bene dei miei cari e per l'avanzamento della società.

"...l'arte vostra quella, quanto pote,
segue, come 'l maestro fa 'l discente;
sì che vostr'arte a Dio quasi è nepote"

Abstract

Today's society is largely based on infrastructures that guarantee necessary goods such as water and electricity, as well as transport and communication networks. Their safeguarding and the saving of resources necessary for their operation is becoming increasingly important in the field of building engineering.
At the same time, materials engineering, thanks to the development of innovative and high performance nanomaterials as graphene, offers several ideas for the construction of durable and multifunctional building materials.
Furthermore, building materials research field is increasingly focused on the re-use of recycled raw materials obtained from industrial by-products, for a more sustainable construction industry and a lower ecological footprint.
The present research aims to sustain these needs through the development of multi-functional binder-based composite with the addition of recycled carbon-based fillers and fibers obtained from industrial by-products. In particular, the enhancement of mechanical strength and durability of the composites have been studied, together with their de-polluting and photocatalytic properties.
The electrical properties of the mixtures have been studied to analyze the Electromagnetic interference shielding capability of carbon-based admixtures, and to provide a basis for the development of strain-sensing materials for structural health monitoring of reinforced concrete constructions.
Pastes and mortars containing graphene or other commercial and recycled carbon-based fillers (from 0.25% to 4.0% on binder weight) and carbon fibers (from 0.05% to 1.6% by mixture volume) were realized. Tests of mechanical resistance (flexural, compressive and tensile splitting strength) and durability (capillary water absorption, hygrometric shrinkage) were performed on the mixtures, together with test for the assessment of pollutants adsorption and photocatalytic properties (NOx abatement).
The electrical properties of the composites have been studied by measuring DC electrical resistivity and AC impedance spectrum. Lastly, the strain-sensitivity has been evaluated by measuring the fractional change in resistivity of the specimens subjected to quasi-static compressive loads.
The results show that the addition of recycled carbon-based fillers leads to a refinement of the cement matrix microstructure, increasing the mechanical compressive strength up to 25% and decreasing the water permeability up to 57%. In contrast, graphene worsens the workability and homogeneity of the mixtures, and leads to an increase in the macroporosity volume within the hardened composites.
The addition of recycled carbon micro-fibers leads to an increase in flexural strengths up to 101% and to a decrease in hygrometric shrinkage strain up to 41%. However, the admixtures do not significantly improve the de-polluting and photocatalytic properties of the composites. The electronic tests demonstrate that the recycled carbon-based materials lead to an increase in electrical conductivity up to several orders of magnitude compared to the traditional cementitious materials (depending on the fillers/fibers concentrations).
However, both the electrical conductivity and the piezoresistivity of the multifunctional composites are strongly influenced by the dispersion degree of the conductive admixtures, and by environmental parameters such as moisture.

La società moderna è in gran parte fondata sul corretto funzionamento di infrastrutture che garantiscono beni di prima necessità, come acqua ed energia, nonché reti di trasporto e mezzi di comunicazione. La loro salvaguardia e il risparmio delle risorse necessarie per il loro funzionamento sta diventando sempre più importante nel campo dell'ingegneria edilizia.

Allo stesso tempo, l'ingegneria della materia, grazie allo sviluppo di nanomateriali innovativi e ad alte prestazioni come il grafene, offre diversi spunti per la realizzazione di materiali da costruzione durevoli e multifunzionali.

Inoltre, il settore della ricerca sui materiali edili si sta focalizzando sempre più sul riutilizzo di materie prime riciclate, ottenute da sottoprodotti industriali, per un'industria edilizia più sostenibile e a minore impatto ecologico.

La presente ricerca si propone di supportare queste esigenze attraverso lo sviluppo di compositi multifunzionali a base di leganti idraulici, con l'aggiunta di filler e fibre a base di carbonio riciclati, ottenuti da sottoprodotti industriali. In particolare, sono stati studiati i miglioramenti in termini di resistenze meccaniche e di durabilità, nonché le loro proprietà disinquinanti e fotocatalitiche.

Sono state studiate le proprietà elettriche delle miscele, in modo da valutare la capacità di schermatura delle interferenze elettromagnetiche delle aggiunte a base di carbonio, e per fornire una base di studio per lo sviluppo di materiali auto-sensibili da utilizzare nel monitoraggio della salute strutturale degli edifici in calcestruzzo armato.

Sono state così realizzate paste e malte contenenti grafene o altri filler a base di carbonio di origine riciclata (da 0.25% al 4% sul peso del legante) e fibre di carbonio (da 0.05% a 1.6% sul volume della miscela). Sui composti sono stati eseguiti test di resistenza meccanica (resistenza a flessione, compressione e trazione indiretta) e durabilità (assorbimento capillare d'acqua e ritiro igrometrico), nonché test per la valutazione dell'adsorbimento degli inquinanti e delle proprietà fotocatalitiche (abbattimento dei NOx). Le proprietà elettriche dei materiali sono state studiate tramite la misura della resistività elettrica in DC e dello spettro di impedenza in AC. Infine, la sensibilità elettrica alla deformazione è stata valutata misurando la variazione percentuale della resistività su provini soggetti a carichi di compressione semi-statici.

I risultati mostrano che l'aggiunta di filler a base di carbonio riciclati contribuiscono a un raffinamento della microstruttura della matrice cementizia, portando a un incremento delle resistenze meccaniche a compressione fino al 25% e a un decremento della permeabilità all'acqua fino al 57%. Al contrario, l'aggiunta di grafene porta a un peggioramento della lavorabilità e dell'omogeneità delle miscele, e a un conseguente aumento del volume di macro-pori all'interno dei composti induriti.

L'aggiunta di micro-fibre di carbonio riciclate contribuisce a incrementare le resistenze meccaniche a flessione fino al 101% e a ridurre le deformazioni da ritiro igrometrico fino al 41%. Le aggiunte, però, non apportano contributi significativi alle proprietà disinquinanti e fotocatalitiche dei materiali.

I test elettronici dimostrano che i materiali riciclati ad alto tenore di carbonio (a seconda della concentrazione) portano a un aumento della conducibilità elettrica di molteplici ordini di grandezza rispetto ai tradizionali materiali cementizi. Tuttavia, è stato dimostrato che sia la conducibilità elettrica sia le proprietà piezoresistive dei composti multifunzionali sono fortemente influenzate dal grado di dispersione delle aggiunte conduttive, nonché da altri parametri ambientali, come il grado di umidità.

Keywords: Mortar, Concrete, Paste, Cement, Lime, Graphene, Carbon-based fillers, Gasification char, Foundry sand, Carbon fibers, Steel fibers, De-polluting, Photocatalysis, Resistivity, Multifunctional cement-based composite, Self-sensing, Structural Health Monitoring, Industrial By-products, Wastes, Recycling.

***Parole chiave**: Malta, Calcestruzzo, Paste, Cemento, Calce, Grafene, Filler a base di carbonio, Char di gassificazione, Sabbia di fonderia, Fibre di carbonio, Fibre in acciaio, Disinquinamento, Fotocatalisi, Resistività, Composti cementizi multifunzionali, Auto-sensoriale, Monitoraggio della salute strutturale, Sottoprodotti industriali, Scarti, Riciclaggio.*

QVI NVNC ES CARBO NEMPE PRVNA FVISTI
PONE ANIMOS FIES MOX CINIS

"You who are now *Carbon*, certainly you were *embers*,
And as soon as you die, you will become *ashes*…"

Janus Pannonius

Contents

Abbreviations

AC	- *Alternating Current*
BSF	- *Brassed Steel Fibers*
CB	- *Carbon Black*
CF	- *Carbon Fibers*
CFRC	- *Carbon Fiber Reinforced Composites*
CNF	- *Carbon Nano-Fibers*
CNT	- *Carbon Nanotubes*
DAQ	- *Data Acquisition System*
DC	- *Direct Current*
EDX	- *Energy Dispersive X-Ray spectroscopy*
EIS	- *Electrochemical Impedance Spectroscopy*
FCR	- *Fractional Change in Resistivity*
FS	- *Foundry Sand*
GCH	- *Gasification Char*
GF	- *Gauge Factor*
GNP	- *Graphene Nano-Platelets*
GO	- *Graphene Oxide*
GONP	- *Graphene Oxide Nano-Platelets*
HPC	- *High Performance Concretes*
MCC	- *Multifunctional Cement-based Composites*
MIP	- *Mercury Intrusion Porosimetry*
MWCNT	- *Multi-Walled Carbon Nanotube*
NRC	- *Nested Reverberation Chamber*
OPC	- *Ordinary Portland Cement*
PAC	- *Powdered Activated Carbon*
PAN	- *Polyacrylonitrile*
PCSS	- *Piezoresistive Cement-based Self-Sensors*
RC	- *Reinforced Concrete*
RCF	- *Recycled Carbon Fibers*
RH	- *Relative Humidity*

SCM - *Supplementary Cementitious Materials*
SEM - *Scanning Electron Microscope*
SF - *Steel Fibres*
SFRC - *Steel Fibers Reinforced Concretes*
SG - *Strain Gauge*
SHM - *Structural Health Monitoring*
SSCC - *Self-Sensing Cement-based Composites*
SWCNT - *Single-Walled Carbon Nanotubes*
UFS - *Used Foundry Sand*
VCF - *Virgin Carbon Fibers*
VOC - *Volatile Organic Compound*

c.m.% - *Cement Mass fraction*
vol.% - *Volume fraction*
wt.% - *Weight fraction*

1 . Chapter
Introduction

Description of the scientific and technological field:
Problems, Aims and methods

1.1 Preface

In recent years, innovations in the field of materials science have transformed construction materials from ordinary structural technologies to a complex instrument for improving the life quality inside and outside buildings.
The development of innovative and performing nanomaterials, such as graphene, provides new ideas for the production of durable and multifunctional building materials. *Graphene* (such as carbon nanotubes and other carbon-based nanomaterials) is characterized by high mechanical strength, photocatalytic properties and high thermal and electrical conductivity.
Moreover, building materials research field is increasingly focused on the use of recycled raw materials obtained from industrial by-products, for a more sustainable construction industry and the reduction of carbon footprint.
This research aims to analyze the technical properties of cement-based composites implemented through the addition of different types of recycled carbon-based materials (fillers and fibers), for the development of more sustainable and low-cost solutions, usable on a large scale in infrastructure engineering. The technological contributions of recycled admixtures have been compared with those of more expensive and high performing nanomaterials, such as graphene and commercial carbon fibers.
This work is also focused on the study of the specific electrical properties of carbon-based fillers and fibers and their potential use for the development of multiple technological solutions, such as finishes for electromagnetic interference shielding and smart cement-based composites usable within self-health monitoring systems, in order to enhance the life-cycle of reinforced concrete buildings.
This experimentation is integrated into the *EnDurCrete* project, which aims to develop a new cost-effective sustainable reinforced concrete for long-lasting and benefit applications (funded by the *Horizon 2020* research and innovation program).
Below, a summary description of the disciplinary sector, the aims of the research and the work methods are described.

1.2 Scientific field and problems

Nowadays, infrastructures have acquired increasing importance within modern society. These regulate resources supply and the proper functioning of communication technologies and modes of transport. Their efficiency and integrity are an essential factor for industry and for economic development.
Concrete is the material on which a large part of the world's building assets is based, as well as one of the fundamental materials for contemporary construction techniques. Since its invention (thousands of years ago) this material has undergone many technological developments, but is still mainly used for its effective structural properties and for its ease of processing.
However, concrete and other cement-based composites are porous materials [1], and therefore they are subject to wear due to the infiltration of pathogens from the external environment. This requires constant and demanding maintenance work, aimed at preserving the functionality of the structure. For this reason, civil and infrastructural

engineering are increasingly focusing on innovative control systems for reinforced concrete structures, that guarantee safety in their use and efficient operation [2][3]. This also includes the introduction of equipment for the non-destructive monitoring, able to investigate the health of concrete structures by the detection of parameters such as pH, humidity, and corrosion rate of reinforcement, or through sensors for the detection of cracks and damages. However, these systems are not always effective, and must be subject to frequent maintenance [4].
In addition to improving strength and durability, another goal that encourages the technological evolution of cement-based materials is the introduction of multiple functions in the same constructive element, in addition to the simple structural use. The needs of modern society have become more complex compared to the past, and a wide range of studies aims to improve the quality of life in buildings through the pollutants removal, the protection of electronic devices and the enhancement of structural safety.
An interesting solution to these different problems is the production of innovative and multifunctional cement-based materials, characterized by high mechanical performance, thanks to the insertion of specific admixtures into the composites.
Material engineering contributes greatly to this field of study thanks to the development of hi-tech nanomaterials, such as *carbon fibers*, *carbon nano-fibers* and *carbon nanotubes*, characterized by high mechanical performance and many other properties, such as high electrical conductivity [5][6][7][8].
However, in recent decades, a new nano-material has attracted concern in this field of study, and in many other areas of research and industry, that is *graphene*.
This novel material, once described in a purely theoretical way, was successively isolated in 2004 and its use has spread to many research fields because of its unique properties (Fig. 1.1) [9]. Graphene is characterized by a very high mechanical resistance, photocatalytic properties and a high thermal and electrical conductivity [10][11].

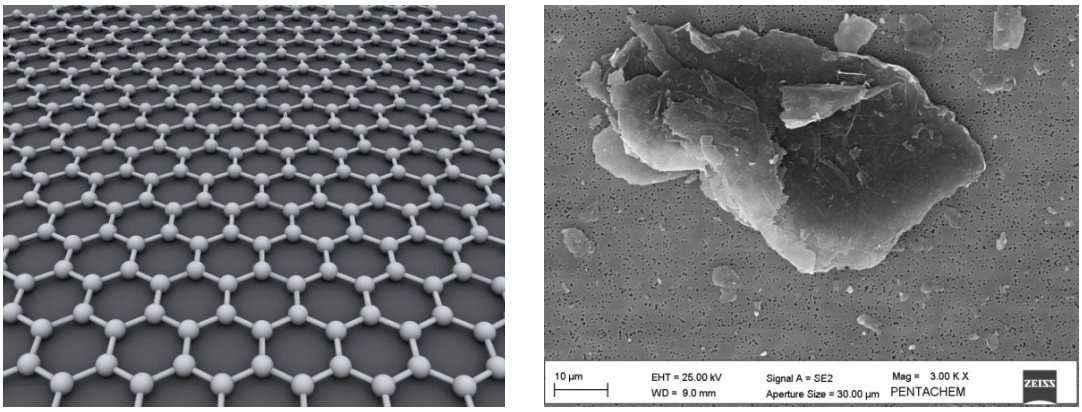

(a) (b)

Figure 1.1. *a) Graphene structure in atomic-scale b) Graphene nanoplatelets (SEM)*

Graphene and other carbon-based fillers, dispersed in a cement-based mixture, form an effective network of high-performance particles, transforming the material in a multifunctional composite [12] (Fig. 1.2).

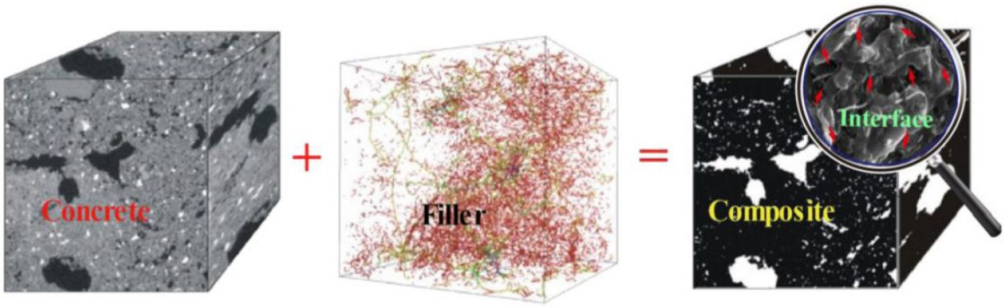

Figure 1.2. *Structure of Multifunctional cement-based composite*

These composites could be used in different applications. For example, they can be integrated as sensors for *structural health monitoring*, since when the hardened composite is subjected to compressive or tensional deformations, the distance between particles change, changing the electrically conductive paths and giving the material strain-sensing properties [13].
However, the introduction of these types of admixtures within the construction materials industry is hampered by several factors. Carbon-based nano-materials, such as graphene or nanotubes, still have very high prices, because of their high technological level and their complex production process. Furthermore, their production techniques are still unable to satisfy the needs of cementitious materials market and its high sales volumes.
The need for high quantities of fillers at low prices could direct this research into the use of recycled carbon-based fillers, obtained by industrial by-products.
In recent years, the use of recycled materials has become of primary importance in cementitious materials research field, for the reduction of the carbon footprint associated with ordinary Portland cement production, and for an eco-friendly building industry.
Nowadays, there are not many studies on multifunctional cement-based materials with recycled fillers addition. Some research have been performed on cementitious composites realized by adding recycled carbon fibers, obtaining good results of mechanical resistance and a remarkable reduction in electrical resistivity [14][15][16].
With regard to recycled powders, some studies have been performed adding vegetable organic-based fillers in cementitious materials, in order to improve their mechanical properties and to reduce their total porosity [17]. Similar tests are carried out on concretes added with foundry sand obtained as a waste industrial by-products of ferrous metallurgy [18][19]. Although the effects of fillers on the cement matrix and on the porosity of the material were analyzed, no tests were performed to study other functions of additions.
The main objective of the present dissertation is to study the effects of new types of recycled carbon-based admixtures on cement-based materials, comparing their effects with those of commercial and high-performance materials such as graphene or virgin carbon fibers. The properties of the multifunctional composites will be investigated in terms of *mechanical strength*, *durability* and *depollutant effect*, in addition to the study of other properties such as *electromagnetic shielding* and *stress-sensitivity* through the increase of their *electrical conductivity*.

1.3 Motivations and objectives

1.3.1 Decreasing the carbon footprint of cement by enhancing the life cycle of concrete

The *construction industry* represents the productive sector with the greatest number of human and technological resources employed and in which the highest number of raw materials are used [20].
Concrete, the most used material in construction, is the most employed human-made product in the world [21][4]. The basic component of this composite is *Portland cement*. European Cement standard EN 197-1:2000 defines 27 distinct common cement products (termed CEM) and their constituents, grouped in five classes (CEM I - CEM V), (Fig. 1.3). Portland Cement clinker (standard symbol K) is the main constituent of CEM cements and it is made by sintering a precisely specified mixture of raw materials (raw meal, paste or slurry) containing elements, usually expressed as oxides, CaO, SiO_2, Al_2O_3, Fe_2O_3 and small quantities of other materials.

CEM cements	Name	% Clinker content (K)
CEM I	Portland cement	>95%
CEM II	Portland composite cement	65-94
CEM III	Blastfurnace cement	5-64
CEM IV	Pozzolanic cement	45-89
CEM V	Composite cement	20-64

Figure 1.3. *EN 197-1, cements classification*

However, the main problem of the construction industry is the high environmental impacts linked to the cement production: global cement industry is responsible for at least 5% of global carbon dioxide emissions and cement production is energy-intensive accounting for 2% of global primary energy consumption; and 5% of global industrial energy consumption (Fig. 1.4) [22]. In particular, each kg of Portland clinker, component strongly correlated with concrete strength and durability, emits almost 1 kg of CO_2 to the atmosphere, contributing heavily to cement and concrete carbon footprint [23].

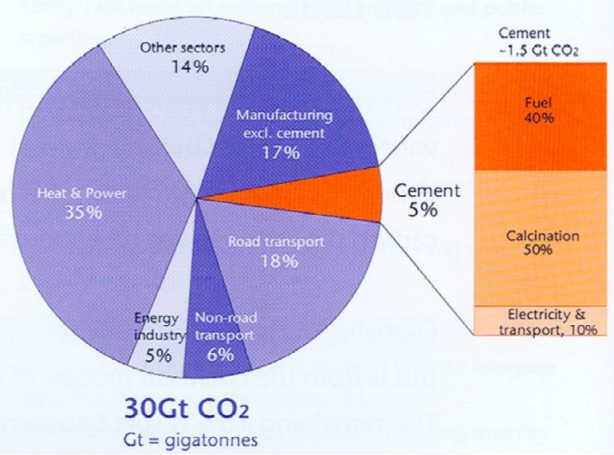

Figure 1.4. *Worldwide CO_2 emissions from cement production* [24]

The improving of production methods and formulations that reduce CO_2 emissions, and raw material use from the concrete and cement manufacturing process is the main objectives of research on building materials and one of the most important topics of the *European Commission agenda* and *European Construction Industry*.
In this context, European and international industries and research centers are investing on improving the environmental friendliness of concrete to make it suitable as a "Green Building" material, by substituting a percentage of Portland clinkers with supplementary materials such as by-products of industrial processes. It is important to note that in a life cycle perspective, the overall energy, material consumption and carbon footprint of concrete can be improved also by increasing the durability of concrete and thus the service life of buildings and infrastructures.
Therefore, further research and innovation efforts are needed from one side to develop innovative sustainable concrete solutions, based on low clicker cement (e.g. < 65%) and from another side to test them in order to assess their high durability when applied also to infrastructures of high economic and social impact and subject to harsh environments where the cost-effectiveness, easy installation and durability of concrete is real added value.
The present dissertation is integrated into this field of study, through the development of structural composites realized with the addition of carbon-based fillers/fibers, in order to decrease the amount of cement in the mixture, but increasing the mechanical properties and durability of the hardened composite. The combined and weighted addition of these materials leads to a reduction in the total porosity of the composite, thus decreasing the risk of pathogens penetration [25][26]. This effect, combined with the mechanical "bridging action" of the fibers [15], allows increasing both the mechanical strength and the durability of the composite, with a lower cost of money and resources for its construction and maintenance.

1.3.2 New functions in cement-based finishes: depolluting properties and electromagnetic interference shielding

In recent years, the progress of medical scientific research has highlighted the problem of pollutants such as VOCs (*Volatile Organic Compounds*) inside buildings, which can lead to health problems due to s*ick building syndrome* [27][28].
Research on building materials is experimenting with new finishes made with high-adsorbent materials, for the reduction of pollutants in building environments. Some types of carbonaceous materials, such as *activated carbon* and other types of charcoal, have a high adsorbent properties, thanks to their high porosity [29], and could be used for the development of plasters with high depolluting power. Other materials, such as graphene, have proven *photocatalytic properties* [30], and could be used for the realization of finishes capable of reducing the concentration of pollutants by photochemical reactions.
Moreover, in modern society the correct functioning of electronic equipment is of fundamental importance, and research is developing electromagnetic shielding systems to avoid interference when using sensitive instruments [31]. The development of finishes and concretes with high electrical conductivity, thanks to the introduction of carbon-based admixtures, could lead to the realization of highly shielding environments for the protection of technologically advanced electronic devices [32][33].

1.3.3 Structural Health Monitoring

The sustainability level linked to building products and infrastructures is closely tied to its maintenance and the promptness of intervention in case of wear and damage. A continuous monitoring of the health state of structure allows a more effective intervention, reducing the repair costs and resources [34][35].
Because of the increasing number of structures that have reached the theoretical limits of their service life [2][36] and because of recent and dire seismic events, a prompt analysis of the conditions of infrastructures has become of primary importance for safety and human health.
Therefore, it is essential to check the actual structural behavior of buildings, in order to identify promptly any signs of incipient damage. Furthermore, the structural monitoring allows optimizing and accelerating the inspection and maintenance operations, with a consequent increase in safety of structures and people.
Strain gauges are a widely used instrument for the measurement of materials deformation. These, applied to the surface of the analyzed element, allow an accurate measurement of its deformation degree, thanks to the piezoresistive effect. *Piezoresistivity* is a physical characteristic of electrically conductive materials which leads to a variation in their electrical resistivity when the element is subject to strain stress [37].
This dissertation studies the development of *smart* mortars and concretes that, in addition to their structural function, are able to diagnose their "state of health", modifying their electrical behavior in presence of strain or damage thanks to the piezoresistivity [38]. The addition of conductive particles, such as carbon-based fillers and fibers, increase the electrical conductivity of cement-based composites, in addition to improve mechanical and durability performances, thanks to the intrinsic electrical properties of carbon and to the reduction in porosity. Moreover, when the composite is subjected to deformation or cracking, the interaction space between the conductive particles changes, modifying the electrical parameters of the multifunctional composite [14][39] (Fig. 1.5).

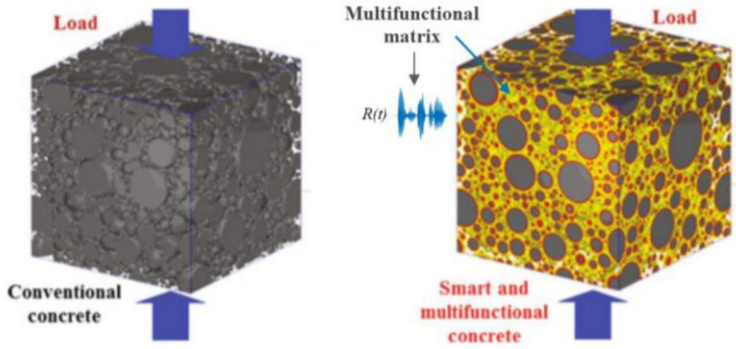

Figure 1.5. *Comparison between conventional and multifunctional concrete*

Other types of monitoring systems have been experimented in concrete structures, such as optic sensors, piezoelectric ceramic, shape memory alloy, and fiber-reinforced polymer bar. However, these sensors have several drawbacks, in particular poor durability, inadequate compatibility and difficulty of application. Furthermore, these systems can be

installed only in critical points of the structure, and do not guarantee a continuous and effective monitoring.
Contrariwise, the multifunctional cement-based materials studied in this dissertation could be applied as traditional mortars or concretes, and could be used on a large scale thanks to their low production cost, thus allowing acquiring a large amount of information about the conditions of the structure.

1.3.4 Recycling of carbon-based industrial by-products

Carbon is at the base of life on earth, and its many allotropic and mineral forms are fundamental elements within industry. Moreover, it is the main component of fossil fuels, indispensable for modern industrial development, and it is the main element of many industrial raw materials. As a result, many industrial processes produce a large volume of carbon-rich by-products. The disposal of these wastes requires labor and economic squander, as well as large amounts of energy, and the removal processes are often harmful for the environment and human health.
This thesis investigates a potential alternative for the recycling and valorizing of carbonaceous wastes within building industry, thus relieving the disposal volume of some industrial sectors in a field with a high demand for raw materials (Fig. 1.6).

(a) (b)

Figure 1.6. *Production processes with carbonaceous waste: a) Gassification plant b) Ferrous metallurgy*

Other types of industrial waste derive from the processing of composites and technologically advanced materials, made of *carbon fibers*. The cutting and milling processes of these elements produce waste microfibres, reusable for other industrial purposes [40][41]. This research will examine the potential of this type of fibers for the production of cementitious materials, as an alternative to traditional “virgin” carbon fibers.

1.3.5 Development of high-performance composites for concrete repair

The experiments performed within this dissertation will also be used for the development of a new generation of mortars with high resistance and high durability for the structural restoration of deteriorated concrete. The project is co-financed by DiaSen s.r.l., located in Sassoferrato (AN, Italy), a company very involved in the green-building sector.

For decades, DiaSen s.r.l. has been producing plasters and buildings finishes entirely realized with eco-friendly, natural or recycled materials. The introduction of a new line of *repair mortars* with carbon-based additions will contribute to the creation of durable and highly compatible systems for the restoration of reinforced concrete structures (Fig. 1.7).

Figure 1.7. *Properties of repair mortars with carbo-based fillers*

1.4 *EnDurCrete* project

The *EnDurCrete* project, which stands for "*New **En**vironmental friendly and **Dur**able con**Crete***", aims to integrate industrial by-products and hybrid systems, by the development of a new eco-friendly and low-cost reinforced concrete [42].
As seen previously, the production process of ordinary Portland cement consumes significant mineral resources, energy and fuel, and creates greenhouse gas emissions. Various efforts are underway to improve the environmental friendliness of concrete, by integrating *Supplementary Cementitious Materials* (SCM) [43], such as by-products of industrial processes. Nevertheless, current state of the art on sustainable solutions based on high substitution rate of Portland cement clinker by SCM occasionally lead to limited performance and durability of concrete structures [44], particularly critical when applied in harsh conditions. All these aspects affect also the resource consumption, waste production, environmental and economic costs of repair and replacement.
In this framework, EnDurCrete Project aims to develop a new cost-effective sustainable reinforced concrete for long lasting and benefit applications [42]. The concept is based on the integration of novel “low-clinker” cement including high value industrial by-products, new nano/micro technologies and hybrid systems ensuring enhanced durability of sustainable concrete structures with high mechanical properties and self-monitoring capacities.
The project is funded under the *Horizon 2020 Call for nanotechnologies, advanced materials, biotechnology and production* (Topic NMBP-06-2017).
Figure 1.8 shows a glance of the overall concept, by a schematic resume of the research areas.

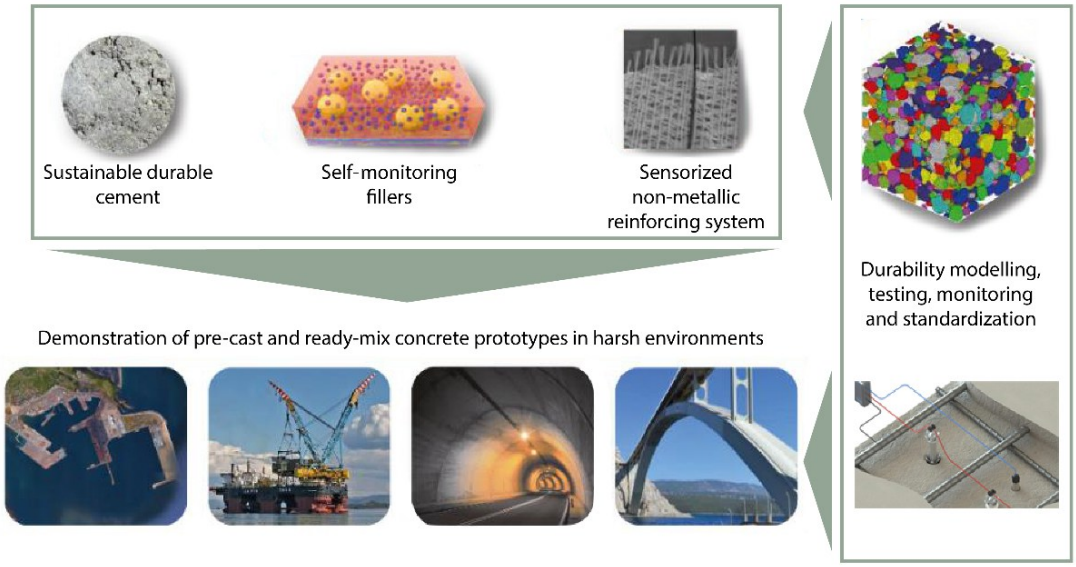

Figure 1.8. *Overall concept of EnDurCrete project*

This dissertation is integrated into the area of experimentation and optimization of the innovative cement-based composite (top-left in Figure 1.8), i.e. in the study of:

- *Novel cement*, produced by including sustainable, high-quality supplementary cementitious materials;
- *New smart fillers,* based on micro carbon-based materials derived from industrial by-products for mechanical and self-sensing properties (the structural self-sensing properties will be complemented with environmental sensors casted in the concrete elements);
- *Concrete non-metallic multifunctional reinforcing systems*, based on electrical conductive and high-strength carbon fibers, enabling both structural reinforcement and continuous structural health monitoring. The systems will be optimized aiming at a proper trade-off between productivity, robustness, and concrete reinforcement adhesion;

In addition, the project pursue the development of advanced non-destructive continuous monitoring and testing tools and procedures, to better exploit the potential of multifunctional cement-based composites with effective measuring instruments.
Lastly, a coupled experimental and computational approach for theoretical and experimental understanding of factors affecting concrete durability will be performed. This will enable long-term durability assessment and resulting service life prediction of the target infrastructures exposed to severe environment.
The technologies developed within the project will be tested under real service conditions, i.e. in working sites of tunnels, ports, and offshore structures, in order to prove the enhanced durability and decreased cost of the new concrete systems in such critical applications. These tests will be the first applications in which the SHM systems will be studied in operational and large-scale infrastructures [4].
Figure 1.9 shows the location and type of working site for the demonstration tests.

Figure 1.9. *Map of infrastructures for demonstration tests: 1) Port of Gijón "El Musel", (Spain), exposed to seawater conditions of the Cantabrian Sea; 2) Mining tunnel facility (Leon, Spain); 3) Ship Yard in a Norwegian cost line (Norway); 4) Krk Bridge, characterized by a very aggressive marine environment (Croatia)*

1.5 Research methods

The different cementitious composites analyzed during the research and the variability of their application fields, led to the need for a detailed study of the state of the art on carbon-based additions, divided into different topics.
Furthermore, an important part of the research will be dedicated to the study of the electrical properties of cement-based composites, in order to evaluate their potential use as smart and multifunctional materials. Whereas methods used for testing the mechanical and durability properties of building materials are widely described and regulated by appropriate regulations (together with the chemical-physical and microstructural characterization), techniques for the evaluation of the electrical resistivity and piezoresistivity of cementitious materials are not standardized, and they can widely change depending on the needs of the study. This requires an in-depth analysis of the measurement configurations and devices used in literature for the evaluation of the electrical parameters of mortars (resistance and resistivity) and the sensitivity of these parameters under mechanical load (piezoresistivity).
Initially, the state of the art of cement-based composites added with carbon-based materials will be analyzed, focusing on the effects provided by fillers and fibers in terms of mechanical strength, durability, depollution and electrical properties.
Subsequently, the electronic theories, at the base of the searched properties will be resumed, in order to understand the mechanisms that regulate the electrical behavior of mortars and concretes. Furthermore, the state of the art connected to techniques for measuring the electrical properties of cementitious composites will be studied, analyzing

the different methods (direct or alternating current) and the configurations for the realization of the specimens (connections, number of electrodes, etc.).
The last part of the preliminary study will concern the selection and characterization of the raw materials for the production of multifunctional cement-based materials, in accordance with the analyses of effectiveness performed in the literature review.
After the phase of preliminary study, the first step of the work will be focused on the study of hydraulic lime pastes added with carbon-based fillers, to better study the effect of fillers on the matrix of a hydraulic binder. In this phase the microstructural properties of fillers and pastes will be analyzed, together with their chemical-physical characteristics. Initially, studies will be performed for the optimization of the dispersion of fillers within the cement matrix. Later, for the verification of the most promising properties of carbon-based materials, tests of mechanical strength, durability (water absorption), depolluting properties (adsorption, photocatalytic feature) and electrical properties (resistivity, electromagnetic shielding) will be carried out.
Thanks to the good results obtained from the conductivity tests and because of the growing interest of the engineering research regarding monitoring systems, the second part of the work will be dedicated to the study of conductive fibers (carbon and steel fibers), materials of proven effectiveness in this research field. Mortars containing different quantity of fibers will be realized, in order to find the best compromise between increase in electrical conductivity, workability and mechanical properties. In addition, durability tests (shrinkage, water absorption) and microstructural tests (porosimetry, SEM) will be performed for the assessment of the potential life cycle of the mixtures.
In the last part of the research, the joint use of fillers and fibers will be investigated to combine the most promising characteristics of both materials. Structural mortars with filler and fiber will be realized, and the addition quantities will be decided in agreement with those that had obtained the best performances in the previous tests. This phase will be focused on the study of "piezoresistivity" of materials, analyzing the variation of the electrical parameters of specimens subjected to cycling loads and strain. Furthermore, tests of mechanical characterization and durability (water absorption) will be performed. This last phase of research was carried out at the *Department of Civil Engineering* (DECivil) of the *University of Aveiro* (Aveiro, Portugal).
The test methods used during the entire research with the relative standards are:

- *Workability* tests and consistence measurement of fresh mortars (UNI EN 1015-3:2007, UNI EN 1015-4:2000);
- Tests of mechanical *flexural* and *compressive strength* (UNI EN 1015-11:2007), and *tensile splitting* tests (UNI EN 12390-6:2010);
- Evaluation of *capillary water adsorption* (UNI EN 1015-18:2004, UNI EN 15801:2010);
- Tests of free *hygrometric shrinkage* (UNI EN 12617-4:2003);
- Electrical resistivity measurement (2 electrodes AC and 4 electrodes DC);
- Tests of *electromagnetic interference shielding* (*Nested Reverberation Chamber*, NRC);
- Piezoresistivity tests (continuous resistivity measurement during load cycles);
- *Pollutant adsorption* tests (reduction of methyl ethyl ketone in gas chromatography);

- Test of photocatalytic properties (measurement of nitrogen oxides reduction, with a plug-flow reactor, UNI 11247:2010);
- Evaluation of the porosimetric characteristics (*Mercury Intrusion Porosimetry*, MIP);
- Microstructural analysis with *Scanning Electron Microscope* (SEM) and *Energy-Dispersive X-ray* (EDX) spectroscopy.

2 . Chapter Multifunctional Cement-based Composites

State of the art on multifunctional cement-based composites added with carbon-based materials

2.1 Introduction

Concretes, mortars and other cement-based composites are the most common structural materials in the construction industry [4].
The hydraulic binders-made composites were discovered and used thousands of years ago, and, thanks to their immediate effectiveness, their modern production techniques have remained very similar to antiquity. However, the great technological development of materials science and nanotechnology in recent decades, has allowed new opportunities for the development of cementitious mixtures, through the introduction of new techniques and innovative materials. This permits creating composites with many additional characteristics (besides structural properties) aimed at improving safety and life quality inside buildings.
This chapter analyzes the evolution of hydraulic binders-based materials in history, until the development of smart and multifunctional composites. Successively, cementitious materials added with carbon-based fillers/fibers are introduced, analyzing the state of the art divided by main topics. Lastly, a review of the effects of carbon-based materials on environment and human health has been performed.

2.2 Cement-based materials: history and evolution

The most used composite material in construction, in which Portland cement is a key component, is concrete. Although modern concrete production techniques have developed just in the last two centuries, artificial conglomerates have a very ancient origin, given that civilizations such as Assyrians [45], Egyptians and, later, Greeks [46] used similar artificial materials.
However, it was the Romans who optimized this constructive technique, with the use of the *Opus caementicium*, producing very advanced works and infrastructures for the time (Fig. 2.1) [47].

(a) (b)

Figure 2.1. *Examples of ancient concrete artefacts: a) Assyrian Jerwan Aqueduct [45], 688 BC b) Roman Pantheon, 128 AD*

After the fall of the Roman Empire, in the 5th century, these constructive techniques were set aside and forgotten, until the humanistic reawakening, after the 14th century, when

the texts of *Pliny the Elder* and *Vitruvius* were rediscovered. In the following centuries, the continuous approach to the rediscovery of concrete led to the discovery of *hydraulic lime*, which marks the technological transition from Roman's Opus caementicium to modern concrete [48]. In these years, there was a development of the chemistry knowledge and of cooking techniques, which led to the manufacture of Portland cement at the beginning of the 19th century [49].
The name "Portland" derived from the similarities found between the "artificial stone", obtained by mixing cement with water and aggregates (today called "concrete" or "mortar"), and the limestone from the British isle of Portland, extensively used as a building stone throughout the British Isles at that time [50].
During the industrial revolution and until the present day, the techniques of production and processing of cement have continuously evolved, and innumerable patents have been registered on further evolutions of the material [4].
Today, cement is used as a binder in a wide range of construction products, with particular emphasis on concretes and mortars. Both are based in similar compositions, which essentially include Portland cement, aggregates and water, being mainly differentiated by the size of the aggregates (coarser in concrete). Cement-based products are generally considered *two-phase* materials, constituted by a cementitious matrix and aggregates. The matrix consists of a cement paste, resulting from the cement hydration, with the function to bind the aggregates together, and create a material similar to an artificial stone (Fig. 2.2).
Several additives can be used to improve or correct workability, setting time, mechanical strength or durability of these mixtures.

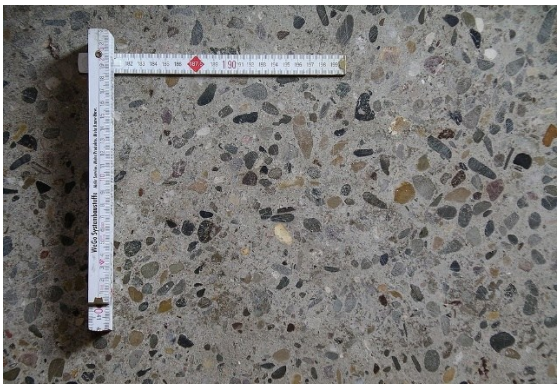

***Figure 2.2**. Traditional concrete surface. Aggregates are distinguishable from the cement matrix*

2.3 Overview of multifunctional cement-based materials

The technology linked to cementitious materials has certainly reached important milestones, but, in recent decades, the needs of the building industry have become numerous and increasingly complex. Buildings are no longer required to have a simple structural function, but to contribute to the daily well-being of its inhabitants [51].
For this reason, the European Union is very active in the production of laws and standards for the regulation of the wholesomeness of living environments and structural safety [52].

This led to the need to implement construction materials with new functions, in order to introduce new technological systems to improve the use of living space. In the last decades, many researchers have been focused in the development of cement-based products capable of performing autonomous tasks without the need of external devices, the so-called *Multifunctional cement-based composites* (MCC) [38].
As already mentioned, cementitious materials such as mortar and concrete can be considered "two-phase" materials: the cement matrix consists of the *reagent* part of the mixture, i.e. the hydraulic binder; the *inert* part is instead represented by the aggregates, held together by the cement paste and which compose the "backbone" of the material. The coarse and fine aggregates traditionally used are gravel and sand, but these can be replaced by other materials, depending on the properties sought in the composite.
Such functionalities are obtained by adding specific admixtures in the compositions, resulting into functional cement matrixes, with rather complex *multi-phase* and *multi-scale* structures (Fig. 2.3) [12].

Figure 2.3. *Concept of Multifunctional cement-based materials*

For example, mortars and plasters can be realized with artificial or natural lightweight aggregates, in order to increase the porosity of the material, obtaining thermal insulation [53], and a similar approach can be used to realize sound-absorbing or sound-insulating plasters (Fig. 2.4) [54].

Figure 2.4. *Hydraulic lime-based plaster realized with natural organic aggregates (cork) for thermal insulation and acoustic absorption*

Adsorbent materials, capable of eliminating pollutants [55], or photocatalyst materials (TiO_2) which decompose harmful products, such as VOCs, can be inserted into the mixtures [56].

The mechanical properties of the cement paste can be improved considerably by inserting steel or carbon fibers [57], which, while not participating in the hardening reaction, improve the mechanical behavior of the composite, in particular the tensile one through the "bridging effect" [58].
Through the insertion of new functionalities, it is also possible to intervene on the traditional problems of concrete structures. One harmful property of concrete is the propitiousness to crack formation, consequence of limited tensile strength. This phenomenon induces carbonation and chloride penetration, leading to the corrosion of the reinforcement and subsequent decrease in the life-span of structures [59].
For this reason, starting from the 90s, multifunctional cementitious materials with *self-healing* properties were studied. The first studies were based on the addition of encapsulated polymers-based products, which are released following the formation of cracks due to thermal effects [60]. In the following years, numerous studies emerged, based on bio-inspired approaches. In turn, the self-healing capacity is induced by mixing bacteria in the concrete [61]. Initially immobilized, bacteria are activated once water permeates into fresh cracks and start to precipitate calcium carbonate-based minerals ($CaCO_3$), filling the interstitial voids (Fig. 2.5) [62].

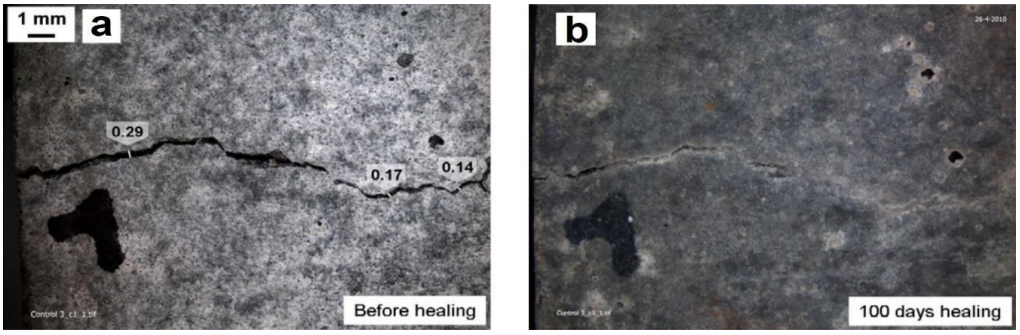

Figure 2.5. *Healing of a crack in a self-healing concrete after 100 days under wet conditions* [63]

Recent studies have shown that it is also possible to produce multifunctional concretes for energy collection, thus creating environmentally friendly and eco-sustainable infrastructures. These composites can accumulate energy deriving from external sources (mechanical energy, thermal and solar energy, etc.) [64][65]. These collectors can turn into widespread energy generators, and support future electric transport systems [38].

2.3.1 Electrical conductive cement-based materials

A parameter that particularly conditions the functionality of a composite is its ability to conduct electric current. Researchers discovered that, by acting on the electrical properties of cementitious materials, it is possible to implement them with many different functions. Thanks to the addition of conductive materials, the electrical conductivity of the whole composite [66] can be increases adding a wide range of new properties.
For example, concrete might generate resistive heating, by imposing an electric current (according to the Joule's law) across two embedded electrodes (Fig. 2.6) [67].

Figure 2.6. *Installation of embedded electrodes and monitoring system in a self-heating concrete pavement* [67]

This effect has the objective of creating simple and effective systems for road surfaces defrosting and improving road safety in cold areas during the winter period (Figure 2.7). This would also eliminate the need for salt and chemical antifreeze products, which will damage the concrete and cause corrosion of the reinforcements.

Figure 2.7. *Operation of a self-heating concrete pavement after a snow fall* [67]

Cement-based materials with high electrical conductivity are also very interesting for electromagnetic shielding functions [68]. Usually, for the absorption of electromagnetic fields, systems composed of highly conductive materials (usually metallic) are used, as for *Faraday cages*. The shielding level depends on the electrical and dimensional properties of the conductive material, such as resistivity and thickness, and the effectiveness depends on the frequency of the electromagnetic waves [69]. In recent years there has been a growing interest for these shielding systems, due to the high diffusion of electronic devices, and the uncertainties related to the effects of electromagnetic radiation on human health.

For this reason, mortars and plasters made with conductive admixtures could be an effective solution for creating building “shells" with shielding properties. Several studies have actually shown an increase in the electromagnetic wave adsorption of cement composites in relation to an increase in electrical conductivity thanks to the addition of carbon nanotubes [70], carbon fibers and carbon black [71].

As seen, multifunctional composites can also be used as energy collectors. The electrical conductivity of cementitious materials also influences this type of functionality. For

example, the accumulation of mechanical energy is possible thanks to the piezoelectric properties of conductive concretes, and the ability of the materials to generate electrical charge from applied voltages [72][73][74].
Recent research has shown that electrically conductive concretes can transform solar energy into electrical energy, if treated with special multilayer coatings realized with titanium dioxide and graphite (Fig. 2.8) [75].

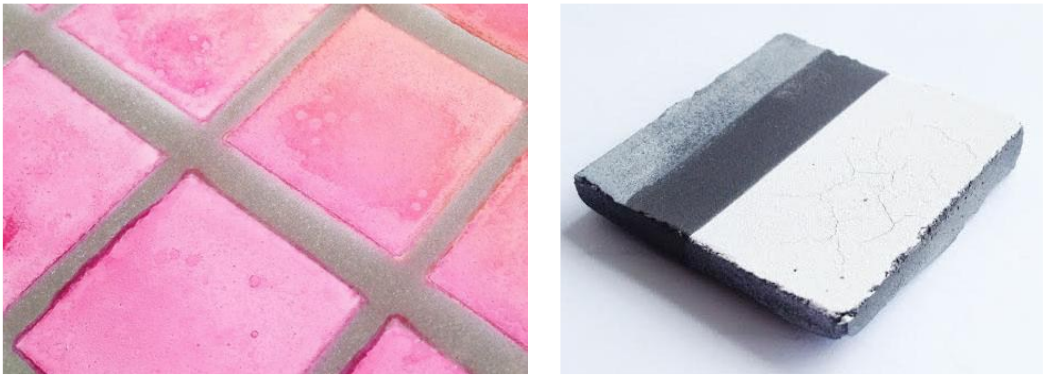

(a) (b)

Figure 2.8. *Fabrication process of solar energy harvesting concrete. a) Currant juice layer and b) Graphitic and TiO_2 layers* [75]

But one of the most interesting features of conductive cement composites is their sensitivity to stress deformation, i.e. their "self-monitoring" ability. Chung et al. [13] have firstly addressed pressure-sensitivity in concrete. The research group demonstrated that the addition of conductive fillers into conventional cement pastes could induce piezoresistivity, after observing linear changes in resistivity upon different external stimuli. This property has been used in various fields of study, e.g. in cement-based sensors for the monitoring of road traffic [76][77][78], elements made with multifunctional mortars or concretes and distributed on road surfaces, able to communicate with precision the passage of means of transport (Fig. 2.9) [79].

(a) (b)

Figure 2.9. *Self-sensing system for traffic monitoring: a) Placement of the cement-based sensor array; b) Overview of the system* [80]

But especially, these materials could be effectively used for the Structural Health Monitoring (SHM) of concrete elements [12]. This work is particularly focusing on this

property, with the aim of creating cement-based sensors for the replacement of some traditional monitoring systems, characterized by various functionality and maintenance problems (Fig. 2.10) [81].

Figure 2.10. *Experiments on a RC frame with embedded cementitious stress-sensitive elements* [81]

However, even cement-based "sensors" may not guarantee optimal control of structural health. Usually, due to the high cost of admixtures and to the dispersion difficulties, they must be applied selectively and locally [8].
Therefore, this dissertation studies the possibility of producing low-cost materials, producible on a large scale, and usable in a widespread way in the infrastructures construction. In this study, the traditional functions of the cementitious material are implemented thanks to the insertion of recycled products with particular properties and widely available from some industry sectors.

2.4 Cement composites and carbon-based fillers: state of the art

Some of the most promising types of admixtures for the production of multifunctional composites are powders (*nano/micro fillers*) with a high content of carbon.
Carbon and its many allotropes form a wide range of high performance materials widely used in the field of nanotechnologies.
The most commonly used nanometric materials for the functionalization of composites are *carbon nano-fibers*, *carbon nanotubes* (single-walled or multiple-walled), different forms of *graphite*, *graphene* and *graphene oxide* (Fig. 2.11).

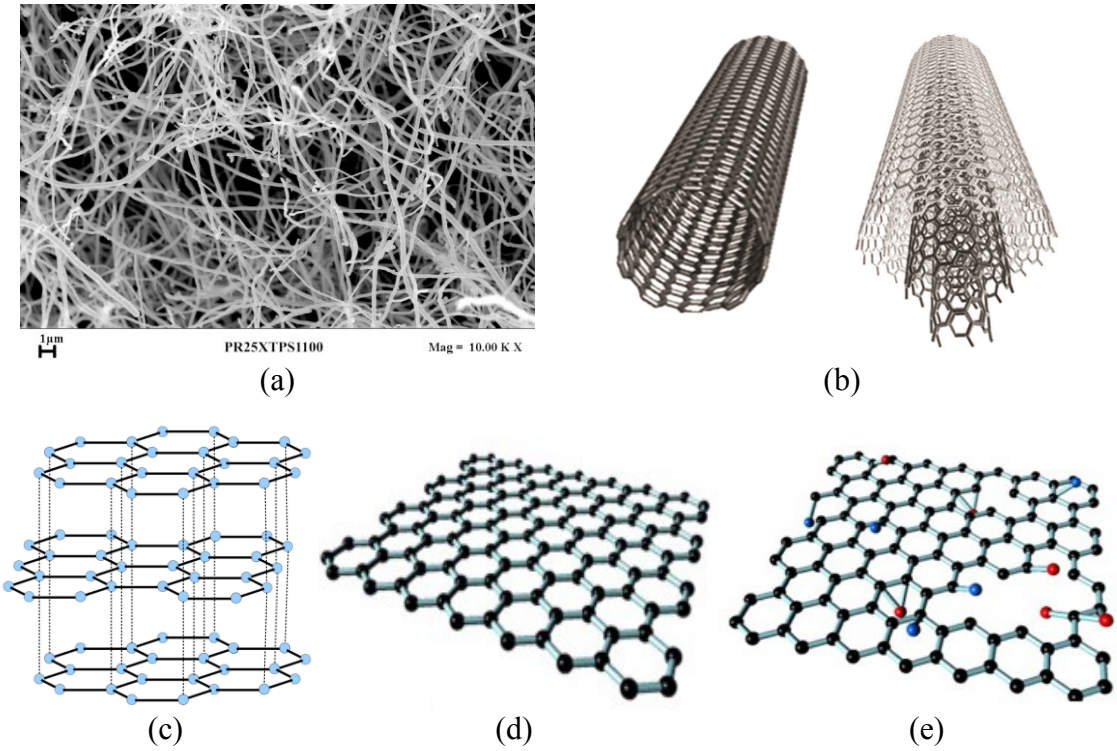

Figure 2.11. *Carbon-based nanometric materials: a) Carbon nanofibers; b) Single-walled and multi-walled carbon nanotubes; c) Graphite; d) Graphene; e) Graphene oxide*

In particular, technologically advanced nano-materials have been widely used in *polymeric materials* production [82] and in sectors such as *biomedical engineering*. Due to their high cost, their use in construction materials research is still very limited.
Therefore, other types of carbon powders, already used in several industrial sectors, have also been studied. Nano-powders such as *carbon black* (Fig. 2.12), widely used as a pigment, in the tire industry and as thermal conductor. Another interesting material is *activated carbon* (Fig. 2.12) [83], already used in the industry because of its high porosity and for its extraordinary adsorbing properties (for this reason it is used in the construction research for the realization of depolluting plasters).

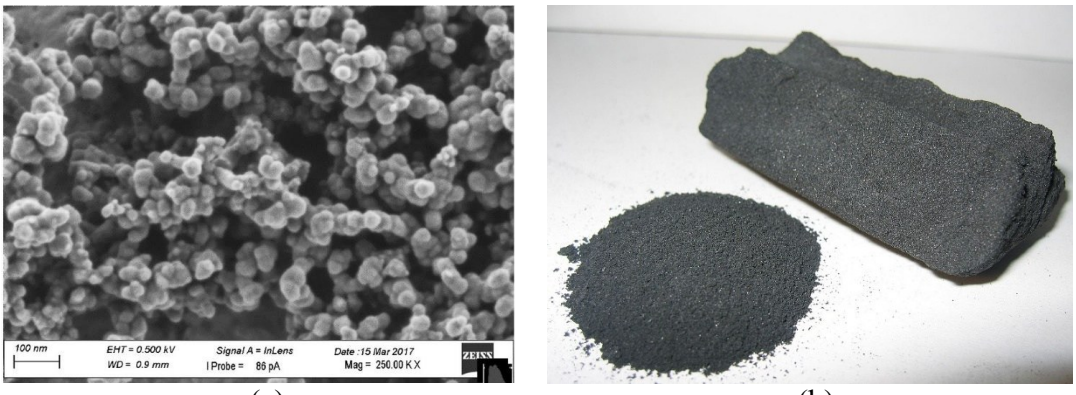

Figure 2.12. *Other types of carbon-based powders: a) Carbon black (particles agglomerates); b) Activated carbon*

In addition, other recycled carbonaceous powders [84] are used, generally obtained by processes of carbonization of organic waste by pyrolysis (*gasification char*) or by grinding the waste obtained from other industrial processes, such as *foundry sand* (Fig. 2.13).

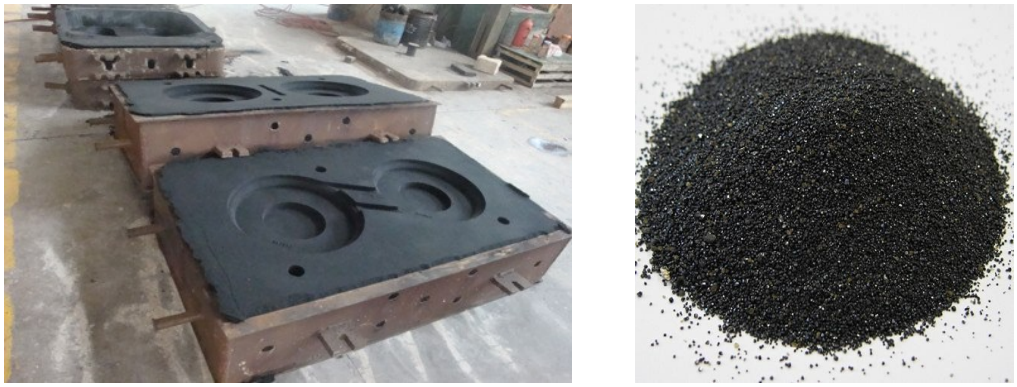

(a) (b)

Figure 2.13. a) Molds used in the steel industry; b) Recycled foundry sand obtained from the molds

Each of these innovative materials has multiple and specific characteristics, and can offer different properties to the composites depending on their microstructure and their chemical nature [5]. Below, the major results obtained from the use of these materials for the production of cement-based composites are summarized, focusing on the specific properties analyzed. The effect of additions on the electrical properties of mixtures is one of the main topics of the dissertation, and it will be better analyzed in the next Chapters.

2.4.1 Mechanical properties

Some allotropic forms of carbon represent the most resistant organic materials in nature. Breaking *carbon-carbon* hybridized bonds requires large amounts of energy, and this makes materials such as carbon nanotubes or graphene extremely more resistant than steel, but in relation to a much lower mass (graphene has a breaking load of 130 GPa and a modulus of elasticity of 1 TPa).
However, within the cement-based materials, their contribution is influenced not only by their physical properties, but also by their surface and microstructural characteristics, and by the interface with the cement matrix.
In general, thoughtful filler quantities show an increase in the mechanical performance of the composites. Hawreen et al. [85], together with other research groups [7][86], demonstrated the effectiveness of carbon nanotubes in improving the flexural and compressive strength of the mortars, as well as increasing the elastic modulus and cracking toughness. This happens thanks to a good dispersion of the admixtures in the materials and to the effective bridging effect of the nanotubes inside the matrix (Fig. 2.14).

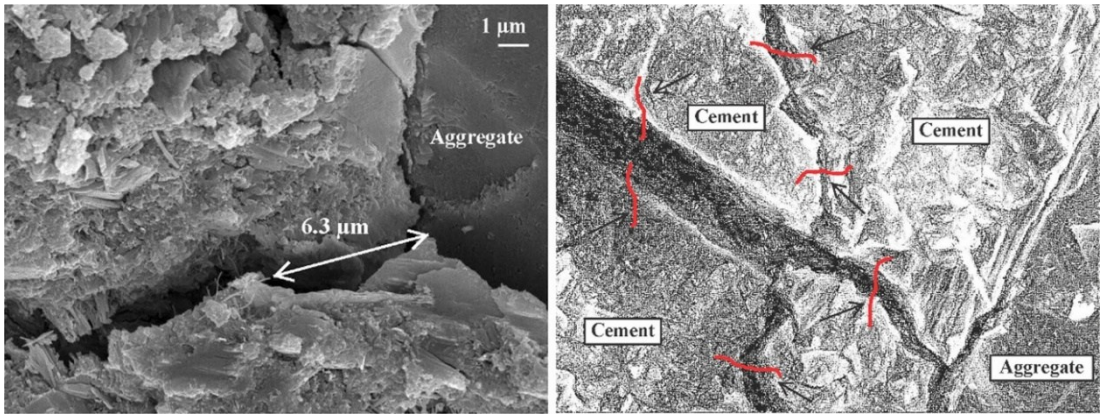

Figure 2.14. *SEM of composite with CNTs addition: a) Detail with aggregate, cement paste and CNT b) Scheme of CNT bridging effect on microcrack* [85]

Jiang et al. studied the mechanical contribution of nano/micro carbon fibers, demonstrating an increase in mechanical performance and an "addition threshold" in which maximum mechanical improvements are obtained (Fig 2.15) [87].

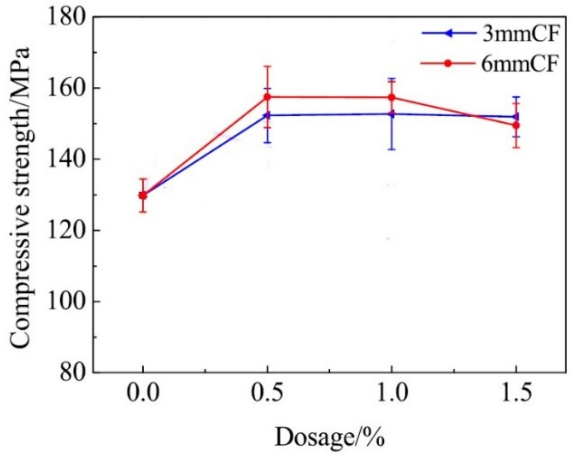

Figure 2.15. *Relation between compressive strength and dosage % of nano and micro fibers on a cement-based composite* [87]

Graphene and its derivative graphene oxide have also shown improvements in the mechanical properties of cementitious materials [88], with increases in flexural, compressive and tensile strength [89]. Graphene lead to a general improvement of the cement matrix, acting on the chemical structure of the binder in the setting and hardening phases [90], regulating the structure of the hydration crystals [91][92][93]. In particular, Tong et al. [94] performed an in-depth chemical and microscopic analysis of cementitious materials with graphene nanoplatelets (GNP) and graphene oxide (GO) addition, demonstrating that the decrease of porous phase and low-density C-S-H gel and the growth of high-density C-S-H gel lead to a denser microstructure for the graphene-reinforced cement paste (Fig. 2.16).

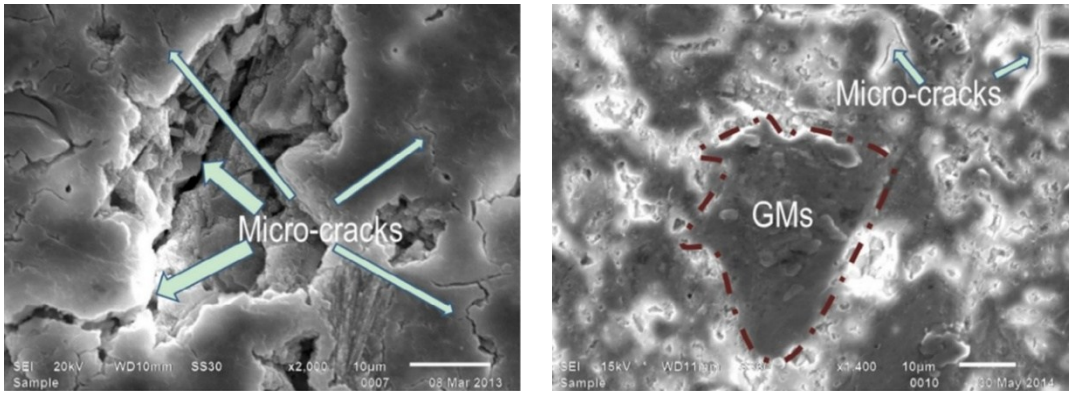

(a) (b)

Figure 2.16. *More dense structure of the cement matrix with GNP addition, compared to the matrix without addition [94]*

Other types of admixtures also lead to improvements in mechanical performance. Monteiro et al. have shown that the addition of carbon black improves the compressive strength and the elastic modulus of mortars, even with high addition doses [95]. This proves that, regardless of the chemical-physical characteristics of the powder, it is possible to obtain an increase in the mechanical strength through the "filler effect", i.e. by reducing the porosity of the material and reducing the *water/solid part* ratio of the mixture.

Other high-carbon recycled powders, such as foundry sand, have shown good results, obtaining a general maintenance of the compressive strength and tensile splitting strength [96]. However, these experiments are focused on the use of foundry sand as an alternative to traditional aggregates, and not as an addition for the production of multifunctional composites. In general, it is always shown that an excessive quantity of addition causes a gradual decrease in the mechanical performance of cement-based material, up to a drastic drop threshold when a specific percentage of addition is exceeded (Fig. 2.17). This is caused by the increase in the water/binder ratio in the mixture, together with the particular interaction of some types of filler with water, which often inhibit the regular process of hydration of the cement [97].

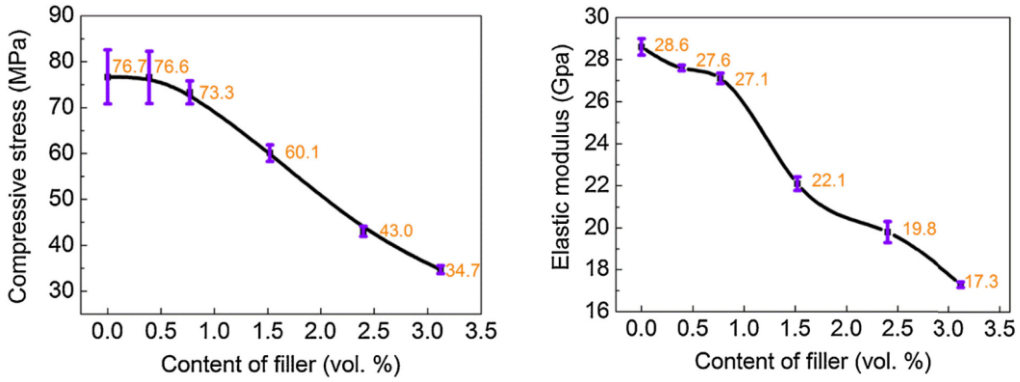

(a) (b)

Figure 2.17. *Effect of the excessive amount of fillers (CNTs and Nano-carbon black) in the compressive strength (a) and in elastic modulus (b) of a cement-based composite* [97]

2.4.2 Durability

The mechanisms that bring additives to increase the mechanical strength in a cementitious material also contribute to the general increase in durability of the composite, thanks to the increase in the microstructure density. However, other factors can influence the life cycle of the material.
As mentioned, the durability of a cement-based material is largely influenced by its water permeability, the main means of transport of aggressive agents within the material. In this way, through the reduction of the porosity of the hardened mixture, it is possible to obtain both an increase in mechanical strength and a lower absorption of water and pathogens.
A detailed study on the durability of concretes with graphene addition was conducted by Tong et al. Using SEM and AFM scans and statistical distribution analyzes, researchers highlighted a significant change in microstructure composition, because a better inter-facial bond is developed between the GNP/GONP and C-S-H gels precipitated around them. Moreover, in deterioration tests, it transpires that the GNP and GONP have the potentials to decelerate chemical attack induced by an acidic solution so as to improve the corrosion resistance of cementitious materials [94].
Lastly, it is demonstrated that the addition of graphene oxide improves the performance of material subjected to freezing and unfreezing cycles.
With GNP addition, the reduction of the critical pore diameter is also obtained, together with a decrease of about 70% of depth penetration of water and of the chloride intrusion coefficient (Fig. 2.18) [98][99].

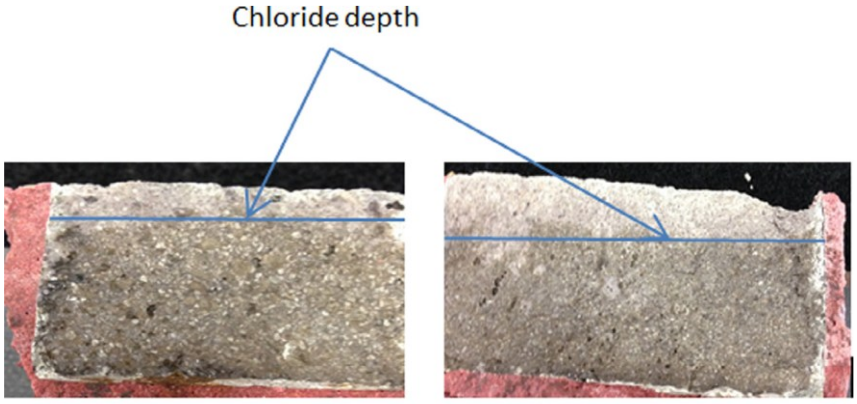

(a) (b)

Figure 2.18. *Penetration of chloride ions into a mixture with GO addition (a) and without GO addition (b)* [98]

Faria et al. studied the graphene oxide behavior also on other types of hydraulic binders. Analyzing mixtures composed of Natural Hydraulic Lime (NHL3.5) and different doses of GONP they have obtained slight improvements, with a decrease in water absorbed by capillarity suction and a higher drying speed [100].
Furthermore, the durability of a cement-based composite is linked to its tendency to crack. Materials with excessive porosity and a low modulus of elasticity can crack due to hygrometric shrinkage, increasing the possibility of infiltration of pathogens for concrete and reinforcing bars.

Carbon nanotubes, due to their morphology, are quite effective for shrinkage reduction. Hawreen et al. have shown a decrease of shrinkage at early ages, increasing the hydration rate due to the nucleation effect of CNT (Fig. 2.19) [85].

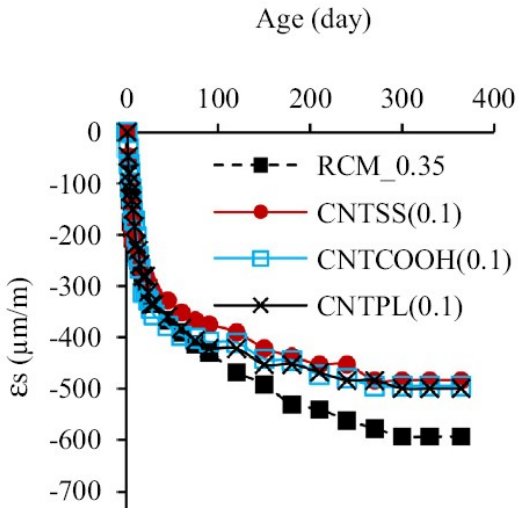

Figure 2.19. *Hygrometric shrinkage of mortars with CNTs compared to a mortar without CNTs (curve with black squares) [85]*

The effect is probably due also to the increase of elastic modulus of the material and to the bridge effect of nanotubes [101]. It is shown that also graphene oxide leads to a decrease in shrinkage, improving the cement matrix and increasing the Young's modulus of the material [90].
Also for the durability properties, the effectiveness of other types of carbon-based powders is demonstrated. Carbon black, thanks to his filler effect, decreases the water absorption coefficient of the mortars, of about 50% approximately [95]. Regarding recycled powders, foundry sand shows good performance in terms of resistance to sulphates and sulfuric acids [19].

2.4.3 De-pollution and photocatalytic properties

Many carbon-based materials could have potential uses as de-polluting materials thanks to their particular properties.
For example, graphene oxide surface is covered by epoxy, hydroxyl and carboxylic groups, which interact with *cations* and *anions* [102], and, dispersed in liquids, shows excellent *absorption properties* (removes copper, cobalt, cadmium, arsenate and organic solvents) [103]. Filters made of graphene oxide are widely used for water purification [104][105].
Another material widely used in this field is Activated Carbon (AC), in its various forms (powdered, granular, extruded, etc.). Its very high microporosity degree increases the active surface for adsorption or chemical reactions [29]. The surface area of 1 g of activated carbon is greater than 3000 m^2 [106]. For this reason, it is widely used in the removal of pollutants in reclaimed waters, in the filtration of drinking water, in air purification and for the elimination of VOCs (Fig. 2.20).

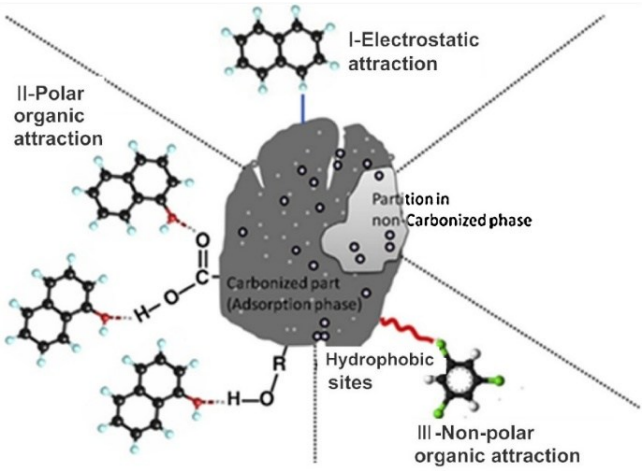

Figure 2.20. *Mechanisms of the interactions of a carbon-based particle with organic contaminants*

The de-polluting properties of these materials can be improved by interacting on their chemical structure. For example, Chowdhury et al. subjected graphene nanosheets to thermal treatment, in order to improve their CO_2 absorption properties [107]. Stőhr et al. have studied methods for improving the catalytic activity of AC through thermal and chemical processes [108].
Another interesting field of application of graphene is related to its potential *photocatalytic properties*. In graphene oxide, the functionality of the oxygen content in the surface structure allows the material to facilitate both ionic and non-ionic interactions with a wide range of molecules [30]. The photocatalytic properties can be activated or increased by functionalizing the material with chemical processes, or by combining carbon-based materials with other highly photocatalytic materials such as titanium dioxide [109].
However, conservation of depolluting properties of carbon-based materials in cementitious composites has not been adequately studied, and the scientific references to indoor air quality improvements are few.
Some studies have been performed to test ozone reduction in indoor environments through the use of activated carbon panels [110].
A study concerning the addition of activated carbon in cement pastes was carried out by Krou et al. [111]. In this study, pastes containing AC seem to decrease the levels of toluene, but, according to the authors, the results require further scientific confirmation.

2.5 Carbon fiber reinforced cement composites: state of the art

A more traditional application in research concerns the reinforcement of cement-based materials through the addition of carbon fibers of variable size and origin. Usually, these are microfibers with length between 3 and 10 mm, and with a diameter of 2-10 μm (Fig. 2.21).

Figure 2.21. *Short carbon fibers used for cement-based composites reinforcement*

Because of their morphological and superficial differences, the mechanisms that regulate the interaction of fillers and fibers in mortars and concretes are different, and require separate and specific studies.
Carbon fibers (CF) are one of the most used materials for the production of high-performance composites, thanks to their very high strength and lightness (Fig. 2.22) [112].

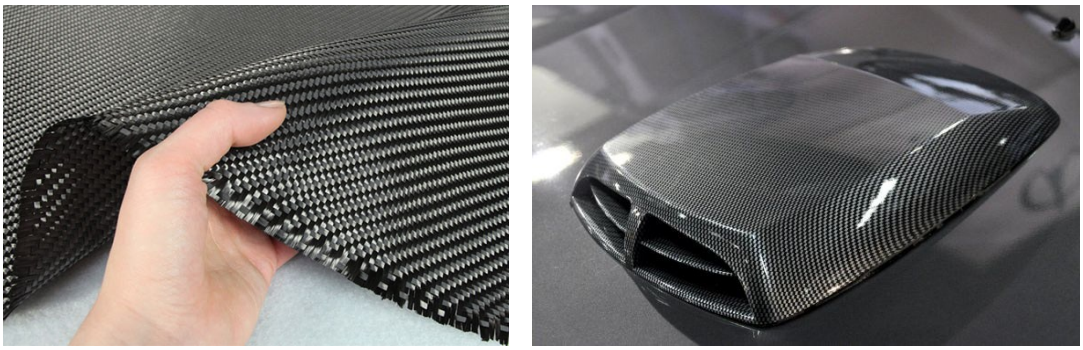

(a) (b)

Figure 2.22. *Example of (a) woven and (b) outline made of carbon fiber*

As seen for other materials, the effects of CF within the cement-based composites are strongly influenced by their interaction and interface with the cement matrix [113]. Many studies have been performed to analyze the influence of these fibers in cementitious materials, according to their dimensional characteristics (aspect ratio) and dispersion modalities. Below is a summary of recent research.

2.5.1 Mechanical properties

Carbon fibers have a tensile strength between 2000 and 7000 MPa, and a Young's modulus between 200 and 600 GPa [114].
When dispersed in a matrix (generally synthetic resin, in the common panels) they form highly resistant composites, intended for applications where high performance is required.
Dispersed in cementitious materials, the fibers form a structure composed of a network of filaments that support the matrix subjected to stress conditions.

Several researches has demonstrated a considerable increase in mechanical strength of cement-based materials with the addition of CF. For example, Shu et al. have shown a good increase in mechanical strength and impact resistance, with the combined use of fibers of different sizes (micro/macro fibers) [115]. These results are confirmed by Chung and Garcés et al., since they achieved an increase in tensile, flexural and compressive strength in cementitious composites [57][116].
Han et al., through accurate SEM analysis and theoretical calculations, studied the microstructural effects of CF of different lengths on concretes [117]. They have shown that the adding of carbon fibers into the cement mortar enhances the mechanical properties of composite up to a maximum value, due to its ability of restraining the growth of microcracks and absorbing energy by overcoming its pull out (Fig. 2.23). The enhancement of compressive strength due to carbon fibers in cement-based composite is linked to a good dispersion of filaments.

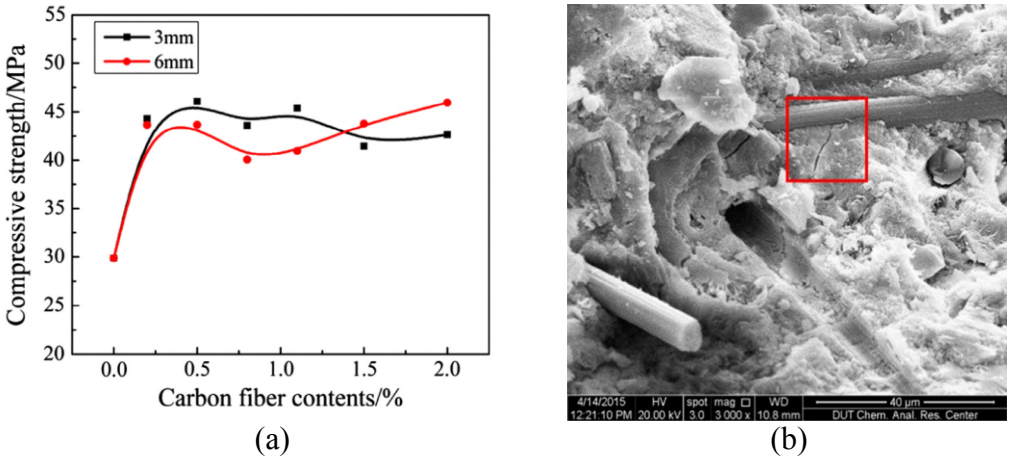

Figure 2.23. *Mortars with addition of different lengths CF: a) Compressive strength at 28 days related with fibers content; b) SEM image of interface between fibers and cement matrix* [117]

However, when the CF content is too high, they clump, causing air voids, decreasing the mechanical performance. The same study shows that, in terms of theoretical calculation, when the fiber content is high, the critical pull-out length of short fiber is larger than actual length and the fibers are pulled out. However, the critical pull-out length of long fiber is still less than actual length (Fig. 2.24). As a result, the maximum stress of long carbon fiber is larger than that of short fiber, resulting in higher tensile strength and compressive strength.

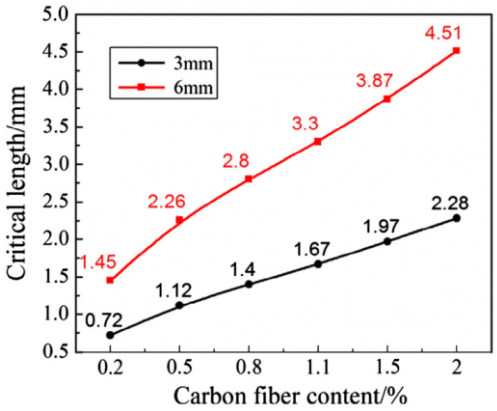

***Figure 2.24**. Relation between critical length and fibers content of 3 mm and 6 mm CF dispersed in a mortar* [117]

Because of the high price of this type of fiber, several researches on building materials have been performed using cheaper recycled carbon fibers.
For example, Mastali et al. have tested the effectiveness of composites obtained from recycled carbon fibers in cementitious materials, demonstrating an improvement in flexural and compressive strength, cracking and impact resistance [15].
Nguyen et al., Have studied two different types of recycled fibers (virgin and mixed with a reinforced polymer), detecting an increase in the flexural strength and stiffness of the composite, and an exceptional increase in fracture energy [14].

2.5.2 Shrinkage

In fiber-reinforced composites, the inclination to shrinkage (and therefore to restrained shrinkage cracking) is not only linked to the microstructure of the cement matrix and to the density of the hardened mixture. The surface forces at the interface between the fiber and the cement paste also influence the shrinkage effects.
For example, Chung et al., shown a reduction of 84% of shrinkage in a concrete with carbon fibers compared to the same material without fibers [57]. These values were obtained despite a lower resistance to compression and a greater content of voids in the mixture with fibers.
Other research groups [118] also demonstrated evident shrinkage reductions, and good results have been achieved, in particular, by combining the effect of CF and CNT (Fig. 2.25) [101].

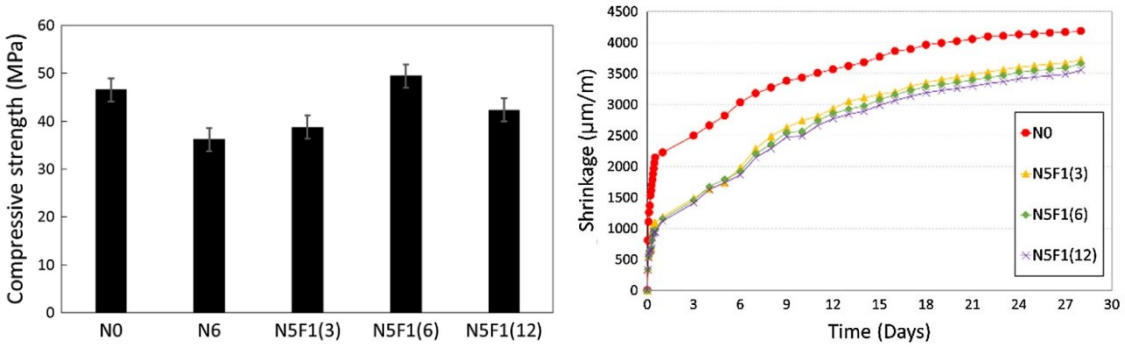

(a) (b)

Figure 2.25. *Comparison between compressive strength and shrinkage in CF reinforced pastes: despite the lower compressive strength (a), pastes with CF show less shrinkage strain (b) compared to the reference N0* [101]

In addition, other studies have highlighted the advantage of treating the surface of carbon fibers with SiH_4, in order to alter the hydrophilic character of the fibers and facilitate the formation of chemical bonds between the surface of the fibers and the cement matrix (thus decreasing the shrinkage phenomenon) [119].

2.5.3 Other properties

Other advantages have been analyzed regarding the use of CF in cementitious materials, in particular with regard to increasing durability and life-cycle of cement products. Concretes with added fibers show greater durability when subjected to freeze-unfreeze cycles, with higher flexural strengths than those of concrete without fibers [57]. This is probably due to the increased cracking toughness of the fiber-reinforced composites, as previously seen.
Moreover, Hou and Chung showed that the increase in electrical conductivity of the concrete, supplied by the carbon fibers, allows reducing the necessary voltage for the cathodic protection of the reinforcing bars [120].

2.6 Dispersion of fillers and fibers within cementitious composites

To achieve the maximum potential of adding carbon-based fillers, an optimal dispersion within the cement matrix is extremely important. Nanoparticles and nanofibers are prone to self-compaction within a suspension, and *Van der Waals forces* cause poor dispersion within cement composites. The poor dispersion can lead to the formation of imperfections in the cement matrix and to a limit of the effects provided by the additions. The resolution of this problem is one of the main challenges in this research field.
Some studies investigated the potential chemical alteration of the surface of the material using covalent or non-covalent bonds. Another widely investigated method is the mechanical dispersion.
The mechanical method consists in the *sonication* of the fillers dispersed inside a liquid. Sonication generates alternately low and high positive pressure waves, which lead to the

formation and collapse of the small vacuum bubbles of the liquid in which the particles are immersed. The energy imparted to the nanoparticles causes the breaking of the weak covalent bonds and therefore the exfoliation of the nanoparticles and the separation of the nanofibers, obtaining the increase in the surface area and greater mobility.
This method is commonly considered a non-destructive technique for the exfoliation of nanofillers such as graphene, which preserves the fundamental surface of the nanoplatelets. However, the sonication generates stress on the surface of the filler, and if used for excessive time the particles can undergo a reduction in size and break (Fig. 2.26) [121][122].

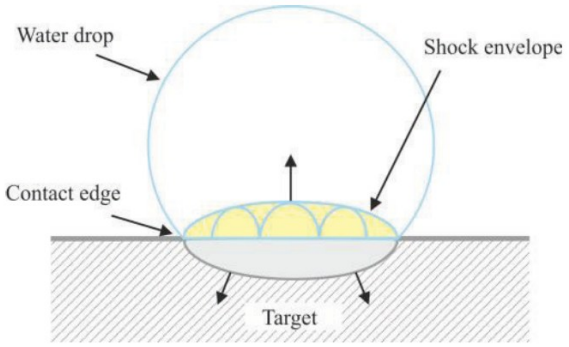

Figure 2.26. *Initial stage of impact between a water drop and a solid target with the contact edge moving faster than the shock velocity in the liquid. The liquid behind the shock envelope is compressed and the target beneath this area (filler particle surface) subjected to high pressure* [122]

The two methods for the distribution of ultrasonic energy in liquids are the *ultrasonic bath* [123][94] and the *ultrasonic probe* (Fig. 2.27) [99].

(a) (b)

Figure 2.27. *Two methods for sonication of suspended fillers: a) Ultrasonic bath. b) Immersion ultrasonic probe*

In the ultrasonic bath, the frequency of alternating current is amplified by a current generator, which produces small mechanical vibrations. These longitudinal vibrations are transmitted to the liquid in the form of ultrasonic waves, which consist in an alternation of compression zones and depression zones. Millions of microscopic bubbles (cavities) are created by these vibrations. When the wavefront advances, the bubbles are subjected

to a positive pressure and grow to an unstable size of about 100 μm in diameter. At the end of this process these bubbles implode creating millions of shock waves. The phenomenon, known as cavitation, lasts a few microseconds and despite the amount of energy released by a bubble is minimal, the cumulative energy of millions of bubbles is extremely high.
In the ultrasonic bath the mechanical vibrational energy is transferred through a liquid (usually water) in which the container is immersed (usually a glass beaker) and the vibrations must overcome the barrier formed by the container before reaching the suspension; these steps dampen the vibration intensity.
This does not happen for the ultrasonic probe. The ultrasonic probe consists of three main components: a *current generator*, a *converter* and a *probe*. The theoretical functioning of this system is similar to the previous one. However, the immersed probe in creates high frequency microvibrations that cause pressure-depression phenomena, in order to confer vibrational energy.
The ultrasonic bath allows to use a higher frequency (40-50 kHz) than the probe (25 kHz). The frequency of the ultrasounds determines the size of the bubbles present in the liquid. Low frequencies generate large bubbles, and the higher the frequencies, the smaller the bubbles are. Consequently, the use of ultrasonic probes is preferable with respect to the ultrasonic baths, in order to obtain larger bubbles and consequently more energy to disperse the filler [124].
Due to the non-suspension capacity of carbon-based nanofillers in water, the use of dispersants is necessary to achieve a stable suspension and to prevent precipitation and floatation of particles [124]. *Superplasticisers* were widely used in literature to disperse and stabilize the particles in aqueous suspension. This additive could be absorbed by the surface of the particles, surrounding them with negative charges in order to create repulsion forces (Fig. 2.28).

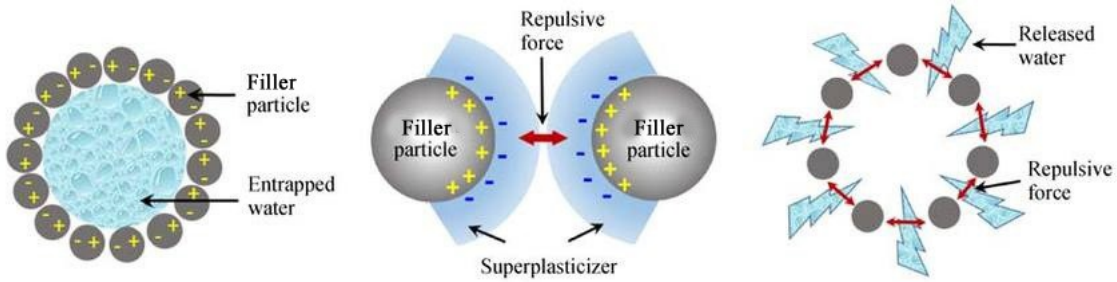

Figure 2.28. *Effect of a polycarboxylate ether superplasticizer on particles in water suspension*

In various experiments, superplasticisers mainly based on *naphthalene sulphonate* [99][71][31][125][126], *methylcellulose* [127][68] and *acetone* [124] were used. Some studies shown that the use of methylcellulose has negative effects on the hydration of the cement matrix and could lead to a reduction of its mechanical properties. Moreover, it has been shown that the use of acetone as a dispersing agent of the particles gives an excellent performance for a time not exceeding 5 minutes. The efficiency of the acetone as a dispersant is also limited by its high evaporation. The naphthalene sulphonate-based superplasticizer allow a good stability in the suspension. The filler particles stabilize the residual charges on their surface, which can be negative or positive. In liquid suspension, the opposite charges present on adjacent particles can generate considerable electrostatic

attractions, causing particles to flocculate (Fig. 2.29). The naphthalene sulphonate molecules interact to neutralize these surface charges and make the surfaces of particles of similar charge. As a result, the particles repel each other, and remain completely dispersed in the liquid suspension.

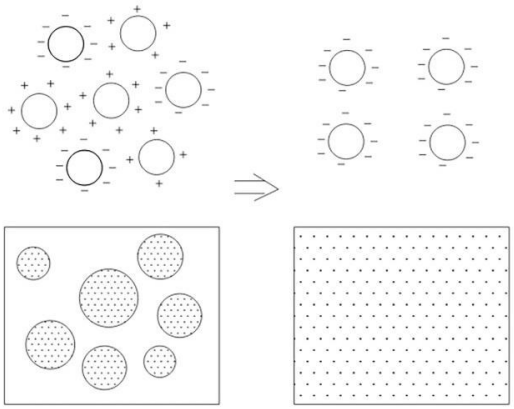

Figure 2.29. *Action of naphthalene sulphonate. Flocculation (left) and dispersion (right)*

2.7 Carbon-based materials: safety and environmental issues

As mentioned, micrometric and nanometric size carbon powders are having a wide diffusion in global industry. Innovative nanometric materials, such as graphene or carbon nanotubes, show a substantial increase in production, and are increasingly used in the development of innovative technologies, thanks to their extraordinary properties [128].
However, due to their recent introduction into research world, the health and environmental risks related to an extensive use of these types of materials are still under discussion.
Recently the medical research is trying to prevent potential problems associated with use of carbon-based nanomaterials, in order to avoid the mistakes caused in the past decades by the thoughtless use of materials such as asbestos, PCBs and Freon.
Carbon is contained in all forms of organic life; it is the second most abundant element in the human body after oxygen and is the basis of organic chemistry. Consequently, it is not a harmful element for life on earth. It has a very low toxicity to humans when taken in millimetric grain size (can be safely ingested in form of graphite or activated carbon).
However, inhalation of micrometric or nanometric scale carbonaceous powder in large quantities can lead to long-term problems. Carbon black, for example, widely used in different industry sectors, may have irritating effects on lung tissue, causing anthracosis, and might increase mortality from lung cancer in case of long exposure [129][130][131].
Targeted studies provide conflicting results, and it is impossible to verify with certainty the danger of this type of material [132]. However, IARC (International Agency for Research on Cancer) has included carbon black in 2B group of "possibly carcinogenic materials".
It is verified that significant health risks are caused by carbon microparticles contained in the exhaust gas of diesel engines. However, it must note that the harmful effects of these

particles could arise from organic chemicals or heavy metal present in them, rather than from the same carbon, because of its remarkable adsorbents properties [133].
In nanometric scale, toxicity of carbon powder it is difficult to quantify, because it is subject to many factors related to the material nature.
Graphene toxicity, for example, is widely discussed in the scientific literature, and research aimed to analyze its environmental impact have shown that it is influenced by factors such as shape and size of particles, purity, steps of production and post-production, oxidative state, functional groups, dispersion state, synthesis methods, mode of application and exposure times [134].
Graphene nanoparticles most used in industry, are not toxic at concentrations lower than 50 mg/ml, because this quantity does not alter the differentiation of stem cells in the human bone marrow, making these concentrations of graphene suitable to be used in biomedical field [135].
Other research has shown how the particular shapes and sizes of graphene particles can be swallowed up by cells, penetrating the cell membranes in solution. The physiological effects of this phenomenon are, however, still uncertain [136][137].
The preliminary research results on carbon nanotubes show difficulty in assessing the degree of toxicity, because of their heterogeneous nature. The chemical, physical and structural parameters of carbon nanotubes (as for graphene) affect their reactivity in contact with organic compounds. Unlike the graphene, however, the particular needle-like shape of the particles (as for asbestos fiber) makes this material extremely dangerous for health [138].
Carbon nanotubes, regardless of mode of synthesis, contribute to cause inflammatory reactions, epithelioid granuloma, fibrosis and biochemical/toxicological functioning mutations of the lungs [139][140].
Due to their needle-like structure, nanotubes can penetrate into the cytoplasm, and cause cell death (Fig. 2.30), causing mesothelioma (similar to those caused by asbestos fibers) [141][142][143][144][145].

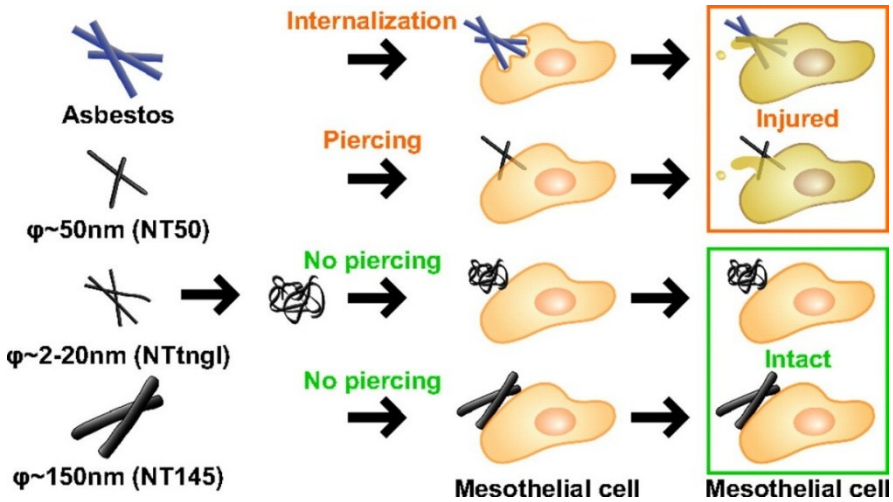

Figure 2.30. *Effect of carbon nanofibres, carbon nanotubes and asbestos fibers on mesothelial cells. The effect is influenced by the thickness and rigidity of the fibers*

In addition, studies have been conducted aimed at analyzing the chemical composition of nanometric carbon-based materials, in order to assess their environmental impact when dispersed in the air, water and soil. The carbon nanoparticles have proven fatal to insects of Drosophila genus [146].
Concerning the environmental dispersion of graphene, the results of physiological and morphological analysis show that graphene significantly inhibited plant growth and biomass production (Fig. 2.31) and led to a reduction in the number and size of leaves in a dose-dependent manner [134]. At 2000 mg/L concentration, ~18–78% root growth inhibition was observed depending on the plant species. Furthermore, leaves show wilting, necrotic lesions and reduction in leaf area. Graphene at high treatment concentrations (>500 mg/L) led to the production of reactive oxygen species leading to necrosis, loss of plasma membrane, and eventual cell death. No toxic effects were observed on lettuce at similar treatment concentrations. These results show that the phytotoxicity of graphene depends on the concentration, exposure time and plant species.

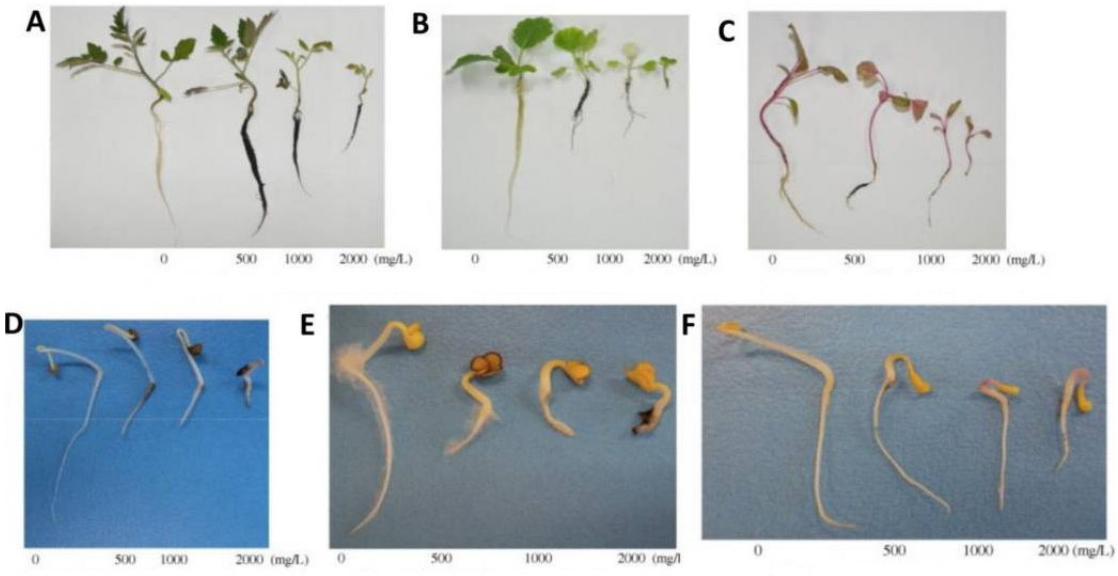

Figure 2.31. *Effect of graphene on growth of seedling and cotyledons (a-c) and root systems of cabbage, tomato and red spinach (d-f) after exposure to 500–2000 mg/L concentration. A dose-dependent reduction in the plant growth and biomass production is observed* [134]

In conclusion, through a resume of the available scientific contributions, it is possible to affirm that graphene is not a particularly hazardous material for human health, whereas carbon nanotubes present greater risks. However, to confirm these data, it is necessary to wait for a greater evolution of this research field.
It is interesting to highlight that many studies have been introduced within the development projects of these materials (in particular by carbon nanotubes producers). There is an obvious desire to contribute to the sustainability of synthesis processes of these innovative materials, inserting environmentalist factors in the product design phases. This represents a turnaround for this industry field, preferring the prevention of future problems, rather than their resolution.

3 . Chapter
Electrical Conductivity in Cement-based Materials

Fundamentals of electronics and electrical conduction in multifunctional cement-based composites. Techniques for resistivity and piezoresistivity measurements

3.1 Introduction

An important part of the present dissertation is focused on the study of the electrical behavior of cement-based materials. As highlighted in the previous chapters, this in-depth study aims to evaluate the self-monitoring properties of cementitious materials added with carbon based additions.
Cement-based materials do not behave as electrically conductive materials, and this leads to theoretical and practical difficulties [147]. When subjected to electrical voltage, their conductive mechanisms reveal typical phenomena of electrically insulating materials (*polarization effect*). However, by electrically conductive admixtures, smart *multi-phase* composites can be created, in which different types of electrical conduction (related to each other) coexist [148].
The combination of these effects and electrical phenomena in multi-functional cement-based materials requires a detailed theoretical study aimed at the optimization of measurement systems and a better results comprehension. This chapter gives an overview of the theoretical electronic fundamentals and physical quantities that underlie this work. Subsequently, the typical electronic phenomena of multifunctional cementitious materials were investigated, together with a study of the scientific literature on measurement systems for the evaluation of resistivity and piezoresistivity. Lastly, a state of the art is reported on the effects of carbon-based fillers and fibers on the electrical properties and piezoresistivity of the composites.

3.2 Fundamentals of electronics

Despite being based on simple principles, the electrical behavior of multifunctional cement-based materials may hide complex phenomena, so a strong knowledge of electronics basics is crucial to not only understand but also operate reliably such composites. Below, the physical scalar quantities and electrical properties of the materials used in this thesis are described.

3.2.1 Electric charge

Electricity is defined as the phenomena that occur due to the presence of electric charge [149]. Charge is created by the movement of charged particles through a conductor, for instance, which in turn does work. Charge can be positive or negative, if carried by protons or electrons, respectively. An element is positively or negatively charged when it has an excess of protons or electrons, respectively. In circuits, charge is carried by moving electrons in conductors. Conventional electrical devices operate using the same basic power source: the movement of electrons to generate work (W), or energy. The standard unit for electric charge is *coulomb* (C). One coulomb is the charge transported by a constant electrical current of one ampere in one second. In some applications, e.g., batteries, it is common to find the charge, i.e., the amount of stored energy, indicated in ampere-hour (Ah) or milliampere-hour (mAh). In quantum physics, electric charge is expressed in number of elementary charges (e), i.e., the charge of a proton ($+e$) or an electron ($-e$), approximately equal to $1.602 \cdot 10^{-19}$ C.

A circuit is a closed loop that allows charge to move from one place to another. Components in the circuit allow us to control this charge and use it to do work.

3.2.2 Voltage

Voltage (*U*) also referred as "potential difference" or "tension", defines the difference in electric potential between two points of a circuit [149]. The voltage between given points A and B in an electric circuit is the work done when a coulomb of charge passes between both points.
The standard units are thus joule per coulomb (energy per unit of charge), corresponding to one *volt* (V). In other words, charge moving through a circuit will lose energy across its various components, which consume it to operate. The difference of energy of a coulomb of charge between two points is the voltage.

3.2.3 Current

Electric current (*I*) is defined as the flow rate of charges. The unit used to quantify current is the *ampere* (A), which is equivalent to the flow of one coulomb of charge per second ($1A = 1Cs^{-1}$), across a section. Thus, similarly to the conservation of liquid, the conservation of charge in the electric circuits is described by the *Kirchoff's Current Law*, which states that the algebraic sum of all currents entering and exiting a node must equal zero. Current is directly proportional to voltage. Accordingly, the higher the voltage imposed in a circuit by a source (e.g., battery or power supply), i.e., the energy of the charges, the higher will be their flow rate. This relation is explained by the *Ohm's law* and the concept of electric resistance.

3.2.4 Ohm's law and Resistance

Electrical resistance (*R*) defines the tendency of certain elements (generally resistors) to oppose a flow of charge (current). As referred previously, *Ohm's law* states that, between two points, the current through a conductor is directly proportional to the voltage [150]. The electrical resistance of a conductor is the constant of proportionality and may be seen as the capacity to decrease the energy of the charges (voltage), per ampere. Resistance is expressed in *ohm* (Ω) and is calculated according to Equation 3.1 (Ohm's law) [151]:

$$R = \frac{U}{I} \tag{3.1}$$

R is the electrical resistance of the element in ohms, *U* is the potential difference in volts and *I* is the current in amperes.
The electrical resistance of an element depends on the material from which it is made and its geometry. Therefore, it is understandable that for the same material, the greater the length, the greater the electrical resistance. Furthermore, the smaller the cross section, the greater will be the electrical resistance because of the bigger difficulty of a current in passing through the element (Fig. 3.1).

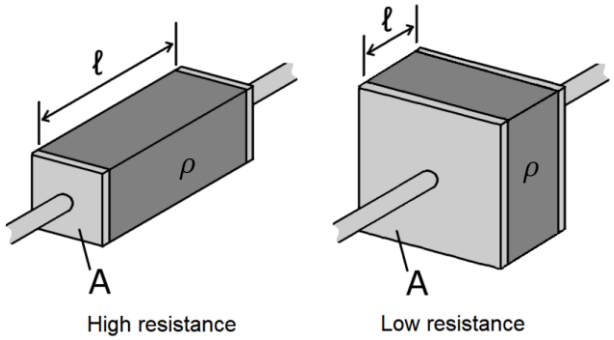

Figure 3.1. *Influence of the geometrical parameters of an element in the electrical resistance*

3.2.5 Resistivity

The *electrical resistivity* (ρ) is the intrinsic property of a material to resist to a current flow. It is the parameter used to quantify the resistive and conductive capacity of materials. Resistivity is the property that defines the electrical resistance of a material, together with its geometry, in accordance with Equation 3.2:

$$R = \rho \frac{l}{A} \tag{3.2}$$

Thus, the greater is the resistivity of the constituent material, the greater will be the electrical resistance.
Given an element similar as seen in Figure 3.1, its resistivity may be determined by measuring voltage and current across the element and combining both Equations 3.1 and 3.2, obtaining the Equation 3.3.

$$\rho = \frac{U}{I}\frac{A}{l} \tag{3.3}$$

However, this relation is only valid for homogeneous and isotropic materials. The *electrical conductivity* (σ) is the inverse of the resistivity (Eq. 3.4).

$$\sigma = \frac{1}{\rho} \tag{3.4}$$

S.I. units of resistivity and conductivity are *ohm meter* (σ·m) and *siemens per meter* (S·m^{-1}), respectively.
It is important to mention that resistivity and conductivity are highly influenced by temperature. Materials may suffer variations in electrical resistivity when subjected to temperature variation. These may be classified having *positive temperature coefficient* (PTC) or *negative temperature coefficient* (NTC). Traditional resistors, have positive temperature gradient, i.e., their resistance rises with the increase in temperature. Piezoresistive cement-based self-sensors (PCSS), for instance, are an example of materials with NTC, as demonstrated by Han et al. [38] and further in the document, i.e., their resistance decreases with the temperature rise.

3.2.6 Capacitance

Capacitance (C) defines the ability of a component (e.g., *capacitor*) to store electric charge, thanks to a property of certain materials, the "*dielectricity*". Dielectric materials are electrical insulators that can be polarized when subjected to an electric field. Electric charges do not flow through a dielectric material as they do in an electrical conductor, but only slightly shift from their average equilibrium positions causing dielectric polarization. Because of dielectric polarization, positive charges are displaced toward the field and negative charges shift in the opposite direction, due to the formation of dipoles. Therefore, when a dielectric material is placed between charged plates, i.e. a capacitor, and subjected to a potential difference, the polarization of the medium produces an electric field opposing the field of the charges on the plate. A capacitor can thus be seen as a component which has the "capacity" to store charge, producing a potential difference across its plates (static voltage), similar to a small rechargeable battery. After the polarization, capacitors are considered "charged" and do not allow more charges to flow, working as open switches (Fig. 3.2).

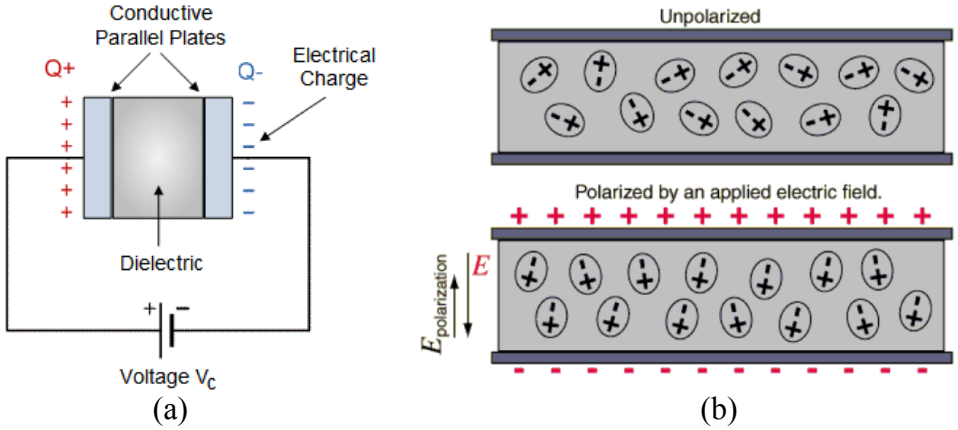

Figure 3.2. *a) Schematic representation of a capacitor [6]. b) Effect of polarization on capacitors induced by an electric field* [152]

The intrinsic capacitance of an element is quantified in *farad* (F) and, similarly to resistivity, it is a function of its geometrical configuration, i.e. area of the plates (A) and spacing between them (l), and the *permitivity* (ε) of the dielectric material between the plates. The latter is the intrinsic property that characterizes the ability of a dielectric to reduce an electric field. Capacitance is thus proportional to the area of the plates and inversely proportional to their spacing (Eq. 3.5).

$$C = \varepsilon \frac{A}{l} \tag{3.5}$$

Where C is the capacitance in farad, the dimensions A and l are in m^2 and the permittivity ε of the dielectric is in $F \cdot m^{-1}$.

Capacitance relates the charge stored per unit of voltage by the Equation 3.6. It is comprehensible, since more charge can be stored into a capacitor by forcing with a higher voltage.

$$C = \frac{Q}{V} \tag{3.6}$$

Figure 3.3 shows a schematic explanation of capacitance. After t = 0, polarization begins, the capacitor starts charging and constrains exponentially the electric field. At its full capacity, the dielectric is polarized and does not allow charges to flow ($I = 0$).

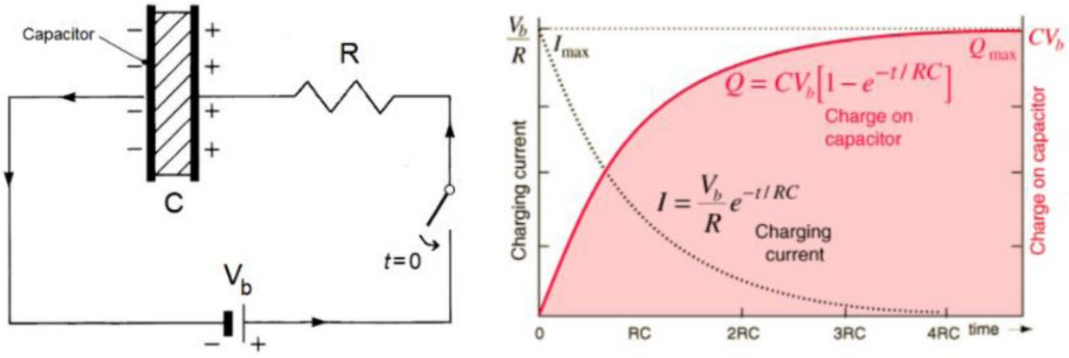

(a) (b)

Figure 3.3. *Schematic explanation of capacitance: a) Capacitor in an electrical circuit. b) Relation between time, charge and charge in the capacitor*

Cement-based materials exhibit capacitance due to the dielectric nature of hydrated cement. Therefore, its understanding plays a very important role in the interpretation of the electrical behavior of multifunctional and piezoresistive cement-based composites and their working principle.

3.2.7 Power

Electric power (P) quantifies the rate at which work is generated, or consumed, between two points. As seen previously, voltage was defined as being the work done by a coulomb of charge between two points. Additionally, current was defined as the flow rate of charges in coulomb per second. The total work rate is thus calculated by multiplying voltage (work done per charge unit) with current (flow of charges per second) and is measured in *watts* (W), equivalent to $J \cdot s^{-1}$. Therefore, the power produced by a charge flow of Q coulomb every t seconds, subjected to a voltage U is defined by the Equation 3.7:

$$P = U\frac{Q}{t} = UI \tag{3.7}$$

3.2.8 Alternating Current

Alternating Current (AC) is a type of electrical conduction obtained from the continuous inversion of the electrical polarity over time. Unlike the direct current, where the polarity is fixed and the current value constant, with AC the positive pole becomes negative and conversely, and the alternation (hence the name) takes place with fixed frequency (usually 50 Hz or 60 Hz). The polarity inversion does not occur suddenly, but with a progressive variation according to a *sinusoidal* pattern (Fig. 3.4).

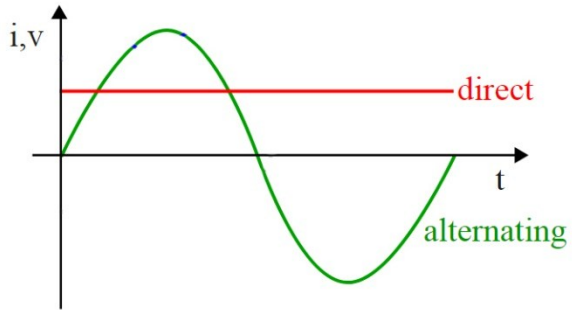

Figure 3.4. *Alternating current (green curve) compared with Direct current (red line). The vertical axis measures current or voltage*

The use of AC requires to generalize the Ohm's law, extending it to the circuits operating in sinusoidal regime. Therefore, the concept of impedance in AC regime arises from the concept of electrical resistance in DC.

3.2.8.1 Impedance

The total opposition to the flow of an alternating current at certain frequency is defined as *impedance*, which is the combination of *ohmic resistance* and *reactance*. Impedance (Z) is generally represented using complex notation (Eq. 3.8) and is expressed with the ohm (Ω) unit.

$$Z = R + jX \tag{3.8}$$

Where, Z = impedance in ohms (Ω); R = ohmic resistance (known as the real part of the impedance) in ohms (Ω); j = imaginary unit; X = reactance, known as the "imaginary part", in ohms (Ω).
Consequently, impedance consists of two parts; ohmic resistance (R) and reactance (X). Due to the effects of reactance, the DC resistance is largely not the same as AC impedance.
Resistance (or ohmic resistance) is known as the "real part" of impedance. The resistance portion of impedance has the following relationship with the phase angle (angle, by which the voltage sine curve lags or leads the current sine curve, Eq. 3.9):

$$R = |Z| \cos\theta \tag{3.9}$$

Where, R = resistance in ohms (Ω); Z = magnitude of impedance in ohms (Ω); θ = phase angle (phase difference between voltage and current) in degrees (°).
According to equation 3.9, purely resistive impedance occurs when the phase angle is zero. Instead, the imaginary part of impedance is referred as reactance (X). Reactance, which may in turn be in the form of *inductive reactance* (X_L) or *capacitive reactance* (X_C) or a combination of the two, also opposes the flow of AC, and as resistance is expressed in ohms (Ω). The resistance portion of impedance has the following relationship with the *phase angle* (Eq. 3.10):

$$X = |Z| \sin\theta \tag{3.10}$$

Where, X = reactance in ohms (Ω); Z = magnitude of impedance in ohms (Ω); θ = phase angle in degrees (°).
When the reactance is positive (X > 0), it is said to be more inductive, whereas a negative reactance (X < 0) implies that the reactance is more capacitive. A reactance of zero (X=0), clearly means that there is no reactance and the impedance is merely resistive.

3.2.8.2 Capacitive and inductive reactance

By definition, *capacitive reactance* (X_C) is the part of reactance that arises from the presence of a capacitor within the circuit (Eq. 3.11). X_C is known to be inversely proportional to the AC signal frequency (f) and capacitance (C):

$$X_C = -\frac{1}{\omega C} = -\frac{1}{2\pi f C} \tag{3.11}$$

Where, X_C = capacitive reactance in ohms (Ω); ω = angular frequency in radians per second (rad/s); C = capacitance of the capacitor in farads; f = signal frequency in hertz (Hz).
Instead, the *inductive reactance* (X_L) is the part of reactance that arises from the presence of an inductor within the circuit (Eq. 3.12). X_L is known to be directly proportional to the AC signal frequency (f) and the inductance (L):

$$X_L = \omega L = 2\pi f L \tag{3.12}$$

Where, X_L = inductive reactance in ohms (Ω); ω = angular frequency in radians per second (rad/s); L = inductance of the inductor in henrys (H); f = signal frequency in hertz (Hz).

3.2.8.3 Frequency

The effects of capacitance and inductance vary with the *frequency* of the alternating current. Thus reactance and consequently impedance vary with frequency. According to Equations 3.11 and 3.12, for a capacitive mechanism, higher frequency leads to lower capacitive reactance and for an inductive mechanism, the lower the frequency, the lower the inductive reactance.
It is generally assumed that resistance is always constant and independent of frequency. Yet this is not always true. In reality, the resistance of a circuit to AC is found to be greater than its resistance to DC. This effect is small at low frequencies. At high frequencies, however, this difference is very pronounced [153].
One of the factors that lead to the increase in the effective resistance in AC with frequency is the "*skin effect*". The skin effect is the tendency of an alternating current to flow in the periphery, or the "skin", of conductors. Thus the effective cross-section of the conductor is reduced, leading to an increase in the effective resistance.

3.3 Electrical conduction in multifunctional cement-based composites

As previously mentioned, traditional cementitious materials are considered *electrical insulators*, due to their high resistivity values (between $2.5 \cdot 10^4$ to $3.5 \cdot 10^4$ Ω·m) [147]. However, the addition of conductive admixtures within the cement matrix, can exponentially increase the conductivity of the composite in relation to the amount of addition, thereby undergoing an insulator-to-conductor transition. Schematizing the evolution of the electrical resistivity of a generic cement-based composite in accordance with the conductive filler concentration, a curve composed by three different sections can be obtained (Fig. 3.5) [12]. The three sections are: the *insulation zone* (A), the *percolation zone* (B) and the *conductive zone* (C) [154][155].

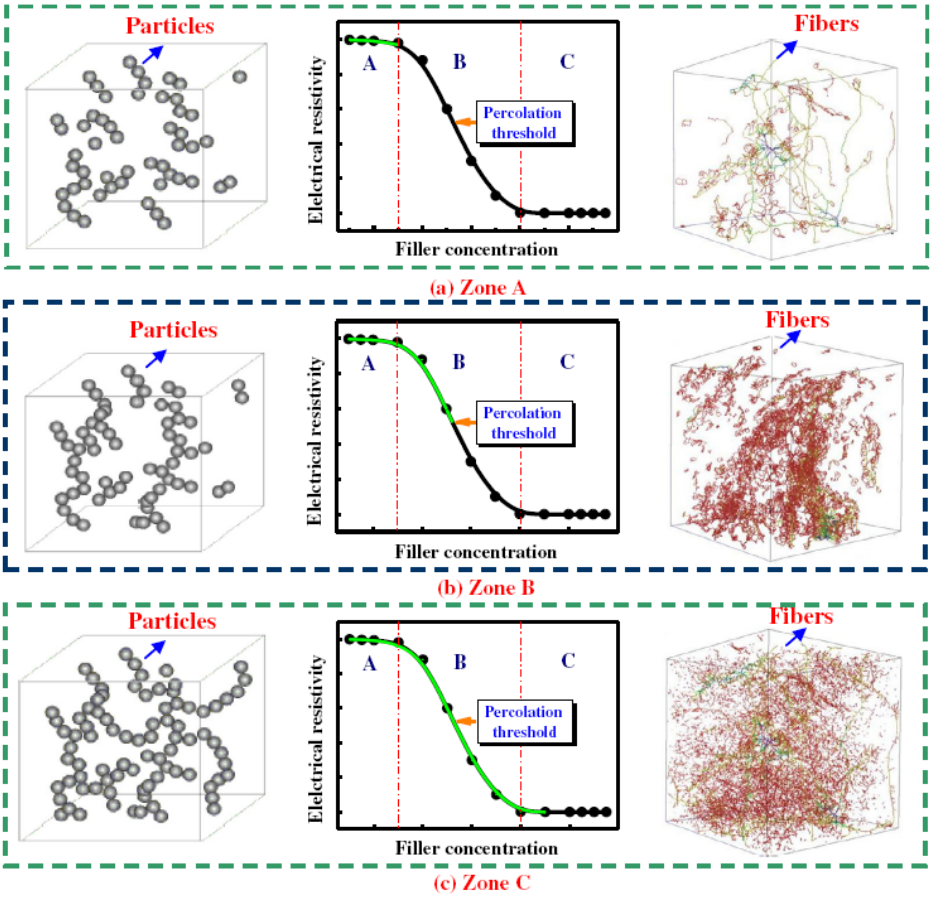

Figure 3.5. *Evolution of the electrical resistivity of a composite, related with the concentration of conductive fillers and fibers [12]*

Composites undergo from insulators to *semi-conductors* and *conductors* at a critical level of filler addition wherein the conductivity is increased by several orders of magnitude, the so-called *percolation threshold* [12]. This is explained by the "percolation theory" [156] and, interestingly, it has been observed that near or below this threshold, compressive loadings may induce or increase the conductivity of composites.

The electrical behavior of this type of composite materials and the phenomena that induce an increase or decrease of the electrical conductivity require a thorough study, because the different components of the materials possess different electrical characteristics, and their interaction greatly affects the conductive properties of the material.
Several types of electrical conduction may occur across a composite, coexisting and interrelating with each other, according with the type of conductive filler, concentration, distribution in the matrix and interface between the cement matrix and conductive filler.
The complex electrical behavior of conductive cementitious composites is due to two basic types of electrical conduction: the *electronic* conduction, divided into *contacting* and *tunnelling* conduction, and the *ionic* conduction [148]. The electronic conduction refers to the free movement of electrons throughout the conductive paths of the matrix and is the responsible for the pressure sensitivity of cement composites. Ionic conduction is related to the movement of ions across the cementitious matrix and derives from its natural dielectric properties.
Studies on the conduction of multifunctional cement-based materials have allowed the development of complex constitutive models, capable of reproducing and predicting their electric behavior.

3.3.1 Electronic conduction

The conductors for which the *Volta's second law* is valid are defined as "*electronic conductors*" (or *I-type* conductors). In the electronic conductors, the flow of electric current is due to the free movement of the electrons [157]. Materials such as metals or semiconductors belong to this category. The materials used as conductive additions in cementitious materials are, generally, I-type conductors.

3.3.1.1 Contacting conduction

Contacting conduction occurs due to direct contact between the conductive particles of the network [12]. This is most likely to occur when using conductive fillers with high aspect ratio, which increases the contact probability. For that reason, in the composites, particles with high aspect ratio require lower concentrations to attain similar conductivity levels, compared to conductive fillers with low aspect ratio.

3.3.1.2 Tunneling conduction

In a composite material, *tunnelling conduction* is associated with the transmission of electrons between the disconnected but close enough filler particles (Fig. 3.6) [4]. Therefore, tunnelling conduction depends on the contact resistance between conductive and cementitious matrix phases. However, contact resistance is a rather complex parameter, which depends on several factors, such as the intrinsic characteristics of the fillers, the inter-particle gaps and the conductivity of the matrix [78]. As explained later, the gaps have a key role in the piezoresistive behavior, since applied loads may lead to considerable changes in the thickness of the matrix between adjacent particles, thus decreasing the tunnelling resistance [39]. This conduction type occurs for critical amounts

of conductive fillers addition, i.e., mainly in composites near the percolation zone (Fig. 3.6).

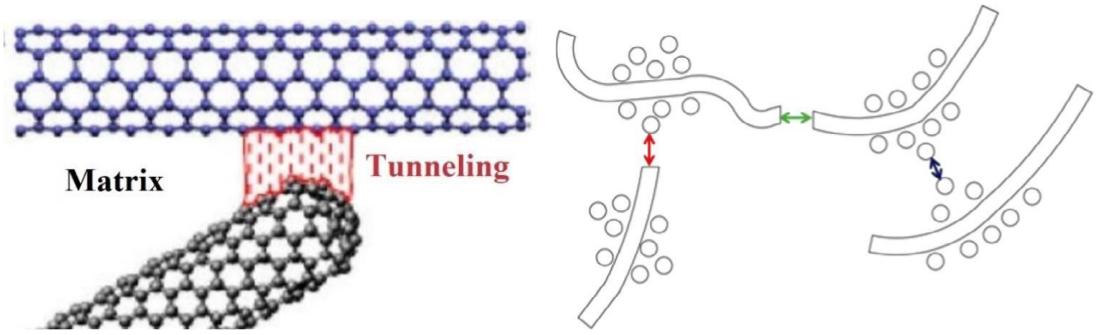

(a) (b)

Figure 3.6. *a) Schematic representation of tunnelling conduction between two nanotubes particles* [78]. *b) Tunnelling effect in hybrid conductive admixtures (fillers and fibers particles)* [39]

3.3.2 Ionic conduction

Conductors that violate the Volta's second law are called *ionic conductors* (or *II-type* conductors). Within ionic conductors, the flow of electric current is due to the free movement of ions which causes chemical reactions [157]. Solutions of acids, bases and salts are, generally, II-type conductors.
Ionic conduction is associated with dielectric materials and, in cement-based materials, arises from the motion of ions across the pore solution of hydrated cement [158]. The presence of free water into the pores leads to the dissolution of Ca^{2+} and OH- ions from the hydration products of Portland cement, namely calcium silicate hydrate (C-S-H) and calcium hydroxide ($Ca(OH)_2$).

3.4 Piezoresistive effect

Piezoresistivity is defined by the ability of certain materials in changing their electrical resistivity when subjected to mechanical strain [159][37][160]. The discovery of this effect dates back to the 19th century (1856), when the British mathematician William Thomson discovered a change of resistance in copper and iron wires when elongated [161]. However, the term "*piezoresistance*" appeared scientifically reported only later in 1935 when John W. Cookson defined the term as the change in conductivity with stress [162]. The term "*Piezo*" is rooted from the term "*piezin*" from the ancient Greek and means "to press".
The parameter that quantifies the piezoresistive ability of a material is usually defined as *Gauge Factor* (GF), also called "strain coefficient" or "strain sensitivity". This parameter is originally defined by the quotient between the variation of the electrical resistance of a metallic filament and its deformation upon tension/compression along the main axis (Eq. 3.8) [158].

$$GF = \frac{\frac{\Delta R}{R}}{\frac{\Delta L}{L}} = \frac{\frac{\Delta R}{R}}{\varepsilon} \tag{3.8}$$

It is generally associated with the conventional piezoresistive extensometers, *strain gauges*, present in most commercial force/pressure/torque transducers (Fig. 3.7). Strain gauges are widely used in various engineering sectors for the accurate measurement of deformations of materials.

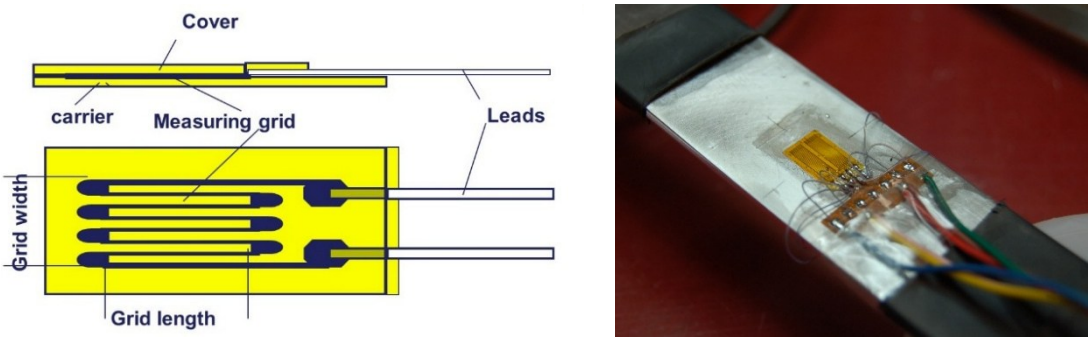

Figure 3.7. *Conventional piezoresistive extensometer: a) schematic illustration of a strain gauge (top view and profile); b) strain gauge applied on a metallic element*

It is important to distinguish *piezoresistivity* from *piezoelectricity*. Although they share a similar root, they are related with two very different effects. Piezoelectricity is related to the generation of electricity upon mechanical stimuli, that is to the change in electric potential.

3.4.1 Piezoresistivity in Cement-based composites

As seen previously, the electrical conductivity of composite materials is influenced by several factors. In the same way, several factors may be behind the conductivity variation upon mechanical strain, e.g., the change of intrinsic resistance of conductive fillers [7], the change of bonding in the interface filler/matrix [163], the change of contacts between functional fillers [12] and the change in distance between adjacent conductive particles [39]. This is understandable, since the conductive interfaces and associated percolation paths change with induced deformations. Theoretically, the closer the conductive particles get, the easier the current flow becomes, leading to the decrease of resistivity (Fig. 3.8). In the elastic regime, this behavior should be completely reversible [164][165].

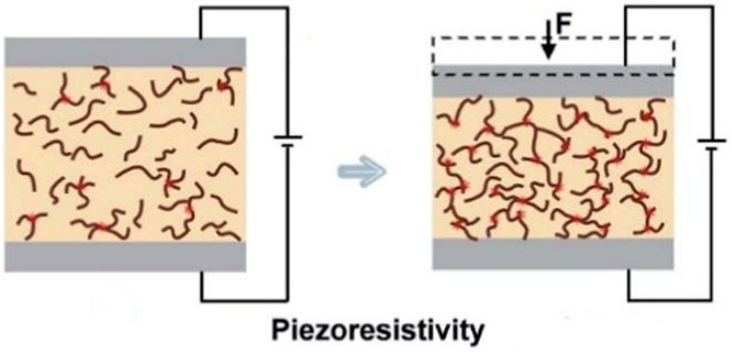

Figure 3.8. *Schematic piezoresistive effect of a cement-based composite with conductive admixtures*

Traditional strain gauges comprise electrically conductive components (usually a metal filament). Likewise, to possess a piezoresistive behavior, a cementitious material must be characterized by a high electrical conductivity, superior to traditional mortars and concretes. For instance, recent studies showed piezoresistive cement-based composites with resistivity between 6×10^{-2} and 1.5×10^{2} Ω·m [7][166][167][168][169][170][6], i.e. from two to four orders of magnitude lower than the respective traditional materials.
With reference to the topic of Section 3.3 (Fig. 3.5), in the insulation zone the concentration of filler is lower than the percolation threshold, with large gaps between conductive particles, with no effective conduction paths. Therefore, composites show null or poor sensing property at this stage. Furthermore, studies demonstrate that ionic conduction prevails in composites with filler concentrations bellow the percolation threshold [4]. Such is detrimental to the stability of piezoresistive cement-based composite, since polarization increases the measured electrical resistance over time.
In the percolation zone, the spacing between adjacent fillers decreases and the conductive particles start creating conductive paths, resulting into a sharp variation in conductivity of the composites. Consequently, compositions from this zone will show high piezoresistive sensitivity. In the conduction zone, the concentration of conductive particles is higher than the percolation threshold. The filler forms a continuous conductive structure and the conductive network becomes hard to change under loading. As a result, the composite will show more stable sensing properties, but lower sensitivity [12]. Usually, a low resistivity is favorable to the piezoresistive sensitivity, since it is helpful to increase the signal to noise ratio. However, high filler concentrations have the drawbacks of lead to strength losses [39]. The right balance can be normally found near the percolation threshold. This is therefore a very important parameter for the design of piezoresistive composites.
However, it is important to highlight that the level of electrical conductivity of the material can be more or less favorable depending on the sought properties. For example, some authors claimed that filler concentrations above the percolation threshold are beneficial to sense tensile stresses and those below the threshold are beneficial to sense compressive stresses [169][171][172].

3.5 Resistivity measurements in multifunctional cement-based composites

In accordance with the concepts detailed in the previous paragraph, the most important parameter for the evaluation of the electrical properties of this type of material is their electrical resistivity. Through an accurate measurement of this parameter (intrinsic of the material) it is possible to evaluate its ability to transmit electrical charges. Furthermore, it is important to develop efficient measurement systems, capable of detecting variations in resistivity in an element (paste, mortar or concrete specimen) depending on its stress. From the resistivity variation detected by the instrument, the piezoresistive capacity of the material is evaluated through the calculation of the *Fractional Change in Resistivity* (FCR, Eq. 3.9):

$$FCR = \frac{\rho_{(t)} - \rho_{(0)}}{\rho_{(0)}} \tag{3.9}$$

Where $\rho_{(t)}$ = resistivity of the specimen at time t; $\rho_{(0)}$ = initial resistivity of the specimen. There are no regulations or standards that describe univocal methods for measuring the resistivity of this type of compound. However, in recent decades, the study of the electrical properties of cementitious materials has been extensively analyzed in literature, because it involves several topics of study in the field of research on building materials. For example, resistivity measurement is frequently used to estimate the permeability to chlorides in reinforced concrete and thus to monitor the corrosion of rebars [59].
Metallic electrodes must be used to apply an electrical field across the element intended to measure. The voltage (U) and current (I) are registered, in order to apply the Equation 3.3 (Paragraph 3.2.5). However, conventional corrosion monitoring uses generally external electrodes, whereas piezoresistive monitoring requires the use of embedded electrodes. Described below are the three main methods used to determine the resistivity in concrete.
Some uncertainties are related to the implementation of systems operating in direct current (DC) or alternating current (AC). These two different measurement methods require different configurations of the electrodes and different instruments and devices. Both types have particular advantages or uncertainties, and it is advisable to choose the best system and configuration according to the nature of the composite and to the investigated properties. Below, a resume of the systems and configurations used in the relevant literature is reported.

3.5.1 Direct Current methods

DC devices provide a continuous detection of the resistivity of a material. This method applies to the material a fixed voltage (or a constant current) eliminating uncertainties and discontinuities related to the charge frequency, as in the AC systems [173]. In piezoresistivity tests, this type of systems may be preferable in applications where it is necessary to detect dynamic variations in resistivity, when the pulse velocity does not allow uncertainties related to the frequency of the voltage (e.g., in the measurement of systems for traffic monitoring [79]). However, DC systems show problems related to the polarization effect of cement-based composites. The time required for stabilization of the specimens leads to uncertainties in the resistivity measurement and hysteresis in the FCR curves in the piezoresistivity analysis. In literature, there are several configurations that use DC systems, depending on the number of electrodes.

3.5.1.1 Two-electrodes method

The *two-electrode method* has been widely used in laboratorial evaluation of concrete resistivity, due to its ease of implementation. Two electrodes are used to apply an electric field across the element, which may be external plates or embedded grids.
In the first setup, two electrodes are applied to the end of the specimen in contact with a wet sponge, to ensure a good electrical transmission (Fig. 3.9a) [174]. The method implemented for measuring cementitious materials consists of the use of electrodes incorporated in the mixture (embedded plates or grids, Fig. 3.9b) [12]. The resistivity is thus calculated by the direct application of the equation 3 by measuring the voltage and current between both electrodes of area A and spacing l. However, the use of this

expression in case of the use of embedded grid, requires further evaluation, due to the ambiguous value of A.

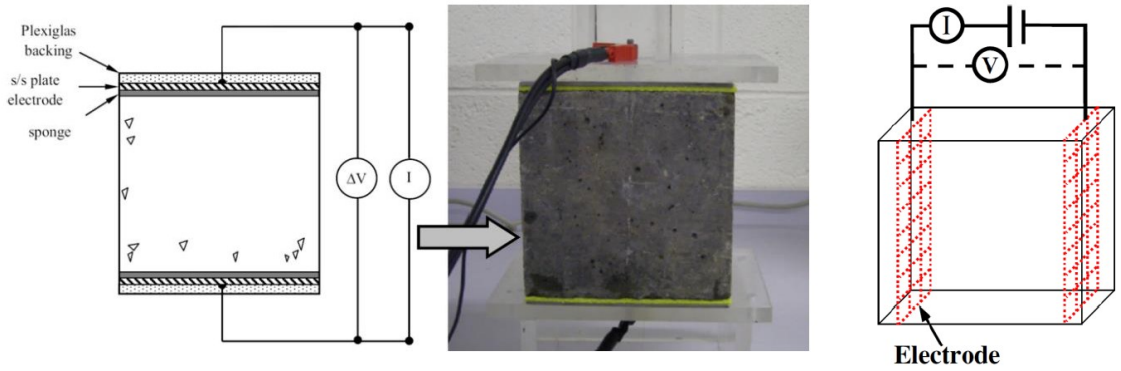

Figure 3.9. *Two-electrode method. a) Evaluation of resistivity in a concrete specimen using two external plate-like electrodes and wet sponges; b) Implementation of the method using embedded grid-like electrodes*

3.5.1.2 Four-electrodes method

This method relies on *four embedded electrodes* (foil- or grid-like), placed in the element during casting. It is based on the same principle of the two-electrode method and makes use of the equation 3 as well. Here, an electric field is imposed through the outer electrodes, where the current *I* is measured, and the voltage *U* is taken between the inner electrodes. The area *A* to consider is the embedded contact area of the electrodes and the spacing *l* is the distance between inner electrodes (Fig. 3.10).

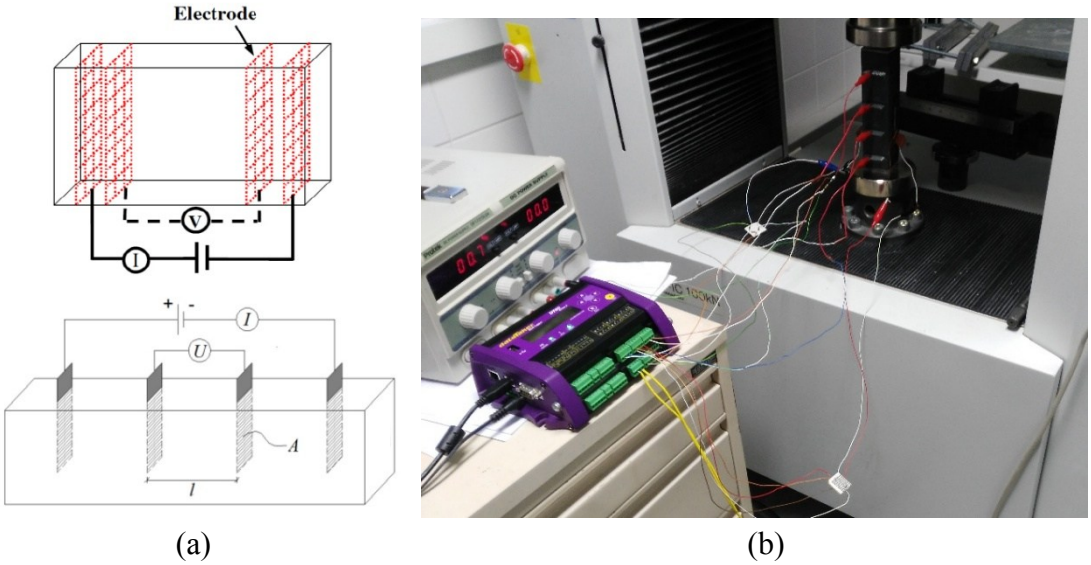

Figure 3.10. *Four-electrode method. a) Schematic illustration with grid-like embedded electrodes. b) Method setup in laboratorial experiment.*

The four-electrode method is considered more accurate than the two-electrode method [16]. Han et al. [6] proved that it may eliminate the contact resistance between the electrodes and the material, which introduces an error in the measured electrical resistance. The potential difference U read by the two-electrode method includes the potential difference derived from the intrinsic resistance of the electrodes (U_E), the potential difference due to the material (U_R) and due to the contact resistance between the electrodes and the material (U_C). By using the internal electrodes, only the resistance of the material itself (U_R) is measured (Fig. 3.11).

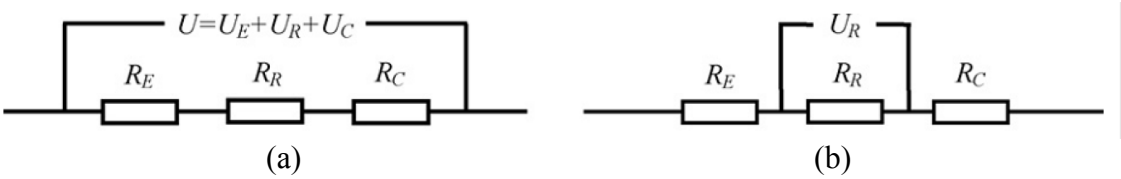

Figure 3.11. *Schematic comparison between two-electrodes method (a) and four electrodes method (b). With the four-electrodes method only the resistance of the material R_R is measured*

Another study by Chiarello and Zinno [175] compares the resistivity values of a cementitious material obtained using the 2-electrode method and the 4-electrode method with different probe configurations (increasing L/A ratio, where L = distance between the electrodes and A = electrodes area).

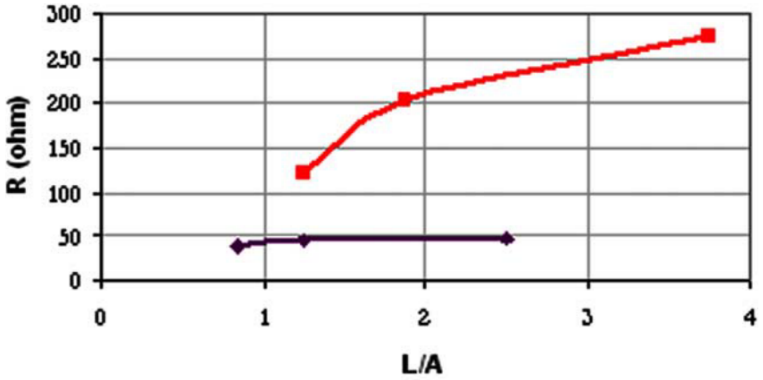

Figure 3.12. *Comparison between two and four-electrodes configurations in relation with L/A ratio [175]*

As it is clear from Figure 3.12, two-probe resistance measurements increase dramatically as L/A ratio increases, whereas the four-probe configuration seems to be relatively unaffected by the specimen design. The four-probe method has also proven to provide higher gauge factors than the two-probe method. In addition, the gauge factor from four-probe measurements tends to vary less with the strain amplitude [176].

3.5.1.3 Wenner-derived method

The *Wenner's method* was initially developed to measure the electrical resistivity of soils [177]. It is a critical factor to consider in the design of underground high voltage networks

and electrical grounding systems, for instance. This method uses four stick-like electrodes, equidistantly placed in the soil (Fig. 3.13).

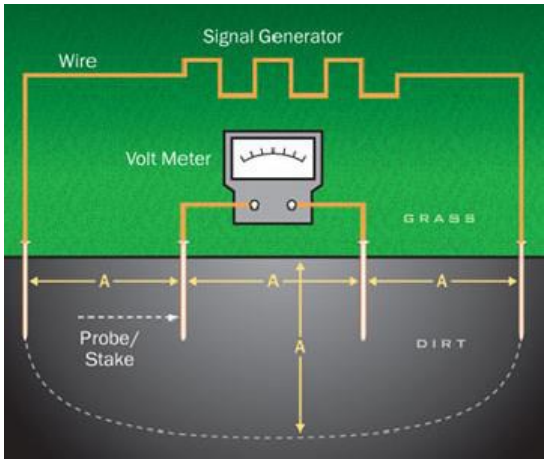

Figure 3.13. *Wenner method applicated in soils*

An electric field is applied between the outer electrodes and the potential difference U and current I are registered as described in previous section. The resistivity is now calculated by Equation 3.10.

$$\rho = 2\pi a \frac{U}{I} \tag{3.10}$$

Where a = electrode spacing. Wenner's method was successfully adapted to measure the surface resistivity of concrete, initially for in-situ evaluations of the corrosion susceptibility of rebars. Here, four spring-mounted pin electrodes are pressed against a concrete element and the surface resistivity is measured using the same equation (Fig. 3.14), following the recommendations of RILEM TC 154 – ECM [178].

Figure 3.14. *Portable Wenner-based device for in situ resistivity measurement of concrete*

Despite measuring surface resistivity, relative variations in surface resistivity have been extrapolated to variations in bulk resistivity in numerous reports. Systems based on the Wenner's method have been widely used in resistivity monitoring of piezoresistive cement-based composites, by installing four external conductive wire by means of a conductive adhesive, e.g., copper or silver paint (Fig. 3.15) [12][179].

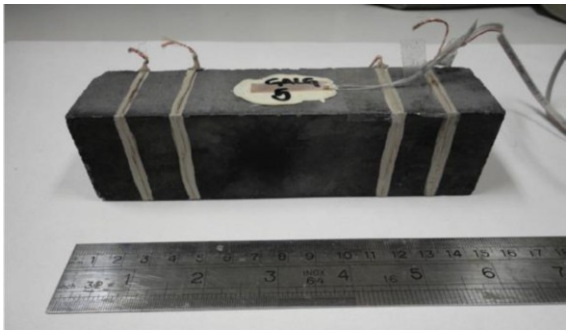

Figure 3.15. *Implementation of the Wenner-derived method in cement-based materials with copper wires and silver adhesive* [12]

3.5.2 Alternating Current methods

As explained in paragraph 3.5.1, systems based on the use of DC devices present problems related to the *polarization effect*. In electronics, when capacitors are subjected to DC voltage (constant), they charge, allowing the current to pass, until they reach their full capacity and block its passage. Because of this phenomenon, a certain period of stabilization of the current in cement-based materials is required before performing reliable measurements. This makes the measurement more complex, and it is not always possible to achieve a sufficient degree of stabilization of the signal, due to a long-term residual capacitor-charging effect. The uncertainties related to this problem could lead to a limited precision in the reading of resistivity, and to the formation of hysteresis in the FCR curves of piezoresistivity tests (because the resistivity value changes regardless of the deformation).

A potential solution to this problem is the use of Alternating Current (AC) systems. Experiments [148] showed that AC voltage could eliminate the effect of capacitor charging, in multifunctional cement-based composites. However, they let AC voltage flow, because high alternating current frequencies do not grant enough time for the capacitor to charge, behaving as an open valve. Using this principle, the charging effect of the cement-based material can be eliminated or attenuated by AC voltage. It has the advantage of eliminating the need of a pre-powering time before the resistance reaches a stable value. A study by Hou and Lynch [180], for instance, observed that, even though some polarization still exists when using AC signals, by increasing the applied AC frequency, it is narrowed to a tolerable range (Fig. 3.16).

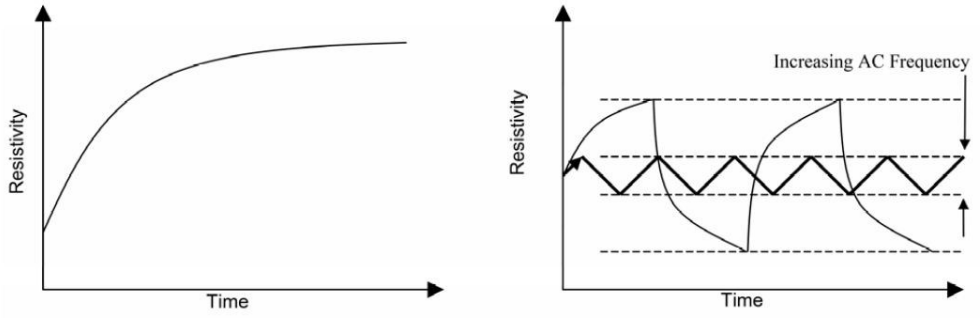

(a) (b)

Figure 3.16. *Polarization effect of cementitious materials when (a) DC and (b) Ac signals are applied* [180]

Moreover, the AC systems do not require 4 electrodes for an optimal measurement, but they work adequately with 2-electrode configurations. This is because the application of alternating voltage in frequency does not cause polarization effects at the interface between electrodes and matrix (as for the capacitor). In this way, the measurement is reliable using the same electrodes for both current application and voltage reading (Fig. 3.17).

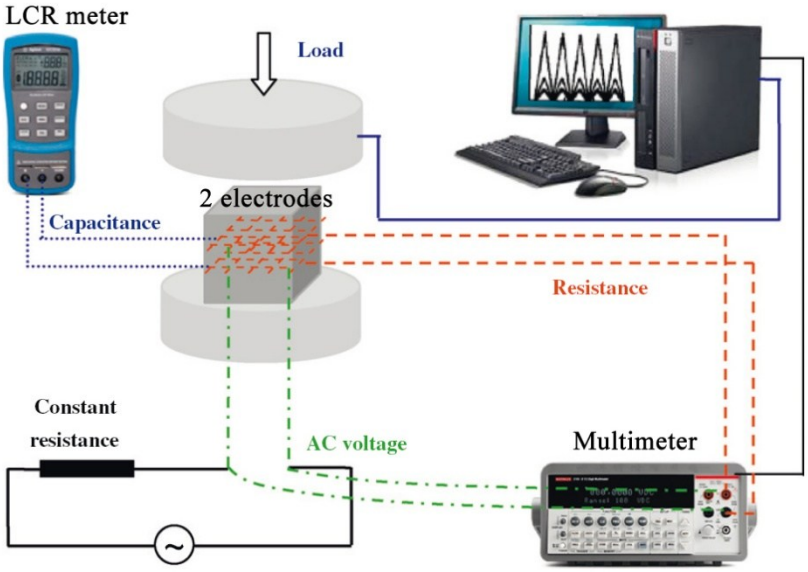

Figure 3.17. *Scheme of piezoresistive test setup in AC*

Nevertheless, the use of AC systems involves other problems related to voltage frequencies. Materials such as cement composites reach a stable resistance after a certain charging time, which varies according to various factors, such as voltage and environmental conditions.

An example is described by Monteiro [173] in the graph in Figure 3.18, which shows the evolution of the resistance over time $R_{s,0(t)}$ of a generic specimen of multifunctional mortar, after applying a current of 2 mA, at 25°C.

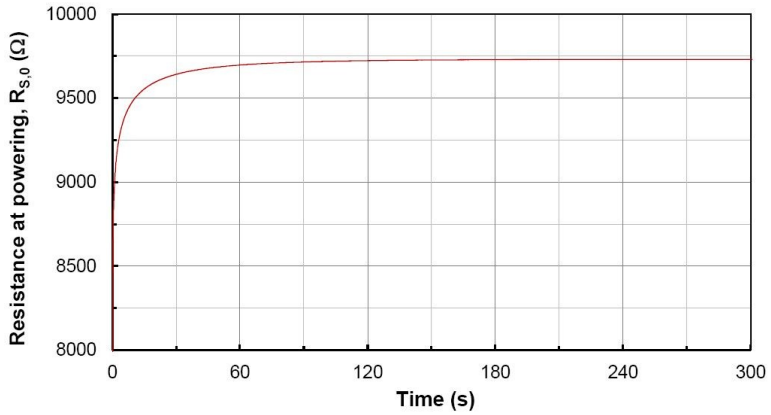

Figure 3.18. *Resistance evolution after powering vs. time, using a current of 2 mA*

In this study the resistance of the specimens after powering is quantified. Immediately after the powering (0.02 s), the specimens reached ~50% of their final resistance, ~85% at 0.1 s, ~98% at 10 s and may be considered completely charged, or polarized, after 180 s. Consequently, analyzing this type of specimens with an AC system, only the instantaneous resistance is taken and it depends on the AC frequency used. In theory, the higher is the frequency, the more effective is the elimination of the polarization effect but the lower is the measured resistance.
In conclusion, the use of AC systems can be advantageous due to the elimination of the polarization effect. However, it is necessary to verify the context of study, and, in piezoresistive tests, if the powering frequency is adaptable to the type of applied load (static, quasi-static or dynamic loads).

3.5.3 Electrodes

In addition to the measurement system and configuration, the composition, shape and size of the electrodes can also influence the resistivity measurement. An *electrode* is a I-type conductor (usually a metal) used to establish an electrical contact with a non-metallic part of a circuit [181]. The electrodes most used in the literature for cement-based materials analyses are steel or copper plates or grids, embedded in the mixtures (Fig. 3.19). Some variants consist in the use of small rods as measuring electrodes, instead of the more bulky plates or grids [4][182].

(a) (b)

Figure 3.19. *Various types of electrodes used for the electronic measurement of cementitious materials: a) Copper foils. b) Stainless steel electrodes with different shapes*

Moreover, as seen in Section 3.5.1.3, metal plates applied to the ends or copper wires wounded on the specimen surface can also be used by means of a conductive adhesive (Fig. 3.20) [179].

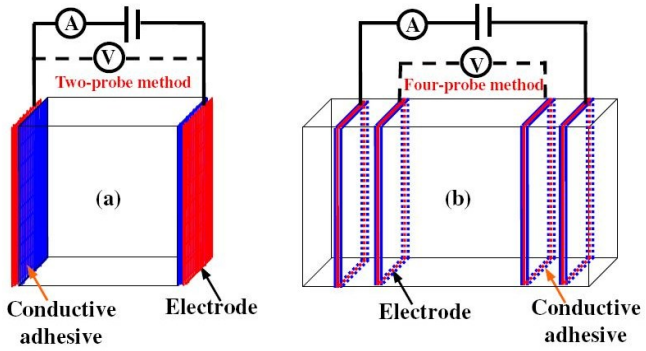

(a) (b)

Figure 3.20. *Two types of external electrodes applied with conductive adhesives: a) System with two-electrodes applied at the extremity. b) Four-electrodes method with copper wires*

This system is minimally invasive and allows easier realization of the specimens. However, measurements made with embedded electrodes are generally recommended, because they eliminate uncertainties related to the adhesion methods and to superficial irregularity of the specimens [183].
The metal grids, compared to the plates, guarantee a better interface with the material and less discontinuity between the electrode and the cement paste [184]. However, the use of grids requires a better analysis of the exact value of the contact area A between the merged electrode and the material. Anyway, some studies have verified that the effective contact area between the mesh and the mixture can be approximated to the general area of the embedded grid (the equivalent area of a plate) without relevant measurement errors [173].
Lastly, the use of stainless steel electrodes is preferable to copper [185], especially in long term measurements, because copper foils lead to uncertainties related to oxidation. In addition, steel has a greater electrochemical compatibility with the cement matrix, and leads to less errors linked to contact resistance between the electrode and the material.

3.5.3.1 Measurement of Cell-costant K

All conductivity meters are characterized by a specific *cell constant* l/A (cm^{-1}) which, in the case of simple geometric shapes, could be theoretically calculated from the length l, and the active section A of the conductor. This relation is used for the calculation of resistivity, according to Equation 3.3 (paragraph 3.2.5). Actually, due to the non-ideal geometry of current lines and the use of complex conducting surfaces, the calculation of resistivity through geometric parameters may not be accurate.
To obtain more precise resistivity values, it is better to determine the cell constant experimentally, i.e. simulating the test configuration and measuring the resistance (R) of a standard solution with a specific known conductance (χ), e.g. a solution of chloride potassium (KCl) of known molarity (Fig. 3.21) [186]. Indeed, the electrical behavior of the cement matrix can be assimilated to the behavior of an ionic conductor (as a salts solution, paragraph 3.3.2).

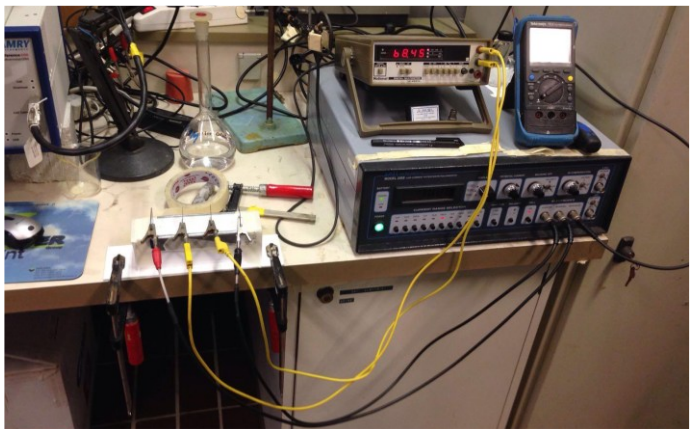

Figure 3.21. *Resistance measurement for the determination of the cell constant of a 4-electrodes configuration. The electrodes are immersed in a box (of the size of the specimen) containing a KCl solution*

By this method, the cell constant of the system can be derived from the second Ohm's law, according to Equation 3.11:

$$C = \chi \frac{A}{l} \tag{3.11}$$

Where C = Conductivity (= 1/R), χ = conductance of the solution (known). From which (Eq. 3.12):

$$K = \frac{l}{A} = \chi R \tag{3.12}$$

The resistivity can thus be calculated more accurately by combining Equation 3.3 and Equation 3.12, from which (Eq. 3.13):

$$\rho = \frac{U}{I}\frac{1}{K} \tag{3.13}$$

3.6 Cement-based composites and Electromagnetic Shielding

Highly conductive cement-based composites are also studied in another field, which has received growing interest, in recent years, thanks to the global technological development, i.e. the *electromagnetic shielding* systems.
Indeed, in the last decades, sources connected to human activities have been added to the natural level of electromagnetic background present on earth. The increasing use of new technologies in the field of radio-telecommunications, as well as new production processes of the industries, have led to a continuous increase of the electromagnetic fields sources (Fig. 3.22). This phenomenon has attracted a growing interest, even in medical research, so as to give rise to the definition of "*electromagnetic pollution*"[187].

Figure 3.22. *Schematic illustration of the main electromagnetic radiations sources*

The term "electromagnetic pollution" refers to *non-ionizing* electromagnetic radiations, i.e. the range of artificial frequencies from 0 Hz up to microwave radiation (from 1 to several hundred GHz, depending on the application field). [188].
A further problem linked to this type of pollution is *Electromagnetic Interference* (EMI), that is the disturbance of sensitive electronic devices, which brings to operation problems [68]. Therefore, numerous researches have investigated the EMI and microwave

absorption for the protection of the environment, and circuits (which are sensitive to the radiation emitted by equipment used in telecommunications [69]).

3.6.1 Electromagnetic radiation and health

The effects of non-ionizing radiation on biological tissues and on health have been intensively studied in the last twenty years [189]. However, reliable data have not yet been obtained, and many effects caused by the electromagnetic radiations of some devices may still be unknown.
Medical studies have been performed in the different frequency ranges of radiation, showing that the biggest problem is linked to the warming of body tissues due to dielectric heating [190]. Low frequency radiation from power lines can lead to a slight cumulation of charge on body surface, with disturbance of nerve and muscle responses [191].
The radio frequency fields used in mobile telephony have been defined as "possibly carcinogenic to humans" by the *World Health Organization* (WHO) [192], but has often been misinterpreted as indicating that of some measure of risk has been observed, however the designation indicates only that the possibility could not be conclusively ruled out using the available data. In 2011, *International Agency for Research on Cancer* (IARC) classified mobile phone radiation as Group 2B "possibly carcinogenic". That means that there "could be some risk" of carcinogenicity, so additional research into the long-term, heavy use of mobile phones needs to be conducted [193].

3.6.2 Literature review on Cement-based composites for EMI shielding

The development of building materials for the electromagnetic radiation shield and absorption has many fields of interest in electronic engineering, computer science, as well as in security [31].
Concrete or shielding finishes can be used for the construction of underground floors containing power transformers and other electronic devices that may be affected by electrical interference. These materials can also be useful in the military field [5] and even in the road safety sector [71].
To implement cementitious materials with shielding properties it is necessary to increase their electrical conductivity, as for the self-sensing properties. This because as soon as an electric field is applied to the surface of a conductor, it induces a current that causes displacement of charge inside the conductor that cancels the applied field inside, at which point the current stops.
Hence, numerous studies on electromagnetic shielding have been performed on multifunctional composite with carbon-based additions. In particular, carbon nanotubes, have been tested by many research groups.
Wang et al. [32] realized mortars with MWCNTs additions up to 0.9 on cement wt.%. The measurements were performed in the frequency range between 2-8 GHz and 8-18 GHz. Mortars show a wave reflection capacity related to the amount of MWCNTs, with a peak of -28 dB at 2.9 GHz (Fig. 3.23)

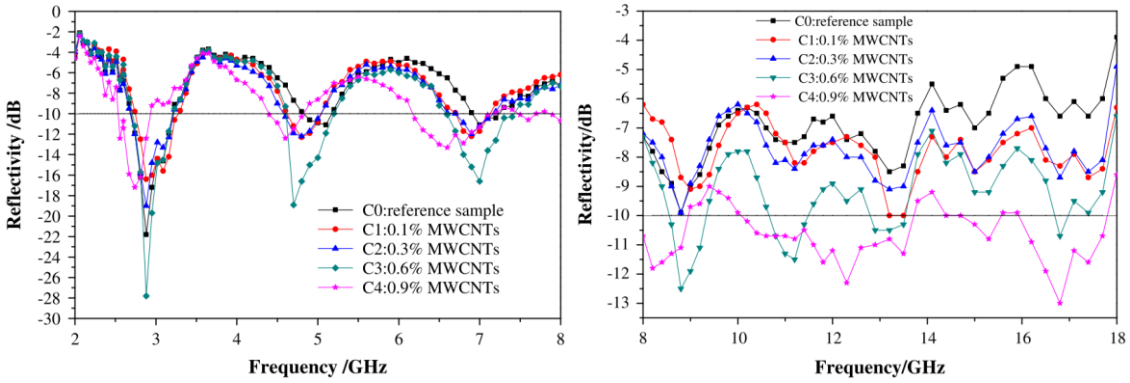

(a) (b)

Figure 3.23. *Influence of MWCNT content on the reflectivity in the frequency range of (a) 2-8 GHz and (b) 8-18 GHz* [32]

Similar results have been shown by Singh et al. [70], that produced composites with greater additions of MWCNTs (up to 15 on cement wt.%). The maximum amount of addition produces a shielding effectiveness (SE) up to 27 dB in the frequency range 8.2-12.4 GHz. Furthermore, the group has shown that the dominant effect in shielding is the absorption of the waves, and in a lesser part from the reflection (Fig. 3.24)

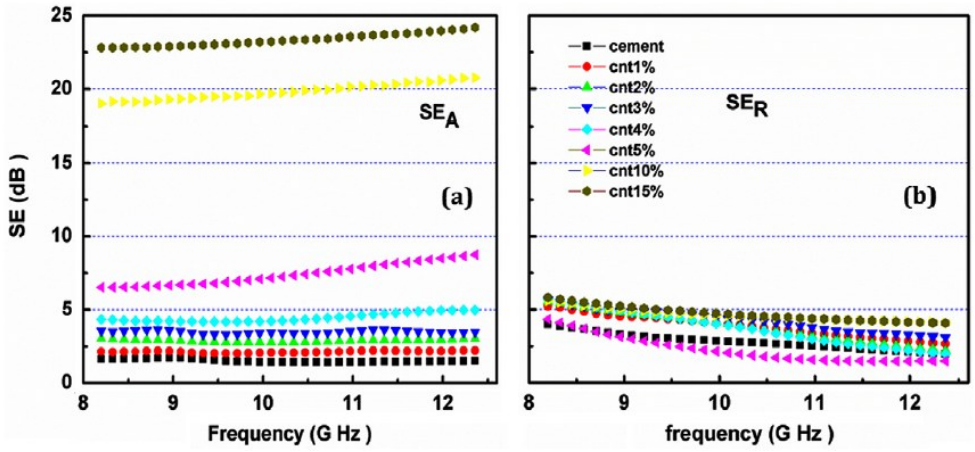

(a) (b)

Figure 3.24. *Dependence of shielding effectiveness: a) Absorption SE; b) Reflection SE (in the frequency range 8.2–12.4 GHz)* [70]

Graphene and grapheme oxide have also been studied in this application, in combination with other admixtures.

For example, Chen et al. [194] studied cement-based composites made with graphene nano-platelets and hollow glass microspheres, measuring the absorption capability of electromagnetic waves. The results show that a GNPs addition of 0.2 by cement wt.% shows good shielding results, with a peak of reflection value of -8.2 dB in the range of 2-18 GHz.

Hybrid additions have also been tested by Donnini et al.[33], which produced mortars containing graphene oxide (up to 10% on cement weight) and steel fibers (2% on cement

weight). Research has shown that the GO does not bring significant shielding improvements, but the combined addition of GO and SF has led to a noticeable increase in SE values (Fig. 3.25) in the 0.8-8 GHz frequency range.

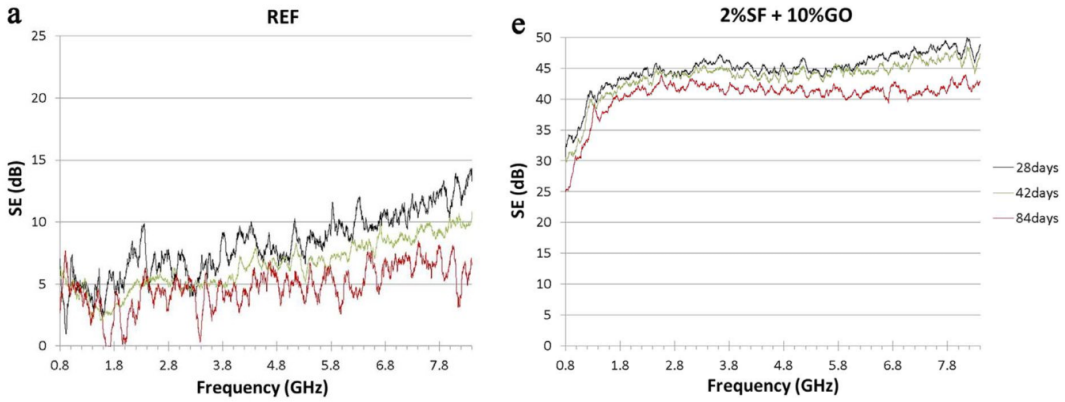

(a) (b)

Figure 3.25. *SE vs. frequency of a Reference mortar (a) and of a mortar with GO and SF addition* [33]

Other types of additions have also been effectively used to increase shielding properties. In a relevant study, D.D.L. Chung [195] compared different types of conductive additions in cement-based pastes, reporting their electrical contribution to the EMI shielding (1 GHz coaxial cable method). The results showed the particular effectiveness of steel fibers with 8 μm of thickness (shielding values up to 59 dB). In the same study, Chung found good values of SE also with carbon nanofibres and Coke powder, with shielding values between 30 dB and 44 dB.

Some research groups have also used recycled carbon-based powders for the evaluation of SE. For example, Khushnood et al. [84], tested cement pastes containing carbonized agricultural residue, such as *carbonized peanut shell* (CPS) and *carbonized hazelnut shell* (CHS), measuring the SE by waves absorption and by waves reflection, in the frequency range 0.2-10 GHz. The results showed an evident effectiveness of the carbon-based residues in increasing the shielding properties of the cement pastes (Fig. 3.26)

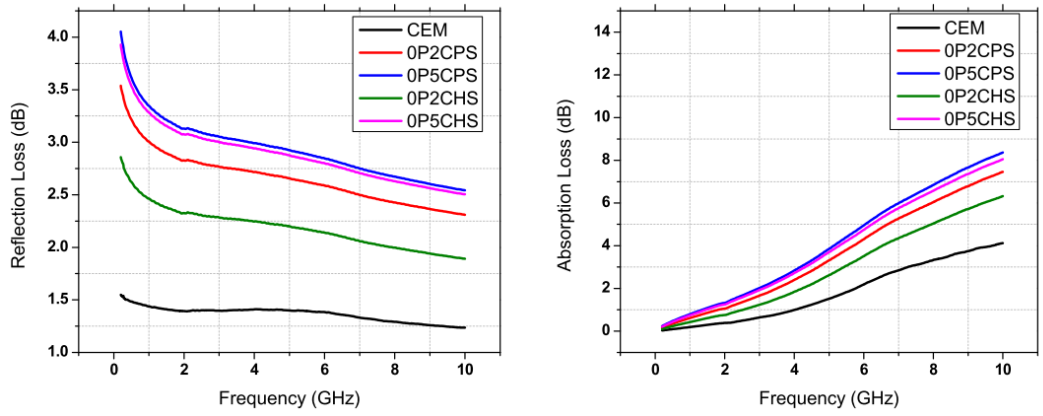

(a) (b)

Figure 3.26. *SE_R (a) and SE_A (b) of 10mm thick cement composite specimen with CHS-CPS and without inclusions* [84]

4 . Chapter

Cement-based Composites for Structural Health Monitoring

Literature review on mortars and concretes with self-sensing properties in laboratory scale and under real service condition.

4.1 Introduction

In the last 30 years interest in the study of conductive cement-based materials for different applications is growing [13]. These studies have evolved according to the demands of society, and the needs born in the new millennium, to combine high technological development with safety, sustainability and energy saving. Obviously, innovations related to the development of technologically advanced composites have been also influenced by the achievements in the fields of chemistry and materials engineering [66]. A line of research started by studying "sensitive" cement-based composites with carbon and steel fibers by the introduction of nanotechnologies and nanomaterials such as carbon nanotubes and, subsequently, graphene [196].
This, together with the development of measurement equipment, has allowed excellent results in creating composites with high stress-sensitivity and repeatability in the measurement. However, considerable problems are still to be solved, in particular the high costs of conductive admixtures and the lack of studies over systems applied in real civil structures. This dissertation aims to provide potential solutions to some of these theoretical gaps, through the study of low-prices materials, easily applicable in real service conditions.
This chapter resume the studies on the effects that influence the electrical and sensitivity properties of cementitious materials with conductive fillers and fibers. Initially, a state of the art over the influence of addition type, mix design and curing conditions in the development of the electrical conductivity of the mixtures is reported.
Subsequently, an overview of the relevant literature on cementitious materials with high piezoresistive properties is reported, shared by type of conductive admixture, and highlighting the quantity of filler, the dispersion method, the measurement configuration and the sensitivity parameters (FCR, GF).

4.2 Enhance the electrical conductivity of cement-based materials: State of the art

As seen in Section 2.3.1, a high electrical conductivity is sought in cementitious materials not only in the research of composites for self-monitoring, but also for a wide set of other properties. In paragraph 3.3, the types of electrical conductivity in cement-based materials have been highlighted. In this section, the factors that regulate the electrical properties of smart multifunctional composites are analyzed, according to a summary of the current state of the art. These factors must be taken into consideration during the realization, curing and testing of electrically conductive materials [197].

4.2.1 Effect of fillers/fibers content

As seen in Section 3.3, the main factor that regulates the increase in electrical conductivity, is the *amount* of conductive filler. The increase in the quantity of filler leads to a growing decrease in electrical resistivity. However, it has been proven that volume fractions higher than a certain threshold are no longer effective in increasing electrical conductivity. In other words, there is a relationship between conductivity and

connectivity of conductive admixtures. This theory deals with the effects of random variation on the number and quality of the existing interconnections (Fig. 4.1) [198].

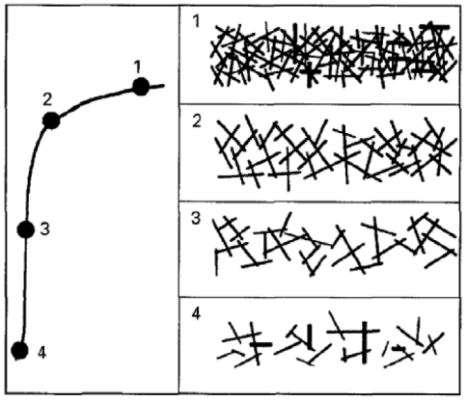

Figure 4.1. *Percolation phenomena: increase in conductivity (left) related to increase of admixtures (fibers) volume*

Xie et al. describe these phenomena using the threshold and post-threshold expressions. Conductivity boosts by several orders of magnitude, when the volume fraction of carbon-based filler reaches a certain critical value, referred to as the percolation threshold. Increasing the fillers/fibers content beyond this threshold, entering the post-threshold region, will only result in marginal increase in electrical conductivity of the composite.
Equation 4.1 [199] describe the *percolation theory* in composites:

$$\sigma\alpha(\varphi - \varphi_c)^t \tag{4.1}$$

Where σ = conductivity of the composite; ϕ = volumetric fraction of conductive fibre; ϕ_c = threshold value of the volumetric fraction; t = positive constant that is independent of the microstructure of the composite.
Xie et al. have proposed Equation 4.2 for a broad range of cement paste and mortars with different water/cement and aggregate/cement ratios:

$$\sigma = 4.10(\varphi - 0.01)^{1.65} \tag{4.2}$$

It should also be noted that particles size and shape of conductive admixtures (aspect ratio) are also important factors in determining the percolation threshold; e.g. the longer the fibers (to a certain extent), the lower the threshold.

4.2.2 Effect of aspect ratio

The shape of conductive particles greatly affects the electrical properties of the composite. An important property for the quantification of the relationship between the shape of the particle and its effect on the matrix is the *aspect ratio* (ratio between the length and the thickness of a single particle or filament).
Usually, the higher the aspect ratio, the more continuous the conductive network and hence the more effective in reducing the electrical resistivity of the cement paste is. However, admixtures with very high aspect ratio, e.g. long fibers, exhibit practical difficulties when mixing, in terms of workability and obtaining a uniform distribution.

As a demonstration of this effect, a study by Chiarello and Zinno [175] investigated the effect of fiber length on the electrical conductivity of carbon fiber reinforced mortar by comparing the conductivities of specimens with three different fiber lengths (Fig. 4.2).

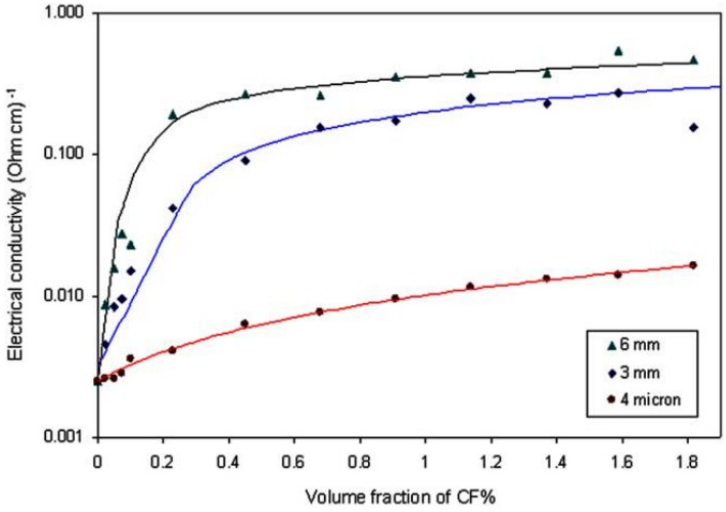

Figure 4.2. *Effect on conductivity of cement-based material with fibers of different length* [175]

This study confirms that specimens with longer fibers (high aspect ratio) attain higher electrical conductivity at a given particles volume fraction, whereas the conductivity of specimens containing very short fibers, increases very gradually with the volume fraction. In other words, the percolation threshold is at much higher volume fractions for filler particles with low aspect ratio. Since a very high quantity of admixture cause inadequate workability and therefore difficulty in mixing, this graph (Fig. 4.2) shows that with an optimum mix of fibers and fillers with different aspect ratio, less admixture content is needed to form a network capable of achieving the threshold conductivity without compromising the workability of the mixture.

4.2.3 Effect of curing and w/c ratio

As a result of hydration, the microstructure of cement paste changes as it cures and its resistivity increases. This holds true for both multifunctional cement-based composites and traditional mortars and concretes, although at higher conductive admixtures dosages, this increase is more gradual. Chacko at al. [166] performed a study on the effect of curing time on the electrical resistivity of cement-based materials with various admixtures contents (carbon fibers, Fig. 4.3).

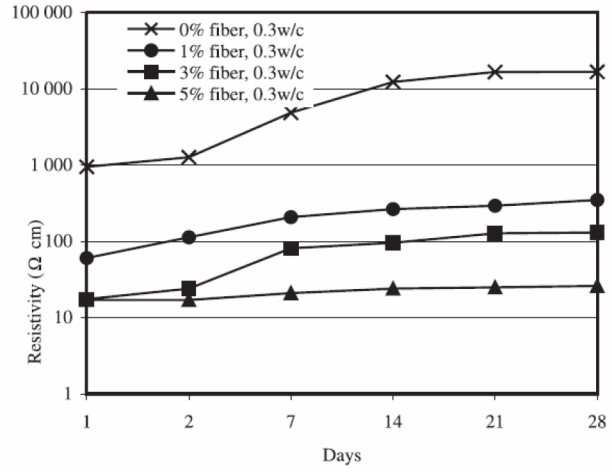

Figure 4.3. *Resistivity as a function of curing time (28 days) at different carbon fibers contents* [166]

Comparing the resistivity values of specimens with and without carbon fibers it is noticed that, although carbon fiber increases the conductivity at all ages, this improvement in conductivity appears to be more pronounced at later ages [200]. This is because, in the first days of curing, the high amount of mixing water increases the electrical conductivity of the material. The progress of hydration and the gradual loss of water, increases the presence of voids within the pores of the material, increasing the resistivity of the hardened composite. In mixtures with carbon-based admixtures, the electrical conductivity is still guaranteed by the conductive network of fillers and fibers, reducing the effect of curing on the resistivity of the composite. Obviously, the greater the quantity of fillers and fibers, the more effective the conductive network, and the less the influence of curing.

Chacko et al. also investigated the effect of the water/cement (w/c) ratio on the increase in resistivity over time (Fig. 4.4). The study shows that a lower ratio (w/c = 0.3) leads to a lower increase in resistivity during the curing period, compared to mixtures with higher ratios (w/c = 0.4 - 0.5).

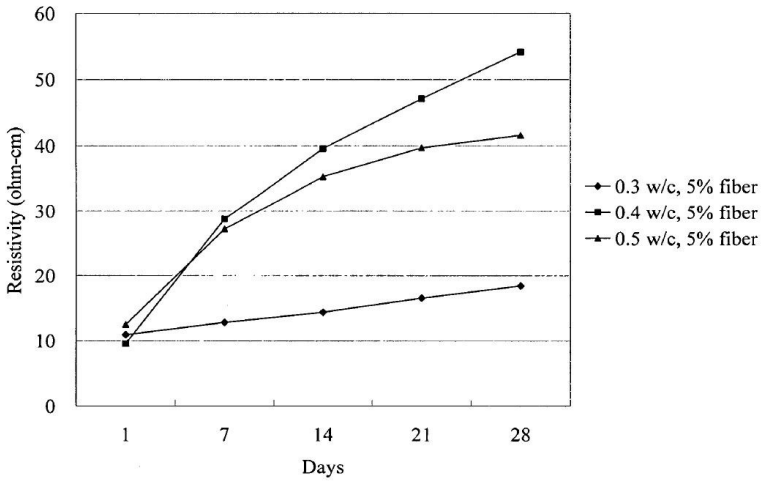

Figure 4.4. *Resistivity as a function of curing time (28 days) at different w/c ratios* [166]

This is due to the lower total quantity of water in the mixtures with lower w/c ratio, which leads to a lower total porosity of the material after the curing period.
At high volume fractions of carbon fibers, the w/c ratio of the mixture does not significantly affect the electrical resistivity because, the carbon fibers provide the primary conduction path, and therefore the amount of un-hydrated water in the composite does not have a large impact on the overall resistivity [201].
Lastly, the study showed that the conservation of specimens in wet conditions (controlled humidity) leads to greater increases in resistivity compared to air curing (Fig. 4.5). This study, however, analyzes the increase in resistivity only for the first 28 days of curing. For longer periods, theoretically, wet conditions should improve the hydration degree of the cement paste, thus leading to a smaller amount of pores within the material, and to a greater electrical conductivity.

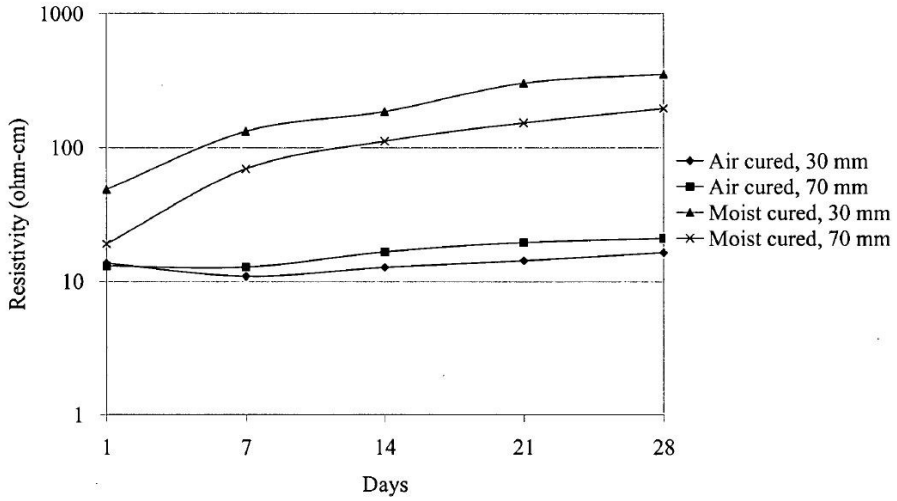

Figure 4.5. *Effect of curing method of specimens (with different length) on resistivity* [166]

4.2.4 Effect of temperature

Another important effect that must be considered during the resistivity tests of cementitious materials is *temperature*. This factor particularly affects the resistivity values of the material, thus influences the sensory capacities of the specimens subjected to load.
A publication by McCarter et al. [202] focuses entirely on this issue. Experiments were conducted on cement mortars with carbon fibers addition over the temperature range of 10–60°C. The specimens were cured for 12 months, ensuring that the influence of age on the electrical resistivity were negligible. The results of this study show that resistivity is related inversely to the temperature, decreasing with an increase in temperature (Fig. 4.6).

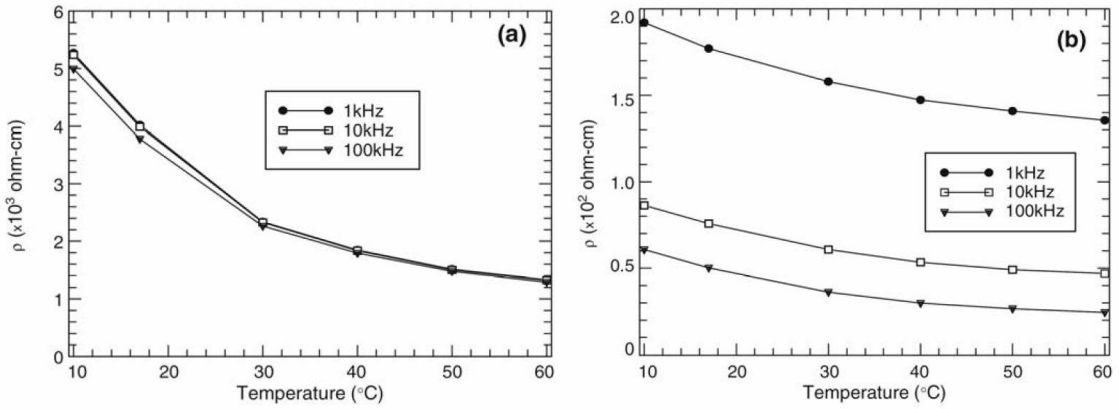

Figure 4.6. *Resistivity variation with temperature at different AC frequencies for (a) traditional cement mortar; (b) mortar containing 3 mm carbon fibers* [202]

It was also concluded that mortar specimens with conductive admixtures are not as sensitive to changes in temperature as the traditional mortar specimens. It is also evident from the Figure 4.6 that at a certain temperature, the resistivity of the specimens of mortars with carbon fibers decreases with the increase in frequency, whereas that of the traditional mortar specimens remains almost unchanged. This implies that, in the composite, carbon fibers are introducing significant scattering in conductivity [202].
It has also been proven that the effect of temperature on cement-based material is reversible, which means that not only resistivity values decrease with the increase in temperature; they also increase with the decrease in temperature [166].
It has become apparent that temperature variation during piezoresistivity tests influences the resistivity values acquired from cement-based sensors. Therefore, appropriate measures should be taken to reduce the effect of temperature on the sensing ability of these sensors; otherwise, temperature correction must be provided.

4.3 Literature review on piezoresistive cement-based materials

As seen, within the multi-phase cement composites various types of electrical conduction are generated, and multiple effects influence the overall electrical properties of the composite material. Other factors influence the variations in the electrical behavior of the material subjected to deformation loads.
In order to better understand these piezoresistive mechanisms, this paragraph provides a thorough overview of the state of the art on additioned cement-based composites with self-sensing properties, outlined by type of admixtures, measurement setup and application field.
Section 2.3.1 describes that piezoresistive cementitious composites are a type of multifunctional cementitious materials that have gained increasing interest in the last decades, thanks to their potential use in SHM systems. More than 20 types of smart mortar and concrete have been developed in the recent 30 years and more new types are still emerging towards the development of intelligent and sustainable materials [38].

Researchers have carried out extensive investigations on design, fabrication methods and performance of multifunctional concretes.
The first notion of piezoresistive concrete dates back to 1993 [13]. A group of *University of Buffalo* led by D.D.L. Chung developed several compositions loaded with small amounts of short carbon fibers and discovered that the electrical resistance varied linearly upon compressive stimuli. Besides the increase in conductivity and sensing ability, the addition of CF was found to enhance flexural and axial strength, freeze-thaw durability and decrease drying shrinkage. Later, subsequent studies focused on the ability of CF-based cementitious materials to perform fatigue and damage monitoring [170] [203] and on the optimization of the measurement setup, in terms of electrodes disposition, to optimize piezoresistive sensitivity [13][162][166][167]. Since 2000s, materials technology has made important developments in the field of carbon-based nanomaterials, thus carbon-based nanoparticles started to be used as conductive filler and gave a notable boost to the development of multifunctional composites [7][8][167][204].
Li et al. [7] experimented the pressure sensitivity of cement pastes using CNT for the first time. A distinct enhancement of the piezoresistive behavior was reported from very low concentrations of filler, as well as the mechanical strength. Despite the advantages of CNT, these are usually rather expensive. This fact may highly affect the diffusion of such technology. On this basis, Li et al. investigated the effectiveness of carbon black as a conductive filler [169] and reported excellent linear piezoresistive responses, despite lower sensitivity levels, compared to CNT and CF-based composites. In the same scope, steel fibers were also experimented [168][200][205]. However, they have demonstrated poor long-term stability, due to their susceptibility of corrosion. Additionally, hybrid fillers were recently tested, e.g., CNT+CF [7], CNT+CB [71][183] and CF+CB [183], trying to bring the benefits of each filler to the composites.
However, in recent years, the excessive costs and uncertainties related to the effects of some carbon-based fillers on human health (such as CNTs and CB) have led to the use of newly discovered nanomaterials. For this reason, graphene, already widespread in various sectors of industry and research, has also become interesting in this field of study.
Starting from 2010s, several research groups have shown the effectiveness of graphene as a conductive filler for the realization of piezoresistive cementitious composites [206]. Pisello et al. [66] have shown a greater effectiveness of the GNPs in increasing of both the electrical and thermal conductivity of cement pastes, compared to CNTs and CFs. However, graphene seems to require greater amounts of addition, compared to CNTs, to achieve a comparable sensitivity to stress and good reading quality. However, adequate quantities of graphene allow high increases in the conductivity of the composites, implementing electronic detection of damage such as cracks and fissures [126].

4.3.1 Fiber-based composites

4.3.1.1 Carbon fibers

Carbon fibers were the first conductive addition used in stimuli sensitive cementitious composites. Since 1993, D.D.L. Chung and colleagues have greatly contributed to the advance of CF-based piezoresistive composites [5] with approaches ranging from stress/strain evaluation to damage and traffic monitoring [13][71][162][170]. For instance, the team studied the ability of cement-based sensors in monitoring strain and

damage using pastes with 0.5% of CF by mass of cement and a four-electrodes configuration in 51×51×152 mm, under compressive and shear cyclic loads [170]. Figure 4.7 depicts the piezoresistive response of a PCSS specimen under compression and shear. Results showed irreversible fractional changes in resistivity (FCR) upon high strain, which could give information about damage in reinforced concrete elements.

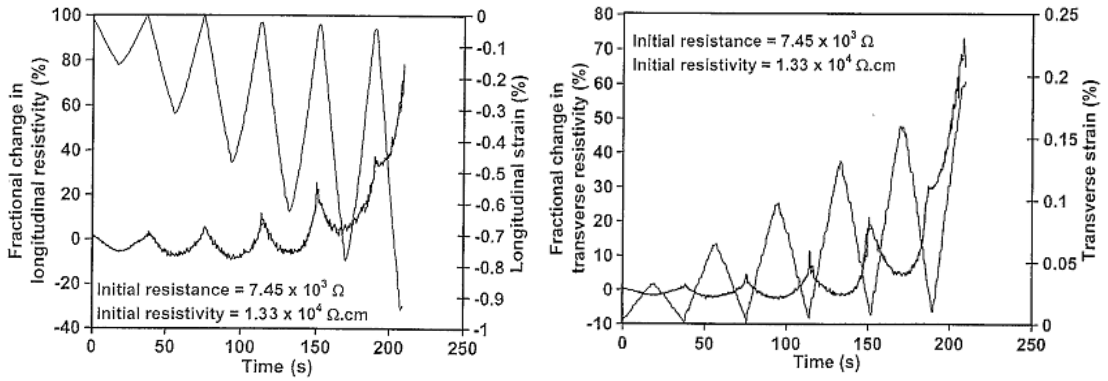

Figure 4.7. *Variation in resistivity (thick curves) vs.: a) longitudinal strain; b) transverse strain (thin curves)* [170]

Wen and Chung have also demonstrated the physical effect of the fibers on the piezoresistive behavior of the composites, thanks to a theoretical model [207]. The model is based on the concept that the piezoresistivity is due to the slight pull-out of crack-bridging fibers during crack opening, and the consequent increase in the contact electrical resistivity of the fiber-matrix interface. This model is based on formulas that estimate the electrical variations of the material by the schematic reproduction of cracks through geometric parameters. The results attained good agreement between model and experiment assessment for both tension and compression stress (Fig. 4.8).

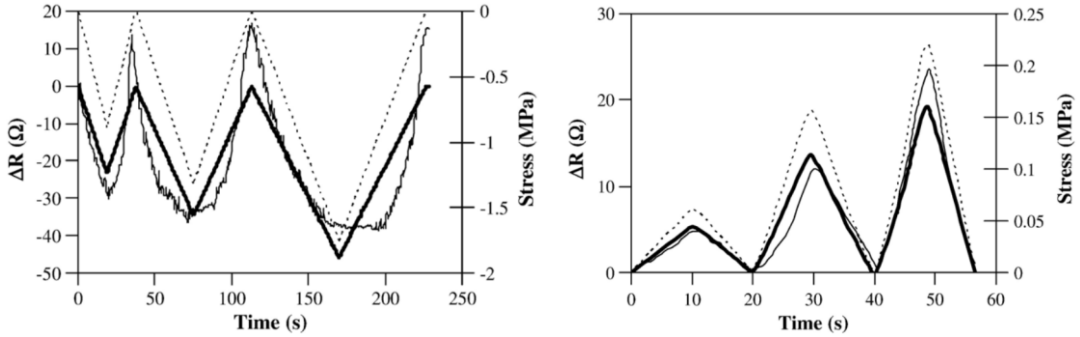

Figure 4.8. *Curves of measured and calculated values of change in electrical resistance vs. time and of the measured stress vs. time under: a) Uniaxial compression; b) Uniaxial tension* [207]

Later in 2007, B. Han et al. [6] also studied CF-based PCSS using paste specimens with fibers concentrations of 3 vol.%. Compressive cyclic tests were performed on specimens equipped with two electrodes, considering two different fixing types (extremity pasted foils and embedded meshes), with a view to compare both solutions in terms of piezoresistive effectiveness (Fig. 4.9a). The plots in Figure 4.9b show the result of a compressive monotonic test, relating the variation in resistivity with the applied stress. Despite the lower stress sensitivity registered for the embedded mesh-based solution, the higher linearity provided demonstrates better suitability.

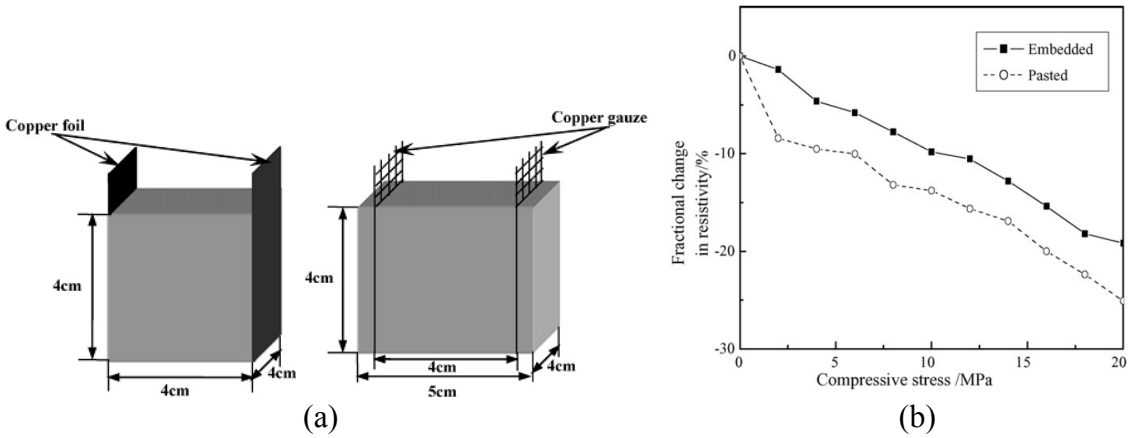

Figure 4.9. *a) Illustration of the two-electrode method using pasted foils and embedded meshes. b) Monotonic compressive stress vs. resistivity variation of both electrode solutions [6]*

In the same period, R. Chacko et al. [166] studied the influence of the electrode spacing in the performance of CF-based PCSS. A cement paste mixture was developed by adding CF in 5 vol.% and the two-electrode method was considered using copper foils and spacing of 30 mm and 70 mm. Figure 4.10 shows the variation in resistivity under monotonic compressive loading until rupture. An electrode spacing of 70 mm demonstrated clearly higher initial linearity and FCR.

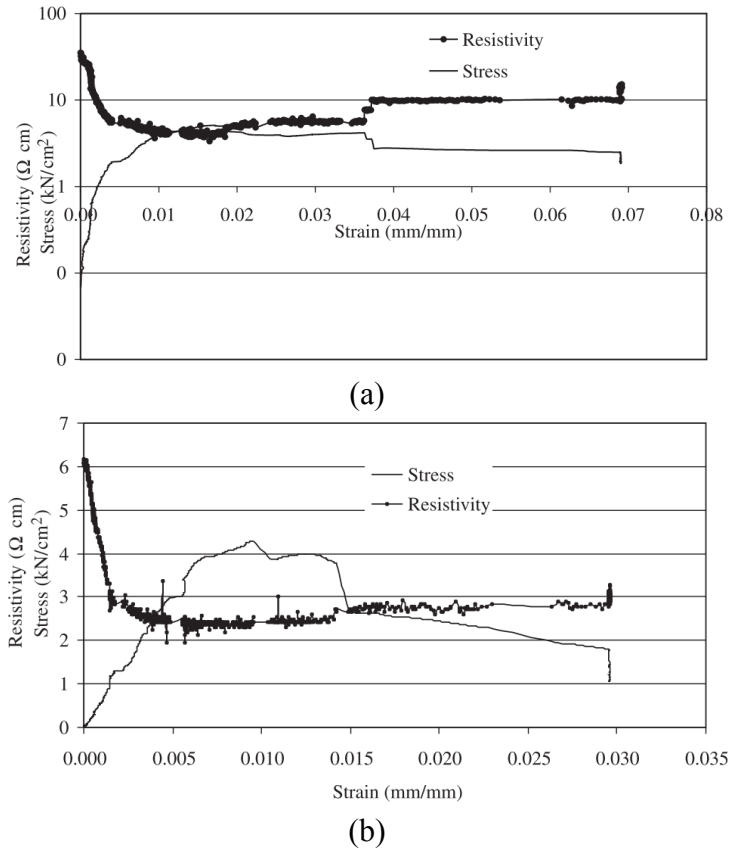

Figure 4.10. *Resistivity vs. strain and stress from electrode spacing of: a) 30 mm and b) 70 mm* [166]

In 2011, R. Howser et al. [185] developed the first experimental study on a short reinforced concrete column (0.3×0.3×0.9 m) fully casted with a CF-based self-compacting concrete. Previous experiments demonstrated more favorable piezoresistive behavior in self-compacting compared to conventional concrete [208]. Filler concentrations of 1 vol. % and embedded mesh-based four-electrode method were used. The columns were experimented under cyclic shear loads, maintaining a constant vertical load while a horizontal load was progressively applied. Figure 4.11a represents the electrodes configuration and the experimental setup. Figures 4.11b and 4.11c show the results of the piezoresistive shear experiments on traditional concrete and CF-based concrete columns, respectively. Although visible variations in the electrical resistance took place during the experiments, no direct association with the loading could be established.

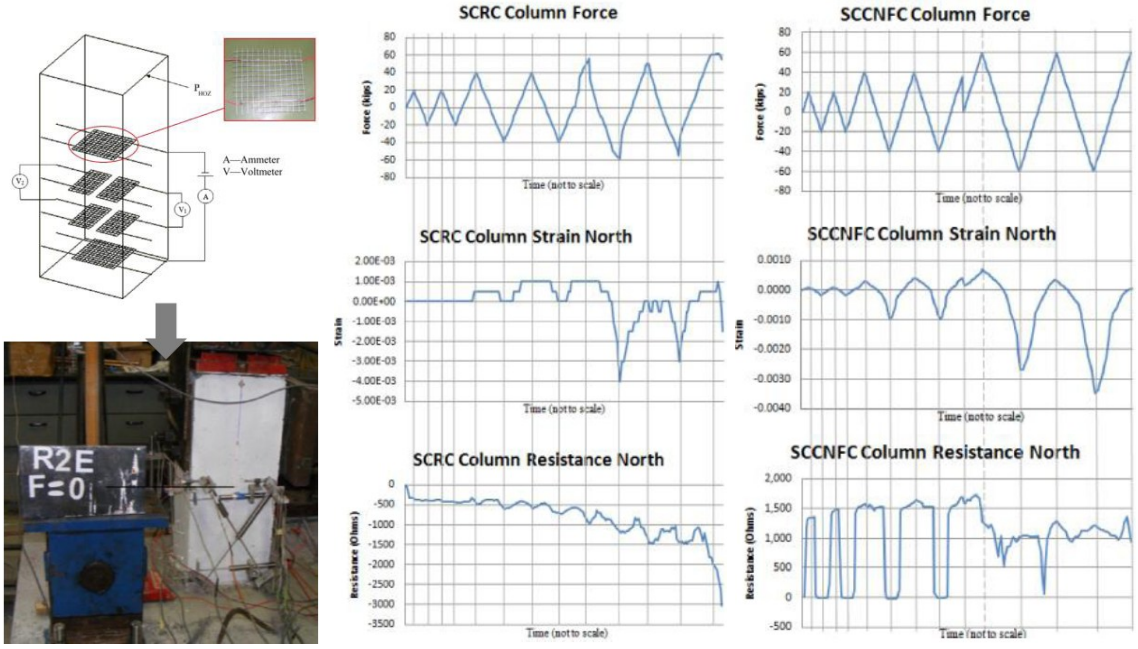

(a) (b) (c)

Figure 4.11. *Arrangement of the electrodes. Results of the shear experiments performed in the column using: b) traditional concrete; c) CF-based concrete* [185]

4.3.1.2 Steel fibers

Steel fibers were recently investigated by Toemete et al. [205]. The purpose of the research was to evaluate the ability of PCSS in detecting cracks by using splitting tensile tests. Six different mixtures were designed; without SF and with 0.2, 0.5, 0.8, 1.0 and 1.5 vol.% of 6 mm SF. The four-electrode method was adopted by embedding copper meshes. Figure 4.12a depicts a cubic (5×5×5 cm) specimen after rupture and Figure 4.12b shows the result obtained from the 1.5 vol.% approach, in terms of resistance variation vs. deformation. A massive GF of 5195 was observed for this composition. However, this magnitude is hardly comparable to other experiments and must be carefully analyzed due to the typology of the test. In addition, the overall linearity was globally low and, curiously, tended to decrease with the SF concentration.

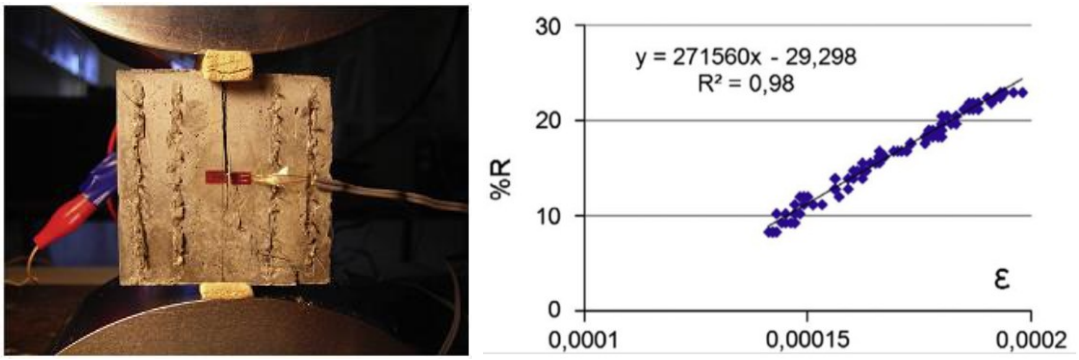

(a) (b)

Figure 4.12. *a) PCSS after splitting tensile test. b) Results of resistance vs. deformation from the tensile strain stress for the specimen with 1.5 vol.%* [205]

The incorporation of SF in PCSS was also addressed by M. Sun et al. [168]. A conductive mixture was specially designed to meet strength criteria of High Resistance Concretes (HPC). Conductive cement paste specimens (4×4×16 cm) loaded with SF in amounts of 0.5 wt.% were embedded in the center of Ø20×80 cm short columns, casted with high resistance concrete. Specimens were sprayed with an epoxy-based coating and fine to prevent undesirable effects from moisture variation and enhance the adherence between PCSS and concrete (Fig. 4.13).

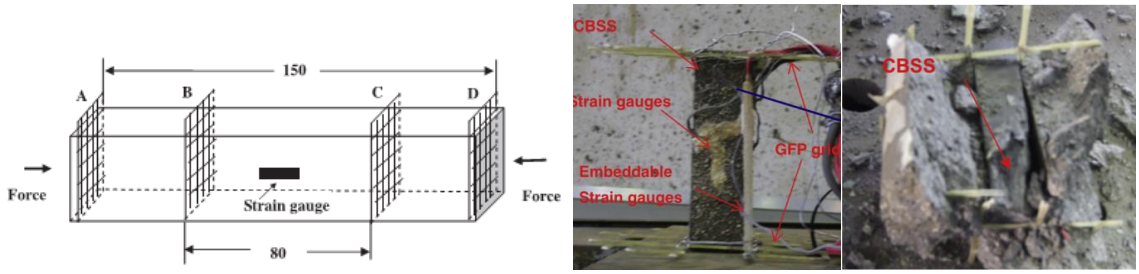

(a) (b) (c)

Figure 4.13. *SF-based high strength PSCC: a) schematic view; b) before embedding; c) after rupture* [168]

Cyclic compressive loadings were carried out (Fig. 4.14a) and revealed linearity until 45 MPa and repeatability impaired by a certain polarization effect. Figure 4.14b shows the FCR vs. compressive strain resulting from a monotonic compressive test until rupture. An initial linear zone was identified until 45 MPa, associated to a GF of 278, followed by a quadratic (45-75 MPa) and linear zone (75-150 MPa). In addition, authors claimed that oven drying the specimens at 60°C increased the GF in 381%.

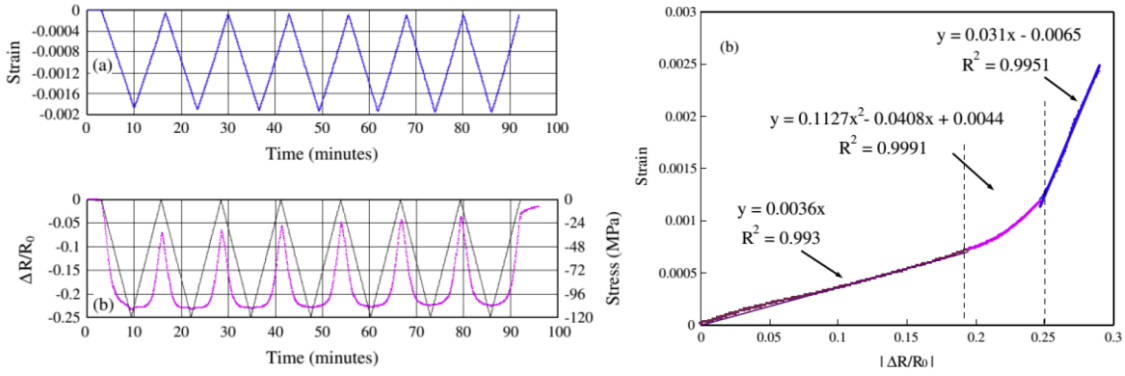

(a) (b)

Figure 4.14. *Piezoresistive experiments on the short column with embedded PCSS: a) cyclic test; b) monotonic test until the failure* [168]

4.3.2 Filler-based composites

4.3.2.1 Carbon nanotubes

Carbon nanotubes were the first carbon-based nanomaterials studied in PCSS. They were first experimented in cement pastes by G. Li et al. [7] in 2006. The piezoresistive response was studied in prismatic specimens (4×4×16 cm) with a CNT concentration of 0.5% by cement mass, under compressive cyclic loads with amplitude of 15 kN. The four-electrode method was implemented with embedded copper foils spaced 40 mm (Figure 4.15a). The authors studied the effect of the CNT treatment by H_2SO_4 (sulfuric acid) on the dispersion effectiveness and piezoresistive response. Two diferent mixtures were considered: using untreated CNT (PCNT) and H2SO4 treated CNT (SPCNT). Figure 4.15b shows the variation in resistivity over time, registered for both approaches. The results demonstrated a pronounced piezoresistive response with excellent repeatability in both mixtures. Nevertheless, the H_2SO_4 treated CNT provided enhanced linearity and sensitivity (higher FCR amplitude). Furthermore, strength tests demonstrated higher compressive strength for the SPCNT-based mixtures.

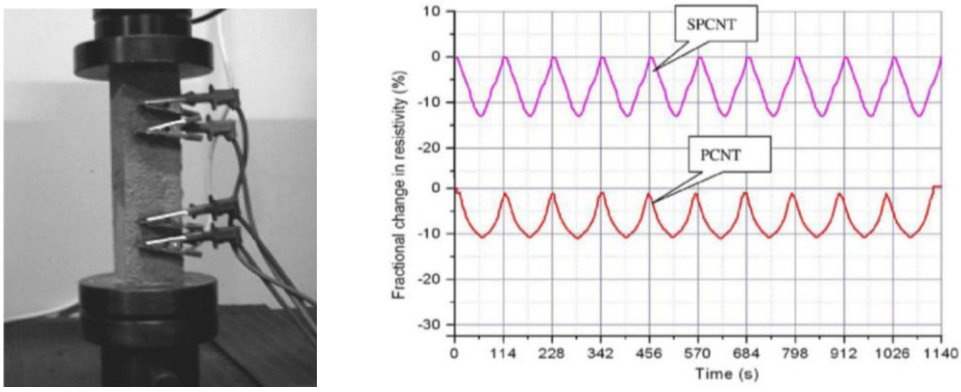

(a) (b)

Figure 4.15. *a) CNT–based PCSS and compression setup. b) Variation of the resistivity over time for both mixtures [7]*

Lately, a research team led by Ubertini, based in the *University of Perugia*, has strongly contributed in the development of CNT-based PCSS. Besides the development of sensitive mixtures, methods for large-scale production [8] and correction methods for the polarization effect [10e] has also been considered (i.e. the main culprit for repeatability issues).
Recently, the team studied MWCNT fillers in a comparative study between cement paste, mortar and concrete [209]. Filler concentrations ranging from 0% to 1.5% with respect to the mass of cement were used in 5.1 cm3 prismatic specimens (Fig. 4.16a). The steady-state resistivity of each mixture was taken (Fig. 4.16b) to determine the percolation threshold and thus the most effective mixtures in terms of piezoresistivity. The compositions with 0.75% of MWCNT were chosen due to their proximity to the threshold. Figure 4.17 depicts the results obtained from the application of cyclic compressive loads with amplitudes of 2 kN, in terms of fractional resistivity variation, in concrete-, mortar-, and paste-like mixtures. The graphs demonstrate that all the typologies of composites exhibit strain sensing capabilities, with GF of ca. 80, 10 and 3 for concrete, mortar and paste, respectively. This is, curiously, the opposite as usually expected, with cement pastes showing the lower sensitivity. However, the high level of noise noticed in the concrete specimens revealed that the use of coarse aggregates is detrimental to the sensing accuracy. Despite good linearity, a visible resistivity drift occurred during the experiments, associated with a strong polarization effect. However, authors claimed that a correction might be easily done by using high pass filtering techniques.

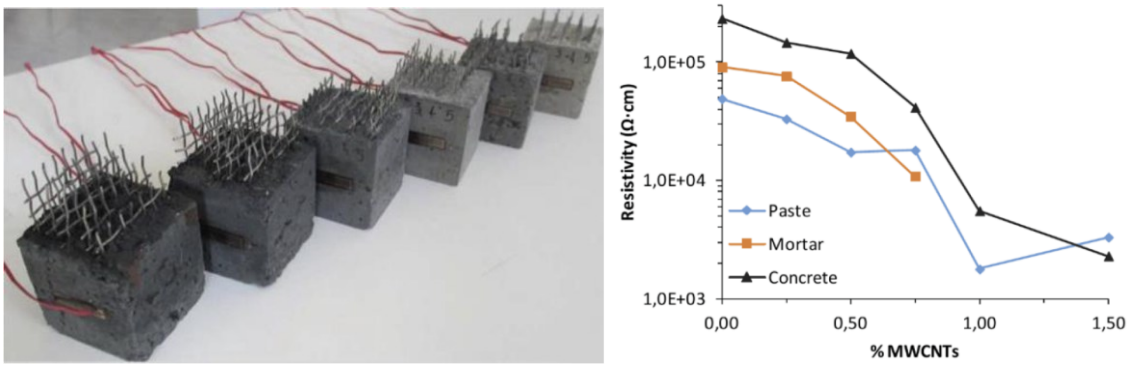

(a) (b)

Figure 4.16. *a) Concrete specimens with 1.5, 1.0, 0.75, 0.5, 0.25 and 0% of MWCNT. b) Electrical resistivity of the composites varying MWCNT concentration* [209]

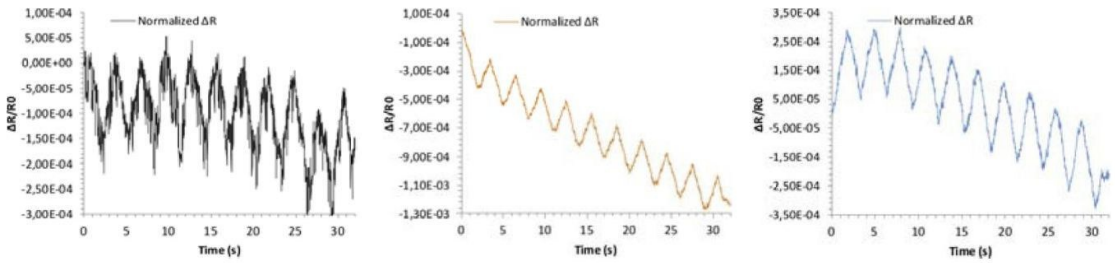

(a) (b) (c)

Figure 4.17. *a) Results of the piezoresistive experiments in mixtures with 0.75% of MWCNT in: a) concrete; b) mortar; c) paste* [209]

The team also focused on the application of CNT-based PCSS for monitoring the dynamic loads in relation to the frequency [210][211]. Conductive cement paste specimens (4×4×16 cm) using 2 % of MWCNT by weight of cement were experimented using a universal testing frame. An average GF of 220 was obtained and the specimens showed decent piezoresistive response under cyclic compressive loading with amplitudes of ca. 2 MPa at frequencies as high as 5Hz [210][211], although slight drifts again registered due to polarization.
Later, the team implemented the above-described sensors in reinforced concrete beams and monitored variations in electrical resistance due to vibrations induced by hammer impacts [211]. Figure 4.18a shows a time history plot of the resistance recorded from a PCSS placed at mid-span during the vibration test. The hammer impacts can be identified by the multiple peaks in the data. Once more, the polarization effect is clearly visible through the drift of the steady-state resistance over time. The latter was eliminated by filtering the low frequencies of the original signal through a high pass filter (Fig. 4.18b). It is worth to mention that this method does not eliminate polarization but only hides it, contrarily to approaches using AC [148] or recently biphasic DC techniques [212].

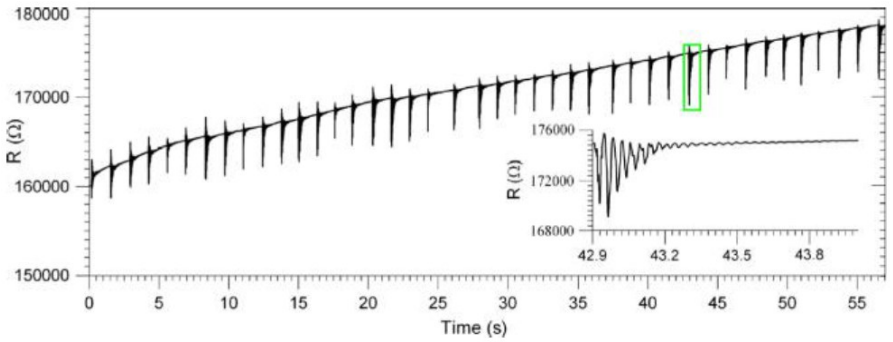

(a)

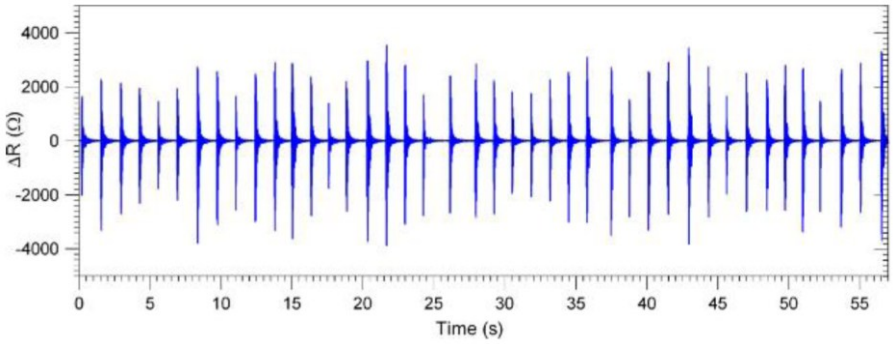

(b)

Figure 4.18. *Sensor output: a) before high-pass filtering; b) after high-pass filtering* [211]

More recently, Dalla et al. experimented the sensitivity to deformation of mortars added with CNTs and CNFs, performing both compressive and flexural tests by three-point bending. The fillers were added to a maximum of 0.6% on the cement weight, i.e. the percolation threshold measured for the CNTs. The results showed a high sensitivity of the mortars, with resistance values that decrease during compression stresses and considerably increase under flexural stresses (Fig. 4.19).

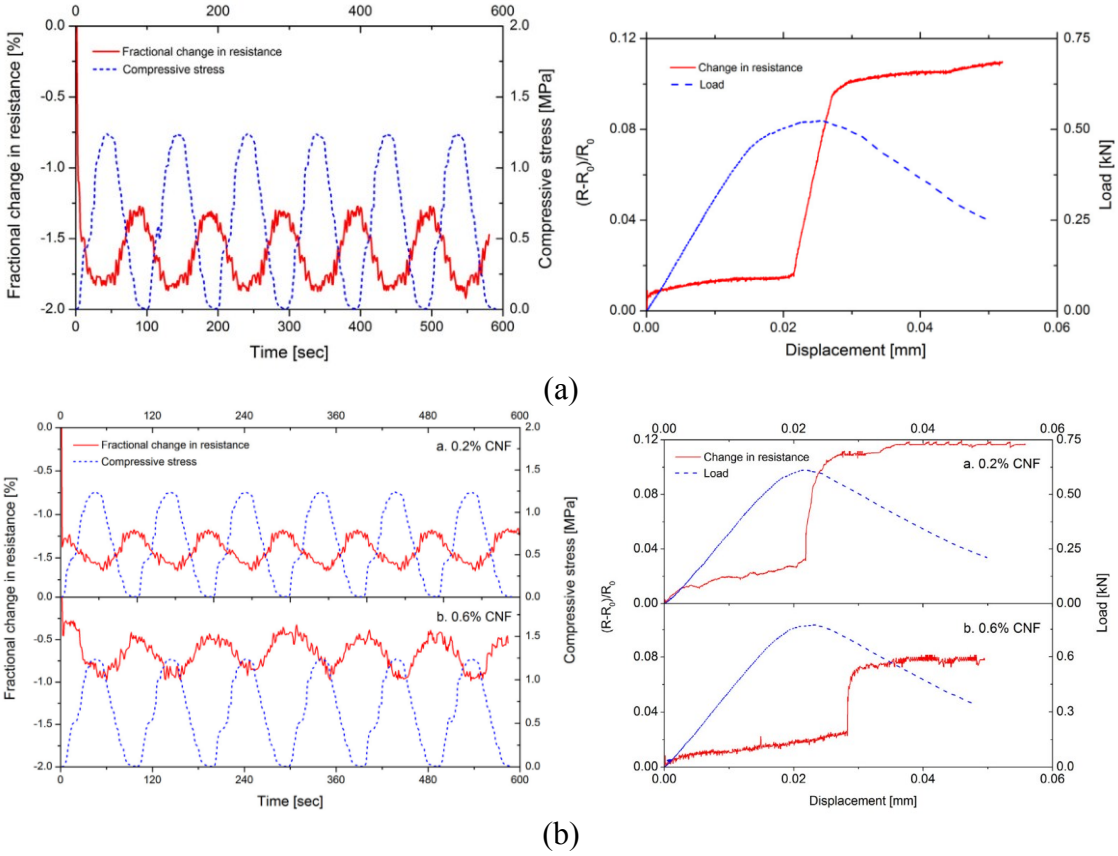

Figure 4.19. *Change in electrical resistance under compressive cyclic loading (left) and under crosshead displacement control three point bending (right) in mortars with 0.6 wt.% of cement CNT (a) and 0.2-0.6 wt.% of cement CNF*

4.3.2.2 Carbon black

Carbon black is a product of incomplete combustion of heavy petroleum products, such as tar, with the addition of a small amount of vegetable oil. To date, it is the only carbon-based powder with an industrial-grade production to have proven effective in the development of the sensitivity properties of cementitious materials. Consequently, it has a much lower cost, compared to other nanomaterials, such as CNT, and therefore it is more suitable for use in mortars and concretes, even in large quantities.

In 2006, Li et al. [169] experimented carbon black nanoparticles as conductive filler in cement paste PCSS using concentrations between 5 and 25% by mass of binder. Small prismatic specimens (3×4×5 cm) were casted and the Wenner-derived four-electrode method was implemented (Fig. 4.19a). The steady-state resistivity of each mixture was taken in order to determine the percolation threshold (Fig. 4.19b). As expected, the resistivity decreases with the addition of carbon black and a pronounced slope indicates the percolation threshold between 12% and 20% of CB addition. Monotonic compressive tests were carried out (Fig. 4.19c) and maximum variations in FRC of ca. 25% were registered in specimens with 15% of CB. Despite favorable results in terms of sensitivity and linearity, the necessary amounts of CB required are ca. 10 times higher compared to

CNT fillers, and those quantities could lead to a strong decrease in the mechanical properties of the composite.

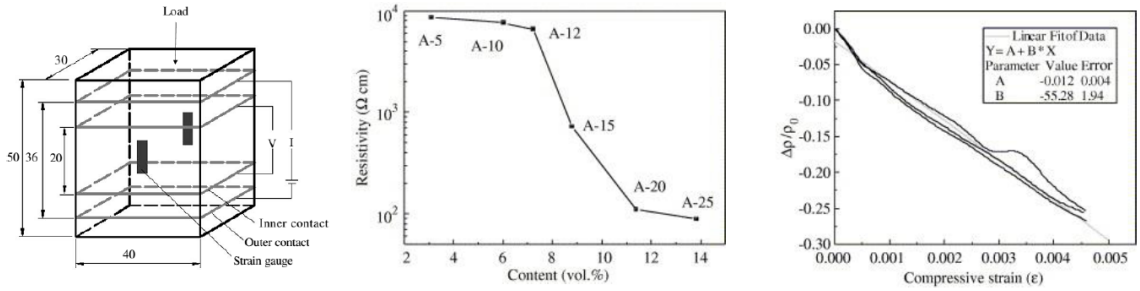

(a) (b) (c)

Figure 4.20. *a) Schematic of the experimental set-up (mm). b) Logarithm of resistivity as a function of CB content. c) Fractional change in resistivity as a function of compressive strain* [169]

The efficacy of lower amounts of CB was tested by Monteiro et al. [95], obtaining good results of sensitivity and repeatability. Prismatic mortar specimens (4x4x16 cm) with 0% to 10% of CB addition by mass of binder, tested with a 4-electrodes configuration and DC devices. By the steady-state resistivity measurement, a percolation threshold was found between 4% and 7% of addition. The specimens were then subjected to 10 loading-unloading cycles, with an amplitude of 9.4 MPa (Fig. 4.20a). The results showed that the specimens with 7% of CB addition reveal the greater sensitivity to strain, with a GF equal to 30 and a high repeatability of the signal (Fig. 4.20b).

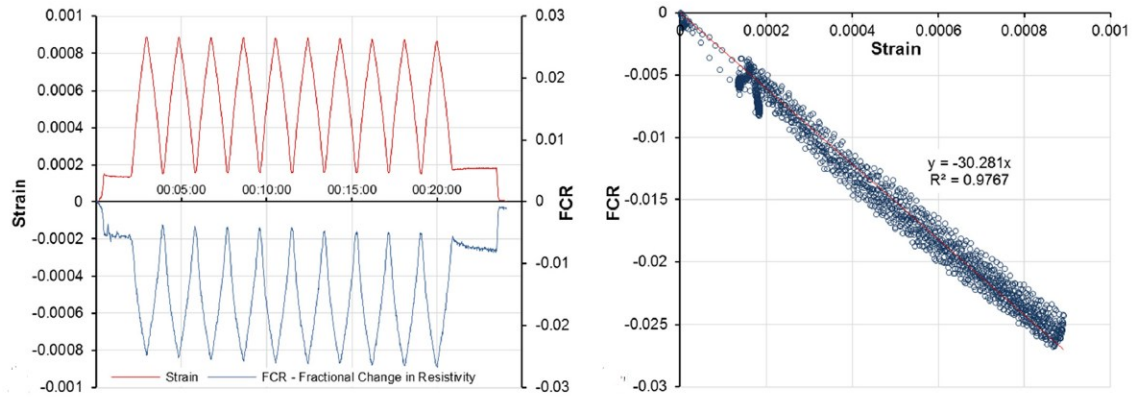

(a) (b)

Figure 4.21*. a) FCR related to strain of a mortar with 7% of carbon black by binder mass. b) FCR vs. strain for 10 load cycles* [95]

These results were obtained using relatively low quantities of CB, unlike the study of Li et al., which also led to an increase in the mechanical resistance (compressive and tensile strength) of mortars, thanks to the "filler effect".
Later studies of the same group investigated the use of the same mixture for traffic monitoring [79], i.e. testing the specimens with compressive loads of variable amplitude and frequency, and optimizing the mixing process and measurement setup.

The sensors showed a high sensitivity and repeatability to all the different load configurations (Fig. 4.22). In the same study, the group also analyzed the influence of temperature on the piezoresistive properties of the composite, detecting a 30% of sensitivity drop when the specimen is heated up to 45°C.

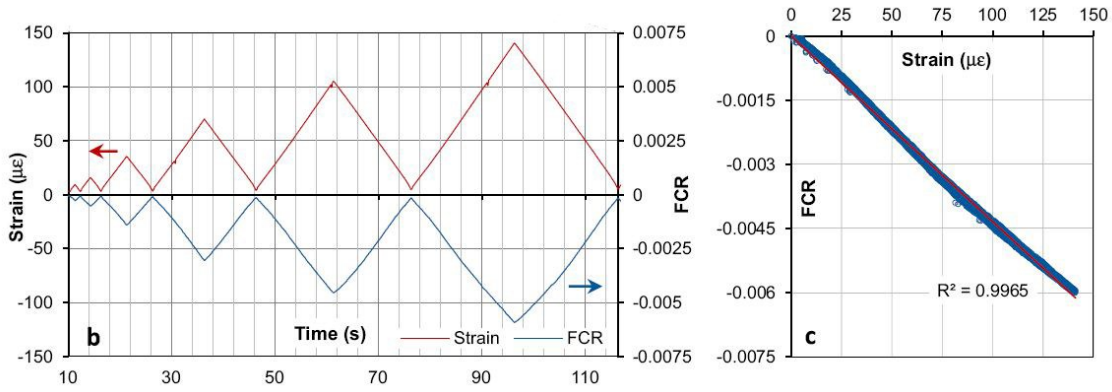

Figure 4.22. *a) FCR vs. strain for a type of load configuration. b) FCR vs. strain for several load cycles* [79]

4.3.2.3 Graphene

Scientific research on SHM materials with *graphene* addition has recently been developed, because of the recent discovery of this nanomaterial (2004). Nevertheless, an in-depth research have been performed by some studies over the sensitivity properties of composite additioned with graphene and graphene oxide nanoplatelets, with a thorough analysis of the dispersion techniques of the filler and the measurements configuration.
A comparison between the piezoresistive properties obtained from GNPs and other carbon-based fillers (CNTs, nanofibers and CB) was performed by Pisello et al. [66]. The group has tested the electrical, thermal and piezoresistive properties of cement pastes with the addition of different types of fillers to 2% on cement mass. The piezoresistive properties have been tested through several rod-like electrodes placed at 1 cm of distance (Fig. 4.23a) with an LCR meter (AC), impressing loads of variable frequency with a maximum amplitude of 14 kN.
The results showed that GNP offer the greatest increases in electrical conductivity compared to other fillers, with a value of $2.6 \cdot 10^{-6}$ $\Omega \cdot cm^{-1}$ ($1.7 \cdot 10^{-7}$ $\Omega \cdot cm^{-1}$ for the reference paste). This data is also related to the greater increase in thermal conductivity of the paste with graphene (1.14 W/mK).
Although graphene offers the greatest increases in electrical conductivity, its contribution to sensitivity properties is uncertain. Indeed, pastes with GNPs show worse results if compared to other fillers, in terms of GF and signal quality (Fig. 4.23b).

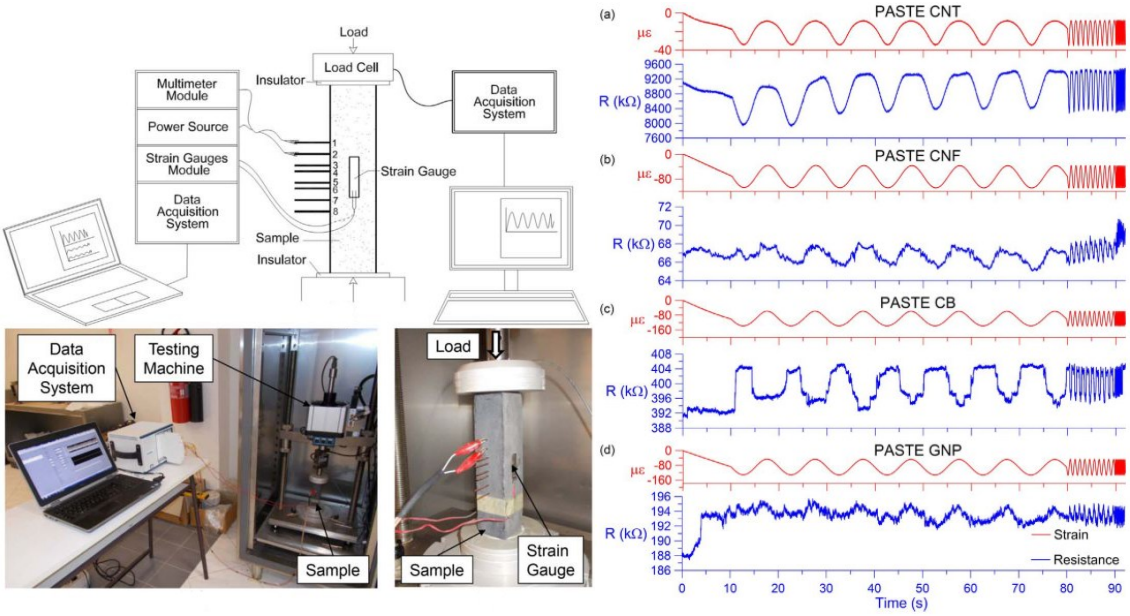

Figure 4.23. *a) Setup of electromechanical tests; b) Time vs. strain and electrical resistance for specimens with MWCNTs, CNFs, CB and GNPs from strain sensing tests* [66]

Better results were obtained by Metaxa and Kourkoulis [206], by the experimentation of sensitive cement-based pastes containing low amount of GNPs (0.15% on cement weight). Prismatic specimens were realized (20x20x80 cm) and the filler was dispersed in the mixing water by sonication through an immersion ultrasonic probe. For the evaluation of the sensitivity properties, a 4-electrode DC configuration was used, applying a monotonic compression load and cyclic compressive loads up to 10 MPa (Fig. 4.24a-4.24b).

The results show a high sensitivity of the pastes, for both monotonic loading and load-unload cycles (Fig 4.24c-4.24d), however, the group does not provide precise information over the sensitivity parameters of the materials (FCR, GF).

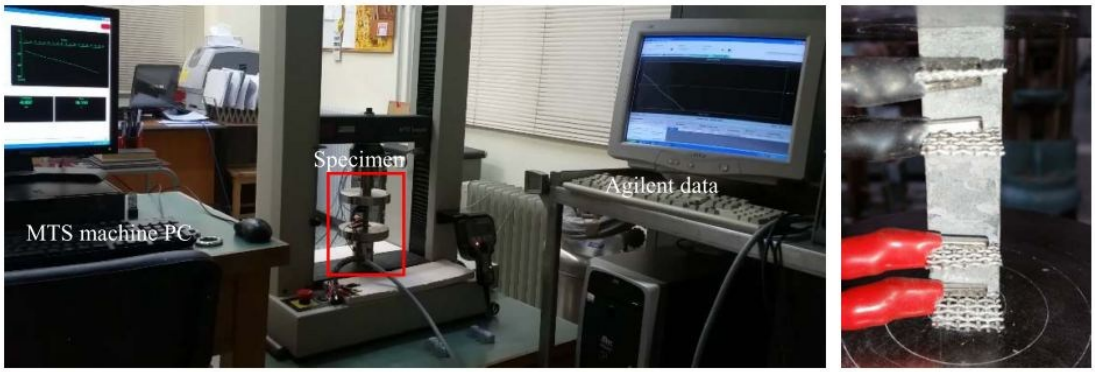

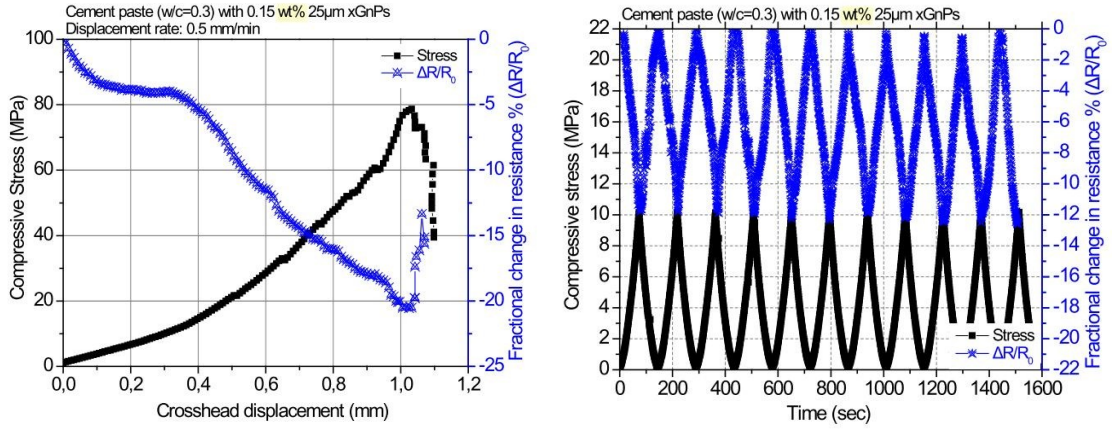

(c) (d)

Figure 4.24. *a) Experimental test set up and. b) Specimen under piezoresistivity test. c) Monotonic compressive strain vs. fractional electrical resistance. d) Cyclic compressive stress and fractional electrical resistance change over testing time* [206]

Liu et al. [196] performed a study using materials more suitable to real service conditions, testing the electrical and piezoresistive properties of structural mortars with several amounts of GNP and Graphene oxide nano-platelets (GONP) added by % on cement mass and with different w/c ratios. The electrical properties were tested with a 2-electrodes configuration (copper grids) and with AC (steady-state resistivity measurement) and DC (resistivity measurements under load) devices (Fig. 4.25a). The group used an ultrasonic bath for the dispersion of GNPs. The sensitivity of mortars was assessed through cyclic compressive tests with an amplitude of 20 kN.
The results showed that the GNPs are more effective than the GONPs for the increase of conductivity, and the high amounts of addition have allowed to detect the percolation threshold (Fig. 4.25b).

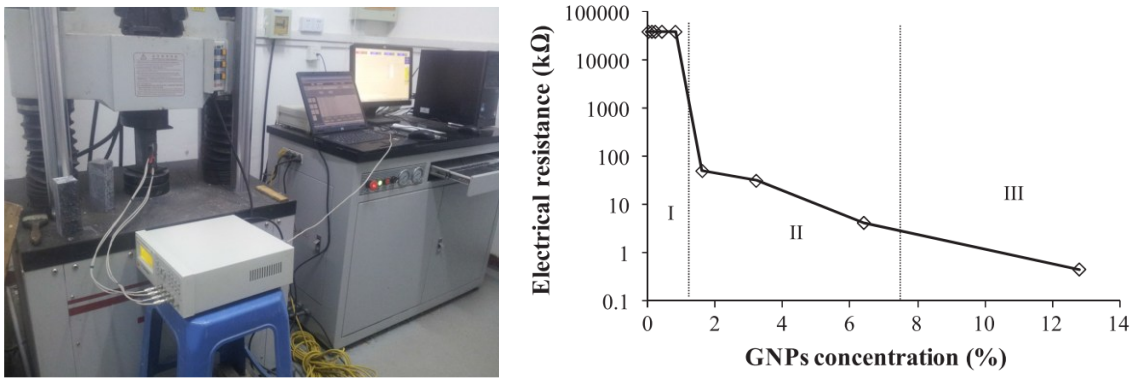

(a) (b)

Figure 4.25. *a) Setup of resistivity measurement under load. b) Relationship between electrical resistance and GNPs concentration* [196]

Figure 4.25b shows a percolation threshold between 1% and 2% of filler addition, and an even higher resistivity decrease with additions above 6%. Piezoresistivity tests clearly show that the higher the amount of GNPs the higher the signal quality (Fig. 4.26).

Furthermore, the FCR of mortars with high filler quantity is higher, but this relationship is not always proportional. Indeed, mortar with 3.2% of GNPs shows a greater sensitivity compared to the mortar with 12.8% of GNPs, despite the worst quality of the signal. The group has also investigated the effect of the drying method on the piezoresistive properties of the specimens, and assessed that the natural air drying of the composites leads to a more stable reading, compared to oven drying.

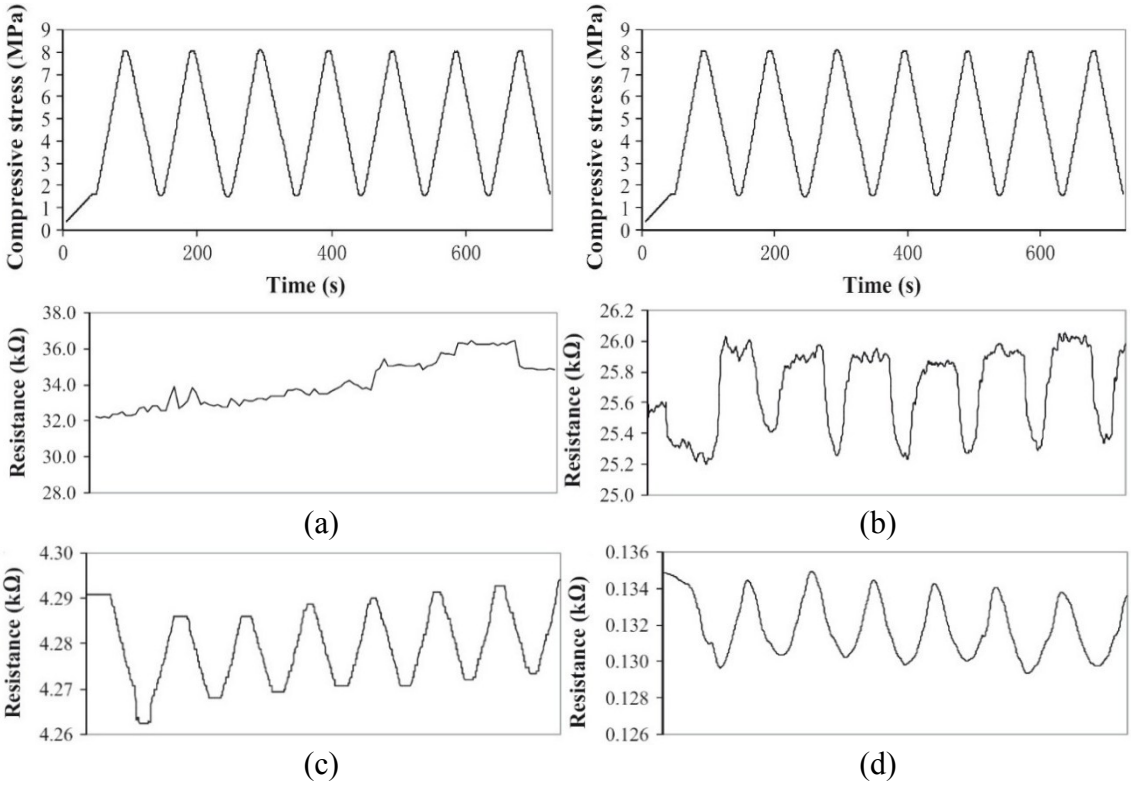

***Figure 4.26**. Piezoresistive reaction of dried specimens: a) 1.6% GNP. b) 3.2% GNP. c) 6.4% GNP. d) 12.8% GNP* [196]

Another interesting study on the implementation of SHM materials with graphene was carried out by Le et al. [126]. The group analyzed the use of GNPs for increasing and stabilizing the electrical conductivity of mortars, thus facilitating the detection of cracks and permanent damage. Structural mortars were realized with different amounts of GNPs, precisely 1.2%, 2.4%, 3.6% and 4.8% on mortar volume. Notches of various thickness (Fig. 4.27a) and increasing depths (0.0D, 0.125D, 0.25D, 0.375D, 0.5D, 0.625D, and 0.75D, where D = specimen depth) were realized in the specimens. The variations in the electrical potential of the specimens were measured with a 4-probe configuration and a DC device, imposing a constant current of 0.5 mA on the materials (Fig. 4.27b).

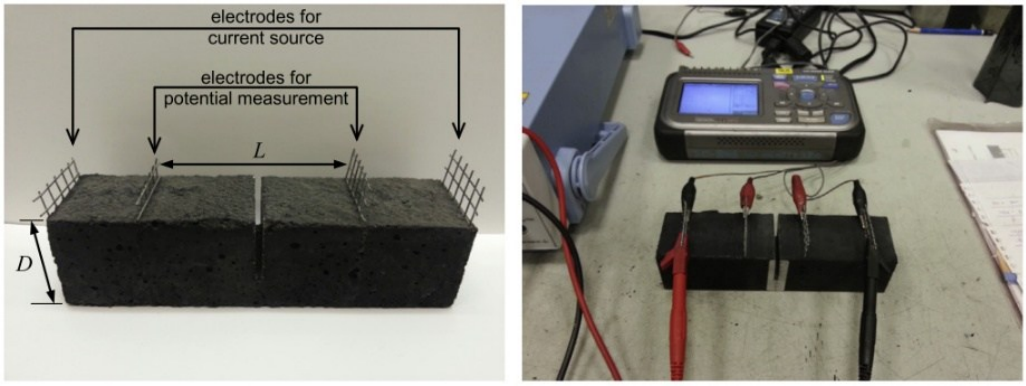

(a) (b)

Figure 4.27. *(a) 4-probe configuration specimen with central notch. (b) Setup for electric potential measurement during testing* [126]

The experimental results identified a percolation threshold, beyond which the high conductivity of the mortar, makes the specimen insensitive to potential variations in resistivity due to humidity (Fig. 4.28b). This allows to obtain accurate electrical data about the state of health of the specimen. The study successively analyzed the increments in electrical resistance of the specimens in relation to the depth and thickness of the notch, thus developing an analytical system for the evaluation of damage degree of the specimens through electrical measurement (Fig. 4.28c).

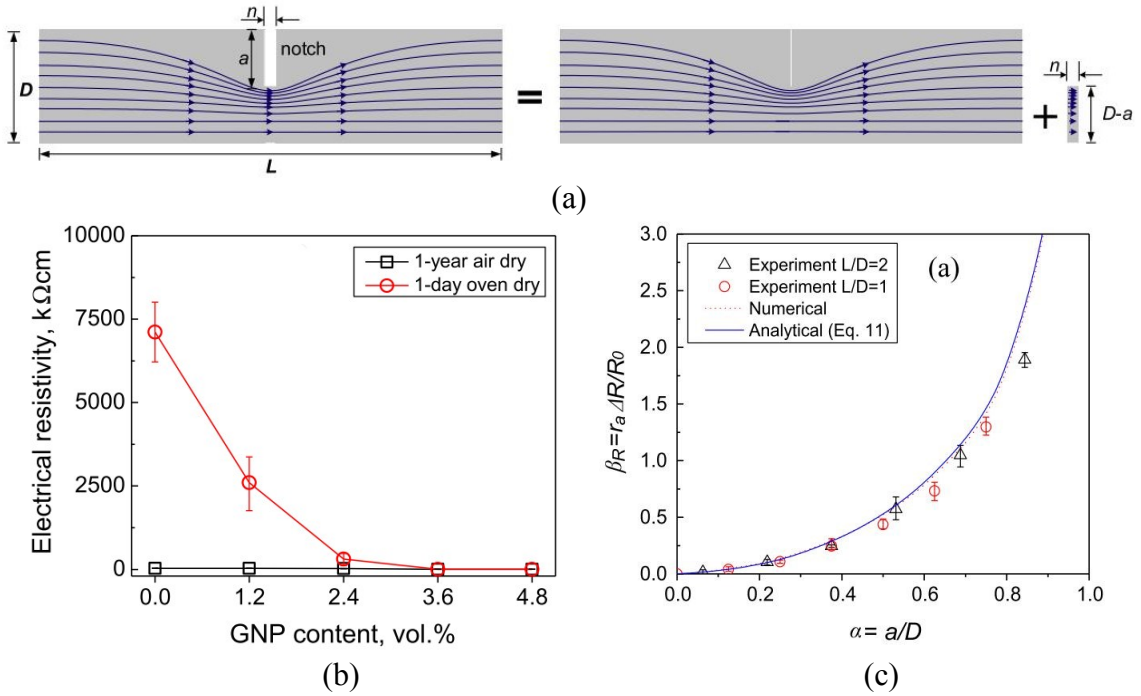

Figure 4.28. *a) Streamlines flowing through a specimen with a finite notch width. b) Electrical resistivity of mortars with different amounts of GNP. c) Comparison between experimental, analytical and numerical results of resistance change as function of thickness* [126]

4.3.3 Hybrid filler-based composites

This dissertation includes an experimentation on the combined effects of different types of conductive admixtures (carbon-based fillers and fibers with different aspect ratios) on the electrical and piezoresistive properties of cementitious materials, called "*hybrid composites*" in literature. Hybrid additions have been experimented with the aim to combine the advantages of each individual filler and create a conductive synergy effect that can proffer superior electrical conductivity and piezoresistivity.
For example, the combination of carbon fibers and carbon nanotubes was studied by Azhari et al. [167]. In their experiments, the team compared the performance of cement pastes using CF and CF/CNT fillers using the Wenner-derived 4-electrode method and compressive cyclic tests with amplitudes of 30 kN. The concentrations of CF and CNT were 15 and 1 vol.%, respectively. Figure 4.29a shows the PCSS specimens and the experimental setup. Figures 4.29b and 4.29c depict the results of the cyclic tests for compositions using CF and CF/CNT fillers, respectively. The addition of the carbon nanoparticles visibly enhanced the piezoresistive behavior in terms of repeatability, leading to a narrower scatter distribution of the plot in Figure 4.29c. However, the linearity remained rather low, with a short initial linear zone in the first 400 με.

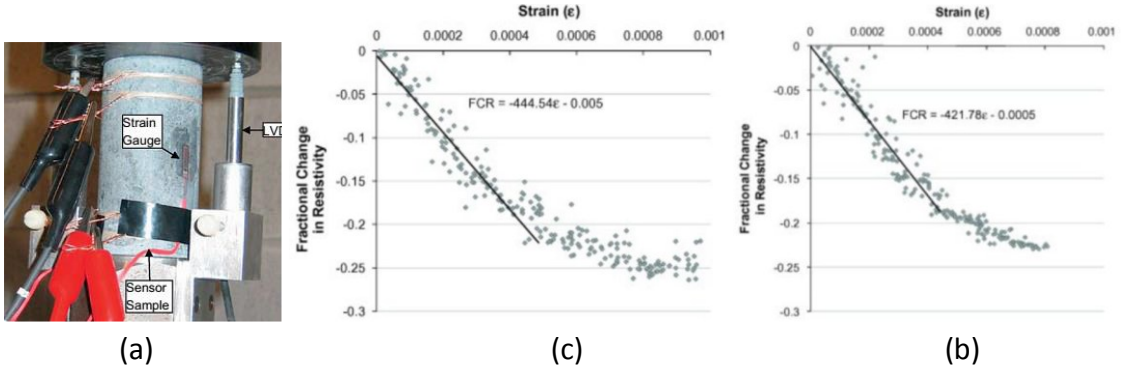

Figure 4.29. *a) Implemented setup. b) and c) electrical resistivity variation after cyclic compressive tests in specimens wit 15% CF and 15% CF + 1% CNT, respectively* [167]

Wen et al. [71] studied the partial replacement (as much as 50%) of CF by CB to reduce the cost of the conductive admixtures. The Wenner-derived 4-electrode method was used in small cubic specimens and compressive cyclic tests with amplitudes from 5 to 25 MPa were performed. The addition of CB diminished the piezoresistive effectiveness by lowering the gauge factor in ca. one order of magnitude. However, it increased significantly the workability of the mixture and allowed lower fabrication costs.
In turn, Han et al. [183] also investigated the combination of CF and CB in PCSS. In their approach, small cement paste specimens were casted and the 4-electrode method was adopted by using copper meshes (Fig. 4.30a). The piezoresistive behavior was evaluated through cyclic compressive loads with amplitudes of 12kN (Fig. 4.30b-4.30c). A linear response and great strain sensitivity with a GF of ca. 227 were found. In comparison to plain CF-based PCSS, the addition of CB demonstrated to enhance significantly the output signals, in terms of linearity and repeatability.

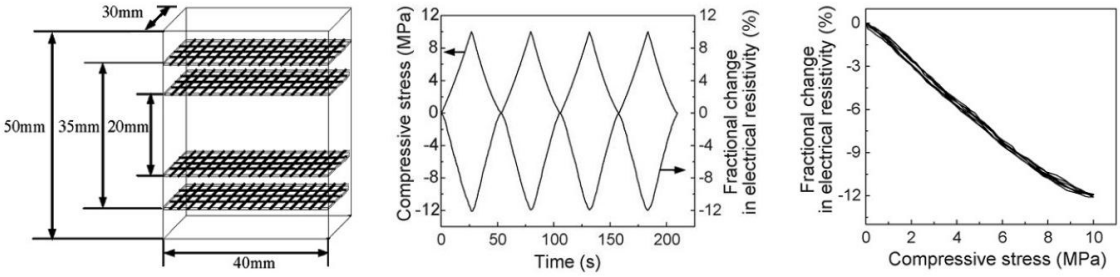

(a) (b) (c)

Figure 4.30. *a) CF/CB PCSS specimen arrangement. b) Compressive stress and FCR vs. time. c) FCR vs. Compressive stress* [183]

Later, the same team combined CNT with CB in fine concrete compositions [39]. CNT and CB were considered in proportions of 40:60 and the hybrid filler was added to the mixtures in concentrations ranging from 0 to 3.12 vol.%. The sensitivity to strain stimuli was carried out by applying cyclic compressive loads on small prisms equipped with two mesh-type electrodes. Figure 4.31a depicts the experimental setup and shows the results of strain sensitivity (GF) obtained for each concentration of filler tested. A GF of 704 was found in PCSS with filler concentration of 2.4 vol.% (Fig. 4.31b). Figure 4.31a shows the resistivity changes upon stress variations of 8 MPa. Figure 4.32b demonstrates that linear response only occurs under 4 MPa and the large scatter distribution transduces a rather poor repeatability.

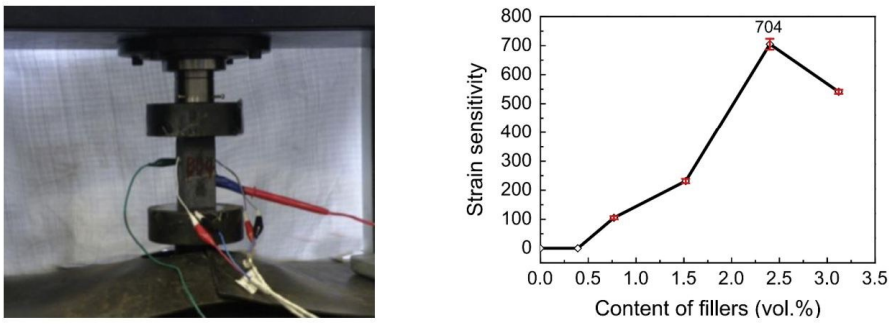

(a) (b)

Figure 4.31. *a) PCSS specimen and setup. b) Strain sensitivity of the composites under compressive loading* [39]

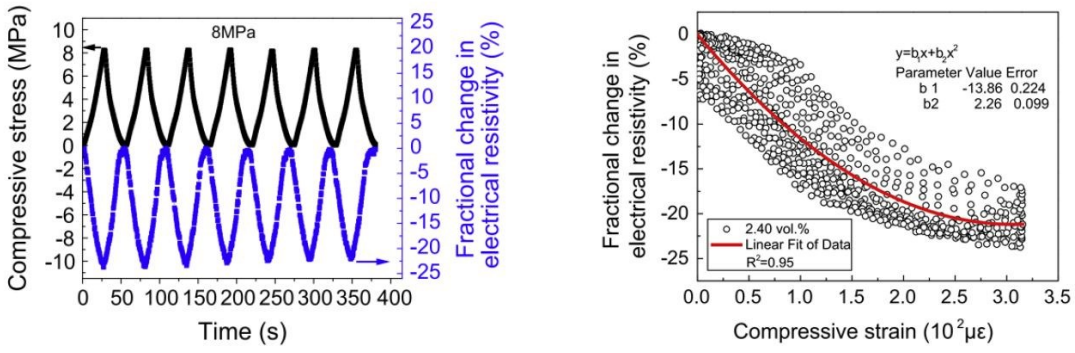

(a) (b)

Figure 4.32. *Piezoresistive experiments of the mixture with 2.4 vol.% of conductive filler: a) FCR under compression cycles. b) Relation between variation in resistivity and strain* [39]

Also studies that analyze the electrical properties of hybrid composites realized by combining CF and GNP are present in literature. However, these researches are few, and no research group has experimented the piezoresistive properties of this type of hybrid.

4.4 Experiments on structural elements

The main goal of developing self-sensing composites is to apply it in civil structures. Owing to the capability of detecting its inside stress, strain, cracking, and damage, self-sensing concrete can replace embedded or attached sensors or detectors, which suffer from high cost, low durability and limited sensing volume. Therefore, self-sensing composites has potential for *structural health monitoring*.
This dissertation does not focus on experimentation of configurations for concrete structure monitoring. However, an overview of the state of the art on the PCSS utilization under real service conditions is interesting, to understand the development degree of this research field.
To date there are few studies on PCSS tested in real civil structures [184]. However, Han et al. [4] carried out an in-depth study on the potential applications of piezoresistive concretes, analyzing different configurations for the monitoring of structural elements (Fig. 4.33).

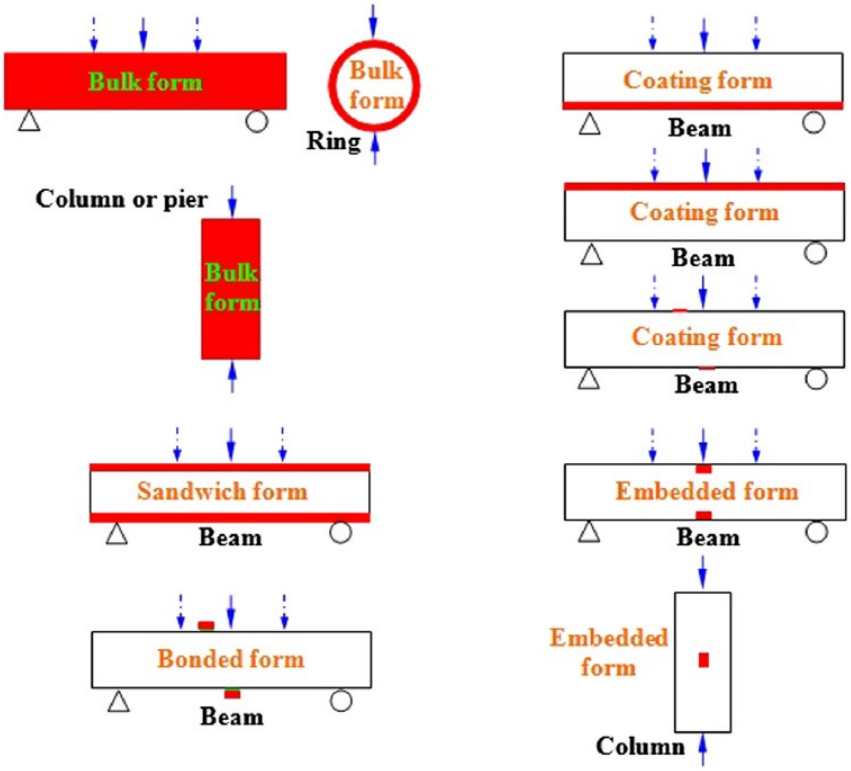

Figure 4.33. *Application forms of self-sensing concrete (red parts) for Structural Health Monitoring on different structural elements* [4]

4.4.1 Embedded form

A possible solution involves the localized installation of concrete sensors in *embedded form*. Embedded form means that self-sensing concrete is prefabricated into standard small-size sensors and then embedded into the structure (Fig. 4.34) [184].
Ou and Han [213] first studied embedded cement paste sensors with hybrid carbon fiber and carbon black into compressive zone of the pure bending region of reinforced concrete beams and into the center of concrete columns, and tested the self-sensing performance of these components under four-point bending and uniaxial compression. They found that these components embedded with cement paste sensors were capable of compressive strain self-sensing.

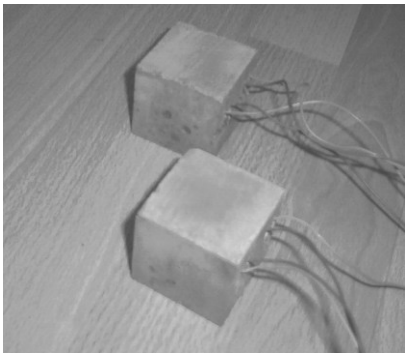

Figure 4.34. *Cement-based strain gauges* [184]

Xiao et al. centrally embedded concrete with carbon black into concrete columns with different compressive strengths (Fig. 4.35a) and tested the self-monitoring ability of the columns under cyclic load and monotonic load [214]. The concrete columns embedded with carbon black–based self-sensing concrete detected the strain (Fig. 4.35b).

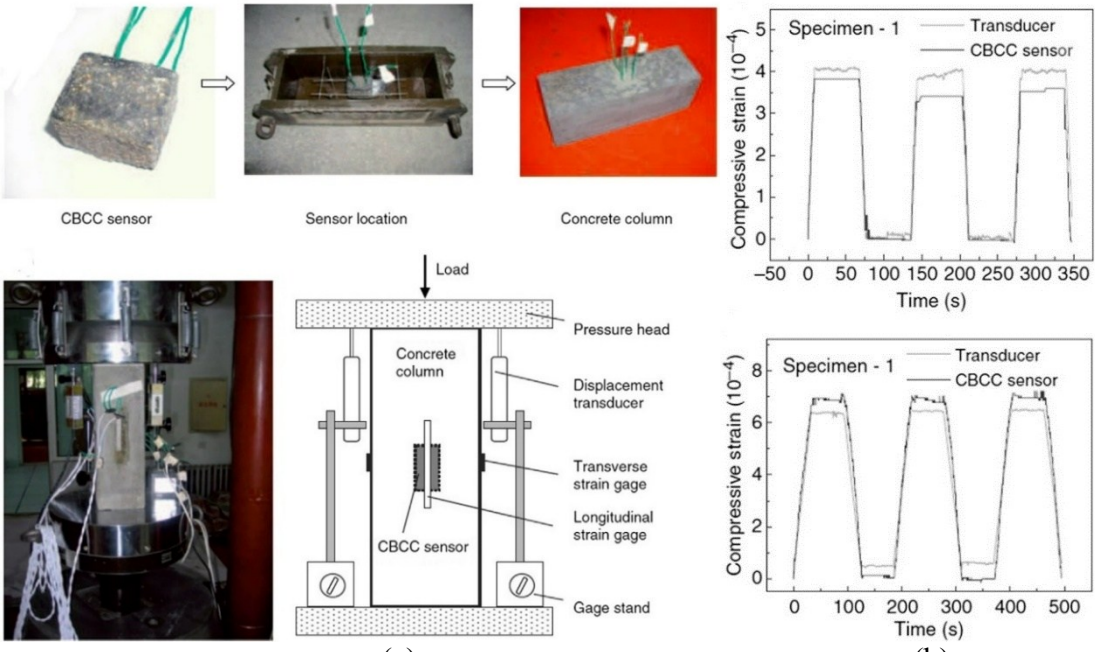

(a) (b)

Figure 4.35. *a) Experimental setup. b) Strain of the columns measured with transducer and concrete sensor* [214]

Xiao et al. also embedded concrete sensors with carbon black into three different stress zones (i.e., uniaxial compression, combined compression and shear, and uniaxial tension zones) of bending reinforced concrete beams and investigated the strain sensing properties of the concrete beams under four-point bending [215]. All sensors embedded under the three different stress zones exhibited reasonable sensing results.

4.4.2 Bonded form

Another possible way for the application of the sensors is in *bonded form*. It means that small sensors made of self-sensing concrete were attached to the concrete component using glue bonding materials and such. Baeza et al. bonded self-sensing concrete containing carbon fibers or carbon nanofibers on the top, bottom, and side of reinforced concrete beam (Fig. 4.36) [216]. They observed that self-sensing concrete with carbon fiber or carbon nanofiber is capable of measuring strains on the surface of a structural element, regardless of whether the local stresses were tension or compression. Furthermore, almost no difference was found between gauge factors calculated for self-sensing concrete with carbon fiber (with equal dimensions) located on the upper and lower sides of the same beam's section. The gauge factor of self-sensing concrete with carbon nanofiber is around 190. Hence, these composites could act as strain sensors, even for severely damaged structures near collapse.

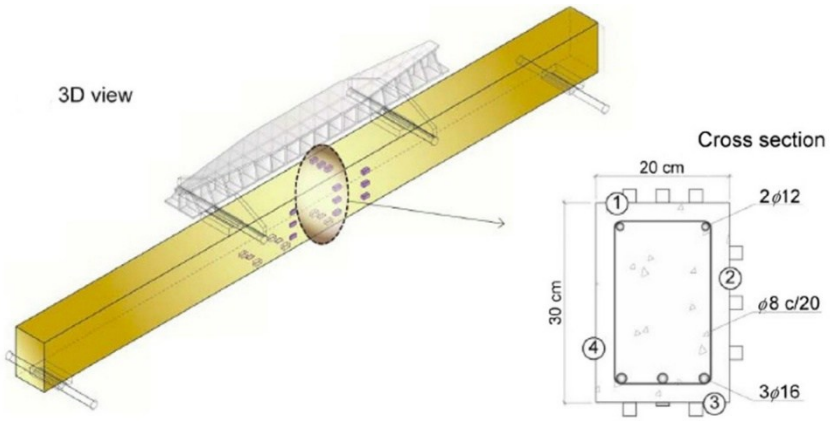

Figure 4.36. *Distribution of self-sensing concrete sensors on the beam* [216]

4.4.3 Coating form

Coating form consist to cover a surface of a structure or component with a layer of self-sensing concrete. Wen and Chung [217] first fixed carbon fiber cement paste coating on either the tensile side or the compressive side of cement paste beams under three-point bending (Fig. 4.37). They observed that the carbon fiber cement paste coating could be used for compressive or tensile strain monitoring of the beam surface.

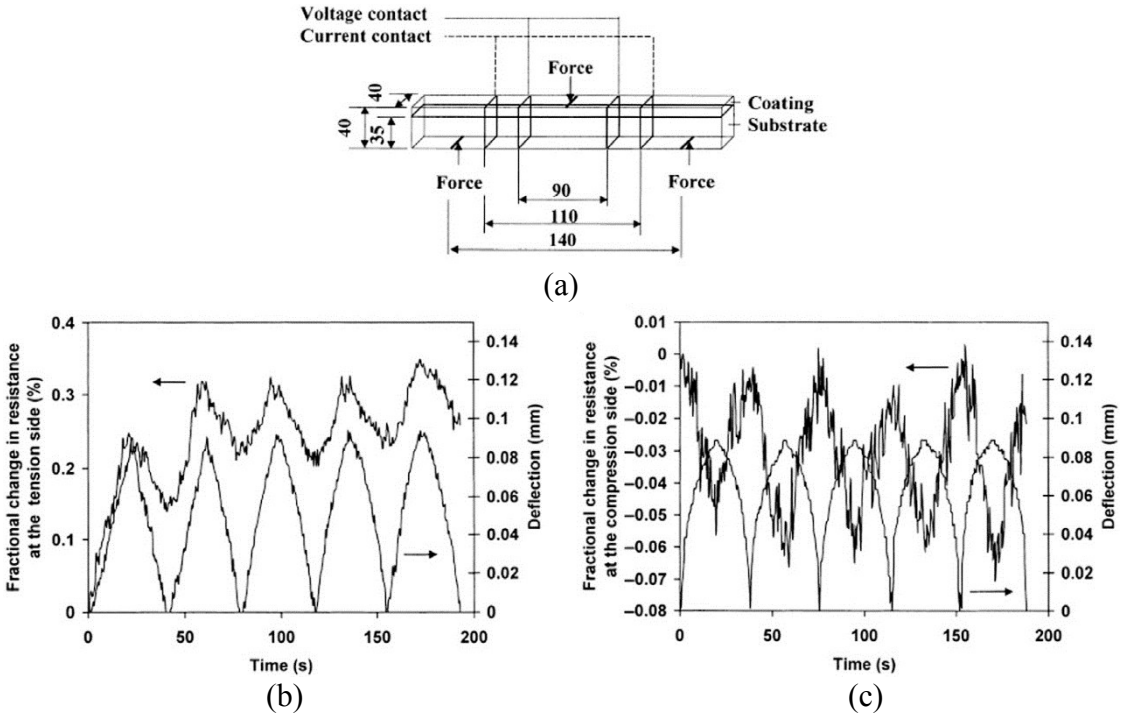

Figure 4.37. *Structural self-sensing behavior of beam cast self-sensing concrete containing carbon fiber on its top or bottom: a) Beam scheme; b) FCR vs. time under tension force; c) FCR vs. time under compression force* [217]

4.4.4 Bulk form

The most interesting configuration for structures monitoring through PCSS consist in the *bulk form* method, i.e. realizing the entire structural element with piezoresistive concrete, without the localized application of small sensors. These type of systems, through an accurate installation of probes, would allow to obtain a continuous and complete reading. This dissertation aims to develop effective and economical piezoresistive composites for this type of system.

Some authors have experimented structural elements made entirely with piezoresistive concretes on a laboratory scale. Zhang et al. [218] fabricated reinforced concrete beams with intrinsic self-sensing carbon fiber concrete. A four-point bending test indicates that the beams have the capability of sensing load and damage in their pure bending region. The same authors also investigated variations in the electrical resistance of carbon fiber concrete beams under monotonous, repeated, and alternating bending loadings. They observed that carbon fiber concrete beams can monitor load and damage in compressive and tensile zones under four-point bending [219]. Lastly, the group studied the feasibility of elastic compressive stress self-monitoring in the pure bending region of carbon fiber concrete beams under four-point bending. The results of a cyclic loading experiment showed that elastic stress self-monitoring of the key section of reinforced concrete beams can be achieved based on the correlation between electrical resistance and the elastic compression strain (Fig. 4.38) [220].

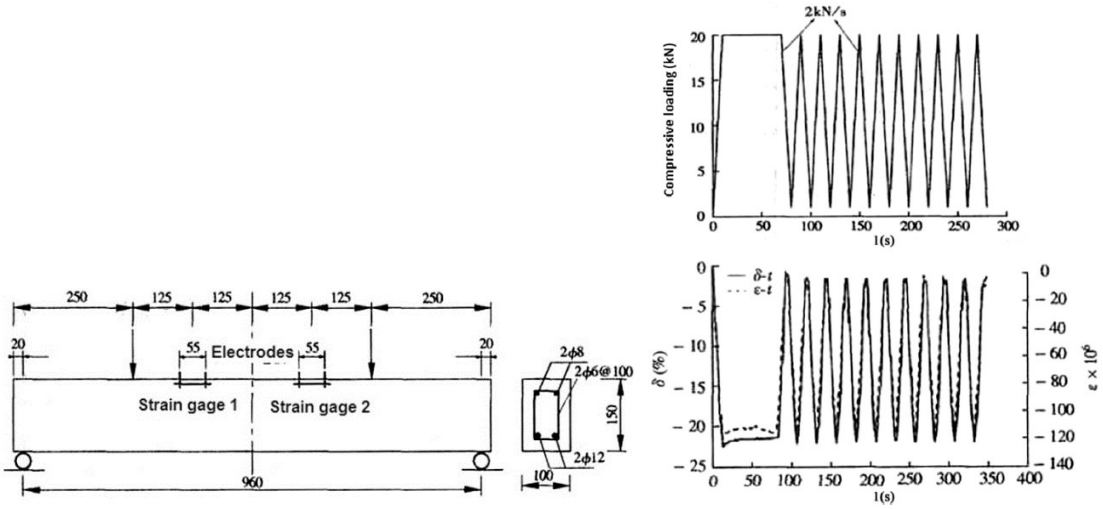

(a) (b)

Figure 4.38. *Diagram of beam structure (a) and Fractional change in electrical resistance of concrete with carbon fiber vs. elastic compression strain (b)* [220]

Wang et al. [221] tested four-point bending beams fabricated with carbon fiber concrete and evaluated the relationship between electrical property and fatigue life under cyclic flexural loading. The test results indicated that carbon fiber concrete can be used to monitor the extent of fatigue damage and predict their fatigue life (Fig. 4.39).

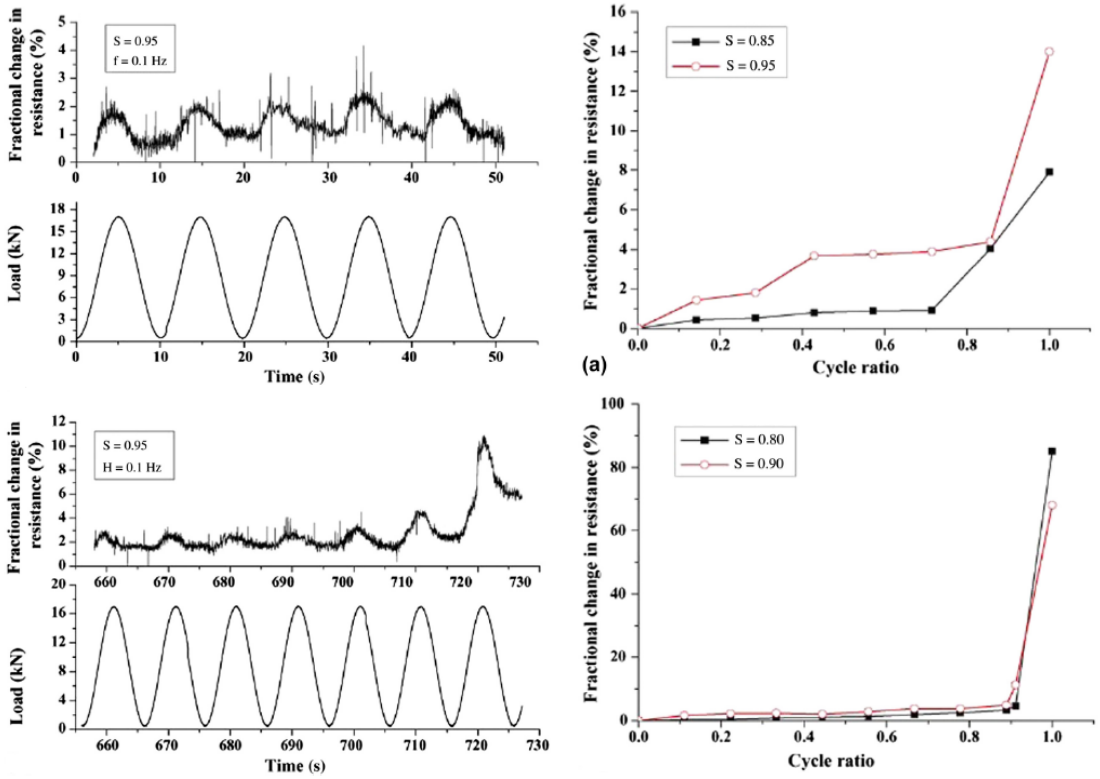

(a) (b)

Figure 4.39. *a) Fractional change in electrical resistance during repeated flexural loading. b) Fractional change in electric resistance vs. cycle ratio (ratio between the individual testing cycle number and the total number of cycles to failure under cyclic flexural loading)* [221]

Howser et al. [185] built shear-critical columns with the carbon nanofiber concrete and tested the self-sensing behavior of concrete columns under a reversed cyclic load. The columns were capable of monitoring their own strain (Fig. 4.40).

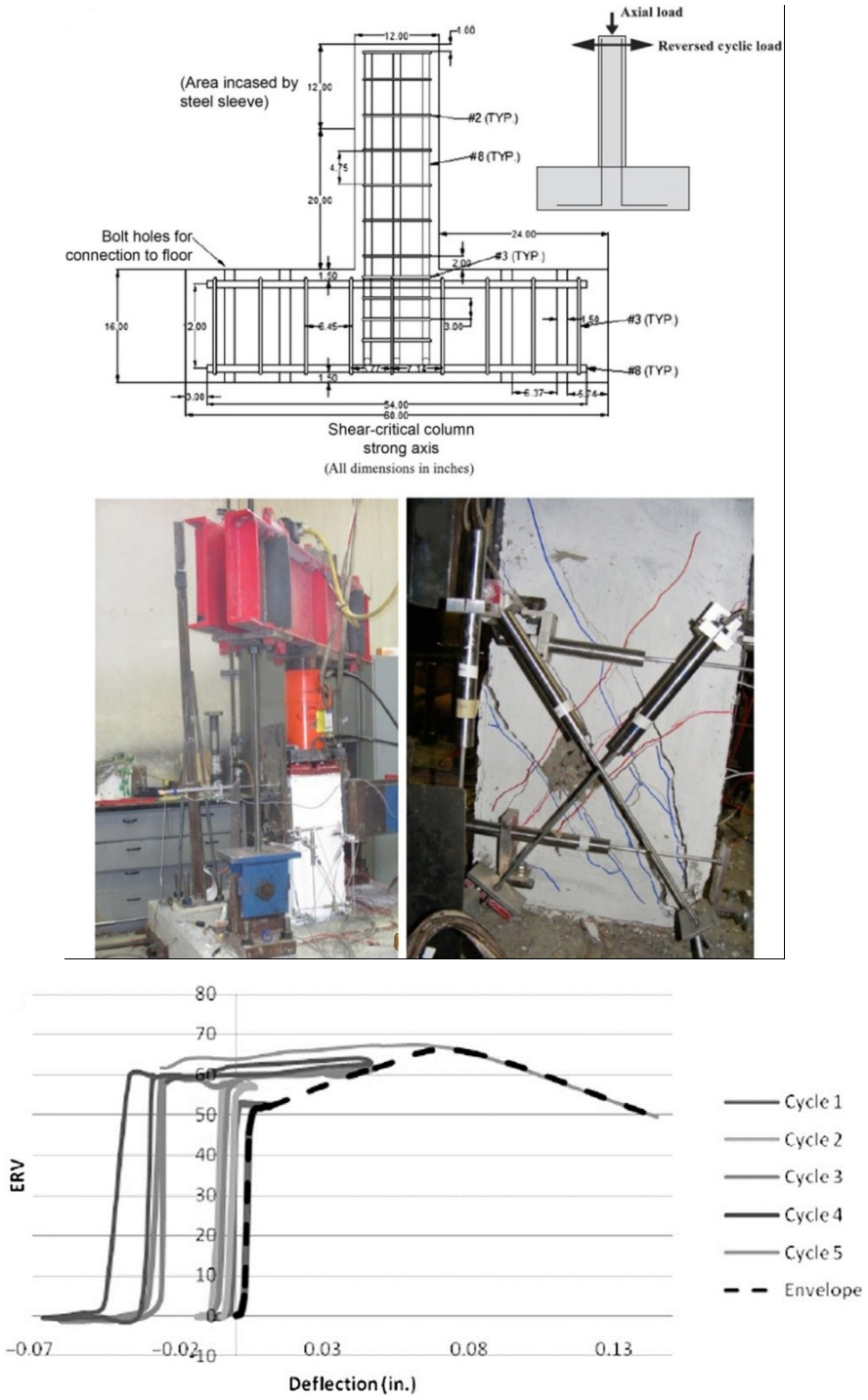

Figure 4.40. Structural self-sensing behavior of columns fabricated with carbon nanofiber self-sensing concrete and loading system. In the graph, the electrical resistance variation (ERV) versus horizontal deflection [185]

4.4.5 Experiments under real service conditions

A single experiment was found in the literature concerning the application of PCSS in SHM. In 2006, J. Ou, et al. [184] have developed small CF-based PCSS (7x5x5cm), relying on the 4-electrode method and grid-like electrodes. Sensors were embedded into the girders of the slabs of *Chongqing Guangyang Island* bridge, in China (Fig. 4.41a-4.41b). Unfortunately, few information is provided about the outputs. Only results from monotonic experiments with one of the sensors are shown (Fig. 4.41c). However, a large variation range was found for the resistance with poor linearity and accuracy at low stresses.

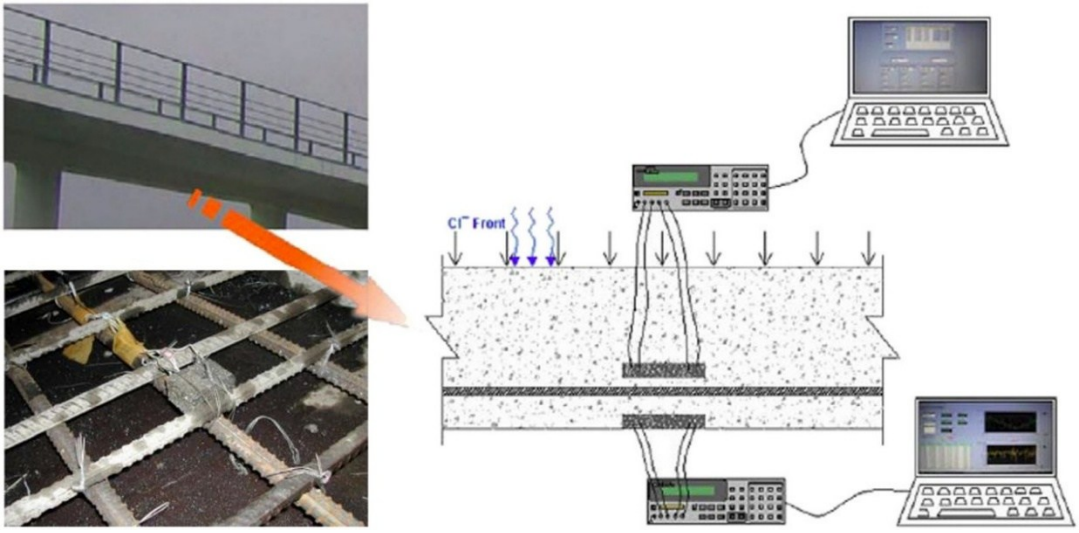

(a)

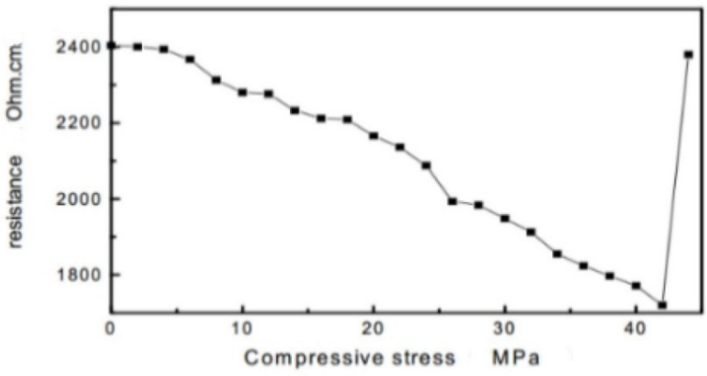

(b)

Figure 4.41. *a) Embedded PCSS into the girders and monitoring setup. b) Results from a monotonic piezoresistive experiment* [184]

5 . Chapter
Materials

Description of materials and conductive admixtures used in the experimentation

5.1 Introduction

The present dissertation aims to develop *hydraulic binders-based composites* by combining the best characteristics of strength, durability and multi-functionality. As seen in section 4.2, the optimization of multiple properties of the composites requires a careful analysis of mix design and a weighted addition of fillers and fibers, combining admixtures with a different aspect ratio. Above all, this is very important to create a continuous and effective electrically conductive network. At the same time, it is convenient to study the exact quantity of fillers and compositional parameters such as the aggregate/binder ratio (a/b) and water/binder ratio (w/b), to obtain composites with suitable mechanical properties.
Furthermore, careful selection of raw materials is necessary for the realization of mixtures. The choice of materials must guarantee the scientific worth of the research, and ensure:

- *Comparability* between the materials developed in the research and similar products already used in the construction sector for the same application;
- *Repeatability* of the tests, i.e. to guarantee the subsequent reproduction of the mixtures and the repetition of the results, as well as to optimize the composites in future researches.

In addition, the principle of *health safety* was considered by selecting harmless materials for the health of experimenters. These type of materials will also be safer for future utilization in real service applications and for a large-scale production.
Therefore, materials have been selected that comply with current European Standards, in order to guarantee a certificated quality of the hardened mixtures and safety in use.
Fillers and fibers have been selected according to the industries needs regarding the waste by-products recycling. However, the chemical-physical homogeneity of the material and a secure supply over time have been guaranteed. In addition, carbon powders harmless to human health have been selected on the basis of an in-depth state of the art (Section 2.7).
The following is an accurate description of the materials used for the realization of mortar and pastes, completed with information from technical data sheets and regulatory references. The microstructural and elemental analyzes (SEM and EDX) of the conductive admixtures are also reported.

5.2 Hydraulic binders

The monolithic properties of mortars and concretes derive from the action of a binder with “hydraulic behavior”.
Hydraulic binders are finely ground inorganic materials. These powders, combined with inert solid elements and mixed with water, form a deformable and workable paste, which gradually hardens both in the air and in water, until it reaches a stone consistency. This property is due to the formation of hydrated compounds, insoluble or poorly soluble, starting from silicates, aluminates and calcium ferrites present in the binder [222]. This makes them solid when exposed to air and water once the process is completed [223].

They are defined as *hydraulic* to differentiate this type of materials from binders such as gypsum and calcium carbonate, which harden only with a direct contact with air. *Cement* is the most used hydraulic binder in construction industry, and the main component of concrete. However, for some types of applications, *hydraulic lime* is preferred, thanks to its transpiring properties and its lower environmental impact.

5.2.1 Cement

Portland cement is an essential building material, and it has "hydraulic properties" since, when mixed with water, it creates a composite with high mechanical properties. Thanks to its wide use on a planetary scale, it is, to date, one of the most marketed products in the world [21].
It is obtained chemically from mineral raw materials with high quantities of: *calcium oxide* (CaO), *silicon oxide* (SiO_2) and *aluminum oxide* (Al_2O_3). These are obtained by cooking limestone and clay at very high temperature (up to 1480°C). The obtained material is the so-called "*Portland clinker*" (Fig 5.1), which is finely ground and added with gypsum (4-6%) as a setting retarder (*primary ettringite*).

Figure 5.1. *Grains of Portland clinker*

After grinding, the ready-to-use cement powder is obtained, which has about 60% of calcium oxide, 20% of silicon oxide, 7% of aluminum oxide and 5% of iron oxide in macro-chemical components.
Portland cement powder consists of four main mineralogical components, which regulate the hydration process:

- *Dicalcium silicate*, $2CaO \cdot SiO_2$ (cement chemist notation C_2S);
- *Tricalcium silicate*, $3CaO \cdot SiO_2$ (C_3S);
- *Tricalcium aluminate*, $3CaO \cdot Al_2O_3$ (C_3A);
- *Tetracalcium alumino ferrite*, $4CaO \cdot Al_2O_3 \cdot Fe_2O_3$ (C_4AF).

Mixed with *water* (H), through complex chemical reactions, these produce hardened cement hydration products:

- $C_3A + H \rightarrow$ C-A-H (*calcium aluminate hydrates*, very fast hydration);
- $C_3S + H \rightarrow$ C-S-H + CH (*calcium silicate hydrates*, fast hydration);
- $C_4AF + H \rightarrow$ C-A-H + C-F-H (*calcium aluminate* and *calcium ferrite hydrates*, fast hydration);
- $C_2S + H \rightarrow$ C-S-H + CH (*calcium silicate hydrates*, slow hydration).

The hardening, and therefore the binding power of the cement, is largely linked to the formation of calcium silicate hydrates, whereas the formation of calcium aluminate hydrates is the main cause of workability loss and setting [224].
The study of the curing process shows how the use of some raw materials rather than others influences the setting or hardening phases. For this reason, the European community regulations, drawn up in recent years, aim at the search for a standardized nomenclature that immediately identifies the characteristics of the different types of binders within the European Market.
The European standard UNI EN 197-1 collects in a single classification all types of cement produced in the member countries, and is the reference paper for the classification of binders according to their composition and their mechanical strength. It identifies five types of cement, twenty-seven subtypes and six strength classes.
The first two types concern Portland cements, divided according to the percentage of clinker (type A> 95%, type B> 65%) and the added raw materials. *Type I* cements are composed entirely of Portland clinker, *Type II* cements are added with other mineral materials, such as slag (S), silica fume (D), pozzolan (P, Q), fly ash (V, W), calcined schist (T) or limestone (L, LL). The standard also describes six different resistance classes based on the mechanical compressive strength developed by a standard mortar after 28 days of curing (Fig. 5.2). For example, a "425N" cement will achieve a compressive strength ≥ 42.5 MPa at 28 days of curing (N highlight a standard initial resistance, whereas R identifies a high initial resistance).

Class	Compressive strength (N/mm^2)				Start setting time (min)
	Initial strength		Normalized strength		
	2 days	7 days	28 days		
32,5 N	-	≥ 16	≥ 32,5	≤ 52,5	≥ 60
32,5 R	≥ 10	-			
42,5 N	≥ 10	-	≥ 42,5	≤ 62,5	
42,5 R	≥ 20	-			
52,5 N	≥ 20	-	≥ 52,5		≥ 45
52,5 R	≥ 30	-			

Figure 5.2. *UNI EN 197-1: Classification of cements according to strength class*

In the present experimentation, two different types of Portland cement were used (Fig. 5.3):

- CEM I 52.5R (COLACEM), pure clinker cement, with very fine particles and high mechanical performances;
- CEM II/B-L 32.5N (CIMPOR), limestone cement with normalized initial strength.

(a) (b)

Figure 5.3. *a) Cement of clinker CEM I 52.5R. b) Calcareous cement CEM II/B-L 32.5N*

5.2.2 Natural Hydraulic Lime

Hydraulic lime is a hydraulic binder primarily composed of calcium hydroxide ($Ca(OH)_2$). The hydraulic lime production differs from Portland cement in the cooking time and in the quality of the clay [225]. Composites made with hydraulic lime show lower mechanical strength and a lower elastic modulus than cement-based materials, due to the lower reactivity of lime powder. However, the hydraulic lime-based materials are more breathable, thanks to their greater porosity.
Hydraulic lime has a lower environmental impact than Portland cement. Its production process is based on the transformation of impure limestone clay, which is crushed and fired at temperatures between 1000°C and 1100°C, much lower than 1400-1500°C necessary for the preparation of Portland clinker [26]. Furthermore, lime is capable of reabsorbing the CO_2 produced during the calcination phase (up to 50%), thus decreasing the production of pollutants.
The chemical composition of the products resulting from the firing are: 60% -70% of *calcium hydroxide*, 10-20% of a hydraulic fraction of *monocalcium aluminate* and *dicalcium silicate*, and 5% -10% of *calcium oxide*. The presence of the hydraulic fraction contributes to provide the material with hydraulic properties similar to those of cement [222].
As for cement, the different types of hydraulic lime are classified according to their compositional characteristics and properties. The European standard UNI EN 459-1:2010 distinguishes between:

- *Natural Hydraulic Lime* (NHL), in which the hydraulic properties are obtained through limestone calcination, without the addition of any additional material;
- *Artificial Hydraulic Lime* (AHL), in which the hydraulic properties are obtained by adding of pozzolan or other hydraulic elements before or after the cooking phase.

Furthermore, NHL is classified, according to the quantity of clay and the consequent mechanical properties, as [226]:

- *Feebly* hydraulic lime (NHL2), which contains a quantity of clay up to 10%, mixed with other impurities;
- *Moderately* hydraulic lime (NHL3.5), which contains clay between 11% and 20%;
- *Eminently* hydraulic lime (NHL5), which contains clay between 21% and 30%;

These three types also define the mechanical strength values. A standard mortar made with NHL2 must achieve a compressive strength ≥ 2 MPa after 28-day of curing.
The hydraulic lime used in this dissertation is Natural Hydraulic Lime NHL5 (Fig. 5.4).

Figure 5.4. *Natural Hydraulic Lime NHL5*

5.3 Aggregates

The *aggregate* is the component of a composite material that contributes to compressive stress and provides a solid structure to the material. It can be defined as "inert", because it does not contribute to the chemical reactions of the hardening process (such as hydraulic binders), but it forms the main framework of the material, held together by the cement paste.
The dimensions of the aggregate differ depending on the application and the sought structural properties. Mortars contain only fine aggregates (sand), whereas concretes contain both fine and large aggregates (gravel).
Theoretically, the ideal aggregate must be selected in order to guarantee a high filling degree; therefore, it must be characterized by a varied grain size [26]. The granulometric curve should be carefully studied to obtain an optimal distribution.
Generally, aggregates are classified according to the particle size as:

- *very fine* (fillers): < 0,075 mm;
- *fine* (sand): 0,075 – 4 mm;
- *coarse*: > 4 mm;
- *fine gravel*: 4 – 15 mm;
- *gravel*: 15 – 40 mm.

Moreover, the aggregates properties vary according to their manufacturing process. They can be extracted from stream beds, quarries or from rock crushing. The former has a more rounded shape, the latter a more angular shape.
Aggregates for structural use must have good mechanical strength, absence of chlorides (harmful to concrete and reinforcement), absence of impurities and must be resistant to frost. The characteristics of the aggregates are regulated by the European standard UNI EN 13055:2003.
The aggregates used in this research for the realization of mortars, are sands with different granulometric curves. They are distinct, based on their petrographic origin and their mineralogical composition, in calcareous sand and silica sand. *Calcareous sand* is originated from calcareous sedimentary rocks, and their main component is calcium carbonate ($CaCO_3$). *Silica sands* are mainly composed by quartz, so their main component is silicon dioxide (SiO_2).
In this work three different types of sand have been used with different granulometric and compositional properties (Fig. 5.5):

- Calcareous sand with grain size ≤ 3 mm;
- Fine silica sand with grain size ≤ 1 mm;
- Silica sand with grain size ≤ 8 mm.

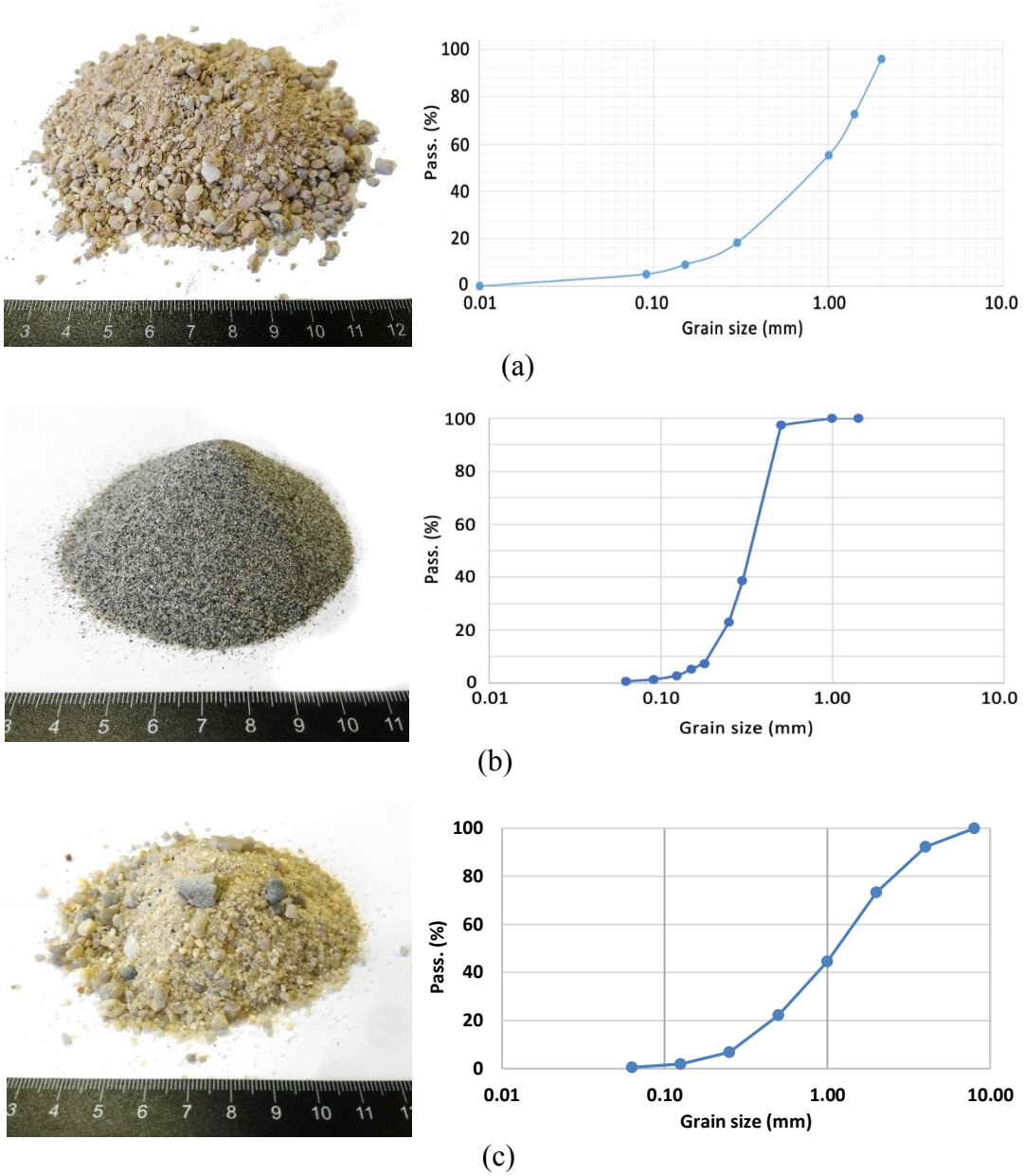

Figure 5.5. *Particle size distribution curves of: a) Calcareous sand 0-3 mm; b) Silica sand 0-1 mm; c) Silica sand 0-8 mm*

5.3.1 Dry surface saturated sand

The humidity of the aggregate is an important factor for the realization of cement composites in laboratory scale, because it can modify the composition ratios of the mixture [55].
For example, an excessively wet sand could release an unexpected amount of water into the mixture, increasing the w/c ratio and thus altering the properties of the cured composite. On the contrary, a dry aggregate could absorb mixing water due to its porosity,

subtracting water from the hydration process of the binder. For this reason, it is advisable to use an aggregate *Saturated* with *Dry Surface* (SSD condition) [227][99].
Therefore, before the experimentation, the humidity degree of the sand was measured by previous drying (possibly in oven). Afterwards, the humidity level in which the aggregate is saturated with dry surface must be measured. This is the sufficient level of humidity to saturate the aggregate, but without an excess of water.
The percentage of humidity of the SSD condition is calculated by gradually moistening of the dry sand, making collapse tests with conical molds (Fig. 5.6). When the sand is wet enough to cause a partial collapse of the form, the SSD condition is reached, and the percentage of maximum absorption of the aggregate USSD is thus calculated according to Equation 5.1:

$$U_{SSD} = \frac{m_{SSD} - m_0}{m_0} \cdot 100 \quad (1)$$

Where m_{SSD} = mass of sand sample in SSD condition; m_0 = mass of dry sand sample.

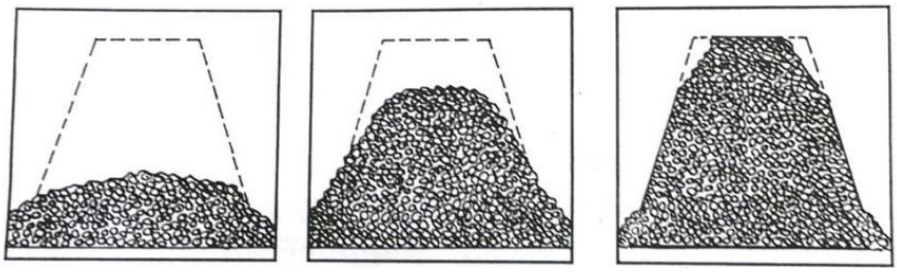

(a) (b) (c)

Figure 5.6. *Mold test on aggregate samples with different humidity. a) Dry sand; b) SSD sand; c) Wet sand*

5.4 Carbon-based Fillers

The term "*fillers*" indicates an aggregates with very small particles (generally micrometric) used to thicken the structure of a generic composite material (mortars and concretes, but also polymers, paints, etc.).
In cementitious materials, traditional fillers are sand or powders with fine particle size added to reduce the porosity of the hardened composite, in order to increase its mechanical strength and durability (the so-called "*filler effect*") [26]. These sands or powders may have a natural origin (calcareous or siliceous) or a recycled origin (by grinded waste from building production). Many different types of powders can be used as fillers in cementitious materials.
For example, many industrial sectors obtain carbon-rich waste powders through combustion, decomposition or thermal degradation processes [228]. These types of fillers have been studied in this thesis for the development of multifunctional cement materials.
In addition, commercial carbon-based *nanopowders* obtained in laboratory by complex production processes, have also been tested [229]. The nanomaterial experimented in this research is graphene, in *nanoplatelets* form. This material was chosen in order to: 1) develop the young research over cementitious materials containing graphene; 2) study composites realized with technologically advanced materials, for the performance

comparison with recycled fillers. Moreover, compared to other carbon-based nanomaterials (Section 2.7), graphene nanoplatelets are considered safe for health [137], and their use does not imply particular precautions.
In addition to graphene, activated carbon has also been studied as commercial filler, and as a material with multiple properties and an interesting depolluting effect.
In conclusion, the following types of fillers have been tested:

- *Commercial* carbon-based fillers:
  - Graphene nanoplatelets (GNP);
  - Activated carbon powder (ACP).
- *Recycled* carbon-based fillers:
  - Gasification char (GCH);
  - Used foundry sand (UFS).

5.4.1 Commercial fillers

5.4.1.1 Graphene Nanoplatelets

Graphene is composed of a layer of carbon atoms arranged according to a hexagonal cell crystal structure [230]. This basic structure has a planar conformation, and the monoatomic layer is a two-dimensional (2D) material. Graphene, whose carbon atoms are sp2 hybridized, can be considered as the basic structure for all other graphitic materials, such as fullerene (0D), carbon nanotubes (1D) and graphite (3D) (Fig. 5.7) [231].

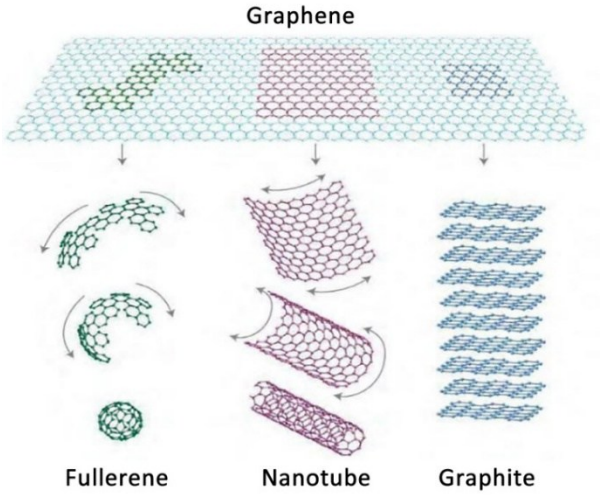

Figure 5.7. *Allotropes of carbon with graphene as structural element*

Until the early 2000s, although it was known as an integral part of graphite materials, graphene was considered a purely "theoretical" material, and its synthesis was considered impossible, due to its thermodynamic instability and its tendency to bend and form other structures (fullerenes and nanotubes).
However, in 2004, Novesolov and Geim isolated a layer of graphene using the adhesive-tape technique (Fig. 5.8). This is the basic method for the production of graphene, and consists in placing the surface of a graphite crystal on an adhesive tape, detaching the

tape and separating some layers of material [232]. The tape with the imprint of the graphite is then folded over itself several times. Each time, the flakes are divided into thinner layers. At the end of the process, the thin flakes are transferred onto an insulating substrate. Mechanical exfoliation is the easiest and most accessible method for isolating graphene platelets of some microns of size, and is a useful technique for basic research on its properties [233]. However, this method is not convenient for a large-scale industrial production.

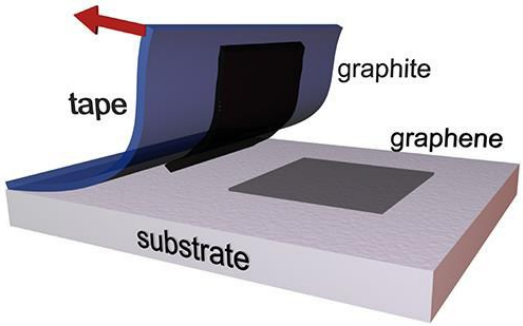

Figure 5.8. *Graphene production by "adhesive-tape" method*

After its discovery, graphene has received worldwide attention thanks to its exceptional properties, and it is studied in many fields of science and engineering, with numerous applications, especially in the electronic field.
The properties of graphene are closely related to its unique 2D structure. The following are the main properties of the filler.

- *Electrical properties*: graphene is a "zero energy gap" semiconductor, with a extremely high electrical conductivity. It is the material with the lowest known resistivity, i.e. $1.0 \cdot 10^{-8}$ $\Omega \cdot m$. With graphene it is possible to obtain current densities of six orders of magnitude higher of those of silver [11];
- *Mechanical properties*: Graphene is currently considered the most resistant material in nature, thanks to its 130 GPa of tensile strength modulus, despite its very low density (Kevlar® resistance modulus is 0.38 GPa). Its elastic modulus is about 1 TPa (the modulus of steel is 0.2 TPa) [234][235];
- *Thermal properties*: graphene is a perfect thermal conductor. Its thermal conductivity is 5000 $W \cdot m^{-1} \cdot K^{-1}$, and is higher than all the values of other carbon structures as nanotubes, graphites and diamonds [236]. This property has implications in electronics, but it is also interesting in the construction field, e.g. for the realization of materials with high thermal exchange, such as heating floors;

In this research, *Pentagraf® graphene nanoplatelets* (PENTACHEM S.r.l.) were used (Fig. 5.9). The following are the technical data of the filler (Tab. 5.1), SEM microstructural analyzes and the EDX analysis (Fig. 5.10) in which the pure carbon content is visible.

Table 5.1. *Graphene nanoplatelets: technical data*

Color	Black, Grey
Carbon content [wt.%]	> 99
Density [g/cm^3]	2.0 ± 0.1
Bulk density [g/cm^3]	0.3 ± 0.05
Particles thickness [nm]	6 - 8
Particles size [µm]	< 5
Specific surface area [m^2/g]	120 - 150
Young's modulus [GPa]	1000
Thermal conductivity [W/(m·K)]	3000
Electrical conductivity [S/m]	10^7

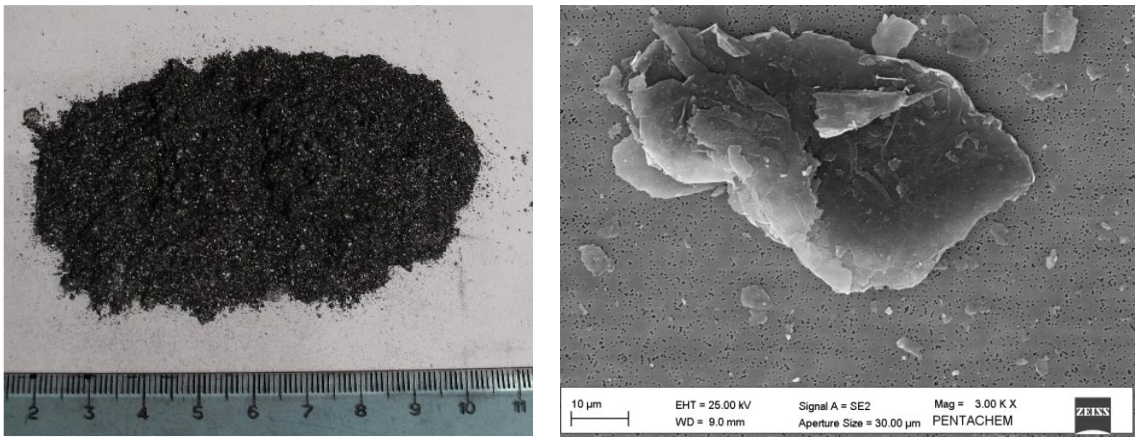

(a) (b)

Figure 5.9. *Graphene nanoplatelets: a) GNP powder; b) SEM analysis*

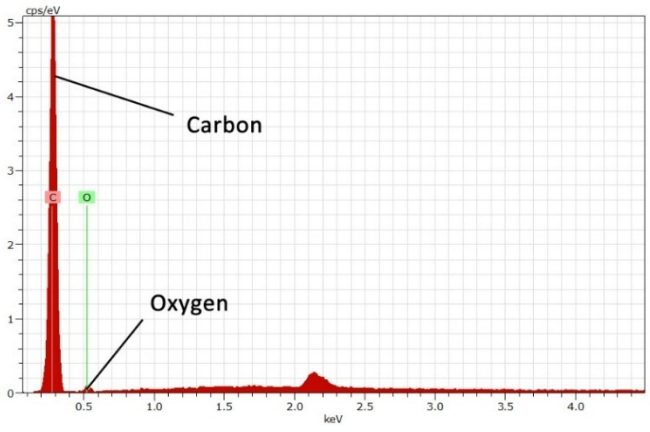

Figure 5.10. *Graphene nanoplatelets: EDX analysis*

Table 5.2. *Graphene nanoplatelets elemental analysis (wt.%)*

C	99.5
O	0.5
Ca	-
K	-
Mg	-
Si	-
Al	-
Na	-
Fe	-

5.4.1.2 Activated carbon

Activated carbon consists mainly of amorphous carbon, and it is characterized by a highly porous structure and a high specific surface area (Fig. 5.11). Thanks to these properties, it is a material with a very high adsorption capacity. It also has a high filtering and purifying capacity thanks to its nano-porosity. The purifying properties of activated carbon were known since antiquity. In India, for example, *wood charcoal* was used to make water drinkable, while in Egypt it was used as a medical adsorbent and purifying agent. It was also used in the 1800s in England to remove odors from the treated water [237].

(a) (b)

Figure 5.11. *Activated carbon: a) Solid and powdered forms. b) AC high porous structure*

It is produced from raw materials with a high carbon content, such as wood, coal, peat, etc. There are two methods for activated carbon production [238]:

- *Chemical activation*: it is generally used for sawdust and peat. It is based on the dehydrating action of some chemical compounds such as folic acid and zinc chloride. The raw material is saturated with a chemical agent, and pyrolyzed at 400-1000°C. In this way a more rich carbon material is obtained with a very high porosity;
- *Gas activation*: a gaseous mixture containing oxide or carbon dioxide is used. At a temperature of 800-1000°C and through a jet of steam, air or carbon dioxide, some of the starting raw materials decompose, producing numerous holes and cracks.

The yield depends on the activation degree: a high activation degree (associated with a low yield) is between 20% and 60%. The activated carbon can be produced using different types of kiln. The most used are rotary kiln, more suitable for the production of AC with several size particle (from dust to granular material).
Activated carbon is generally used in two types of particle sizes [239]: 1) Granular form (*Granular Actived Carbon*, GAC) with grains of about 0.8 mm, when a material with small pores and a high specific surface area is required; 2) Powder form (*Powdered Actived Carbon*, PAC), with micrometric particles, when a material with larger pores, and a smaller specific surface area is required.
As previously mentioned, the adsorption power is the most interesting property of this material (Fig 5.12), linked to its very high specific surface area, between 500 and 2500 m^2/g. The specific surface of 1 gram of activated carbon is comparable to the area of a football field [240]. The adsorption power of AC is evaluated by specific parameters such as the benzene index, the molasses index (ability to absorb large molecules), iodine index (ability to absorb inorganic compounds at high molecular weight, i.e. small molecules), methylene blue index (indicative of the AC unit with particular reference to its microporosity).

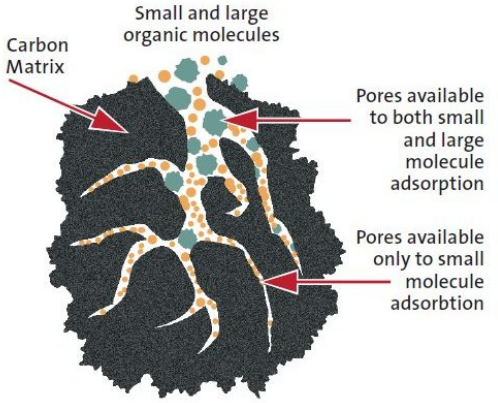

Figure 5.12. Schematic adsorption effect of an AC particle

In the present dissertation, *Norit® Cap super-WJ powdered activated carbon* (CABOT Inc.) is used (Fig. 5.13), whose technical specifications are described below (Table 5.3). SEM and EDX analysis are reported below (Fig 5.14, Tab. 5.4).

Table 5.3. *Powdered Activated Carbon: technical data*

Color	Black
Carbon content [wt.%]	> 95
Density [g/cm^3]	0.5 ± 0.05
Bulk density [g/cm^3]	0.2 ± 0.05
Particles size [µm]	< 40
Specific surface area [m^2/g]	1800
Molasses number	100
Iodine number [mg/g]	900
Methylene blue adsorption [g/100g]	38

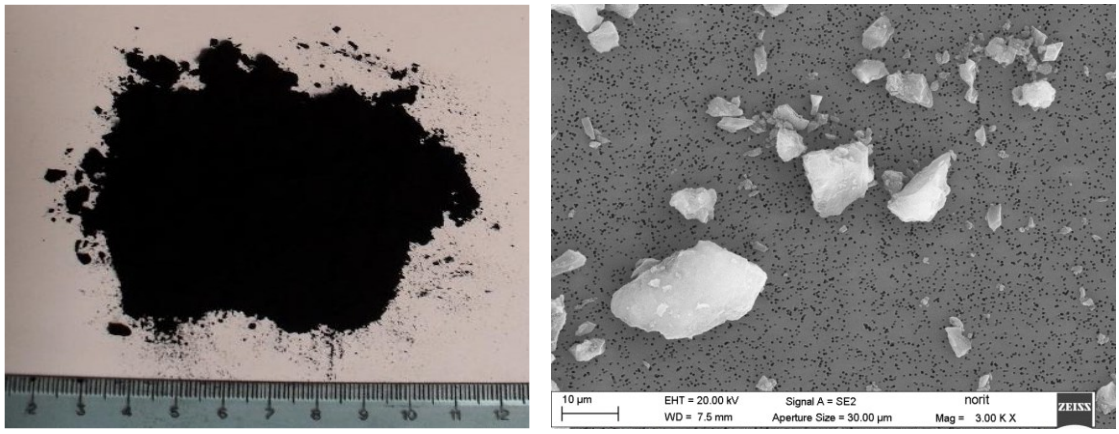

(a) (b)

Figure 5.13. *Activated carbon: a) AC powder; b) SEM analysis*

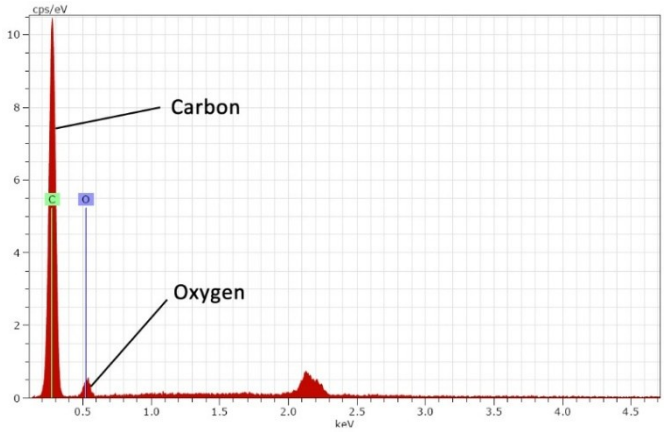

Figure 5.14. *Powdered activated carbon: EDX analysis*

Table 5.4. *Powdered activated carbon: elemental analysis (wt.%)*

C	95.2
O	4.8
Ca	-
K	-
Mg	-
Si	-
Al	-
Na	-
Fe	-

5.4.2 Recycled fillers

5.4.2.1 Gasification Char

Gasification is a chemical process that converts carbon-rich material, such as coal, oil, or biomass, into carbon monoxide, hydrogen, and other gaseous compounds. The thermal

degradation process occurs at high temperatures (above 700-800°C), through an oxidizing agent, typically air (oxygen) or steam [241]. The resulting gaseous mixture is a synthesis gas (syngas) and it is a fuel. Gasification is a method for obtaining energy from different types of organic materials, i.e. to convert a solid fuel into a gaseous fuel, and it is also used in the thermal treatment of waste.
To date, there are few plants that produce synthetic fuels from gasification and these mainly use coal as raw material. The gasification of fossil fuels is widely used in industry to produce electricity [242]. However, some gasification plants use raw materials not born as fuels, such as *organic waste* and *biomass* (Fig 5.15).

Figure 5.15. *Woodchips processed in gasification plants*

The thermal degradation of these organic materials through gasification produces a waste ash (Fig. 5.16), the so-called "*gasification char*".
Char is the porous carbonaceous solid residual, collected directly in the ashtray of the gasification plant. It is an amorphous, disordered, isotropic material, with a heterogeneous structure containing mainly elemental carbon (from 50% to 90% by weight), but also oxygen, hydrogen, nitrogen and minerals such as potassium, calcium, sodium, silicon and magnesium [243]. This ash is considered a waste, and its disposal is a problem for the managers of the gasification plants, because it requires money and resources. Methods for recycling char as fuel in combustion chambers, domestic charcoal, and fertilizer have been investigated [244]. This dissertation will study its potential recycling in the construction materials sector.

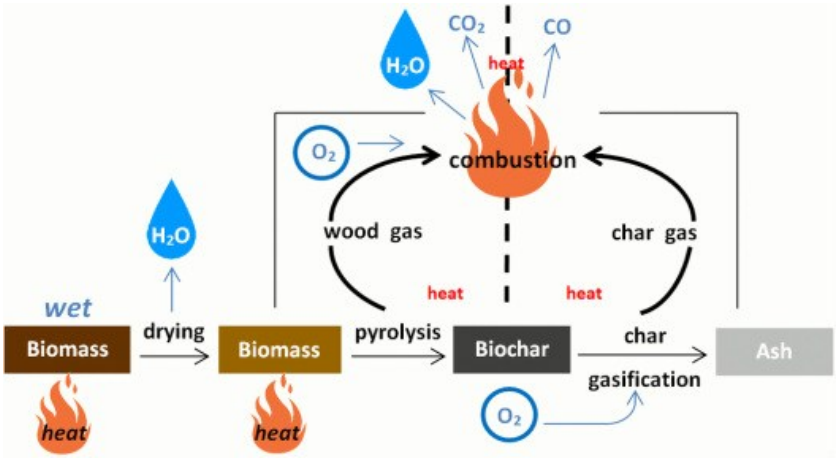

Figure 5.16. *Scheme of char production by biomass gasification*

Char produced from biomass is generally much more porous than the char obtained from mineral coal, and is therefore much more reactive.
In the present research, char obtained from the gasification process of fine woodchips is used (Tab. 5.5). The material has been manually grounded in order to obtain a powder with particle size ≤ 75 µm, and comparable with the other fillers used.
The following are the technical data [245], and the SEM-EDX analyzes (Figg. 5.17-5.18) performed on the material (Tab. 5.6).

Table 5.5. *Gasification Char: technical data*

Color	Black
Carbon content [wt.%]	> 75
Density [g/cm^3]	2.1 ± 0.1
Bulk density [g/cm^3]	0.3 ± 0.05
Particles size [µm]	< 75
Specific surface area [m^2/g]	400 – 600

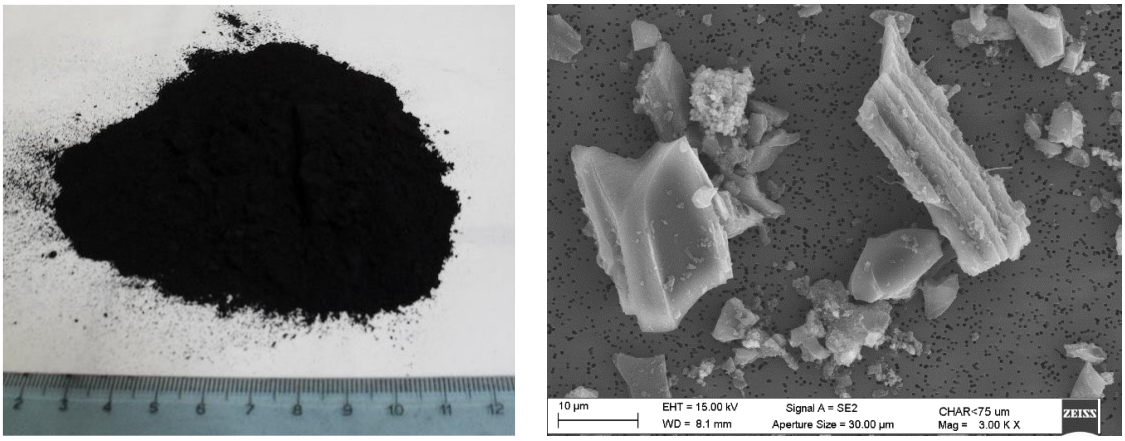

(a) (b)

Figure 5.17. *Gasification char < 75 µm: a) GCH powder; b) SEM analysis*

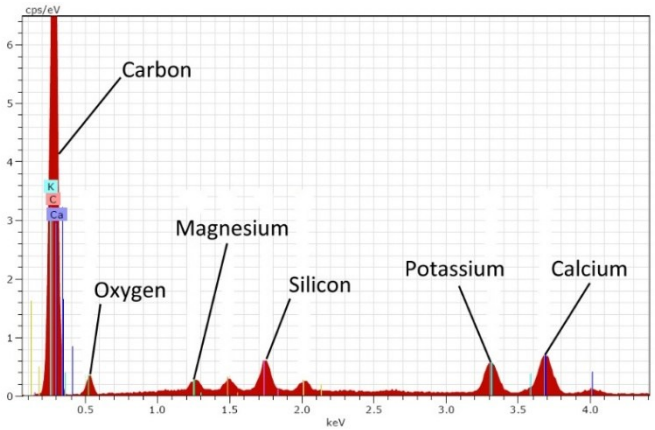

Figure 5.18. *Gasification char: EDX analysis*

Table 5.6. *Gasification char: elemental analysis (wt.%)*

C	76.7
O	14.9
Ca	5.4
K	2.0
Mg	0.6
Si	0.4
Al	-
Na	-
Fe	-

5.4.2.2 Used Foundry Sand

Foundry sand is generally a high quality silica sand with uniform physical characteristics [246]. Exhausted foundry sand is a waste product in the smelting industry of ferrous and non-ferrous materials, where it has been appreciated for centuries for its thermal conductivity properties (Fig. 5.19). The characteristics of this waste depend on the type of casting adopted and the origin industrial sector.

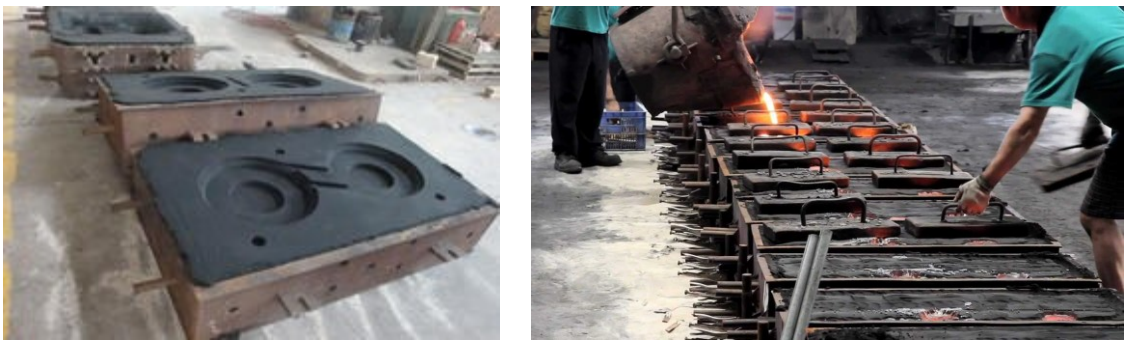

(a) (b)

Figure 5.19. *a) Foundry sand molds (green sand). b) Steel casting in molds*

Foundries recycle and successfully reuse the same sand several times. However, after many uses, the sand loses its characteristics of cleanliness and uniformity, and its use is not further repeatable. Consequently, the exhausted sand is the bigger waste product of the foundry and takes the name of *Used Foundry Sand* (UFS) [96]. The automotive industry and its suppliers are the main producers of foundry sand (about 95% of the total existing USF). These industries employ about 1 ton of foundry sand for each ton of steel produced, and this leads to a worrying environmental impact. Each year, the melting processes generate approximately 9.4 million of tons of foundry sand [247].
There are several drawbacks linked to this trend: landfill saturation, soil pollution (in case of unmanaged waste), economic impact (in particular due to logistics), transport costs and environmental impact linked to CO_2 emissions [248].
UFS has been classified as *non-hazardous material* by the EU, paving the way for many possible re-uses in various industrial sectors (including the construction materials production field [249]).

The physical and chemical characteristics and the behavior of foundry sand depend strictly on the type of casting process, on the industry of origin, and in particular on the type of binder systems used for mold forming. Typically, there are two types of binders with different physical and environmental characteristics: clay and chemical binders. The most used systems are the clay-based, from which the so-called "green sand" is obtained. The used foundry sand employed in this experimentation is a dark granular powder, analyzed by ECAM RICENT Company (Fig. 5.22a). The original sand has large particles and conglomerates. Thus (as for gasification char) the sand was refined by manual grinding, and sieved, in order to obtain a powder with particle size ≤ 75 μm. Following, the technical data (Tab. 5.7) and the SEM-EDX performed on the material are reported (Figg. 5.20b - 5.21, Tab. 5.8).

Table 5.7. *Used foundry sand: technical data*

Color	Black
Carbon content [wt.%]	> 30
Density [g/cm^3]	1.9 ± 0.1
Bulk density [g/cm^3]	0.8 ± 0.1
Particles size [μm]	< 75

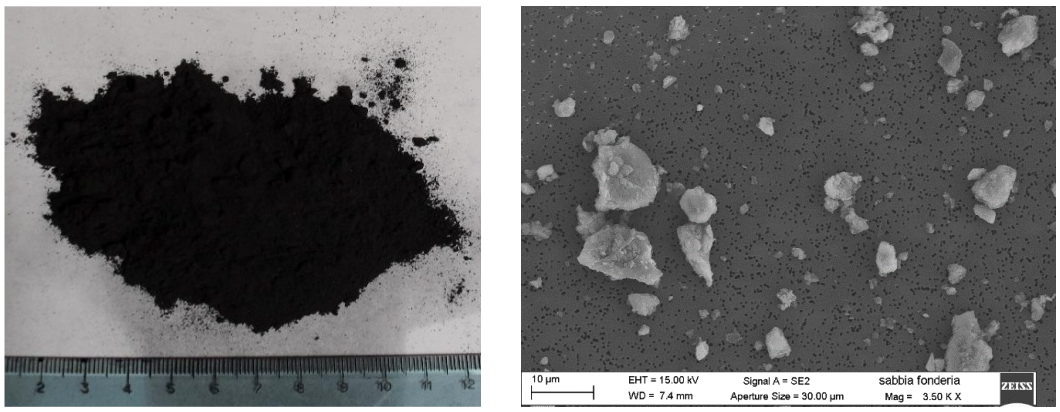

(a) (b)

Figure 5.20. *Used foundry sand < 75 μm: a) UFS powder; b) SEM analysis*

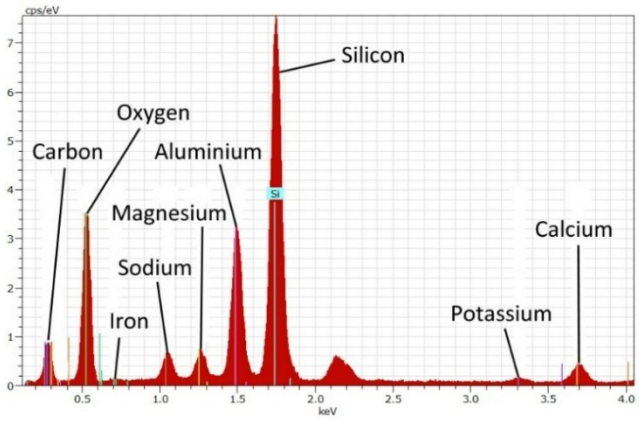

Figure 5.21. *Used foundry sand: EDX analysis*

Table 5.8. *Used foundry sand: elemental analysis (wt.%)*

C	32.9
O	37.9
Ca	1.9
K	0.7
Mg	1.2
Si	14.8
Al	6.4
Na	2.0
Fe	2.3

5.4.3 Dimensional and morphological analysis of filler particles

As seen in section 4.2.2, the shape of filler particles has considerable influence on the final properties of the cement-based composite. In fibrous additions, the aspect ratio is a very important parameter for the development of the mechanical and electrical properties of the cementitious material. In powders with quasi-spherical grain, there are other factors to consider, but an accurate dimensional analysis of the grains is still important to understand the effect of the filler on the cement matrix.
For this reason, *dimensional* and *morphological* analyzes of fillers were carried out through SEM investigation (Fig. 5.22).

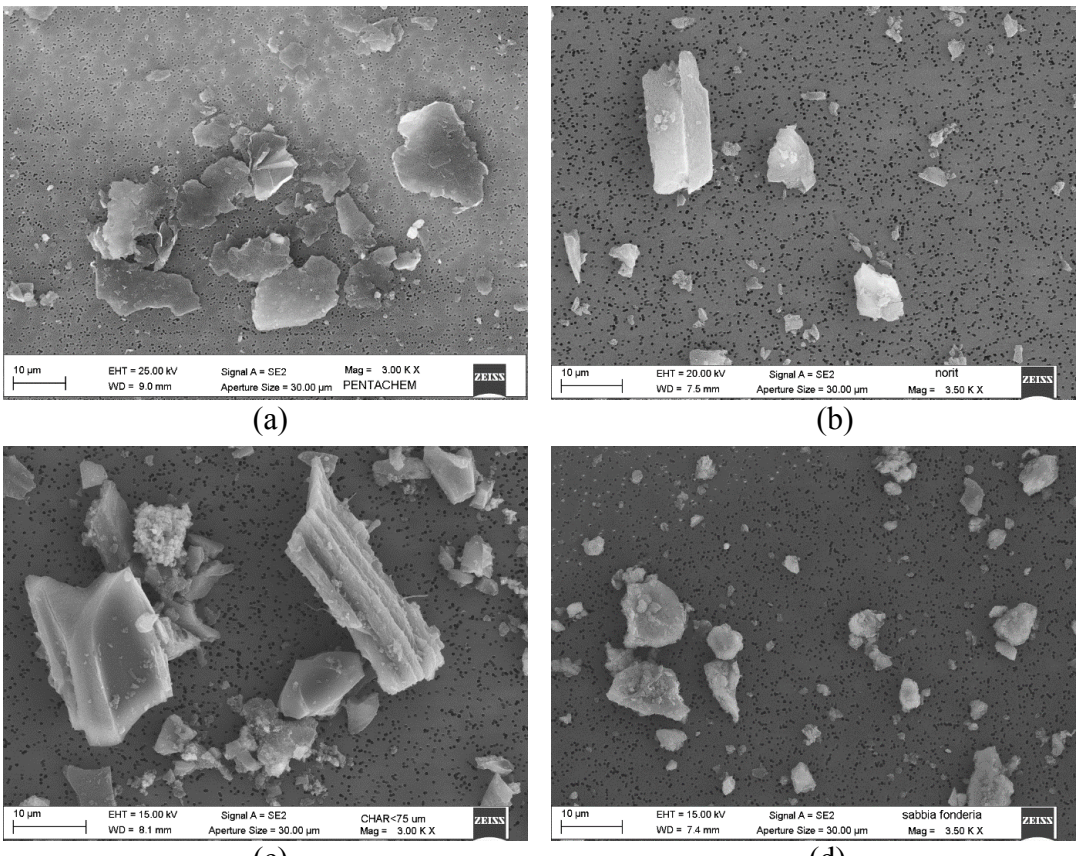

Figure 5.22. *SEM analysis: a) Graphene nanoplatelets; b) Powdered activated carbon; c) Gasification char > 75 µm; d) Used foundry sand > 75 µm*

SEM and *ImageJ* processing software have been used to evaluate the morphology of the elongated particles (PAC and GCH) and to measure both the particle size and size distribution. An image analysis method was conducted, since indirect advanced methods (e.g. those involving scattered, diffracted light or laser) assume the particle being spherical, which was not the predominant case of PAC and GCH samples. Indeed, for those particles that show an irregular shape, assuming them regular and geometrical will result in an oversimplification. A spherical particle dimension can be approximated using a single number - the diameter - because each dimension is identical, whereas non-spherical particles should be described using different length and width measures. Therefore, the irregular particles have been described by the diameter of a circle of equal projection area (d_{EC}), *Feret's diameter* (d_F) and *minimal Feret's diameter* (Min d_F) [250][251]. The circle considered to determine d_{EC} is drawn on the projection of the particle as it appears on the SEM image plan. The d_F is the longest distance between any two points along the selection boundary, also known as maximum caliper. The Min d_F is the minimal Feret's diameter calculated after considerations of all possible orientations (0°-180°, Fig. 5.23).

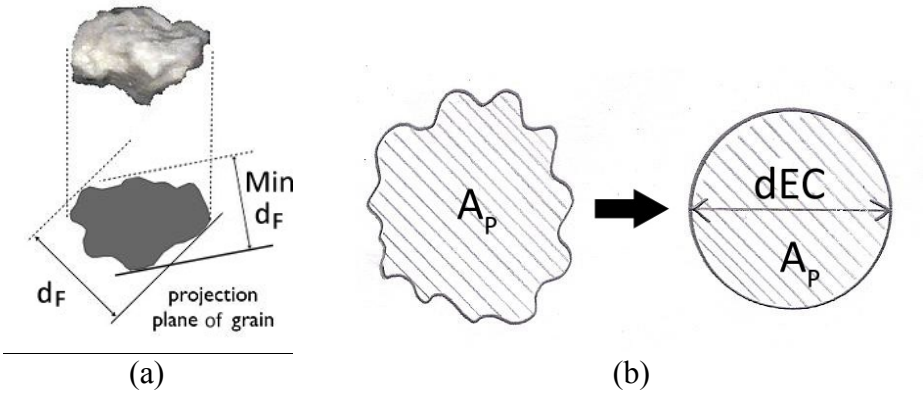

Figure 5.23. *Evaluation of particle diameter: a) Feret's diameter (d_F) and minimal Feret's diameter (Min d_F); b) Equivalent spherical diameter (d_{EC})*

For each sample, 15 images have been acquired assuring a minimum quantitative of particles according to the standard ISO 13322-1:2004. A sample with *Geometric Standard Deviation* (GSD) of 1.15 needs, in fact, 1460 particles to achieve mass median diameter within 5% error with 95% probability. In Table 5.9, the results of GCH and PAC samples are showed.

Table 5.9. *Mean values and standard deviations (STD) of d_{EC}, d_F and Min d_F for GCH and PAC*

Filler	d_{EC} (μm)	d_F (μm)	Min d_F (μm)
GCH	1.6 ÷ 2.5	2.5 ÷ 3.5	1.5 ÷ 2.3
PAC	2.8 ÷ 3.2	4.7 ÷ 4.5	2.9 ÷ 3.0

Contrarily, for GNP and UFS, the particle size distribution was determined by laser diffraction analysis, since both types of filler showed a predominant spherical

morphology (Fig. 5.22a and 5.22d). The results are showed in Figure 5.24: foundry sand sieved at 75 µm is finer than GNP that has also a broader grain size distribution.

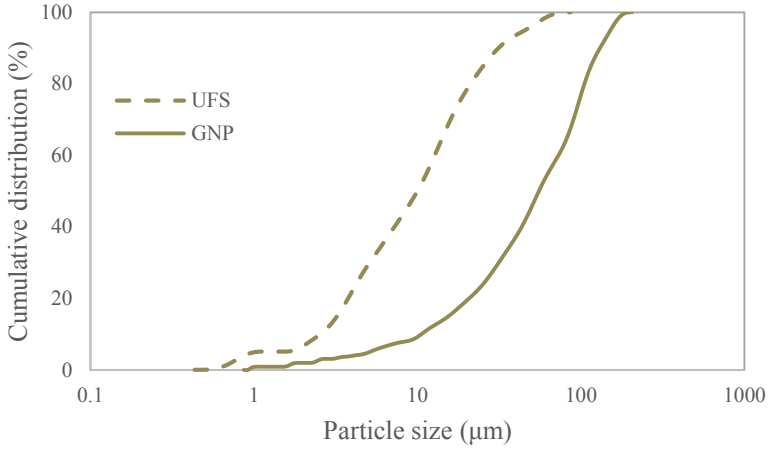

Figure 5.24. *Particle size distribution of graphene nanoplatelets, and used foundry sand*

5.5 Conductive fibers

In recent decades, the extensive use of fibers in the construction materials sector derives from the advantage of using a material with a lower density, but higher strength and modulus than the constituent material of the composite [26]. Fibers are the traditional addition to create multifunctional materials, with greater mechanical strength, together with a greater lightness.
The advantages in the construction of fiber-reinforced building materials were already known in antiquity [252]. An example is the dried bricks made of clay and straw used by the Mesopotamian civilizations, but also other types of filaments with organic origin were used (e.g. horsehair).
At a mechanical and durability level, the fibers do not directly improve the flexural strengths and do not appreciably decrease the hygrometric shrinkage. Instead, the effect of the fibers is shown in increasing the ductility of the concrete after the cracking phenomenon, i.e. increasing the toughness of the material. Moreover, the fibers reduce the propagation of cracks due to hygrometric shrinkage thanks to their "*sewing*" action, thus also decreasing the capillary water absorption of the material [26].
As seen previously (Section 4.3.1) this behavior also affects the electrical and sensitivity properties of the fiber-reinforced PCSS. The bridging action of the fibers influences the *pull-out effect* between the fiber and the cement matrix, a fundamental parameter for the piezoresistivity of the composite [207]. When the pull-out effect of the conductive fibers is in the elastic phase, the piezoresistive effect is created (Fig. 5.25). The fibers are usually distinguished according to their material, the coating type and their aspect ratio. This last feature affects the mechanical properties of the composite, since the greater the aspect ratio, the greater the adhesion forces between fiber and cement paste [26]. Likewise, the aspect ratio also affects the electrical properties of the mixture (see section 4.2.2), in particular through the tunneling effect and the pull-out effect.

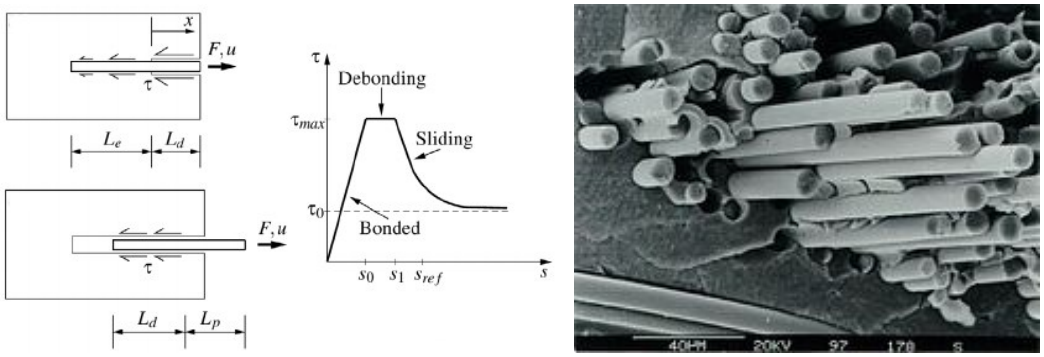

(a) (b)

Figure 5.25. *a) Diagram of the pull-out effect of fibers by tension forces. b) SEM of debonded fibers in a composite*

In this research, three different types of conductive fibers were selected, based on their electrical properties and dimensional characteristics:

- *Virgin Carbon Fibers* (VCF);
- *Recycled Carbon Fibers* (RCF);
- *Brassed Steel Fibers* (BSF).

5.5.1 Carbon fibers

Carbon fibers are the most used materials for producing high performance composites, thanks to their numerous properties. They are usually weaved to product carbon fabrics. The fabrics are immersed in a matrix (generally epoxy) and formed, so as to create a very light material with high mechanical strength and thermal resistance.
Carbon fibers can also be used for other applications, e.g. as loose filaments to improve the properties of composites with different matrices, for example cement-based materials [253].
The first carbon-based filaments were synthesized in 1860 [254], but only after 1960 their technology was advanced and were introduced into the market, thanks mainly to the needs of the aviation industry.
The atomic structure of carbon fiber is similar to that of graphite, consisting of aggregates of carbon atoms with a flat structure (grapheme sheets) arranged according to regular hexagonal symmetry (Fig. 5.26) [255]. The difference between fibers and graphite are the types of interconnected graphene sheets and their chemical bonds.

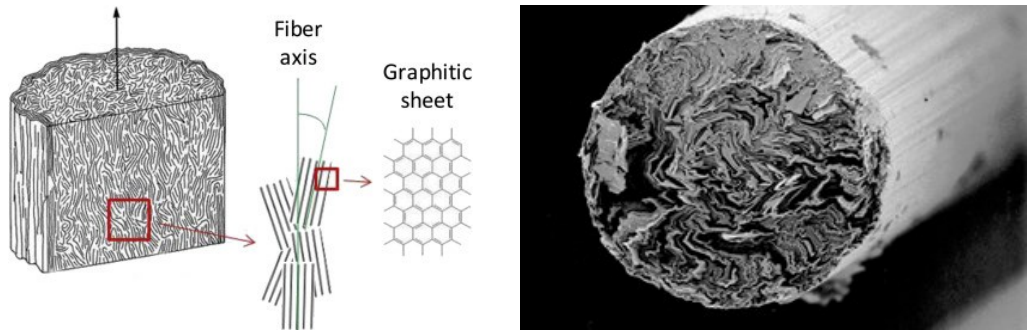

(a) (b)

Figure 5.26. *Cross-section of carbon fiber filament. a) Schematic structure; b) SEM scan*

Each single carbon filament has a cylindrical shape with a diameter of 5-8 μm, and is composed almost entirely of carbon (≥ 92%) [114]. The mechanical tensile strength of the fibers varies between 2-7 GPa depending on the type of filament, and they resist temperatures up to 1000 K.
There are different techniques for the synthesis of carbon fibers, but most are produced by stabilization, carbonization, and high temperature treatment of *polyacrylonitrile* (PAN) (Fig. 5.27) [256]. This type of fibers has a "turbostatic" structure, that is a crystalline structure formed by deviated planes, and the sheets of carbon atoms are randomly joined or folded (Fig. 5.26).

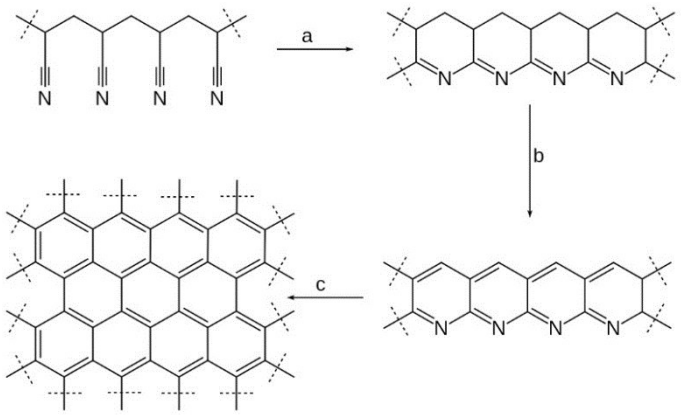

Figure 5.27. *Synthesis of CF from polyacrylonitrile (PAN): a) cyclization; b) dehydrogenation; c) elimination of nitrogen*

The fibers are commercially classified, according to their mechanical properties, in:

- *General performance* (GP), fibers with lower mechanical strength, and Young's modulus ≤ 200 GPa;
- *High performance* (HP), fibers with higher mechanical strength, and Young's modulus ≥ 200 GPa.

The loose carbon fibers are also classified according to the length in:

- *Very short* (or ground), between 0.03 and 3 mm;
- *Short cut*, approximately 6 mm;
- *Long cut*, between 10 and 50 mm.

The commercial carbon fibers used in this research are 6 mm fibers (STW), obtained from PAN precursors, graphitized at 2000°C, with epoxy-based coating (Figure 5.28). Additional technical data are shown in Table 5.10.

Table 5.10. *Virgin carbon fibers: technical data*

Color	Black
Carbon content [wt.%]	> 92
Surface coating	Epoxy
Density [g/cm^3]	1.78
Thickness (diameter) [μm]	7.0
Filament length [mm]	6.0
Specific surface area [m^2/g]	0.229
Young's modulus [GPa]	230 - 250
Tensile strength [MPa]	4000
Average resistivity [Ω·cm]	0.0015

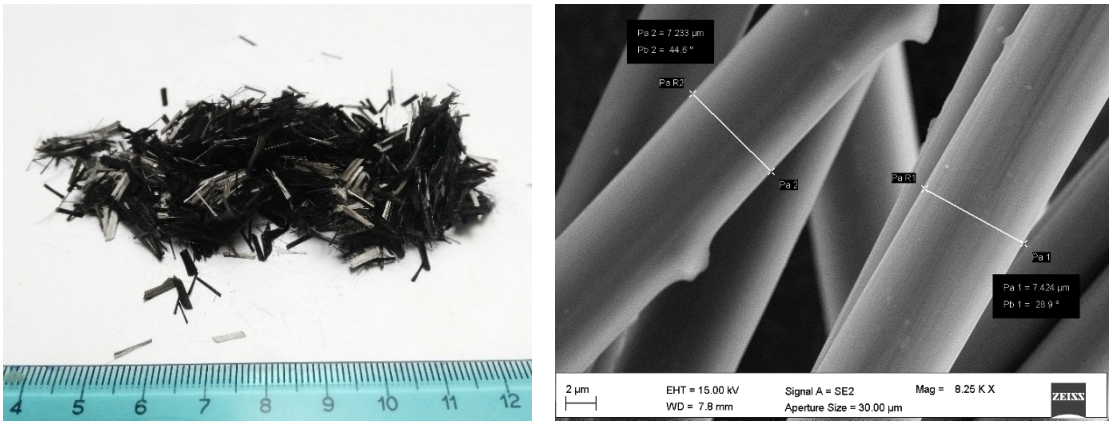

(a) (b)

Figure 5.28. *a) 6 mm Virgin carbon fibers; b) VCF SEM analysis*

5.5.2 Recycled carbon fibers

The production sector of carbon fiber components is constantly growing, thanks to the continuous progress of the automotive sector, and mechanical and materials engineering. The increase in production leads to an increase in waste produced by manufacturing processes. In particular, the realization of CF profiles produces many waste from the cutting processes of panels and fabrics, and from milling operations (up to 10-20% by weight of the raw material, Fig. 5.29) [257]. These wastes can be reused within the same industry, but when this is not possible they can be recycled into other fields, for example in the building sector [258].

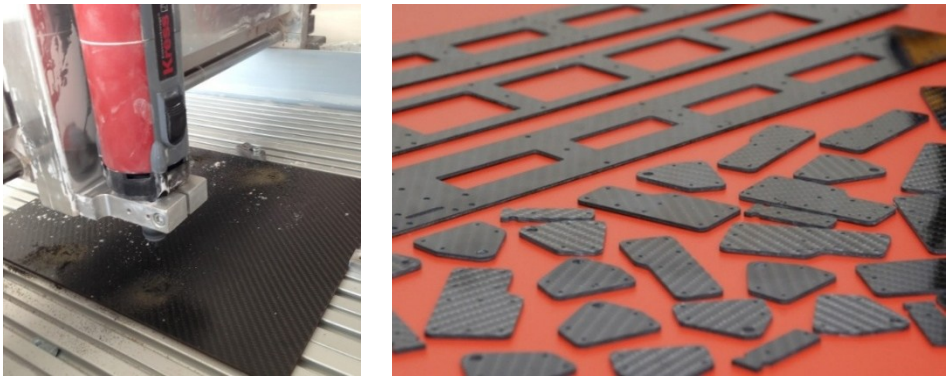

(a) (b)

Figure 5.29. *a) Milling of a CF panel. b) Small CF profiles from panel cutting*

The industrial by-products used in the building sector can be of two types: 1) filaments of loose carbon fibers, obtained from the cutting processes of fabrics or coils; 2) fragments of composite panels (Fig. 5.30), consisting of carbon fiber (at least 70%) and a forming polymer (epoxy) [46].

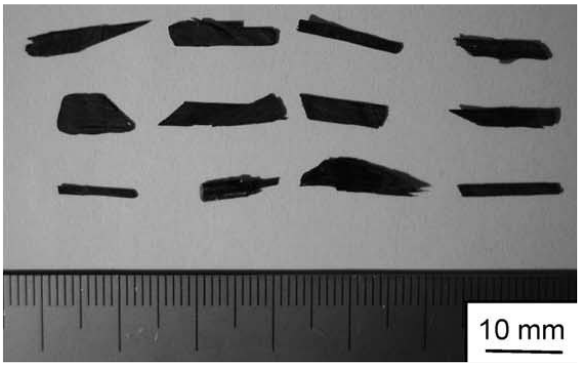

Figure 5.30. *Crushed carbon fiber reinforced polymer used for reinforcement*

The recycled carbon fibers used in this research are 6 mm (APPLYCARBON) filaments of *ex-PAN* graphitic structure and glycerol-based coating, recycled from the cutting of pure carbon fiber coils (Fig. 5.31). The technical characteristics of the recycled fibers are shown in Table 5.11.

Table 5.11. *Recycled carbon fibers: technical data*

Color	Black
Carbon content [wt.%]	94 (> 92)
Surface coating	Glycerol
Density [g/cm^3]	1.7 – 2.0
Thickness (diameter) [μm]	7.0 ± 2.0
Filament length [mm]	6.0 ± 0.5
Young's modulus [GPa]	230
Tensile strength [MPa]	3500
Average resistivity [Ω·cm]	0.0015

Figure 5.31. *6 mm Recycled carbon fibers*

SEM analyzes of recycled fibers show that their shape and structure are the same of VCF. However, the recycled fibers also contain a fraction of *fine particles* (made entirely of carbon), originated from mechanical cutting processes, which make their surface more irregular (Fig. 5.32).

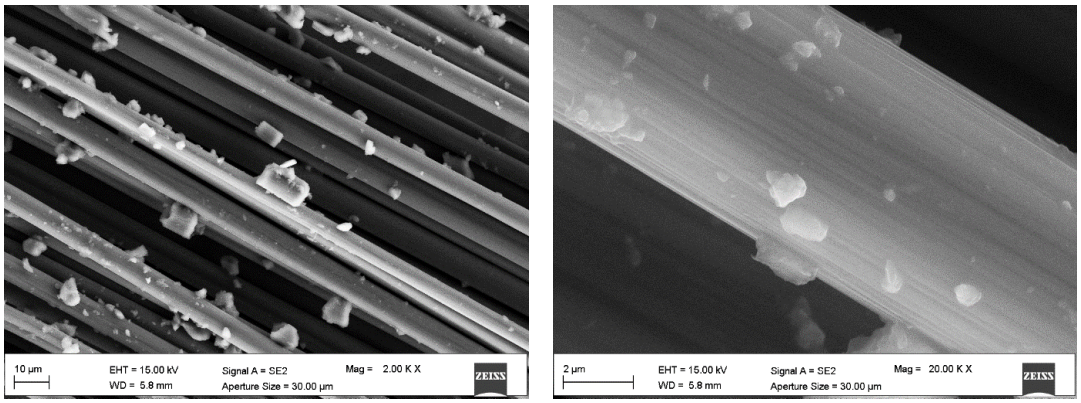

(a) (b)

Figure 5.32. *SEM images of recycled carbon fibers*

5.5.3 Steel fibers

The fibers used in the building sector are subdivided, according to their performance, into *non-structural* and *structural* fibers. The most common structural fibers for concrete production are *steel fibers*. These are used to ensure the improvement of tensile strength in the post-crack phase of concrete [26]. This function aims to a partial (or complete) replacement of reinforcements (bars or mesh), thus reducing casting speed.
Steel Fiber Reinforced Concrete (SFRC) are also used for industrial flooring in substitution of electro-welded mesh, in prefabricated elements and in *shotcrete* (spray concrete) [259].
The use of steel fibers in concrete is regulated by various European standards, such as UNI EN 14889-1:2006, and UNI EN 14651:2005. The latter classifies the fiber-reinforced composites according to its residual post-cracking tensile strength by CMOD measuring (*Crack Mouth Opening Displacement*), test described in the following sections. The steel fibers modify the fragile behavior of the concrete transforming it into a ductile material (Fig. 5.33), with post-crack resistance, impact and fatigue strength. The fiber must oppose to the increase in crack opening, and must deform slowly during the

pull-out process. For this reason, not only the resistance to slippage is important, but also the distribution and homogeneity of the fibers, together with their tensile strength.

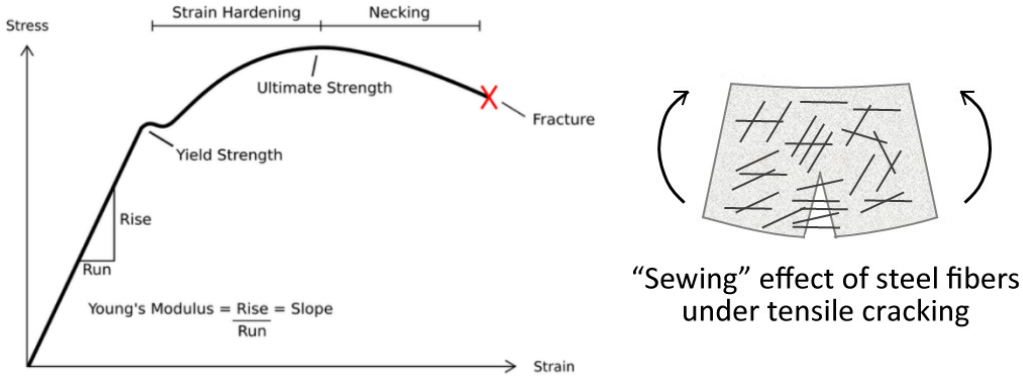

Figure 5.33. *Ductile behavior of a SFRC (stress-strain curve)*

Steel fibers differ according to the type of metal in: fibers with low carbon content (C ≤ 0.2%), fibers with a high carbon content (C > 0.2%), or *stainless steel fibers* (low carbon content and chromium content ≥ 12%) [260]. The type of steel also influences the corrosion behavior of the fibers. To avoid corrosion, steel fibers are often coated with an anticorrosive layer based on zinc or brass. The coating also improves the chemical interaction between fiber and cement matrix, increasing adhesion and resistance to slippage. Metal fibers can be obtained from two different production processes:

- *cold drawing* of a steel wire: a section of semi-finished steel passes through a truncated-conical hole called a "die-cutter". Matrices with progressively lower diameter are used, until reaching a product with the desired dimensions. With the "cold" drawing, a notable hardening of the material is obtained, together with an increase of the mechanical resistances;
- from *cutting* of metal sheets.

In the cutting phase, they can be *laminated*, i.e. compressed between two rotating cylinders; the shape variation is obtained with a series of passages through various pairs of cylinders. The fibers reach a final length between 6 mm and 70 mm, and a final equivalent diameter between 0.15 mm and 1.20 mm.
The metal fibers used in this experimentation are the straight *Brassed Steel Fibers* (BSF) *Dramix*® (BEKAERT), with 6 mm of length (Fig. 5.34), produced by cold drawing of high quality and high ductility steel. The technical data are shown in Table 5.12.

Table 5.12. *Brassed steel fibers: technical data*

Color	Yellow, Gold
Surface coating	Brass
Density [g/cm^3]	7.87
Thickness (diameter) [μm]	160
Filament length [mm]	6.0
Tensile strength [MPa]	2600
Average resistivity [Ω·cm]	$1.4 \cdot 10^{-6}$

Figure 5.34. *6 mm Brassed steel fibers*

The SEM analysis shows the high morphological regularity of the steel fibers (Fig. 5.35a). However, by analyzing their surface, some scratches and cracks are noticed (Fig. 5.35b), probably caused by the production and transport processes. Furthermore, the EDX analysis was performed, and confirms the chemical surface composition of the fibers (Fig. 5.36).

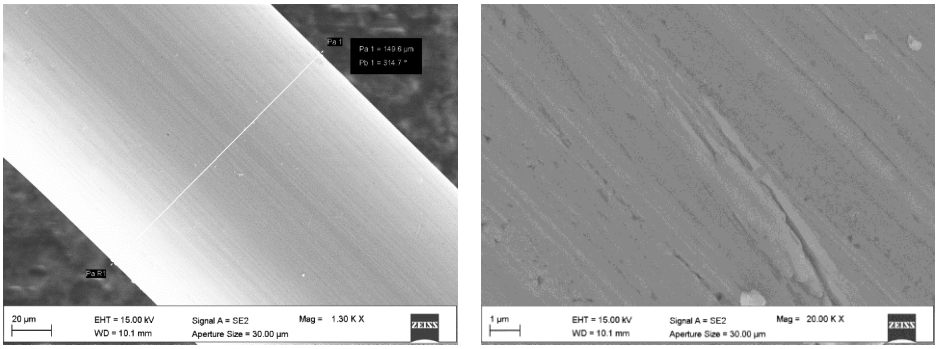

(a) (b)

Figure 5.35. *a) SEM image of brassed steel fibers. b) In-depth surface analysis*

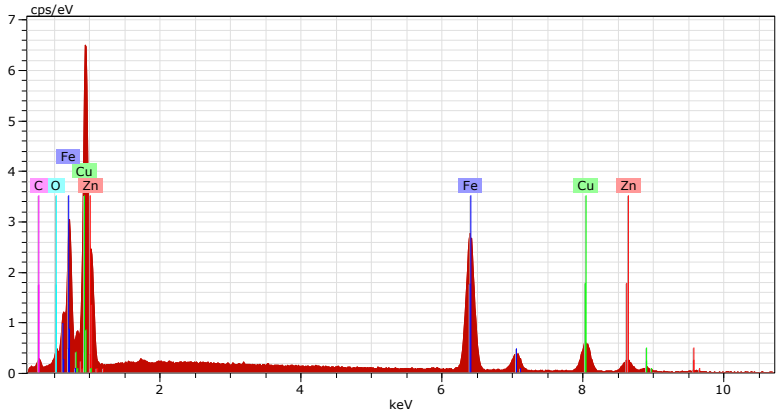

Figure 5.36. *Brassed steel fibers: EDX analysis*

Table 5.13. *Brassed steel fibers elemental analysis (wt.%)*

Fe	52.5
Cu	27.8
Zn	15.4
C	3.0
O	1.3

5.6 Additives (Superplasticizers)

Additives are chemical products added to mortars or concretes in order to improve their performance. A type of additives are *superplasticizers* (SP), polymers with very effective dispersing and surfactants capability [26]. These are very common in the field of cement-based materials, but they are also used in chemistry, in the production of high dispersion particle suspensions. Within the cementitious materials, they allow to improve the workability of the mixture without increasing the w/c ratio, thus without compromising the mechanical properties of the hardened composite [261]. They are also used for the realization of *self-compacting* concretes and *self-leveling* cement floors. Superplasticizers are added in small amounts, as a percentage of binder weight.
In the research field of multifunctional cementitious materials, SPs are widely used for two reasons: 1) their contribution to the dispersion of the filler within the composite (combined with ultrasonic dispersion techniques) [262]; 2) the improvement of the low workability of mixtures with high content of conductive fibers [263].
All superplasticizers are based on water-soluble polymers. The first synthesized SP were based on *poly-naphthalen-sulfonates* or *poly-melamine-sulfonates* (invented by Hattori and Anigesberger in the 1970s) [261]. The dispersing action of these compounds derives from their organic polymers nature, bearing a high quantity of negative electrical charges: these are wrapped around the cement particles, creating repulsion forces.
Dispersants of more recent conception are *polycarboxylated ethers* (PCE), characterized by the absence of sulphonic groups, whose action is not based on electrostatic repulsion, but on spherical repulsion [264].
PCE's backbone, which is negatively charged, permits the adsorption on the positively charged colloidal particles. Because of PCE adsorption, the zeta potential of the suspended particles changes, due to the adsorption of the COO^- groups on the colloid surface. This displacement of the polymer on the particle surface ensures to the side chains the possibility to exert repulsion forces, which disperse the particles of the suspension and avoid friction (Fig. 5.37) [265].

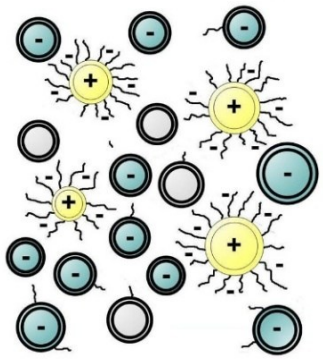

Figure 5.37. *Polycarboxylate displacement on a multi-phase suspension*

Two types of superplasticizers additives have been used in this dissertation:

- Naphthalene sulphonate-based superplasticizer *N200* (MAPEI);
- PCE superplasticizer *Melflux 4930 F* (BASF).

6 . Chapter
Preliminary Tests in lime Pastes

Evaluation of carbon-based fillers behavior in NHL pastes

6.1 Introduction

The first phase of the research was focused on the properties induced by carbon-based fillers on preliminary experimental composites as *hydraulic lime-based pastes*.
Initially, the research focused on the effects of carbonaceous fillers on the mechanical and durability properties of cement-based materials. As previously mentioned (Section 1.3.1) the production and use of Portland cement involves serious problems related to ecological sustainability [22], and research on building materials is increasingly focused on innovative composites realized using recycled industrial by-products [23].
One way to reduce the environmental impact of Portland cement is to improve the durability of mortars and concretes. The durability of mortars/concretes is strongly influenced by their aptitude to transport aggressive agents through the connected porosities [266]. Aggressive ions, dissolved in water, such as sulphates and chlorides in polluted areas and coastal zones [267][268], promote concrete deterioration and corrosion of embedded reinforcements [269].
Mortar/concrete protection through hydrophobic treatments, which make concrete less susceptible to water saturation [270][271][272], enhances their durability. Furthermore, the addition of fillers in the mix design, thanks to the refinement of the paste microstructure, leads to an increase in both the mechanical and durability performances [10][273] [274].
Carbon-based fillers, thanks to their high strength, combined with their lightness and high specific surface, have promising potentials in this field. In addition, these materials possess a large number of other features, which have been carefully studied in this research.
The high electrical properties of carbon-based nanomaterials can be exploited in various applications, such as SHM, but also for the development of conductive finishes for Electromagnetic Interference (EMI) shielding [84]. Nowadays, electronic devices and communication systems are contaminating our surrounding with electromagnetic (EM) radiations. These signals, particularly at high frequencies such as the radio ones, may interfere with electronic devices, such as computers [5][68][71][125][275]. Some medical studies also investigated if an excessive exposure to such radiations can enhance the probability of cancer development in humans [276][277]. For this reason, different shielding systems are being studied, potentially usable on a large scale to devices protection and to increase the living comfort inside buildings.
Some carbon-based materials also have a high de-polluting capability, linked to their high specific surface area and their absorbing power. This characteristic can be exploited to realize finishes for increasing indoor air quality, through absorption and reduction of volatile organic compounds (VOCs) [29].
In this preliminary experimentation phase, lime pastes were added with commercial carbon-based fillers with proven electrical and de-polluting properties, such as graphene and activated carbon. Those materials are generally very expensive and difficult to disperse in polar liquids as water, due to their high specific surface where Van der Waals forces create bundles and agglomerates [278].
Therefore, the effects of these two fillers were compared with those of carbon-based powders obtained from industrial by-products that, even much more cheaply, can exhibit comparable properties to those of commercial ones. Moreover, thanks to a less specific

surface area and/or a different chemical composition, due to the presence of functional groups which contain other elements than carbon (as Mg, Al, Ca, Si, Na, K, Fe, O), the fillers result more compatible with water and then easily dispersible in polar liquids [84]. The recycled fillers used in this work are char obtained from biomass gasification and used foundry sand (Section 5.4.2).
Initially, studies on the dispersion techniques of fillers inside the mixtures have been performed. Later, pastes were produced containing three different filler amounts, as a percentage of the binder weight, evaluating the workability of the fresh mixtures. Tests of mechanical strength (tensile splitting and compression) and durability (capillary water absorption) were carried out on the composites.
The special properties of the fillers were analyzed by means of electronic tests (resistivity measurement and evaluation of the EMI shelding effectiveness), and depolluting tests (pollutant adsorption, photocatalysis).
The results were supported by microstructural analysis, through scanning electron microscopy (SEM) and mercury intrusion porosimetry.
Below is a description of the produced composites and of investigation methods, together with a critical discussion of the results.

6.2 Materials and Mix design

Natural hydraulic lime (NHL 5, according to UNI EN 459-1:2010) was used for the realization of pastes. This type of binder has been selected because of its most environmentally friendly nature, compared to ordinary Portland cement. Moreover, the lower mechanical properties and greater porosity of lime-based materials are more functional for the study of the fillers effects, in terms of differences evidence. This choice is also functional on a scientific viewpoint, since the literature does not report research studies regarding the effect of carbonaceous fillers in the properties of lime based matrixes.
Graphene Nanoplatelets (GNPs) and *Activated Carbon Powder* (PAC) were selected as commercial carbon-based fillers, and *Gasification Char* (GCH) and *Used Foundry Sand* (UFS) as recycled fillers. For a better description of the materials and their technical specifications, see chapter 5.
To better disperse each carbonaceous addition, fillers were put into a blend composed by the entire amount of mixing water and superplasticizer (SP); the compound was at first manually stirred and then it was submitted to sonication with an ultrasonicator for 10 minutes. Two types of liquid superplasticizer were compared: a naphthalene sulphonate superplasticizer (N200) (Mapefluid N200, Mapei S.p.A.) and an acrylic superplasticizer (SP1) (Dynamon SP1, Mapei S.p.A.).
The amount and type of SP for preparing the final mixes were chosen by visual evaluation of GNP dispersion in water after ultrasonication for 10 minutes (Fig. 6.1). Fig. 6.1a shows results obtained by using the acrylic superplasticizer (SP1) and Fig. 6.2b shows results obtained by using the naphthalene sulphonate one (N200). The addition of N200 to the water had ensured a better and homogeneous dispersion of the GNP compared to that reached by using the SP1; when the dosage of N200 is 1 wt.% of the binder, the best dispersion can be obtained (specimen in the middle, Fig. 6.1b). The use of naphthalene

sulphonate superplasticizer as dispersing agent for carbonaceous fillers is suggested also by other authors [99][31][126].

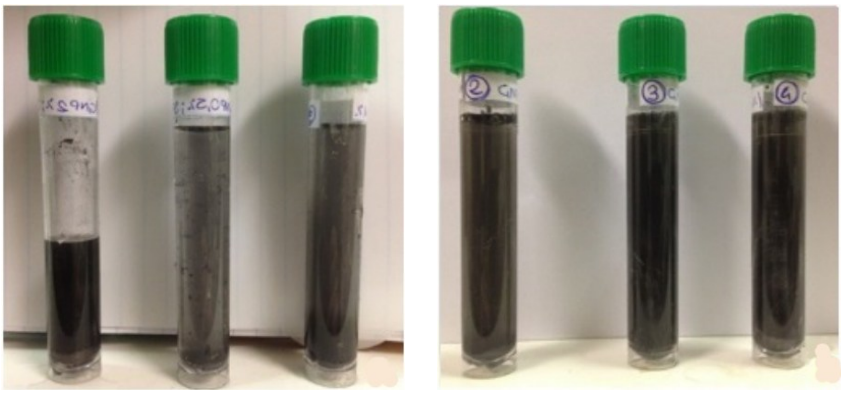

(a) (b)

Figure 6.1. *Fillers dispersion after 10 min of sonication: a). left (1% GNP + 2% SP1), centre (0.5% GNP + 0.5% SP1) and right (0.5% GNP + 1% SP1); b) left (0.5% GNP + 0.5% N200), centre (0.5% GNP + 1% N200) and right (1% GNP + 0.5% N200)*

Pastes were manufactured mixing lime and water with a w/b ratio = 0.32 in order to reach a stiff consistency (flow value ≤ 140 mm, UNI EN 1015:3-2010), with superplasticizer and different amounts of carbonaceous fillers (0.25, 0.50 and 1.00 wt.% on lime). As reference (REF), a paste without filler addition was prepared. Mix proportion and workability of pastes are reported in Table 6.1.

Table 6.1. *Mix proportions and slump flow values of lime pastes*

Mixtures	*NHL 5 (g/L)*	*Water (g/L)*	*N200 (g/L)*	*GNP (g/L)*	*PAC (g/L)*	*GCH (g/L)*	*UFS (g/L)*	*w/b*	*Flow value (mm)*
REF	1375	441	13.75	-	-	-	-	0.32	117
GNP 0.25	1375	441	13.75	3.44	-	-	-	0.32	112
GNP 0.50	1375	441	13.75	6.87	-	-	-	0.32	112
GNP 1.00	1375	441	13.75	13.75	-	-	-	0.32	107
PAC 0.25	1375	441	13.75	-	3.44	-	-	0.32	112
PAC 0.50	1375	441	13.75	-	6.87	-	-	0.32	107
PAC 1.00	1375	456	13.75	-	13.75	-	-	0.33	107
GCH 0.25	1375	441	13.75	-	-	3.44	-	0.32	109
GCH 0.50	1375	441	13.75	-	-	6.87	-	0.32	113
GCH 1.00	1375	441	13.75	-	-	13.75	-	0.32	110
UFS 0.25	1375	441	13.75	-	-	-	3.44	0.32	112
UFS 0.50	1375	441	13.75	-	-	-	6.87	0.32	115
UFS 1.00	1375	441	13.75	-	-	-	13.75	0.32	112

Superplasticizer was manually stirred with the mixing water, after carbonaceous fillers were added to the liquid. Fillers were dispersed for 10 minutes by means of an ultrasonicator *Vibra CellTM VCX 130* (Sonics & Materials, Inc.) equipped with a probe that works with a frequency of 20 kHz by setting an amplitude of 70% (Fig. 6.2).

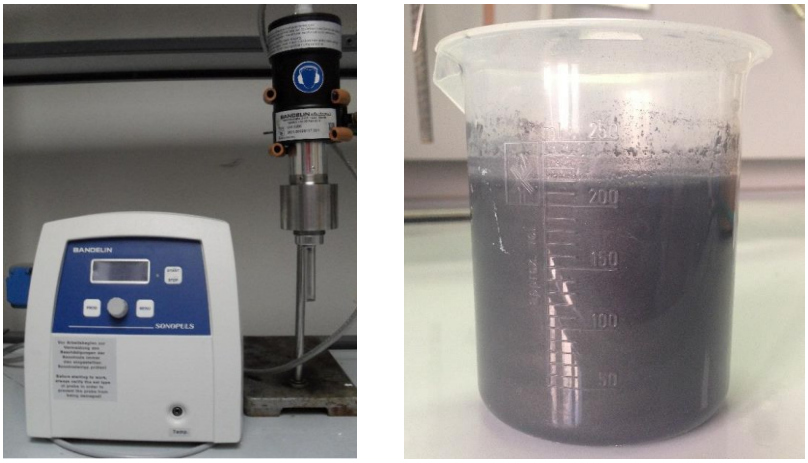

(a) (b)

Figure 6.2 *. a) Vibra CellTM VCX 130 sonicator with ultrasonic probe. b) Suspension with filler, SP and water after sonication*

After sonication, the suspensions were added to NHL5 and mixed for 3 minutes, until homogeneous mixtures were obtained (Fig. 6.3).
Pastes were poured into different moulds, according to tests to be carried out, and cured at T = 20 ± 1°C and a RH = of 95 ± 5% for 7 days, then maintained at T = 20 ± 1°C and RH = 50 ± 5% until testing.

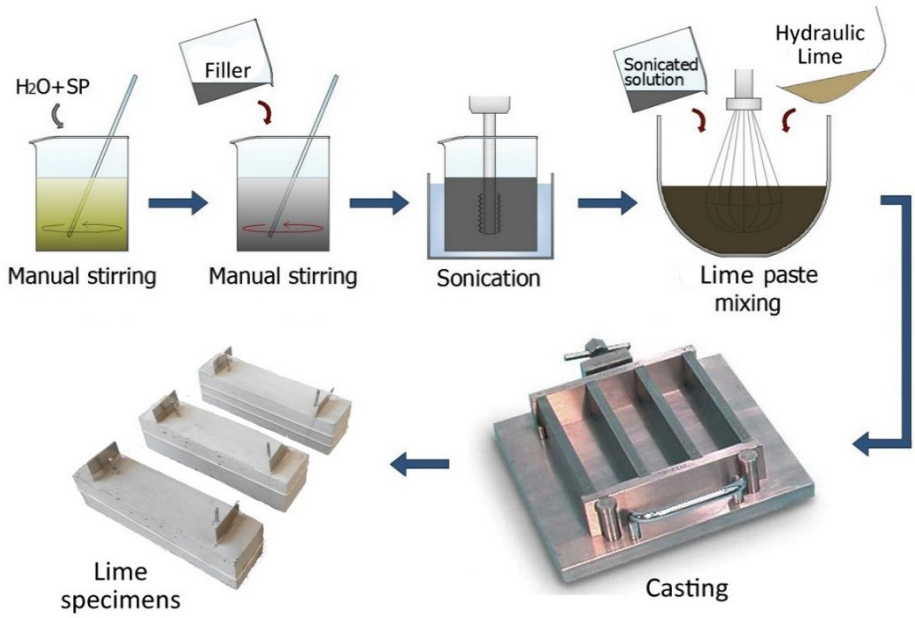

Figure 6.3. *Scheme of paste specimens fabrication process*

6.2.1 Workability

The workability of the pastes has been evaluated by means of slump test to the *flow table*, according to UNI EN 1015-3:2007 standard (Fig. 6.4).

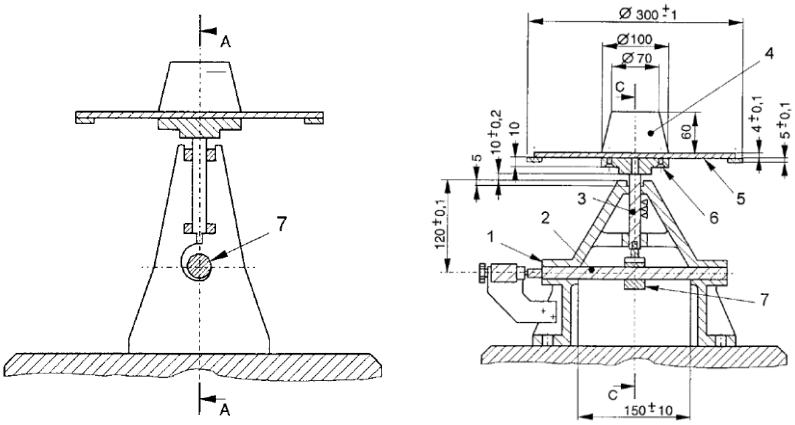

Figure 6.4. *Schematic structure of the flow table apparatus, UNI EN 1015-3:2007*

The test evaluates the *percentage consistency* (C%) of the fresh mixture by measuring the expanded diameter of the sample after 15 bumps at the flow table, through Equation 6.1:

$$C(\%) = \frac{d_f - d_i}{d_i} \cdot 100 \quad (6.1)$$

Where d_f = sample diameter after 15 bumps; d_i = initial diameter of the sample (100 mm). The results show that all pastes reach a stiff consistency ($d_f \leq 140$ mm) according to UNI EN 1015-3:2010. Table 6.2 shows the flow and consistency values of the pastes.

Table 6.2. *Flow values and C% of pastes (UNI EN 1015-3:2007)*

Mixtures	*Flow value (mm)*	*C (%)*
REF	117	17
GNP 0.25	112	12
GNP 0.50	112	12
GNP 1.00	107	7
PAC 0.25	112	12
PAC 0.50	107	7
PAC 1.00	107	7
GCH 0.25	109	9
GCH 0.50	113	13
GCH 1.00	110	10
UFS 0.25	112	12
UFS 0.50	115	15
UFS 1.00	112	12

All mixtures show similar flow values, therefore the workability of pastes with carbon-based fillers are comparable to that of the reference.
However, a high stiffness and some mixing difficulties were detected in the pastes with high contents of GNP and PAC. High amounts of graphene compromise the workability

of the mixtures due to its high bulk density and its hydrophobicity. The loss of workability of mixtures with GNP addition is a recurring problem in literature [33].
Instead, PAC tends to absorb mixing water, due to its high porosity. Contrariwise, no problem arose during the mixing of the pastes with recycled fillers.

6.3 Methods

6.3.1 Mechanical properties

In order to investigate the effect of fillers on the mechanical properties of pastes, 40x40x160 mm specimens were manufactured and submitted to both *compression* and *tensile splitting* tests after 2, 7 and 28 days of curing according to UNI EN 1015-11:2007 and UNI EN 123906:2010, respectively.
Mechanical tests were performed with a hydraulic press equipped with a load cell (Fig. 6.5). The force values were elaborated in order to calculate the tensile splitting strength (f_{ct}, Fig. 6.6a) and the compressive strength (R_c, Fig. 6.6b) according to Equations 6.2 and 6.3 respectively:

$$f_{ct} = \frac{2 \cdot F_{ct}}{\pi \cdot L \cdot d} \quad (6.2)$$

Where F = maximum tensile force (N); L = contact length of the specimen (40 mm); d = nominal length of the cross section (40 mm).

$$R_c = \frac{F}{A} \quad (6.3)$$

Where F = maximum compression force (N); A = load area of the specimen (1600 mm^2).

Figure 6.5. *Hydraulic press for mechanical tests*

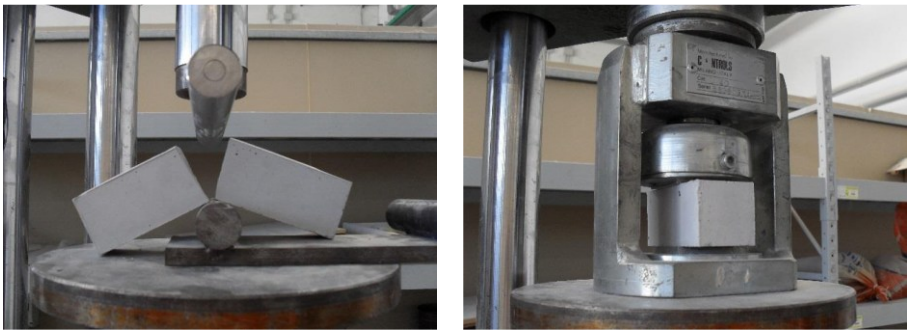

(a) (b)

Figure 6.6. *Paste specimens subjected to: a) tensile splitting test, b) compressive test*

6.3.2 Capillary water absorption

Water is the medium and the main carrier of aggressive ions (Cl^-, SO_4^{2-}, etc.). For this reason, the study of *water absorption* is of primary importance to give information on the durability of a construction material (Fig. 6.7). The durability of pastes was studied through *capillary* absorption tests carried out both for short and for long periods of contact with water, evaluating the amount of water absorbed by a dried specimen through capillary suction by monitoring the specimen mass against time. For *short periods* of contact with water, the absorption coefficient (C) was calculated on 40x40x80 mm paste specimens according to UNI EN 1015-18:2004. For *long periods* of contact with water, the water absorbed per unit area (Q_i) on the same specimens was measured for 8 days according to UNI EN 15801:2010.

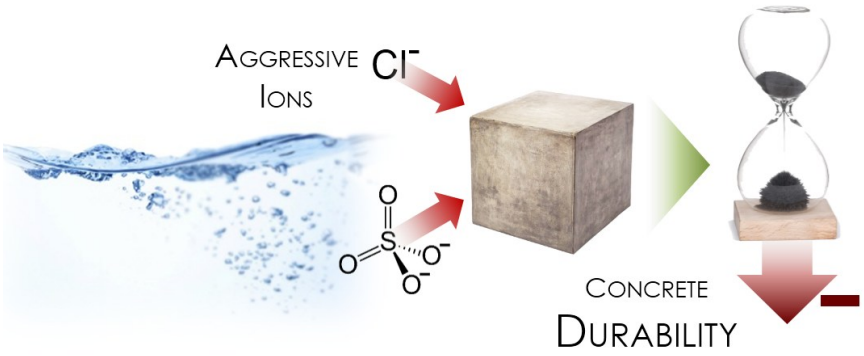

Figure 6.7. *Effect of ions in concrete deterioration*

6.3.2.1 Water absorption in short periods (UNI EN 1015-18:2004)

The water absorption capability in the short period was measured by immersing the paste specimens in water (direct contact) for 90 minutes, according to UNI EN 1015-18:2004 standard. The specimens of dimensions 40x40x80 mm (previously dried in oven) were cut, and the cut surface was immersed in a bucket with water, up to a contact height of about 10 mm (Fig. 6.8).
The capillary absorption coefficient C (kg/(m^2·√min)) has been thus calculated through the weight difference of the specimens, using Equation 6.4:

$$C = 0.1 \cdot (M_{90} - M_{10}) \quad (6.4)$$

Where M_{90} = specimen mass after 90 min of immersion; M_{10} = specimen mass after 10 min of immersion.

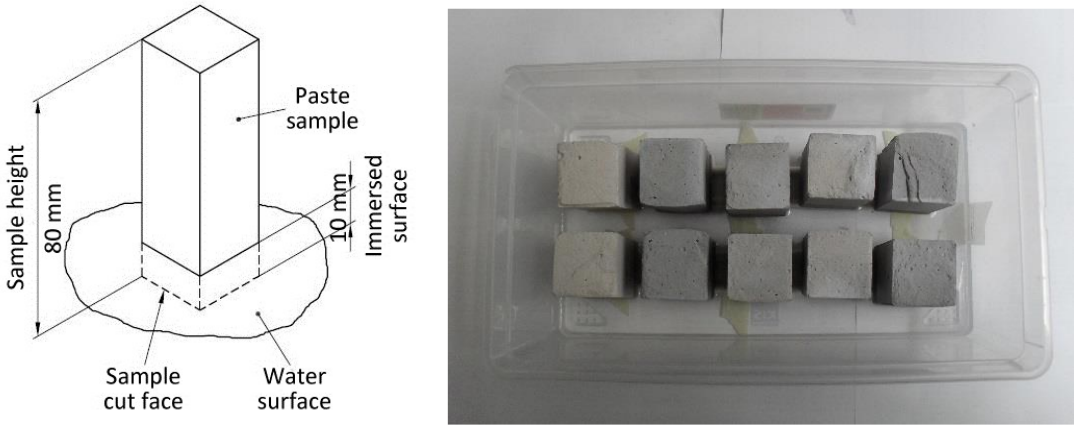

(a) (b)

Figure 6.8. *a) Test method configuration. b) Paste specimens during test (UNI EN 1015-18:2004)*

6.3.2.2 Water absorption in long periods (UNI EN 15801:2010)

The long-term absorption cabability of water was measured by placing the paste specimens in contact with blotting paper sheets (drenched in water) for 8 days, according to the UNI EN 15801:2010 standard (Fig. 6.9). The cut and dried specimens (the same ones previously seen) were weighed at regular time lapse, i.e. at 10 min, 20 min, 30 min, 60 min, 4 hours, 6 hours, 24 hours and at subsequent 24-hour periods.
The amount of absorbed water Q_i (kg/m^2) was measured in relation to time, using Equation 6.5:

$$Q_i = \frac{m_0 - m_i}{A} \tag{6.5}$$

Where m_0 = mass of dry specimen (kg); m_i = specimen mass at time t_i (kg); A = contact area of the specimen with the wet sheet (m^2).

Figure 6.9. *Tested paste specimens on wet paper sheets (UNI EN 15801:2010)*

6.3.3 Microstructural characterization

In order to correlate the obtained results with microstructure, *mercury intrusion porosimetry* (MIP) was performed using a *Thermo Fisher 240 Pascal* porosimeter to analyse the pore distribution and the *total porosity volume* (V_p) of pastes (Fig. 6.10a). Three small fragments for each composition were tested after 28 days of curing and the average results were reported. Moreover, *Scanning Electron Microscopy* (SEM) observations were performed using a *SEM PHILIPS XL20* equipment (Fig. 6.10b) on small pieces of graphite coated paste specimens after 28 days of curing.

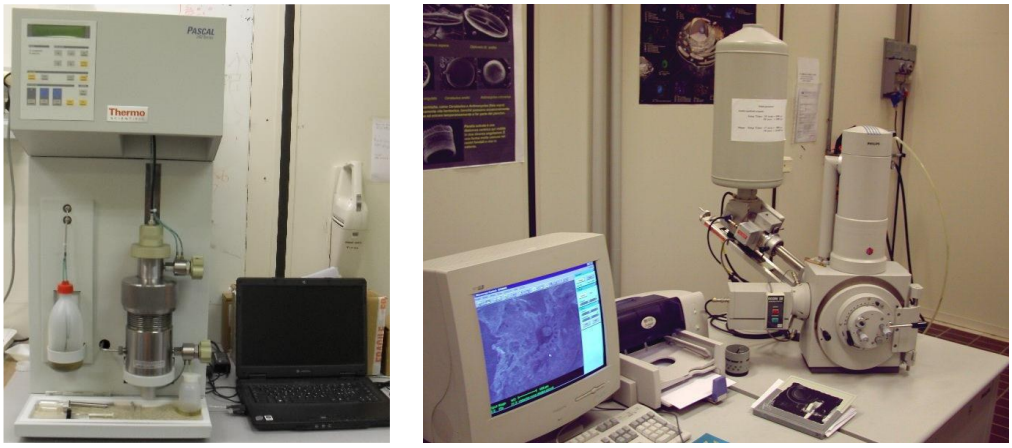

(a) (b)

Figure 6.10. *Instrumentation for microstructural characterization: a) Mercury intrusion porosimeter, b) Scanning electron microscope (SEM)*

6.3.4 Depolluting tests

In order to investigate if the carbonaceous fillers additions adopted in this work could give a certain *depolluting activity* to lime based materials, the depollution properties of different pastes were evaluated after 28 days of curing. Two different experimental tests were carried out: *in-batch*, to explore the adsorbent properties of the carbonaceous fillers, and *in continuous*, by flow test methods inside a reactor to highlight the possible effect of the carbonaceous fillers on the photocatalytic ability of pastes.

6.3.4.1 In batch test

The *in-batch* condition was analysed by Gas Chromatography. The batch test was carried out by monitoring in time the concentration of Methyl-ethyl-ketone (MEK) in a 16.65 L sealed glass box containing the specimen (Fig. 6.11a) [48,49]. Inside the test box a fan guarantees a continuous air recirculation. The specimens had the same dimension of those used for the flow test. Air samples inside the box were collected by a micro-syringe every 8 min and analysed with a gas chromatograph (*GC 8000 Top Carlo Erba instruments*®, injector split 1:15, carrier control by flow; capillary column characteristics: length 25 m, thickness 0.52 µm, Ø 0.32 mm, crosslinked Methyl Siloxane, isotherm 50°C, FID Detector, Fig. 6.11b). The initial amount of MEK injected into the test box was 50 µL

that corresponds to 2402 mg/m^3 (approximately four times the Threshold Limit Value – TLV). The monitoring of data started after 20 min from the first injection to guarantee that all MEK was vaporised. Then, the results were plotted as a percentage of concentration detected (C_i) with respect to the initial concentration (C_0). Tests were conducted in dark condition (absence of irradiation).

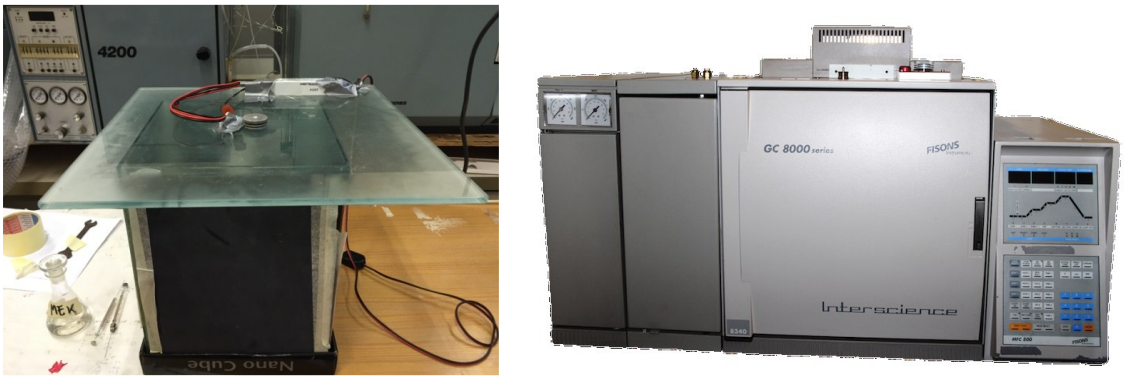

(a) (b)

Figure 6.11. *a) Test box with vaporized MEK. b) Gas chromatograph GC 8000 for MEK concentration measurement*

6.3.4.2 Flow test

The continuous *flow test* was performed according to UNI 11247:2010. The specimen (cylinder with an exposed area of 5026 mm^2) was placed inside a borosilicate glass chamber of 3.58 L (Fig. 6.12a) on a tripod to irradiate the surface with UVA irradiation provided by an UVA metal-halogen quartz lamp (power 400 W) with mercury vapour, peak at 360 nm. The distance between the surface of the sample and the lamp guarantees a specimen radiance of about 20 W/m^2. The inlet gas was a mixture of synthetic air and NOx. The chamber was linked to an analyzer Monitor Labs, *Nitrogen Oxides Analyser model 8841* (Fig. 6.12b). The inlet concentration guaranteed was of 500 ppb of NOx and the *abatement coefficient* in terms of A_c (the percentage of NOx abated) is evaluated according to the standard UNI 11247:2010.

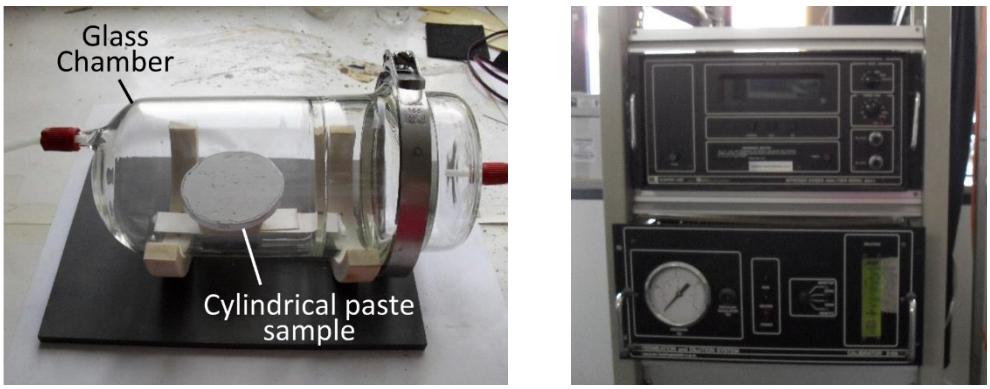

(a) (b)

Figure 6.12. *a) Borosilicate glass chamber for UVA irradiation. b) Flowmeter Nitrogen Oxides Analyser model 8841*

6.3.5 Electrical conductivity

The electrical conductivity measurements play an important role, given the main purpose of this research. For this reason, an in-depth analysis of the literature was carried out, in order to select the most reliable and effective testing system.
Subsequently to these studies (reported in Section 3.5), paste specimens were made with different configurations and different types of electrodes (Fig. 6.13).

Figure 6.13. *Lime specimens with different tested configurations: stainless steel plates and rods placed at variable distance*

Resistance measurements in DC and AC were carried out on these specimens. Following this study, a reliable *four-electrodes* configuration was selected, analyzing the validity of the values during the curing period of the mixtures.
Therefore, during casting, two AISI 304 stainless steel sheets (30x50x1 mm dimensions) were immersed in each specimen for a length of 30 mm (leaving out the remaining length of 20 mm, on the top of the surface) and at a distance of 120 mm. At the same way, two AISI 304 stainless steel rods (Ø 3 mm) were immersed in the paste specimens for a length of 20 mm and placed at a distance of 100 mm: each one, 10 mm far from the corresponding sheet, at the same specimen side (Fig. 6.14).

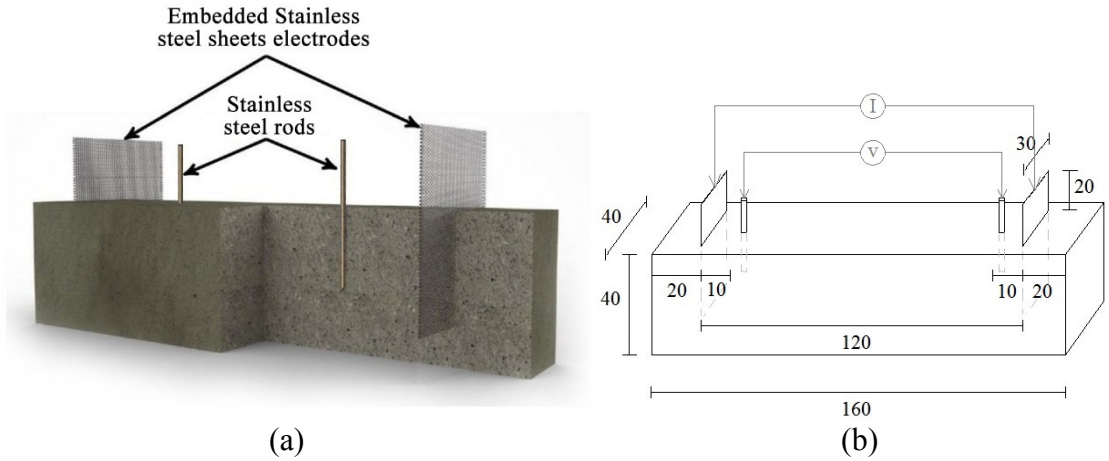

Figure 6.14. *Electrical resistivity tests configuration: a) 3D model; b) dimensions and measures*

On these type of specimens, two different test methods were carried out, with different instruments: direct current and alternating current measurements.

6.3.5.1 Direct Current measurements

Through the DC method the *electrical resistivity* (ρ) of the pastes was determined by means of a four-probe approach on specimens at 7, 14, 21 and 28 days of curing. The four-probe approach was used to determine the potential difference across the specimens, after the application of a set constant current, eliminating the polarization effect of the electrodes (see Section 3.5.1.2). The voltage was applied by an *Amel Mod. 2059* potentiostat/galvanostat on the outer two current probes (stainless steel sheets), while the potential difference was measured using a high impedance digital multimeter between the inner two voltage probes (stainless steel rods, Fig. 6.15).

Figure 6.15. *Paste specimen subjected to DC resistivity measurement*

Since each electrolytic cell, as the studied paste specimens, is characterized by its own specific geometry (Section 3.5.3.1), a *cell-constant* K must be determined for it, considering that this particular conductor obeys to the Ohm's Law (Eq. 3.2)
The cell-constant K is given by l/A ratio (cm^{-1}), while ρ (Ω·cm) is the resistivity of the electrolytic conductor, whose inverse (1/Ω) is its conductivity σ ($\Omega^{-1}\cdot cm^{-1}$ or $S\cdot cm^{-1}$; S = siemens). Considering that an ideal cell, with well-defined geometrical dimensions, does not exist, for real cells, K is determined by immersing the four-probes in the same configuration showed in the figure in an aqueous solution having a known σ value. Therefore, using the same equipment described above, the resistance R is measured and K is calculated using the Ohm's Law. The solution used for this purpose was KCl 0.01 M, having σ = 1.408 $mS\cdot cm^{-1}$ at 25°C [279]. Actually, instead of this value, the conductivity of this solution was experimentally measured with an electrical conductivity meter *AMEL Mod. 160* obtaining this value: σ = 1.442 $mS\cdot cm^{-1}$.
With more details, to obtain the value of the resistance R of the cell with KCl solution and of all specimens, at first, the potential difference (ΔV_0) between the two rods was measured in absence of current, then, a constant current I was applied between the two sheets in the range 5 – 10000 μA and the new potential difference (ΔV_i) was measured. These measurements were plotted in a (ΔV_i - ΔV_0) vs. I diagram (Fig. 6.16): interpolating the values that showed a linear trend, the value of the electrical resistance R was obtained.

In particular, with value R corresponding to the cell containing KCl solution, a cell-constant of 0.6849 cm^{-1} was calculated. Using the Ohm's Law and this σ value, from R determinations, ρ values were calculated for all specimens as a function of curing time.

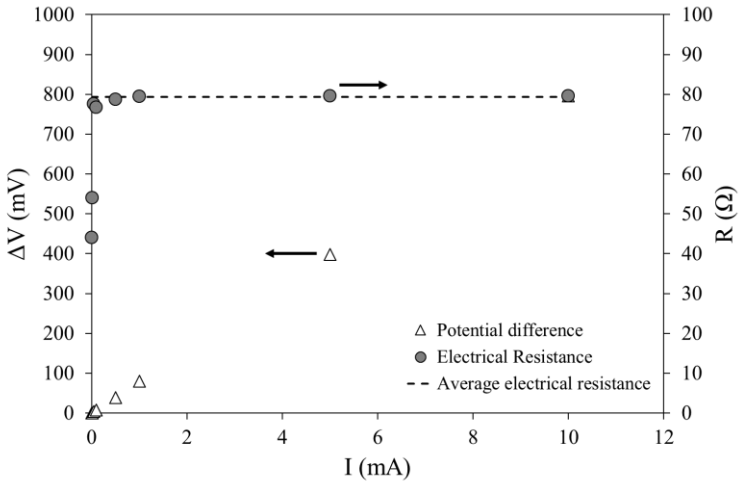

Figure 6.16. *Example of determination of the electrical resistance (R) through potential difference (ΔV_i - ΔV_0) and current (I) measurements*

6.3.5.2 Alternating Current measurements

AC measurements were performed similarly to the *electrochemical impedance spectroscopy* (EIS) measurement approach. For this purpose, a potentiostat (*EG&G PAR Mod. 273*) connected to a frequency spectrum analyzer (*Solartron Mod. 1255*) was used. This instrumentation uses a two-probe configuration typical of AC systems. One of the two external steel plates acts as a *working electrode* (W), while the cables relative to the *counter electrode* (C) and to the *reference* (R) are connected to the other steel plate (Fig. 6.17).

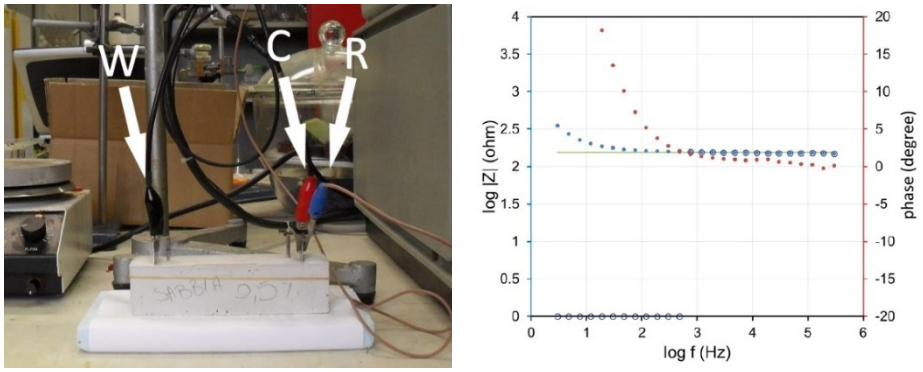

(a) (b)

Figure 6.17. *Measurements in AC: a) specimen tested with relative connections, b) example of Bode diagram for data processing*

Between the two steel plates, a voltage was applied, with variable frequency (in the range 300-3 Hz) and amplitude equal to 10 mV or 50 mV. For each frequency, the instrument software provides a modular *impedance value* |Z| and phase θ, obtaining the *Bode diagrams*, merged into a single graph (Fig. 6.17b).

Through a specifically developed algorithm, the resistivity of the sample was determined by the average log |Z|, which corresponds to a phase close to 0° (circled values in Figure 6.17b). Except for the experimental error, these values of log |Z| indicate a resistive electrical behavior of the tested sample.

6.3.6 Electromagnetic shielding properties

The *electromagnetic shielding effectiveness* (SE) was evaluated on mortars prepared with a water/binder (w/b) ratio of 0.49, calcareous sand (Section 5.3) with a maximum grain size of 3 mm (sand/lime ratio = 3) and by adding a *shrinkage reducing* admixture (SRA) (Mapecure SRA, Mapei S.p.A.) and a CaO expansive agent (Expancrete, Mapei S.p.A.) in amounts equal to 2 and 5 wt.% on lime, respectively, in order to prevent detachment or cracking of mortars due to shrinkage from the specimen holder used in SE measurements. In mortars, carbon-based fillers were added at the same dosage weight of dry materials used for pastes (Tab. 6.1). The type and amount of fillers with gave the best electrical conductivity performances (lower resistivity values) were used in these tests, compared to a reference mortar without additions. The fillers dispersion was carried out with the same procedure used for pastes. Mortars compositions are reported in Table 6.3.

Table 6.3. *Mix proportions of mortars tested in terms of electromagnetic shielding effectiveness*

Mixtures	*NHL5 (g/L)*	*Water (g/L)*	*N200 (g/L)*	*GNP (g/L)*	*AC (g/L)*	*CH (g/L)*	*FS (g/L)*	*Sand (g/L)*	*CaO (g/L)*	*SRA (g/L)*	*w/b*
MREF	524	256	13.75	-	-	-	-	1611	26.19	10.47	0.49
MGNP 0.50	524	256	13.75	6.87	-	-	-	1611	26.19	10.47	0.49
MPAC 0.50	524	256	13.75	-	6.87	-	-	1611	26.19	10.47	0.49
MGCH 1.00	524	256	13.75	-	-	13.75	-	1611	26.19	10.47	0.49
MUFS 1.00	524	256	13.75	-	-	-	13.75	1611	26.19	10.47	0.49

The electromagnetic shielding properties of materials can be evaluated in different ways. In this work, a *reverberation chamber* (RC) was used. The RC facility is able to reproduce a real environment, where the electromagnetic field is statistically uniform, isotropic and with random polarization [280]. In this way, the specimens was excited from all possible directions (polarization and incident angle), as a real life scenario. In order to evaluate the SE, a smaller chamber with an aperture, called nested chamber, was used. The sample under test was mounted on the aperture [281]. Figures 6.18 and 6.19 show the measurement setup. The outer RC which excites the material under test has dimensions of 6x4x2.5 m^3, whereas the inner chamber has dimensions 1.2x0.9x0.8 m^3. Within the outer RC, vertical and horizontal stirrers made of metallic rotating paddles provided the field mixing. The sample was placed on the aperture (Fig. 6.18b). In order to have an optimal contact between the sample edges and the aperture perimeter, avoiding field leakages [282], electromagnetic gaskets have been used (Fig. 6.18b). Moreover, to improve the contact between the sample and the aperture a multi-hole frame (Fig. 6.18c) with screws was used, that element pushes the sample towards the underlying gaskets (Fig. 6.18d).

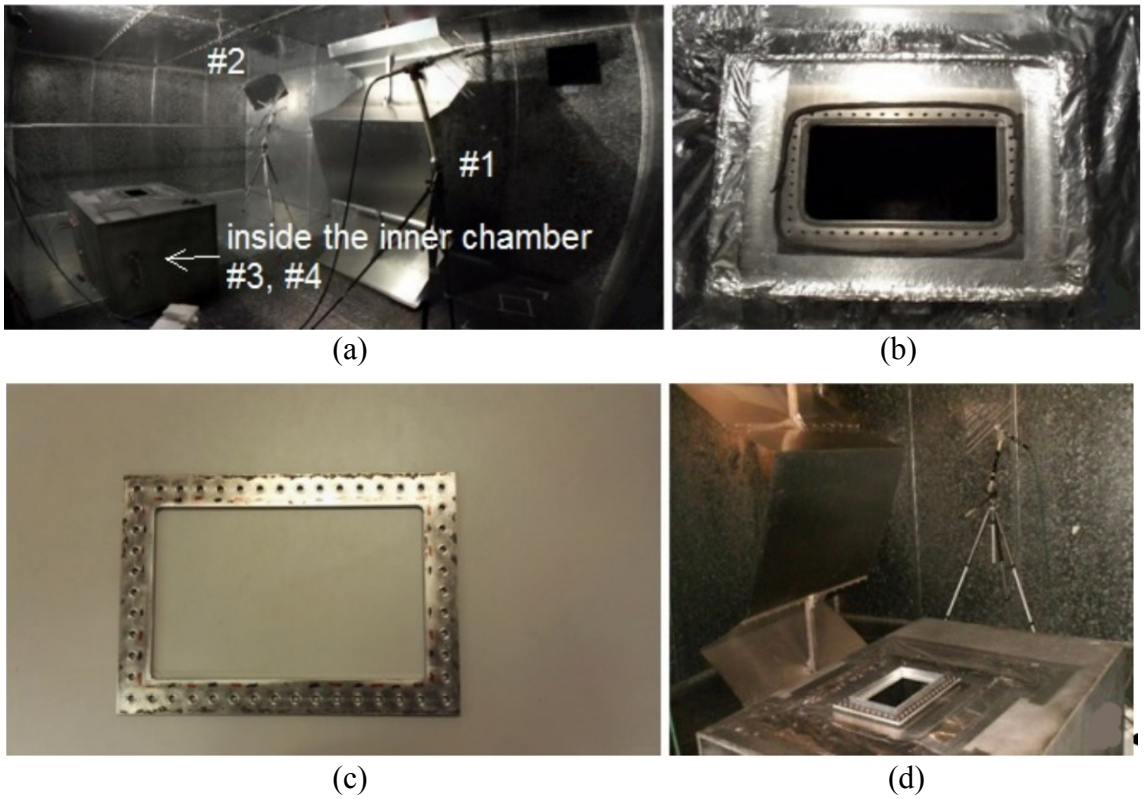

Figure 6.18. *a) Measurement set-up: outer RC equipped by vertical and horizontal stirrers, two log-periodic antennas and nested RC with the aperture on the top; b) aperture of the nested RC where both the gaskets used to avoid field leakages and the holes, where the multi-hole frame was mounted with screws to fasten the specimens and to provide a good contact, are visible; c) multi hole frame, used to improve the mechanical contact between the sample and the aperture; d) multi hole frame mounted on the aperture*

The outer reverberation chamber is fed by a log-periodic antenna (#1 in Fig. 6.18) and the resulting energy exciting the sample is monitored by a second antenna (#2) of the same type (Fig. 6.19). The field inside the nested chamber is picked up by two double ridge antennas, receiving (#3) and transmitting (#4). A four port *Vector Network Analyze*r (VNA) is connected to the system to measure the scattering parameters between the four antennas: (#1) and (#2) for the outer chamber and (#3) and (#4) for the inner one. The power received is given by $|S_{ij}|^2$, where S is the complex scattering coefficient measured by the VNA, i and j are the receiving and transmitting antennas, respectively. In this case, the power received inside the outer and inside the inner reverberation chamber and the power between the outer to inner chamber are $|S_{21}|^2$, $|S_{43}|^2$ and $|S_{31}|^2$, respectively. In fact, the material also exhibits effective absorption of electromagnetic energy, thus reducing the quality factor of both the reverberation chambers [283]. The SE is evaluated by means of Equation 6.6:

$$SE = -10\log\left(\frac{\langle|S_{21}|^2_{ns}\rangle\langle|S_{41}|^2_{s}\rangle\langle|S_{43}|^2_{ns}\rangle}{\langle|S_{21}|^2_{s}\rangle\langle|S_{41}|^2_{ns}\rangle\langle|S_{43}|^2_{s}\rangle}\right) \quad \text{.....(6.6)}$$

Where $\langle \cdot \rangle$ is the ensemble averaged over the chamber realizations, the subscripts s means “the case with the specimen” and ns means “the case without the specimen”. A

single chamber realization, of the outer RC, corresponds at each stirrer position. On the contrary, within the inner chamber, due to the limited space, there is not a stirrer. In the inner chamber, a bandwidth with a frequency step of 250 kHz was considered, and the frequency stirring [284] was applied by using 400 frequency points, each of the correspondent to a chamber realization. The investigated band was from 0.8 to 8.4 GHz, divided into several sub-bands of 400 MHz, where 1601 frequency points were acquired by the VNA, sampled by steps of 250 kHz. The stirrers worked in a synchronous way, more precisely, they have the same angle step and 9 stirrer positions are considered for both, 40 degrees shifted for each position.

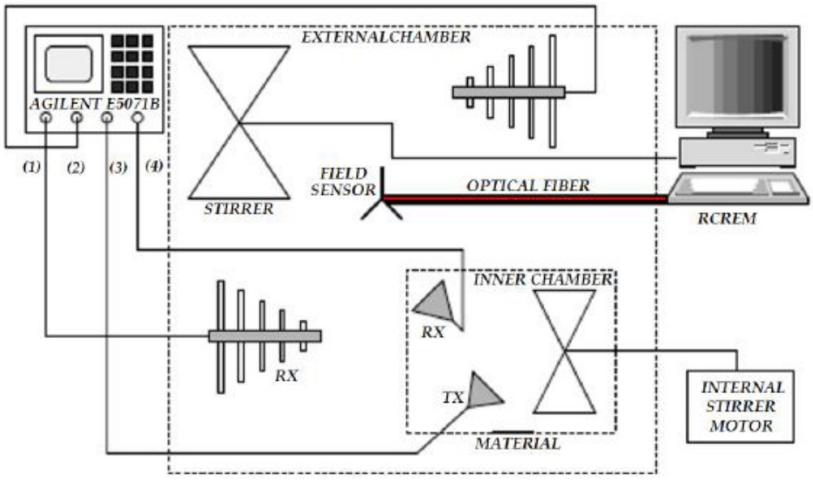

Figure 6.19. *NRC measurement setup for SE tests*

6.4 Results and discussions

6.4.1 Mechanical and microstructural characterization

The carbon fillers provided a general increase in the mechanical strength of the pastes, with values not always proportional to the addition content.
The overall results of tensile (f_{ct}) and compressive strength (R_c) of pastes carried out during the first 28 days, together with the values of the porosimetric analyzes, are reported in Table 6.4.

Table 6.4. *Tensile strength (f_{ct}), compressive strength (R_c), total porosity (V_p) and average pore diameter (d_p) of pastes*

Mixtures	*f_{ct} (MPa)*			*R_c (MPa)*			*V_p (%)*	*d_p (μm)*
	2 days	*7 days*	*28 days*	*2 days*	*7 days*	*28 days*		
REF	0.20	0.56	0.82	1.2	4.2	10.8	41	0.116
GNP 0.25	0.30	0.50	0.92	1.9	4.8	13.0	37	0.082
GNP 0.50	0.30	0.65	0.88	2.0	3.5	13.8	39	0.103
GNP 1.00	0.40	0.66	1.17	2.3	3.7	13.5	39	0.104
PAC 0.25	0.30	0.48	0.99	1.2	4.4	12.8	38	0.093
PAC 0.50	0.30	0.60	0.97	1.8	4.3	13.3	38	0.096
PAC 1.00	0.40	0.58	0.99	1.7	4.4	11.1	39	0.096
GCH 0.25	0.34	0.56	0.69	2.6	4.2	12.7	38	0.111
GCH 0.50	0.39	0.47	0.82	2.7	4.3	12.1	40	0.111
GCH 1.00	0.39	0.59	0.82	2.8	5.1	13.6	39	0.110
UFS 0.25	0.51	0.85	0.88	3.7	6.4	15.8	37	0.086
UFS 0.50	0.57	0.97	0.82	3.5	7.5	13.3	36	0.084
UFS 1.00	0.43	0.58	0.79	3.0	5.2	13.1	36	0.099

Concerning f_{ct} values, all pastes showed the same behavior, with a gradual increase of tensile strength during time (Fig. 6.20). Only specimens manufactured with foundry sand, UFS 0.25% and UFS 0.50%, reached approximately the maximum strength after the first week of curing. This effect is related to the presence of alkaline salts in the foundry sand (see Tab. 5.7, Section 5.4.2.2) [285], which have worked as quick setting agents, contributing to a great development of mechanical strength during the first days after casting.

The maximal enhancement of tensile strength was registered for pastes manufactured with the two commercial fillers, which showed a 20% higher strength for those prepared with PAC at any percentage and even more than 40% when the amount of GNP is 1.00 wt.% on the binder content. Gong et al. [286] found that the use of graphene oxide (GO) inside cement Portland pastes increase the tensile strength more than 40% when used at 0.03 wt.% on the binder content. The little amount of addition in this case is related to the great capacity of oxidized graphene platelets to be dispersed in water with respect to graphene nanoplatelets, due to its hydrophilic nature. Instead, the addition of waste carbon-based fillers (GCH and UFS) has produced no effect on the tensile strength after 28 days, showing comparable results to that of the paste without fillers (REF).

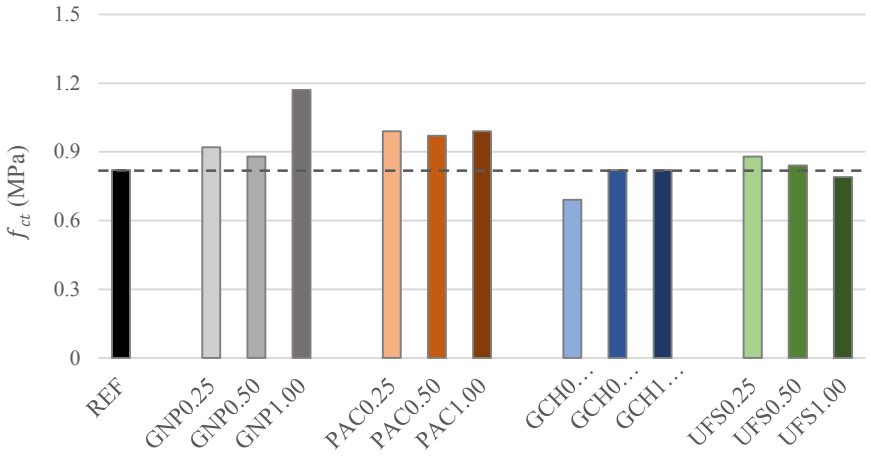

Figure 6.20. *Final Tensile strength (f_{ct}) of pastes after 28 days of curing*

In general, the presence of carbonaceous fillers within the paste has contributed to an increase of the mechanical compressive strength already after 2 days of curing, compared to the R_c of the REF paste, with values two and three times higher when GCH and UFS are added, respectively. As for tensile strength, this behavior is related to the presence of alkaline salts inside the two waste carbon-based fillers which acted as quick setting agents. Furthermore, each addition has increased the final mechanical strength (R_c at 28 days) with respect to REF paste at each percentage (Fig. 6.21), except for PAC 1.00 one. This result is related to the fact that at a such great content of activated carbon, the workability of the paste has decreased much more than with the other fillers, due to its high specific surface area (1800 m^2/g), and additional water was necessary to reach a slump flow value comparable to that of all other pastes (Tab. 6.1). The additional water has changed the w/b ratio from 0.32 to 0.33, leading to a decrease of the R_c after 28 days with respect to the other pastes with fillers addition [26]. The ability of nano/micro fillers to increase the mechanical strength of cementitious materials already at early ages, is known as "filler effect" [273][287]. This behavior is also related to the fact that such materials work as nucleation sites for C-S-H [287][288] accelerating the degree of hydration as well as the mechanical properties development of hardened composites, thanks to their high specific surface area [10].

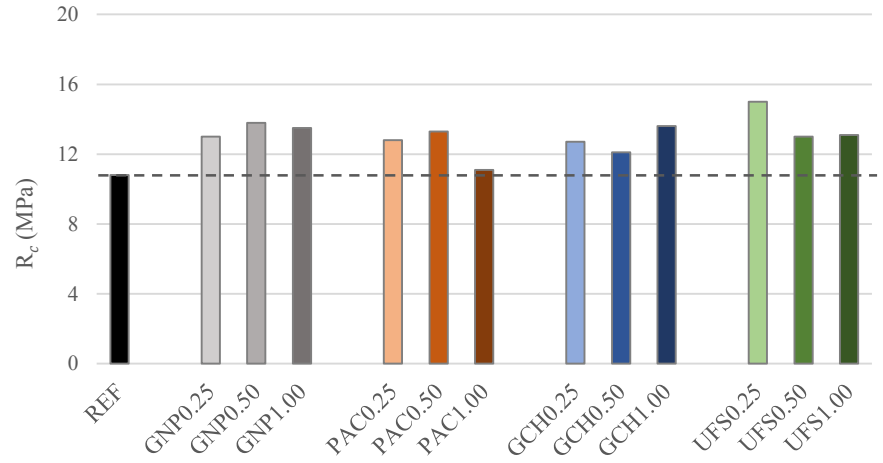

Figure 6.21. *Final compressive strength (R_c) of pastes after 28 days of curing*

Moreover, it is well-known that the addition of fillers contributes to the refinement of the paste, lowering the total porosity (V_p) of the composite and by shifting the average pore diameter (d_p) to smaller dimensions. Such effect is well visible in Table 6.4, where the REF paste showed a V_p of 41% and all other pastes had a lower total porosity, that reached the lowest value of 36% when foundry sand is added. This effect is probably due to the best dispersion obtained by the UFS filler because of the small and spherical shape of its particles (Section 5.4.3). Moreover, all the manufactured pastes are characterized by smaller d_p than the REF, confirming the ability of pore refinement of the matrix also for carbonaceous filler wastes. Figure 6.22 shows the curves obtained from the porosimetric tests, where it is highlighted that all the pastes with fillers addition show both a lower pore volume, and pores with smaller diameter.

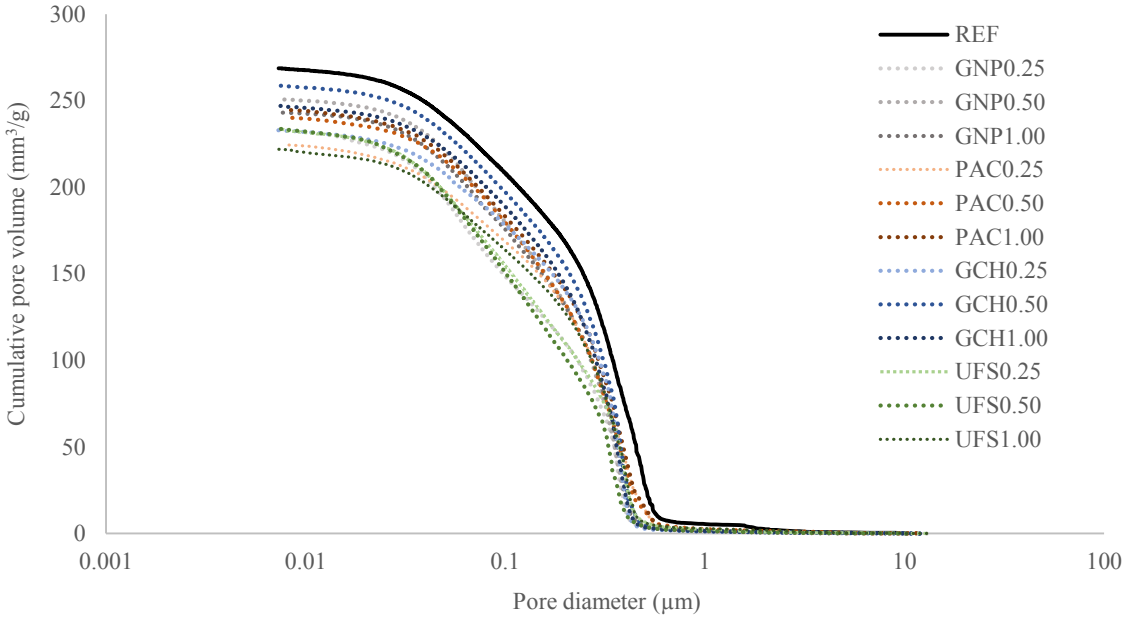

Figure 6.22. *Porosimetric curves of pastes*

The lower porosity of pastes with carbonaceous additions is also visible from SEM images of the REF paste and all the other one manufactured with 0.5 wt.% of carbon-based fillers (Fig. 6.23). The reference paste (Fig. 6.23a) shows a microstructure characterized by a diffuse porosity, whereas all the other pastes appear more compact and homogeneous. In PAC 0.50 and UFS 0.50 specimens the presence of the carbonaceous addition was not visible (Figg. 6.23c and 6.23e), whereas in GNP 0.50 two agglomerates of graphene nanoplatelets partially embedded in the matrix can be noted in the upper left side (Fig. 6.23b), confirming the more difficulty to disperse GNP with respect to the other fillers. In GCH 0.50 specimen, the presence of one particle of char perfectly adhered to the paste is visible in the middle of Fig. 6.23d.

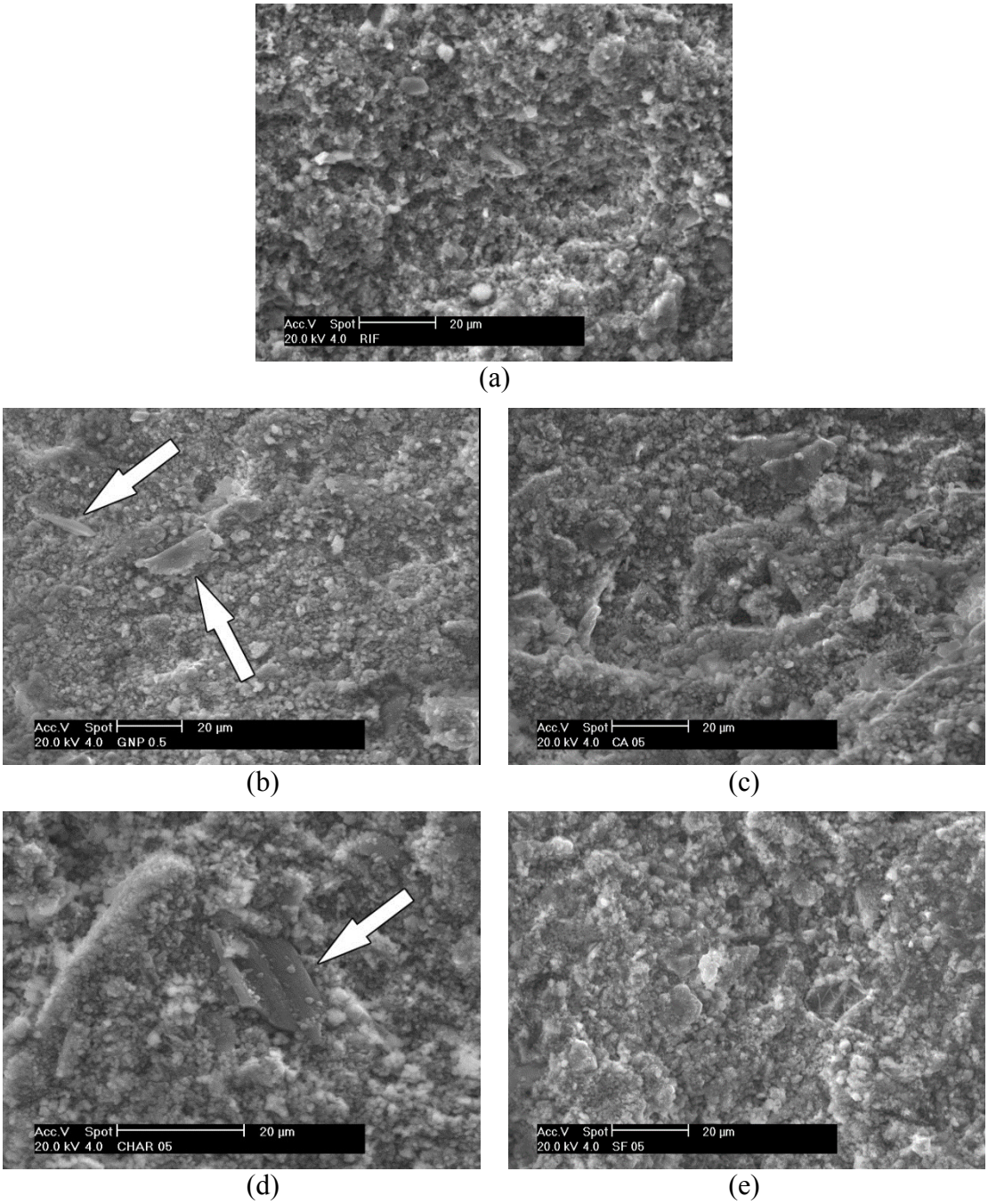

Figure 6.23. *SEM of pastes: a) REF; b) GNP 0.50; c) PAC 050; d) GCH 0.50; e) UFS 0.50. Arrows indicate the carbonaceous particles*

6.4.2 Capillary water absorption

The durability of pastes was studied through capillary water absorption tests, and the results showed an evident contribution of fillers in decreasing the amount of water absorbed in both short and long period.

Regarding the water absorption coefficient (C), the addition of carbonaceous fillers had a great influence in decreasing the water uptake of pastes (Fig. 6.24) at short periods of contact with water (90 min). All the studied mixtures showed a lower value of the C coefficient with respect to the reference paste, reaching values even lower than half of that of REF when GNP and UFS fillers are used. In general, increasing the content of the carbon-based fillers, the water suction decreased, especially for pastes prepared with the commercial admixtures, since both activated carbon [289][290] and graphene nanoplatelets [291][292] are hydrophobic materials. This behavior is much less evident for pastes with char from gasification, whose C values remained always around 76% of REF, since in this type of pastes the average pore diameter d_p is higher than that of the pastes manufactured with other fillers, regardless of the GCH amount (Tab. 6.4). It is demonstrated that the saturation of the capillary pores with higher dimensions occurs faster than that of the smaller ones [293].
On the other hand, the water absorption coefficient has a reversal trend when UFS is used, seeing that C increased with the amount of this filler, with absorption equal to 43% and 54% of REF when 0.25% and 1.00% of UFS are respectively added. This effect can be explained by the fact that with the increase of UFS also the presence of clay impurities [285][248] increases: it is well-known that clay is hydrophilic and thus much more prone to the absorption [26]. However, the very low absorption coefficients in UFS specimens are related both to their low total porosities and their small average pore diameters d_p (Tab. 6.4).

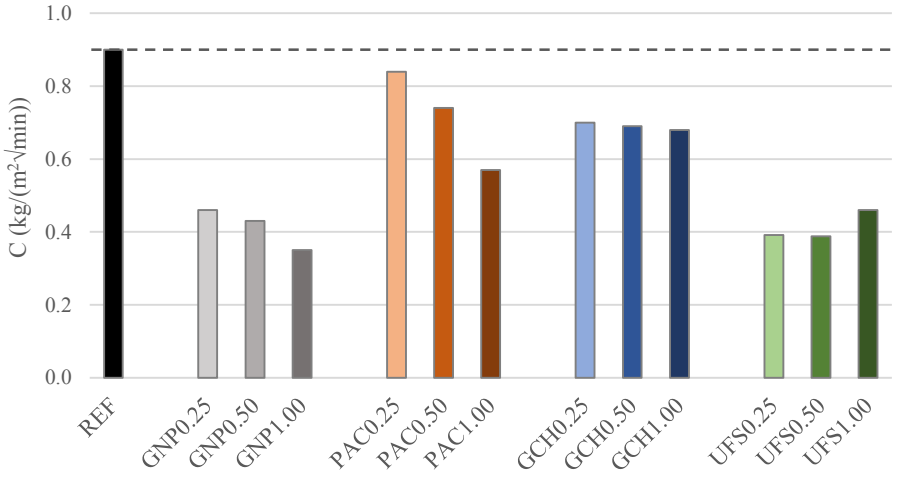

Figure 6.24. *Water absorption coefficient (C) of pastes after 28 days of curing*

The water absorbed per unit area (Q_i) of pastes after 28 days of curing is reported in Fig. 6.25. Also for longer time of contact with water (8 days), all pastes, if manufactured with carbonaceous fillers, showed a lower absorption compared to that of the reference one. In particular, best results (lower absorptions) are registered for those prepared with GNP (Fig. 6.25a), confirming again the hydrophobic nature of the material. Also pastes with UFS exhibited very low water absorptions during time (Fig. 6.25d), similar to those of pastes prepared with GNP, thanks to their lowest total porosity (Tab. 6.4). For these two types of pastes the lowest amounts of water absorbed in time are reached by the specimens manufactured with 0.50 wt.% of filler on the binder weight. For UFS 0.50 this is due to

the smaller average pore diameter (Tab. 6.4). For the GNP 0.50 specimen, the low absorption of water is due to the hydrophobicity of graphene, since neither the total porosity nor the average pore diameter were the smallest among all the pastes with GNP addition (Tab. 6.4).
The Q_i trend of pastes manufactured with activated carbon (Fig. 6.25b) shows an opposite trend compared to that of the water absorption coefficient (Fig. 6.24). In fact, whereas for the latter increasing the PAC content the absorption (C) decreases, for the former the situation was opposite: the lower the addition, the lower the amount of the water absorbed. This situation is related to the fact that PAC has an hydrophobic behaviour only at early ages thanks to its non-polar surface characteristics [294], whereas for long periods of time it becomes hydrophilic [289].

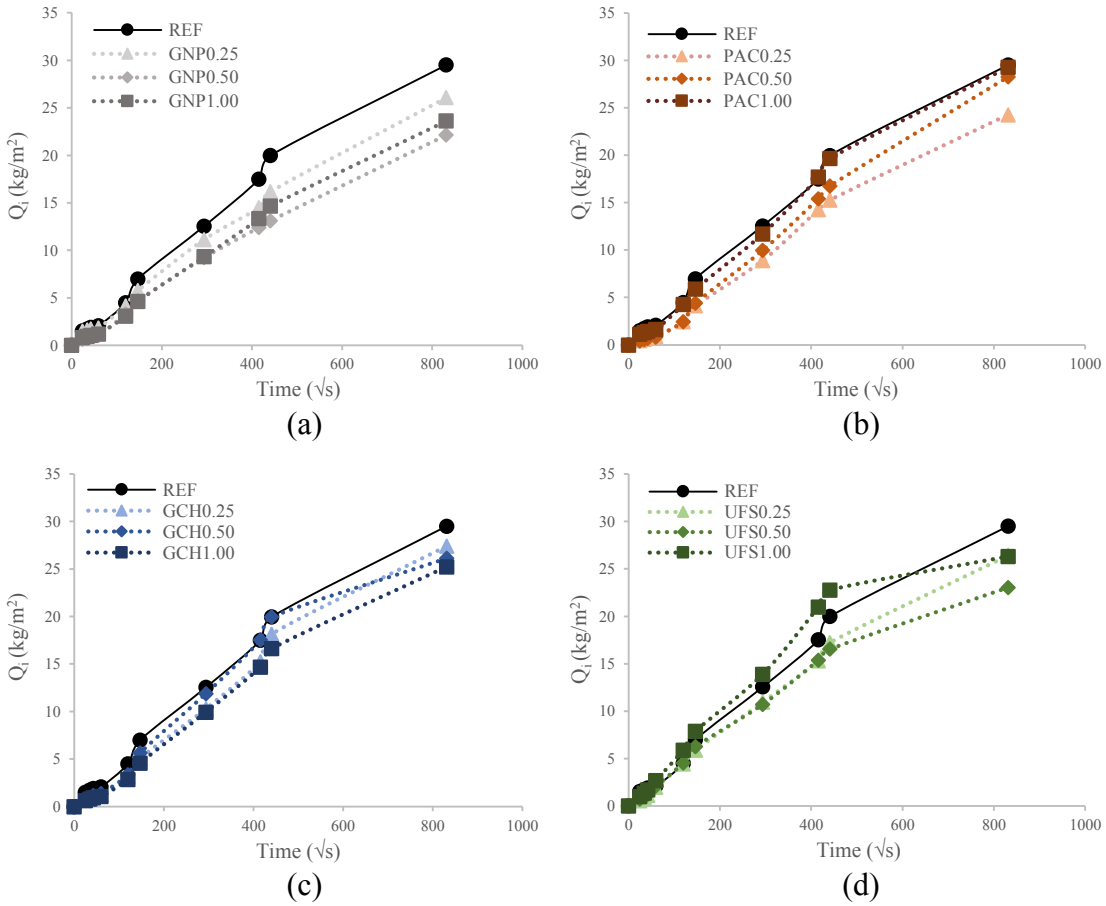

Figure 6.25. *Water absorbed per unit area (Q_i) of pastes after 28 days of curing. Comparison between REF and: a) GNP, b) PAC, c) GCH, d) UFS*

6.4.3 Depollution tests

6.4.3.1 In batch test

The depollution capacity of pastes under dark condition is displayed in Fig. 6.26, where the residual percentage of MEK inside the box is plotted against time. Trend line starts at 20 min because this time is necessary to MEK to vaporize completely.

The graph shows that almost all pastes containing carbon-based fillers have higher adsorption properties compared to the REF. The best results were obtained from foundry sand, in particular in UFS 0.25 paste, with MEK decreases of up to 50%. However, even the GCH and the PAC demonstrate good adsorption capability.

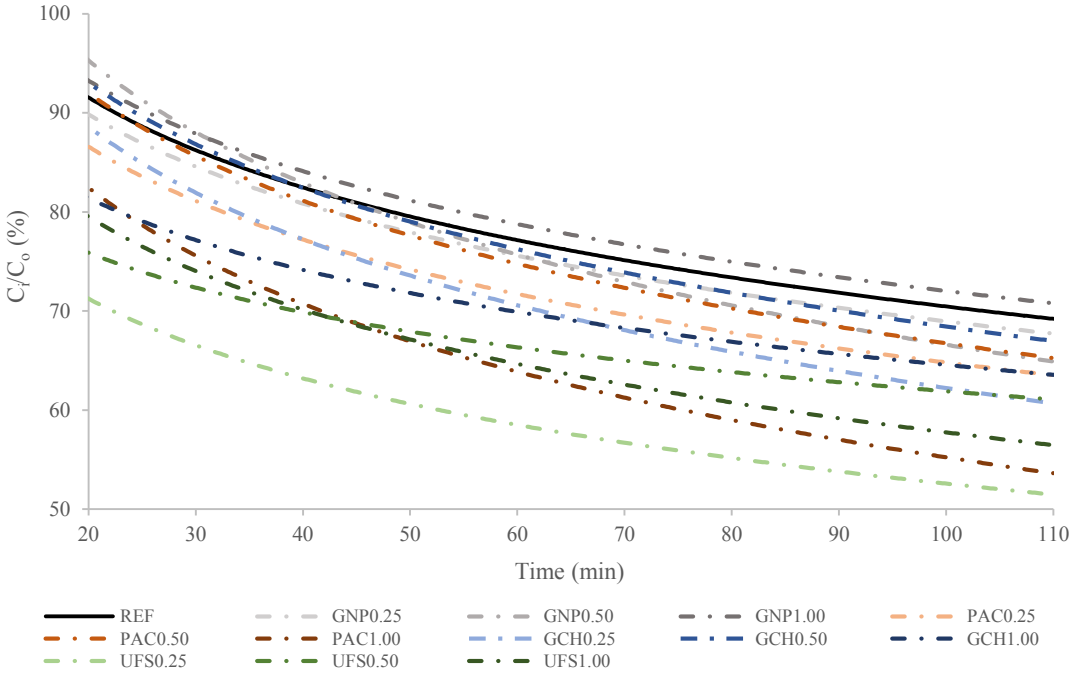

Figure 6.26. *Residual percentage of MEK during depollution tests performed on pastes after 28 days of curing*

To better analyze and compare the results, MEK residual concentration in percentage inside the box with the different specimens, measured after 120 min of test under dark condition, is reported in Figure 6.27.

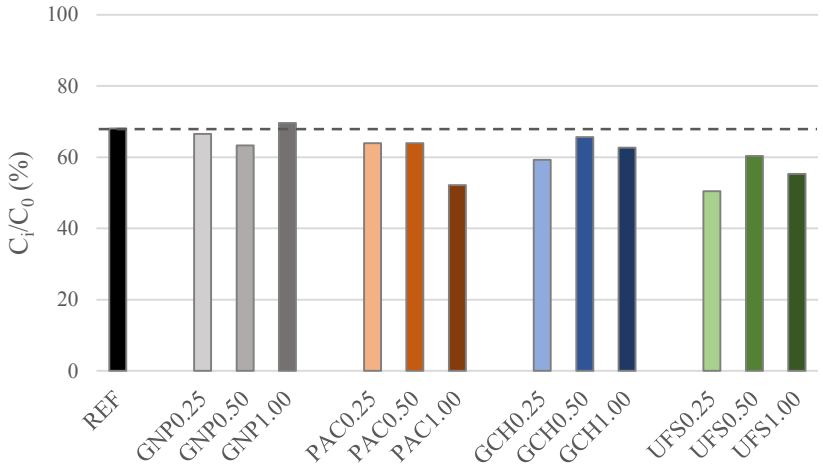

Figure 6.27. *Residual MEK concentration inside test box after 120 min*

6.4.3.2 *Flow test*

Results of the photocatalytic efficiency of pastes tested in terms of NOx abatement under UVA radiation are shown in Figure 6.28.
It is evident that the addition of both commercial and waste carbonaceous fillers has not modified the behavior of the lime pastes. In fact, the REF paste has shown a NOx abatement of 6.5%, which cannot be considered as a photocatalytic behavior. The presence of fillers of different typologies and at any percentage did not improve the photocatalysis of pastes and sometimes has even reduced the effect in comparison with the reference one.

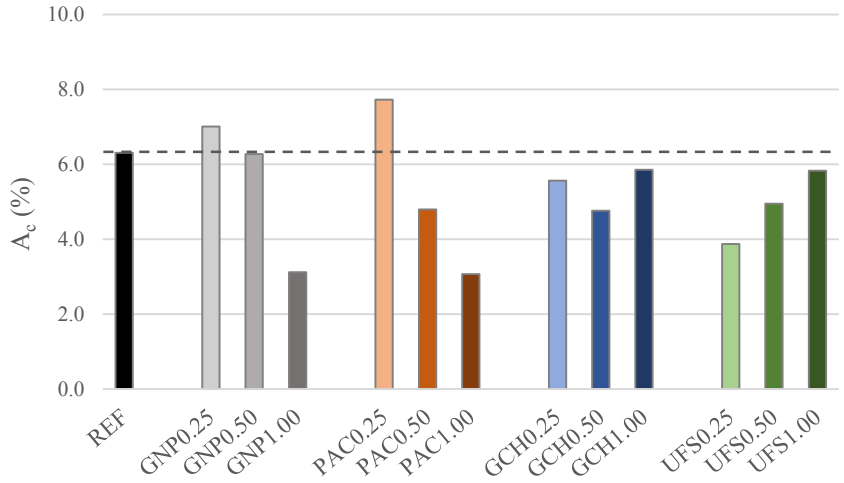

Figure 6.28. *Photocatalytic efficiency under UVA radiation of pastes (NOx abatement)*

For this reason, it was decided to test some selected pastes with the addition of nano-TiO_2, which is known for being an efficient photocatalytic agent [295], to evaluate if the carbonaceous filler additions could in some way affect (enhance) the photocatalytic activity of TiO_2. Pastes with carbonaceous additions were manufactured at a 0.50 wt.% of filler and *AEROXIDE® TiO_2 P 25* (Evonik Resource Efficiency GmbH) at 1.00 wt.% on the hydraulic lime. Pastes compositions with TiO_2 addition are reported in Table 6.5.

Table 6.5. *Mix proportions of pastes with TiO_2 submitted to depolluting analysis (flow test)*

Mixtures	*NHL 5 (g/L)*	*Water (g/L)*	*N200 (g/L)*	*GNP (g/L)*	*PAC (g/L)*	*GCH (g/L)*	*UFS (g/L)*	*TiO_2 (g/L)*	*w/b*
REF T	1434	545	14.34	-	-	-	-	14.34	0.39
GNP0.50 T	1434	545	14.34	7.17	-	-	-	14.34	0.39
PAC0.50 T	1434	545	14.34	-	7.17	-	-	14.34	0.39
GCH0.50 T	1434	545	14.34	-	-	7.17	-	14.34	0.39
UFS0.50 T	1434	545	14.34	-	-	-	7.17	14.34	0.39

Results of the photocatalytic efficiency of pastes with TiO_2 addition are reported in Fig. 6.29. When the nano-photocatalyst is added to the plain paste (REF T), the NOx abatement reached values of 25%, four times higher than that of the same paste without

TiO_2 (REF specimen, Fig. 6.28). In general, also with carbonaceous fillers, all pastes with TiO_2 showed a great enhancement of the photocatalytic action. In particular, GNP0.50 T and PAC0.50 T showed an A_c around the 20%, which were four and three times higher than that of GNP0.50 and PAC0.50, respectively (Fig. 6.28). Referring to the waste carbon-based additions, the lowest NOx abatement was found for GCH0.50 T that showed an abatement coefficient equal to 15%, three times the one registered for GCH 0.50 specimen. On the contrary, the specimen manufactured with TiO_2 and foundry sand, UFS0.50 T, showed the same photocatalytic efficiency of the REF T, five times higher than that of the same without photocatalytic agent (Fig. 6.28).

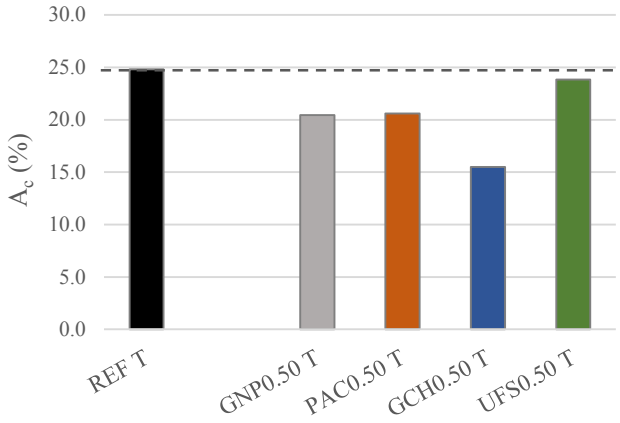

Figure 6.29. *Photocatalytic efficiency under UVA radiation of pastes (NOx abatement) with TiO_2 addition*

Summarizing results of Figg. 6.28-6.29, it is evident that the addition of a photocatalytic agent is the necessary parameter for having a NO_x abatement under UVA irradiation. Moreover, the addition of the carbonaceous fillers has always worsened the depolluting behavior of the pastes with respect to the reference one: only in the case of UFS, the TiO_2 has ensured a similar result of that of REF T paste. This effect could be related to the coloration that specimens acquired because of the filler addition, since all carbonaceous fillers have a black color that has darkened the paste (Fig. 6.30). Only the paste manufactured with UFS showed a color similar to that of the reference specimen (Fig. 6.30a and 6.30e). It is reported that the addition of pigments that provide a significant coloration on finishing products can induce a moderate decrease of the photocatalytic activity in terms of NOx abatement [296][297].

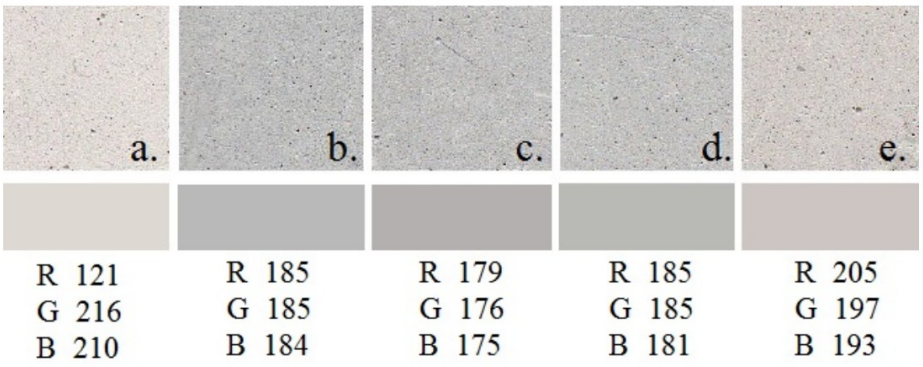

Figure 6.30. *Scan images of the specimens surface (up) and average RGB value measured in five different points (down): a) REF T, b) GNP0.50 T, c) PAC0.50 T, d) GCH0.50 T, e) UFS0.50T*

Moreover, results obtained demonstrate that the addition of GNP without specific treatments is not efficient for increasing the photocatalytic behavior of the titanium dioxide. This effect can be only achieved by functionalization methods [298], like hydrothermal [299][300] or sol-gel [301] treatments.

6.4.4 Electrical resistivity

From the results of the electrical conductivity tests, it is confirmed that all types of carbon-based fillers, both commercial and recycled, decrease the resistivity values of the mixtures, and therefore increase their conductivity. The DC electrical resistivity (ρ) measurements conducted on paste specimens at 7, 14, 21 and 28 days of curing are displayed in Fig. 6.31.

After the first week of curing (Fig. 6.31a), the REF paste has registered an electrical resistivity of 170 Ω·cm. All the other specimens showed similar ρ values independently from carbonaceous addition (ranging from 190 to 170 Ω·cm), unless if prepared with the UFS fillers. Moving towards 0.25 to 0.50 and 1.00 percentages of UFS, the resistivity decreases showing values equal to 790, 360 and 210 Ω·cm, respectively. Moreover, already at early ages the electrical resistivity of UFS pastes decrease with the increasing amount of carbonaceous addition, as reported in the literature for GNP [126], carbon black [71][31], carbon coke [125], graphite [302] and fly ash or silica [303] additions. The use of foundry sand for decreasing the electrical resistivity of cementitious materials was never tested before.

After another week (14 days of curing), the electrical resistivity of pastes increased of one order of magnitude, because of the loss of mixing water, and the increase of voids. (Fig. 6.31b). The ρ measured for REF paste was equal to about 3400 Ω·cm, whereas all the other specimens containing a carbon-based addition, regardless if commercial or waste type, showed a lower electrical resistivity if compared to it.

In general, a clear trend related to the different additions of the same filler and electrical resistivity is not visible; only those with FS maintained the same trend observed at 7 days of curing. At 21 days from the cast (Fig. 6.31c), ρ of specimens continued to increase, especially for the REF paste which achieved a value around 10000 Ω·cm. Also at this

curing period, all pastes containing carbonaceous fillers assumed lower values of the resistivity than the REF one, even if those manufactured with GNP showed a trend reversal for that reported in the literature, since the higher the amount of carbon-based fillers, the higher the resistivity. This effect could be related to the not optimally dispersed graphene nanoplatelets [127], as observed in Fig. 6.23. It is reported that the decrease of electrical resistivity with the increase of carbon-based fillers dosage is obtained only when the amount remains under the percolation threshold (Section 4.2.1) and particles are well dispersed or, if above this value, the segregation occurs along the conduction paths [304]. When the activated carbon was used, the electrical resistivity showed a decrease from 0.25 to 0.50% PAC addition and then ρ increased at 1.00% addition. It is possible that, also for PAC specimens, the increase of ρ values is due to the agglomeration of particles, which have discontinued the available current paths. Regarding GCH specimens, the electrical resistivity was approximately the same for each addition and around 4000 Ω·cm. Results of UFS specimens continued to maintain the same trend registered at 7 and 14 days.

At 28 days (Fig. 6.31d) the electrical resistivity increased again and, for the REF paste it became even more than double of the value registered at 21 days and equal to 22000 Ω·cm. For specimens with carbonaceous additions, the general trend measured at 21 days was confirmed. In general, at 21 and 28 days of curing, the lowest ρ values were found for GNP 0.25, for all specimens with GCH and for UFS 1.00.

The resistivity measurements performed with the AC system confirm the results obtained in DC in terms of comparisons between the pastes (Fig. 6.31). All mixtures containing fillers show lower resistivity values than the reference. The pastes containing GCH are always the most conductive, in particular that with maximum quantity (GCH 1.00). The trend of the electrical resistivity with respect to the filler quantity is approximately the same for all types of admixtures (the higher the GNPs content the higher the resistivity, whereas the higher the UFS content the lower the resistivity).

However, the values obtained from the DC method and those obtained from the AC tests show some differences, in particular after the first two weeks of curing. Up to 14 days of curing, the two measurement systems show similar results and widely comparable values. After 21 days of curing, the resistivity of mortars increases considerably, and the results obtained by the AC tests diverge, with higher values than those obtained by the DC tests. At the end of the detection period (28 days) the REF resistivity measured in DC is 21689 Ω·cm, against the 47997 Ω·cm obtained with the AC method. In general, the resistivity values obtained with the AC method are higher if compared to those obtained with the DC method, for all types of pastes (with increases up to 100%, Fig. 6.31).

This phenomenon is probably linked to the polarization effect, which increases when the material becomes more capacitive, that is when its resistivity increases [152]. This leads to reading differences between DC system and AC system (in which the polarization effect does not occur) [148].

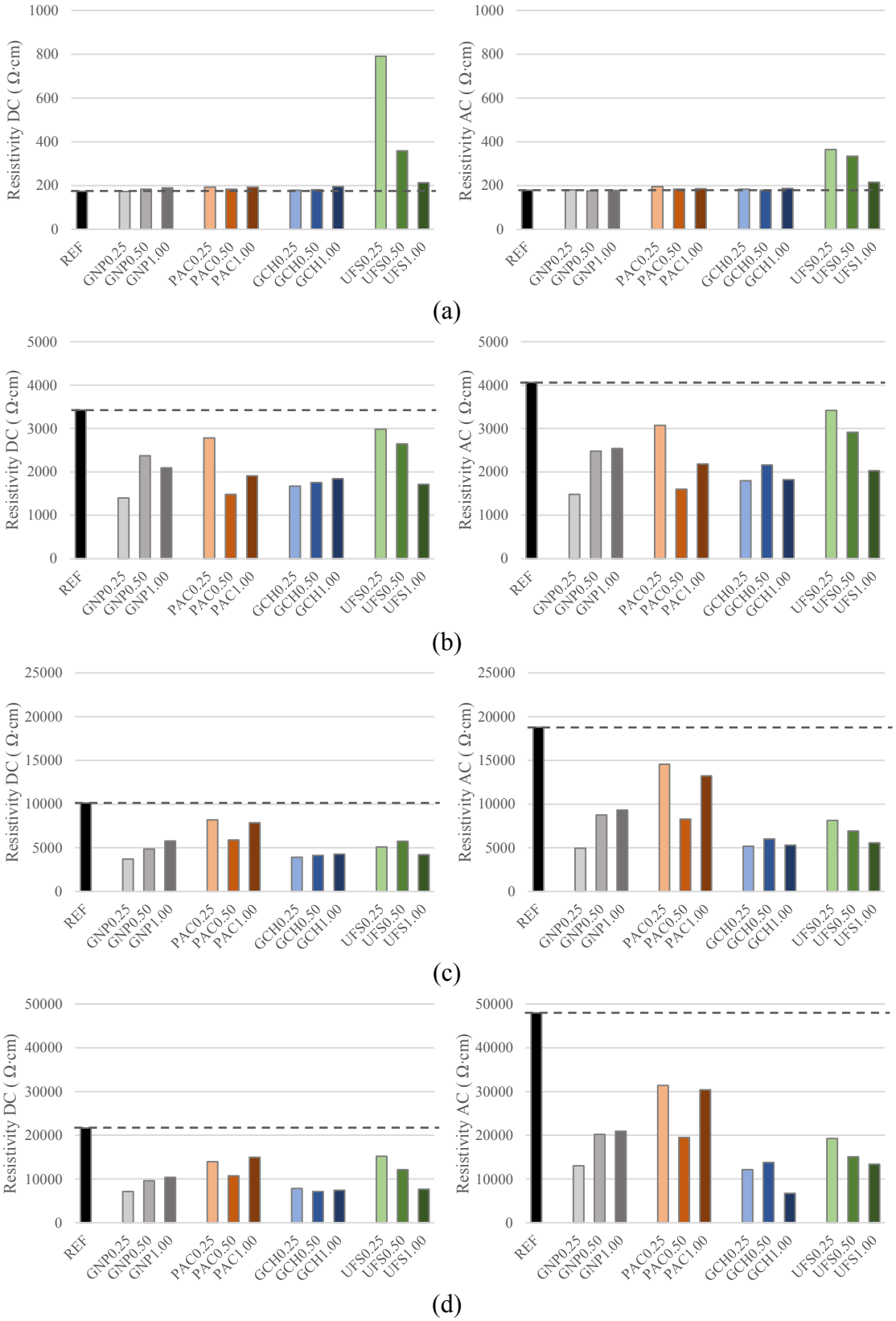

Figure 6.31. *DC (left) and AC (right) electrical resistivity (ρ) of pastes after: a) 7, b) 14, c) 21, and d) 28 days of curing*

6.4.5 Electromagnetic shielding properties

It is well-known that generally at the lowest electrical resistances, thus at the highest electrical conductivities, the best results are found for the SE [71][125][305]. Since the lowest electrical resistivity values were found for waste carbonaceous fillers at the highest percentages (1.00 wt.% on the lime, 13.75 g/L) and for the commercial one at a content of 0.50 wt.% on the binder (6.87 g/L), the SE was determined only on specimens with these filler dosages.
The SE was measured on mortars, since a perfect adhesion between the specimens and the mold used for the test should be ensured. Results obtained are given in Fig. 6.32.
In general, the SE of mortars was very low, since they were manufactured with hydraulic lime. This is because the NHL-based composites have a lower density compared to the materials made realized with ordinary Portland cement, due to the lower reactivity of the lime. This leads to a reduction in EMI shielding properties, which are also influenced by the mass of the material [306]. All mortars with carbonaceous additions registered a higher SE, or at least similar, to that of the reference one (M REF). Only M PAC 0.50 specimen showed a lower SE than M REF at each investigated frequency value. On the contrary, the M GNP 0.50 mortar showed a SE always 1 or 2 dB higher than the reference one.

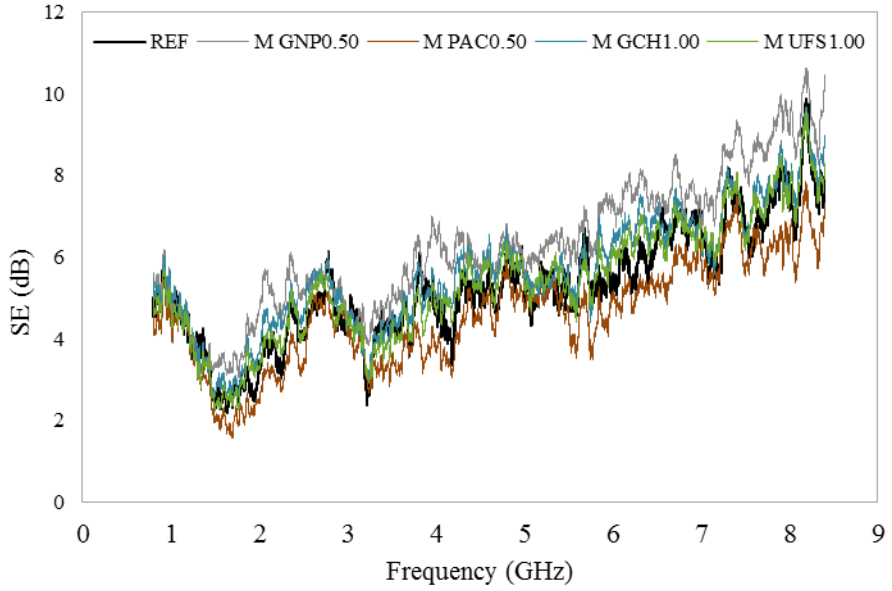

Figure 6.32. *Shielding effectiveness (SE) of mortars after 21 days of curing*

To analyze with more details results, Fig. 6.33 reports figures enlarged at 2 – 3 GHz, 4 – 5 GHz and 6 – 7 GHz, since in these ranges differences between all the manufactured mortars were more visible. These frequencies are mostly familiar with wireless communication systems. Frequencies of 2.1 GHz and 2.6 GHz are used for telecommunication mobile phones, Universal Mobile Telecommunications System (UMTS) and fourth generation Long Term Evolution (4G-LTE), respectively. Moreover, 2.45 GHz for the Bluetooth standard, whereas 2.4 GHz and 5 GHz are used for wireless networks. The frequency of 7 GHz is dedicated for point-to-point narrow band systems,

as *Plesiochronous Digital Hierarchy/Synchronous Digital Hierarchy* (PDH/SDH). In these frequency ranges, the increase of the SE was around 30% with respect to the reference mortar when M GNP 0.50 was tested. Also carbonaceous waste fillers enhanced the SE at 2 – 3 GHz, 4 – 5 GHz and 6 – 7 GHz compared to the M REF mortar, even though the general improvement was around the 6% for M GCH 1.00 mortar. These results confirmed that the two types of fillers that gave the lowest electrical resistivity to pastes are those that gave the higher SE values. Therefore, even if GNP is surely the most effecting filler for enhancing the electromagnetic shielding properties of binder-based materials, also waste carbonaceous fillers, with no cost, can slightly improve this property.

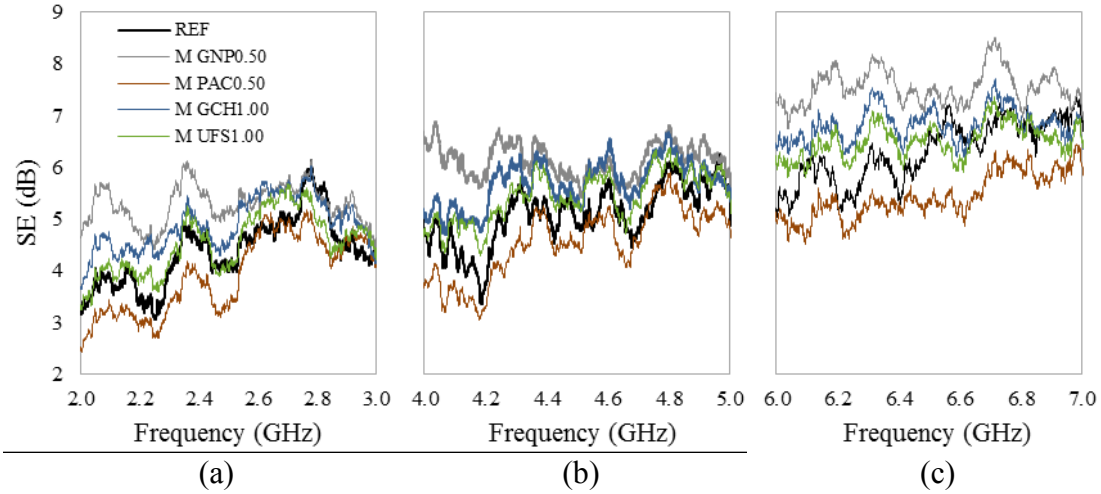

Figure 6.33. *Shielding effectiveness (SE) of mortars after 21 days of curing in the ranges of frequencies between a) 2 – 3 GHz, b) 4 – 5 GHz, and c) 6 – 7 GHz*

6.5 Conclusions

In this first part of the research, the use of both commercial and waste carbon-based micro-fillers in hydraulic lime pastes and mortars was evaluated in terms of mechanical, durability, electrical and electromagnetic properties. As commercial fillers, graphene nanoplatelets (GNP) and powdered activated carbon (PAC) were used. As waste fillers, a char (GCH) obtained by gasification process of biomasses and the finer fraction of a used foundry sand (UFS) were chosen. Fillers were added at 0.25, 0.50 and 1.00 wt.% on the lime weight.
The obtained results suggest the following conclusions:

- The addition of the carbonaceous fillers in the paste, regardless of their nature and amount, is essential to lower the *total porosity* and reduce the *pores size* of the paste. The resulting "filler effect" enhances the tensile strength of 40% and 20% when GNP and PAC are added at 1.00 wt.% on the lime, respectively. Especially compressive strength is increased for all type of additions, both commercial and waste;
- The reduced porosity and the decrease of the average pore diameter lower the *capillary water absorption* of pastes at each percentage and type of carbonaceous

addition, both at short and long time of contact with water. In particular, at early ages, the capillary water absorption is decreased more than 50% with GNP and UFS;

- The *depollution capability* of pastes, in terms of MEK adsorption, enhanced mostly by the addition of 1.00% of PAC. However also both waste fillers, at all percentages, showed very good adsorption capacity, even equal to 50% when foundry sand is added;
- No one of the carbonaceous fillers is effective in giving a *photocatalytic activity* to pastes in absence of a photocatalytic agent. Under UVA radiation and in the presence of TiO_2, the carbonaceous fillers even decrease the photocatalytic behavior because of the darkening of the paste;
- Both commercial and recycled carbon fillers effectively reduce the *electrical resistivity* of pastes, with average decreases of 50%. This effect is linked to the refinement of the microstructure and to the carbonaceous nature of the admixtures. The most effective powders are GCH and GNP, which decrease the resistivity up to 70%. This results could be particularly interesting for the development of "self sensing" mortars/concretes for SHM systems;
- Fillers that provide greater conductivity increases (GCH and GNP) are also those that ensured the highest *electromagnetic interference shielding effectiveness*, by 6% in the case of GCH and even by 30% in the case of GNP.

In view of the obtained results, it can be stated that the various recycled carbon-based fillers achieve the same performance of commercial fillers for all the analyzed functionalities. Foundry sand proved to be particularly effective in increasing the mechanical performance and durability of the pastes, by reducing total porosity. Gasification char has instead effectively improved the electrical conductivity of the mixtures, with better results compared to graphene.
On the other hand, no type of filler has shown interesting results in terms of depolluting capacity, and they have shown only poor improvements in electromagnetic shielding.
However, it is evident that recycled industrial by-products have shown potentials that are broadly comparable with those of the more expensive commercial nano-fillers, such as graphene, carbon nanotubes or carbon black.
Therefore, the next phase of the research was mainly focused on the promising electrical properties of recycled fillers, analyzing their potential use for the production of strain-sensing mortars and concretes.

7 . Chapter

Development of conductive mortars by Carbon/Steel fibers addition

Assessment of electrical, mechanical and durability properties of structural mortars with conductive fibers addition

7.1 Introduction

In the first part of the experimentation on lime paste, the electrical conductivity tests provided the most interesting results. In particular, recycled carbon-based fillers showed better results than an expensive and technologically advanced nanomaterials such as graphene, decreasing the electrical resistivity of compounds up to 70%. These results have focused the research interest on the potential of conductive cement materials in the civil engineering sector for structural monitoring.
In recent years there has been a growing awareness on *infrastructures safety*, especially in countries with a high seismic risk, where the nature of the territory constantly endangers the existing building heritage (Fig. 7.1a) [307].
To date, the need for efficient monitoring systems is deeply felt, due to recent catastrophic events caused by the lack of adequate interventions on concrete works, resulting in serious economic and human loss [308] (Fig. 7.1b).

(a) (b)

Figure 7.1. *a) Seismic damage of a reinforced concrete structure (crisis of the pillar-beam node), b) Morandi bridge (Genoa, Italy) after collapse (August, 2018)*

As seen, a promising research strand for the introduction of durable and effective monitoring systems is represented by electrically conductive and *self-sensing concretes* for self-monitoring systems. The recycled fillers analyzed in the preliminary experimentation could be inserted in this sector, for the realization of low-cost conductive concretes that can be used on a large scale.
The next phase of experimentation aims to increase the potential of fillers through the combined effect of these powders and other additions with proven electrical effectiveness, i.e. through the production of hybrid composites [71][183] entirely made with recycled materials.
From the literature review reported in Chapter 4, the high effectiveness of carbon fibers has been found, i.e. the first conductive additions used for the realization of piezoresistive concretes [13]. It has long been recognized that the addition of carbon fibers to concrete offers convenient and practical improvements in various mechanical properties of the structural material, such as enhanced toughness, fatigue resistance, impact resistance, tensile strength, flexural strength, reduced creep and shrinkage and improvements in the post-cracking behavior [202].

Furthermore, some research demonstrated that the addition of even a small amount of CF to cement paste significantly reduces the resistivity of the material.
CFs also offer a great contribution to the piezoresistivity of the material, thanks to their particular interaction with the cement matrix (because of the *tunneling* and *pull-out* effect, Fig. 7.2 [207]).

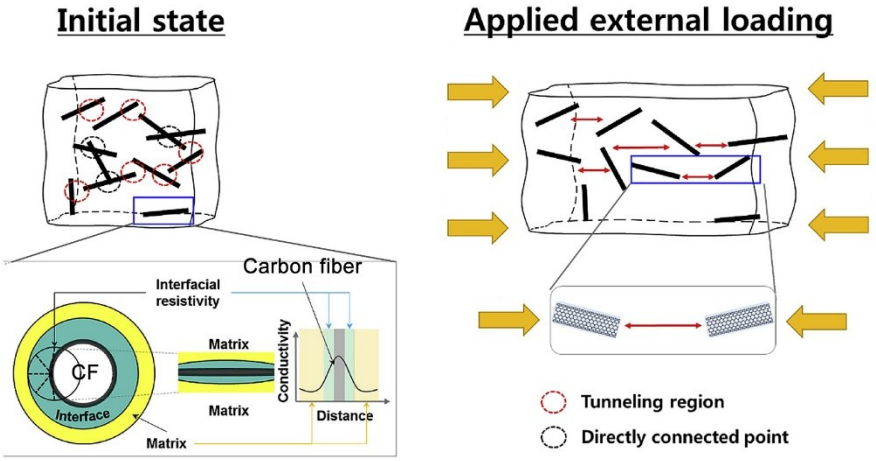

Figure 7.2. *Schematic illustration of the piezoresistive effect of CFs in cement based materials* [309]

By combining the effects of fillers and fibers, a multifunctional hybrid composite could be created, integrating the electrical and mechanical properties of the fibers with the improvement of the cement paste microstructure offered by the fillers, creating a more resistant, durable and stress-sensitive material [183].
In this part of the research, the effects of carbon-based fibers on structural mortars were studied, analyzing a high number of concentrations, in order to identify the electric percolation thresholds and the optimal dosages in terms of mechanical performances. This is a preparatory study phase to the last part of the research, where hybrid composites will be realized combining filler and fiber additions, evaluating their electrical and piezoresistive properties.
Two types of carbon fibers have been selected: virgin carbon fibers of commercial use and recycled carbon fibers obtained by industrial processes. The recycled fibers have been studied with the aim of creating cheaper and eco-friendly composites.
Furthermore, a third type of metal fiber has been tested, that is steel fibers with a brassed coating. This type of fiber is widely used in the production of reinforced mortars and concretes, and their proven mechanical and electrical properties are useful as comparison for the obtained results.
The mortars were realized by dispersing the 3 types of fibers in 7 different concentrations. Tests of workability, mechanical resistance (flexural strength, tensile splitting strength, compression and CMOD), durability (free hygrometric shrinkage, capillary water absorption) and electrical conductivity were carried out on the mortar specimens. As for the previous study phase, the results obtained have been enhanced through microstructural SEM and porosimetric analysis. The following are the production methods and the compositional characteristics of the mortars, together with the description of test methodologies and the analysis of the results.

7.2 Materials and Mortars composition

An *ordinary Portland cement* (OPC) COLACEM CEM I 52.5R (according to UNI EN 197-1) was used for the production of mortars. This type cement endows the hardened composite with high mechanical strength, thanks to its high fineness and reactivity (Section 5.2.1), and has been selected to obtain a greater workability of the mixtures [33], in particular with high fibers concentrations. For the same reason, a fine aggregate was selected, i.e. *silica sand* with grain size ≤ 1 mm (Section 5.3). Some study demonstrated that the use of finer cements and aggregates improves the workability of composites with high contents of fillers and fibers [95][33].
An aggregate/cement (a/c) ratio of 1.5 was used, according to many studies performed on CFRC (where values are generally placed between 1.0 and 2.0) [81][310][311]. The w/c ratio is equal to 0.5.
The three different types of used conductive fibers are: short cut *Virgin Carbon Fibers* (VCF) *SFC-EPB* from STW, *Recycled Carbon Fibers* (RCF) *CGF-6* from APPLY CARBON and *Brassed Steel Fibers* (BSF) *Dramix® OL6/.16* from BEKAERT (Fig. 7.3). All fibers have a length of 6 mm, which has provided good conductivity increases in several experiments [175]. Table 7.1 shows a summary of the dimensional characteristics. For a better description of fibers and their technical specifications, see Chapter 5.

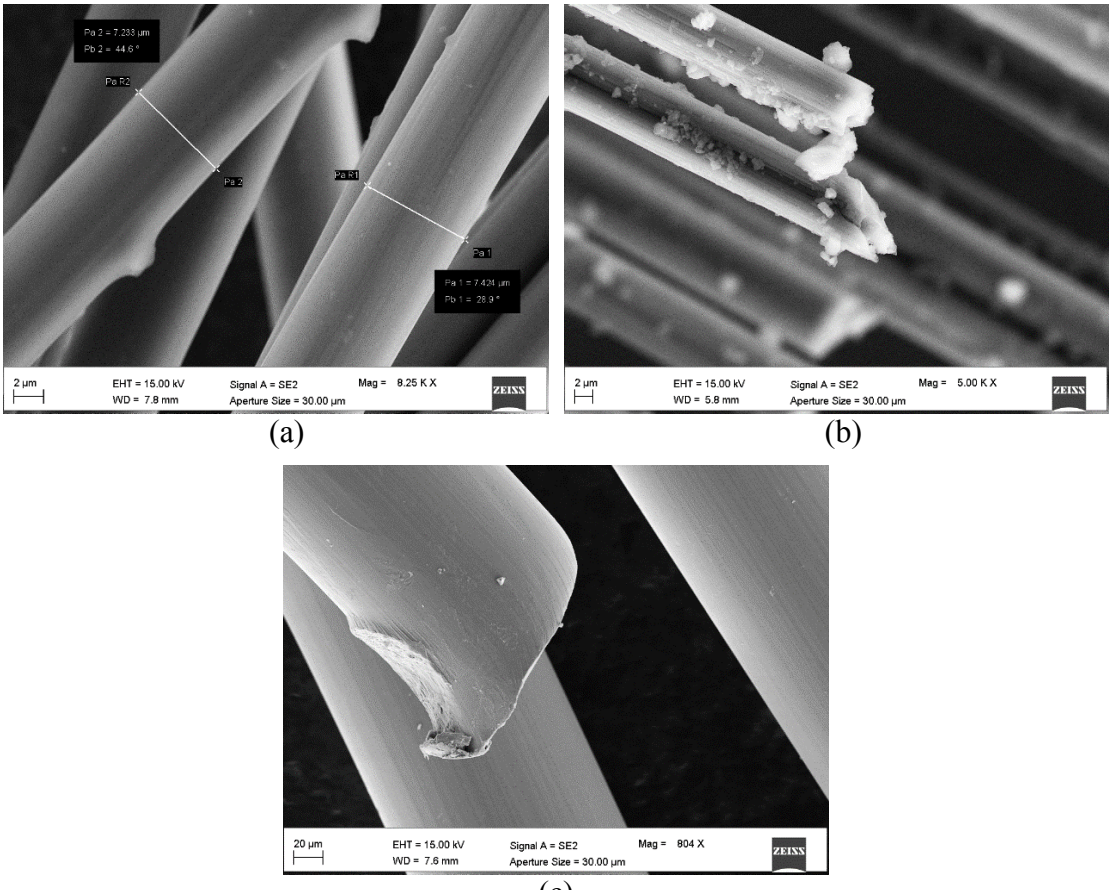

(a) (b)

(c)

Figure 7.3. *SEM scanning on the conductive fibers: a) Virgin carbon fibers, b) Recycled carbon fibers, c) Brassed steel fiber*

Table 7.1. *Physical and dimensional characteristics of fibers*

Fibers	Commercial name	Length (mm)	Diameter (μm)	Aspect ratio	Specific Surface area (m^2/g)	Density (g/cm^3)
VCF	SFC-EPB	6	7	857	0,229	1.78
RCF	CFG-6	6	5-9	857	0,195	1.7-2.0
BSF	OL 6/.16	6	160	38	0.003	7.87

The fibers were added in 7 different concentrations as a percentage of the mortar volume. 4 dosages were chosen based on the quantities frequently used in the production of fiber-reinforced premixed mortars [312], i.e.: 0.05, 0.1, 0.2, 0.4 vol.%. Moreover, three high concentrations were analyzed, in order to maximize the electrical properties of the materials [205][168], i.e.: 0.8, 1.2, 1.6 vol.%.
To facilitate the mixing of mortars with high contents of CFs, a high-performance polycarboxylate ether SP *Melflux® 4930F* (BASF) was added [16][101], proportionally to the amount of fibers (from 0.9 to 1.8 on cement wt.%). Overall, 21 different fiber-reinforced mortars were produced, together with a plain mortar without fibers addition (REF). Mix proportion of mortars are reported in Table 7.2.

Table 7.2. *Mix proportions of mortars*

Mixtures	OPC (g/L)	Water (g/L)	Sand ≤ 1mm (g/L)	Fibers (g/L)			SP (g/L)	w/b	Fibers volume (cm^3/L)
				VCF	RCF	BSF			
REF	720	360	1080	-	-	-	-	0.5	-
0.05VCF	720	360	1080	0.9	-	-	-	0.5	0.5
0.1VCF	720	360	1080	1.8	-	-	-	0.5	1.0
0.2VCF	720	360	1080	3.6	-	-	-	0.5	2.0
0.4VCF	720	360	1080	7.3	-	-	-	0.5	4.0
0.8VCF	720	360	1080	14.5	-	-	6.6	0.5	8.0
1.2VCF	720	360	1080	22.0	-	-	9.4	0.5	12.0
1.6VCF	720	360	1080	29.0	-	-	12.9	0.5	16.0
0.05RCF	720	360	1080	-	0.9	-	-	0.5	0.5
0.1RCF	720	360	1080	-	1.8	-	-	0.5	1.0
0.2RCF	720	360	1080	-	3.6	-	-	0.5	2.0
0.4RCF	720	360	1080	-	7.3	-	-	0.5	4.0
0.8RCF	720	360	1080	-	14.5	-	6.6	0.5	8.0
1.2RCF	720	360	1080	-	22.6	-	9.4	0.5	12.0
1.6RCF	720	360	1080	-	30.3	-	12.9	0.5	16.0
0.05BSF	720	360	1080	-	-	4.0	-	0.5	0.5
0.1BSF	720	360	1080	-	-	8.0	-	0.5	1.0
0.2BSF	720	360	1080	-	-	16.1	-	0.5	2.0
0.4BSF	720	360	1080	-	-	32.2	-	0.5	4.0
0.8BSF	720	360	1080	-	-	64.3	-	0.5	8.0
1.2BSF	720	360	1080	-	-	96.3	-	0.5	12.0
1.6BSF	720	360	1080	-	-	128.3	-	0.5	16.0

The mortars were initially prepared by manually mixing OPC and sand, then pouring the water and the SP (Fig. 7.4). During blending, through a Hobart mixer, the fibers were gradually added to ensure a better dispersion within the mortar. The final composite was mixed at variable speed, to ensure a homogeneous material [313], for at least 5 min. The fresh mortars were poured into molds, in order to realize 40x40x160 mm specimens, also using mechanical vibration, for a better compaction of the material [313].
Specimens were cured under controlled environmental conditions: at T = 20 ± 1°C and a RH = of 95 ± 5% for 7 days, then maintained at T = 20 ± 1°C and RH = 50 ± 5% until testing.

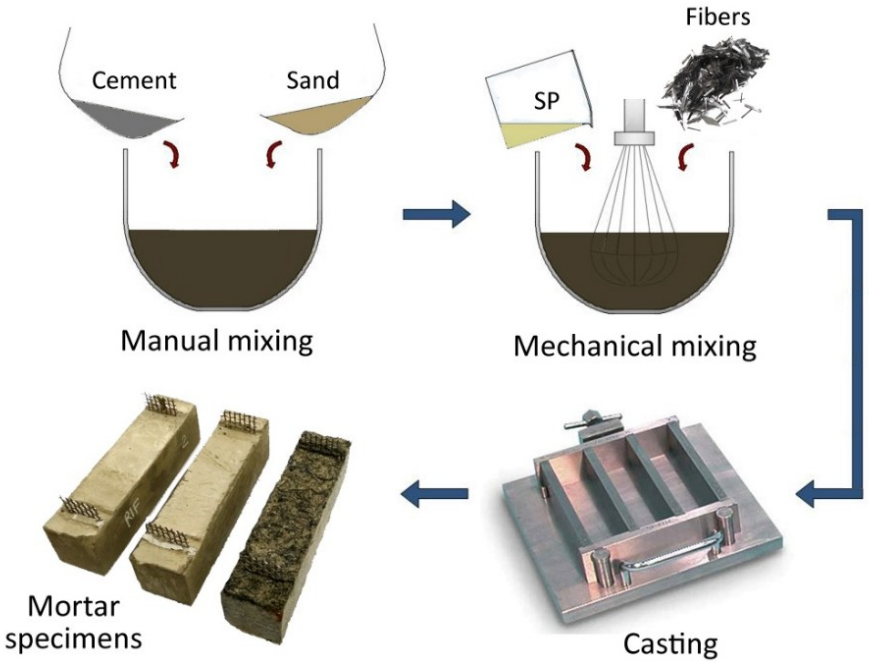

Figure 7.3. *Scheme of mortar Specimens fabrication process*

7.2.1 Workability

As in the preliminary experimentation on pastes (Section 6.2.1), the *workability* of the mixtures has been evaluated by means of slump test to the flow table and the relative calculation of the % consistency, according to UNI EN 1015-3:2007 standard. Results are reported in Table 7.3.

Table 7.3. *Flow values and C% of mortars (UNI EN 1015-3:2007)*

Mixtures	Flow value (mm)	C (%)
REF	199	99
0.05CCF	150	50
0.1CCF	151	51
0.2CCF	149	49
0.4CCF	144	44
0.8CCF	137	37
1.2CCF	122	22
1.6CCF	114	14
0.05RCF	182	82
0.1RCF	165	65
0.2RCF	139	39
0.4RCF	126	26
0.8RCF	130	30
1.2RCF	122	22
1.6RCF	116	16
0.05BSF	149	49
0.1BSF	145	45
0.2BSF	162	62
0.4BSF	158	58
0.8BSF	160	60
1.2BSF	150	50
1.6BSF	143	43

The results show the high flow values (C% ≥ 50) of reference mortar and mortars with the addition of BSF (both high and low quantity), and low quantities of VCF and RCF. These mixtures have all shown good workability, and good amalgamation.
Contrariwise, the mixing of mortars with a high content of carbon fibers (≥ 0.8 vol%) proved to be problematic, due to the hygrometric behavior of CF. In fact, the carbon fibers agglomerates tend to absorb mixing water, worsening the workability of the mortar during the mixture. Subsequently, when the fresh mortar undergoes mechanical stress (e.g. during casting), the fiber tufts release the absorbed water, creating bleeding and segregation effects (Fig. 7.4). This problem has been partially solved by adding SP. However, beyond a certain threshold, the addition of SP does not provide any further effect.

(a) (b)

Figure 7.4. *Effect of fibers during blending: a) fresh 0.8 BSF mortar, b) 0.8 VCF with water bleeding*

The difficulties in mixing of composites with a high content of carbon fibers are well known in literature [113][314], and this factor influences the microstructural properties of the mortars, as will be seen in the experimentation results (Section 7.4). In general, an increasing amount of carbon fibers decreases the C% (Table 7.3). This trend does not occur with BSF, whose values are between 40% and 60% regardless of the fibers concentrations.

7.3 Methods

7.3.1 Mechanical properties

The effect of conductive fibers on the mechanical properties of mortars are investigated by flexural (R_f), tensile splitting (f_{ct}) and compressive (R_c) strength tests on 40x40x160 mm specimens, according to UNI EN 1015-11:2007 and UNI EN 123906:2010.
Flexural strength R_f was evaluated by three-point bending test, according to Equations 7.1:

$$R_f = 1.5 \frac{F \cdot L}{b \cdot h^2} \tag{7.1}$$

Where F = maximum flexural force; L = distance between the bending supports (100 mm); b = specimen width (40 mm); h = specimen height (40 mm).
Tensile splitting strength and compressive strength were calculated as seen in the previous tests on pastes (Section 6.3.1).

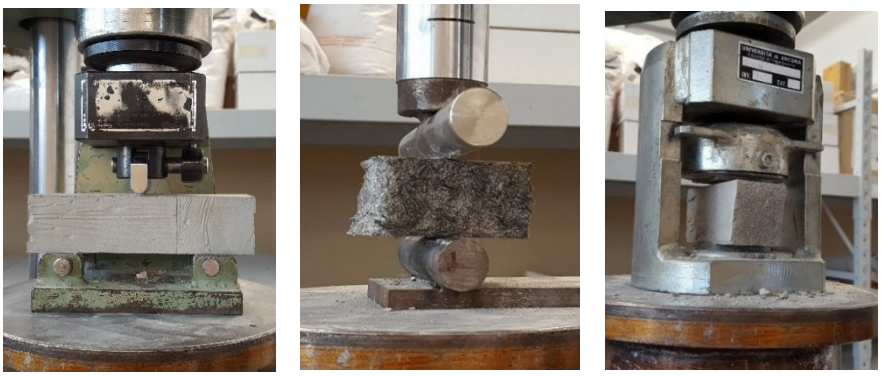

(a) (b) (c)

Figure 7.5. *Mechanical strength tests on fiber-reinforced mortars: a) Flexural strength, b) Tensile splitting strength, c) Compressive strength*

7.3.1.1 Crack Mouth Opening Displacement measurement

The post-cracking mechanical contribution of conductive fibers and the ductility of the fiber-reinforced composites were evaluated by means of flexural tests with a *Crack Mouth Opening Displacement* extensometer (CMOD test), according to UNI EN 14651:2007 and RILEM TC-50 standards.
Specimens of fiber-reinforced mortars 40x40x160 mm were used for this test. In the specimens a notch was cut with a depth of 10 mm (1/4 of the section height) and 1 mm of thickness, in order to obtain a controlled cracking during opening (Fig. 7.6).
The specimens were subjected to three points bending tests, continuously measuring the opening of the crack by a displacement transducer installed on a slot at the base of the notch (Fig. 7.6a).

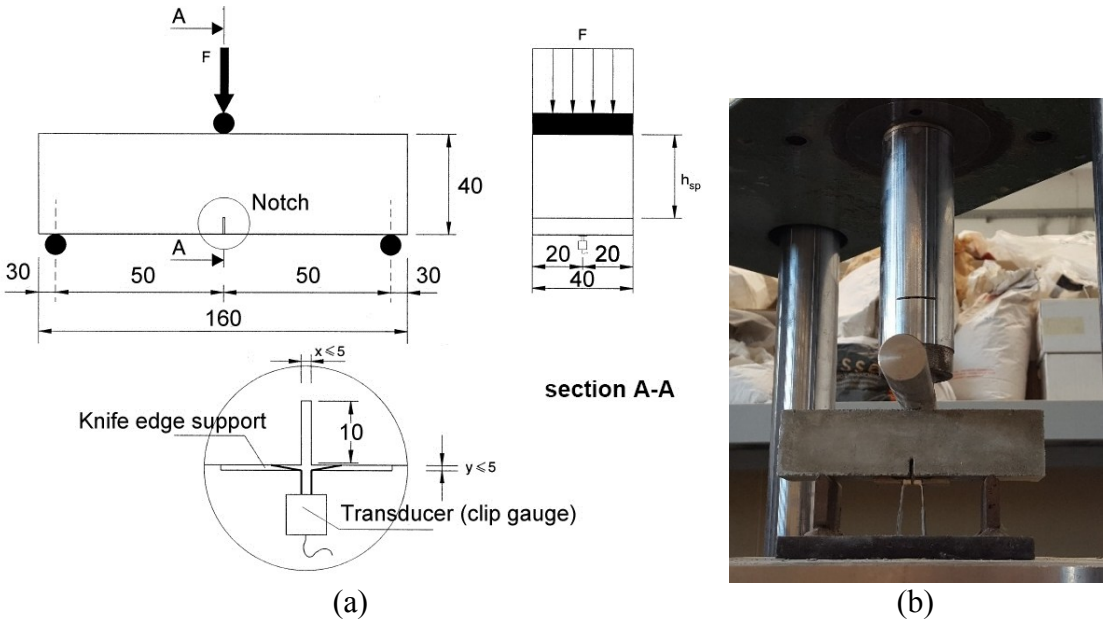

(a) (b)

Figure 7.6. *Measurement of the CMOD: a) Schematic setup and instrumentation, b) Fiber-reinforced mortar specimen under test*

Measuring the bending force (F) and the corresponding crack opening value, the σ_f - CMOD curves were obtained, where σ_f = flexural stress (MPa), *CMOD* = Crack opening deformation (mm/m). From the σ_f - CMOD graphs, the reinforcing properties of fibers were studied, by calculation of:

- *Ultimate CMOD* value, opening of the crack to the maximum load;
- $f_{R,j}$, strength at maximum load;
- E_f, the crack Young's modulus (N/mm^2), calculated in the portion of the load-CMOD curve preceding the limit of proportionality (LOP), in accordance with the RILEM recommendations [315];
- Cracking *toughness*, from the area under the σ_f – CMOD curve (Eq.7.3).

$$toughness = \int_0^{CMOD} f(\sigma_f) dCMOD \tag{7.3}$$

7.3.2 Durability

7.3.2.1 Capillary water absorption

As in the experimentation on the pastes, the durability of the mortars has been assessed by means of *capillary water absorption* tests in the short and long period (Section 6.3.2), i.e. through the calculation of the absorption coefficient C according to UNI EN 1015-18:2004 and the water absorbed in the unit area Q_i, according to UNI EN 15801:2010, respectively.

7.3.2.2 Drying shrinkage

The durability of the mortars was also studied through tests for the evaluation of *hygrometric shrinkage*. The free drying shrinkage measurement is an important parameter to appraise the propensity to crack of cement-based material in presence of mechanical constraints, such as reinforcing bars or supports. This phenomenon greatly affects the life cycle of concrete. The drying process of the material during the curing period (or at very low humidity) triggers mechanical stresses, due to the different drying speeds between the surface and the internal areas. If these stresses exceed the tensile strength of concrete, cracks arise, which cause the degradation process, facilitating the infiltration of pathogens elements [224][316].
Generally, the lower the hygrometric shrinkage during the material drying, the lower the occurrence of cracking phenomena [26].
The effectiveness of the fibers in reducing the shrinkage cracks opening has been extensively studied and demonstrated in the literature [259]. In this research, the effect of conductive fibers in free drying shrinkage of composites was assessed by measuring the longitudinal strain of a mortar specimen, related to the water loss during the curing period. Specimens of dimensions 40x40x160 mm have been used for this test, realized by embedding steel linchpins at the ends of the specimens, to fit the measuring instruments. Specimens have been maintained at T = 20 ± 1°C and a RH = of 95 ± 5% for 24 h. After the first 24 h, the specimens were removed from the molds, and their longitudinal size was measured using a micrometer (sensitivity 5 μm). The *shrinkage strain* of the specimens ε_s (mm/m) was measured during the curing period by their differences in length ΔL, measured with a fixed length reference steel bar (Fig 7.7), according to Equation 7.3:

$$\varepsilon_s = \frac{\Delta L_i}{L_0} = \frac{L_i - L_0}{L_0} \tag{7.3}$$

Where, L_i = specimen length at time i, L_0 = specimen initial length.

(a) (b)

Figure 7.7. *Measurement equipment of shrinkage strain: a) Comparison measure of steel reference bar, b) Measurement of a mortar specimen*

Furthermore, the *weight loss* by the specimens was measured during the curing period, as a percentage of the initial weight, in order to relate the hygrometric shrinkage strain to the amount of water lost.
The measurements were performed for 82 days. After the first 24 hours, specimens were maintained at T = 20 ± 1°C and RH = 50 ± 5% until the end of experiments.

7.3.3 Microstructural characterization

As in the preliminary experimentation on the pastes, the data obtained from the tests on mortars have been validated by microstructural analyzes after 28 days of curing (see Section 6.3.3).
The *total porosity* V_p and the *pore distribution* of the mixtures were analyzed with a MIP Thermo Fisher 240 Pascal.
Microscopy and EDX analyzes were performed through a scanning electron microscope *ZEISS NEON* High Resolution SEM (Fig. 7.8).

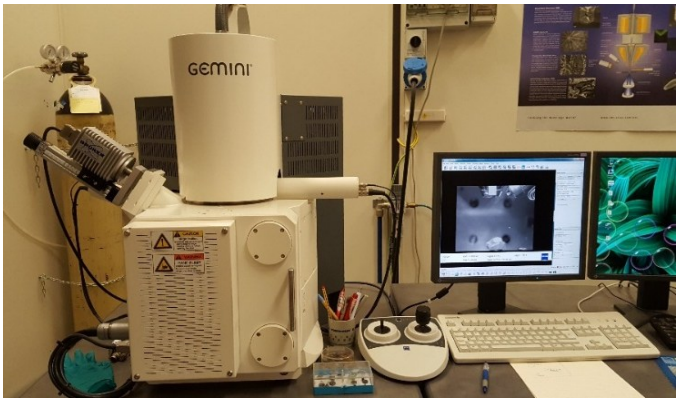

Figure 7.8. *ZEISS NEON High Resolution SEM*

7.3.4 Electrical conductivity

The main objective of this research phase is the study of the electrical contribution of different types of conductive fibers, in order to identify the percolation thresholds and the optimal concentrations for the realization of highly conductive composites, maintaining good workability and high mechanical strength.
For this reason, an accurate study of the measurement system is important for obtaining scientifically reliable data and an effective comparison of results.
As seen in Chapter 3 (Section 3.3), within the multifunctional cement composites, various types of conductive paths are implemented, some linked to conductive additions (electronic conduction) and some linked to the cement matrix (ionic conduction) [317]. High fiber content mortars have a characteristic electrical behavior, which requires a thorough analysis of the results. Preliminary investigations on electronic measurements setup have been carried out to study the best configuration and the best test methodology.

7.3.4.1 Preliminary investigations

For the optimization of the measurement system, specimens with 2 different configurations (Fig. 7.9) and different types of electrodes were realized. 3 different types of stainless steel grids were used as external electrodes: 1) #16 Mesh, with 1.03 mm of aperture; 2) #6 Mesh, with 3.50 mm of aperture; 3) #4 Mesh, with 5.45 mm of aperture. The grids were chosen to study a better cohesion at the interface between the electrode and the matrix [6][184]. Stainless steel rods (Ø 3 mm) were used as internal electrodes, placed at variable distances from the external electrodes (from 20 mm to 45 mm), in order to study the effect of distance in the DC measurements.

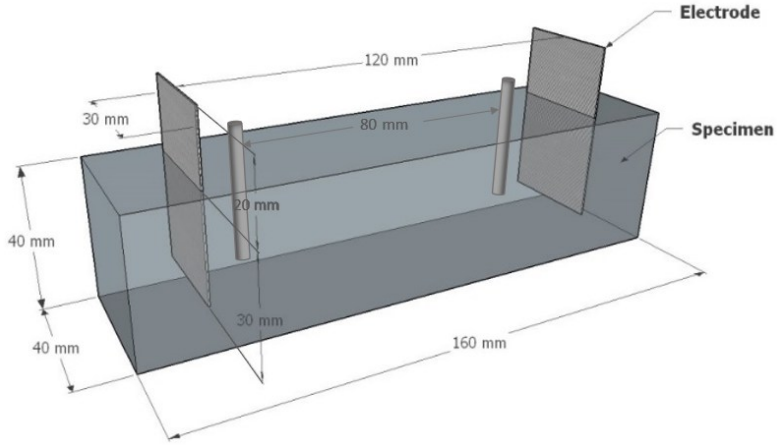

(a)

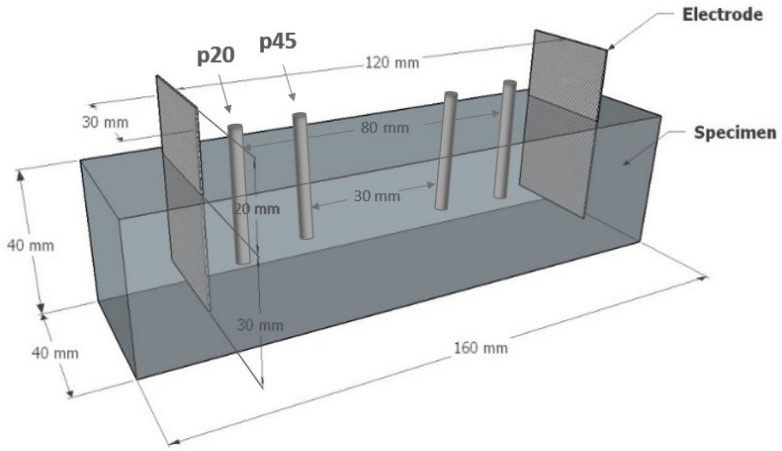

(b)

Figure 7.9. *Dimensional characteristics of the configurations studied in the preliminary electrical tests: a) 4-probe system, b) 4-probe system with different distances between the internal electrodes*

After measuring the cell constants K for both types of configuration (as explained in Section 6.3.5.1), resistivity measurements through both DC and AC devices were performed at 2, 7 and 19 days of curing. The results are shown in Figure 7.10.

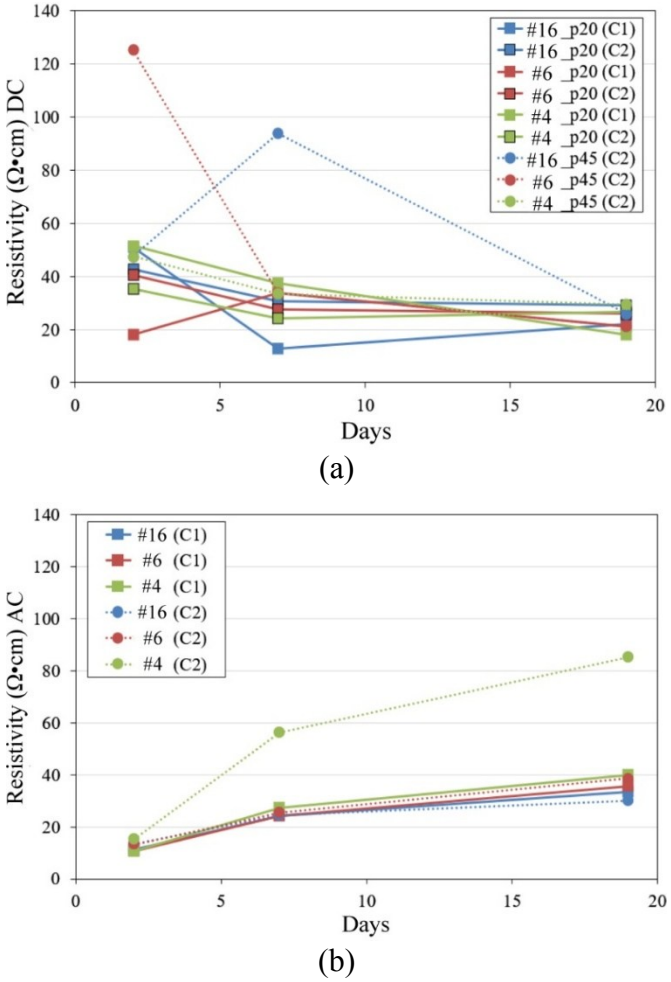

Figure 7.10. *DC (a) and AC (b) resistivity measurements on preliminary configurations (p20-45, C1-C2) with different types of grid*

The results obtained from DC tests show unusual values, since the resistivity of the mixtures decreases during the curing period. This effect is contradictory to the traditional behavior of cement-based materials [173][197], and does not derives from the different distances between the probes and the different types of grids. This phenomenon is probably due to the high content of CF, which, in a 4-probe system, create a continuous conductive paths between the external electrodes (grids) and the close internal probes (rods), thus eliminating the electrical contribution of the cement matrix (ionic conduction).

Contrariwise, the AC tests showed consolidated results, with an almost linear increase in resistivity during the curing period [197], thus analyzing the combined effect of the conductive fibers and cement matrix.

Because of these more reliable results, experimentation continued using the AC system with a two-probe configuration. The different meshes used for external electrodes did not bring significant measurement differences between them. Thus, for the final configuration, the intermediate grid Mesh #6 has been chosen, which guarantees a good incorporation.

7.3.4.2 AC resistivity measurement

Because of the results of the preliminary tests, an AC impedance measurement system was used for the electrical characterization of the mortars, detecting the electrical resistivity ρ at 2, 7, 14, 21, 28, 49, 70 and 91 days of curing.
40x40x160 mm specimens with embedded two stainless steel #6 grids with 3.5 mm of aperture and 0.71 mm of wire diameter were realized for the tests. By this configuration, a cell constant K of 0.7681 cm^{-1} was measured.
The dimensional characteristics of the specimens are shown in Figure 7.11.

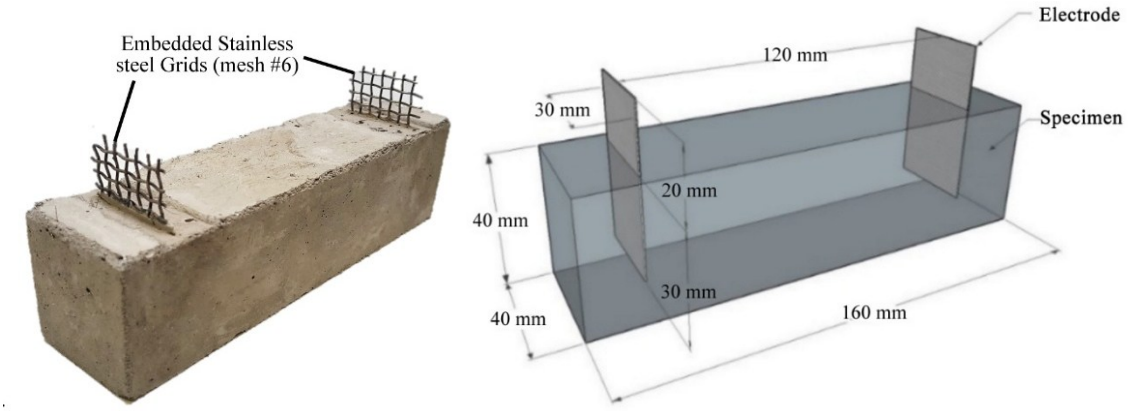

(a) (b)

Figure 7.11. *Specimen realized for electronic tests (a) and its dimensional characteristics (b)*

As seen in Section 3.5.2, AC impedance measurements with high frequency electrical signals are often used to avoid the polarization effect of the electrodes, and therefore, to measure only the resistivity of composite systems [314][318][319][320]. The electrical conductivity of the cement-based composites with metal/carbon-based fibers is divided into two types of conductive mechanisms: electrolytic and electronic (Section 3.3) [182][175]. Therefore, the resistivity of this composite system is determined in one hand by the *electrolytic resistivity* of the cement-based matrix, which contains the mobile ionic species coming from the mixing of the binder with the water [321], and on the other hand, by the *electronic resistivity* related to the transportation of free electrons through the conductive phase, which is constituted in this case by the carbon fibers. In particular, at AC high frequencies, a "*composite resistance*" [182], determined by the combination of both described mechanism, can be obtained.
Considering that the polarization contribution of the electrodes must not be included in impedance response, the low frequency limit of the measuring range was set to a relatively low value, corresponding to 10 Hz. The impedance measurements scan started from 1 MHz up to this low frequency limit. The whole range was swept by setting 10 points/decade in a *Gamry Reference 600* potentiostat (Fig. 7.12a). The AC signal had an amplitude of 10 mV.
The two steel grids (electrodes) were connected to the *working cable* (W-WS) and to the *counter cable* (C), respectively. The counter connection was short-circuited with the *reference* (R) connection, in order to set a two-probe configuration measurements (Fig. 7.12a) [182].

The *impedance data* (Z) were automatically imported and elaborated by setting a *phase angle threshold* (PAT), in order to select a set of impedance data having a phase angle within the range defined by ± PAT values.
Initially, PAT has been set to 1° and it has been varied, if necessary, to higher values in order to select at least a number of five impedance measurement data, from which the average value of log |Z| was calculated. In any case, PAT never exceeded 5° because the set of selected Z data must have a resistive reactance in order to be representative of the resistive behavior of the tested composite material: this means phase angles as close as possible to 0°. The |Z|-frequency and the phase-frequency relationships have been studied through the *Bode plots* (Fig. 7.12b).
The *resistance* R (Ω) of the fiber-reinforced specimens was then calculated using Equation 7.4:

$$R = 10^{\overline{\log|Z|}} \tag{7.4}$$

Using this procedure, the selected Z data ranged in the high frequency region of the impedance spectrum, approximately within 10-100 kHz, where R calculated from Equation 7.4 corresponds to the above-mentioned composite resistance (as better explained later).
The characteristic *resistivity* of the material ρ was thus calculated from the ratio between the resistance R and the cell constant K (Section 3.5.3.1, Eq. 3.13).

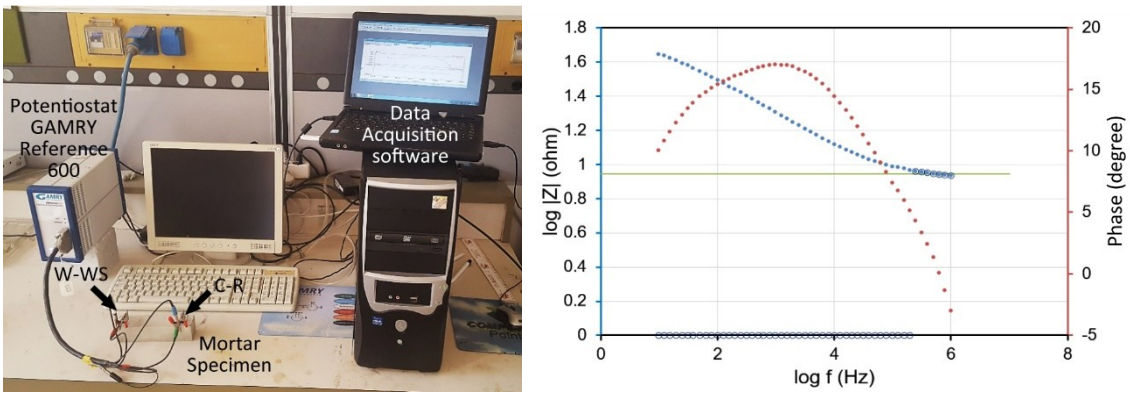

(a) (b)

Figure 7.12. *a) AC measurement equipment and specimen under test. b) Example of a Bode plot for data processing: The circled blue points are those selected for the measurement of |Z| (phase angle close to 0°)*

7.4 Results and discussions

7.4.1 Mechanical and microstructural characterization

The addition of fibers within the mortars has led to a noticeable increase in mechanical strength, particularly under flexural and tensile stress.
The development of mechanical strength of the mixtures during the curing period is shown in Table 7.4.

Table 7.4. *Flexural strength (R_f), Tensile strength (f_{ct}), Compressive strength (R_c) of the mortars (results are reported as percentage of the reference value on the right)*

Mixtures	R_f (MPa)			f_{ct} (MPa)			R_c (MPa)			REF comp. 28 days (%)		
	2 days	7 days	28 days	2 days	7 days	28 days	2 days	7 days	28 days	R_f	f_{ct}	R_c
REF	5.4	6.0	6.9	2.0	2.6	2.8	32.6	43.3	48.1	-	-	-
0.05VCF	6.0	7.0	7.5	2.8	3.7	3.9	43.3	47.5	54.4	109	136	113
0.1VCF	6.9	7.0	8.0	2.6	3.7	4.0	42.5	47.3	55.7	116	142	116
0.2VCF	6.8	7.5	8.5	2.5	3.9	4.7	38.3	44.4	56.6	124	167	118
0.4VCF	7.2	7.3	9.2	3.7	3.9	4	35.5	48.2	51.2	135	142	106
0.8VCF	8.6	9.1	11.2	4.2	4.3	4.7	30.2	37.6	45.1	163	166	94
1.2VCF	8	10.6	11.5	3.4	4.4	4.7	25.7	31.5	40.0	168	166	83
1.6VCF	6.3	10.6	11.8	2.4	4.1	5.0	15.2	35.7	44.4	171	174	92
0.05RCF	6.2	6.8	7.6	3.2	3.4	4.6	40.9	49.3	59.0	111	162	123
0.1RCF	6.2	6.9	7.4	3.8	4.6	4.9	41.1	51.0	53.3	107	173	111
0.2RCF	7.3	8.5	8.7	3.4	3.5	4.4	39.5	47.7	53.5	127	153	111
0.4RCF	8.5	8.9	9.7	4.2	4.4	4.4	37.6	47,4	54.7	141	156	114
0.8RCF	6.8	7.5	7.9	3.6	4.1	4.4	33.8	37.7	50.5	115	154	105
1.2RCF	9.0	10.8	12	4.0	4.7	5.4	29.6	40.1	46.2	175	192	96
1.6RCF	10.4	11.3	13.9	4.0	5.2	5.3	30.7	37.4	46.7	202	187	97
0.05BSF	7.1	8.0	8.3	3.3	3.6	4.5	46.6	54.4	64.6	120	157	134
0.1BSF	6.8	7.4	9.0	3.2	4.5	4.9	44.3	56.6	63.3	130	174	132
0.2BSF	6.9	7.2	8.8	3.9	4.4	4.6	43.2	54.3	66.1	128	161	138
0.4BSF	6.8	7.8	9.1	3.8	4.5	4.7	42.9	48.9	63.8	133	165	133
0.8BSF	8.0	8.6	8.8	3.5	4.5	5.1	46.2	55.2	65.3	128	181	136
1.2BSF	8.4	8.8	9.0	3.6	5.0	5.5	45.1	55	65.3	131	195	136
1.6BSF	9.7	9.9	10.6	5.1	5.4	6.0	46.2	58.5	64.6	154	211	134

The prominent contribution of fibers is visible from the three points bending tests results and from the R_f values (Fig. 7.13). All types of fibers provide an increase in mechanical strengths related to the amount of addition (the higher the fiber concentration, the higher the strength values), but this effect is less evident for BSF.

Table 7.4 shows the fast development of the flexural mechanical strength of fiber-reinforced mortars in the first days of curing, with an average value of 80% at 2 days and 90% at 7 days, compared to the final ones (28 days). The best results were obtained by CFs, in particular from the recycled ones, with increases up to 102% compared to REF (mortar 1.6 RCF).

The best results of VCF and RCF compared to BSF is due to their greater aspect ratio. As widely demonstrated in the literature, the aspect ratio has a considerable influence on the mechanical properties of fiber-reinforced composites [322]. The CF, with the same volume of addition, create more connections than the BSF, amplifying the stitching effect in the micro-cracks, the adhesion forces and the bridging effect [58].

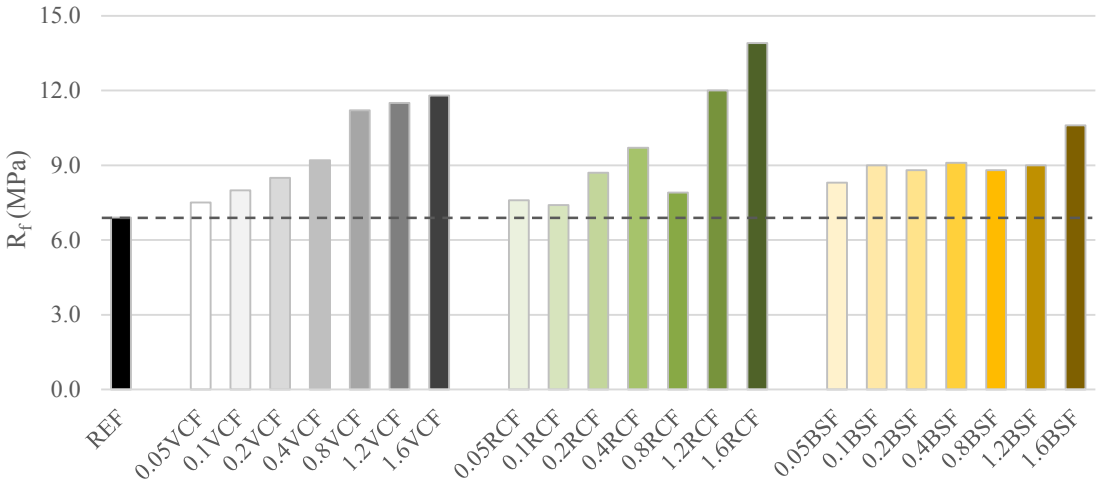

Figure 7.13. *Flexural strength R_f of mortars at 28 days of curing*

Similar results were obtained from tensile splitting strength tests (Fig. 7.14). The f_{ct} values are evidently related to the fibers content of the mixtures, although this connection is less evident than the flexural strength tests. Generally, all fiber-reinforced mortars (even with low fiber contents) show higher mechanical resistances than the reference, with increases ranging from 36% to 111% (for the 1.6BSF mortar).
The RCFs again show better results than VCF, particularly at low concentrations (0.05-0.1%). The best results of BSF are related to the relationship between tensile splitting strength and compressive strength for this type of test (*Brazilian test*, UNI EN 12390-6:2010) [323][324].

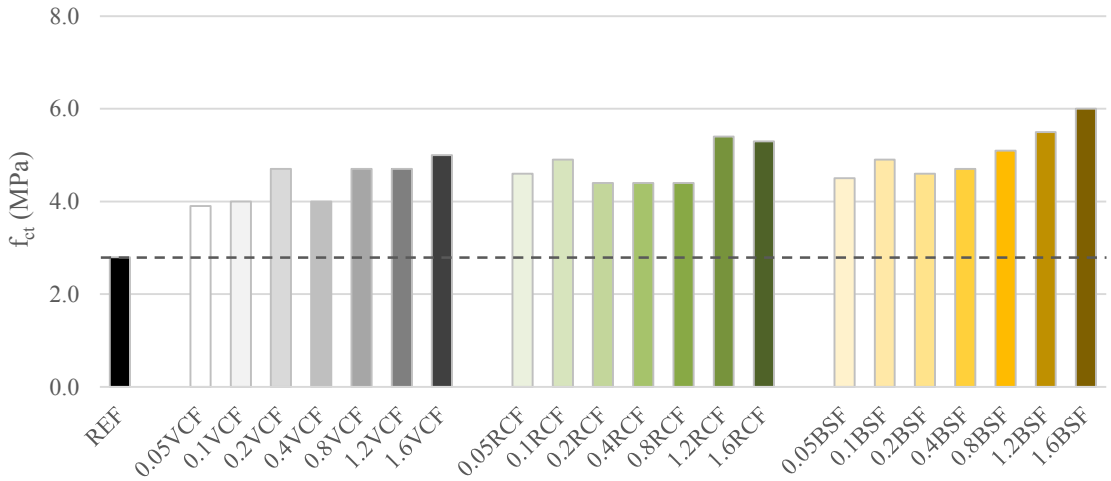

Figure 7.14. *Tensile splitting strength f_{ct} of mortars at 28 days of curing*

The values obtained from the compressive strength tests show a different trend compared to R_f and f_{ct}. In particular, there are clear differences between the R_c values of the mortars with low and high CF content. Generally, an increase in the amount of VCF and RCF leads to a decrease of compressive strengths. This trend does not occur with steel fibers reinforced mortars, which show similar R_c values, regardless of the amount of addition.

As can be seen from Table 7.4, the growth of compression strength is quite fast, since values reach 85% of the final resistances at 7 days.
The best results were obtained by 0.2 BSF mortar, with an increase of 38% compared to the REF value, while the mixtures with a high CF content slightly decreased the resistances compared to the traditional mortar (by 17%, for 1.2VCF). The best mechanical compression performances of BSFs are probably related to the structure of the specimens. As demonstrated [325][326], the fibers and their aspect ratio largely influence the flexural behavior of composite, but they have less effect on the compressive strengths, which are more dependent on other factors, such as the material density [26][260].
The adding of carbon fibers into the cement mortar up to a certain concentration enhances the mechanical properties thanks to its ability of restraining the growth of microcracks and absorbing energy by overcoming its pull out. However, when the carbon fiber content is too high, they will clump and cause air void, thus reducing mechanical compression performances [117].
As seen in paragraph 7.2.1, high doses of CF compromise the workability of the mixtures during the casting phase, increasing the macroporosity and segregation phenomena inside the specimens. This phenomenon does not occur with BSF, which do not interact with mixing water, allowing a better compaction of the mixture in the molds even with high fibers concentrations.

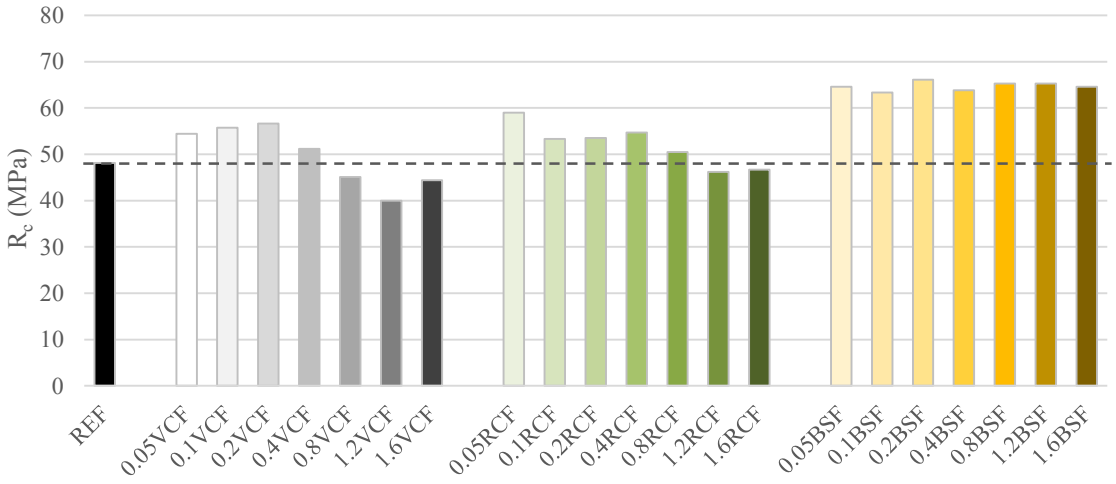

Figure 7.15. *Compressive strength R_c of mortars at 28 days of curing*

To provide further information to support the mechanical characterization and durability tests, porosimetric analyzes were performed on mortars containing both low and high fiber quantity (0.1 and 0.8 vol%), as well as on reference mortar. Table 7.5 shows the obtained V_p and d_p values.

Table 7.5. *Total porosity (V_p) and average pore diameter (d_p) from the porosimetric analysis of mortars*

Mixtures	V_p (%)	d_p (μm)
REF	21.3	0.080
0.1VCF	18.7	0.074
0.8VCF	15.1	0.052
0.1RCF	19.3	0.068
0.8RCF	15.0	0.056
0.1BSF	17.5	0.071
0.8BSF	15.3	0.068

The results showed that all types of conductive fibers interact with the cement matrix microstructure, reducing microporosity. Both CF and BSF decrease the total volume of micropores by approximately 29% compared to the reference. Both the pore volume and the critical pore diameter are related to the quantity of fibers, since the greater the concentrations of fibers, the lower the V_p and d_p values. Other authors have found relationships between the increase in the amount of CF and the decrease in microporosity of cementitious materials [327][328].
Figure 7.16 shows the porosimetric curves of the analyzed mixtures, where the fiber-reinforced mortars show both a smaller cumulative pores volume and a smaller pores diameter compared to the traditional mortar.

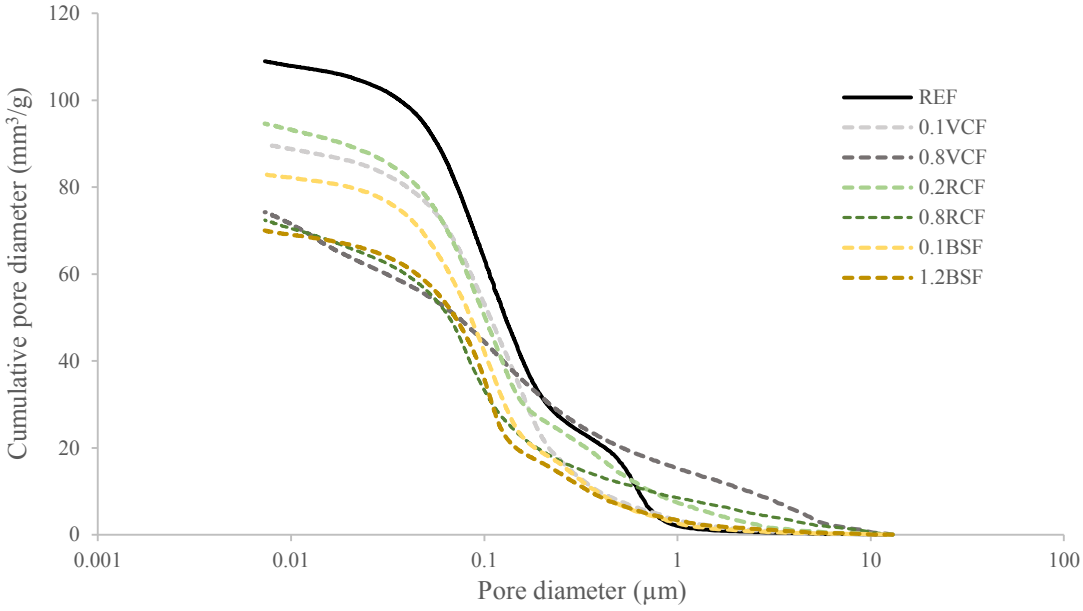

Figure 7.16. *Porosimetric curves of mortars*

However, the porosimeter used in this analysis is not able to detect the macroporities within the composite. Despite their low content of micropores, mortars with high concentration of CF could contain a large number of pores with diameters > 100 μm, due to the poor workability in casting phase and the consequent incorporation of air voids. Visual analysis on the surface of mortars with high CF amounts clearly shows irregularities due to the presence of macroporosity (Fig. 7.17). These macropores are not present in mortars with a high BSF content, which show a regular and smooth surface, similar to the reference mortar.
This phenomenon could be the reason for the lower R_c values of mortars with high contents of VCF and RCF (≥ 0.8 vol%).

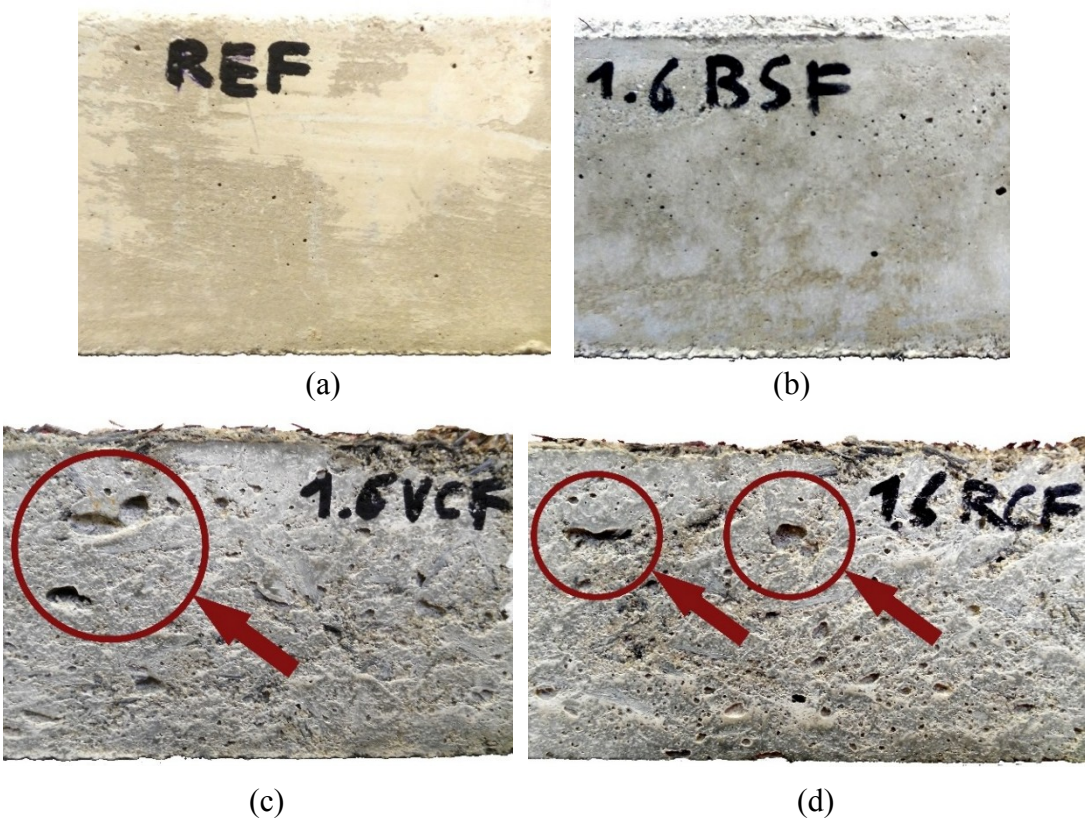

Figure 7.17. *Photographic investigation on mortar specimens surfaces: a) REF, b) 1.6 BSF, c) 1.6 VCF, d) 1.6 RCF*

More information on the fiber-reinforced mortars behavior in the post-cracking phase has been obtained through the CMOD tests. These measurements showed a very different behavior between mixtures with low or high fiber concentrations, as well as between mortars reinforced with CF or SF. The values of flexural strength $f_{R,j}$, Ultimate CMOD, E_f and toughness are shown in Table 7.6.

Table 7.6. *Post-cracking parameters of mortars: $f_{R,j}$, Ultimate CMOD, E_f and toughness*

Mixtures	$f_{R,j}$ (MPa)	Ultimate CMOD (mm)	E_f (MPa)	Toughness (MPa)
REF	6.0	0.020	22.9	-
0.05VCF	6.2	0.017	19.8	3.1
0.1VCF	7.4	0.033	16.5	3.9
0.2VCF	7.9	0.026	20.7	5.0
0.4VCF	9.2	0.060	20.3	11.7
0.8VCF	13.2	0.155	20.6	8.8
1.2VCF	15.2	0.170	17.7	15.2
1.6VCF	16.0	0.190	15.7	14.7
0.05RCF	6.0	0.014	23.7	0.0
0.1RCF	7.9	0.014	25.5	0.0
0.2RCF	8.3	0.014	24.2	0.1
0.4RCF	7.8	0.015	23.6	0.0
0.8RCF	12.1	0.106	16.8	7.2
1.2RCF	14.8	0.132	17.8	9.0
1.6RCF	15.1	0.113	18.1	11.2
0.05BSF	7.1	0.018	21.9	4.6
0.1BSF	7.1	0.017	21.0	6.8
0.2BSF	6.9	0.016	22.2	3.8
0.4BSF	8.8	0.019	21.3	7.9
0.8BSF	11.7	0.641	20.7	37.1
1.2BSF	16.7	0.724	24.2	52.5
1.6BSF	16.3	0.719	20.9	53.6

As can be seen from the results, the low-fiber mortars (≤ 0.4 vol%) show a fragile behavior, similar to REF. These mortars show a high cracking elastic modulus E_f, and very low toughness values (Fig. 7.18). In these mixtures, the bridge effect of the fibers in the slit is very small, and consequently also the value of Ultimate CMOD.
The cracking toughness of mortars increases by increasing the fibers concentration, especially in mixtures with additions ≥ 0.8 vol.%. In particular, mortars with a high CF content show a lower E_f, but high toughness and ultimate CMOD values [329].

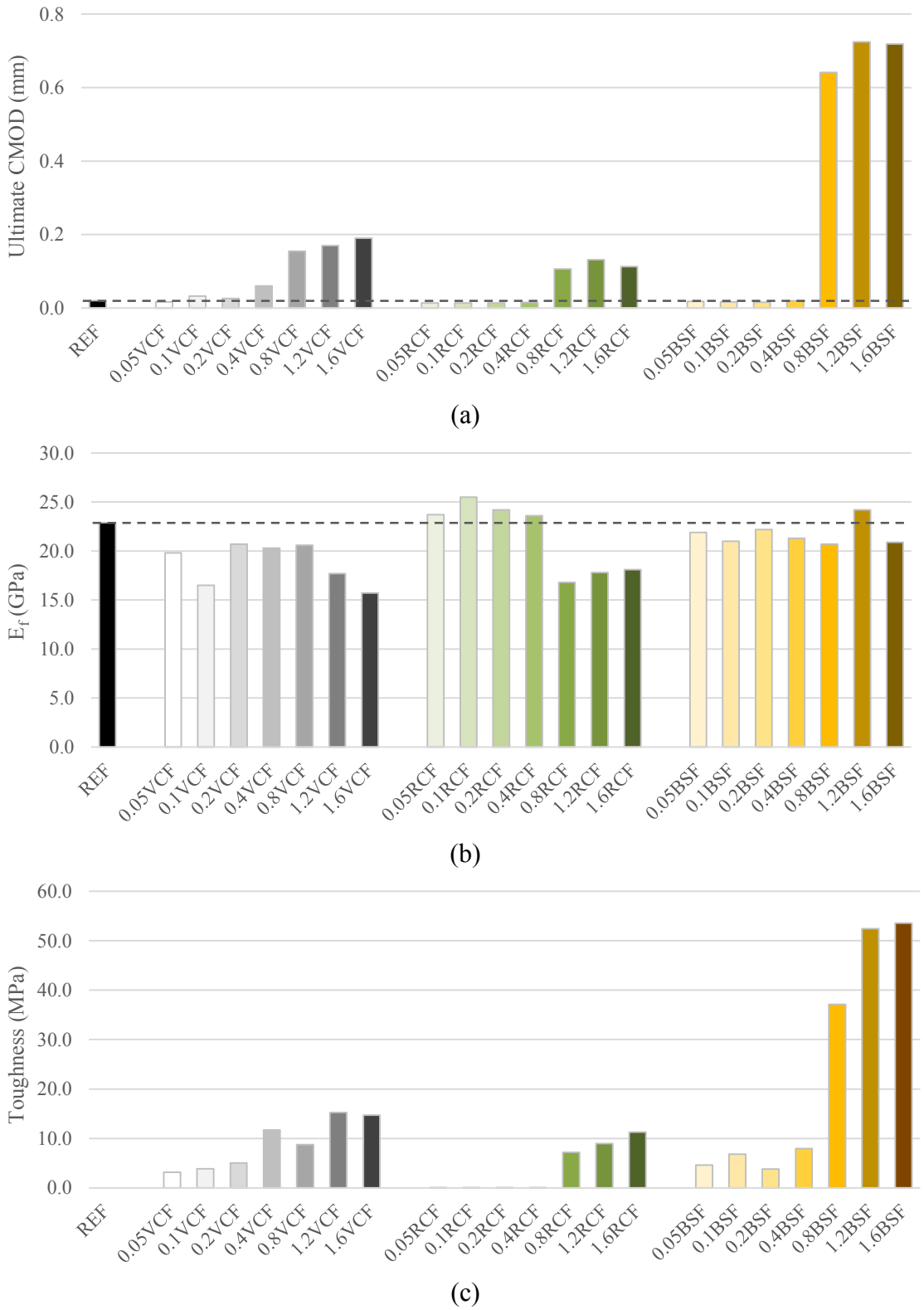

Figure 7.18. *CMOD tests results: a) Ultimate CMOD, b) Cracking elastic modulus E_f, c) Cracking toughness*

However, the best post-cracking mechanical performances were obtained by steel fibers. BSF cracking toughness is 350% greater than the maximum value of the CFs (Fig. 7.18c), and the crack mouth reaches an opening of about 0.7 mm before breaking (compared to 0.19 mm of 1.6VCF, Fig. 7.18a).
SEM investigations were used to analyze the crack behavior. Figure 7.19 shows the analysis of CFs and SFs immersed in cement paste.

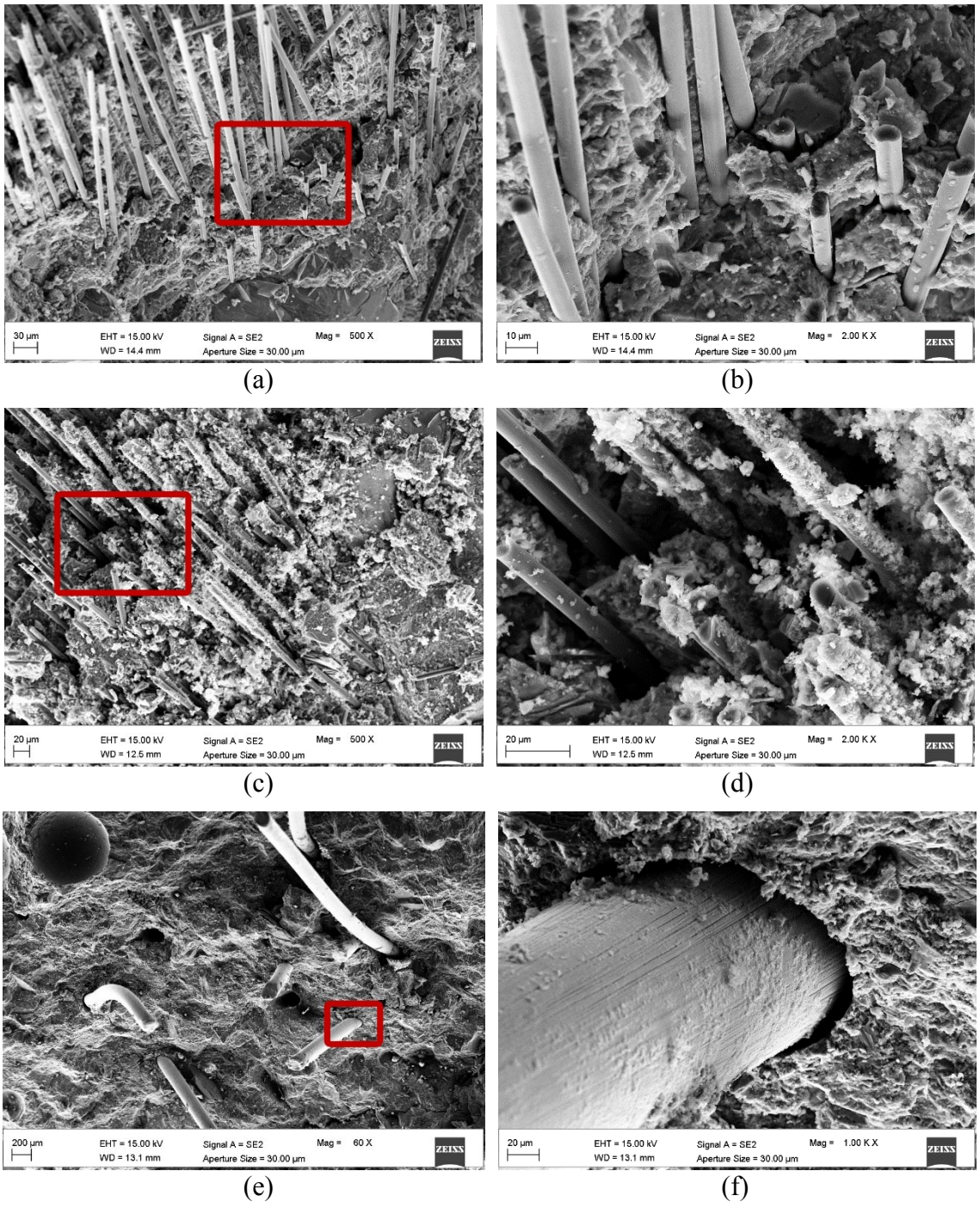

Figure 7.19. *SEM investigation. Fibers agglomerated (left) and enlargement on fibers-cement matrix interface (right): a-b) VCF, c-d) RCF, e-f) BSF*

The images show that VCF and RCF are effectively incorporated within cement paste. In particular, the recycled fibers are covered with agglomerates of cement paste particles (Figg. 7.19c-7.19d). The carbon-based microparticles on the RCFs surface (Fig. 7.20) increase the specific surface, creating nucleation points for the formation of C-S-H and C-A-H on the filaments, thus improving their interaction with the matrix [14][330].
This analysis explains the high mechanical performance of mortars with RCFs (Figg. 7.13-7.15).

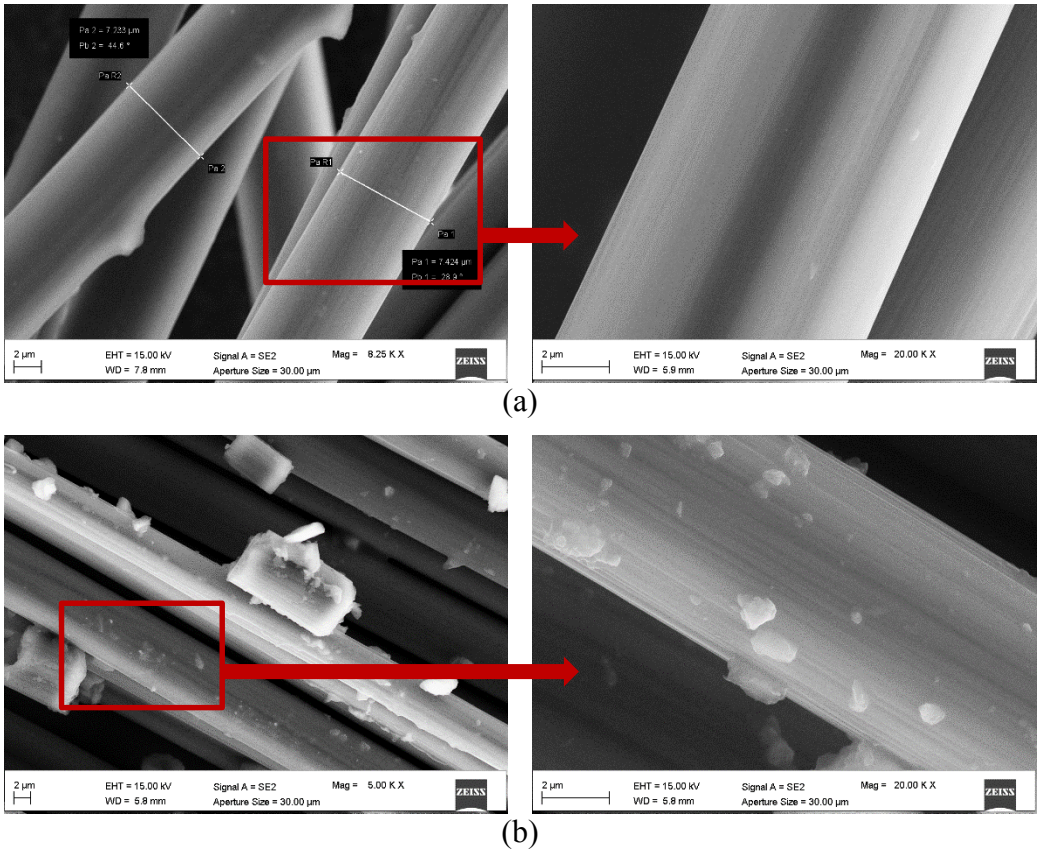

Figure 7.20. *SEM images of VCF and RCF at different magnifications. The carbon micro-particles on the surface of RCF are clearly visible*

In contrast, BSFs exhibit slight detachments at the interface with the paste (Fig. 7.19f). However, these separations could be due to subsequent mechanical stresses occurred during the preparation of SEM specimens. The greater cracking toughness of BSFs is probably linked to the high intrinsic flexural stiffness of the SF filaments, due to their higher diameter. Indeed it is demonstrated that a higher diameter of SF increases the cracking toughness and the maximum crack opening [331]. Furthermore, the ends of the BSFs are more irregular (Fig. 7.3c) and this increases their pull-out resistance.
Figure 7.21 shows the σ_f-CMOD curves of mortars with high fiber content ($\geq$ 0.8 vol%), where the greater toughness of BSF compared to VCF and RCF is evident.

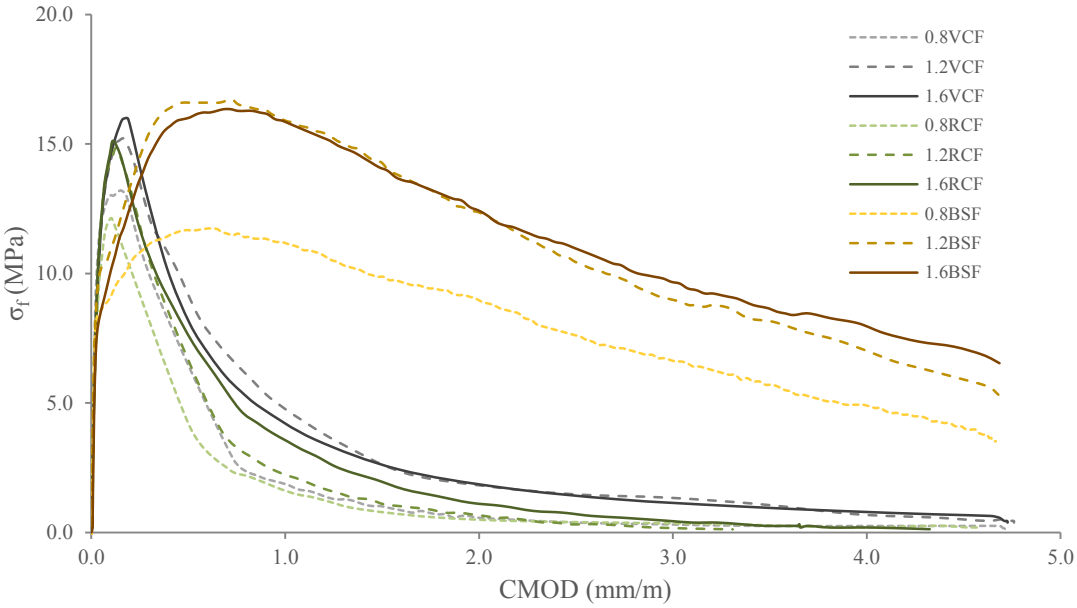

Figure 7.21. *σ_f vs. CMOD curves of fiber-reinforced mortars*

7.4.2 Durability

7.4.2.1 Capillary water absorption

The results of the capillary absorption tests show that all fiber-reinforced mortars show less water suction, both in the short and long period.
In particular, Figure 7.22 shows that all types of fibers addition lead to a decrease in the values of absorption coefficient C, and therefore to a lower quantity of water absorbed through direct immersion. However, the values are in no way proportional to the amount of fibers. The best results were obtained by RCF and BSF, with decreases of C up to 30% (mixtures 0.4RCF and 0.1BSF).

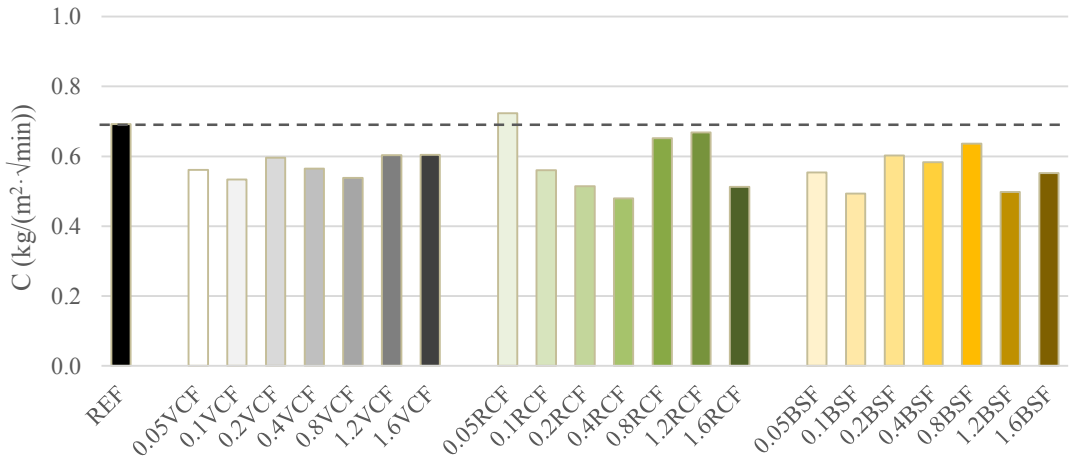

Figure 7.22. *Water absorption coefficient (C) of mortars*

The effect of the fibers content is more influential in the long-period water absorption tests. Here too all the fiber-reinforced mixtures show a greater resistance to capillary suction, since the Q_i values are always lower than the REF during the measurement period (Fig. 7.23). Moreover, a greater quantity of fibers leads, on average, to a lowering of total Q_i (Fig. 7.24). The mortars with maximum quantities of VCF and BSF are the most waterproof, with Q_i values 22% lower than REF.

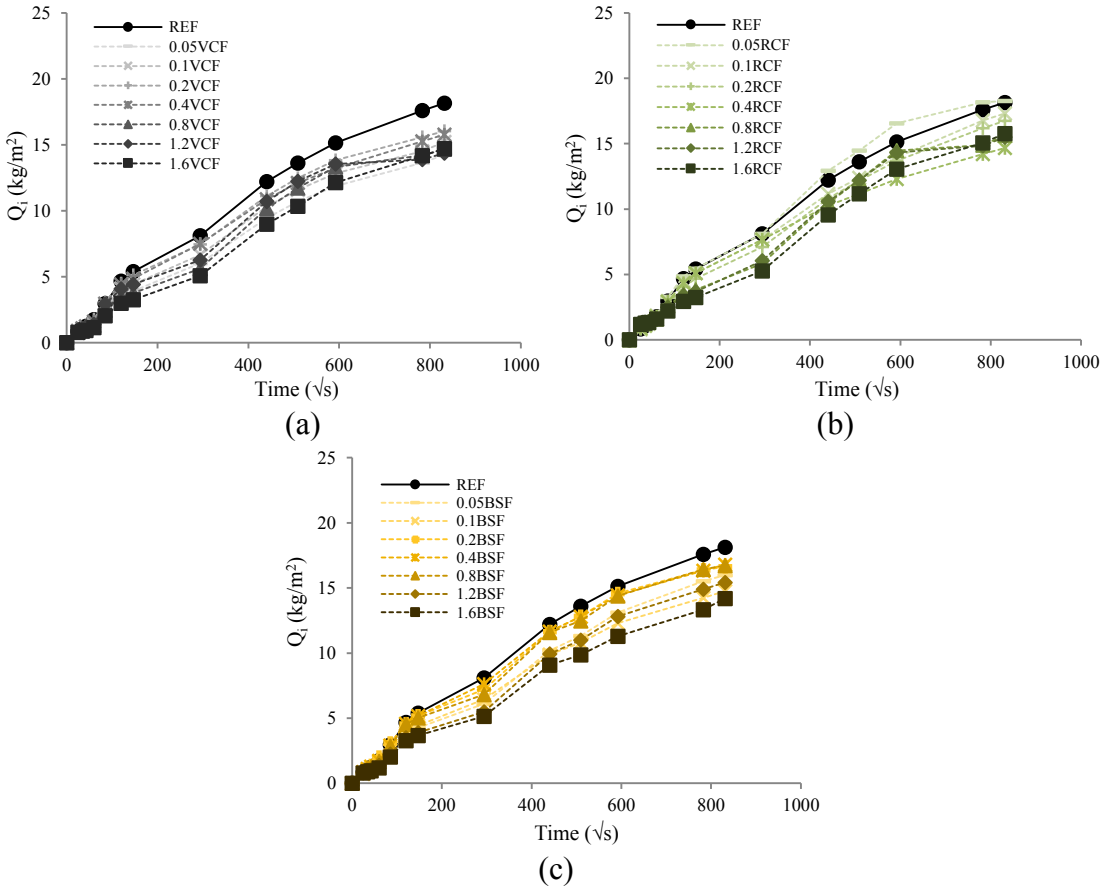

Figure 7.23. *Water absorbed per unit area (Q_i). Comparison between REF and mortars reinforced with: a) VCF, b) RCF, c) BSF*

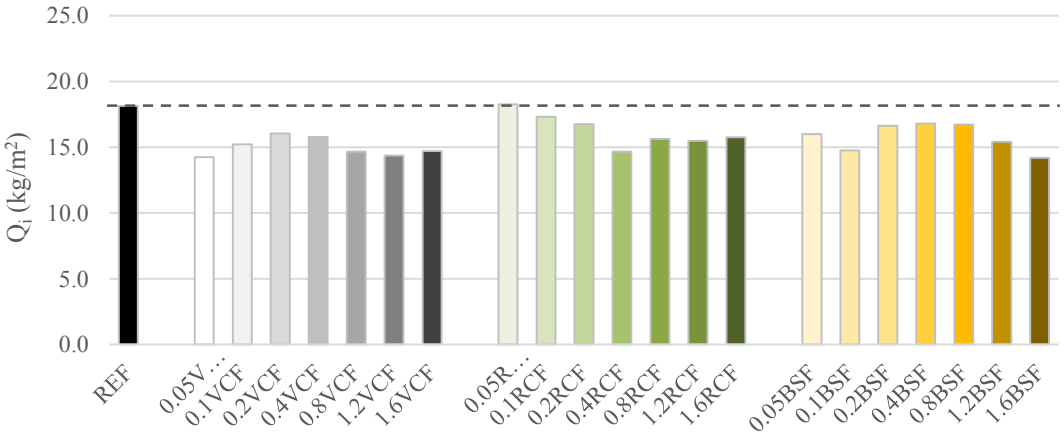

Figure 7.24. *Total Q_i of mortars after 8 days of test*

The lower C and Qi values of the fiber-reinforced mortars are related to their lower total porosity V_p compared to the reference (Table 7.5). In particular, mortars with high concentrations of fibers (≥ 0.8 vol%) have both lower V_p and low volumetric content of capillary pores (Fig. 7.16), particularly with diameter < 1 μm, i.e. the voids that mainly promote water absorption. For this reason, high fiber content mortars show a high resistance to capillary absorption.

7.4.2.2 Drying shrinkage

The results of free drying shrinkage tests show that all types of conductive fibers decrease the hygrometric shrinkage of the mortars. The curves of the shrinkage strain ε_s vs. time are shown in Figure 7.25.

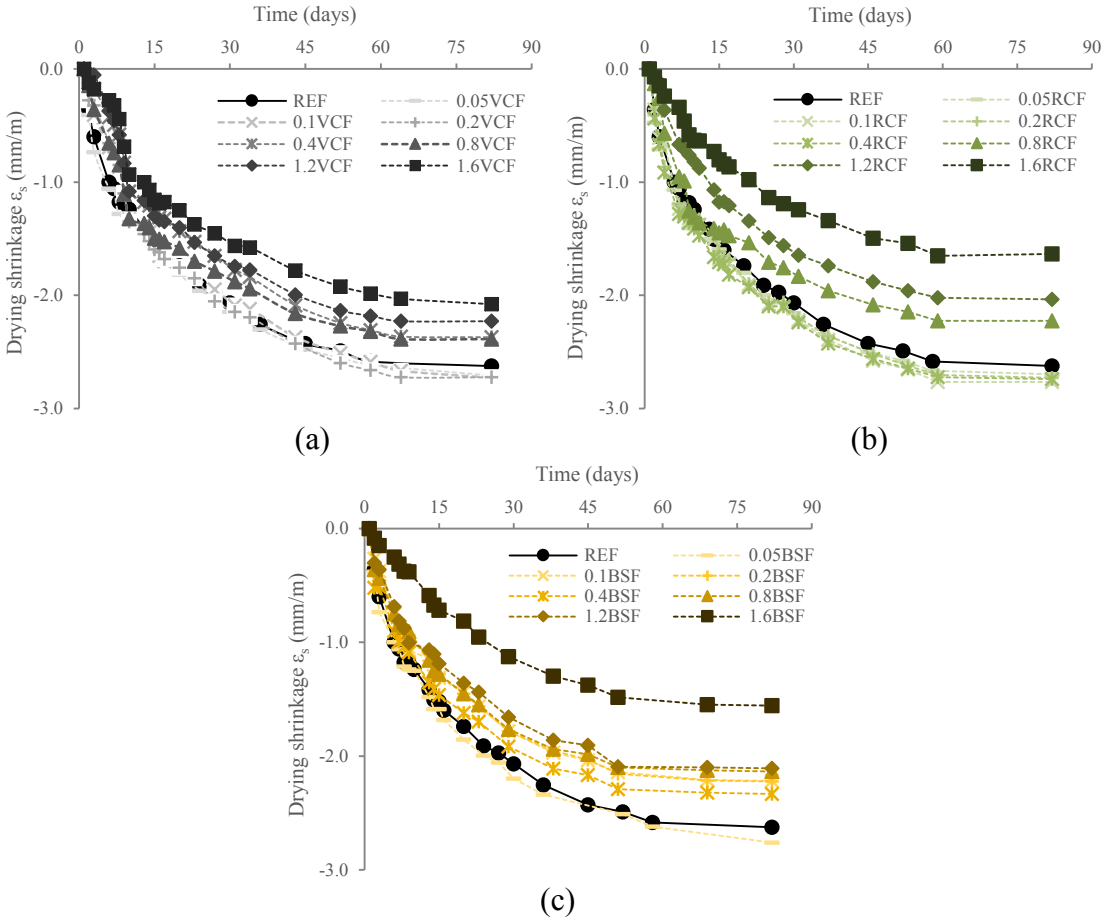

Figure 7.25. *Drying shrinkage (ε_s). Comparison between REF and mortars reinforced with: a) VCF, b) RCF, c) BSF*

The curves show that shrinkage of the mortar specimens stabilize after 50-60 days of curing (i.e. the deformation is almost complete).

All fiber-reinforced mortars show lower shrinkage strain compared to REF, except mixtures with low fiber content, which show similar curves to plain mortar. Moreover, a higher fibers concentration leads to a decrease in hygrometric shrinkage, both for CF and for BSF. The largest decreases were measured in mortars with high content of RCF and BSF (Figg. 7.25b-7.25c), which show final ε_s values 38% lower than the reference (1.6RCF and 1.6BSF).

The low hygrometric shrinkage of the mortars with conductive fibers is linked to their porosimetric characteristics. It is well known that the shrinkage phenomenon is strongly influenced by the surface tension of the water within the capillary pores [332]. Following the gradual loss of water in unsaturated steam environments (RH < 95%), water meniscus are formed, which attract the hydrated cement particles surfaces (mainly consisting of calcium hydrated silicate fibers, C-S-H). The attraction between C-S-H fibers determines the hygrometric shrinkage [26]. The lower V_p and the lower content of capillary pores of the fiber-based mortars (Table 7.5) leads to a reduction in their shrinkage strain. In particular, mortars with a high content of CF and BSF contain a very low volume of pores with diameter <50 nm, the most responsible for deformation [224].
The lower deformation of RCF-based mortars compared to mortars with VCF is linked to the filler effect of the carbon microparticles obtained from the fibers processing (Fig. 7.3b), and to their better interaction with the cement paste (Fig. 7.19d), which have considerably reduced the capillary porosity volume (Fig. 7.16).
Moreover, the proportional lower presence of cement paste in the hardened compound (replaced by the volume of fibers) has probably led to the lower ε_s of the high fiber content mortars. Usually, the shrinkage behavior is closely linked to the weight loss by the material, since the greater the amount of water lost during the curing period, the greater the strain stress within the pores of the specimen [266]. The amount of water lost by the mortars in the curing period (as a percentage of their initial weight) is shown by the curves in Figure 7.26.

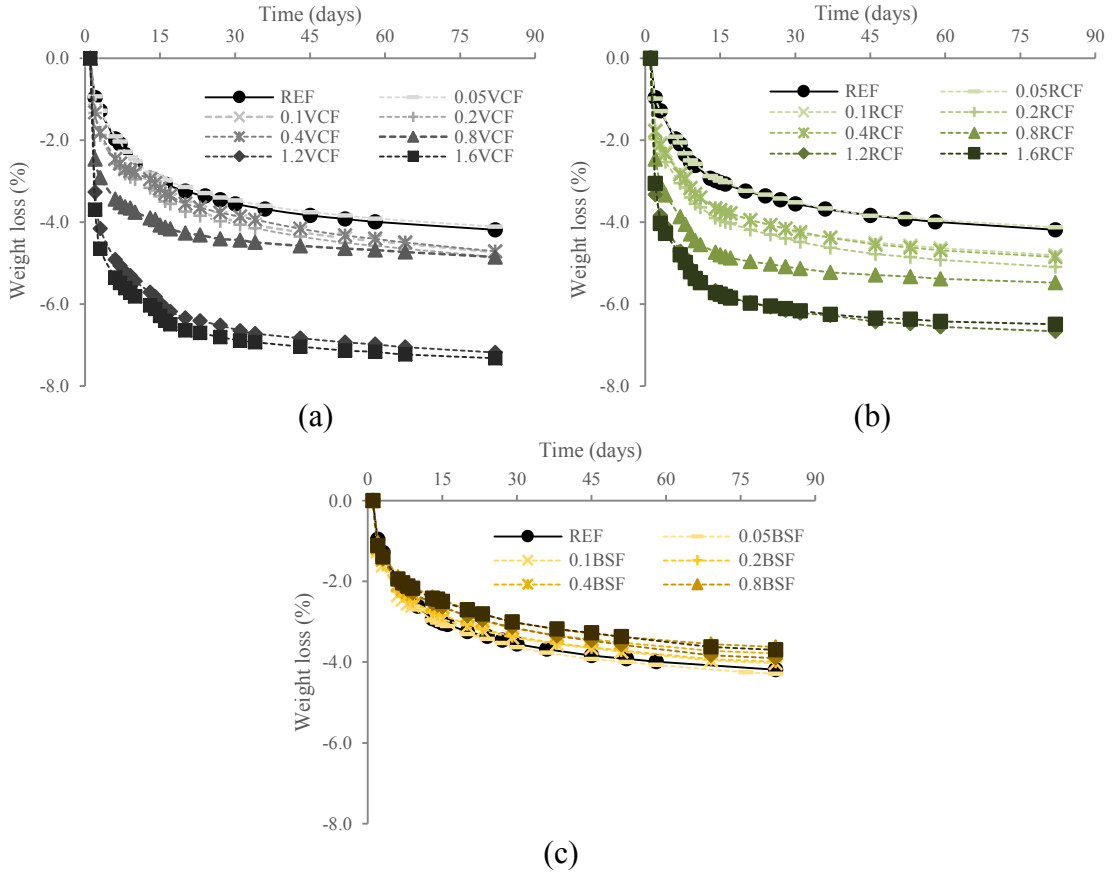

Figure 7.26. *Weight loss (%) in the curing period. Comparison between REF and mortars reinforced with: a) VCF, b) RCF, c) BSF*

Weight loss curves show differences between CF mortars and BSF mortars.
The amount of water lost from mixtures containing BSF is similar to that of REF, with slightly lower values in high fiber content mortars, because of the lower proportional water content. Moreover, these mixtures are characterized by a usual weight loss-ε_s relationship, i.e. a smaller quantity of water lost, corresponding to a lower hygrometric shrinkage [26].
In contrast, mortars containing CF show very high water losses (78% more than REF). In the case of VCF and RCF, the greater the concentration of fibers, the greater the amount of weight drop, but the lower the shrinkage deformation.
This phenomenon confirms the previous hypothesis regarding the high content of macropores of CF-based mixtures (Section 7.4.1). The high presence of mixing water contained within the large-size pores, has led to high weight losses of the specimens with CF during the curing period. However, the total volume of macroporosity is less influential than the micropores volume on shrinkage strains, which in mixtures with a high content of VCF and RCF, is very low.

7.4.3 Electrical resistivity

The results of the electrical measurements confirmed the high efficiency of the conductive fibers in decreasing the electrical resistivity of the mortars. In particular, an exponential enhancement in conductivity was detected by adding increasing concentrations of CF.
The characteristic electrical properties of mixtures containing VCF and RCF has led to a thorough analysis of the electrical behavior of multi-phase cement-based composites. As widely reported in literature, the different types of conduction within multifunctional cement-based materials lead to the interaction between two different electrical contributions: electronical and electrolytic conductivity. In AC measurements, this leads to noticeable differences between the values of impedance Z measured at low frequencies and those measured at high frequencies. In the first case, the effect of the polarization of the cement matrix is greater due to the longer charging time, in the second case, the polarization effect is eliminated, and the electrical contribution of the fibers is more evident [182].
This effect is clearly visible through *Electrochemical Impedance Spectroscopy* (EIS), a widely used technique to study the dielectric properties of cementitious materials [333][334][335][336][337].
In the *Nyquist plot* (Fig. 7.27), in which the relationship between the *imaginary part* ($-Z_{Im}$) and the *real part* (Z_{Re}) of impedance is shown, the impedance spectrum of plain cementitious materials is characterized by a *single arc* describing the material behavior (*material arc*) and a *spurious arc* occurring at lower frequencies ascribed to polarization effects at the specimen-electrode interface (electrode arc) [338].

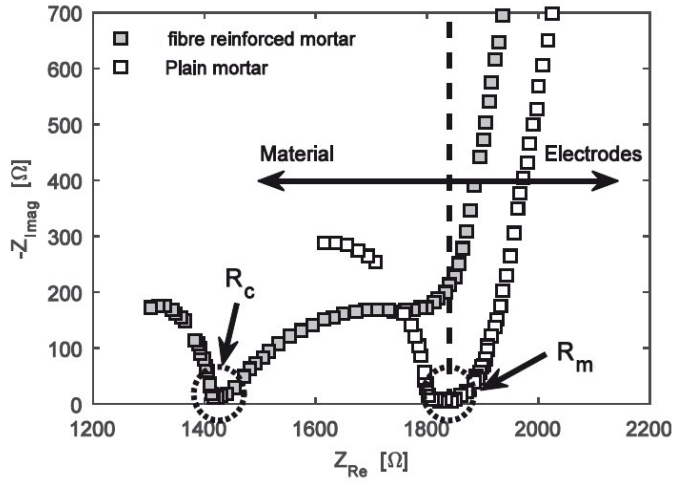

Figure 7.27. *Impedance spectra for a plain mortar specimen and a conductive fiber reinforced mortar. The AC matrix resistivity R_m, related to ionic current within the pore solution, and the composite resistivity R_c, accounting for both the ionic flow and the electronic current through the fibers are indicated* [182].

The value of the real impedance axis at the *cusp* between both arcs is regarded as the electric resistivity of the material, which is comparable to the resistivity measured under DC. The incorporation of conductive fibers, e.g. SF or CF, into the matrix of a cementitious material with fiber dosages that exceed the percolation threshold, results in a notable change of the impedance spectrum, as reported in several studies [339][340][341][342][343].

The main effect of the conductive fibers in the curves of the Nyquist plot is the partition of the single arc of the cement-based material into two arcs (Fig. 7.27). This feature, sometimes referred to as "*double arc*" [339], highlights the "multiphase" nature of the composite, since the "*matrix resistance*" and the "*composite resistance*" describe a different behavior of the material at different frequency ranges. In Figure 7.26, the matrix resistance, R_m, represents the resistance to ionic current through the pore solution, acting as electrolyte, corresponding to the junction between the middle material arc and the rightmost spur resulting from polarization effects at the matrix-electrode interface.

Instead, at higher frequencies, the composite resistance R_c, which corresponds to the cusp between the two material arcs and accounts for the combined transfer of ionic current through the electrolyte and electronic current through the carbon fibers [342].

This effect is also clearly visible in the Bode plot. E.g., the *|Z|-frequency* and *phase-frequency* curves of a CF-based mortar specimen (0.8 RCF) are shown in Figure 7.28. The extremes of the phase-frequency curve (red points) reveal two ranges of points with PAT near 0°, corresponding to two distinct range of points of the curve |Z|-frequency (blue points) related to a purely resistive behavior of the material [182].

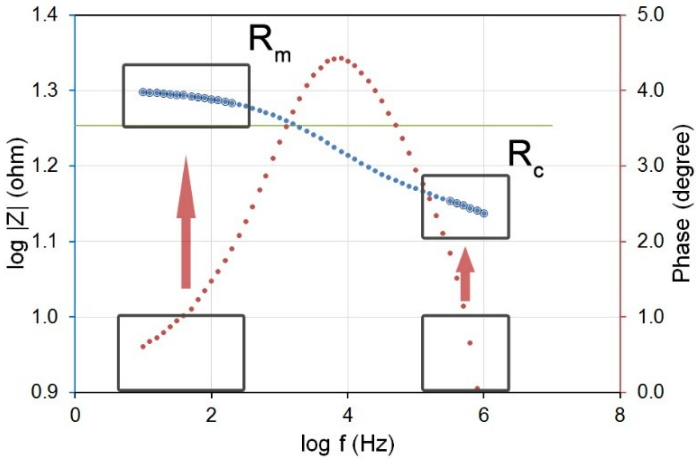

Figure 7.28. *Bode plot of a RCF-based mortar specimen. The two extremes of the phase-frequency curve (red points) correspond to two sets of points of the curve |Z| -frequency (blue points), i.e. two different resistive behaviors of the composite*

This results in two different impedance values, which correspond to the resistance of the material R_m measured at low frequencies (blue points on the left) and the resistance of the composite R_c measured at high frequencies (blue points on the right). Figure 7.29 shows the corresponding Nyquist plot, where R_c is identified by the cusp of the two material curves (lower resistance values) and R_m is identified by the spurious arc connected to the contact resistance between the material and the electrode (*arc of the electrode*, higher resistance values).

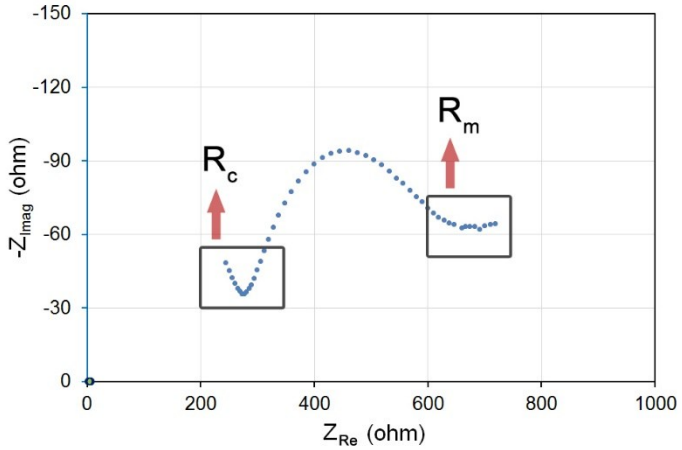

Figure 7.29. *Nyquist plot of the same RCF-based mortar. The extremes of the double arc curve represent the matrix impedance (on the right, higher values of |Z|) and the composite impedance (on the left, lower values of |Z|).*

After this analysis, for the calculation of the specific resistivity of the mortars, only the impedance values obtained at high frequencies were evaluated, i.e. the values that show the contribution of the fibers in the electrical behavior of the composite.
The conclusive data of resistivity measurements carried out throughout the curing period are shown in Table 7.7.

Table 7.7. *Electrical resistivity ρ of mortars during 91 days of curing*

Mixtures	Electrical Resistivity ρ (Ω·cm)							
	2 days	7 days	14 days	21 days	28 days	49 days	70 days	91 days
REF	901	1382	2258	2469	3144	4332	5493	7265
0.05VCF	694	1070	1512	1893	2344	4100	5368	8907
0.1VCF	460	686	958	1120	1456	2578	3482	5941
0.2VCF	174	260	358	426	550	914	1277	2070
0.4VCF	108	158	217	253	329	532	707	1167
0.8VCF	12	13	18	20	24	28	28	33
1.2VCF	7	10	12	14	16	21	24	28
1.6VCF	6	8	12	13	15	19	22	25
0.05RCF	194	306	490	581	704	1004	1476	1934
0.1RCF	163	227	373	441	530	751	1064	1392
0.2RCF	80	101	146	164	184	232	303	355
0.4RCF	48	56	74	81	89	106	126	142
0.8RCF	7	12	12	15	16	19	20	20
1.2RCF	7	10	11	13	16	18	19	20
1.6RCF	6	8	10	10	13	15	16	16
0.05BSF	1295	1904	2269	3137	4357	5554	7659	11202
0.1BSF	1276	1819	2116	3071	4122	5164	7480	10565
0.2BSF	1070	1502	1756	2613	3414	4349	6312	9506
0.4BSF	765	1180	1431	2132	2842	3507	5303	8573
0.8BSF	504	862	1165	1505	1527	2465	3336	4089
1.2BSF	404	666	933	1138	1121	1777	2387	2953
1.6BSF	309	535	733	860	908	1413	2103	2609

The values show a regular increase in resistivity of the mixtures during the curing period (Fig. 7.30). An increasing amount of fiber enhance the conductivity already in the first days, and leads to smaller resistivity increase in the following weeks, because the electrical conductivity of the fibers overpowers the ionic conductivity of the solution within the pores. Particularly, RCFs bring to a high decrease in resistivity already in the early days also at low concentrations, and the values remain low until the end of the measurements (Fig. 7.30b).

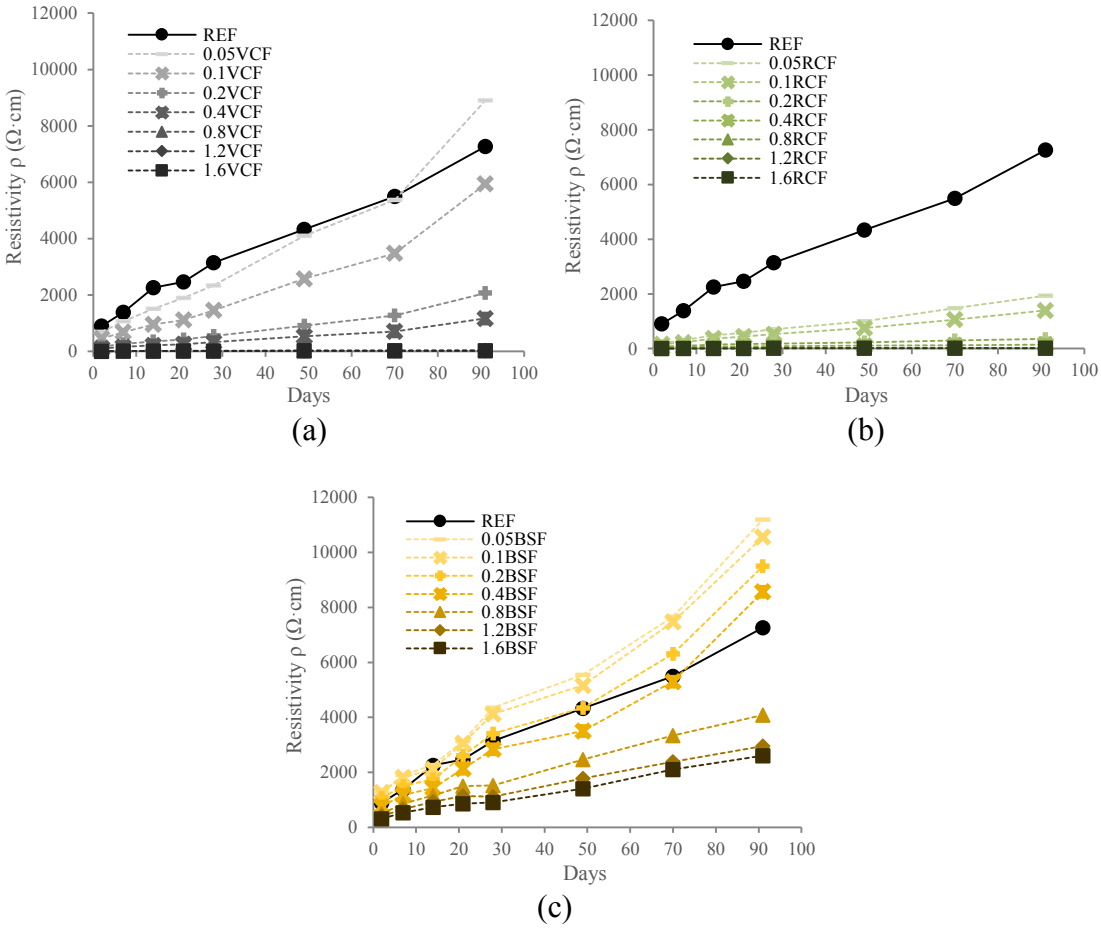

Figure 7.30. *Electrical resistivity (ρ) in the curing period. Comparison between REF and mortars reinforced with: a) VCF, b) RCF, c) BSF*

Figure 7.31 shows the final resistivity values of the mortars (91 days). ρ is reported in a logarithmic scale, due to the very different electrical properties of the composites.

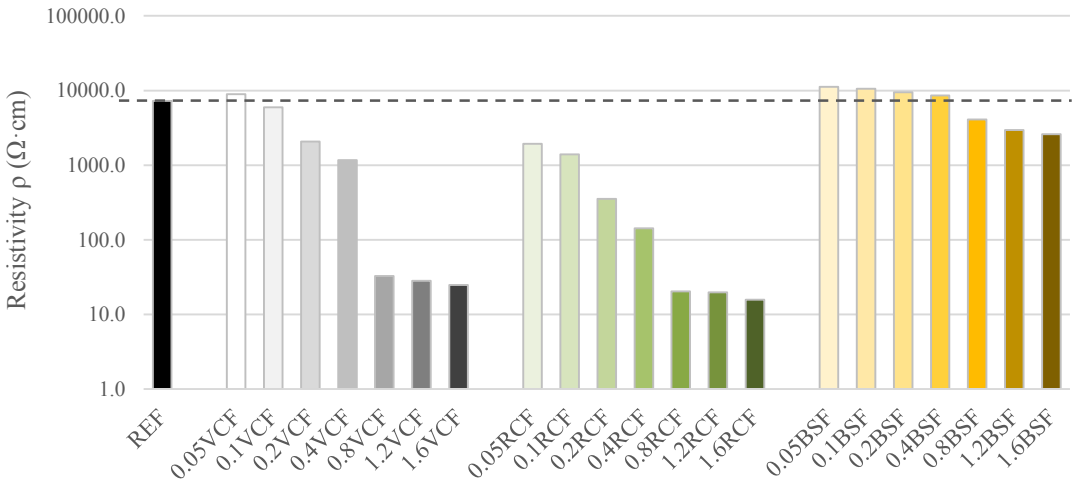

Figure 7.31. *Electrical resistivity ρ of mortars at 91 days of curing (logarithm)*

The most evident fact is the very high efficacy of CF in increasing the electrical conductivity of the mixtures. Mortars with high VCF and RCF contents (≥ 0.8 vol%) show resistivity values of two orders of magnitude lower than the reference. Even at intermediate concentrations (0.2-0.4 vol.%) the effect of VCF and RCF is very effective. 0.2 VCF and 0.2 RCF additions lead to 72% and 95% resistivity decreases, respectively (compared to REF). Contrariwise, BSFs require high doses to significantly enhance conductivity, since the 1.6 BSF addition shows only a 64% resistivity decrease.
The relationship between resistivity ρ and the amount of conductive fibers is shown in Figure 7.32.

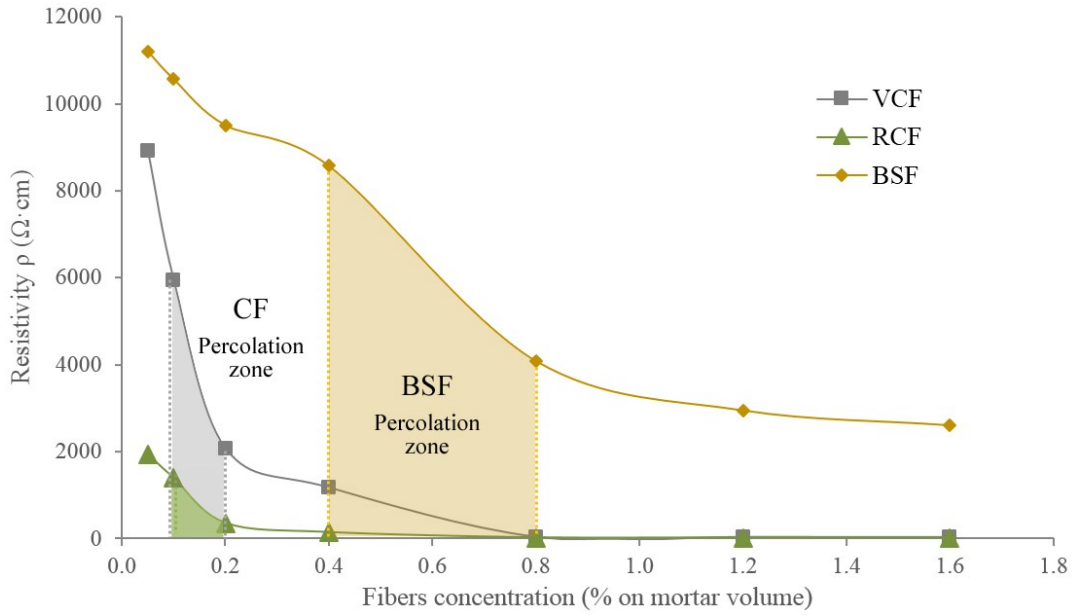

Figure 7.32. *Resistivity ρ of mortars vs. fibers concentrations*

The curves show a remarkable decrease in the electrical resistivity of the mortars with concentrations of VCF and RCF between 0.1 and 0.2 vol.%, which are considered the extremes of the percolation zone of carbon fibers [12]. In this area, VCFs decrease the resistivity of the mixture from 5941 to 2070 Ω·cm, or 65%. The effect of the RCF is more evident, decreasing from 1392 Ω·cm of 0.1 RCF to 355 Ω·cm of 0.2RCF, with a difference of one order of magnitude approximately. Instead, the percolation threshold of BSFs is placed between 0.4 and 0.8 vol.%. In this range, the steel fibers lead the resistivity of the mortar from 8573 to 4089 Ω·cm, with a decrease of 52%.
However, Table 7.7 shows that these are not the only fiber concentrations that lead to a marked increase in electrical conductivity. Figure 7.33 shows the same curves, where the resistivity ρ is reported in logarithmic scale.

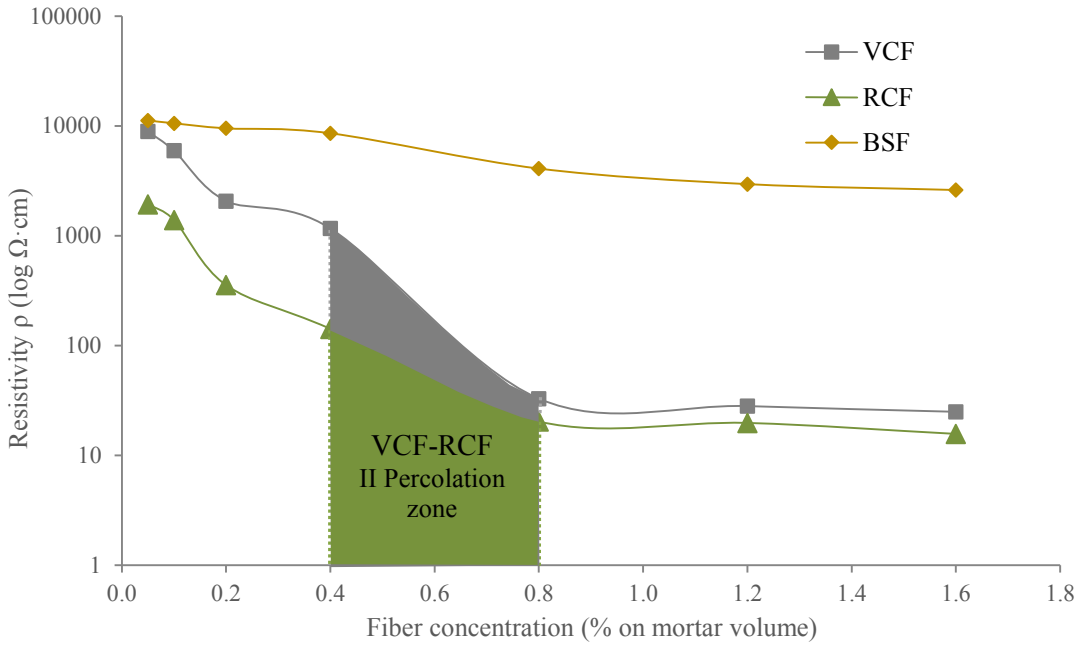

Figure 7.33. *Resistivity ρ of mortars (logarithm) vs. fibers concentrations*

The greatest decrease in resistivity was obtained with a CF addition between 0.4 and 0.8 vol.%. In this range, the VCFs lead to a decrease from 1167 to 33 Ω·cm (two orders of magnitude less). Similarly, RCFs pass from 142 Ω·cm of 0.4 RCF to 20 Ω·cm of 0.8 RCF, i.e. a decrease of 86%. This effect is linked to a percolation threshold in which the very high quantity of fibers leads to the domain of the electronic contact conductivity on the ionic conductivity of the cement matrix [117][199] [314]. This is also demonstrated by the low resistivity increases of mortars with high CF content (≥ 0.8 vol.%) during the curing period (Table 7.7), with values rising from 6-12 Ω·cm at 2 days, to only 16-33 Ω·cm at 91 days.

The most evident result of the electronic tests is the high effectiveness of RCFs in increasing the electrical conductivity of the mortars, even at low dosages. 0.05 RCF mortar shows a 91 day resistivity of 1934 Ω·cm, 73% less than plain mortar, with a concentration of only 0.9 g/L of fibers. This behavior is related to the high quantity of carbon microparticles present on the surface of the RCFs (Fig. 7.2b), which increase the functional electrical surface, creating more effective conductive paths even at low concentrations. Furthermore, these microparticles act as fillers, decreasing the porosity of the matrix and thus decreasing the resistivity (Section 7.4.1, Fig. 7.19d).

The lower efficacy of BSFs is linked both to the lower electrical properties of SF [200] and to their lower aspect ratio. As widely demonstrated in the literature, fibers with a lower aspect ratio form a less effective conductive network [175], decreasing the electrical contact bridges and conducting the tunneling effect. Mortars containing low doses of BSF (≤ 0.4 vol%) have a resistivity even higher than plain mortar REF. This unexpected effect requires further analysis, and may be linked to discontinuity at the interface between SF and cement paste (Fig. 7.19f) [344] and to an increase in porosity, or to a particular electrochemical behavior of the fibers coating.

Furthermore, it must be stressed that BSF-based mortars do not exhibit the typical multi-phase AC electrical behavior of conductive cement-based composites, due to their lower electrical effectiveness. The Nyquist plot of a specimen with high steel fibers content (1.6 BSF) shows a trend similar to that of the plain mortar (Fig. 7.34), in which the purely resistive behavior of the material is identified by the cusp between the two arches, and there is no distinction between the matrix resistance R_m and the composite resistance R_c.

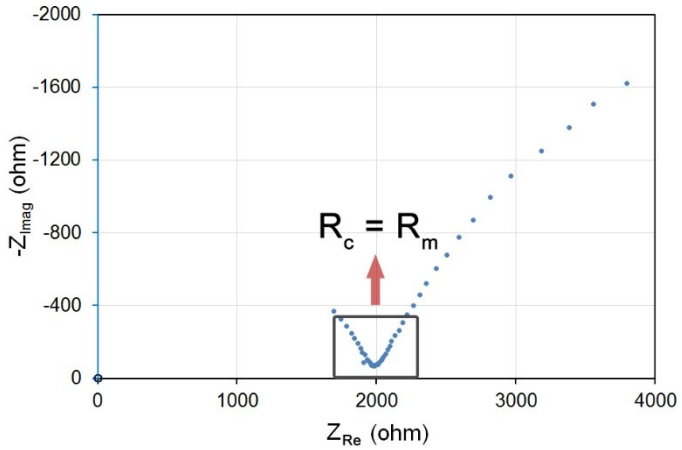

Figure 7.34. *Nyquist plot of 1.6 BSF mortar, where the set of points of the cusp represent both the resistance of the matrix R_m and the resistance of the composite R_c*

For a better analysis of the results, in Appendix A the Bode and Nyquist plots obtained by the EIS tests on all the fiber-reinforced mixtures are reported.

7.5 Conclusions

In the second part of the research, the effect of 3 different types of conductive fibers added in 7 different concentrations was investigated in terms of mechanical strength (pre and post-cracking), durability and electrical properties of mortars. Two types of 6 mm carbon fibers (CF) were studied: commercial virgin carbon fibers (VCF) and recycled carbon fibers (RCF), together with 6 mm brassed steel fibers (BSF). Fibers were added at 0.05, 0.1, 0.2, 0.4, 0.8, 1.2 and 1.6 % on the mortar volume.
The obtained results suggest the following conclusions:

- *Mechanical strength* tests demonstrate the high effectiveness of CF in increasing flexure strength of the mixtures, thanks to their high aspect ratio and to the bridging effect. In particular, RCF increase the R_f values by 101% compared to the plain mortar. All types of fibers enhance the tensile splitting strength of the mortars. The highest values were obtained by the 1.6 BSF addition, which increases the f_{ct} value by 114% compared to the REF. Both R_f and f_{ct} are related to the fibers content, since the higher the CF/SF quantities, the greater the mechanical performances. Also the mechanical compressive strength increases with the addition of fibers, but high concentratios of VCF and RCF lead to a decrease of the R_c values, since the poor workability of the mixtures leads to an increase of the macropores volume inside the composite;

- High fiber amounts greatly improve the *post-cracking* toughness of the mixtures. Particularly, BSF revealed high performances, with toughness values above 50 MPa (250% more than CF), and ultimate CMOD values up to 0.72 mm;
- SEM investigations showed high compatibility and good adhesion to the interface between CF and cement paste. The carbon-based nano/micro-particles on the RCFs surface act as nucleation points for the growth of C-S-H and C-A-H agglomerate, attached to the filaments. The BSFs present slight detachments at the interface with the cement paste, due to mechanical stresses. Porosimetric analyzes prove that a growing quantity of conductive fibers leads to a decrease in *total porosity* V_r and *average pores diameter* d_p. However, mortars with a high CF concentration probably contain a high volume of macropores, which cannot be detected by the used porosimetric instrumentation;
- The lower total porosity and the lower volume of capillary pores also leads to an enhancement in durability of fiber-reinforced mortars, as shown by the *capillary water absorption* and *hygrometric shrinkage* tests. The additions of VCF, RCF and BSF lead to a lower water absorption capability in both the short and long period, with lower capillary coefficient C and Q_i values that decrease by increasing the fibers concentrations. 0.4RCF reached the higher resistance to water absorption, with C and Qi values of 31% and 19% lower compared to the reference, respectively. The lower capillary pores volume and the lower amount of cement also leads to the lower free drying shrinkage of high fiber content mixtures. Mixtures 1.6 RCF and 1.6 BSF achieved the lowest shrinkage strain ε_s values, with a decrease of 38% compared to the plain mortar;
- The *electrical resistivity* measurements showed the high effectiveness of CF in increasing the electrical conductivity of cement compounds. Through the impedance measurements by AC EIS, 2 percolation thresholds were identified in 3 different amounts of VCF and RCF: the first between 0.1 and 0.2 vol.% and the second between 0.4 and 0.8 vol.%, in which the resistivity values decrease by several orders of magnitude compared to REF. In particular, the RCFs showed a very high effectiveness, with noticeable conductivity enhancements even at low additions. This contribution is related to the high number of carbon microparticles in RCFs, which increase the specific conductive surface. The impedance spectra of CF-based mortars highlighted the multiphase nature of the composites, with a clear distinction between electrical resistance of the matrix R_m and the resistance of the matrix-fibers system R_c detected by the Nyquist and the Bode plots. This subdivision does not occur with the BSF-based mortars, because of the lower electrical properties of SF due to their lower aspect ratio.

The results obtained during this research demonstrated the conductive fibers effectiveness in increasing the electrical conductivity of cement-based composites, and confirm the enhancement in mechanical strength and durability of fiber-reinforced mortars.
In particular, the experimentation provides results related to a wide range of different fibers concentrations, useful for the optimization of multifunctional fiber-reinforced cement-based composites, with the aim of obtaining the best compromise between electrical properties and mechanical performances.

The most important result obtained by the tests is the high electrical efficiency of the recycled carbon fibers addition, which bring great increases in conductivity even at low dosages. These data could promote the production of cheaper conductive cement-based composites for self-sensing systems and other applications, as well as a new waste recycling system within the production of carbon fiber profiles.
The last part of the dissertation will study the combined effect of carbon-based fillers and fibers for the realization of multifunctional composites, analyzing their electrical and mechanical properties, and focusing on their strain sensitivity.

8 . Chapter

Piezoresistive composites by combined fillers and fibers addition

Production of mortars with hybrid carbon-based fillers and fibers addition: setting of the piezoresistivity measurement system and evaluation of the electrical sensitivity of the composites

8.1 Introduction

The data obtained from previous experiments, particularly from electrical characterization tests, have progressively approached the research to the development of *Self-sensing Cement-based Composites* (SSCC) for SHM systems, especially through the use of waste industrial by-products. This interest is shared by a substantial sector of building materials engineering and of research on cement composites [345][346]
The natural process of sensitizing of the modern society towards the problems linked to sustainability encourage the construction sector to focus on innovative processes, which aim to resources saving and improving the durability of infrastructures [4][21] [23].
Numerous research projects are focused on the production of innovative cement-based composites by the reuse of recycled industrial by-products [347][348], and the European Union is very active in funding the most promising scientific contributions.
As seen in Section 1.4, the experiments related to this dissertation are an integral part of the *EnDurCrete* project, which aims at the development of sustainable and low-cost multifunctional concretes [42].
The aim of the project is the production of a new type of concrete with a lower environmental impact (less use of OPC) through the integration of SCM and carbon-based admixtures obtained from industrial waste, without compromising the mechanical properties and durability of the composite. The development of the novel concrete also involves the use of non-metallic reinforcement materials with high mechanical strength and high electrical conductivity (carbon fibers), to increase both the life cycle and the strain-sensing properties of the material.
The combination of these different needs requires a thorough study of the mix-design, in order to hold the production costs, or weighing the use of the most expensive raw materials.
The previous study steps provided many information on the potentialities of the different types of additions and on their different concentrations. The last phase of the work involves the optimization of the techniques and amount of addition, through the study of the combined effects of carbon-based fillers and fibers. The hybrid additions have been tested on mixtures more similar to the traditional structural materials, i.e. OPC-based mortars with larger aggregates (grain size $\leq$ 8 mm) and high workability (flow value $\approx$ 200 mm). The additions have been characterized according to the mechanical and electrical properties of the composites, as well as to their sensitivity to deformation, for which a suitable piezoresistivity measurement setup has been studied.
Three types of carbon-based fillers have been studied:

- 2 types of recycled fillers: *Gasification char* (GCH) and *Used foundry sand* (UFS);
- 1 type of commercial filler: *Graphene nanoplatelets* (GNP), as comparison;

Together with two types of carbon fibers:

- *Recycled carbon fibers* (RCF);
- *Virgin carbon fibers* (VCF);

Mixtures were realized by adding fillers and fibers in 2 different concentrations, or combining the two types of carbon-based materials. The specimens were tested for mechanical resistance (flexural and compressive strength), durability (capillary water

absorption in short and long period), electrical conductivity and fractional change in resistivity under load (piezoresistivity).
The last part of the work of this Thesis, i.e. the realization process of the specimens and the tests of mechanical strength, electrical conductivity and piezoresistivity, was performed at the *Departamento de Engenharia Civil* (DECivil), of the *Universidade de Aveiro* (University of Aveiro), a research center that boasts relevant scientific contributions in the field of piezoresistive cement-based composites [95][79][263].
The following are the production methods and the compositional characteristics of the mortars, together with the description of test methodologies and the analysis of the results.

8.2 Materials and Mix-design

An ordinary Portland cement CIMPOR CEM II/B-L 32.5N (UNI EN 197-1) was used for the production of mortars. This limestone cement with normalized initial strength is a widely used binder in common applications, and has been selected to provide data reproducible on large-scale. To create mortars more similar to a traditional concrete for formwork casting, a medium-large aggregate was selected, i.e. a silica sand with grain size ≤ 8 mm (Section 5.3), and an aggregate/cement ratio = 3. The w/c ratio is equal to 0.5, in order to obtain a high workability.
Three different types of carbon-based powders have been studied (Fig. 8.1): 2 recycled fillers appropriately ground and sieved, with particle size < 75 μm, i.e. *Gasification Char* (GCH) and *Used Foundry Sand* (UFS), together with a non-recycled nano-powder, i.e. *Graphene Nanoplatelets* (GNP) *Pentagraf* (PENTACHEM), as a reference commercial filler. For a better description of the dimensional properties of the fillers and their technical specifications, see Chapter 5, Section 5.4.

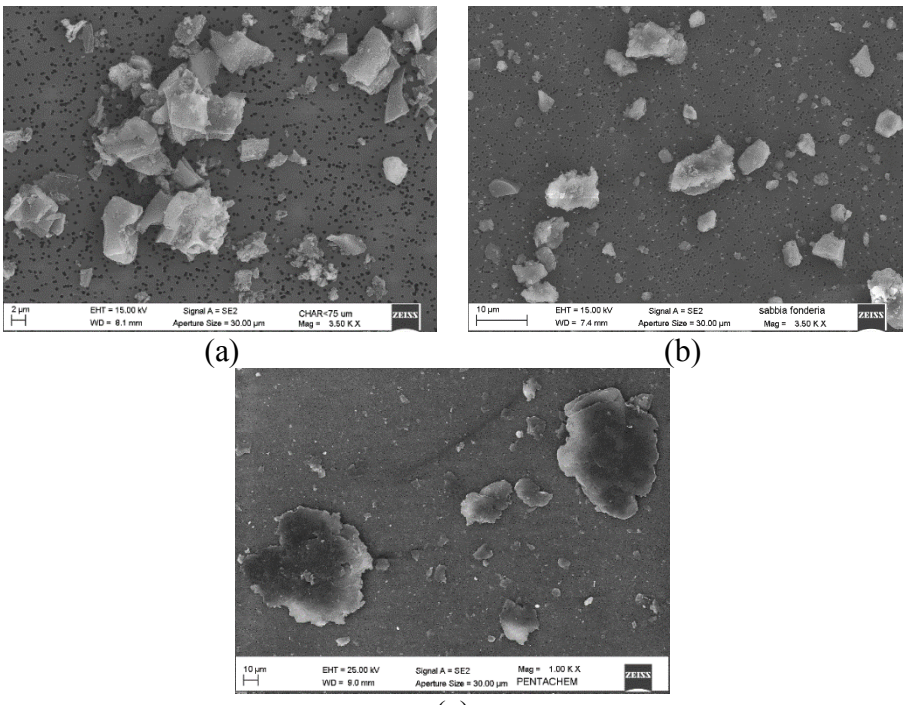

(a) (b)
(c)

Figure 8.1. *SEM analysis of fillers particles: a) Gasification Char, b) Used foundry sand, c) Graphene nanoplatelets*

Two types of carbon fibers have been selected as conductive filaments (Fig. 8.2): short cut *Virgin Carbon Fibers* (VCF) *SFC-EPB* from STW, and *Recycled Carbon Fibers* (RCF) *CGF-6* from APPLY CARBON, both with length 6 mm. More information on the technical characteristics of CFs are reported in Section 5.5 and 7.2.

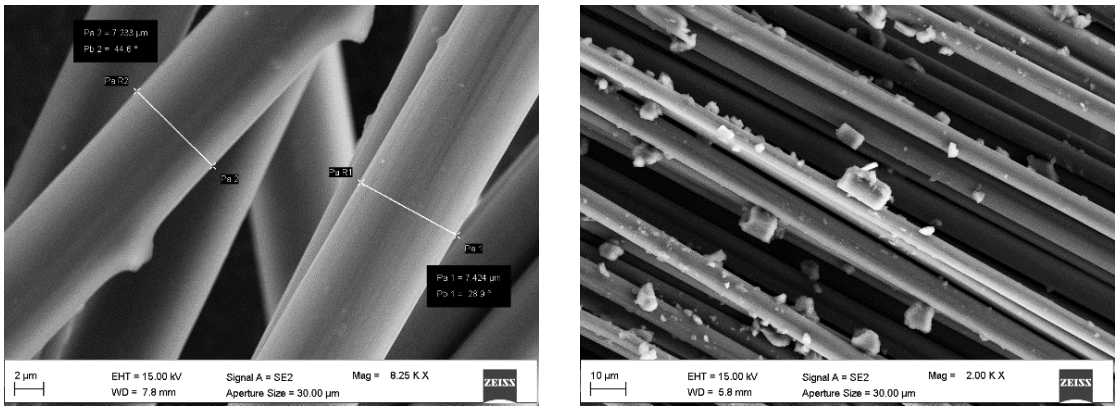

(a) (b)

Figure 8.2. *SEM analysis of conductive filaments: a) Virgin carbon fibers, b) Recycled carbon fibers*

Carbon-based fillers were added in two different concentrations: 4% and 7% on the cement weight. These amounts have proven to be effective in the implementation of SSCC according to the work of several authors [95][79][126].
CFs were also analyzed in two different concentrations: 0.05% and 0.2% on the mortar volume. These amounts were selected thanks to the good performances shown in the previous research phase, since they combine high mechanical strength and high workability of the mixtures (Section 7.4). The 0.2% concentration is also the maximum limit of the percolation zone detected in the previous electrical resistivity tests (Section 7.4.3).
The effects of the hybrid additions were studied by combining the two concentrations of VCF and RCF with an amount of 4 wt.% of the three types of filler. Therefore, 6 mortars were added with carbon-based fillers, 4 mortars with carbon fibers and 12 mortars with hybrid filler-fiber additions, thus producing 22 mixtures, together with a plain mortar without addition used as a reference (REF). Mix proportion of mortars are reported in Table 8.1.

Table 8.1. *Mix proportions of mortars*

Mixture	CEM (g/L)	Water (g/L)	Sand ≤ 8mm (g/L)	GNP (g/L)	GCH (g/L)	UFS (g/L)	Fibers (g/L)		SP (g/L)
							VCF	RCF	
REF	512	256	1535	-	-	-	-	-	-
GNP4	512	256	1535	20.5	-	-	-	-	0.96
GNP7	512	256	1535	35.8	-	-	-	-	2.40
GCH4	512	256	1535	-	20.5	-	-	-	0.64
GCH7	512	256	1535	-	35.8	-	-	-	1.12
UFS4	512	256	1535	-	-	20.5	-	-	1.28
UFS7	512	256	1535	-	-	35.8	-	-	1.28
0.05VCF	512	256	1535	-	-	-	0.9	-	0.16
0.2VCF	512	256	1535	-	-	-	3.4	-	0.48
0.05RCF	512	256	1535	-	-	-	-	0.9	0.32
0.2RCF	512	256	1535	-	-	-	-	3.7	0.64
GNP4-0.05VCF	512	256	1535	20.5	-	-	0.9	-	1.12
GNP4-0.2VCF	512	256	1535	20.5	-	-	3.4	-	1.92
GNP4-0.05RCF	512	256	1535	20.5	-	-	-	0.9	1.76
GNP4-0.2RCF	512	256	1535	20.5	-	-	-	3.7	2.40
GCH4-0.05VCF	512	256	1535	-	20.5	-	0.9	-	1.12
GCH4-0.2VCF	512	256	1535	-	20.5	-	3.4	-	1.28
GCH4-0.05RCF	512	256	1535	-	20.5	-	-	0.9	1.12
GCH4-0.2RCF	512	256	1535	-	20.5	-	-	3.7	1.44
UFS4-0.05VCF	512	256	1535	-	-	20.5	0.9	-	1.76
UFS4-0.2VCF	512	256	1535	-	-	20.5	3.4	-	1.92
UFS4-0.05RCF	512	256	1535	-	-	20.5	-	0.9	2.08
UFS4-0.2RCF	512	256	1535	-	-	20.5	-	3.7	2.08

To improve the homogeneity of the composites, a powdered polycarboxylate ether SP *Melflux® 4930F* (BASF) was used. This type of high-performance dispersants is widely used to increase the dispersion degree of carbon-based nanomaterials particles [8][33][349].

The carbon-based powders were previously dispersed within the whole amount of mixing water, together with a fraction of SP. After a preliminary manual stirring, the suspensions were sonicated by ultrasonic bath for approximately 30 min. The total volume of the suspension has been divided into several containers (beakers) in order to maximize the effects of ultrasonic excitation. The actual mortars were realized by manually mixing sand and cement. Then, the CFs were gradually dispersed within the aggregate-binder composite, mixing manually and mechanically to ensure the maximum dispersion of the filaments. Suspensions of water and filler were then added to the solid components, and the mixtures were blended by means of a *Hobart* mixer at different speeds for at least 5 min (Fig. 8.3). If necessary, further SP was added to the mortars during blending, to improve the workability of the composites.

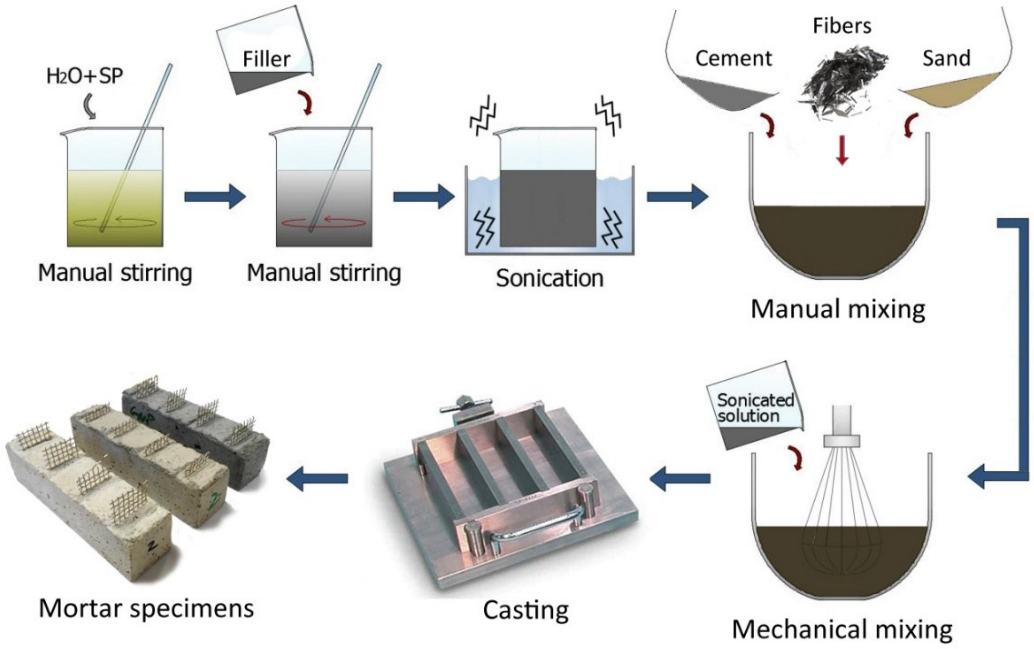

Figure 8.3. *Scheme of mortar specimens fabrication process*

The fresh mortars were poured to realize 40x40x160 mm specimens, subjecting the molds to mechanical vibration, for a better compaction of the material [313].
Specimens were cured under controlled environmental conditions: at T = 20 ± 1°C and a RH = of 95 ± 5% for 7 days, then maintained at T = 20 ± 1°C and RH = 50 ± 5% until testing.

8.2.1 Workability

As in the previous experimentations (Section 6.2.1 - 7.2.1), the workability of the mixtures has been evaluated by means of slump test to the flow table and the calculation of the percentage consistency, according to UNI EN 1015-3:2007 standard.
During the production of the mixtures, the addition of SP was carefully adjusted so as to obtain a fresh mortar consistency of about 100%, i.e. a flow value of ≈ 200 mm. In this way, very workable composites were obtained, with a consistency similar to the concretes normally used during the casting in formwork and between the reinforcement bars.
Therefore, the realized mixtures are *plastic mortars* according to the UNI EN 1015-6: 2007 standard (mortars with flow value from 140 mm to 200 mm).
The characterization parameters of fresh mortars and their SP concentrations are reported in Table 8.2.

Table 8.2. *SP amounts, Flow values and C% of mortars (UNI EN 1015-3:2007)*

Mixtures	SP (g/L)	Flow value (mm)	C (%)
REF	-	185	85
GNP4	0.96	173	73
GNP7	2.40	200	100
GCH4	0.64	183	83
GCH7	1.12	183	83
UFS4	1.28	164	64
UFS7	1.28	174	74
0.05VCF	0.16	177	77
0.2VCF	0.48	170	70
0.05RCF	0.32	205	105
0.2RCF	0.64	177	77
GNP4-0.05VCF	1.12	200	100
GNP4-0.2VCF	1.92	177	77
GNP4-0.05RCF	1.76	193	93
GNP4-0.2RCF	2.40	177	77
GCH4-0.05VCF	1.12	204	104
GCH4-0.2VCF	1.28	202	102
GCH4-0.05RCF	1.12	208	108
GCH4-0.2RCF	1.44	193	93
UFS4-0.05VCF	1.76	180	80
UFS4-0.2VCF	1.92	178	78
UFS4-0.05RCF	2.08	187	87
UFS4-0.2RCF	2.08	183	83

As can be seen from the results, all mortars show similar flow values, thanks to the well-balanced use of SP. The plain mortar shows a high workability, with a consistency of 85% without dispersant addition. Mortars with UFS addition are those with less workability, obtaining slightly lower flow values than the other mixtures, despite the greater quantity of SP.
Some hurdles arose in the production process of mortars containing GNP, especially in high concentrations (GNP7). The high hydrophobicity of graphene led to segregation phenomena and to mixing water rejection during the pouring inside molds (Fig. 8.4b).

(a) (b)

Figure 8.4. *Interaction between GNPs and mixing water: a) Separation of the water-filler suspension (red arrow); b) water rejection after casting in mold*

At high doses of GNP, the mortars acquire a foamy appearance, and a separation between the different phases of the mixture (water-filler suspension and solid part) is clearly visible (Fig. 8.4a). The workability problems related to the use of graphene in cementitious materials have already been analyzed in the previous studies of this work (Section 6.2.1) and in literature [100][33] [196].

8.3 Methods

8.3.1 Mechanical properties

The effect of singular and hybrid addition of carbon-based filler and fibers on the mechanical properties of mortars were investigated by *flexural* (R_f) and *compressive* (R_c) strength tests on 40x40x160 mm specimens, according to UNI EN 1015-11:2007.
The measurement setup and the calculation methods for data processing are the same as reported in previous tests (Sections 6.3.1-7.3.1).

8.3.2 Durability

8.3.2.1 Capillary water absorption

As in previous experiments, the durability of the mortars has been assessed by means of *capillary water absorption* tests in the short and long period (Sections 6.3.2–7.3.2), i.e. through the calculation of respectively the absorption coefficient C according to UNI EN 1015-18:2004 and the measurement of water absorbed in the unit area Q_i, according to UNI EN 15801:2010.

8.3.3 Microstructural characterization

Results obtained from mechanical, durability and electrical tests have been validated by microstructural analyzes after 28 days of curing (see Section 6.3.3).

The *total porosity* V_p and the *pores distribution* curves of the mixtures were analyzed through a mercury intrusion porosimeter *Thermo Fisher 240 Pascal*.

8.3.4 Electrical conductivity and self-sensing properties

The electrical and self-sensing properties of the mortars have been individually studied, by measuring both the electrical resistivity of the specimens during the curing period and the fractional change of electrical resistance under mechanical stress (*piezoresistivity*).
The assessment of reliable resistivity values is important to relate the strain sensitivity of the composites with their actual electrical properties.
Therefore, two different systems have been used, and a piezoresistivity measurement setup has been configured, capable of continuously acquiring all the data for assessing the sensitivity of the mortars.

8.3.4.1 Resistivity measurements

The resistivity of the mortars throughout the curing period was measured with a 4-probe DC system. 40x40x160 mm specimens with embedded four stainless steel #6 grids (3.50 mm of aperture and 0.71 mm of wire diameter) were realized. The grids (electrodes) are placed at a distance of 40 mm from each other. To calculate the cell constant K, the geometric parameters of the configuration were used, according to Equation 3.12 (Section 3.5.3.1). From the ratio between l (40 mm) and A (900 mm2) a cell constant K = 44.4 m^{-1} is obtained (Fig. 8.5).

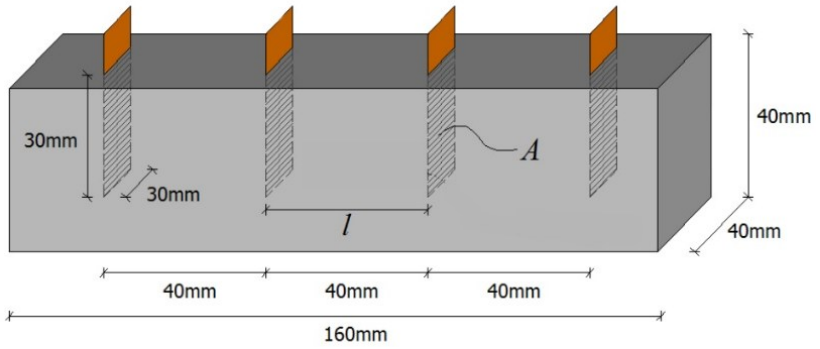

Figure 8.5. *Dimensional characteristics of specimens realized for electronic tests*

The measurement setup is similar to that used for experimenting with pastes (Section 6.3.5.1). An electric tension was applied to the external steel grids, equivalent to a current I (mA) read through a 120 Ω *Shunt resistor*, by using a *DC power supply PROTEK*. Through the two internal electrodes, the voltage U (mV) was read, using a data acquisition device (DAQ) *Data Taker DT80*. The measurements were performed with currents variable in a range from 5 to 5000 μA, and reading the average R values (Fig. 8.6), from which the resistivity ρ was then calculated by Equation 3.3.
The measurements were carried out at 2, 7, 14, 21 and 28 days of curing, and on the dried specimens.

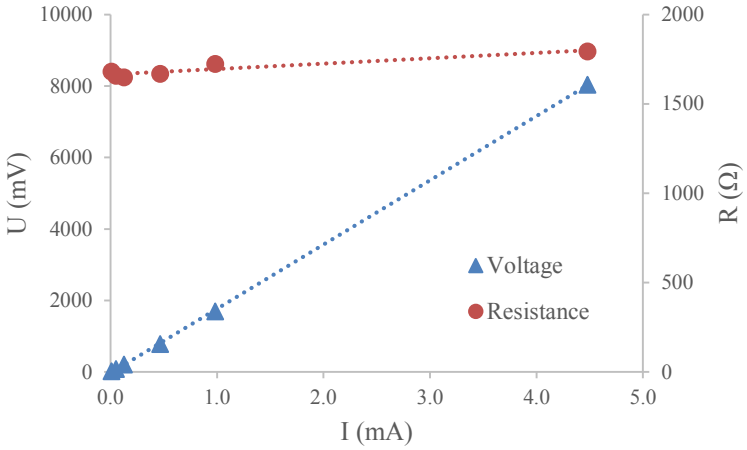

Figure 8.6. *Example of determination of electrical resistance (R) through potential difference (U) and current (I) measurements*

For a complete analysis of the electrical behavior of the specimens, impedance measurements were performed, using a 2-probe configuration and AC devices.
The impedance spectra of dried specimens were evaluated by EIS tests, using a Gamry Reference 600 potentiostat, and performing measurements with a frequency range between 10 Hz and 1 MHz and a signal width of 1000 mV. The test setup and the formulas for data processing and calculation of resistivity ρ are the same of the previous experiments (Section 7.3.4.2).

8.3.4.1 Piezoresistivity tests

The resistivity tests under cyclic loads were performed with a 4-probe DC system, i.e. an extension of the measurement configuration seen in the previous paragraph. Specimens were exposed to quasi-static cyclic compression loads, while their resistivity and their axial deformation were calculated.
An electric current $I_{(t)}$ of at least 5 μA was used, by applying a variable voltage to the external electrodes of the specimens, depending on the conductivity of the material, with a DC power supply. The electric tension was maintained for at least 30 minutes before testing, until the depletion of polarization effect and the stabilization of the resistance values.
Subsequently the stress was applied through a *Shimadzu* press *AG-IC*, isolating the specimen from the press by using plastic plates. An initial load of 2 kN was applied and maintained for 2 min, until the stabilization of the resistivity value. Later, 10 loading/unloading cycles were performed, with increments/decreases of 250 N/s. Three different types of quasi-static loading tests were performed, i.e. with amplitudes of 15 kN, 20 kN and 25 kN, wich led to stresses of 9.4 MPa, 12.5 MPa and 15.6 MPa, respectively. Figure 8.7 shows the execution of a test, and the different devices.

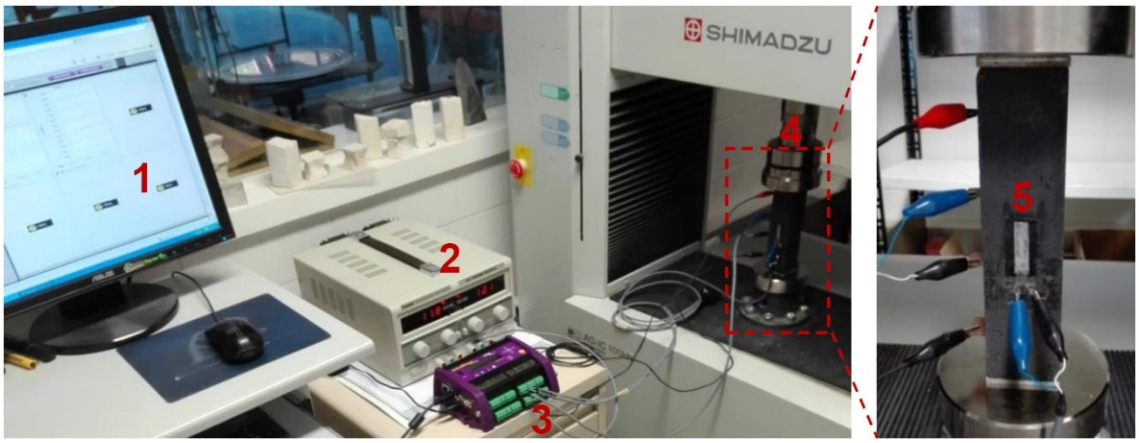

Figure 8.7. *Piezoresistivity test of a mortar specimen and experimental set-up: 1) Computer interface, 2) DC power supply, 3) Data acquisition device, 4) Press actuator, 5) Strain gauge.*

The axial deformation of the composite was measured through a 25 mm 120 Ω strain gauge (Fig. 8.8), with GF = 2.07, paste to the center of the specimen. During the tests, the strain gauge was connected to the DAQ by means of a *Wheatstone bridge*, to obtain an instantaneous and accurate reading of the axial με.

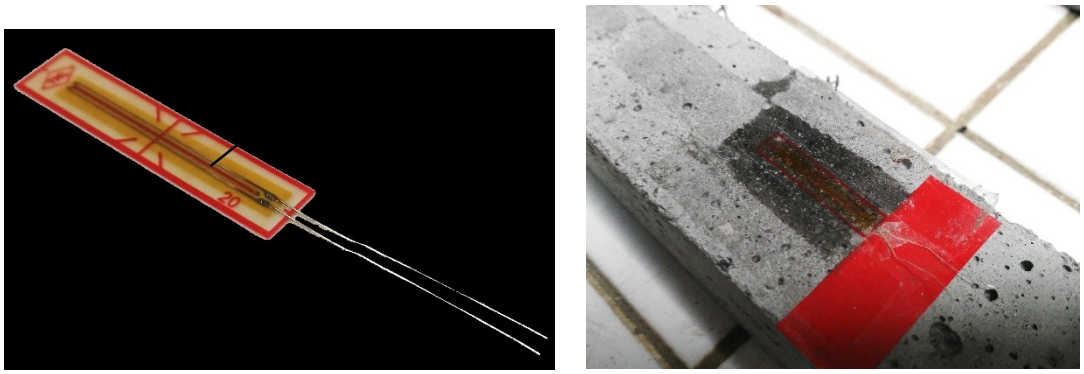

(a) (b)

Figure 8.8. *120 Ω strain gauge used for piezoresistivity tests: a) Working elements; b) Strain gauge paste on a mortar specimen*

The test equipment, i.e. DC power supply and Shimadzu press, were also coupled to the DAQ connected to a software, thus simultaneously detecting the load force, strain, current, voltage, and the resulting electrical resistance of the material. Figure 8.9 shows a schematic illustration of the tests configuration.

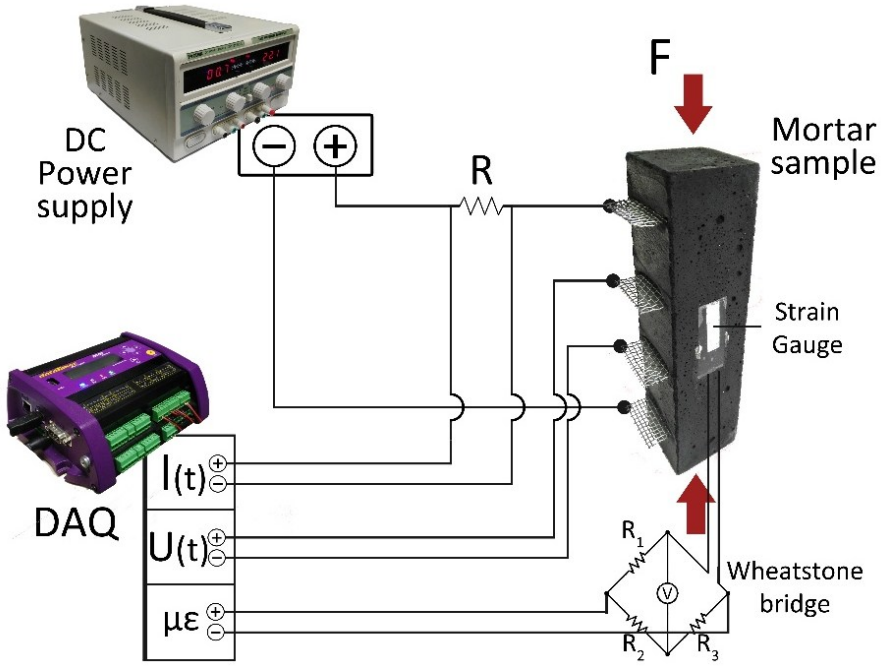

Figure 8.8. *Representation of the setup adopted for strain-sensing measurements*

The specimens were subjected to piezoresistivity tests after 28 days of curing, to ensure the full development of their mechanical properties. At the end of the tests in wet conditions, the specimens were placed in oven at 60°C for several days, until a constant mass was reached, in order to eliminate the influence of the moisture in the electrical behavior of the composites. The tests were thus repeated on specimens in dry conditions. The self-sensing properties of the mortars were assessed through the identification of three parameters: *Gauge Factor* (GF), *Fractional Change in Resistivity* (FCR), and *stress sensitivity*.

The first is the most important technical parameter for strain gauges (Section 3.4), and relates the variation in resistivity of an element with its deformation (Eq. 8.1):

$$GF = \frac{\frac{\Delta\rho}{\rho}}{\frac{\Delta L}{L}} = \frac{\frac{\Delta\rho}{\rho}}{\varepsilon} \tag{8.1}$$

FCR measures the change in resistivity ρ as a function of time, compared to the initial value (Eq. 8.2)

$$FCR = \frac{\rho_{(t)} - \rho_0}{\rho_0} \tag{8.2}$$

Lastly, stress sensitivity relates FCR with the axial stress σ (Eq. 8.3):

$$Sensitivity = \frac{FCR}{\Delta\sigma} \tag{8.3}$$

8.4 Results and discussions

8.4.1 Mechanical characterization

The results of mechanical strength tests showed that recycled filler addition leads to an increase in mechanical resistance of mortars, contrary to graphene, which tends to decrease the performance of the composites. CFs have a notable effect on the mechanical properties of mortars. The growth of mechanical strengths of the mixtures during the curing period is shown in Table 8.3.

Table 8.3. *Flexural strength (R_f) and Compressive strength (R_c) of mortars (percentage comparison with reference on the right)*

Mixtures	R_f (MPa)			R_c (MPa)			REF comp. 28 days (%)	
	2 days	7 days	28 days	2 days	7 days	28 days	R_f	R_c
REF	4.4	5.3	6.9	13.6	20.8	31.5	-	-
GNP4	4.2	5.0	6.4	13.0	19.0	29.3	94	93
GNP7	2.2	5.7	7.0	6.5	18.7	24.4	102	78
GCH4	4.1	5.4	7.3	15.2	23.9	34.5	106	110
GCH7	2.7	5.7	6.6	11.0	25.0	31.6	96	101
UFS4	4.5	5.6	8.6	15.8	23.3	34.4	125	109
UFS7	2.4	5.1	6.3	8.3	22.9	31.9	92	101
0.05VCF	3.3	5.2	7.5	11.3	19.3	29.3	109	93
0.2VCF	3.7	4.8	7.2	13.6	20.9	30.2	105	96
0.05RCF	2.0	5.0	6.7	5.9	19.1	28.3	98	90
0.2RCF	2.4	5.7	7.3	8.1	20.9	29.0	106	92
GNP4-0.05VCF	4.9	5.3	6.7	15.7	19.0	27.4	97	87
GNP4-0.2VCF	4.5	4.9	6.6	16.1	18.2	27.7	96	88
GNP4-0.05RCF	4.3	5.0	6.0	14.7	17.6	25.7	87	82
GNP4-0.2RCF	4.1	4.6	5.8	13.2	15.8	25.2	85	80
GCH4-0.05VCF	4.6	5.6	6.8	17.7	22.7	34.0	99	108
GCH4-0.2VCF	5.1	5.9	6.9	18.3	22.8	31.3	101	99
GCH4-0.05RCF	3.9	5.9	6.5	15.3	22.7	32.2	94	102
GCH4-0.2RCF	5.0	6.2	6.5	17.0	24.0	31.4	94	100
UFS4-0.05VCF	5.2	5.2	6.6	19.4	23.0	33.6	97	107
UFS4-0.2VCF	5.1	5.3	7.4	20.2	20.5	34.9	108	111
UFS4-0.05RCF	4.8	5.1	7.0	18.3	22.1	33.5	102	106
UFS4-0.2RCF	5.4	5.4	6.7	18.8	22.7	32.7	98	104

The results underline the rapid development of the flexural strength in the first days of curing, with values reaching 59% and 78% of the final resistances, respectively at 2 and 7 days. The growth trend of R_f values is similar for all mortars, and it is not related to the type and amount of admixtures.
The values at 28 days of curing (Fig. 8.9) show that the additions do not significantly alter the flexural strength of the mortars. However, slight improvements have been obtained with the addition of VCF and RCF, thanks to the bridging effect of the filaments, which confirm the results obtained in the previous experiments (Section 7.4.1) and in literature [58][116][117]. The addition of recycled fillers also shows slight increases, in particular the UFS4 mixture, with a R_f value greater than 25% compared to REF.
The lowest values were obtained by the GNP-CF hybrid additions, with decreases up to 15% compared to the plain mortar.

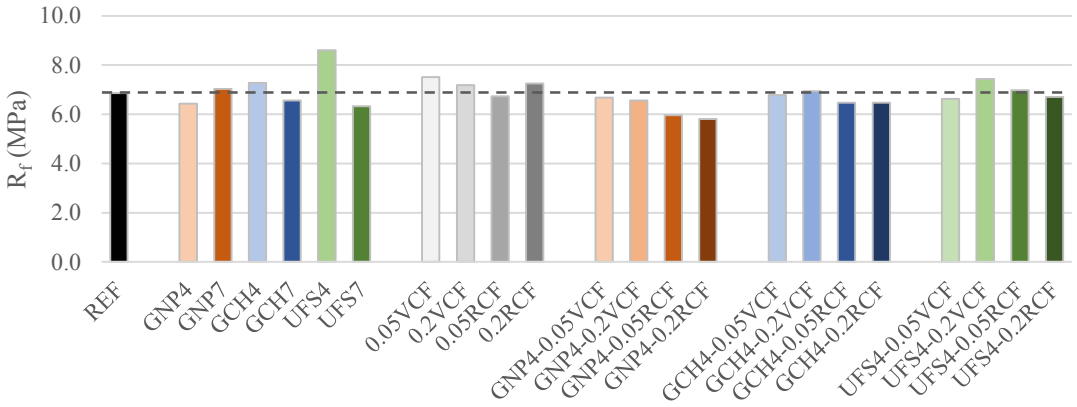

Figure 8.9. *Flexural strength R_f of mortars at 28 days of curing*

The differences between the effect of graphene and the other fillers is also visible from the results of compressive strength tests (Fig. 8.10).
The addition of GCH and UFS leads to an increase in R_c values. Even the mortars with hybrid additions of GCH/UFS and CF show an increase in compressive strength. The highest values have been obtained by GCH4 and UFS4-0.2VCF mortars, with increments of 10% compared to REF.
In contrast, the addition of GNP bring to a decrease in mechanical compression strengths, both individually and in hybrid additions with CFs. At higher concentrations, GNP further reduce the mortar resistance, with a decrease of 22% compared to the plain mortar.

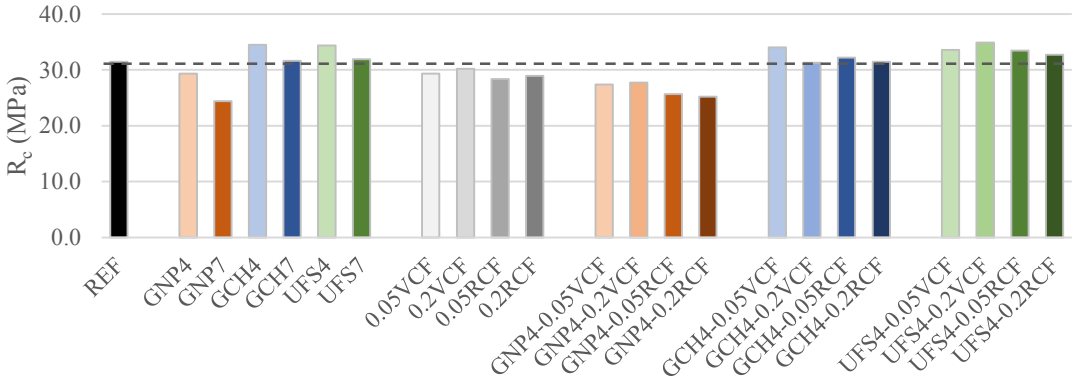

Figure 8.10. *Compressive strength R_c of mortars at 28 days of curing*

The lower mechanical performances of the mortars with GNP are linked to the difficulties encountered during their mixing and casting (Section 8.2.1). The addition of graphene, due to its bulk density and its interaction with water, leads to a lack of homogeneity of the mixture and to the formation of a large number of voids within the hardened composite [33]. Furthermore, the high hydrophobicity of graphene contrast the proper hydration of the cement, and leads to a lower development of mechanical performance [122][286].
From the analysis of the inner macrostructure of the specimens (Fig. 8.11) a large presence of large voids in the mortars with graphene is clearly visible. These macro-pores are the main cause of the lower mechanical resistance of mortars with GNP and with hybrid GNP-CF additions.
Contrariwise, the inner structure of mortars with GCH and UFS is more compact (Figures 8.11b-8.11c), and show a lower presence of voids compared to REF, confirming the higher values obtained in the mechanical strength tests.
As seen in Chapter 6 (Section 6.4.1) the presence of micro-fillers reduces the porosity of the cement matrix, working as nucleation sites for C-S-H [273][287][288], and improving the hydration degree as well as the mechanical properties of hardened composites.

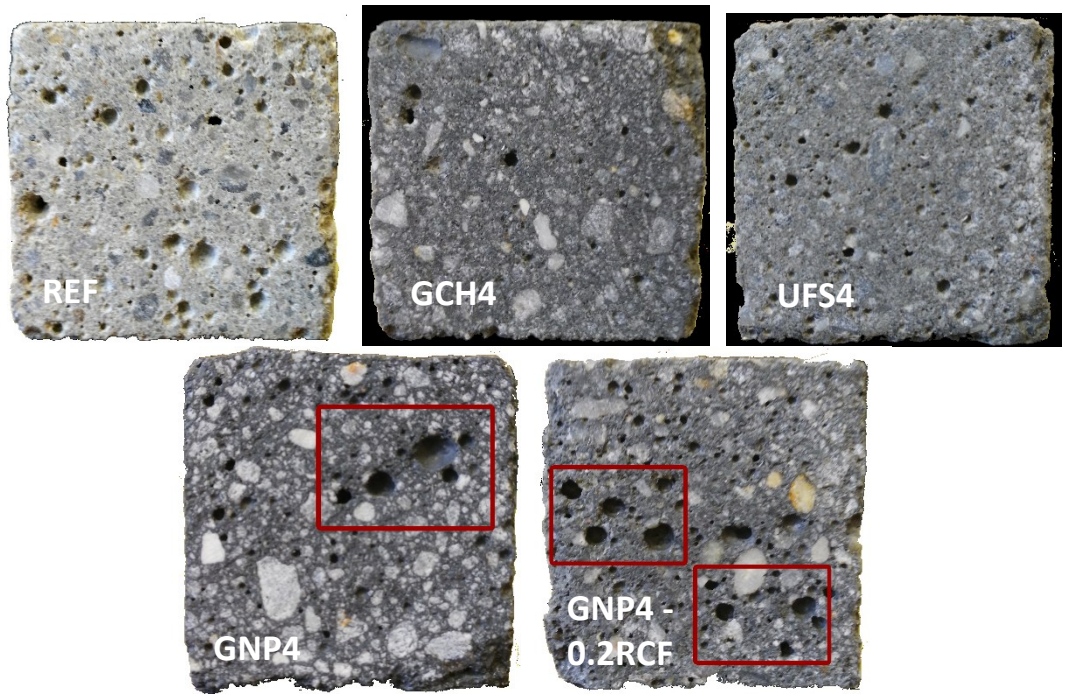

Figure 8.11. *Analysis of the inner macrostructure of mortars: below the macroporosity of the specimens with grapheme are highlighted*

8.4.2 Durability and microstructural characterization

The results of the porosimetric tests confirm that the carbon-based admixtures lead to a refinement of the cement paste microstructure, decreasing the total volume of microporosity and the average diameter of pores. All mortars have similar absorption properties, but the mortars with filler addition show greater waterproof in the short period.

The tests were performed on specimens containing fillers and fibers in both concentrations, in order to study the effect of each individual addition on the microstructure of mortars, and the results are shown in Table 8.4.

Table 8.4. *Total porosity (V_p) and average pore diameter (d_p) from the porosimetric analysis of mortars*

Mixtures	V_p (%)	d_p (μm)
REF	17.4	0.090
GNP4	17.1	0.080
GCH4	16.5	0.075
UFS4	16.7	0.072
GNP7	16.2	0.068
GCH7	15.9	0.067
UFS7	15.5	0.066
0.05VCF	18.4	0.093
0.2VCF	15.7	0.078
0.05RCF	13.9	0.103
0.2RCF	16.5	0.078

An increasing concentration of carbon-based fillers leads to an increasing reduction in the volume of micropores, since mortars with 4% of fillers addition show lower V_p values compared to REF, and the mortars with additions of 7% show even lower values. The average diameter of the pores d_p also follows this trend, decreasing as the amount of filler increases. In contrast, mortars with VCF and RCF show uncertain results, and their values of V_p and d_p do not appear related to the fibers concentration.
The UFS shows a high filler effect, which leads to the best microstructure, with a volume of microporosity equal to 15.5% for the mortar UFS7, or 11% less than the plain mortar. These data also explain the greater mechanical performance of mortars with UFS and UFS + CF. Figure 8.12 shows the porosimetric curves of the analyzed mortars, where it is quite evident that a greater quantity of fillers leads to both a lower amount of micropores and a lower size of pores.

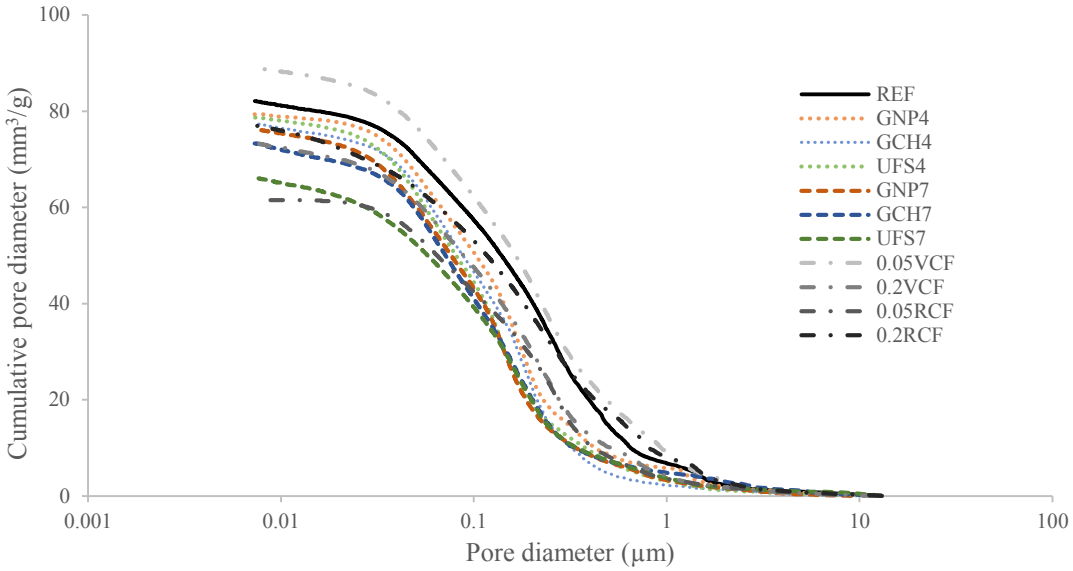

Figure 8.12. *Porosimetric curves of mortars*

The microstructural characteristics of the mixtures also influence their absorption properties. Figure 8.13 shows that the values of water absorption coefficient C of mortars with fillers addition are lower than the reference. The insertion of fibers does not affect the capillary absorption, but the combined use of fillers and CF leads to a further decrease of C, with values up to 27% lower compared to REF (mortars GNP4-0.2RCF and UFS4-0.2VCF). Generally, a greater addition of fillers or fibers leads to a higher resistance to water absorption of the mortar in the short period (lower values of C).

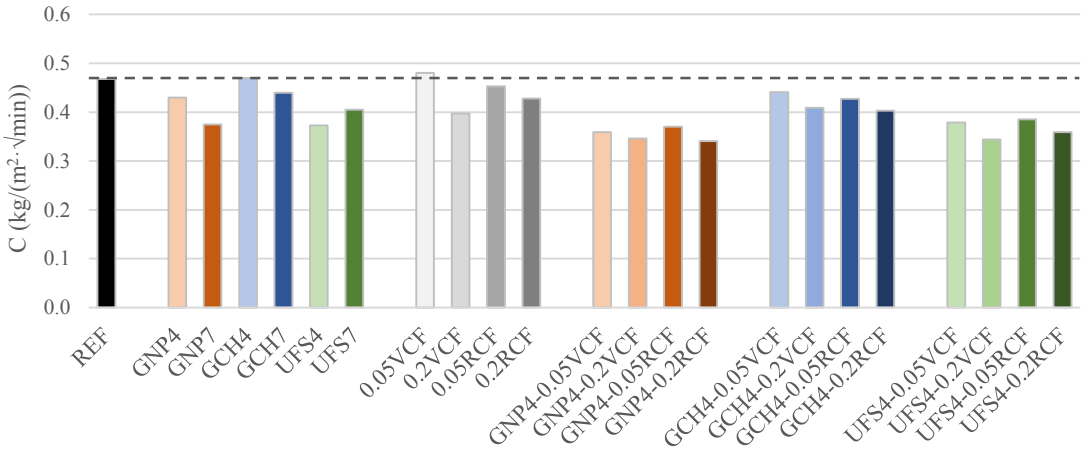

Figure 8.13. *Water absorption coefficient (C) of mortars*

The Q_i vs. time curves (Fig. 8.14) do not show substantial differences between REF and the other mortars in terms of amount of water absorbed in the long period.

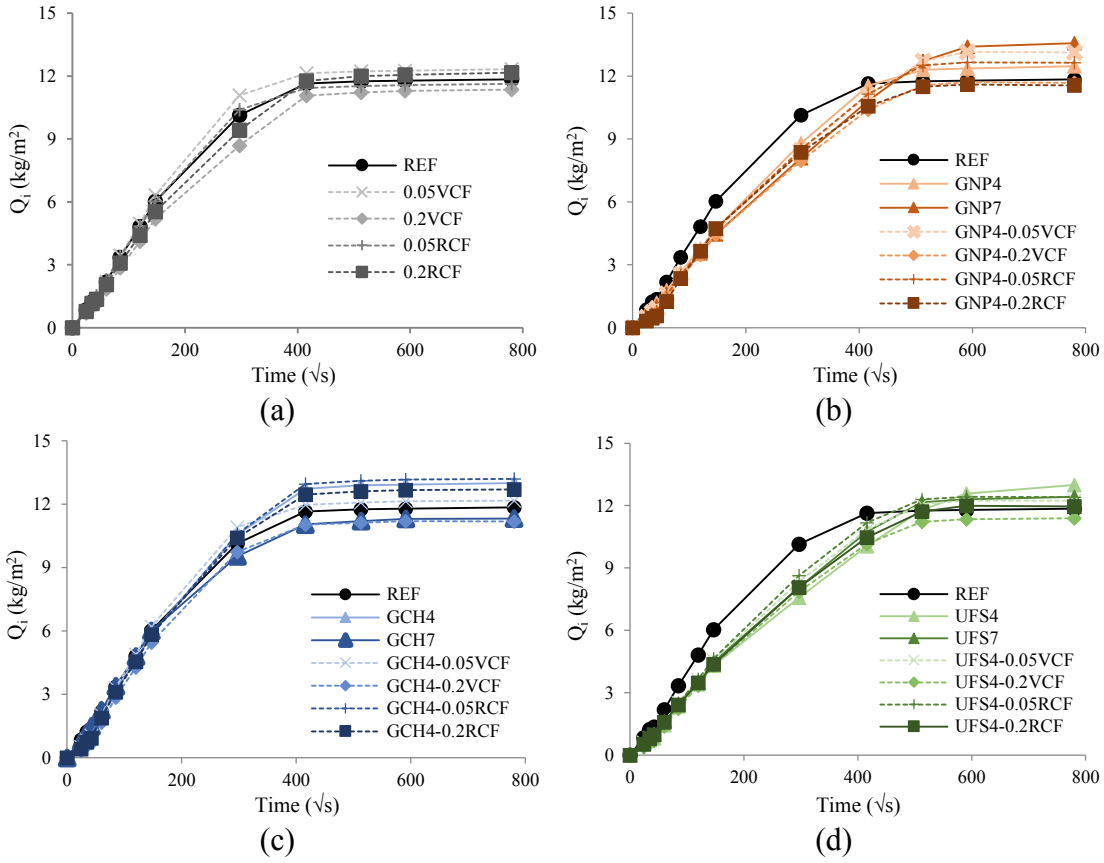

Figure 8.14. *Water absorbed per unit area (Q_i). Comparison between REF and mortars containing: a) CFs, b) GNP and GNP+CFs, c) GCH and GCH+CFs, d) UFS and UFS+CFs*

The results show that mortars containing GNP, UFS and the combination GCH+CFs absorb smaller quantities of water in the first period of moisture exposure. This is also demonstrated by absorption coefficient (AC) values calculated by the slope of the first linear section of the Q_i vs. time curves (first hours of testing, Fig. 8.15).

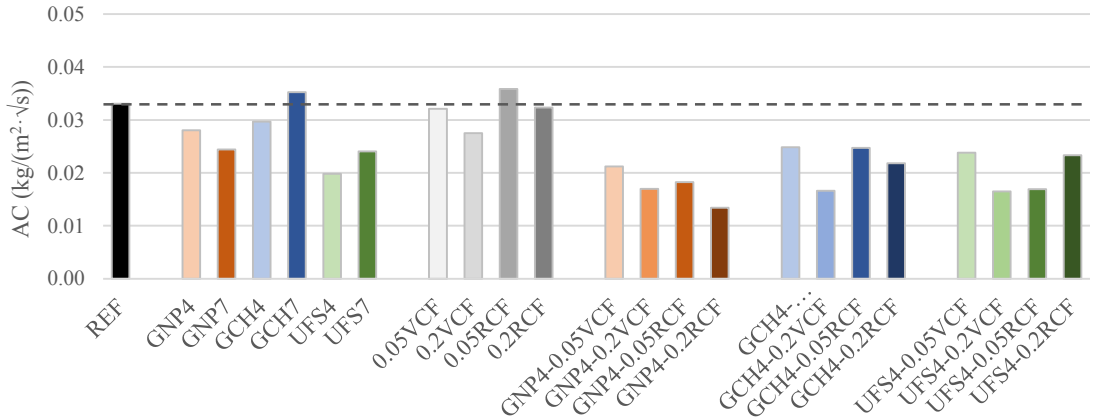

Figure 8.15. *Water absorption coefficient (AC) of mortars calculated from the first linear part of the Q_i vs. time curves*

The high concentration of macropores within the mortars with GNP (Fig. 8.11) did not affect their absorption properties. Indeed, it is well known that the capillary suction of water mainly concern pores of size ≤ 10 μm, and is practically nil within pore sizes > 100 μm. Despite the incorporation of air voids into the composites, the GNP has led to an improvement in the microstructure, and thus to a lower presence of capillary pores compared to the reference (Table 8.4).

8.4.3 Electrical properties and strain-sensing

8.4.3.1 Electrical resistivity

The results of the electronic tests have shown the remarkable influence of carbon-based additions on the electrical conductivity of the mixtures, but also the effect of other parameters, such as moisture. The different test methods showed different electrical behaviors of the composites, which required an in-depth analysis of the data.
During the first 28 days of curing, the DC measurements showed a linear increase in the resistivity values of almost all the mortars, as shown in Figure 8.16.

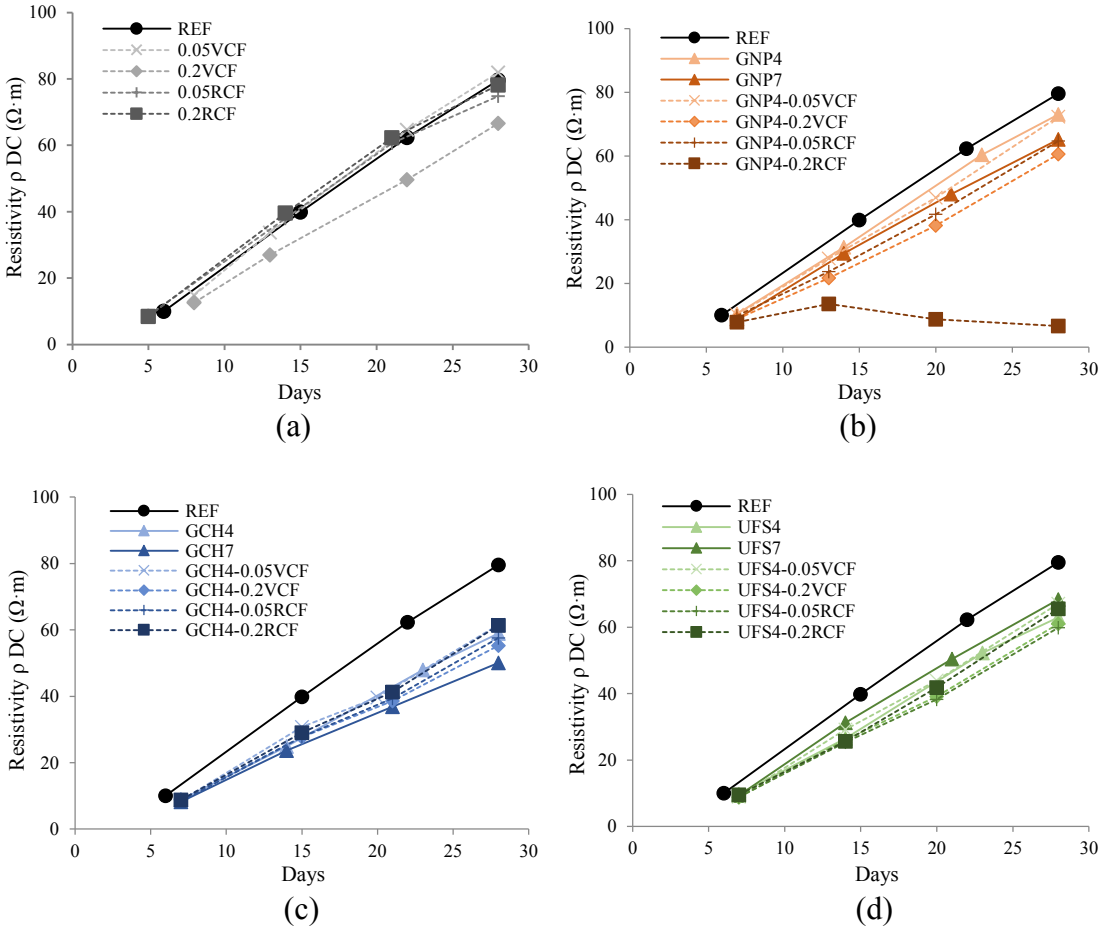

Figure 8.16. *Electrical resistivity (ρ) in the first 28 days of curing. Comparison between REF and mortars containing: a) CFs, b) GNP and GNP+CFs, c) GCH and GCH+CFs, d) UFS and UFS+CFs*

The singular addition of fibers does not lead to variations in the electrical properties of the composites, with the exception of 0.2VCF (Fig. 8.16a); while fillers or hybrid fillers-fibers insertion bring to a substantial decrease of ρ values in the first curing periods. The most effective additions are GCH and GCH-CF hybrids, with average decreases of 29% compared to REF (Fig. 8.16c).
Only one mixture does not show a linear growth of electrical resistivity in time, that is the mortar with hybrid GNP4-0.2RCF addition, with values of ρ almost unchanged in the first weeks. This is also the most electrically conductive mixture, with a resistivity of 6.7 Ω·m at 28 days, i.e. 90% less than the reference (Fig. 8.17).
In most cases, a higher amount of fillers and/or fibers leads to an increase in electrical conductivity, but this effect does not always occur.

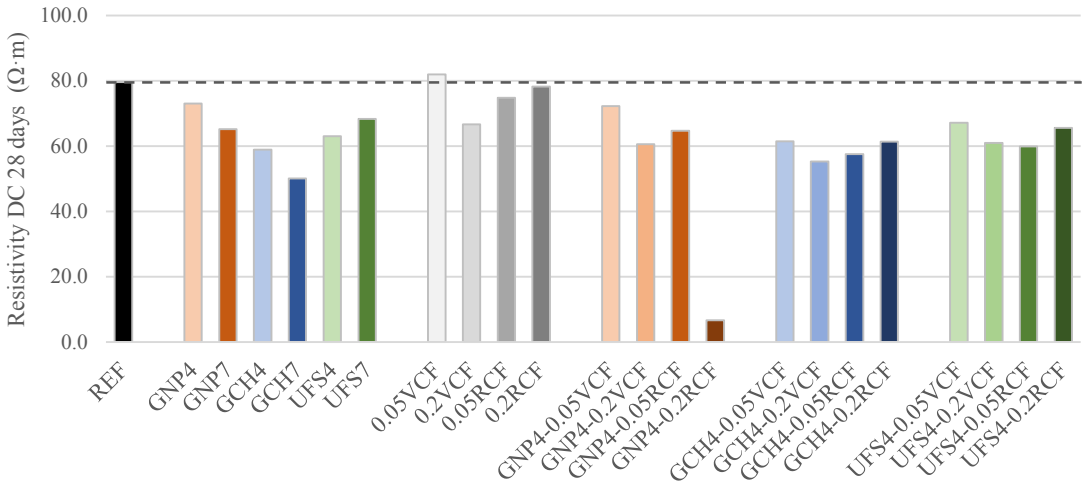

Figure 8.17. *Electrical resistivity ρ of mortar specimens at 28 days of curing*

To distinguish the electrical contribution of carbon-based admixtures from the influence of moisture within the porosity of the composites, the DC resistivity tests were repeated on the specimens dried in oven. The results are shown in Figure 8.18.

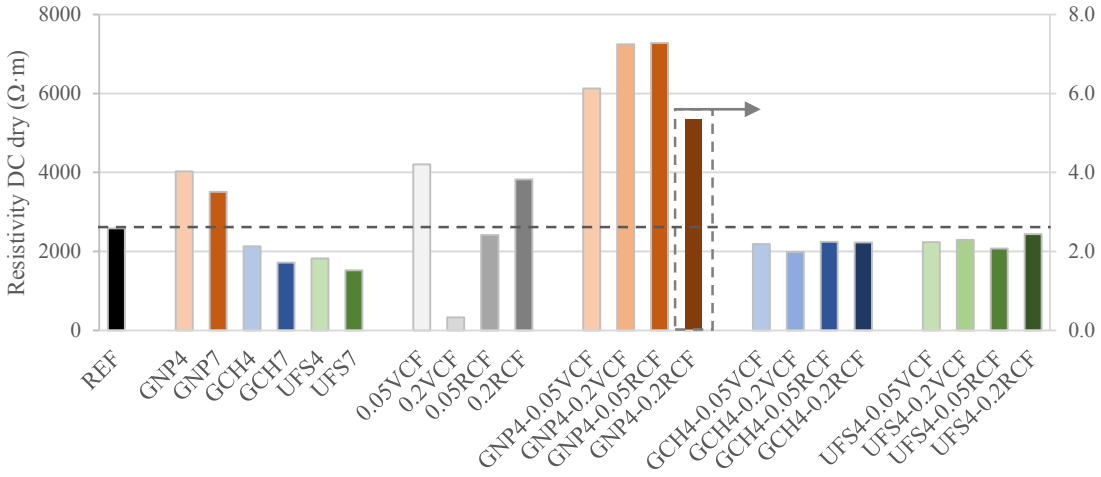

Figure 8.18. *Electrical resistivity ρ of dry mortar specimens (GNP4-0.2RCF refers to the scale on the right)*

It is clearly visible that the conductivity of the materials decreases drastically after the elimination of water inside the pores, since the resistivity increases by approximately two orders of magnitude compared to the values measured at 28 days. The removal of water amplify the differences in the electrical behavior of the mixtures, as can be seen from the greater variability of the values.
The most evident result is the high electrical resistivity of the mortars containing GNP, which increases by 100 times compared to the values measured at 28 days, and up to 280% compared to the value of the plain mortar (GNP4-0.2VCF and GNP4 0.05RCF).
This effect is due to the macrostructure of the GNP-mixtures cement-matrix. As previously analyzed, the lack of homogeneity of fresh mortars containing GNP (Section 8.2.1) and the high hydrophobicity of graphene have led to a high number of large pores within the hardened composite (Section 8.4.1, Fig. 8.11). In the first curing period, their effect on electrical properties is hidden by the within water, which decreases resistivity by ionic conduction [12][197]. However, after drying and water removing, the large number of voids creates electrical discontinuities, which prevail the effect of conductive powders in the electrical properties of the composites.
This phenomenon also occurs with the individual additions of VCF and RCF, which probably hindered the good compaction of the mixture inside molds, contributing to the formation of voids, as suggested by the previous experimentation (Section 7.4.1, Fig. 7.17) and by the lower mechanical compressive strengths (Fig. 8.10).
Contrariwise, GCH and UFS produce a good contribution for the electrical properties of mortars, whether used singularly or in combination with CF. Furthermore, it is demonstrated that a greater content of filler leads to an increase in conductivity, since mortars GCH7 and UFS7 show a lower resistivity of 34% and 41% respectively compared to REF.
This effect is linked to the electrical properties of these admixtures, but also to the filler effect of GCH and UFS powders, which leads to a decrease of both micro- and macro-porosity (Fig. 8.11, Tab. 8.4).
Another clear result of the tests is the very different behavior of the 0.2VCF and GNP4-0.2RCF mixtures, which show a significantly higher conductivity compared to the other composites. The 0.2VCF specimens, after drying, show an average resistivity of 333.3 Ω·m, or 87% less than the plain mortar.
The GNP4-0.2RCF mixture does not even show any conductivity decrements after the elimination of water, and its resistivity of 5.4 Ω·m is almost 3 orders of magnitude lower than the other mortars.
The unexpected differences between these two mixtures and other mortars are probably due to a perfect and homogeneous distribution of conductive admixtures within the cement matrix, which has created very effective electronic conduction paths.
These results require further analysis for a better understanding of the multi-phase behavior of the composites. EIS tests were thus performed, and the impedance spectra obtained from the mixtures were carefully analyzed. The resistivity values measured in AC are reported in Figure 8.19.

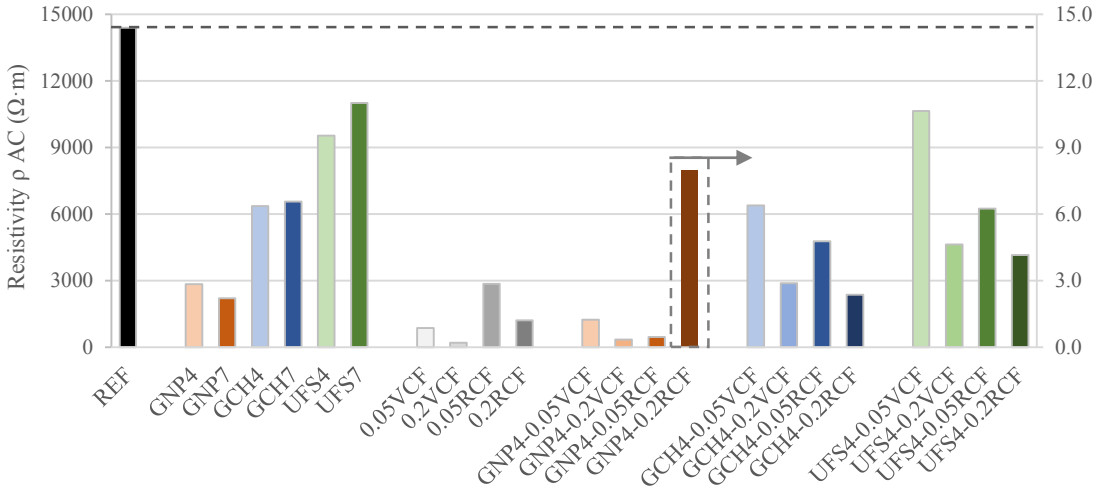

Figure 8.19. *Electrical resistivity ρ of dry mortar specimens by AC measurements*

The results show that the electrical contribution of carbon-based additions is much more visible with this measurement system, since all mixtures containing fillers and fibers show less resistivity than REF. Furthermore, the effect of the insertion of highly conductive materials is more noticeable, since the mortars with a higher content of GNP and CFs show a much lower electrical resistivity compared to the plain mortar (GNP7, 0.2VCF, 0.2RCF, GNP4-0.2VCF).
The differences between the values obtained from the tests performed in DC by a digital multimeter and the values obtained through EIS in AC are linked to the multi-phase nature of the mixtures, and to the electrochemical phenomena seen in the previous Chapter (Section 7.4.3).
The values of resistance R obtained in DC are comparable to the values obtained at low frequencies with AC devices, related to the resistance of the matrix R_m, steered by ionic conduction and more influenced by the microstructure of the cement paste.
Instead, the impedance spectrum consisting of the |Z| values detected in a wide range of frequencies (10^1-10^6 Hz) allows to analyze the resistance of the composite R_c (high frequencies), connected both to the ionic conduction of the matrix and to the electronic conduction of the admixtures (Fig. 7.27).
For this reason, the macro-porosity inside the GNP-mixtures entail a great increase in resistivity values obtained by the DC measurements, while their effect is less influential in the AC measurements, where the conductive paths created by graphene (tunneling conduction [4][12]) decrease the R_c values.
The presence of GNP or CF within the specimens involve the formation of a double arc in their impedance spectrum, in which the values of |Z| of the cusp represent the resistance of the composite R_c (Fig. 8.20).

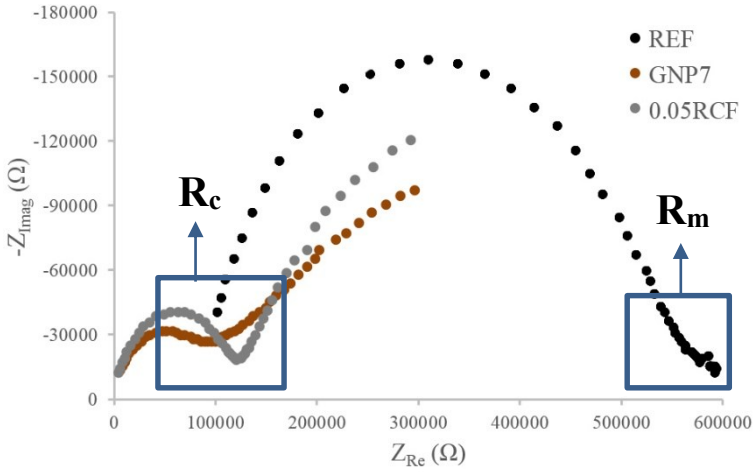

Figure 8.20. *Nyquist plot of REF, GNP7 and 0.05RCF mortars: the double arc cusp formed by the presence of GNP and CFs is the set of points that identifies the resistance of the composite* R_c

This effect is not visible in the specimens with GCH and UFS, which show a curve similar to that of the plain mortar. The electrical contribution of recycled fillers is however visible from the lower values of ρ (Fig. 8.19). In particular, the single addition of GCH decreases the resistivity by 56%. The GCH-CF hybrid additions lead to even greater decrements, with resistivity up to 2367 Ω·m (GCH4-0.2RCF), or 84% less than REF.
The singular addition of recycled fillers improves the conductivity of the composites mainly by acting on the mortars microstructure, i.e. decreasing the porosity thanks to the filler effect. This behavior has already been studied in DC measurements (Fig. 8.18), and is confirmed by the Nyquist plots obtained from the EIS, where only the resistance of the cement matrix is visible (GCH7, Fig. 8.21).
The addition of CFs improves the electrical contribution of recycled fillers, increasing the electronic conduction paths, thus forming a double-arc diagram typical of multi-phase composites (GCH4-0.2RCF, Fig. 8.21).

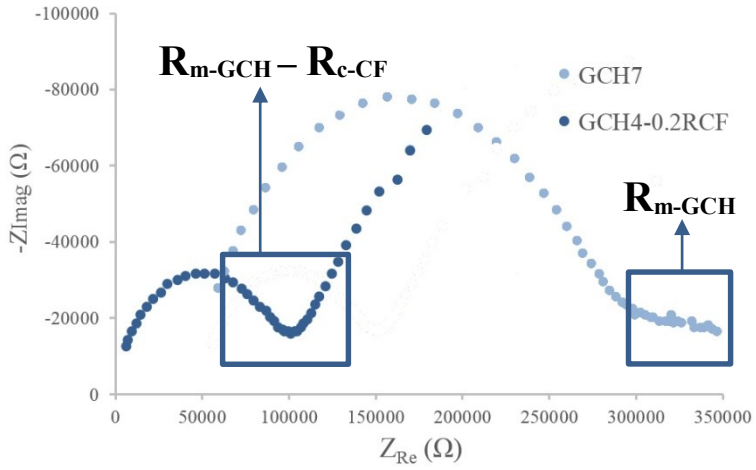

Figure 8.21. *Nyquist plot of GCH7 and GCH4-0.2RCF. The presence of CFs forms the cusp wich identifies the electric contribution of GCH, CFs e cement matrix*

Lastly, the EIS tests confirmed the highly conductive nature of the 0.2VCF and GNP4-0.2RCF mixtures, which show very low resistance values, similar to those obtained in the DC measurements.
As supposed, a very effective dispersion of these additions has probably led to a dominance of the electronic conduction on the ionic conduction of the matrix, a phenomenon also described by the very accentuated cusp of the impedance spectra (Fig. 8.22).

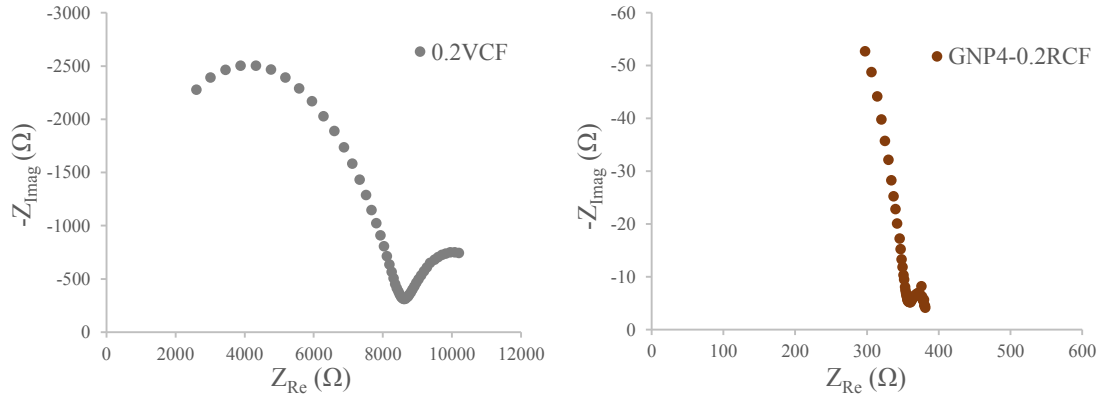

Figure 8.22. *Nyquist plot of 0.2VCF and GNP4-0.2RCF*

For a better analysis of the results, in Appendix B the Bode and Nyquist plots obtained by the EIS tests on all the mixtures are reported.

8.4.3.2 Strain-sensing

The measurements of conductivity under load showed the great influence of moisture on the sensorial properties of the mortar specimens.
After short periods of curing (28 days) the high content of water inside the pores cancels the stress sensitivity of the material. This effect does not change regardless of the type and amount of addition, as seen in Figure 8.23, which shows the *FCR vs. time* and the *Strain vs. time* trends of some mixtures subjected to load cycles. The FCR values of the 0.2VCF mortar show no relation to the compression strain of the specimen, while the electrical resistances of GCH4-0.2VCF and UFS4-0.2VCF show only slight decreases during application of the maximum load.

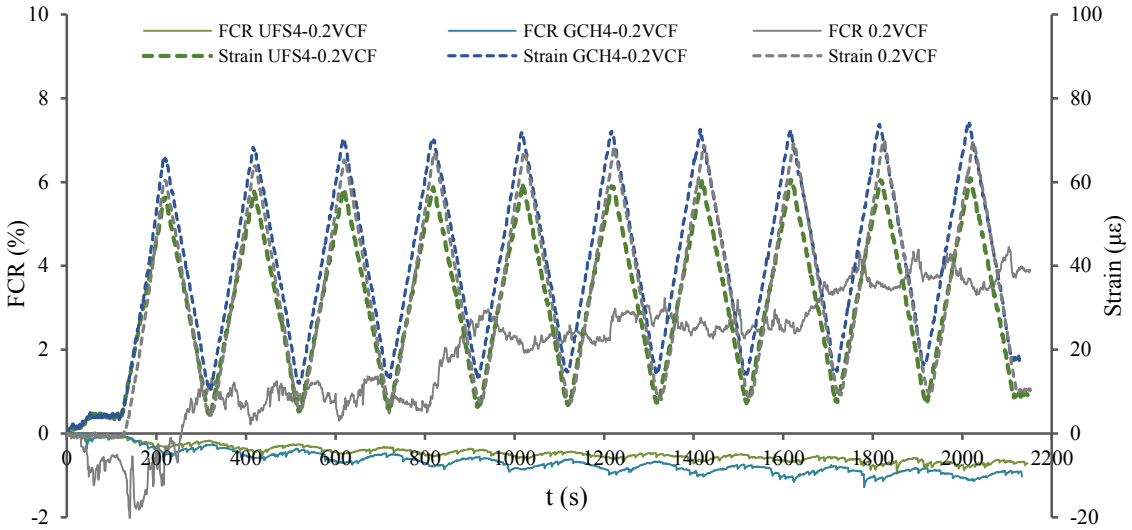

Figure 8.23. *Piezoresistivity tests at 28 days of curing: FCR and strain vs. time of mortars under compressive load cycles*

Indeed, it has been shown in the literature that humidity conditions have a significant influence on the piezoresistive properties of multifunctional composites [168][197]. This influence is overcome only with concentrations of fillers and fibers above the percolation threshold [126].
Successively, the uncertainty related to humidity was eliminated by drying the specimens, i.e. simulating the conditions of specimens subjected to long periods of curing. The tests were then repeated on dry specimens, and the analysis of FCR values showed a very different behavior between highly conductive mortars (0.2VCF and GNP4-0.2RCF) and other composites.
Low conductivity mortars, including REF, denote an unusual piezoresistive behavior, i.e. an emphasized increase in resistivity when subjected to compressive load cycles. Contrariwise, highly conductive mortars show a traditional piezoresistive behavior, that is, their electrical resistivity decreases when the specimen is subjected to compression strain (reduction of distance between conductive particles).
The piezoresistive parameters obtained from stress-sensitivity tests are shown in Table 8.5.

Table 8.5. *Electrical and piezoresistive parameters of mortars*

Mixtures	ρ_0 DC (Ω·m)	max. Strain (με)	max. FCR (%)	GF	Stress sensitivity (MPa^{-1})
REF	2587.3	69.7	14.8	2124	$9.5 \cdot 10^{-3}$
GNP4	4030.9	74.5	-	-	-
GNP7	3509.2	98.1	-	-	-
GCH4	2134.4	55.9	4.0	724	$2.6 \cdot 10^{-3}$
GCH7	1716.4	78.2	4.7	602	$3.0 \cdot 10^{-3}$
UFS4	1820.4	46.5	8.3	1789	$5.3 \cdot 10^{-3}$
UFS7	1524.6	62.0	15.0	2428	$9.6 \cdot 10^{-3}$
0.05VCF	4208.4	72.3	9.0	1250	$5.8 \cdot 10^{-3}$
0.2VCF	333.3	80.5	-4.8	-593	$-3.1 \cdot 10^{-3}$
0.05RCF	2414.3	70.5	3.2	454	$2.1 \cdot 10^{-3}$
0.2RCF	3825.3	74.2	6.4	869	$4.1 \cdot 10^{-3}$
GNP4-0.05VCF	6121.8	85.5	-	-	-
GNP4-0.2VCF	7244.5	85.1	-	-	-
GNP4-0.05RCF	7278.5	70.2	-	-	-
GNP4-0.2RCF	5.4	92.8	-2.2	-232	$-1.4 \cdot 10^{-3}$
GCH4-0.05VCF	2187.0	62.2	5.6	902	$3.6 \cdot 10^{-3}$
GCH4-0.2VCF	1986.9	69.3	15.4	2229	$9.9 \cdot 10^{-3}$
GCH4-0.05RCF	2240.8	66.5	7.8	1171	$5.0 \cdot 10^{-3}$
GCH4-0.2RCF	2228.3	90.0	11.4	1262	$7.3 \cdot 10^{-3}$
UFS4-0.05VCF	2232.6	78.2	-	-	-
UFS4-0.2VCF	2293.3	78.5	14.4	1831	$9.2 \cdot 10^{-3}$
UFS4-0.05RCF	2070.7	81.9	12.9	1572	$8.2 \cdot 10^{-3}$
UFS4-0.2RCF	2435.4	71.7	17.9	2498	$11.5 \cdot 10^{-3}$

As can be seen from the results, most of the mixtures (including REF) obtained high positive FCR values, which led to high values of GF and stress sensitivity. This piezoresistive behavior is not related to the amount of admixtures, since the plain mortar shows a high sensitivity despite the lack of carbon-based fillers and fibers. Figure 8.24 shows the relationship between deformation and resistivity change during load cycles of the reference and other mortars containing recycled fillers and hybrid additions.

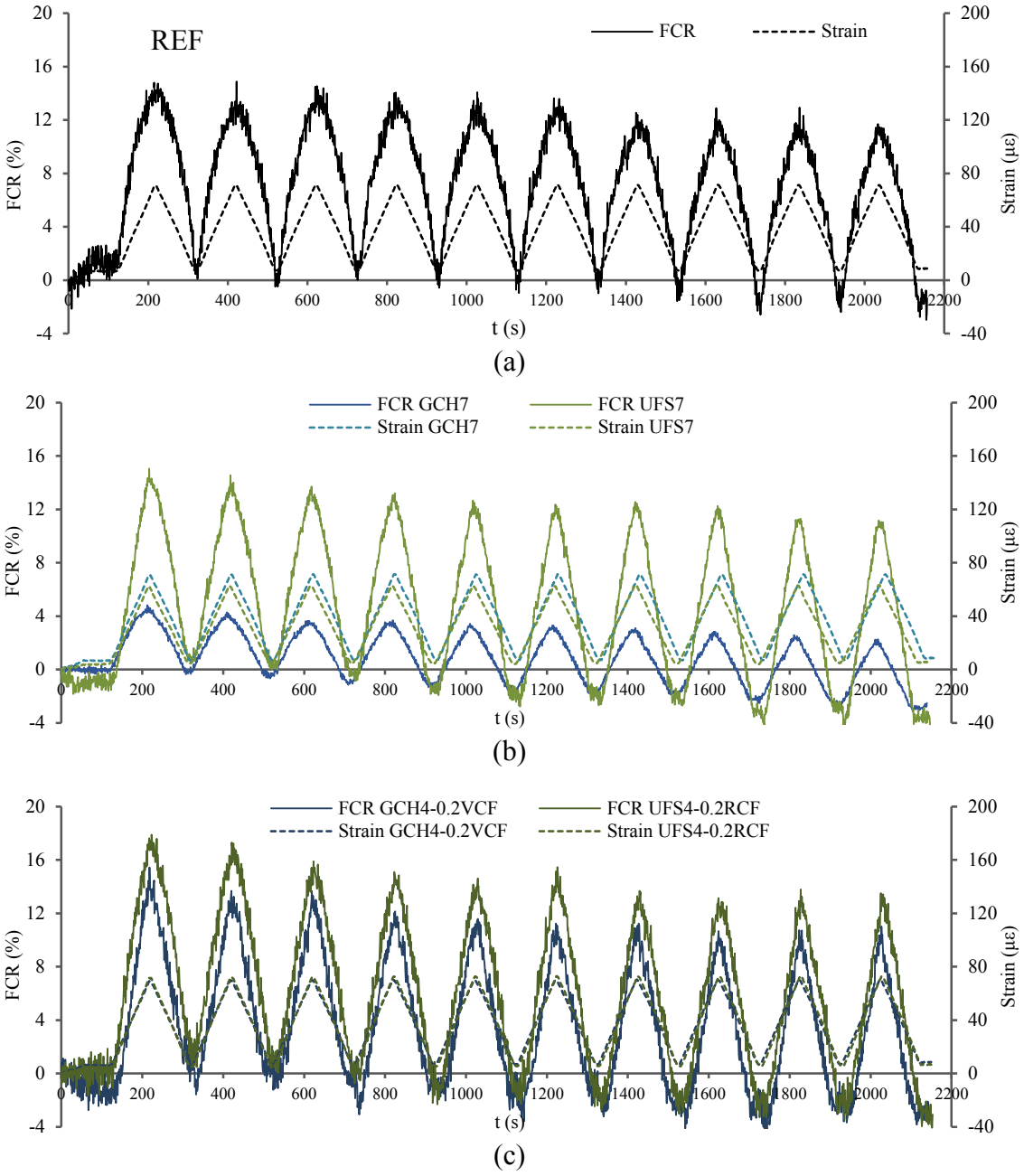

Figure 8.24. *Piezoresistivity tests on dry specimens. FCR and strain vs. time of: a) REF, b) Mortars with recycled carbon fillers, c) Mortars with hybrid recycled fillers and CFs addition*

The graphs show an increase and a decrease in the electrical resistivity linked to an increase and decrease of the compressive stress, respectively. The FCR values are very high, both in the reference (variations up to 14.8%) and in the other mixtures. The largest percentage changes were achieved by UFS4-0.2RCF, with a Max. FCR equal to 17.9%, from which the highest values of Gauge factor and stress sensitivity were obtained (respectively 2498 and $11.5 \cdot 10^{-3}$ MPa^{-1}).

Figure 8.25 shows the linear relationship between FCR and Strain considering all load cycles. The graphs also show a high repeatability of the measurements, with slight

hysteresis due to the electrical stabilization of the specimens [173][183]. The mortars with hybrid additions show a greater scattering of the points, and therefore a lower accuracy of the reading compared to the mixtures without carbon fibers.

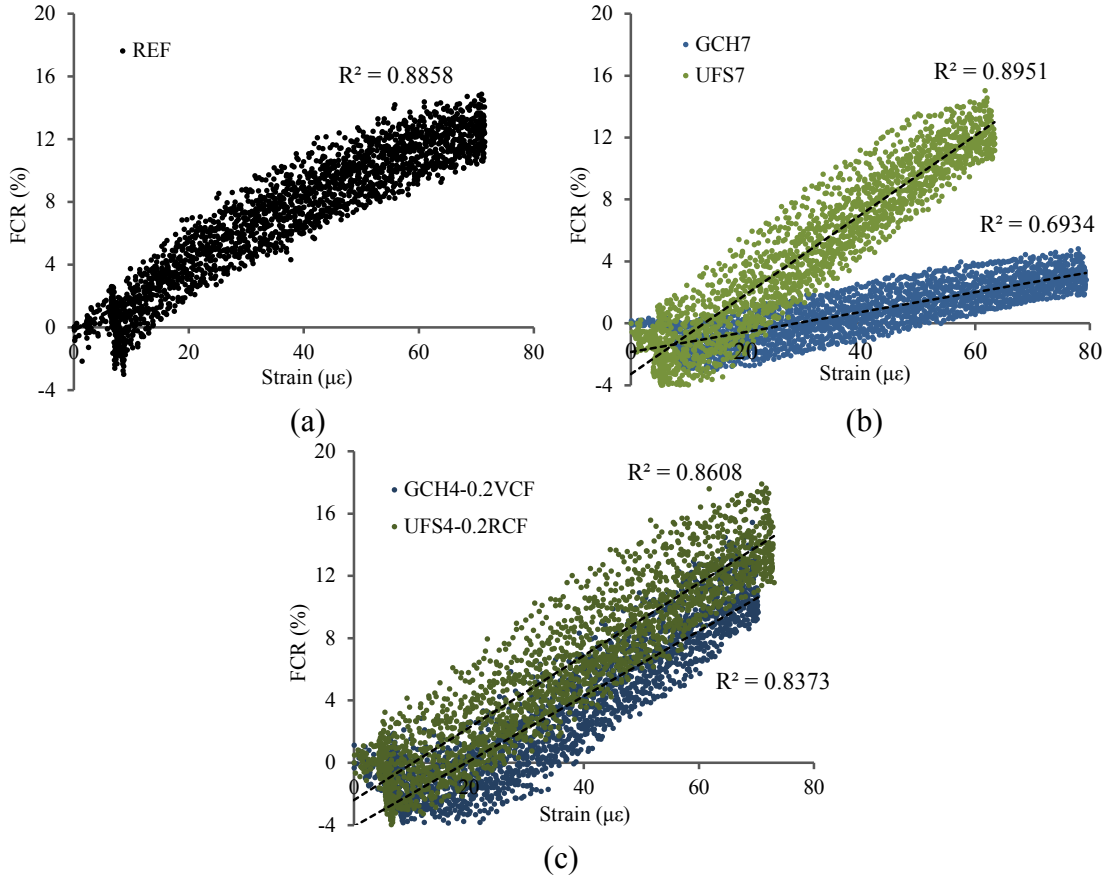

Figure 8.25. *FCR vs. Strain for 10 load cycles: a) REF, b) Mortars with recycled fillers (GCH7, UFS7), c) Mortars with hybrid additions (GCH4-0.2VCF, UFS4-0.2RCF)*

In contrast, mortars with graphene show very low stress sensitivity, as shown in Figure 8.26. As seen previously, the electrical resistivity of the GNP-based mortars measured in DC is very high, due to the great influence of the macrostructure of the material. This factor led to problems in measuring the resistance variations, linked to very low currents inside the material, as well as to high scattering phenomena (GNP4-0.2VCF).

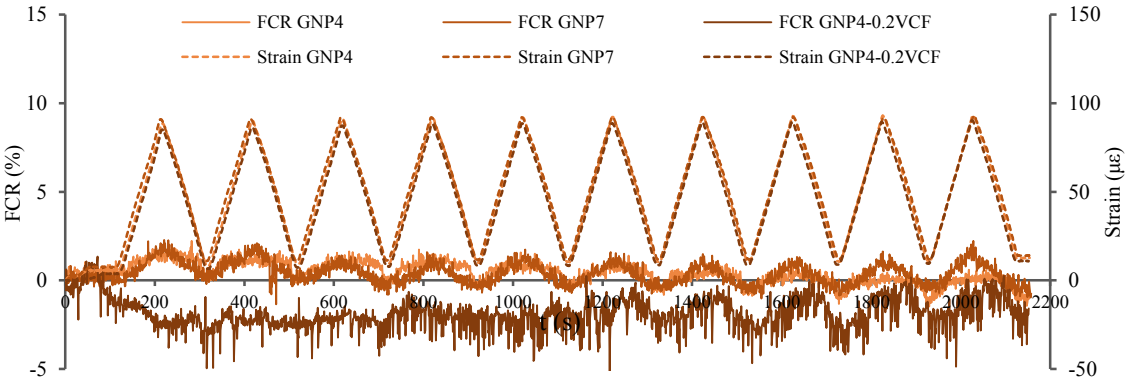

Figure 8.26. *FCR and strain vs. time of GNP-based mortars*

However, the data obtained require further theoretical insights, since the piezoresistive effects analyzed do not have a clear comparison in literature. As seen in Chapter 4 (Sections 4.3-4.4), most of the studies on the self-sensing properties of cement-based materials show a decrease in the electrical resistivity of the specimens subjected to compression loads, due to the shortening of the electric paths and the approach of conductive particles (tunneling effect).
The opposite phenomenon obtained in this experimentation could be an intrinsic effect of some mixtures or could be connected to other factors, e.g. to the measurement system and to the interaction between electrodes and cement matrix.
For example, the application of compressive stresses could lead to the formation of micro-cracks inside the material and to a slight pull-out effect of the fibers, and therefore to the formation of electrical discontinuities studied in literature through theoretical models. [207].
This phenomenon is not present in the measurements carried out for short periods of maturation (see the results of the tests at 28 days), but appears after the drying of the specimens and the considerable increase in their resistivity.
Contrariwise, the highly conductive mortars 0.2VCF and GNP4-0.2RCF showed a traditional piezoresistive behavior, with negative FCR values when the compression load is applied, as shown in Table 8.5 (highlighted values). Figures 8.27 and 8.28 show the relationship between strain and resistivity variation of these two mortars.

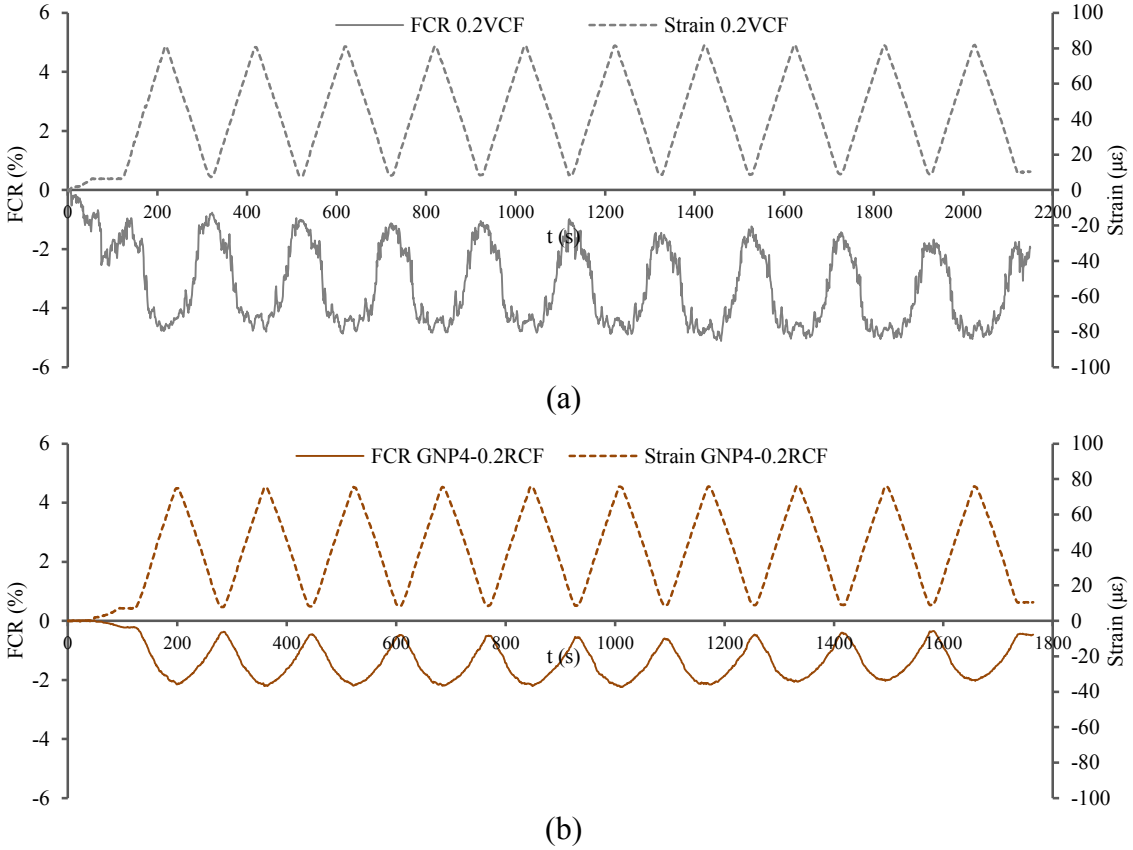

Figure 8.27. *FCR and strain vs. time: a) 0.2VCF, b) GNP4-0.2RCF*

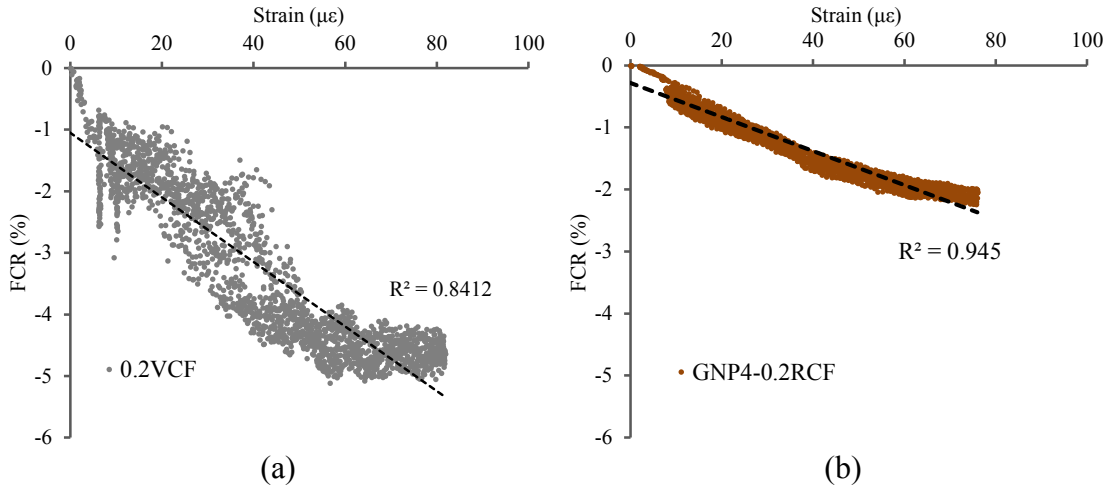

Figure 8.28. *FCR vs. Strain for 10 load cycles: a) 0.2VCF, b) GNP4-0.2RCF*

The 0.2VCF mortar has higher sensing properties than GNP4-0.2RCF, with a GF of 593 and a stress sensitivity equal to $3.1 \cdot 10^{-3}$ MPa^{-1}. However the GNP4-0.2RCF mortar show a higher precision of measurements, and a very low scattering of the points ($R^2 = 0.945$), thanks to the very high conductivity (behavior more similar to a traditional strain gauge). Indeed, it is widely demonstrated in literature that a higher conductivity of cement-based composites does not always lead to an increase in stress sensitivity, but greatly increases the accuracy and the repeatability of the results, through the stabilization of the reading of electrical resistance [95][66][173].

Through an overall analysis of the results, it can be stated that the 4-probe DC measurement system provides information on the piezoresistivite behavior of the cement paste. As analyzed in the previous paragraph, the resistivity measured in DC is influenced by the micro- and macro-structure of the matrix, rather than by the presence of electrically conductive admixtures.

This is demonstrated by the very low sensitivity of the mortars containing GNP, characterized by a very high resistivity due to the high macroporosity. This effect is exceeded by measuring elements with a high conductivity, such as 0.2VCF and GNP4-0.2RCF mortars, where a good dispersion of the additions has led to a prevalence of the electronic conductivity of the carbon-based materials on the ionic conduction of the matrix.

To better understand the results obtained from piezoresistivity tests, additional verification measurements were made using AC instrumentation, and measuring the electrical sensitivity to stress of the reference mortar and other mixtures added with carbon-based fillers fibers.

The resistivity of the specimens was measured by a conductivity meter AMEL 160, operating at a frequency of 1 kHz and with an amplitude of 50 mV. The tests were performed by applying a compression strain equal to 0.033 mm/s on the specimens through a press connected to a software, with an increasing compression force up to a maximum of 25 kN, equivalent to a stress of 15.6 MPa. The measurement set-up is shown in Figure 8.29.

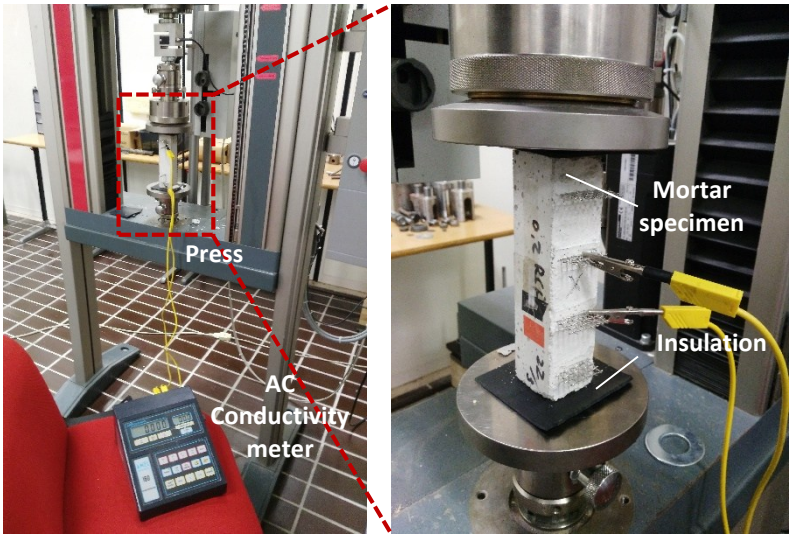

Figure 8.29. *AC stress-sensitivity measurements: Set up and instrumentations*

The resistivity of the specimens was measured at different loads, to determine the value of FCR as a function of stress. The data obtained are reported in Figure 8.30 and Table 8.6.

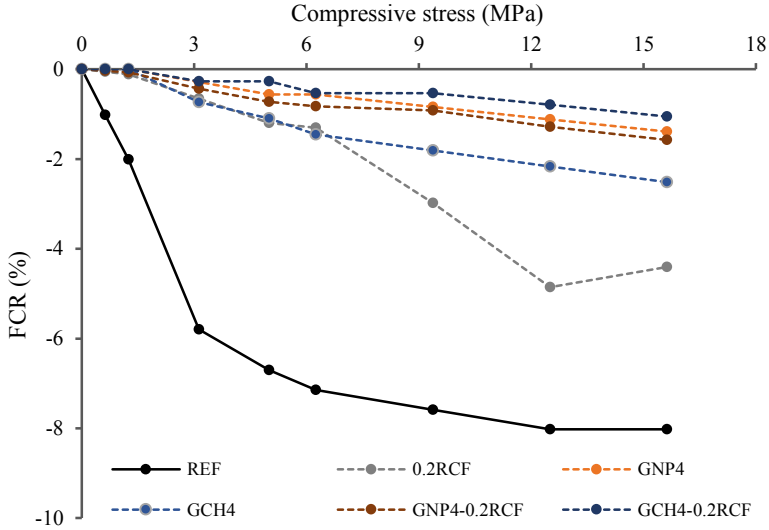

Figure 8.30. *FCR vs. stress*

Table 8.6. *Electrical and piezoresistive parameters of mortars (AC measurements)*

Mixture	ρ_0 AC (Ω·m)	Max. FCR (%)	GF	Stress sensitivity (MPa^{-1})
REF	14397	-8.0	1150	$5.1 \cdot 10^{-3}$
GNP4	2842	-1.4	186	$0.9 \cdot 10^{-3}$
GCH4	6358	-2.5	450	$1.6 \cdot 10^{-3}$
0.2RCF	1218	-4.4	593	$2.8 \cdot 10^{-3}$
GNP4-0.2RCF	8	-1.6	169	$1.0 \cdot 10^{-3}$
GCH4-0.2RCF	2366	-1.1	117	$0.7 \cdot 10^{-3}$

As seen from the curves, all the analyzed mixtures show a decrease of the electrical resistivity with the increase of the compressive stress. This trend is reverse to that obtained in DC, and demonstrates the marked difference between these two measurement systems. On the other hand, the parameters that influence the conductivity measurements in AC are very different from those of the DC methods, as demonstrated in the previous paragraph.
Another noticeable result is the high stress sensitivity of the traditional mortar, which shows a higher FCR value compared to the other mixtures, with a GF equal to 1150. However, the reading of REF conductivity during the test was very unstable, due of the very high resistivity of the mortar. Indeed, the mixtures added with fillers and CFs show lower FCR values, but a greater stability of the electric signal and a higher proportionality between compression stress and resistivity change with respect to the plain mortar.
For a better analysis of the results, in Appendix C the *FCR-Strain vs. time* and *FCR vs. Strain* of all mixtures obtained by DC resistivity tests under load cycles are reported.

8.5 Conclusions

In the last part of the research, the effect of three different types of carbonaceous fillers and two types of carbon fibers were studied in terms of mechanical resistance (flexural and compressive strength), durability (capillary water absorption), electrical properties and stress-sensitivity of the mortars. Two types of recycled fillers have been studied: Gasification char (GCH) and Used foundry sand (UFS), whose effects have been compared with those of Grapheme nanoplatelets (GNP) as commercial filler. Two types of carbon fibers were studied: commercial virgin carbon fibers (VCF) and recycled carbon fibers (RCF). Their effects were studied by adding 4% and 7% of fillers on the cement weight and 0.05% and 0.2% of fibers on the mortars volume, together with hybrid additions composed of 4% of fillers and both amounts of fibers. The obtained results suggest the following conclusions:

- During the production of mixtures, the insertion of graphene caused segregation problems on the fresh mortar, due to the physical and dimensional characteristics of the GNPs and to their hydrophobicity. This led to bleeding phenomena during casting and to the formation of macroporosity within the hardened composites. Contrariwise, the addition of CFs and recycled fillers did not affect the *workability* and homogeneity of the materials;
- Three-point bending and compression strength tests demonstrated that the addition of carbon-based fillers and fibers does not significantly influence the *mechanical performance* of the mixtures. However, slight improvements in terms of flexural strength were obtained by CFs and UFS, with increases in R_f values up to 9% and 25%, respectively. The highest compressive strength values were obtained by mixtures containing GCH and UFS and through the hybrid additions GCH-CFs and UFS-CFs, thanks to the filler effect of the recycled powders, with increments of up to 10%. In contrast, the inclusion of GNP has led to a significant decrease in both flexural and compressive strength. The R_c value of the mortar with the highest concentration of graphene (GNP7) is 22% compared to REF. This

is because the lack of homogeneity of the mortars containing GNP has led to the formation of a high volume of macropores during the casting process;

- *Microstructural* analyzes have shown that an increasing amount of fillers leads to a greater refinement of the microstructure, decreasing both the total volume and the average diameter of micropores. In particular, the UFS7 addition led to a decrease in V_p equal to 11%. The lower micropores volume also leads to less capillary water absorption in the short period of filler-based mortars. On average, UFS-based mortars show the highest resistance to water absorption, with C values 27% lower than REF;
- Measurements performed by using DC instruments mainly analyze the *electrical behavior* of the cement matrix, while AC instruments provide more information about the electrical properties of fillers and fibers and of the composite material. The results showed a linear increase in mortars resistivity in the first weeks of curing, and a significant increase in ρ values after the specimens drying. The greatest increases were obtained by the GNP-based mortars, since the elimination of water from their numerous macroporities brought to a high increase in electrical gaps. In contrast, mortars containing recycled fillers show greater conductivity compared to REF, thanks to their lower porosity. The impedance spectra obtained from the EIS tests instead highlighted both the electrical behavior of the matrix and of the composite. The resistivity values measured in AC reveal the high electrical conductivity of the mortars containing GNP and CFs, and their effect is clearly visible from the Nyquist diagrams. Mixtures with GCH-CFs hybrid additions also showed low resistivity values, thanks to the effect of recycled filler on the ionic conduction of the matrix, and to the effect of fibers on the electronic conduction of the composite. 0.2VCF and GNP4-0.2RCF mixtures showed an extremely high conductivity compared to the other mixtures, i.e. ρ values of 2 and 3 orders of magnitude lower than the REF, respectively. This effect is probably linked to an optimal internal distribution of these admixtures, which has created very effective conductive paths;
- *Stress-sensitivity* tests revealed that the piezoresistive behavior of the mixtures is strongly influenced by moisture and electrical resistivity of the materials. Moreover, the results obtained by the 4-probe DC measuring system and by the measurements performed with the AC conductivity meter show significant differences. At short curing periods (28 days) no mixtures are sensitive to compression stress, because the high water content within the porosity hides the piezoresistive properties of the composites. After drying, the DC tests detect a considerable increase in resistivity on the specimens subjected to compressive loads, with high values of FCR both for the reference mortar (14.8%) and for the other types of mixtures. AC resistivity measurements under load did not confirm this trend, rather showing an increase in the electrical conductivity of specimens subjected to compression deformations. Both the DC and AC measurements confirm that a higher conductivity of the mixtures (i.e. a greater amount of fillers and fibers) does not increase their stress sensitivity, but improves the accuracy and repeatability of the electrical signal. This factor is strongly demonstrated by the highly conductive mixture GNP4-0.2RCF, which shows a linear relationship between FCR and compressive strain.

This final part of the research has shown that the restrained addition of carbon-based fillers and fibers can lead to significant enhancements in mechanical strength and durability of cementitious materials. Unlike graphene, the insertion of low-cost recycled fillers within the mixtures does not entail problems of workability and does not worsen the macrostructure of hardened composite. Indeed, the addition of recycled powders improves the mechanical performance and leads to a refinement of the cement matrix.
Gasification char and Used foundry sand are less effective than graphene in improving the electrical conductivity of mortars, but their filler effect, combined with the electrical properties of carbon fibers, produces hybrid composites much more conductive than traditional cement-based materials. However, the electrical parameters measured on the materials vary considerably depending on the used measuring system. Further research is required for a better understanding of the electrical behaviors of the multi-phase cement-based materials, aimed at the optimization of the measurement system, and the development of techniques for the evaluation of the actual sensorial properties of multifunctional composites.

9 . Chapter
Final Remarks

Conclusions, critical analysis of results and future developments

The present dissertation investigated the integration of the traditional structural use of concrete with further functions, through the development of multifunctional cement-based materials with a large number of properties, in order to improve the quality of life inside buildings, and the safety and efficiency of infrastructures.
In particular, this study focused on the effects of high-performance carbonaceous admixtures inserted into cement composites, following the technological boosts linked to the recent introduction of graphene and other innovative carbon-based nanomaterials.
The research mainly focused on the comparison between the use of commercial nanofillers (graphene) and waste carbon-based micro-powders, to promote the recycling of industrial by-products and a more sustainable construction industry.
In this last chapter, after the description of the research development, a critical analysis of the results is reported, together with a study on the potential applications of the developed materials and on the future objectives of the research.

9.1 Research progress

Initially, the aims of the project have been identified thanks to a careful analysis of the state of the art on smart cement materials, and on the various technological solutions in which they can be used. The previous studies about the enhancement of the mechanical and durability properties of mortars and concretes by the use of carbon-based fillers and fibers have been thoroughly investigated.
The main uses of high-carbon materials are related to their high electrical properties. Therefore, after a theoretical summary of the electronics fundamentals, an accurate study on the technological potential of high conductivity cementitious materials was performed. Furthermore, today's methods for measuring the electrical resistivity of cement-based materials have been investigated.
The last part of the bibliographic research summarizes the most important studies on the self-sensing properties of cement-based composites added with carbon-based materials, for the potential use of highly conductive concretes within Structural Health Monitoring systems.
Carbon-based fillers and fibers were chosen according to their physico-chemical properties and their technical characteristics.
In the first part of the experimentation, the functionality of carbon-based fillers was investigated by means of a wide range of tests performed on lime pastes. Two types of commercial fillers (graphene nanoplatelets and powdered activated carbon) and two types of recycled carbonaceous powders (gasification char and used foundry sand) were added in three different concentrations (0.25%, 0.5% and 1% on binder weight), and their effects were analyzed in terms of mechanical strength, durability, depolluting and photocatalytic properties, electrical conductivity and shielding of electromagnetic interference.
In the following part, the electrical properties of carbon in cementitious materials have been scrutinized by inserting high conductivity fibers into structural mortars. Two types of carbon fibers (virgin and recycled) and one type of brassed steel fibers have been added in several concentrations, from 0.05% to 1.6% on mixtures volume. Their effects have been studied in terms of pre- and post-cracks mechanical strength, durability, and enhancement of electrical conductivity.

The final part of the work analyzed the combined use of carbon-based fillers and fibers, by using the best concentrations studied in previous experiments, for the development of innovative, durable and low-cost materials. Graphene, gasification char and used foundry sand were added to 4% and 7% on cement weight; virgin and recycled carbon fibers were added to 0.05% and 0.2% on mortars volume. The effects of individual and combined additions have been studied in terms of mechanical strength, durability, electrical properties and sensitivity to stress of the composites.
The following is an overall analysis of the results, in which the strengths and weaknesses of the experimentation work are carefully examined.

9.2 Overall analysis of results and conclusions

During the experimentation cycles, the properties of the mixtures were studied through a large number of tests, which provided large quantities of information on the effects of the different admixtures at different concentrations. Sometimes different instruments have been used to analyze the same parameter, in order to obtain a more complete collection of data.
Furthermore, during the long research work, very different materials were analyzed, such as NHL pastes and different types of structural mortars produced with different types of cements, and consequently carbon-based admixtures showed different behaviors depending on the matrix in which they were inserted.
The following is a concluding analysis of the results, i.e. a summary of the general effects of fillers/fibers on the specific characteristics of cement-based materials.

9.2.1 Effects on microstructure and enhancement of mechanical properties

All the microstructural microscopic investigations carried out on composites showed the effectiveness of the filler effect of carbon-based powders. A greater amount of fillers in the mixture (lime paste or cement mortar) leads to a reduction in total porosity and in pore size. In the case of recycled powders, this effect leads to an increase in both flexural and compressive strength, even at high filler concentrations. GCH and UFS particles work as nucleation points for C-S-H, improving the hydration degree of cement. In contrast, high concentrations of graphene, such as 4% or 7% by binder weight, lead to a gradual decrease in mechanical resistances, due to mixing difficulties of the fresh mortars and the increase in macroporosity within the hardened composites.
The mechanical tests performed on fiber-reinforced mortars confirmed the effectiveness of the sewing action of carbon fibers, which significantly increase flexural and tensile splitting strengths, as well as the post-cracks toughness of the composites thanks to their bridging effect. The best results were obtained by recycled fibers, and SEM analyzes have verified the high compatibility between these type of filaments and the cement matrix, since carbon fibers micro-scraps act as nucleation points for the growth of C-S-H (such as carbon-based fillers). However, as for graphene, a high quantity of fibers leads to a severe reduction in workability, with consequent segregation and bleeding phenomena, and a consequent decrease in mechanical compressive strength.

9.2.2 Durability: capillary water absorption and reduction of drying shrinkage

The addition of fillers and fibers bring to a lower quantity of water absorbed by the mixture, thanks to the microstructure refinement and to the smaller volume of capillary porosity. This effect is entirely related to the porosimetric characteristics of the mixtures, and is not influenced by the type of binder (Hydraulic lime or cement). Generally, a higher concentration of addition leads to greater resistance to water absorption in the short period and to a lower amount of water absorbed in the long time. Used foundry sand has led to greater decreases in the permeability of both lime pastes and cement mortars.
The addition of carbon fibers also leads to a reduction in drying shrinkage, thanks to the reduction of the capillary porosity and to the adhesion forces between the filaments and the cement paste. The results demonstrated that the higher the quantity of fibers within the mixture, the smaller the shrinkage deformations of the hardened composites. The effect of carbon-based fillers on shrinkage strains of mixtures has not been analyzed in this research, but it will be studied in future experimentations.

9.2.3 Enhancement of de-pollution properties and photocatalytic efficiency

The tests performed on hydraulic lime pastes show that the addition of carbon-based fillers leads to a higher pollutants reduction compared to traditional composites. The best adsorption properties were measured on mixtures containing used foundry sand and powdered activated carbon. The capability of fillers to adsorb methyl-ethyl-ketone is not proportional to their concentrations.
On the contrary, no depolluting properties by photocatalysis were detected on mixtures, since none of the fillers showed a photocatalytic efficiency. NOx reduction tests under UVA radiation have shown that carbon-based fillers decrease the abatement rates, even after the addition of TiO_2. This effect is due to the darker coloring of the pastes containing carbonaceous fillers.

9.2.4 Electrical conductivity

The different techniques for the electrical resistivity measurement have shown that carbon-based fillers and fibers increase the electrical conductivity of hydraulic binders-based composites. Both lime pastes and structural cement mortars show decreases of ρ values up to different orders of magnitude, depending on the type and amount of carbon-based admixture.
However, the comparisons between obtained by the different types fillers and fibers are strongly influenced by the type of matrix and by the system for the measurement of electrical current. During the experimentation, the technological development of the mixtures was followed by a gradual optimization of the electrical measurement systems, aimed at obtaining a more truthful reading of the electrical contribution of the additions.
The results have shown that recycled carbon-based fillers improve the conductivity of the mortars by acting on their microstructure and porosity, i.e. decreasing the electrical resistance of the matrix measured by DC and AC systems. Highly conductive materials, such as graphene and carbon fibers, increase the electrical properties of the composite by

creating electronic conduction paths from direct contact and through the tunneling effect. These effects were verified by comparing the resistivity data obtained from the DC measurements and the impedance spectra obtained from the AC measurements.
Gasification char proved to be the most effective recycled powder in increasing the electrical conductivity of both lime- and cement-based mixtures, thanks to the refining of microstructure and to its high carbon content. Carbon fibers have proved extremely effective in increasing electrical conductivity of the composites. From the results, percolation thresholds were identified, related to two different concentrations of filaments. In particular, recycled carbon-based fibers have led to large increases in conductivity even at low doses (between 0.05% and 0.2% on mortar volume). However, the effect of these low concentrations of fibers is hardly detectable with DC instrumentations. The combined insertion of recycled fillers and carbon fibers lead to considerable increases in conductivity, thanks to the effect of fillers on the cement matrix and to the multiphase electric behavior originated by the fibers.

9.2.5 EMI shielding effectiveness

The increase in electrical conductivity through the insertion of carbon-based fillers has also led to improvements in electromagnetic shielding properties of the mixtures. In general, the powders that provided higher electrical conductivity also provided greater shielding effectiveness, i.e. graphene and gasification char, with average improvements of 30% and 6% compared to the reference, respectively.
However, the shielding values vary depending on the frequency range, and they are generally negligible. This is because the studies were performed on mortars realized with NHL5 hydraulic lime, a low-reactive hydraulic binder with low mechanical properties. The low density of lime pastes has led to low attenuation of EMI, since it is well known that the greater the density of the material, the greater its shielding effect. In the future, the studies will be repeated on higher density finishes produced with high performance binders.

9.2.6 Self-sensing properties

Piezoresistivity tests have shown variable results depending on the different measurement systems used, and the data obtained require further studies for a better explanation. All mortars produced in the last phase of the research showed electrical sensitivity to stress, but with different trends depending on the method used for FCR measurement. The specimens subjected to compression strain showed a traditional decrease in the resistivity values measured with an AC conductivity meter, while a marked increase was measured by a 4-probe DC system.
From the overall analysis of the results, it can be stated that the addition of conductive fillers and fibers does not improve the strain-sensitivity of the composites, but improves the stability of the signal and the accuracy of the measurement, through the increase of electrical conductivity. The plain mortar shows high FCR values at the maximum load (between 8% and 15%) regardless of the measurement system used, but also shows a high scattering of the FCR vs. strain curves, because of its high electrical resistivity.

Contrariwise, composites with higher electrical conductivity show a higher linearity between FCR and strain and a greater repeatability of readings.
However, the analysis of piezoresistive effect of these type of composites requires further studies, to better understand the electrical behavior of multi-phase mortars and concretes both in stationary conditions and under mechanical strain. The data obtained in this research will be used as a basis for the development of an effective system for the assessment of self-sensing properties.

9.3 Scientific contribution and future developments

The present dissertation opens a new line of study on the improvement of concrete with new functionalities, and adds knowledge to the field of multifunctional cement-based materials through the development of novel smart composites.
The search for new techniques and formulations for the enhancement of mechanical properties and life cycle of cementitious materials has been followed by the development of other functionalities, in particular by increasing the electrical conductivity of the composites.
Heretofore, research on multifunctional and electrically conductive cement-based materials has focused on the use of high performance nanomaterials (sometimes dangerous for health), which have led to the development of functional but very expensive composites, which can only be used in the laboratory scale.
On the contrary, this research focused on the production of low-cost composites, easily producible and usable on a large scale, thanks to the introduction of recycled powders and to a balanced use of carbon fibers.
The results obtained propose new methods for the recycling of industrial waste with a high carbon content within the building sector. The used foundry sand powder proved to be very effective in increasing the mechanical strength and durability of the composites, by refining of the microstructure and reducing their porosity. The gasification char has proven effective in increasing the electrical conductivity of the mortars, thanks to the filler effect and to its high carbon content.
However, some analyzed parameters showed scientific gaps, which require a theoretical investigation and further steps of experimentation. In particular, the electrical behavior of multi-phase cement-based materials requires a better understanding, in order to eliminate the uncertainties related to the different results obtained by the different measurement systems. This is also necessary to evaluate the actual strain-sensing properties of the materials.
Future research work will be aimed at:

- The optimization of materials through the study of further filler and fiber concentrations, i.e. analyzing a higher number of hybrid combinations. The mixtures will be realized with more performing binders to analyze the electrical properties of higher density composites;
- Further studies on the durability of composites, through the measurement of free and restrained hygrometric shrinkage, and of resistance to sulphate and chlorides attack;

- A better understanding of the electrical behavior of composites comparing the results of electrical resistivity measurements in DC and electrochemical impedance spectroscopy in AC;
- The optimization of an effective system for the measurement of fractional change in resistivity of mortar specimens subjected to mechanical loads;
- More detailed assessment of the electrical sensitivity of mixtures by subjecting the specimens to different mechanical stress conditions, i.e. variable compression cycles, bending and induced cracking;
- Evaluation of the effect of environmental parameters, such as humidity and temperature, on the sensorial properties of the mixtures.

The future developments of the research involve the study of the effects of carbon-based additions within novel concretes produced with high-performance binders, within the EnDurCrete project. Successively, these smart concretes will be tested in infrastructures under real service conditions, as described in Section 1.4.

This dissertation represents a small step towards a construction industry more close to the needs of the society and of the environment, based on the use of technology to improve the security of infrastructure and the quality of life of human beings.

References

[1] D. Roy, P. Brown, D. Shi, B. Scheetz, W. May, Concrete Microstructure Porosity and Permeability, Strateg. Highw. Res. Program, Natl. Res. Counc. ,Washingt. DC. (1993).

[2] J.M.W. Brownjohn, Structural health monitoring of civil infrastructure, Philos. Trans. R. Soc. A Math. Phys. Eng. Sci. 365 (2007) 589–622. doi:10.1098/rsta.2006.1925.

[3] A.B. Noel, A. Abdaoui, T. Elfouly, M.H. Ahmed, A. Badawy, M.S. Shehata, Structural Health Monitoring Using Wireless Sensor Networks: A Comprehensive Survey, IEEE Commun. Surv. Tutorials. 19 (2017) 1403–1423. doi:10.1109/COMST.2017.2691551.

[4] B. Han, X. Yu, J. Ou, Self-Sensing Concrete in Smart Structures, 2014. doi:10.1016/C2013-0-14456-X.

[5] D.D.L. Chung, Carbon materials for structural self-sensing, electromagnetic shielding and thermal interfacing, Carbon N. Y. 50 (2012) 3342–3353. doi:10.1016/j.carbon.2012.01.031.

[6] B. Han, X. Guan, J. Ou, Electrode design, measuring method and data acquisition system of carbon fiber cement paste piezoresistive sensors, Sensors Actuators, A Phys. 135 (2007) 360–369. doi:10.1016/j.sna.2006.08.003.

[7] G.Y. Li, P.M. Wang, X. Zhao, Pressure-sensitive properties and microstructure of carbon nanotube reinforced cement composites, Cem. Concr. Compos. 29 (2007) 377–382. doi:10.1016/j.cemconcomp.2006.12.011.

[8] A. D'Alessandro, M. Rallini, F. Ubertini, A.L. Materazzi, J.M. Kenny, Investigations on scalable fabrication procedures for self-sensing carbon nanotube cement-matrix composites for SHM applications, Cem. Concr. Compos. 65 (2016) 200–213. doi:10.1016/j.cemconcomp.2015.11.001.

[9] N.A.A. Ghany, S.A. Elsherif, H.T. Handal, Revolution of Graphene for different applications: State-of-the-art, Surfaces and Interfaces. 9 (2017) 93–106. doi:10.1016/j.surfin.2017.08.004.

[10] S. Chuah, Z. Pan, J.G. Sanjayan, C.M. Wang, W.H. Duan, Nano reinforced cement and concrete composites and new perspective from graphene oxide, Constr. Build. Mater. 73 (2014) 113–124. doi:10.1016/j.conbuildmat.2014.09.040.

[11] D.R. Cooper, B. D'Anjou, N. Ghattamaneni, B. Harack, M. Hilke, A. Horth, N. Majlis, M. Massicotte, L. Vandsburger, E. Whiteway, V. Yu, Experimental review of graphene, 2012 (2011). doi:10.5402/2012/501686.

[12] B. Han, S. Ding, X. Yu, Intrinsic self-sensing concrete and structures: A review, Meas. J. Int. Meas. Confed. 59 (2015) 110–128. doi:10.1016/j.measurement.2014.09.048.

[13] P.W. Chen, D.D.L. Chung, Carbon fiber reinforced concrete for smart structures capable of non-destructive flaw detection, Smart Mater. Struct. 2 (1993) 22–30. doi:10.1088/0964-1726/2/1/004.

[14] H. Nguyen, T. Fujii, K. Okubo, V. Carvelli, Cement mortar reinforced with recycled carbon fiber and CFRP waste, ECCM 2016 - Proceeding 17th Eur. Conf. Compos. Mater. (2016).

[15] M. Mastali, A. Dalvand, The impact resistance and mechanical properties of self-compacting concrete reinforced with recycled CFRP pieces, Compos. Part B Eng. 92 (2016) 360–376. doi:10.1016/j.compositesb.2016.01.046.

[16] G. Faneca, I. Segura, J.M. Torrents, A. Aguado, Development of conductive cementitious materials using recycled carbon fibres, Cem. Concr. Compos. 92 (2018) 135–144. doi:10.1016/j.cemconcomp.2018.06.009.

[17] M. Bołtryk, A. Krupa, E. Pawluczuk, Modification of the properties of the cement composites with the organic filler, Constr. Build. Mater. 167 (2018) 143–153. doi:10.1016/j.conbuildmat.2018.02.025.

[18] J.M. Khatib, B.A. Herki, S. Kenai, Capillarity of concrete incorporating waste foundry sand, Constr. Build. Mater. 47 (2013) 867–871. doi:10.1016/j.conbuildmat.2013.05.013.

[19] N. Makul, G. Sua-Iam, Innovative utilization of foundry sand waste obtained from the manufacture of automobile engine parts as a cement replacement material in concrete production, J. Clean. Prod. 199 (2018) 305–320. doi:10.1016/j.jclepro.2018.07.167.

[20] E. Commission, Internal Market, Industry, Entrepreneurship and SMEs Directorate General, Eur. Constr. Sect. A Glob. Partn. (2016) 2016.

[21] S.Vaclav, Making the Modern World: Materials and Dematerialization, Lulu Press. (2016).

[22] P. Fred, The concrete jungle overheats, New Sci. 2091. (1997) 14.

[23] J. Davidovits, Carbon-Dioxide Greenhouse-Warming: What Future for Portland Cement, Proceedings, Emerg. Technol. Symp. Cem. Concrees Glob. Environ. Portl. Cem. Assoc. Chicago, Illinois. (1993).

[24] M.J. Gibbs, P. Soyka, D. Conneely, CO2 emissions from cement production, Good Pract. Guid. Uncertain. Manag. Natl. Greenh. Gas Invent. (n.d.) 175–182.

[25] S. Lv, J. Liu, T. Sun, Y. Ma, Q. Zhou, Effect of GO nanosheets on shapes of cement hydration crystals and their formation process, Constr. Build. Mater. 64 (2014) 231–239. doi:10.1016/j.conbuildmat.2014.04.061.

[26] M. Collepardi, Il Nuovo Calcestruzzo, 3rd Edition, (2003).

[27] C. Brauer, The sick building syndrome revisited, Copenhagen. (2005).

[28] M. Murphy, Sick Building Syndrome and the Problem of Uncertainty, (2006). doi:10.1215/9780822387831.

[29] Properties of Activated Carbon, CPL Caron Link. (2012).

[30] L.K. Putri, L.L. Tan, W.J. Ong, W.S. Chang, S.P. Chai, Graphene oxide: Exploiting its unique properties toward visible-light-driven photocatalysis, Appl. Mater. Today. 4 (2016) 9–16. doi:10.1016/j.apmt.2016.04.001.

[31] Y. Dai, M. Sun, C. Liu, Z. Li, Electromagnetic wave absorbing characteristics of carbon black cement-based composites, Cem. Concr. Compos. 32 (2010) 508–513. doi:10.1016/j.cemconcomp.2010.03.009.

[32] B. Wang, Z. Guo, Y. Han, T. Zhang, Electromagnetic wave absorbing properties of multi-walled carbon nanotube/cement composites, Constr. Build. Mater. 46 (2013) 98–103. doi:10.1016/j.conbuildmat.2013.04.006.

[33] A. Mazzoli, V. Corinaldesi, J. Donnini, C. Di Perna, D. Micheli, A. Vricella, R. Pastore, L. Bastianelli, F. Moglie, V. Mariani Primiani, Effect of graphene oxide and metallic fibers on the electromagnetic shielding effect of engineered cementitious composites, J. Build. Eng. 18 (2018) 33–39. doi:10.1016/j.jobe.2018.02.019.

[34] W.R. De Sitter Jr., Costs for Service Life Optimisation, the Law of Fives, Proc. CEB-RILEM Int. Work. "Durability Concr. Struct. Copenaghen, Denmark,. (1983) 131–134.

[35] K. Tuutti, Corrosion of Steel in Concrete, Swedish Found. Concr. Res. Stoccolma. (1982).

[36] B.F. Harms T., Sedigh S., Structural health monitoring of bridges using wireless sensor networks, IEEE, Instrum. Meas. Mag. 8 (2010) 13–14.

[37] S. Zhu, D.D.L. Chung, Analytical model of piezoresistivity for strain sensing in carbon fiber polymer-matrix structural composite under flexure, Carbon N. Y. 45 (2007) 1606–1613. doi:10.1016/j.carbon.2007.04.012.

[38] and J.O. B. Han, L. Zhang, Smart and Multifunctional Concrete Towards Sustainable Infrastructures, Springer Singapore. (2017) 2017.

[39] B. Han, L. Zhang, S. Sun, X. Yu, X. Dong, T. Wu, J. Ou, Electrostatic self-assembled carbon nanotube/nano carbon black composite fillers reinforced cement-based materials with multifunctionality, Compos. Part A Appl. Sci. Manuf. 79 (2015) 103–115. doi:10.1016/j.compositesa.2015.09.016.

[40] S. Pimenta, S.T. Pinho, Recycling carbon fibre reinforced polymers for structural applications: Technology review and market outlook, Waste Manag. 31 (2011) 378–392. doi:10.1016/j.wasman.2010.09.019.

[41] S.J. Pickering, Recycling Technologies For Thermoset Composite Materials, Adv. Polym. Compos. Struct. Appl. Constr. ACIC 2004. 37 (2004) 392–399. doi:10.1016/B978-1-85573-736-5.50044-3.

[42] New Environmental friendly and Durable concrete – EnDurCrete, Horizon 2020 research and innovation Programme, Available from Http//Www.Endurcrete.Eu/Home. (n.d.) 2020.

[43] S. Samad, A. Shah, Role of binary cement including Supplementary Cementitious Material (SCM), in production of environmentally sustainable concrete: A critical review, Int. J. Sustain. Built Environ. 6 (2017) 663–674. doi:10.1016/j.ijsbe.2017.07.003.

[44] S. Liu, T. Zhang, Y. Guo, J. Wei, Q. Yu, Effects of SCMs particles on the compressive strength of micro-structurally designed cement paste: Inherent characteristic effect, particle size refinement effect, and hydration effect, Powder Technol. 330 (2018) 1–11. doi:10.1016/j.powtec.2018.01.087.

[45] T. Jacobsen, Sennacherib's Aqueduct at Jerwan, Orient. Inst. Publ. 24 (1935).

[46] A.C. Sparavigna, D. Fisica, P. Torino, Ancient concrete works, Anc. Concr. Work. (2011).

[47] The History of Concrete, Dept. Mater. Sci. Eng. Univ. Illinois, Urbana-Champaign. (2012).

[48] N. Gromicko, The History of Concrete, Int. Assoc. Certif. Home Insp. (2013).

[49] B. Herring, The Secrets of Roman Concrete, Romanconcrete.Com. (2012).

[50] R. Courland, Concrete planet : the strange and fascinating story of the world's most common man-made material, Amherst, N.Y. Prometh. Books. (2015).

[51] A. Schieweck, E. Uhde, T. Salthammer, L.C. Salthammer, L. Morawska, M. Mazaheri, P. Kumar, Smart homes and the control of indoor air quality, Renew. Sustain. Energy Rev. 94 (2018) 705–718. doi:10.1016/j.rser.2018.05.057.

[52] The European Commission's science and knowledge service, Improving safety in construction, avaible from: https://ec.europa.eu/jrc/en/research-topic/improving-safety-construction, (n.d.).

[53] S. Mounir, K. Abdelhamid, Y. Maaloufa, Thermal Inertia for Composite Materials White Cement-cork, Cement Mortar-cork, and Plaster-cork, Energy Procedia. 74 (2015) 991–999. doi:10.1016/j.egypro.2015.07.830.

[54] Q. Zeng, T. Mao, H. Li, Y. Peng, Thermally insulating lightweight cement-based composites incorporating glass beads and nano-silica aerogels for sustainably energy-saving buildings, Energy Build. 174 (2018) 97–110. doi:10.1016/j.enbuild.2018.06.031.

[55] F. Tittarelli, C. Giosuè, A. Mobili, M.L. Ruello, Influence of binders and aggregates on VOCs adsorption and moisture buffering activity of mortars for indoor applications, Cem. Concr. Compos. 57 (2015) 75–83. doi:10.1016/j.cemconcomp.2014.11.013.

[56] K. Loh, C.C. Gaylarde, M.A. Shirakawa, Photocatalytic activity of ZnO and TiO2'nanoparticles' for use in cement mixes, Constr. Build. Mater. 167 (2018) 853–859. doi:10.1016/j.conbuildmat.2018.02.103.

[57] D.D.L. Chung, Cement reinforced with short carbon fibers: A multifunctional material, Compos. Part B Eng. 31 (2000) 511–526. doi:10.1016/S1359-8368(99)00071-2.

[58] K. Ogi, T. Shinoda, M. Mizui, Strength in concrete reinforced with recycled CFRP pieces, Compos. Part A Appl. Sci. Manuf. 36 (2005) 893–902. doi:10.1016/j.compositesa.2004.12.009.

[59] F. Tittarelli, Monitoraggio per la manutenzione preventiva e programmata delle strutture in c.a., Enco J. 31 (2005) 27–29.

[60] D. Carolyn, Matrix cracking repair and filling using active and passive modes for smart timed release of chemicals from fibers into cement matrices, Smart Mater. Struct. 3 (1994) 118–123. doi:10.1088/0964-1726/3/2/006.

[61] M. Wu, B. Johannesson, M. Geiker, A review: Self-healing in cementitious materials and engineered cementitious composite as a self-healing material, Constr. Build. Mater. 28 (2012) 571–583. doi:10.1016/j.conbuildmat.2011.08.086.

[62] K. Van Tittelboom, N. De Belie, Self-healing in cementitious materials-a review, 2013. doi:10.3390/ma6062182.

[63] V. Wiktor, H.M. Jonkers, Quantification of crack-healing in novel bacteria-based self-healing concrete, Cem. Concr. Compos. 33 (2011) 763–770. doi:10.1016/j.cemconcomp.2011.03.012.

[64] D.D.L. Chung, Enhancing the Seebeck effect in carbon fiber-reinforced cement by using intercalated carbon fibers, Cem. Concr. Res. 30 (2000) 1295–1298.

[65] D.D.L. Chung, Thermoelectric behavior of carbon–cement composites, Carbon N. Y. 30 (2002) 2495–2505.

[66] A.L. Pisello, A. D'Alessandro, S. Sambuco, M. Rallini, F. Ubertini, F. Asdrubali, A.L. Materazzi, F. Cotana, Multipurpose experimental characterization of smart nanocomposite cement-based materials for thermal-energy efficiency and strain-sensing capability, Sol. Energy Mater. Sol. Cells. 161 (2017) 77–88. doi:10.1016/j.solmat.2016.11.030.

[67] Y. Sherif, Conductive Concrete Overlay for Bridge Deck Deicing, Mater. J. 96 (n.d.).

[68] J. Chen, D. Zhao, H. Ge, J. Wang, Graphene oxide-deposited carbon fiber/cement composites for electromagnetic interference shielding application, Constr. Build. Mater. 84 (2015) 66–72. doi:10.1016/j.conbuildmat.2015.03.050.

[69] M.S. Cao, W.L. Song, Z.L. Hou, B. Wen, J. Yuan, The effects of temperature and frequency on the dielectric properties, electromagnetic interference shielding and microwave-absorption of short carbon fiber/silica composites, Carbon N. Y. 48 (2010) 788–796. doi:10.1016/j.carbon.2009.10.028.

[70] A.P. Singh, B.K. Gupta, M. Mishra, Govind, A. Chandra, R.B. Mathur, S.K. Dhawan, Multiwalled carbon nanotube/cement composites with exceptional electromagnetic interference shielding properties, Carbon N. Y. 56 (2013) 86–96. doi:10.1016/j.carbon.2012.12.081.

[71] S. Wen, D.D.L. Chung, Partial replacement of carbon fiber by carbon black in multifunctional cement-matrix composites, Carbon N. Y. 45 (2007) 505–513. doi:10.1016/j.carbon.2006.10.024.

[72] N. Kaur, Combined energy harvesting and structural health monitoring potential of embedded piezo-concrete vibration sensors, J. Energy Eng. 141 (2014) 4014001.

[73] W.T. Park, Piezoresistivity, in Encyclopedia of Nanotechnology, B. Bhushan, Ed. (2012) 2111–2117.

[74] and Y.H. M. Sun, Q. Liu, Z. Li, A study of piezoelectric properties of carbon fiber reinforced concrete and plain cement paste during dynamic loading, Cem. Concr. Res. 30 (2000) 1593–1595.

[75] E. Montalbano, Solar Energy-Harvesting Concrete Makes For Sustainable Buildings, Materials & Assembly, Altern. Energy. (2015) 2015.

[76] B. Han, X. Yu, E. Kwon, A self-sensing carbon nanotube/cement composite for traffic monitoring, Nanotechnology. 20 (2009) 445501. doi:10.1088/0957-4484/20/44/445501.

[77] B. Han, K. Zhang, T. Burnham, E. Kwon, X. Yu, Integration and road tests of a self-sensing CNT concrete pavement system for traffic detection, Smart Mater. Struct. 22 (2013). doi:10.1088/0964-1726/22/1/015020.

[78] F. Report, Intelligent Pavement for Traffic Flow Detection – Phase II, (n.d.).

[79] A.O. Monteiro, A. Loredo, P.M.F.J. Costa, M. Oeser, P.B. Cachim, A pressure-sensitive carbon black cement composite for traffic monitoring, Constr. Build. Mater. 154 (2017) 1079–1086. doi:10.1016/j.conbuildmat.2017.08.053.

[80] X. Yu, Intelligent Pavement for Traffic Flow Detection – Phase II, (2012) 26.

[81] P.W. Chen, D.D.L. Chung, Concrete as a new strain stress sensor, Compos. Part B-Engineering. 27 (1996) 11–23. doi:10.1016/1359-8368(95)00002-x.

[82] Le potenzialità di impiego del grafene in ambito industriale, (n.d.).

[83] M. Frías, R. Vigil de la Villa, R. García, S. Martínez, E. Villar, I. Vegas, Effect of a high content in activated carbon waste on low clinker cement microstructure and properties, Constr. Build. Mater. 184 (2018) 11–19. doi:10.1016/j.conbuildmat.2018.06.216.

[84] R.A. Khushnood, S. Ahmad, P. Savi, J.M. Tulliani, M. Giorcelli, G.A. Ferro, Improvement in electromagnetic interference shielding effectiveness of cement composites using carbonaceous nano/micro inerts, Constr. Build. Mater. 85 (2015) 208–216. doi:10.1016/j.conbuildmat.2015.03.069.

[85] A. Hawreen, J.A. Bogas, A.P.S. Dias, On the mechanical and shrinkage behavior of cement mortars reinforced with carbon nanotubes, Constr. Build. Mater. 168 (2018) 459–470. doi:10.1016/j.conbuildmat.2018.02.146.

[86] C. Tzileroglou, M. Stefanidou, S. Kassavetis, S. Logothetidis, Nanocarbon materials for nanocomposite cement mortars, Mater. Today Proc. 4 (2017) 6938–6947. doi:10.1016/j.matpr.2017.07.023.

[87] S. Jiang, D. Zhou, L. Zhang, J. Ouyang, X. Yu, X. Cui, B. Han, Comparison of compressive strength and electrical resistivity of cementitious composites with different nano- and micro-fillers, Arch. Civ. Mech. Eng. 18 (2018) 60–68. doi:10.1016/j.acme.2017.05.010.

[88] I. Rhee, Y.A. Kim, G.O. Shin, J.H. Kim, H. Muramatsu, Compressive strength sensitivity of cement mortar using rice husk-derived graphene with a high specific surface area, Constr. Build. Mater. 96 (2015) 189–197. doi:10.1016/j.conbuildmat.2015.08.016.

[89] S. Lv, Y. Ma, C. Qiu, T. Sun, J. Liu, Q. Zhou, Effect of graphene oxide nanosheets of microstructure and mechanical properties of cement composites, Constr. Build. Mater. 49 (2013) 121–127. doi:10.1016/j.conbuildmat.2013.08.022.

[90] E. Horszczaruk, E. Mijowska, R.J. Kalenczuk, M. Aleksandrzak, S. Mijowska, Nanocomposite of cement/graphene oxide - Impact on hydration kinetics and Young's modulus, Constr. Build. Mater. 78 (2015) 234–242. doi:10.1016/j.conbuildmat.2014.12.009.

[91] X. Li, W. Wei, H. Qin, Y. Hang Hu, Co-effects of graphene oxide sheets and single wall carbon nanotubes on mechanical properties of cement, J. Phys. Chem. Solids. 85 (2015) 39–43. doi:10.1016/j.jpcs.2015.04.018.

[92] Q. Wang, J. Wang, C. Lu, B. Liu, K. Zhang, C. Li, Influence of graphene oxide additions on the microstructure and mechanical strength of cement, New Carbon Mater. 30 (2015) 349–356. doi:10.1016/S1872-5805(15)60194-9.

[93] Z. Pan, L. He, L. Qiu, A.H. Korayem, G. Li, J.W. Zhu, F. Collins, D. Li, W.H. Duan, M.C. Wang, Mechanical properties and microstructure of a graphene oxide-cement composite, Cem. Concr. Compos. 58 (2015) 140–147. doi:10.1016/j.cemconcomp.2015.02.001.

[94] T. Tong, Z. Fan, Q. Liu, S. Wang, S. Tan, Q. Yu, Investigation of the effects of graphene and graphene oxide nanoplatelets on the micro- and macro-properties of cementitious materials, Constr. Build. Mater. 106 (2016) 102–114. doi:10.1016/j.conbuildmat.2015.12.092.

[95] A.O. Monteiro, P.B. Cachim, P.M.F.J. Costa, Self-sensing piezoresistive cement composite loaded with carbon black particles, Cem. Concr. Compos. 81 (2017) 59–65. doi:10.1016/j.cemconcomp.2017.04.009.

[96] T. Manoharan, D. Laksmanan, K. Mylsamy, P. Sivakumar, A. Sircar, Engineering properties of concrete with partial utilization of used foundry sand, Waste Manag. 71 (2018) 454–460. doi:10.1016/j.wasman.2017.10.022.

[97] L. Zhang, B. Han, J. Ouyang, X. Yu, S. Sun, J. Ou, Multifunctionality of cement based composite with electrostatic self-assembled CNT/NCB composite filler, Arch. Civ. Mech. Eng. 17 (2017) 354–364. doi:10.1016/j.acme.2016.11.001.

[98] A. Mohammed, J.G. Sanjayan, W.H. Duan, A. Nazari, Incorporating graphene oxide in cement composites: A study of transport properties, Constr. Build. Mater. 84 (2015) 341–347. doi:10.1016/j.conbuildmat.2015.01.083.

[99] H. Du, S.D. Pang, Enhancement of barrier properties of cement mortar with graphene nanoplatelet, Cem. Concr. Res. 76 (2015) 10–19. doi:10.1016/j.cemconres.2015.05.007.

[100] P. Faria, P. Duarte, D. Barbosa, I. Ferreira, New composite of natural hydraulic lime mortar with graphene oxide, Constr. Build. Mater. 156 (2017) 1150–1157. doi:10.1016/j.conbuildmat.2017.09.072.

[101] G.M. Kim, H.N. Yoon, H.K. Lee, Autogenous shrinkage and electrical characteristics of cement pastes and mortars with carbon nanotube and carbon fiber, Constr. Build. Mater. 177 (2018) 428–435. doi:10.1016/j.conbuildmat.2018.05.127.

[102] F. Li, X. Jiang, J. Zhao, S. Zhang, Graphene oxide: A promising nanomaterial for energy and environmental applications, Nano Energy. 16 (2015) 488–515. doi:10.1016/j.nanoen.2015.07.014.

[103] X. Ren, J. Li, X. Tan, X. Wang, Comparative study of graphene oxide, activated carbon and carbon nanotubes as adsorbents for copper decontamination, Dalt. Trans. 42 (2013) 5266–5274. doi:10.1039/c3dt32969k.

[104] W. Gao, M. Majumder, L.B. Alemany, T.N. Narayanan, M.A. Ibarra, B.K. Pradhan, P.M. Ajayan, Engineered graphite oxide materials for application in water purification, ACS Appl. Mater. Interfaces. 3 (2011) 1821–1826. doi:10.1021/am200300u.

[105] R.K. Joshi, P. Carbone, F.C. Wang, V.G. Kravets, Y. Su, I. V. Grigorieva, H.A. Wu, A.K. Geim, R.R. Nair, Precise and ultrafast molecular sieving through graphene oxide membranes, Science (80-.). 343 (2014) 752–754. doi:10.1126/science.1245711.

[106] E.C. Dillon, J.H. Wilton, J.C. Barlow, W.A. Watson, Large surface area activated charcoal and the inhibition of aspirin absorption, Ann. Emerg. Med. 18 (1989) 547–552. doi:10.1016/S0196-0644(89)80841-8.

[107] S. Chowdhury, R. Balasubramanian, Highly efficient, rapid and selective CO2 capture by thermally treated graphene nanosheets, J. CO2 Util. 13 (2016) 50–60. doi:10.1016/j.jcou.2015.12.001.

[108] B. Stőhr, Enhancement of the catalytic activity of activated carbons in oxidation reactions by termal treatment with ammonia or hydrogen cyanide and observation of a superoxide species as a possible intermediate, Carbon N. Y. 29 (1991) 707–720.

[109] C. Xu, J. Zhu, R. Yuan, X. Fu, More effective use of graphene in photocatalysis by conformal attachment of small sheets to TiO2spheres, Carbon N. Y. 96 (2016) 394–402. doi:10.1016/j.carbon.2015.09.088.

[110] D.A. Kunkel, E.T. Gall, J.A. Siegel, A. Novoselac, G.C. Morrison, R.L. Corsi, Passive reduction of human exposure to indoor ozone, Build. Environ. 45 (2010) 445–452. doi:10.1016/j.buildenv.2009.06.024.

[111] N.J. Krou, I. Batonneau-Gener, T. Belin, S. Mignard, I. Javierre, I. Dubois-Brugger, M. Horgnies, Reactivity of volatile organic compounds with hydrated cement paste containing activated carbon, Build. Environ. 87 (2015) 102–107. doi:10.1016/j.buildenv.2015.01.025.

[112] W.J. Cantwell, J. Morton, The impact resistance of composite materials - a review, Composites. 22 (1991) 347–362. doi:10.1016/0010-4361(91)90549-V.

[113] P. Stynoski, P. Mondal, C. Marsh, Effects of silica additives on fracture properties of carbon nanotube and carbon fiber reinforced Portland cement mortar, Cem. Concr. Compos. 55 (2015) 232–240. doi:10.1016/j.cemconcomp.2014.08.005.

[114] Carbon fibres types, IUPAC Gold B. (n.d.).

[115] X. Shu, R.K. Graham, B. Huang, E.G. Burdette, Hybrid effects of carbon fibers on mechanical properties of Portland cement mortar, Mater. Des. 65 (2015) 1222–1228. doi:10.1016/j.matdes.2014.10.015.

[116] P. Garcés, E. Zornoza, E.G. Alcocel, Ó. Galao, L.G. Andión, Mechanical properties and corrosion of CAC mortars with carbon fibers, Constr. Build. Mater. 34 (2012) 91–96. doi:10.1016/j.conbuildmat.2012.02.020.

[117] B. Han, L. Zhang, C. Zhang, Y. Wang, X. Yu, J. Ou, Reinforcement effect and mechanism of carbon fibers to mechanical and electrically conductive properties of cement-based materials, Constr. Build. Mater. 125 (2016) 479–489. doi:10.1016/j.conbuildmat.2016.08.063.

[118] T. Wongtanakitcharoen, A.E. Naaman, Unrestrained early age shrinkage of concrete with polypropylene, PVA, and carbon fibers, Mater. Struct. Constr. 40 (2007) 289–300. doi:10.1617/s11527-006-9106-z.

[119] Y. Xu, D.D.L. Chung, Reducing the drying shrinkage of cement paste by admixture surface treatments, Cem. Concr. Res. 30 (2000) 241–245. doi:10.1016/S0008-8846(99)00239-2.

[120] J. Hou, D.D.L. Chung, Cathodic protection of steel reinforced concrete facilitated by using carbon fiber reinforced mortar or concrete, Cem. Concr. Res. 27 (1997) 649–656. doi:10.1016/S0008-8846(97)00058-6.

[121] Z.Y. Xia, S. Pezzini, E. Treossi, G. Giambastiani, F. Corticelli, V. Morandi, A. Zanelli, V. Bellani, V. Palermo, The exfoliation of graphene in liquids by electrochemical, chemical, and sonication-assisted techniques: A nanoscale study, Adv. Funct. Mater. 23 (2013) 4684–4693. doi:10.1002/adfm.201203686.

[122] J. Foldyna, V. Foldyna, M. Zeleňák, Dispersion of carbon nanotubes for application in cement composites, Procedia Eng. 149 (2016) 94–99. doi:10.1016/j.proeng.2016.06.643.

[123] L. Coppola, A. Buoso, F. Corazza, Electrical Properties of Carbon Nanotubes Cement Composites for Monitoring Stress Conditions in Concrete Structures, Appl. Mech. Mater. 82 (2011) 118–123. doi:10.4028/www.scientific.net/AMM.82.118.

[124] H. Sixuan, Multifunctional graphite nanoplatelets (gnp) reinforced cementitious composites, Thesis Submitt. Degree master Eng. Dep. Civ. Eng. Natl. Univ. SINGAPORE. (2012).

[125] J. Cao, D.D.L. Chung, Coke powder as an admixture in cement for electromagnetic interference shielding, Carbon N. Y. 41 (2003) 2433–2436. doi:10.1016/S0008-6223(03)00289-6.

[126] J.L. Le, H. Du, S.D. Pang, Use of 2-D Graphene Nanoplatelets (GNP) in cement composites for structural health evaluation, Compos. Part B Eng. 67 (2014) 555–563. doi:10.1016/j.compositesb.2014.08.005.

[127] A. Al-Dahawi, O. Öztürk, F. Emami, G. Yildirim, M. Şahmaran, Effect of mixing methods on the electrical properties of cementitious composites incorporating different carbon-based materials, Constr. Build. Mater. 104 (2016) 160–168. doi:10.1016/j.conbuildmat.2015.12.072.

[128] B. Denise, Minimizing the environmental impacts of CNTs, Dep. Civ. Environ. Eng. Massachusetts Inst. Technol. (2008) 2008.

[129] D. Kuempel Eileen, Identification of Research Needs to Resolve the Carcinogenicity of High-priority IARC Carcinogens, Views Expert Opin. an IARC/NORA Expert Gr. Meet. Lyon, Fr. 30 June – 2 July 2009. IARC Tech. Publ. No. 42. Lyon, Fr. Int. Agency Res. Cancer. 42. 42 (2012) 61–72.

[130] T. Sorahan, A ‘“ Lugged ”’ Analysis of Lung Cancer Risks in UK Carbon Black Production Workers , 1951 – 2004, Am. J. Ind. Med. 564 (2007) 555–564. doi:10.1002/ajim.20481.

[131] E.M. Ward, P.A. Schulte, K. Straif, N.B. Hopf, J.C. Caldwell, T. Carreón, D.M. Demarini, B.A. Fowler, B.D. Goldstein, K. Hemminki, C.J. Hines, K.H. Pursiainen, E. Kuempel, J. Lewtas, R.M. Lunn, E. Lynge, D.M. McElvenny, H. Muhle, T. Nakajima, L.W. Robertson, N. Rothman, A.M. Ruder, M.K. Schubauer-Berigan, J. Siemiatycki, D. Silverman, M.T. Smith, T. Sorahan, K. Steenland, R.G. Stevens, P. Vineis, S.H. Zahm, L. Zeise, V.J. Cogliano, Research recommendations for selected IARC-classified agents, Environ. Health Perspect. 118 (2010) 1355–1362. doi:10.1289/ehp.0901828.

[132] P. Morfeld, R.J. McCunney, Carbon black and lung cancer: Testing a new exposure metric in a German cohort, Am. J. Ind. Med. 50 (2007) 565–567. doi:10.1002/ajim.20491.

[133] K. Donaldson, V. Stone, A. Clouter, L. Renwick, W. Macnee, Ultrafine Particles, Occup Env. Med. 58 (2001) 211–216. doi:10.1136/oem.58.3.211.

[134] G. Lalwani, M. D’Agati, A.M. Khan, B. Sitharaman, Toxicology of graphene-based nanomaterials, Adv. Drug Deliv. Rev. 105 (2016) 109–144. doi:10.1016/j.addr.2016.04.028.

[135] Y. Talukdar, J.T. Rashkow, G. Lalwani, S. Kanakia, B. Sitharaman, The effects of graphene nanostructures on mesenchymal stem cells, Biomaterials. 35 (2014) 4863–4877. doi:10.1016/j.biomaterials.2014.02.054.

[136] “Jagged graphene can slice into cell membranes”. Avaible from (https://news.brown.edu/articles/2013/07/graphene). (2013), News from Brown. Brown Edu. (2013) 2013.

[137] Y. Li, H. Yuan, A. von dem Bussche, M. Creighton, R.H. Hurt, A.B. Kane, H. Gao, Graphene microsheets enter cells through spontaneous membrane penetration at edge asperities and corner sites, Proc. Natl. Acad. Sci. 110 (2013) 12295–12300. doi:10.1073/pnas.1222276110.

[138] Current Intelligence Bulletin 65: Occupational Exposure to Carbon Nanotubes and Nanofibers, Natl. Inst. Occup. Saf. Heal. (2013).

[139] L.M. Fatkhutdinova, T.O. Khaliullin, O.L. Vasil'yeva, R.R. Zalyalov, I.G. Mustafin, E.R. Kisin, M.E. Birch, N. Yanamala, A.A. Shvedova, Fibrosis biomarkers in workers exposed to MWCNTs, Toxicol. Appl. Pharmacol. 299 (2016) 125–131. doi:10.1016/j.taap.2016.02.016.

[140] J. Kolosnjaj, Toxicity studies of carbon nanotubes, Adv. Exp. Med. Biol. 620 (2007) 181–204.

[141] C.A. Poland, R. Duffin, I. Kinloch, A. Maynard, W.A.H. Wallace, A. Seaton, V. Stone, S. Brown, W. MacNee, K. Donaldson, Carbon nanotubes introduced into the abdominal cavity of mice show asbestos-like pathogenicity in a pilot study, Nat. Nanotechnol. 3 (2008) 423–428. doi:10.1038/nnano.2008.111.

[142] C. Corredor, W.C. Hou, S.A. Klein, B.Y. Moghadam, M. Goryll, K. Doudrick, P. Westerhoff, J.D. Posner, Disruption of model cell membranes by carbon nanotubes, Carbon N. Y. 60 (2013) 67–75. doi:10.1016/j.carbon.2013.03.057.

[143] A.E. Porter, M. Gass, K. Muller, J.N. Skepper, P.A. Midgley, M. Welland, Direct imaging of single-walled carbon nanotubes in cells, Nat. Nanotechnol. 2 (2007) 713–717. doi:10.1038/nnano.2007.347.

[144] Z. Ralph, Approaches to Safe Nanotechnology: Managing the Health and Safety Concerns Associated with Engineered Nanomaterials, Natl. Inst. Occup. Saf. Heal. NIOSH Publ. 125. 125 (2009).

[145] C. Lam, J.T. James, R. McCluskey, S. Arepalli, R.L. Hunter, A Review of Carbon Nanotube Toxicity and Assessment of Potential Occupational and Environmental Health Risks, Crit. Rev. Toxicol. 36 (2006) 189–217. doi:10.1080/10408440600570233.

[146] Carbon Nanoparticles Toxic To Adult Fruit Flies But Benign To Young, ScienceDaily. (2009).

[147] F. Rajabipour, J. Weiss, Electrical conductivity of drying cement paste, Mater. Struct. Constr. 40 (2007) 1143–1160. doi:10.1617/s11527-006-9211-z.

[148] B. Han, K. Zhang, X. Yu, E. Kwon, J. Ou, Electrical characteristics and pressure-sensitive response measurements of carboxyl MWNT/cement composites, Cem. Concr. Compos. 34 (2012) 794–800. doi:10.1016/j.cemconcomp.2012.02.012.

[149] R.G. Seippel, Fundamentals of electricity: basics of electricity, electronics, controls and computers, Am. Tech. Soc. (1974) 1974.

[150] R.A. Millikan, Elements of Electricity: A Practical Discussion of the Fundamental Laws and Phenomena of Electricity and Their Practical Applications in the Business and Industrial World, Am. Tech. Soc. (1917).

[151] J.C. Shedd, Popular Science Monthly, in Self-Sensing Concrete in Smart Structures, T.S. Press. Ed. Elsevier Sci. (1913) 599.

[152] Polarization of Dielectric, Available from Http//Hyperphysics.Phyastr. Gsu.Edu/Hbase/Electric/Dielec.Html. (2000) 2000.

[153] A. Robbins, W.C. Miller, Circuit Analysis: Theory and Practice, Thomson Delmar Learn. (2003).

[154] H. Ying, Conductive mechanism research based on pressure-sensitive conductive composite material for flexible tactile sensing, Int. Conf. Inf. Autom. (2008).

[155] M.H. Al-Saleh, A review of vapor grown carbon nanofiber/polymer conductive composites, Carbon N. Y. 47 (2009) 2–22.

[156] D. Stauffer, Introduction To Percolation Theory, (1994).

[157] G. Bianchi, Elettrochimica, (1976).

[158] D.M. Stefanescu, Handbook of Force Transducers: Principles and Components, Springer Berlin Heidelb. (2011).

[159] F. Carmona, Piezoresistivity of heterogeneous solids, J. Appl. Phys. 61 (1987) 2550.

[160] Y. Cao, Giant piezoresistivity in polymer derived amorphous SiAlCO ceramics, J. Mater. Sci. 51 (2016) 5646–5650.

[161] W. Thomson, On the Electro-Dynamic Qualities of Metals:--Effects of Magnetization on the Electric Conductivity of Nickel and of Iron, Proc. R. Soc. London. 8 (1856) 546–550. doi:10.1098/rspl.1856.0144.

[162] S. Zhu, D.D.L. Chung, Theory of piezoresistivity for strain sensing in carbon fiber reinforced cement under flexure, J. Mater. Sci. 42 (2007) 6222–6233. doi:10.1007/s10853-006-1131-3.

[163] D.D.L. Chung, Piezoresistive Cement-Based Materials for Strain Sensing, J. Intell. Mater. Syst. Struct. 13 (2002) 599–609.

[164] B. Chen, Damage in carbon fiber-reinforced concrete, monitored by both electrical resistance measurement and acoustic emission analysis, Constr. Build. Mater. 22 (2008) 2196–2201.

[165] D.M. Bontea, Damage in carbon fiber-reinforced concrete, monitored by electrical resistance measurement, Cem. Concr. Res. 30 (2000) 651–659.

[166] R.M. Chacko, Carbon-fiber-reinforced cement-based sensors, Can. J. Civ. Eng. 34 (2007) 284–290.

[167] F. Azhari, N. Banthia, Cement-based sensors with carbon fibers and carbon nanotubes for piezoresistive sensing, Cem. Concr. Compos. 34 (2012) 866–873. doi:10.1016/j.cemconcomp.2012.04.007.

[168] M.Q. Sun, R.J.Y. Liew, M.H. Zhang, W. Li, Development of cement-based strain sensor for health monitoring of ultra high strength concrete, Constr. Build. Mater. 65 (2014) 630–637. doi:10.1016/j.conbuildmat.2014.04.105.

[169] H. Li, H. gang Xiao, J. ping Ou, Effect of compressive strain on electrical resistivity of carbon black-filled cement-based composites, Cem. Concr. Compos. 28 (2006) 824–828. doi:10.1016/j.cemconcomp.2006.05.004.

[170] S. Wen, Effects of Strain and Damage on Strain-Sensing Ability of Carbon Fiber Cement, J. Mater. Civ. Eng. 18 (2006) 355–360.

[171] B.G. Han, Effects of the content level and particle size of nickel powder on the piezoresistivity of cement-based composites/sensors, Smart Mater. Struct. 19 (2010) 65012.

[172] S. Mohamed, Wireless and embedded carbon nanotube networks for damage detection in concrete structures, Nanotechnology. 20 (2009) 395502.

[173] A.O. Monteiro, Development of a multifunctional carbon black/cement composite for traffic monitoring, PhD Thesis, Univ. Aveiro, Dep. Eng. Civ. (2017).

[174] W.J. McCarter, H.M. Taha, B. Suryanto, G. Starrs, Two-point concrete resistivity measurements: Interfacial phenomena at the electrode-concrete contact zone, Meas. Sci. Technol. 26 (2015). doi:10.1088/0957-0233/26/8/085007.

[175] M. Chiarello, R. Zinno, Electrical conductivity of self-monitoring CFRC, Cem. Concr. Compos. 27 (2005) 463–469. doi:10.1016/j.cemconcomp.2004.09.001.

[176] S. Wen, D.D.L. Chung, Piezoresistivity-based strain sensing in carbon fiber- reinforced cement, ACI Mater.J. 104 (2007) 171–179.

[177] F. Wenner, A method of measuring earth resistivity, Bur. Stand. Washington, D.C. (1915) 10.

[178] R. Polder, Test methods on site measurement of resistivity of concrete, RILEM TC 154-EMC, Mater. Struct. 33 (2000) 603–611.

[179] O. Galao, F.J. Baeza, E. Zornoza, P. Garcés, Strain and damage sensing properties on multifunctional cement composites with CNF admixture, Cem. Concr. Compos. 46 (2014) 90–98. doi:10.1016/j.cemconcomp.2013.11.009.

[180] T.-C. Hou, J.P. Lynch, Conductivity-based strain monitoring and damage characterization of fiber reinforced cementitious structural components, Smart Struct. Mater. 2005 Sensors Smart Struct. Technol. Civil, Mech. Aerosp. Syst. SPIE-Int. Soc. Opt. Eng, San Diego, CA, USA,. (2005) 419–429.

[181] M. Faraday, On Electrical Decomposition, Philos. Trans. R. Soc. (1834).

[182] C.G. Berrocal, K. Hornbostel, M.R. Geiker, I. Löfgren, K. Lundgren, D.G. Bekas, Electrical resistivity measurements in steel fibre reinforced cementitious materials, Cem. Concr. Compos. 89 (2018) 216–229. doi:10.1016/j.cemconcomp.2018.03.015.

[183] B. Han, J. Ou, Embedded piezoresistive cement-based stress/strain sensor, Sensors Actuators, A Phys. 138 (2007) 294–298. doi:10.1016/j.sna.2007.05.011.

[184] J. Ou, Research and practice of intelligent sensing technologies in civil structural health monitoring in the mainland of China - art. no. 61761D, Nondestruct. Eval. Heal. Monit. Aerosp. Mater. Compos. Civ. Infrastruct. V. 6176 (2006) D1761. doi:10.1117/12.663993.

[185] R.N. Howser, H.B. Dhonde, Y.L. Mo, Self-sensing of carbon nanofiber concrete columns subjected to reversed cyclic loading, Smart Mater. Struct. 20 (2011) 85031.

[186] A. from Http://www.analytical-chemistry.uoc.gr/files/items/6/618/agwgimometria_2.pdf, Radiometer Analytical SAS, Conductivity: Theory and Practice, (n.d.) 618.

[187] G. Redlarski, B. Lewczuk, A. Zak, A. Koncicki, M. Krawczuk, J. Piechocki, K. Jakubiuk, P. Tojza, J. Jaworski, D. Ambroziak, Ł. Skarbek, D. Gradolewski, The influence of electromagnetic pollution on living organisms: Historical trends and forecasting changes, Biomed Res. Int. 2015 (2015). doi:10.1155/2015/234098.

[188] Kwan-Hoong Ng, Non-Ionizing Radiations - Sources, Biological Effects, Emissions and Exposures, Proc. Int. Conf. Non-Ionizing Radiat. UNITEN. (2003) 1–16. http://www.who.int/peh-emf/meetings/archive/en/keynote3ng.pdf.

[189] WHO, Electromagnetic fields and public health: mobile phones, (2018).

[190] M. Repacholi, Systematic review of wireless phone use and brain cancer and other head tumors, Bioelectromagnetics. 33 (2012) 187–206.

[191] D.G. Sutton, C.J. Martin, "Practical Radiation Protection in Healthcare," OUP Oxford; Second Ed. (2015) 2015.

[192] B. JD, Cell phones, cancer, and children, J. Natl. Cancer Inst. 103 (2011) 1211–3. doi:10.1080/01402390.2011.569130.

[193] WHO, IARC Classifies radiofrequency electromagnetic fields as possibly carcinogenic to humans, Int. Agency Res. Cancer. (2011).

[194] X. Lv, Y. Duan, G. Chen, Electromagnetic wave absorption properties of cement-based composites filled with graphene nano-platelets and hollow glass microspheres, Constr. Build. Mater. 162 (2018) 280–285. doi:10.1016/j.conbuildmat.2017.12.047.

[195] D.D.L. Chung, Electrically conductive cement-based materials, Adv. Cem. Res. 16 (2004) 167–176. doi:10.1680/adcr.16.4.167.46658.

[196] Q. Liu, Q. Xu, Q. Yu, R. Gao, T. Tong, Experimental investigation on mechanical and piezoresistive properties of cementitious materials containing graphene and graphene oxide nanoplatelets, Constr. Build. Mater. 127 (2016) 565–576. doi:10.1016/j.conbuildmat.2016.10.024.

[197] F. AZHARI, Cement-Based Sensors for Structural Health Monitoring, (2008).

[198] P. Xie, P. Gu, J.J. Beaudoin, Electrical percolation phenomena in cement composites containing conductive fibres, J.Mater.Sci. 31 (1996) 4093–7. doi:10.1016/j.jmgm.2005.11.005.

[199] R. Zallen, Physics of Amorphous Solids, Wiley, New York. (1983) 135–204.

[200] N. Banthia, S. Djeridane, M. Pigeon, Electrical resistivity of carbon and steel micro-fiber reinforced cements, Cem. Concr. Res. 22 (1992) 804–814. doi:10.1016/0008-8846(92)90104-4.

[201] R. Farhad, Volume electrical resistivity of carbon fiber cement composites, ACI Mater.J. 98 (2001) 25–35.

[202] W.J. McCarter, G. Starrs, C. G., B. T. M., Activation energy and conduction in carbon fibre reinforced cement matrices, J.Mater.Sci. 42 (2007) 2200–3.

[203] X. Fu, D.D.L. Chung, Self-monitoring of fatigue damage in carbon fiber reinforced cement, Cem. Concr. Res. 26 (1996) 15–20.

[204] X. Yu, E. Kwon, A carbon nanotube/cement composite with piezoresistive properties, Smart Mater. Struct. 18 (2009) 55010.

[205] E. Teomete, O.I. Kocyigit, Tensile strain sensitivity of steel fiber reinforced cement matrix composites tested by split tensile test, Constr. Build. Mater. 47 (2013) 962–968. doi:10.1016/j.conbuildmat.2013.05.095.

[206] Z.S. Metaxa, S.K. Kourkoulis, Cement Based Nanocomposites With Self-Diagnostic Characteristics, (2017) 20–25.

[207] S. Wen, D.D.L. Chung, Model of piezoresistivity in carbon fiber cement, Cem. Concr. Res. 36 (2006) 1879–1885. doi:10.1016/j.cemconres.2006.03.029.

[208] G. Di, Electrical resistance of carbon-nanofiber concrete, Smart Mater. Struct. 18 (2009) 95039.

[209] A. D'Alessandro, F. Ubertini, A.L. Materazzi, Self-sensing concrete nanocomposites for smart structures, World Acad. Sci. Eng. Technol. Int. J. Civ. Environ. Eng. 10 (2016) 599–604.

[210] A.L. Materazzi, F. Ubertini, A. D'Alessandro, Carbon nanotube cement-based transducers for dynamic sensing of strain, Cem. Concr. Compos. 37 (2013) 2–11. doi:10.1016/j.cemconcomp.2012.12.013.

[211] F. Ubertini, A.L. Materazzi, A. D'Alessandro, S. Laflamme, Natural frequencies identification of a reinforced concrete beam using carbon nanotube cement-based sensors, Eng. Struct. 60 (2014) 265–275. doi:10.1016/j.engstruct.2013.12.036.

[212] A. Downey, A. D'Alessandro, F. Ubertini, S. Laflamme, R. Geiger, Biphasic DC measurement approach for enhanced measurement stability and multi-channel sampling of self-sensing multi-functional structural materials doped with carbon-based additives, Smart Mater. Struct. 26 (2017) 0–12. doi:10.1088/1361-665X/aa6b66.

[213] B. Han, Properties, sensors and structures of pressure-sensitive carbon fiber cement paste, Diss. Dr. Degree Eng. China Harbin Inst. Technol. (2005).

[214] H. Xiao, H. Li, J. Ou, Self-monitoring properties of concrete columns with embedded cement- based strain sensors, J Intell Mater Syst Struct. 22 (2011) 191–200. doi:10.1080/01402390.2011.569130.

[215] H. Xiao, H. Li, J. Ou, Strain sensing properties of cement-based sensors embedded at various stress zones in a bending concrete beam, Sens Actuators Phys. 167 (2011) 581–7. doi:10.1080/01402390.2011.569130.

[216] F. Baeza, O. Galao, E. Zornoza, P. Garces, Multifunctional cement composites strain and damage sensors applied on reinforced concrete (RC) structural elements, Materials (Basel). 6 (2013) 841–55.

[217] S. Wen, D.D.L. Chung, Carbon fiber-reinforced cement as a strain-sensing coating, Cem. Concr. Res. 31 (2001) 665–667. doi:10.1016/S0008-8846(01)00474-4.

[218] D. Zhang, Z. Luo, Z. Luo, S. Wu, Sensitivity of reinforced components of CFRC, J Harbin Inst Technol. 36 (2004) 1411–3.

[219] D. Zhang, S. Wu, B. Ma, J. Zhao, Sensitivities of carbon fiber reinforced concrete under bending loading, J Jilin Univ Eng Technol Ed. 34 (2004) 679–683.

[220] W. Zhang, H. Xie, J. Liu, B. Shi, Experimental study on elastic stress self-monitoring of carbon fiber reinforced smart concrete beams, J Southeast Univ Nat Sci Ed. 34 (2004) 647–650.

[221] W. Wang, S. Wu, H. Dai, Fatigue behavior and life prediction of carbon fiber reinforced concrete under cyclic flexural loading, Mater Sci Eng A. 434 (2006) 347–51.

[222] L. Burlamacchi, Capire il calcestruzzo, Hoepli, 1994.

[223] A. Weyer, E. Glos, European Illustrated Glossary Of Conservation Terms For Wall Paintings And Architectural Surfaces, Petersberg, Michael Imhof. (2015) 381.

[224] V.A. Rossetti, Il calcestruzzo: materiali e tecnologia, 2003.

[225] M. Couvreux, Selecting a Natural Hydraulic Lime - What to Look For, (2014) 8–10. http://www.limes.us/wp-content/uploads/2014/03/TheLastStraw.pdf.

[226] UNI EN 459-1:2010, Standard. (n.d.).

[227] H.K. Kim, I.W. Nam, H.K. Lee, Enhanced effect of carbon nanotube on mechanical and electrical properties of cement composites by incorporation of silica fume, Compos. Struct. 107 (2014) 60–69. doi:10.1016/j.compstruct.2013.07.042.

[228] Thermal Gasification of Biomass, Int. Energy Agency Task 33, Www.Gastechnology.Org. (2011). doi:10.1080/01402390.2011.569130.

[229] B. Jayasena, S. Subbiah, A novel mechanical cleavage method for synthesizing few-layer graphenes, Nanoscale Res. Lett. 6 (2011) 1–7. doi:10.1186/1556-276X-6-95.

[230] Cambridge-dictionaries, Graphene definition, meaning – what is graphene, Br. English Dict. Thes. (n.d.). doi:10.1145/2503368.2503369.

[231] M.I. Katsnelson, Graphene: carbon in two dimensions, Mater. Today. 10 (2007) 20–27.

[232] A.K. Geim, A.H. MacDonald, Graphene: Exploring carbon flatland, Phys. Today. (2007) 35–40. doi:10.1111/j.1468-2982.2004.00639.x.

[233] K.S. Novoselov, A.K. Geim, S. V Morozov, D. Jiang, Y. Zhang, Electric Field Effect in Atomically Thin Carbon Films, Science (80-.). 306 (2004) 666–669. doi:10.1126/science.1102896.

[234] C. Lee, X. Wei, J.W. Kysar, J. Hone, Measurement of the elastic properties and intrinsic strength of monolayer graphene, Science (80-.). 321 (2008) 385–388.

[235] C. Lee, X. Wei, Q. Li, R. Carpick, J.W. Kysar, J. Hone, Elastic and frictional properties of graphene, Phys. Status Solidi. 246 (2009) 2562–2567.

[236] V. Singh, D. Joung, L. Zhai, S. Das, S.I. Khondaker, S. Seal, Graphene based materials: Past, present and future, Prog. Mater. Sci. 56 (2011) 1178–1271. doi:10.1016/j.pmatsci.2011.03.003.

[237] Adsorbed Methane Film Properties in Nanoporous Carbon Monoliths, Bull. Am. Phys. Soc. 58 (2013).

[238] A. Russo, Produzione ed utilizzo dei carboni attivi, Master Degree Thesis Environ. Eng. Univ. Naples, Federico II (2014). (2014).

[239] Activated carbon monoliths for methane storage, Bull. Am. Phys. Soc. 57 (2012).

[240] Activated Carbon Basics, Haycarb, Avaible from Http//Www.Haycarb.Com/Activated-Carbon. (n.d.). doi:10.1159/000030320.

[241] K.D. McCranie, M. Faulkner, D. French, G.A. Daddis, J. Gow, A. Long, Review of Technologies for Gasification of Biomass and Wastes, NNFCC project 09/008, Natl. Non-Food Crop. Cent. (2011). doi:10.1080/01402390.2011.569130.

[242] C. Higman, M. Van der Burgt, Gasification, Second Edition, (2008).

[243] C. Guizani, M. Jeguirim, R. Gadiou, F.J. Escudero Sanz, S. Salvador, Biomass char gasification by H2O, CO2and their mixture: Evolution of chemical, textural and structural properties of the chars, Energy. 112 (2016) 133–145. doi:10.1016/j.energy.2016.06.065.

[244] J.J. Hernández, M. Lapuerta, E. Monedero, Characterisation of residual char from biomass gasification: effect of the gasifier operating conditions, J. Clean. Prod. 138 (2016) 83–93. doi:10.1016/j.jclepro.2016.05.120.

[245] V. Benedetti, F. Patuzzi, M. Baratieri, Gasification Char as a Potential Substitute of Activated Carbon in Adsorption Applications, Energy Procedia. 105 (2017) 712–717. doi:10.1016/j.egypro.2017.03.380.

[246] R. Siddique, G. de Schutter, A. Noumowe, Effect of used-foundry sand on the mechanical properties of concrete, Constr. Build. Mater. 23 (2009) 976–980. doi:10.1016/j.conbuildmat.2008.05.005.

[247] About Metal Casting, Am. Foundry Soc. (AFS), Available from Http//Www.Afsinc.Org/Content/View /62/122/. (n.d.).

[248] S. Monosi, D. Sani, F. Tittarelli, Used foundry sand in cement mortars and concrete production, Open Waste Manag. J. 3 (2010).

[249] R. Bakis, H. Koyuncu, A. Demirbas, An investigation of waste foundry sand in asphalt concrete mixtures, Waste Manag. Res. 24 (2006) 269–274.

[250] A. Mazzoli, O. Favoni, Particle size, size distribution and morphological evaluation of airborne dust particles of diverse woods by Scanning Electron Microscopy and image processing program, Powder Technol. 225 (2012) 65–71. doi:10.1016/j.powtec.2012.03.033.

[251] A. Mazzoli, G. Moriconi, Particle size, size distribution and morphological evaluation of glass fiber reinforced plastic (GRP) industrial by-product, Micron. 67 (2014) 169–178. doi:10.1016/j.micron.2014.07.007.

[252] Y. Wang, H.C. Wu, V.C. Li, Concrete reinforcement with recycled fibers, J. Mater. Civ. Eng. (2000) 314–319.

[253] D.D.L. Chung, Carbon Fiber Composites, (1994).

[254] American Chemical Society, High Performance Carbon Fibers, Natl. Hist. Chem. Landmarks. Am. Chem. Soc. (2014).

[255] Fibers, 5. Synthetic Inorganic - Carbon Fibers, Ullmann's Encycl. Ind. Chem. (2002).

[256] V.I. Kostikov, Fibre Science and Technology, 1995.

[257] T. Tanaka, K. Yagi, N. Kojima, K. Kimura, H. Katsumata, Retrofit method with carbon fiber reinforced concrete structures, Adv Compos Mater. 4 (1994) 183–95.

[258] L. Ye, K. Friedrich, C. Weimer, Y. Mai, Surface treatment and adhesion bonding between concrete and a CFRP composite, Adv Compos Mater. 7 (1998) 47–91.

[259] ACI 544.3R-93: Guide for Specifying, Proportioning, Mixing, Placing, and Finishing Steel Fiber Reinforced Concrete, ACI Mater. J. (1998). doi:10.14359/4046.

[260] C. Pierini, Calcestruzzo fibrorinforzato con fibre di acciaio (SFRC), Caratterizzazione del materiale e progettazione strutturale, Ingenio. 41 (2016) 46.

[261] Speciale Additivi, Enco J. 59 (2013).

[262] B. Zou, S.J. Chen, A.H. Korayem, F. Collins, C.M. Wang, W.H. Duan, Effect of ultrasonication energy on engineering properties of carbon nanotube reinforced cement pastes, Carbon N. Y. 85 (2015) 212–220. doi:10.1016/j.carbon.2014.12.094.

[263] A.O. Monteiro, P.B. Cachim, P.M.F.J. Costa, Electrical Properties of Cement-based Composites Containing Carbon Black Particles, Mater. Today Proc. 2 (2015) 193–199. doi:10.1016/j.matpr.2015.04.021.

[264] F. Winnefeld, S. Becker, J. Pakusch, T. Götz, Effects of the molecular architecture of comb-shaped superplasticizers on their performance in cementitious systems, Cem. Concr. Compos. 29 (2007) 251–262. doi:10.1016/j.cemconcomp.2006.12.006.

[265] L. Ferrari, J. Kaufmann, F. Winnefeld, J. Plank, Interaction of cement model systems with superplasticizers investigated by atomic force microscopy, zeta potential, and adsorption measurements, J. Colloid Interface Sci. 347 (2010) 15–24.

[266] A. Mobili, A. Belli, C. Giosuè, T. Bellezze, F. Tittarelli, Metakaolin and fly ash alkali-activated mortars compared with cementitious mortars at the same strength class, Cem. Concr. Res. 88 (2016) 198–210. doi:10.1016/j.cemconres.2016.07.004.

[267] V. Corinaldesi, G. Moriconi, F. Tittarelli, Thaumasite: Evidence for incorrect intervention in masonry restoration, Cem. Concr. Compos. 25 (2003) 1157–1160. doi:10.1016/S0958-9465(03)00158-6.

[268] I. Ozga, N. Ghedini, C. Giosuè, C. Sabbioni, F. Tittarelli, A. Bonazza, Assessment of air pollutant sources in the deposit on monuments by multivariate analysis, Sci. Total Environ. 490 (2014) 776–784. doi:10.1016/j.scitotenv.2014.05.084.

[269] G. Roventi, T. Bellezze, G. Giuliani, C. Conti, Corrosion resistance of galvanized steel reinforcements in carbonated concrete: Effect of wet-dry cycles in tap water and in chloride solution on the passivating layer, Cem. Concr. Res. 65 (2014) 76–84. doi:10.1016/j.cemconres.2014.07.014.

[270] G. Moriconi, F. Tittarelli, V. Corinaldesi, Review of silicone-based hydrophobic treatment and admixtures for concrete, Indian Concr. J. 76 (2002) 637–642.

[271] M. Carsana, F. Tittarelli, L. Bertolini, Use of no-fines concrete as a building material: Strength, durability properties and corrosion protection of embedded steel, Cem. Concr. Res. 48 (2013) 64–73. doi:10.1016/j.cemconres.2013.02.006.

[272] F. Tittarelli, M. Carsana, M.L. Ruello, Effect of hydrophobic admixture and recycled aggregate on physical-mechanical properties and durability aspects of no-fines concrete, Constr. Build. Mater. 66 (2014) 30–37. doi:10.1016/j.conbuildmat.2014.05.043.

[273] V. Bonaventi, V. Rahhal, E. Irassar, Studies on the carboaluminate formation in limestone filler-blended cements, Cem. Concr. Res. 31 (2001) 853–859.

[274] F. Tittarelli, Effect of low dosages of waste GRP dust on fresh and hardened properties of mortars: Part 2, Constr. Build. Mater. 47 (2013) 1539–1543. doi:10.1016/j.conbuildmat.2013.06.086.

[275] C.H. Phan, M. Mariatti, Y.H. Koh, Electromagnetic interference shielding performance of epoxy composites filled with multiwalled carbon nanotubes/manganese zinc ferrite hybrid fillers, J. Magn. Magn. Mater. 401 (2016) 472–478. doi:10.1016/j.jmmm.2015.10.067.

[276] C. Beall, E. Delzell, P. Cole, I. Brill, Brain Tumors among Electronics Industry Workers, Epidemiology. 7 (1996) 125–130.

[277] K. Andrews, D. Savitz, Accuracy of industry and occupation on death certificates of electric utility workers: Implications for epidemiologic studies of magnetic fields and cancer, Langmuir. 20 (1999) 512–518. doi:10.1002/(SICI)1521-186X(199912)20.

[278] G. Mittal, V. Dhand, K.Y. Rhee, S.J. Park, W.R. Lee, A review on carbon nanotubes and graphene as fillers in reinforced polymer nanocomposites, J. Ind. Eng. Chem. 21 (2015) 11–25. doi:10.1016/j.jiec.2014.03.022.

[279] D. Lide, Handbook of Chemistry and Physics, 82nd Ed. Boca Raton, Florida, USA CRC Press. (2001).

[280] D.A. Hill, Electromagnetic Theory of Reverberation Chambers, NIST Tech. Note 1506, Natl. Inst. Stand. Technol. Boulder, Color. (1998).

[281] D. Micheli, A. Vricella, R. Pastore, A. Delfini, R. Bueno Morles, M. Marchetti, F. Santoni, L. Bastianelli, F. Moglie, V. Mariani Primiani, V. Corinaldesi, A. Mazzoli, J. Donnini, Electromagnetic properties of carbon nanotube reinforced concrete composites for frequency selective shielding structures, Constr. Build. Mater. 131 (2017) 267–277. doi:10.1016/j.conbuildmat.2016.11.078.

[282] M. Albano, D. Micheli, G. Gradoni, R.B. Morles, M. Marchetti, F. Moglie, V. Mariani Primiani, Electromagnetic shielding of thermal protection system for hypersonic vehicles, Acta Astronaut. 87 (2013) 30–39. doi:10.1016/j.actaastro.2013.02.003.

[283] L. Bastianelli, S. Capra, G. Gradoni, D. Micheli, A. Vricella, V. Corinaldesi, Shielding effectiveness statistical evaluation of random concrete composites, 3rd IEEE Int. Work. Metrol. Aerospace, Metroaerosp. (2016) 172–176. doi:10.1109/MetroAeroSpace.2016.7573207.

[284] D.A. Hill, Electronic Mode Stirring for Reverberation Chambers, IEEE Trans. Electromagn. Compat. 36 (1994) 294–299. doi:10.1109/15.328858.

[285] S. Monosi, F. Tittarelli, C. Giosuè, M.L. Ruello, Effect of two different sources and washing treatment on the properties of UFS by-products for mortar and concrete production, Constr. Build. Mater. 44 (2013) 260–266. doi:10.1016/j.conbuildmat.2013.02.029.

[286] K. Gong, Z. Pan, A.H. Korayem, L. Qiu, D. Li, F. Collins, C.M. Wang, W.H. Duan, Reinforcing Effects of Graphene Oxide on Portland Cement Paste, J. Mater. Civ. Eng. 27 (2015) A4014010. doi:10.1061/(ASCE)MT.1943-5533.0001125.

[287] H. Moosberg-Bustnes, B. Lagerblad, E. Forssberg, The function of fillers in concrete, Mater Struct. 37 (2004) 74–81. doi:10.1617/13694.

[288] E. Berodier, K. Scrivener, Understanding the filler effect on the nucleation and growth of C-S-H, J. Am. Ceram. Soc. 97 (2014) 3764–3773. doi:10.1111/jace.13177.

[289] R. Yang, Gas Separation by Adsorption Processes, Stoneham Butterworth Publ. (1987).

[290] M. Gonçalves, M. Molina-Sabio, F. Rodriguez-Reinoso, Modification of activated carbon hydrophobicity by pyrolysis of propene, J. Anal. Appl. Pyrolysis. 89 (2010) 17–21. doi:10.1016/j.jaap.2010.04.009.

[291] S. Ranjan, N. Dasgupta, Nanoscience in Food and Agriculture 5, 2017. doi:10.1007/978-3-319-58496-6.

[292] S.G. Prolongo, R. Moriche, A. Jiménez-Suárez, M. Sánchez, A. Ureña, Advantages and disadvantages of the addition of graphene nanoplatelets to epoxy resins, Eur. Polym. J. 61 (2014) 206–214. doi:10.1016/j.eurpolymj.2014.09.022.

[293] Y. Benachour, C.A. Davy, F. Skoczylas, H. Houari, Effect of a high calcite filler addition upon microstructural, mechanical, shrinkage and transport properties of a mortar, Cem. Concr. Res. 38 (2008) 727–736. doi:10.1016/j.cemconres.2008.02.007.

[294] F. Çeçen, A. Özgür, Activated carbon for water and wastewater treatment: Integration of adsorption and biological treatment, John Wiley Sons. (2011).

[295] F. Pacheco-Torgal, S. Jalali, Nanotechnology: Advantages and drawbacks in the field of construction and building materials, Constr. Build. Mater. 25 (2011) 582–590. doi:10.1016/j.conbuildmat.2010.07.009.

[296] D. Enea, G. Guerrini, Photocatalytic Properties of Cement-Based Plasters and Paints Containing Mineral Pigments, Transp Res Rec J Transp Res Board. (2010) 52–60. doi:10.3141/2141-10.

[297] W. Daoud, Self-Cleaning Materials and Surfaces: A Nanotechnology Approach, John Wiley Sons. (2013). doi:10.1002/9781118652336.

[298] V. Georgakilas, M. Otyepka, A. Bourlinos, V. Chandra, N. Kim, K. Kemp, Functionalization of graphene: Covalent and non-covalent approaches, derivatives and applications, Chem Rev. 112 (2012) 156–214. doi:10.1021/cr3000412.

[299] H. Zhang, X. Lv, Y. Li, Y. Wang, J. Li, P25- graphene composite as a high performance photocatalyst, ACS Nano. 4 (2009) 380–386. doi:10.1021/nn901221k.

[300] X. Pan, Y. Zhao, S. Wang, Z. Fan, TiO2/graphene nanocomposite for photocatalytic application, Mater Process Energy Commun Curr Res Technol Dev. (2013) 913–920.

[301] X. Zhang, Graphene/TiO2 nanocomposites: synthesis, characterization and application in hydrogen evolution from water photocatalytic splitting, J Mater Chem. (2010) 2801–2806. doi:10.1039/b917240h.

[302] J. Cao, D.D.L. Chung, Colloidal graphite as an admixture in cement and as a coating on cement for electromagnetic interference shielding, Cem. Concr. Res. 33 (2003) 1737–1740. doi:10.1016/S0008-8846(03)00152-2.

[303] J. Cao, D.D.L. Chung, Use of fly ash as an admixture for electromagnetic interference shielding, Cem. Concr. Res. 34 (2004) 1889–1892. doi:10.1016/j.cemconres.2004.02.003.

[304] D. Chung, Dispersion of Short Fibers in Cement, J Mater Civ Eng. 17 (2005) 379–383. doi:10.1061/(ASCE)0899-1561(2005)17.

[305] D. Chung, Multifunctional Cement-Based Materials, CRC Press. (2003).

[306] P. Clayton, Introduction to Electromagnetic Compatibility, Wiley-Interscience, 2 Ed. (2006).

[307] M.A. Zanini, L. Hofer, C. Pellegrino, A framework for assessing the seismic risk map of Italy and developing a sustainable risk reduction program, Int. J. Disaster Risk Reduct. (2018) 1–20. doi:10.1016/j.ijdrr.2018.09.012.

[308] A. Brenchic, Ponte Morandi a Genova , una tragedia annunciata?, Ing. Available from Http//Www.Ingegneri.Info/News/Infrastrutture-e-Trasporti/Ponte-Morandi-Genova-Analisi-Infrastrutturale/. (2018).

[309] H. Souri, J. Yu, H. Jeon, J.W. Kim, C.M. Yang, N.H. You, B.J. Yang, A theoretical study on the piezoresistive response of carbon nanotubes embedded in polymer nanocomposites in an elastic region, Carbon N. Y. 120 (2017) 427–437. doi:10.1016/j.carbon.2017.05.059.

[310] S. Erdem, S. Hanbay, M.A. Blankson, Self-sensing damage assessment and image-based surface crack quantification of carbon nanofibre reinforced concrete, Constr. Build. Mater. 134 (2017) 520–529. doi:10.1016/j.conbuildmat.2016.12.197.

[311] P.W. Chen, X. Fu, D.D.L. Chung, Improving the bonding between old and new concrete by adding carbon fibers to the new concrete, Cem. Concr. Res. 25 (1995) 491–496. doi:10.1016/0008-8846(95)00037-D.

[312] G. Plizzari, Il calcestruzzo fibrorinforzato per le applicazioni strutturali, Shah's 5 Days Concr. Technol. Course L'Aquila, Fac. Di Ing. - 16 Dicembre 2008. (2008).

[313] W. Chuang, J. Geng-sheng, L. Bing-liang, P. Lei, F. Ying, G. Ni, L. Ke-zhi, Dispersion of carbon fibers and conductivity of carbon fiber-reinforced cement-based composites, Ceram. Int. 43 (2017) 15122–15132. doi:10.1016/j.ceramint.2017.08.041.

[314] J. Donnini, T. Bellezze, V. Corinaldesi, Mechanical, electrical and self-sensing properties of cementitious mortars containing short carbon fibers, J. Build. Eng. 20 (2018) 8–14. doi:10.1016/j.jobe.2018.06.011.

[315] S.P. Shah, Determination of fracture parameters (K(Formula presented.) and CTODc) of plain concrete using three-point bend tests, Mater. Struct. Matériaux Constr. 23 (1990) 457–460. doi:10.1007/BF02472029.

[316] M. Collepardi, Durabilità del calcestruzzo: teoria, pratica e prescrizioni di capitolato - Parte I: cause di degrado di tipo chimico, Ind. Ital. Del Cem. 671 (1992) 1992.

[317] S. Wen, D.D.L. Chung, The role of electronic and ionic conduction in the electrical conductivity of carbon fiber reinforced cement, Carbon N. Y. 44 (2006) 2130–2138. doi:10.1016/j.carbon.2006.03.013.

[318] M. Sahmaran, G. Yıldırım, G. Aras, S. Keskin, O. Keskin, M. Lachemi, Self healing of cementitious composites to reduce high CO2 emissions, Mater. J. 114 (2017) 93–104. doi:10.1111/j.1469-7610.2010.02280.x.

[319] R. Spragg, C. Villani, K. Snyder, D. Bentz, J. Bullard, J. Weiss, Factors That Influence Electrical Resistivity Measurements in Cementitious Systems, Transp. Res. Rec. J. Transp. Res. Board. 2342 (2013) 90–98. doi:10.3141/2342-11.

[320] G. Monfore, The electrical resistivity of concrete, J. PCA Res. Dev. Lab. (1968) 35–48.

[321] H. Whittington, J. McCarter, M. Forde, The conduction of electricity through concrete, Mag. Concr. Res. 33 (1981) 48–59.

[322] R. Hameed, A. Turatsinze, F. Duprat, A. Sellier, Metallic fiber reinforced concrete : effect of fiber aspect ratio on the flexural properties, 4 (2009) 67–72.

[323] M. Mastali, A. Dalvand, A.R. Sattarifard, Z. Abdollahnejad, M. Illikainen, Characterization and optimization of hardened properties of self-consolidating concrete incorporating recycled steel, industrial steel, polypropylene and hybrid fibers, Compos. Part B Eng. 151 (2018) 186–200. doi:10.1016/j.compositesb.2018.06.021.

[324] L. Ferrara, R. Gettu, Size effect in splitting tests on plain and steel fiber-reinforced concrete: A non-local damage analysis, Fract. Mech. Concr. Struct. (2001) 677–684. doi:10.1016/j.compstruct.2007.04.006.

[325] H. Wu, G.M. Ren, Q. Fang, J.Z. Liu, Effects of steel fiber content and type on dynamic tensile mechanical properties of UHPCC, Constr. Build. Mater. 173 (2018) 251–261. doi:10.1016/j.conbuildmat.2018.04.040.

[326] J. Domski, J. Katzer, M. Zakrzewski, T. Ponikiewski, Comparison of the mechanical characteristics of engineered and waste steel fiber used as reinforcement for concrete, J. Clean. Prod. 158 (2017) 18–28. doi:10.1016/j.jclepro.2017.04.165.

[327] W. Baomin, Z. Yuan, M.A. Hainan, Porosity and Pore Size Distribution Measurement of Cement/Carbon Nanofiber Composites by Low Field Nuclear Magnetic Resonance, J. Wuhan Univ. Technol. Sci. Ed. 29 (2014) 82–88. doi:10.1007/s11595-014-0871-1.

[328] O.C. Sola, C.D. Atis, B. Sayin, Investigation of mechanical properties of mortars with carbon fiber using multi slice computed tomography, Rev. La Construcción, Esc. Construcción Civ. Pontif. Univ. Católica Chile. 16 (2017) 167–173. doi:10.7764/RDLC.16.1.167.

[329] H. Nguyen, V. Carvelli, T. Fujii, K. Okubo, Cement mortar reinforced with reclaimed carbon fibres, CFRP waste or prepreg carbon waste, Constr. Build. Mater. 126 (2016) 321–331. doi:10.1016/j.conbuildmat.2016.09.044.

[330] M. Mastali, A. Dalvand, A. Sattarifard, The impact resistance and mechanical properties of the reinforced self-compacting concrete incorporating recycled CFRP fiber with different lengths and dosages, Compos. Part B Eng. 112 (2017) 74–92. doi:10.1016/j.compositesb.2016.12.029.

[331] L. Vandewalle, Postcracking Behaviour of Hybrid Steel Fiber Reinforced Concrete, 6th Int. Conf. Fract. Mech. Concr. Concr. Struct. (2007) 17–22.

[332] J. Rhodes, D. Carreira, J. Beaudoin, B. Gamble, H. Geymayer, B. Goyal, B. Hope, J. Keeton, C. Kesler, ACI 209R-92, Prediction of Creep, Shrinkage, and Temperature Effects in Concrete Structures, Rep. by ACI Comm. 209. 29 (2000) 143–148. doi:10.1080/03064220008536699.

[333] W. McCarter, S. Garvin, N. Bouzid, Impedance measurements on cement paste, J. Mater. Sci. Lett. 7 (1988) 1056–1057. doi:10.1007/ BF00720825.

[334] W.J. McCarter, R. Brousseau, The A.C. response of hardened cement paste, Cem. Concr. Res. 20 (1990) 891–900. doi:10.1016/0008- 8846(90)90051-X.

[335] P. Gu, Z. Xu, P. Xie, J. Beaudoin, Application of A.C. impedance techniques in studies of porous cementitious materials, Cem. Concr. Res. 23 (1993) 531–540. doi:10.1016/0008-8846(93)90003-R.

[336] C. Scuderi, T. Mason, H. Jennings, Impedance spectra of hydrating cement pastes, J. Mater. Sci. 26. 26 (1991) 349.353. doi:10.1007/ BF00576526.

[337] S. Ford, J. Shane, T. Mason, Assignment of features in impedance spectra of the cement-paste/steel system, Cem. Concr. Res. 28 (1998) 1737–1751.

[338] R. Coverdale, B. Christensen, H. Jennings, T. Mason, D. Bentz, E. Garboczi, Interpretation of impedance spectroscopy of cement paste via computer modelling, J. Mater. Sci. 30 (1995) 712–719. doi:10.1007/BF00356331.

[339] J.M. Torrents, T.O. Mason, E.J. Garboczi, Impedance spectra of fiber-reinforced cement-based composites: A modeling approach, Cem. Concr. Res. 30 (2000) 585–592. doi:10.1016/S0008-8846(00)00211-8.

[340] J. Torrents, T. Mason, A. Peled, S. Shah, E. Garboczi, Analysis of the impedance spectra of short conductive fiber-reinforced composites, J. Mater. Sci. 36. 36 (2001) 4003–4012.

[341] A. Hixson, L. Woo, M. Campo, T. Mason, E. Garboczi, Intrinsic conductivity of short conductive fibers in composites by impedance spectroscopy, J. Electroceram. 7 (2001) 189–195.

[342] T.O. Mason, M.A. Campo, A.D. Hixson, L.Y. Woo, Impedance spectroscopy of fiber-reinforced cement composites, Cem. Concr. Compos. 24 (2002) 457–465. doi:10.1016/S0958-9465(01)00077-4.

[343] A.D. Hixson, L.Y. Woo, M.A. Campo, T.O. Mason, The origin of nonlinear currentevoltage behavior in fiber-reinforced cement composites, Cem. Concr. Res. 33. 33 (2003) 835–840. doi:10.1016/S0008-8846(02) 01062-1.

[344] G. Šahmenko, A. Krasnikovs, A. Lukašenoks, M. Eiduks, Ultra High Performance Concrete Reinforced with Short Steel and Carbon Fibers, Environ. Technol. Resour. Proc. Int. Sci. Pract. Conf. 1 (2015) 193. doi:10.17770/etr2015vol1.196.

[345] D. Yoo, I. You, G. Zi, S. Lee, Effects of carbon nanomaterial type and amount on self-sensing capacity of cement paste, Measurement. (2017) submitted. doi:10.1016/j.measurement.2018.11.024.

[346] DAlessandro, Ubertini, Materazzi, Il Calcestruzzo Nanocomposito " Intelligente " per il Monitoraggio delle Costruzioni : Prospettive di Impiego nell ' Ingegneria Sismica, XVI Convegno ANIDIS L'Aquila 2015. (2015).

[347] A. Mehta, R. Siddique, An overview of geopolymers derived from industrial by-products, Constr. Build. Mater. 127 (2016) 183–198. doi:10.1016/j.conbuildmat.2016.09.136.

[348] B. Bhardwaj, P. Kumar, Waste foundry sand in concrete: A review, Constr. Build. Mater. 156 (2017) 661–674. doi:10.1016/j.conbuildmat.2017.09.010.

[349] N. Yazdani, V. Mohanam, Carbon Nano-Tube and Nano-Fiber in Cement Mortar: Effect of Dosage Rate and Water-Cement Ratio, Int. J. Mater. Sci. 4 (2014) 45. doi:10.14355/ijmsci.2014.0402.01.

Appendix A.

Electrochemical Impedance Spectroscopy of mortars reinforced with VCF, RCF and BSF at 91 days of curing. Bode plots (left) and Nyquist plots (right).

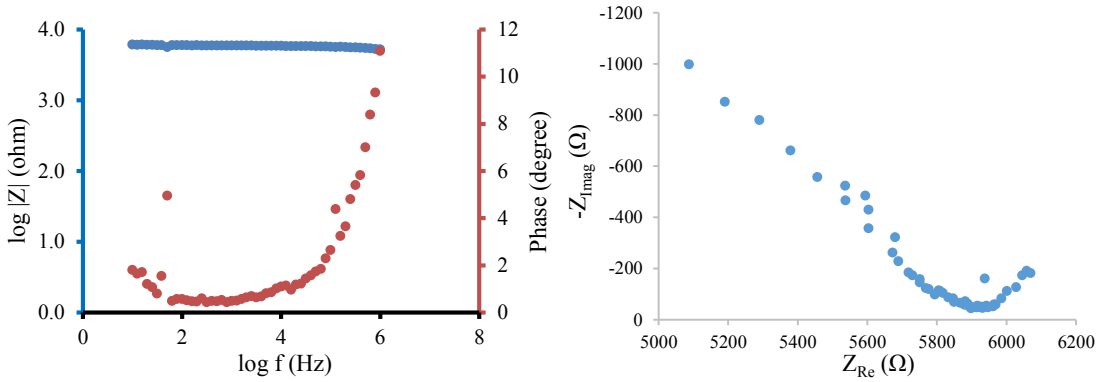

Figure A.1. *REF*

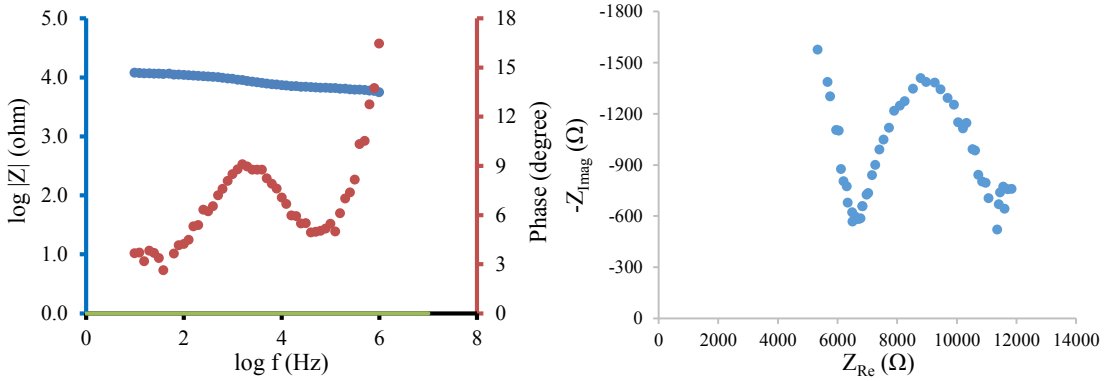

Figure A.2. *0.05 VCF*

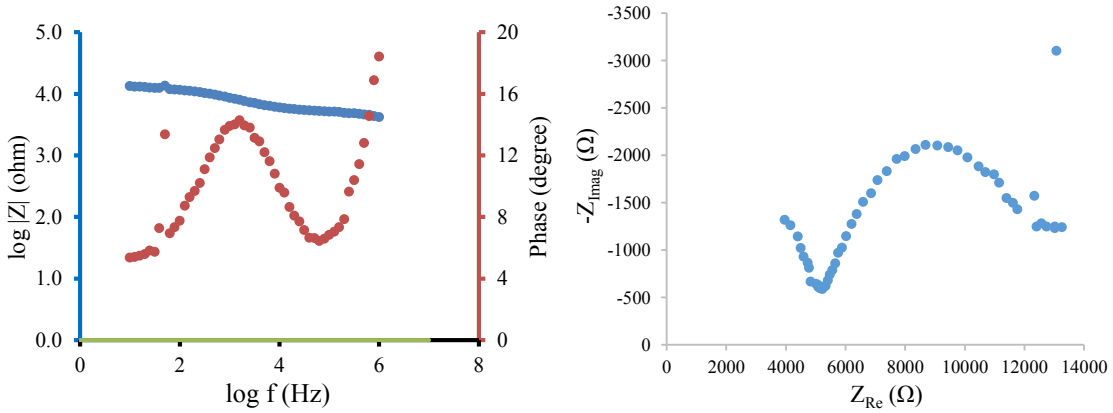

Figure A.3. *0.1 VCF*

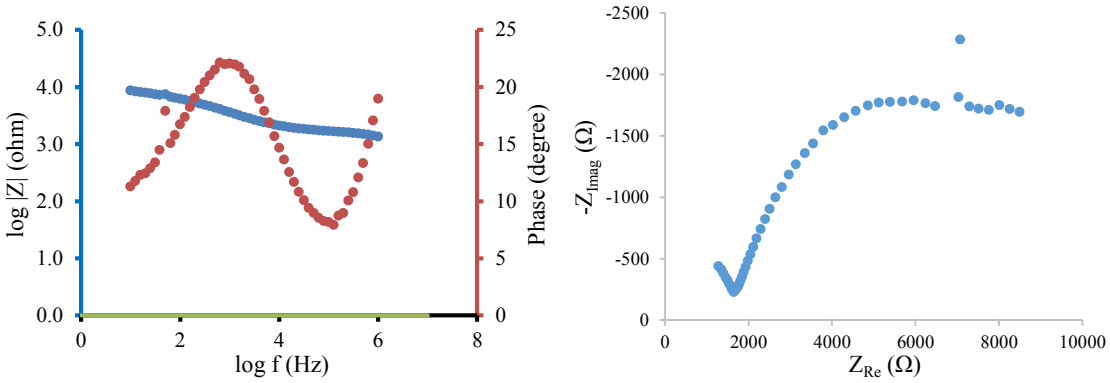

Figure A.4. *0.2 VCF*

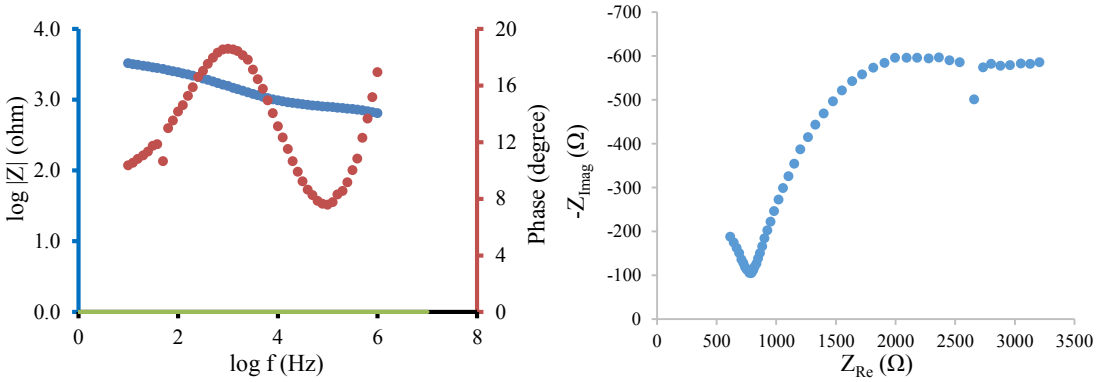

Figure A.5. *0.4 VCF*

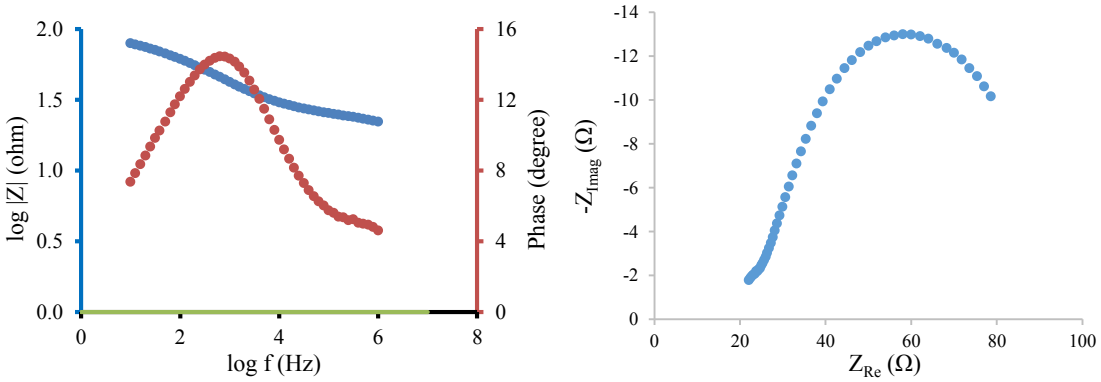

Figure A.6. *0.8 VCF*

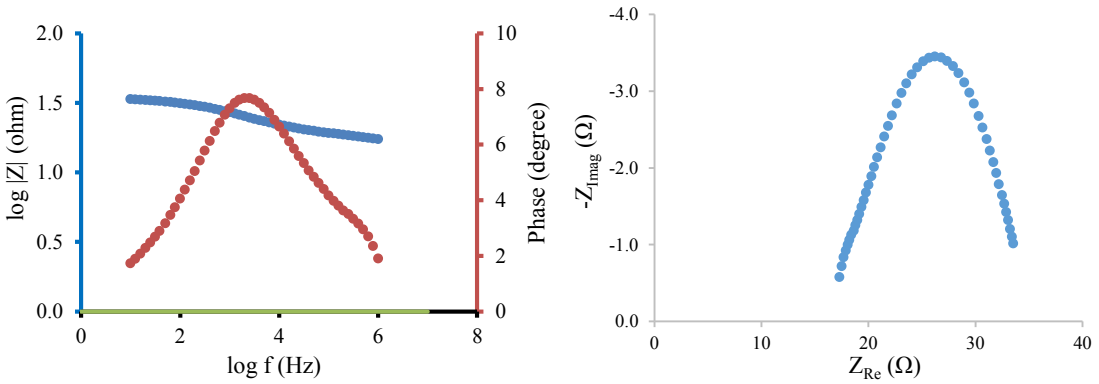

Figure A.7. *1.2 VCF*

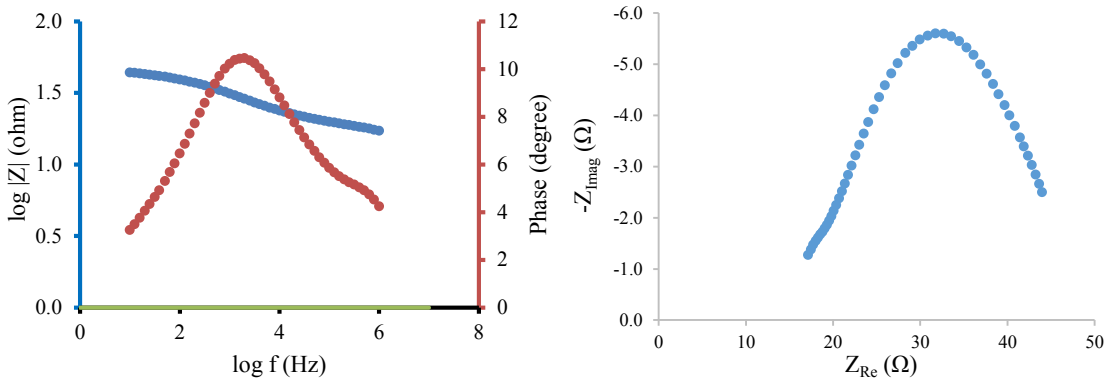

Figure A.8. *1.6 VCF*

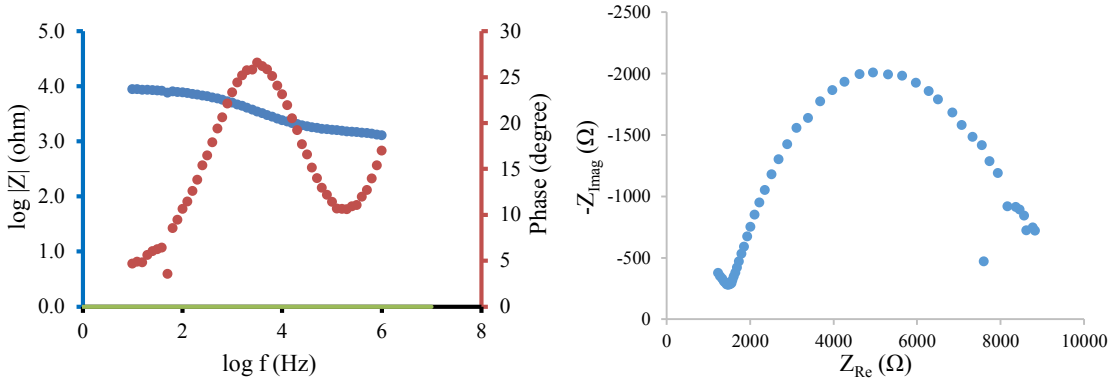

Figure A.9. *0.05 RCF*

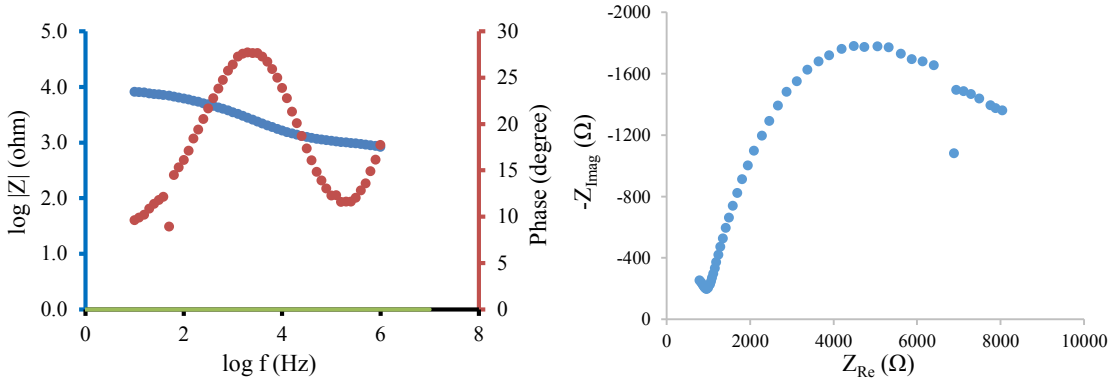

Figure A.10. *0.1 RCF*

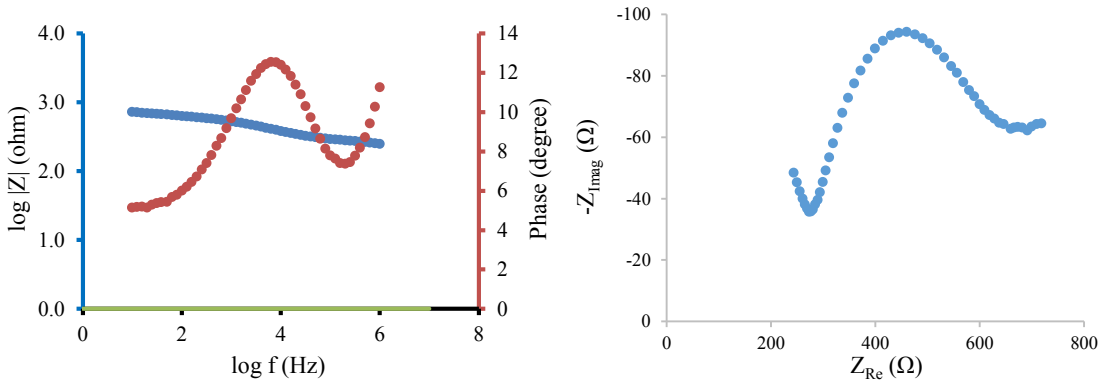

Figure A.11. *0.2 RCF*

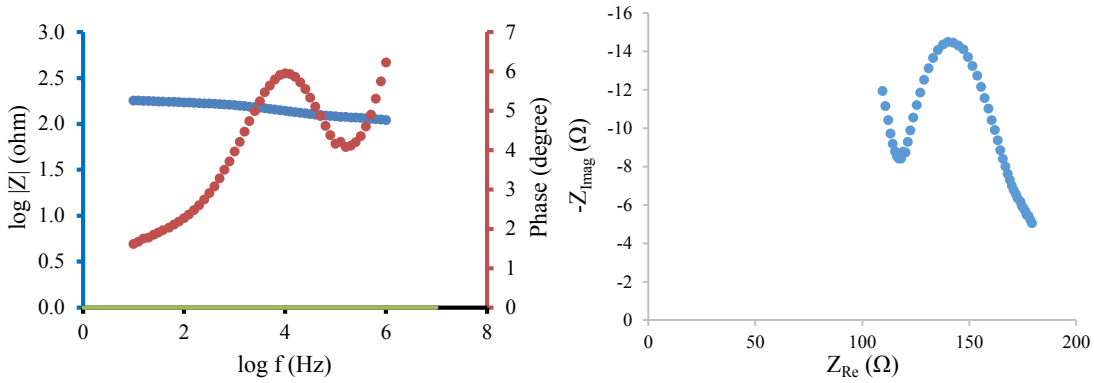

Figure A.12. *0.4 RCF*

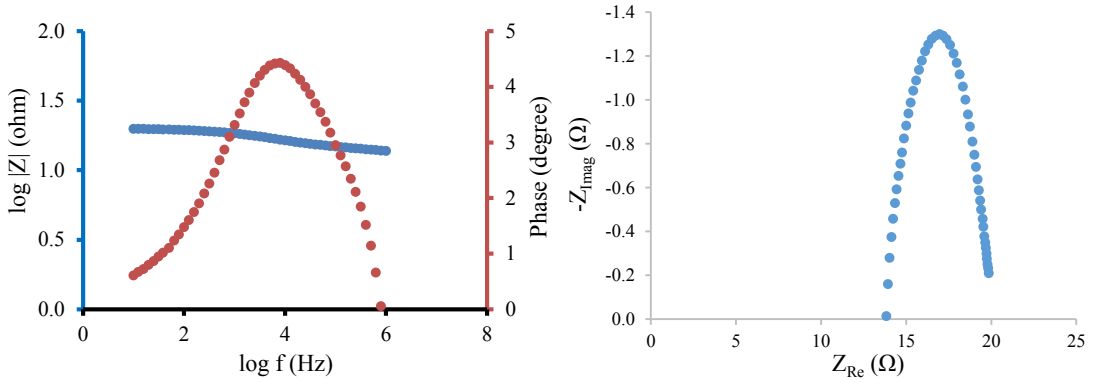

Figure A.13. *0.8 RCF*

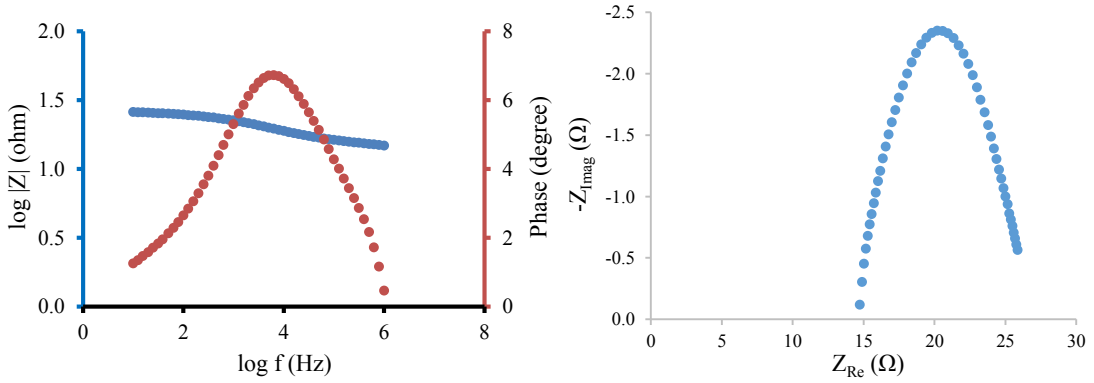

Figure A.14. *1.2 RCF*

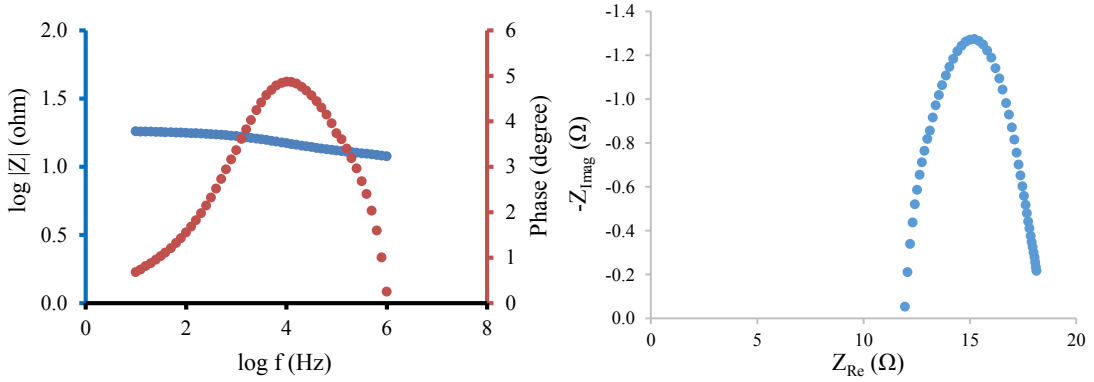

Figure A.15. *1.6 RCF*

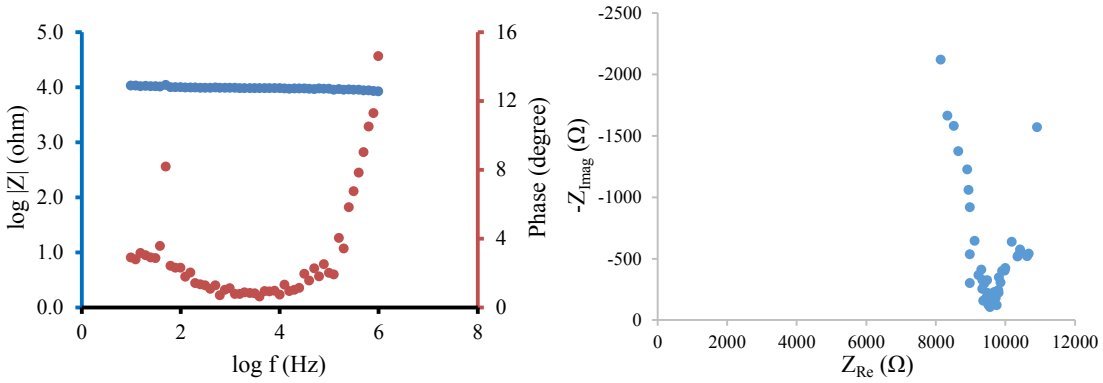

Figure A.16. *0.05 BSF*

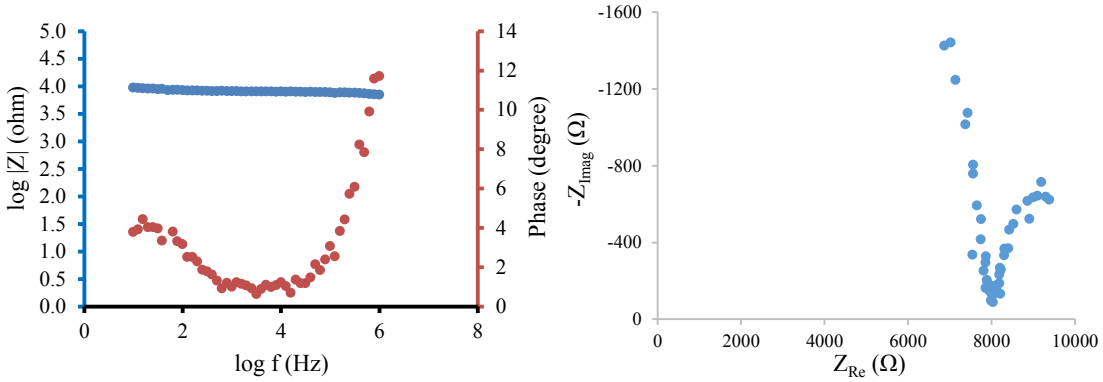

Figure A.17. *0.1 BSF*

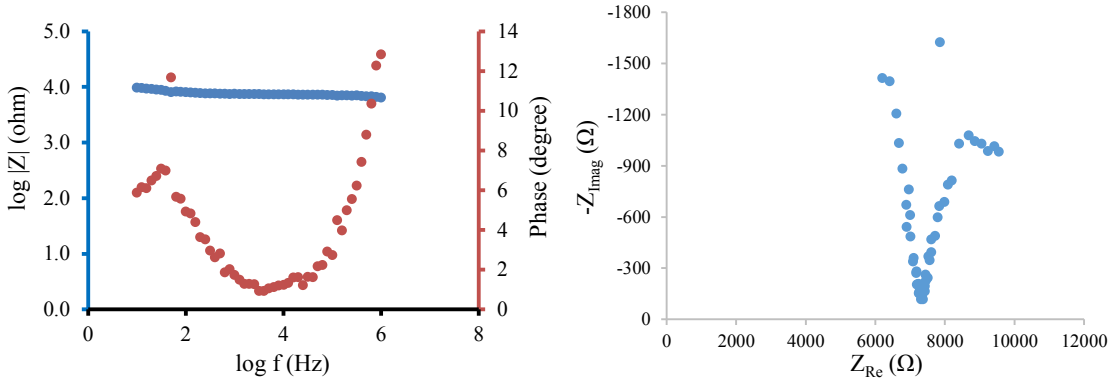

Figure A.18. *0.2 BSF*

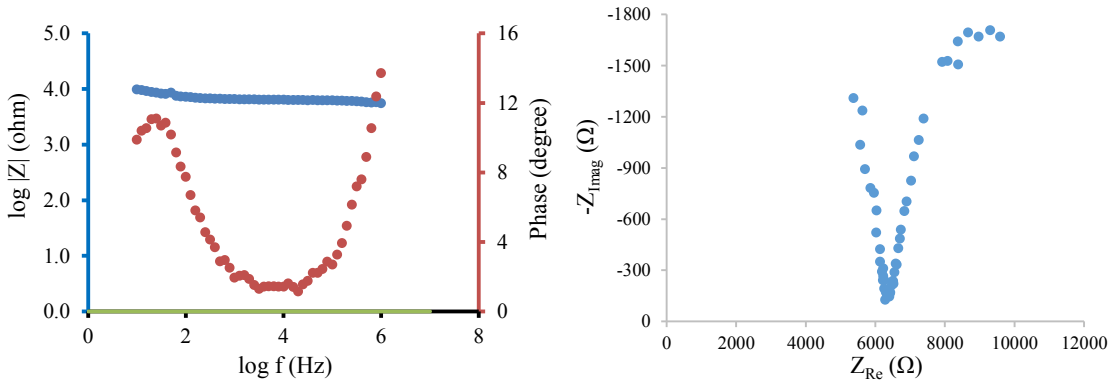

Figure A.19. *0.4 BSF*

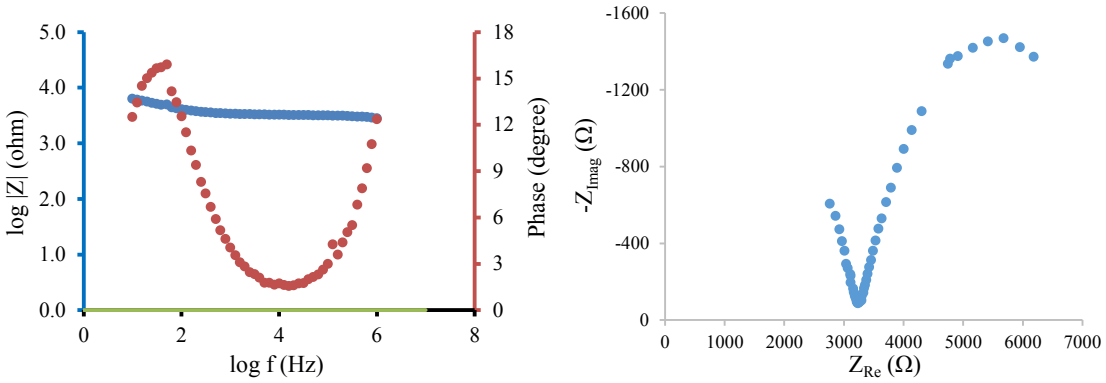

Figure A.20. *0.8 BSF*

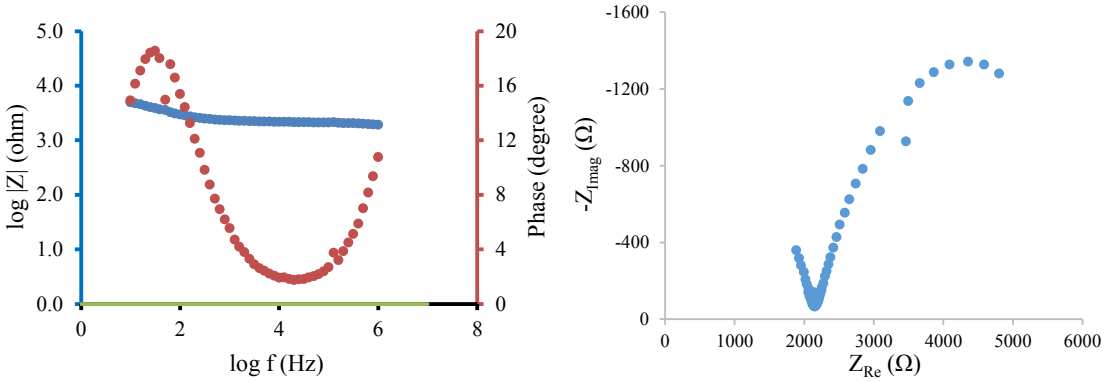

Figure A.21. *1.2 BSF*

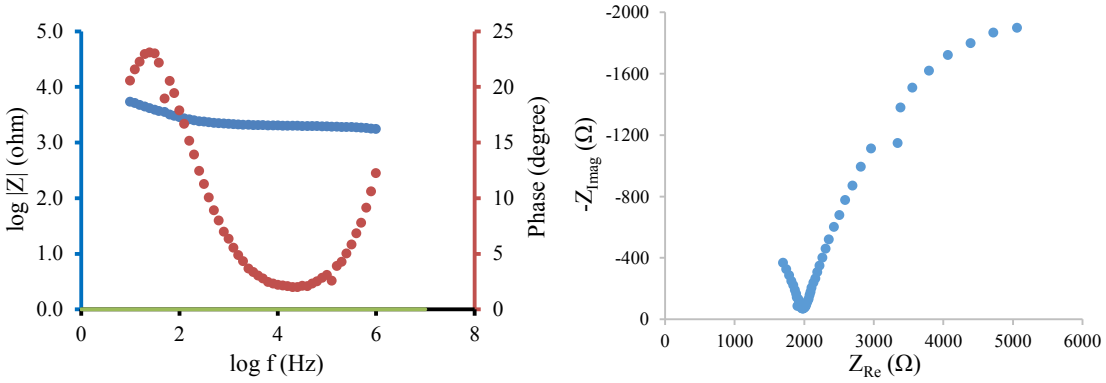

Figure A.22. *1.6 BSF*

Appendix B.

Electrochemical Impedance Spectroscopy of mortars with individual and combined additions of fillers (GNP, GCH, UFS) and fibers (VCF, RCF). Bode plots (left) and Nyquist plots (right) obtained by tests on dry specimens.

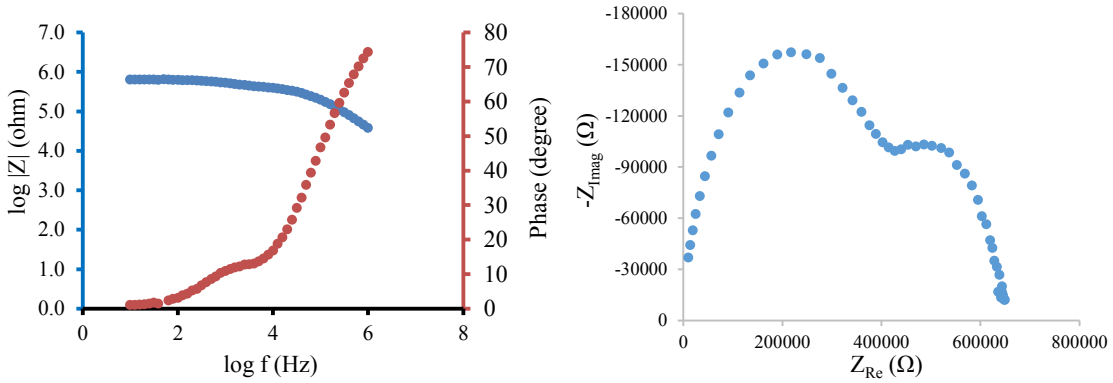

Figure B.1. *REF*

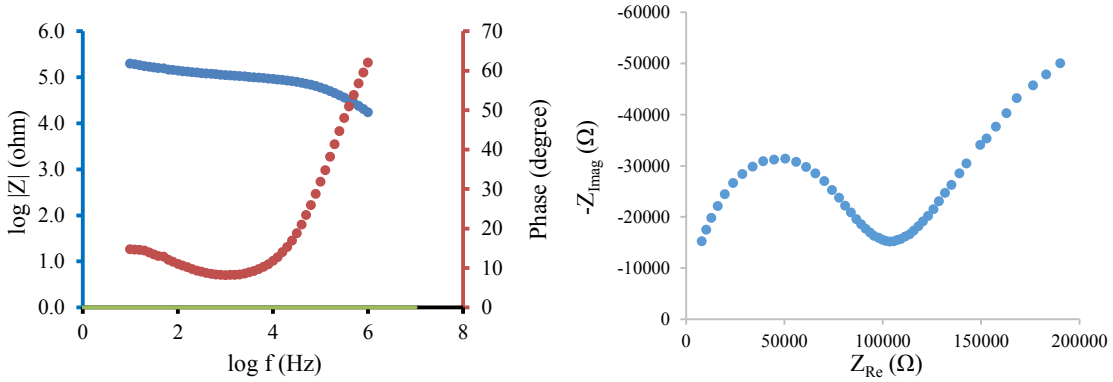

Figure B.2. *GNP4*

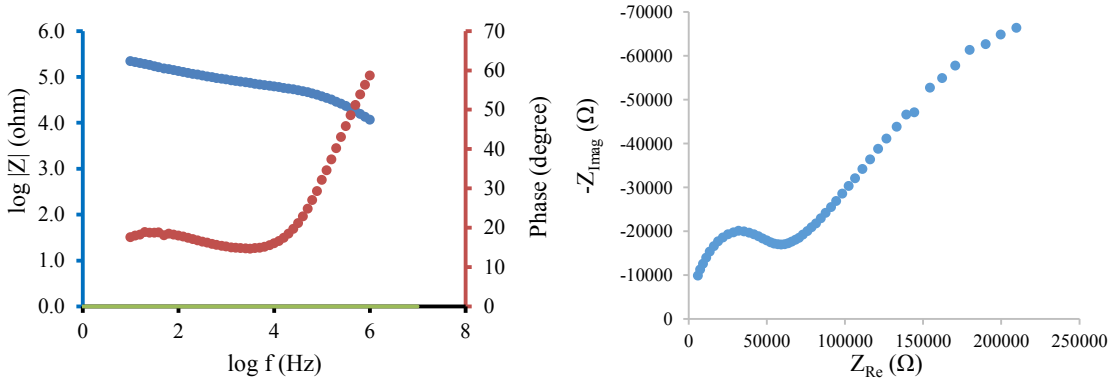

Figure B.3. *GNP7*

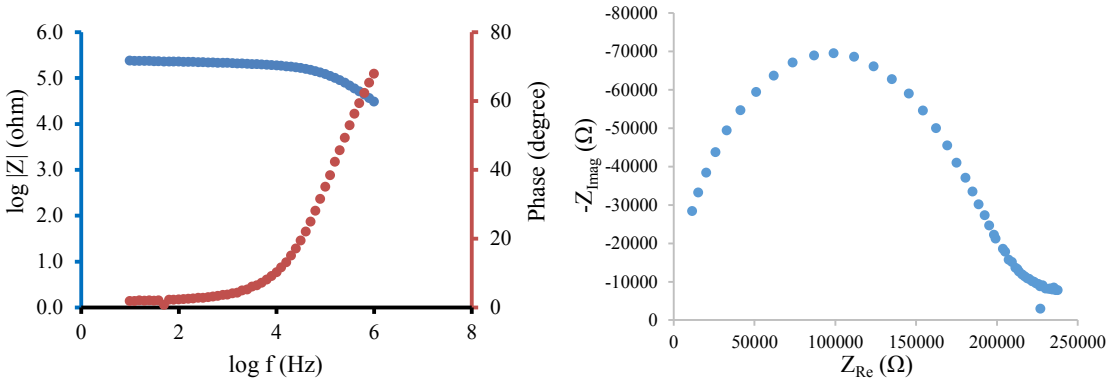

Figure B.4. *GCH4*

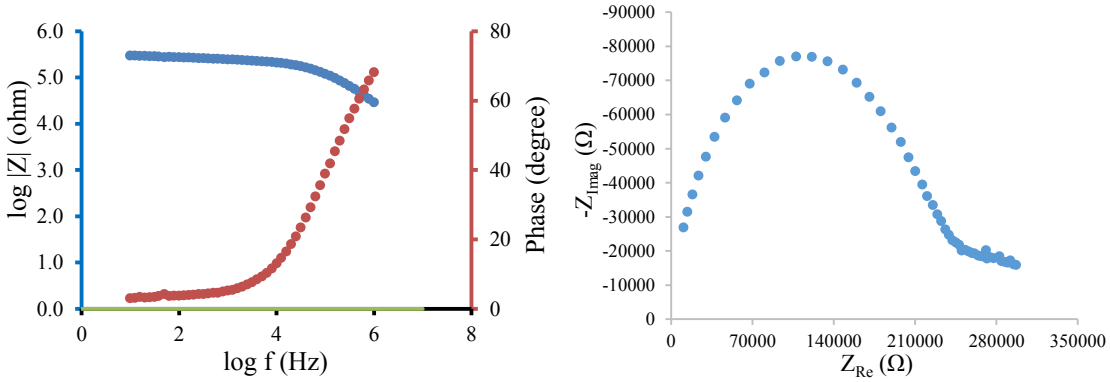

Figure B.5. *GCH7*

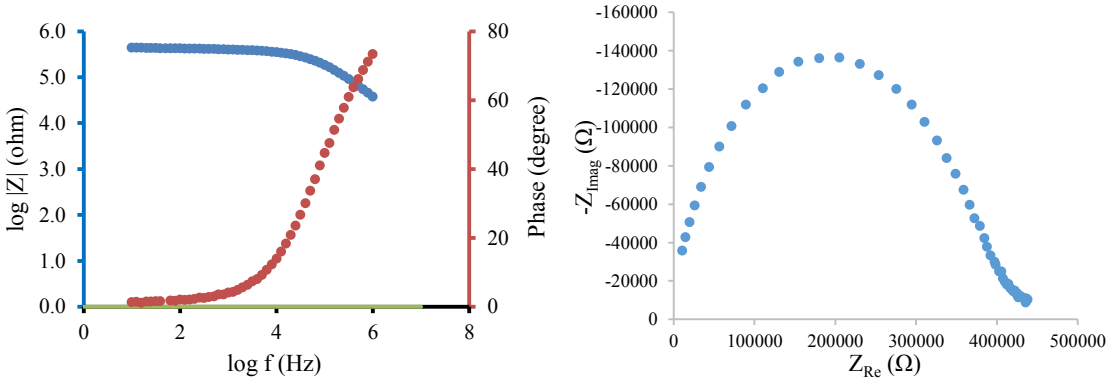

Figure B.6. *UFS4*

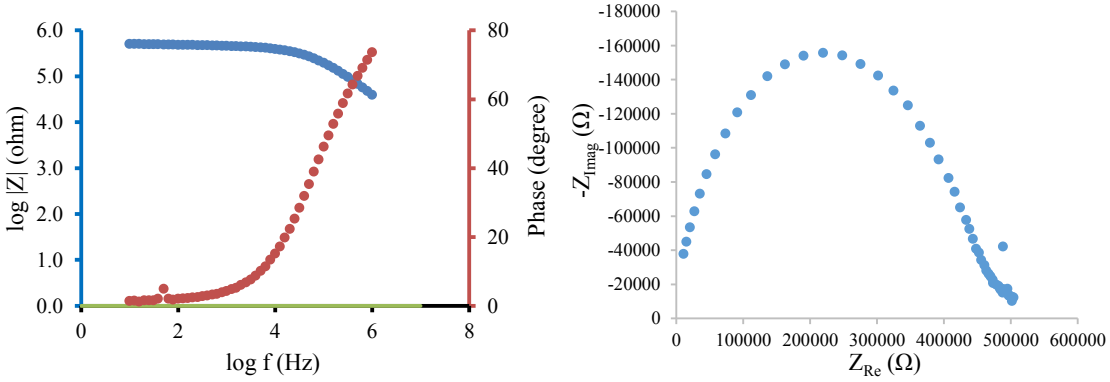

Figure B.7. *UFS7*

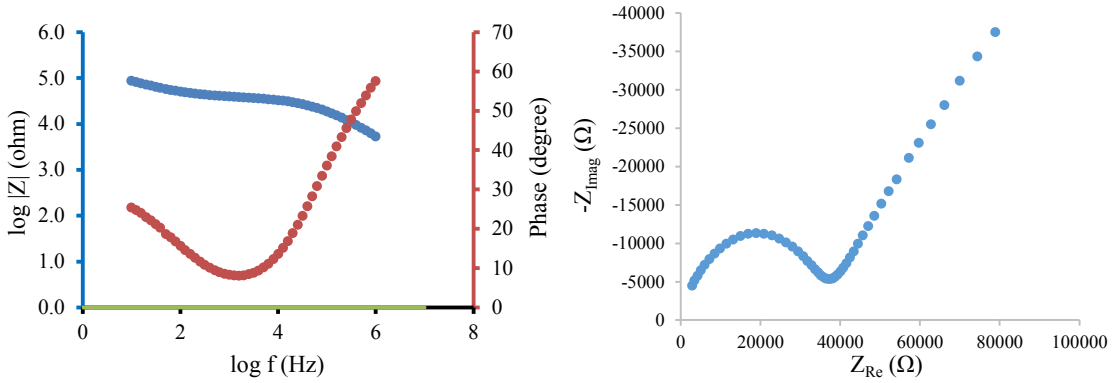

Figure B.8. *0.05 VCF*

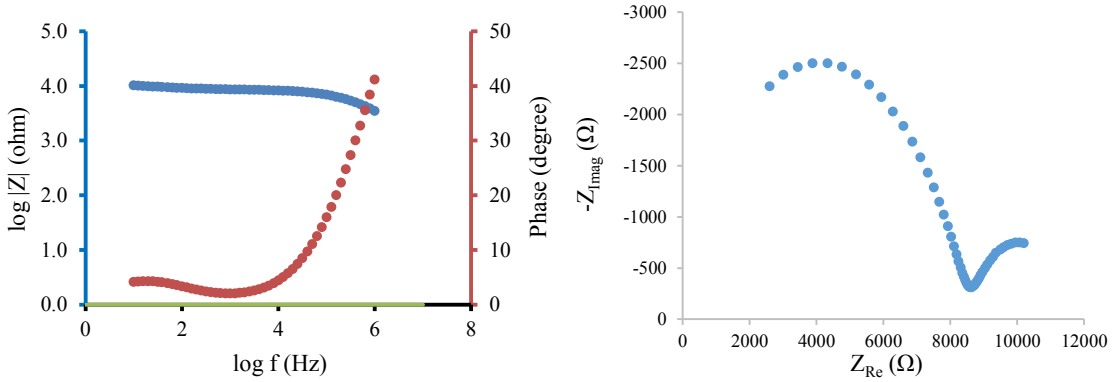

Figure B.9. *0.2 VCF*

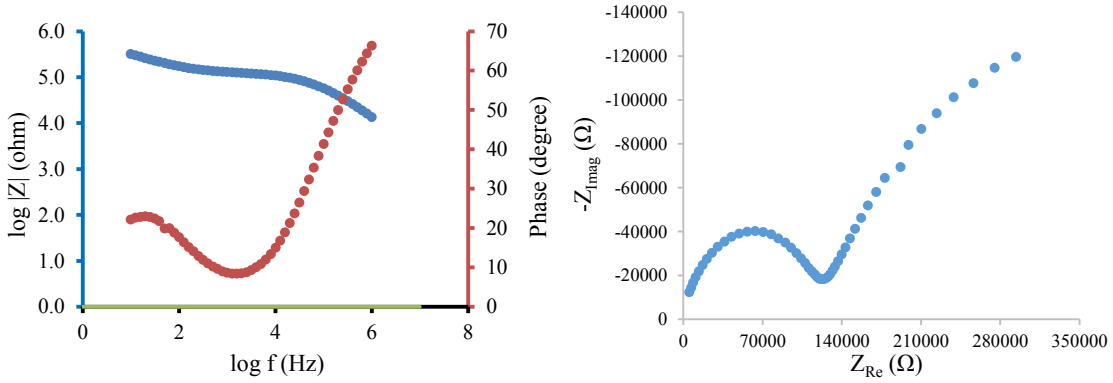

Figure B.10. *0.05 RCF*

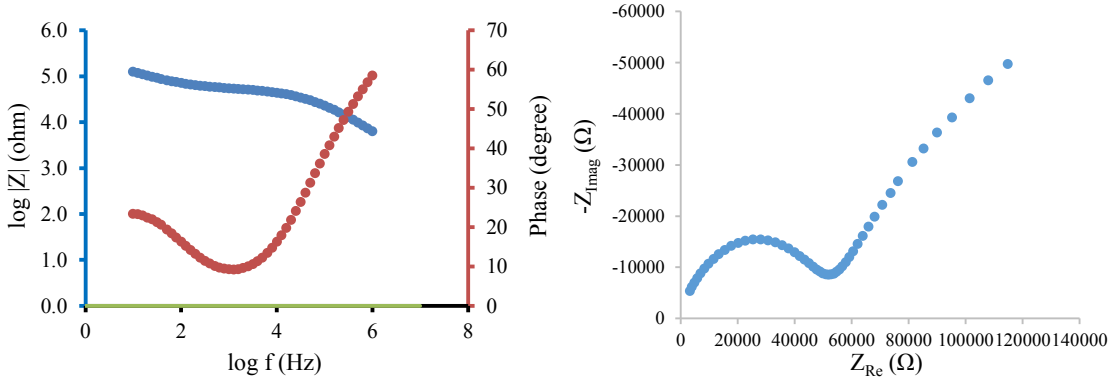

Figure B.11. *0.2 RCF*

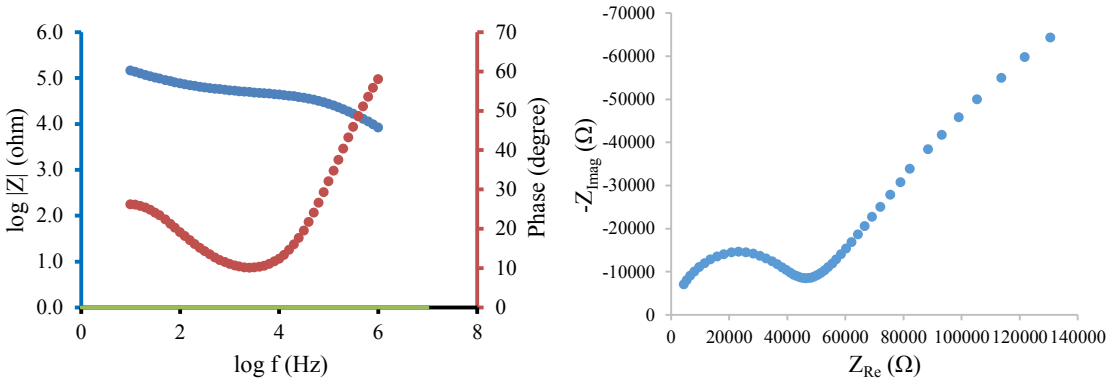

Figure B.12. *GNP4 - 0.05VCF*

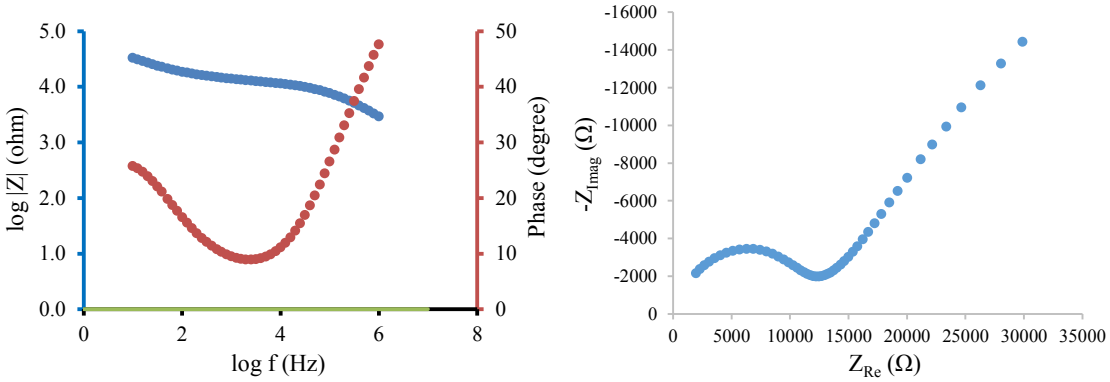

Figure B.13. *GNP4 - 0.2VCF*

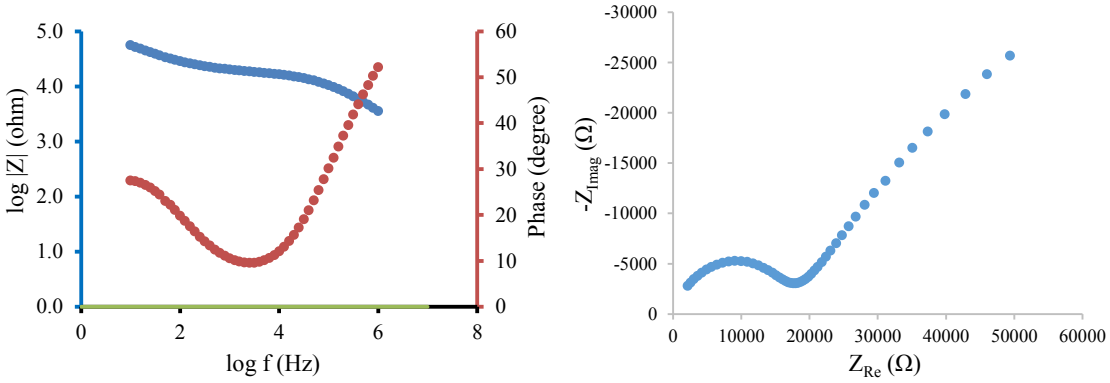

Figure B.14. *GNP4 - 0.05RCF*

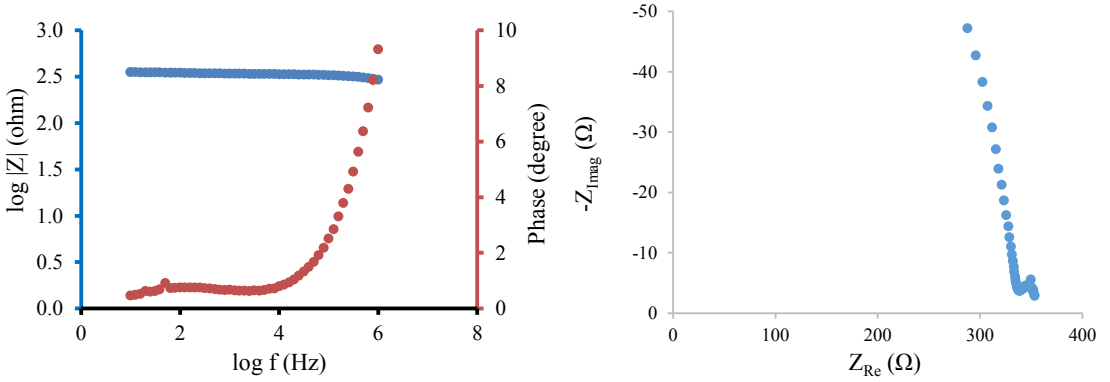

Figure B.15. *GNP4 - 0.2RCF*

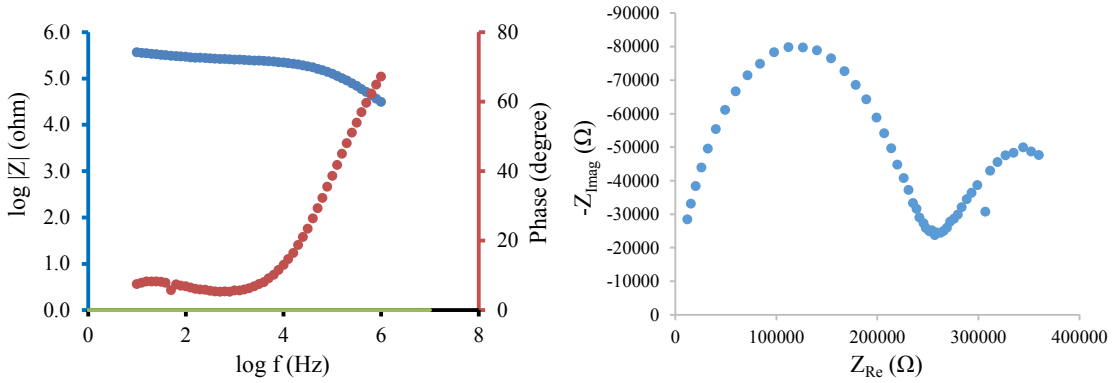

Figure B.16. *GCH4 – 0.05VCF*

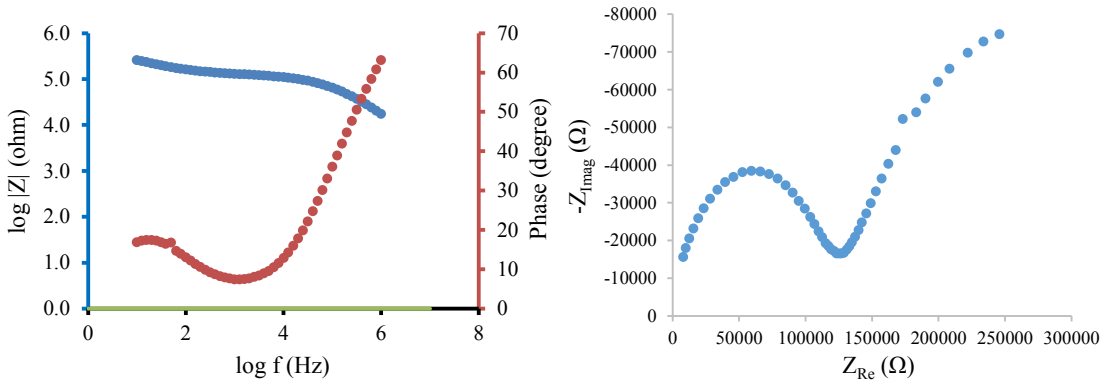

Figure B.17. *GCH4 – 0.2VCF*

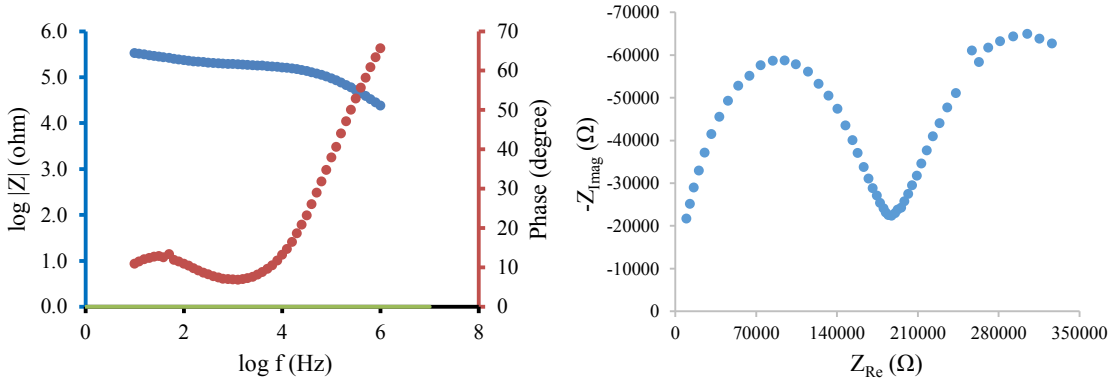

Figure B.18. *GCH4 – 0.05RCF*

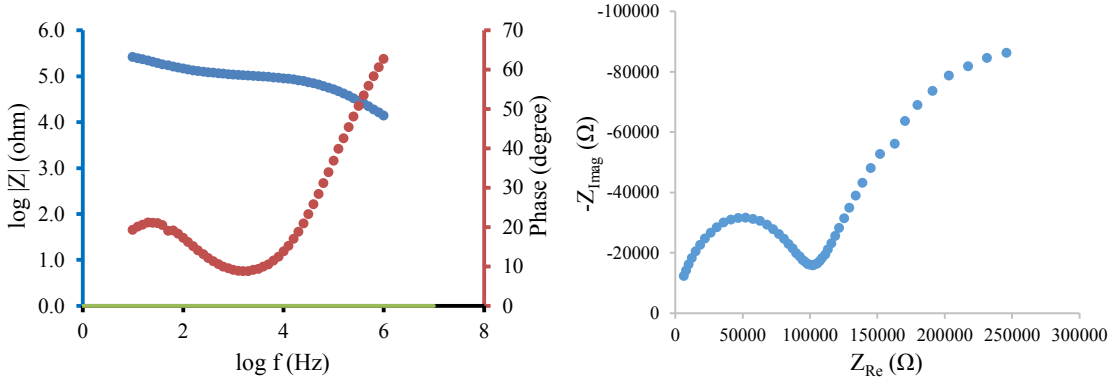

Figure B.19. *GCH4 – 0.2RCF*

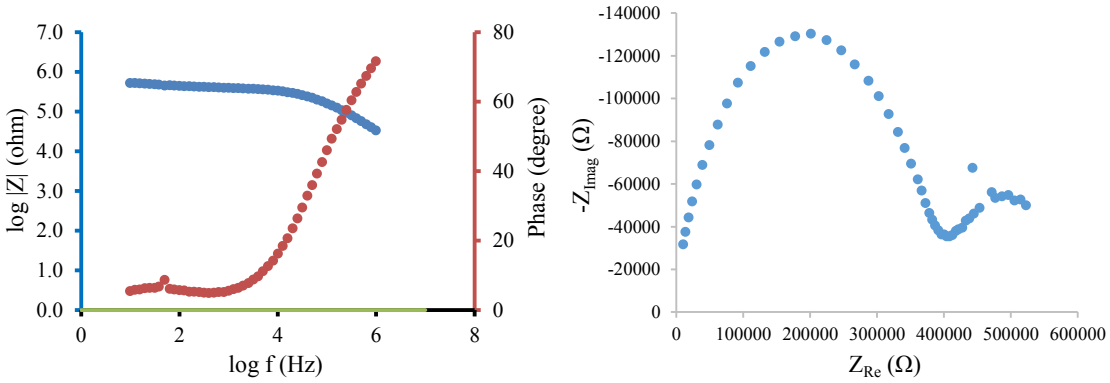

Figure B.20. *UFS4 – 0.05VCF*

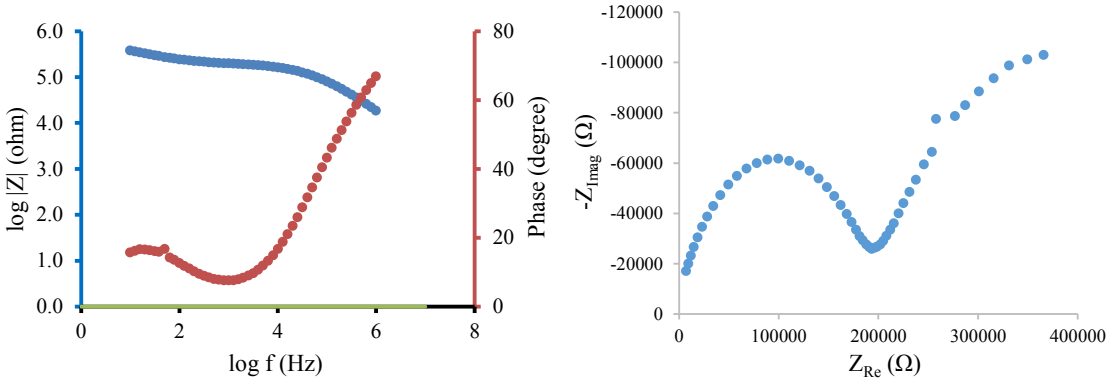

Figure B.21. *UFS4 – 0.2VCF*

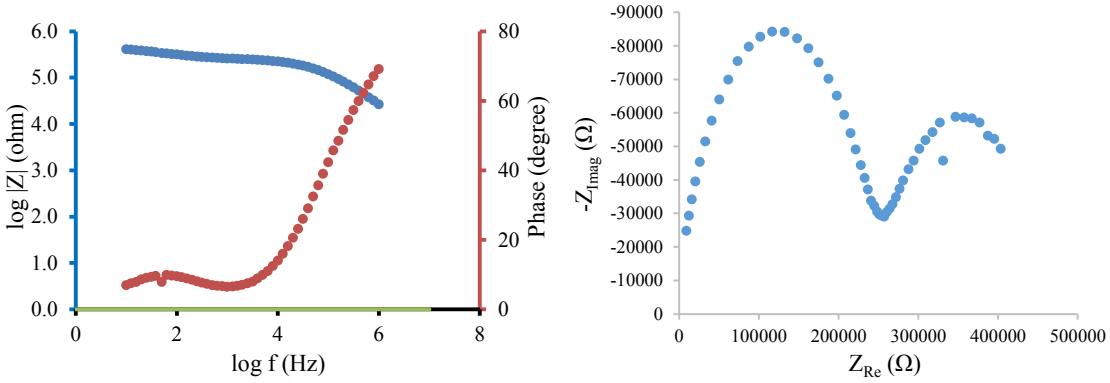

Figure B.22. *UFS4 – 0.05RCF*

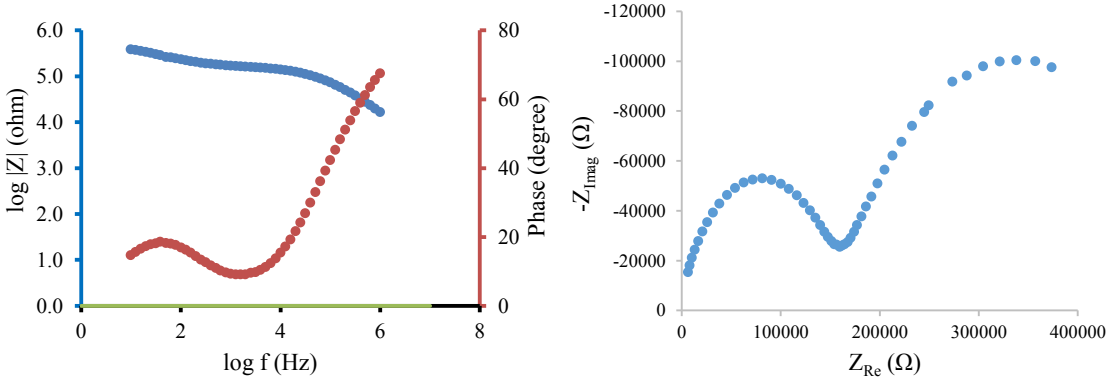

Figure B.23. *UFS4 – 0.2RCF*

Appendix C.

Piezoresistivity tests on mortars with individual and combined additions of fillers (GNP, GCH, UFS) and fibers (VCF, RCF). FCR and Strain vs. time (left) and FCR vs. strain (right) measured by 4-probe DC system.

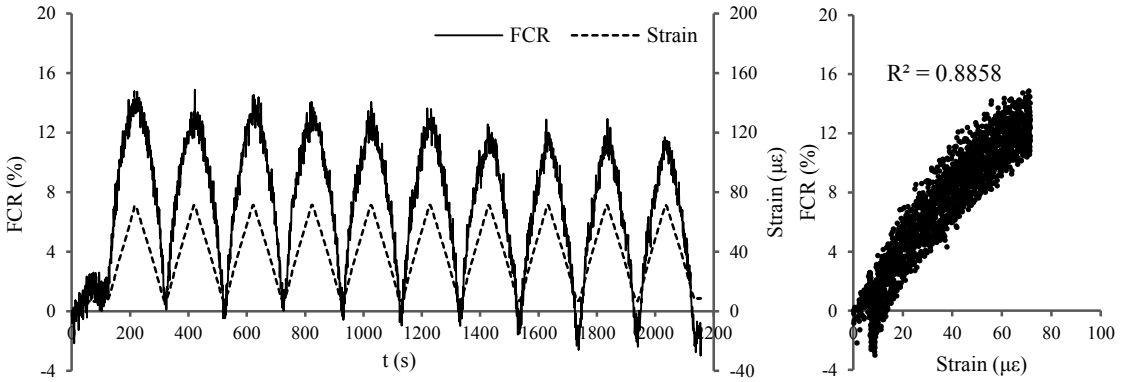

Figure C.1. *REF*

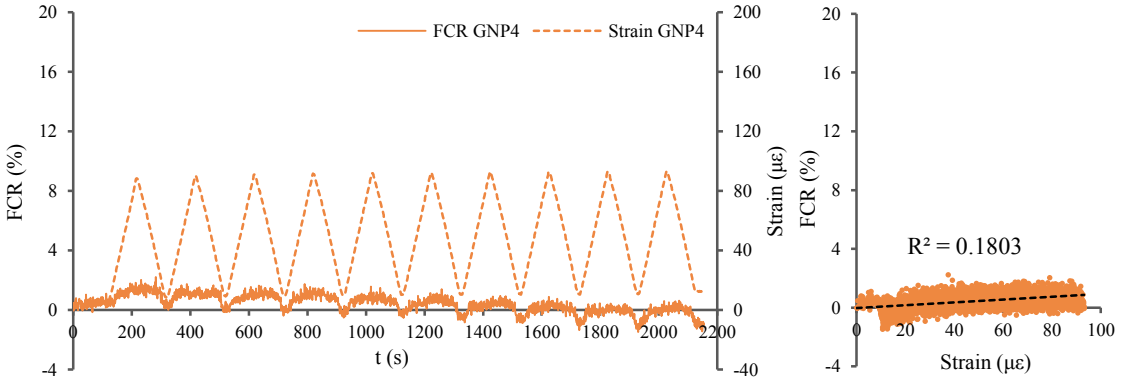

Figure C.2. *GNP4*

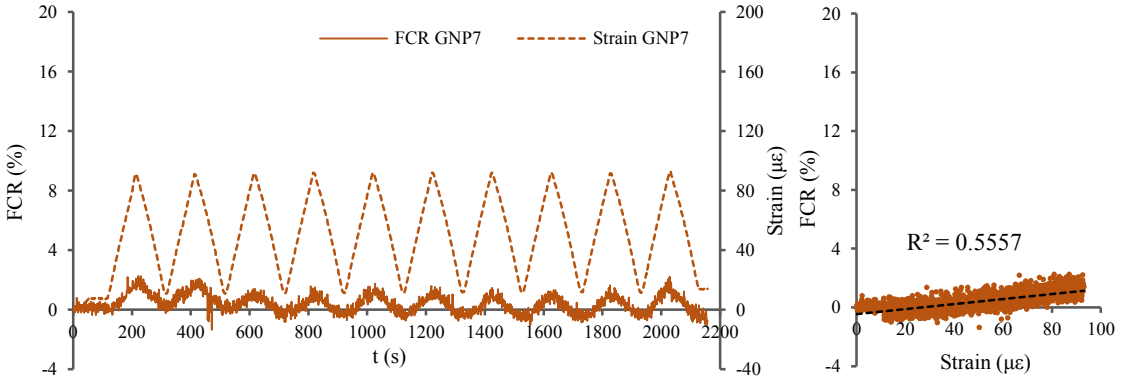

Figure C.3. *GNP7*

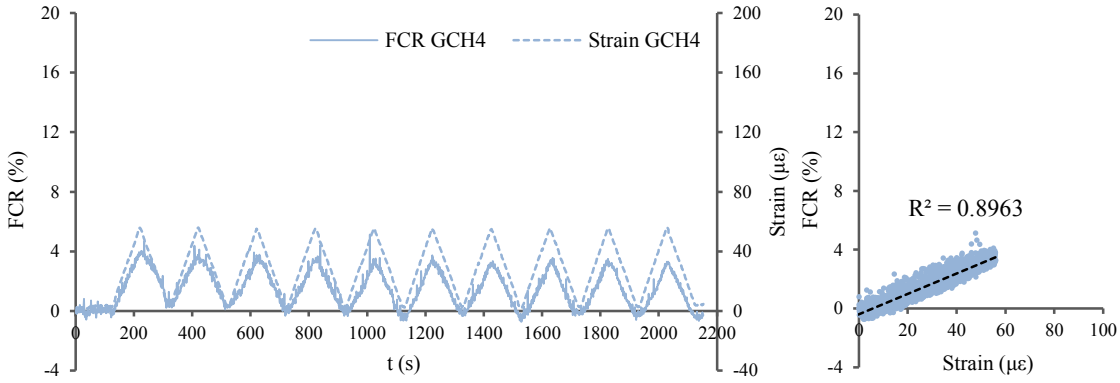

Figure C.4. *GCH4*

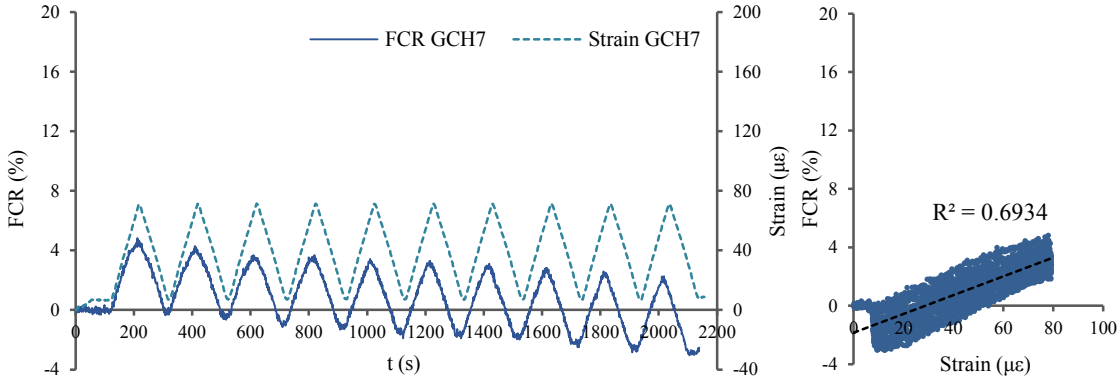

Figure C.5. *GCH7*

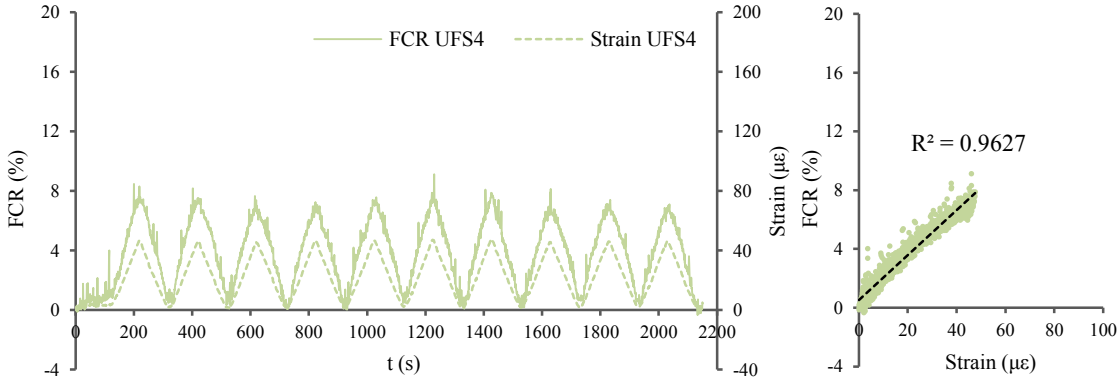

Figure C.6 *UFS4*

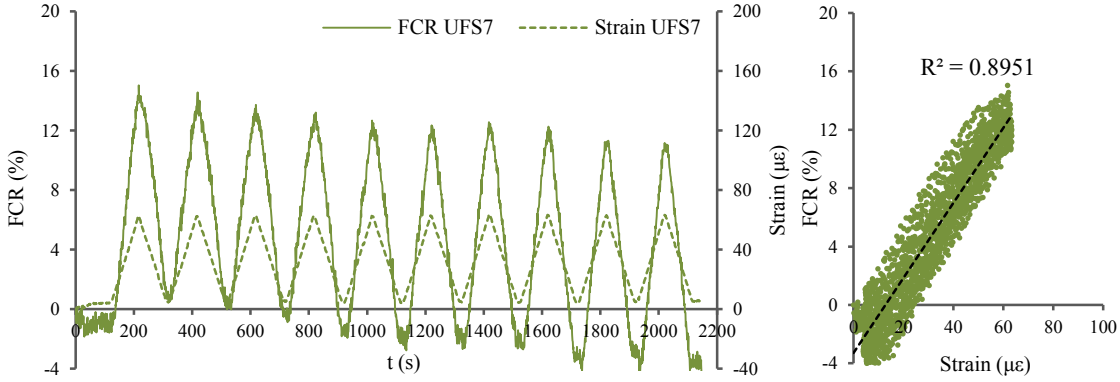

Figure C.7. *UFS7*

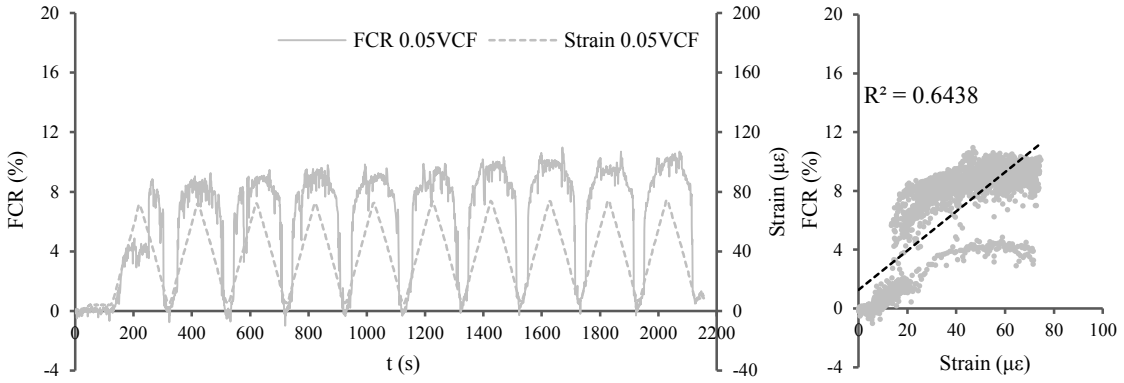

Figure C.8. *0.05 VCF*

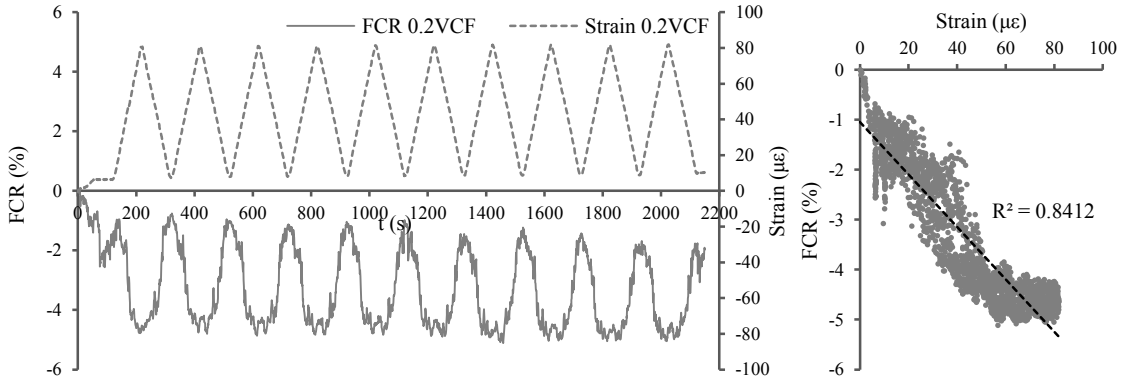

Figure C.9. *0.2 VCF*

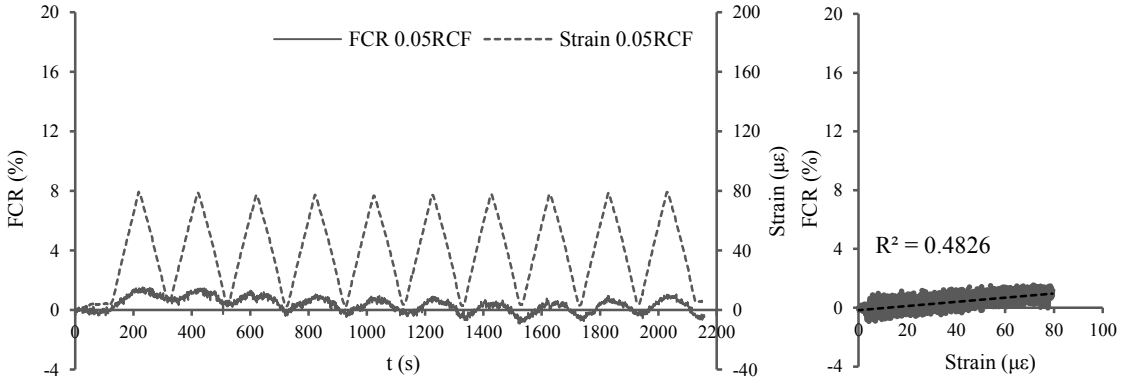

Figure C.10. *0.05 RCF*

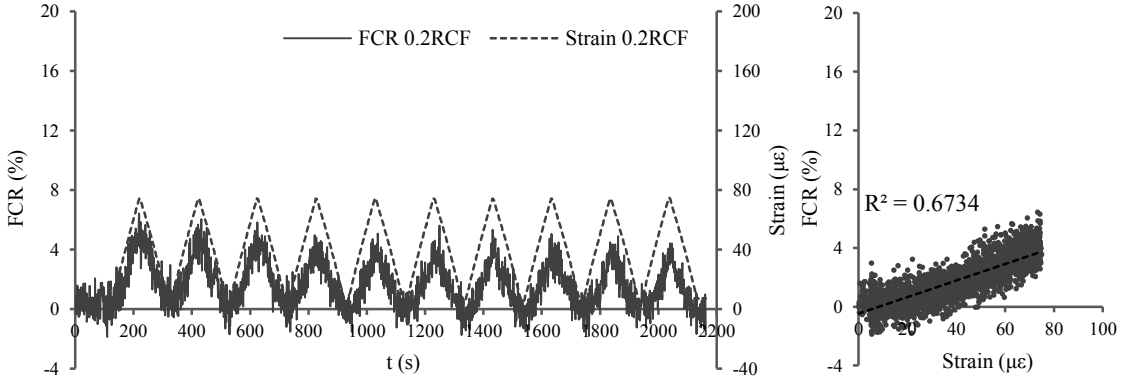

Figure C.11. *0.2 RCF*

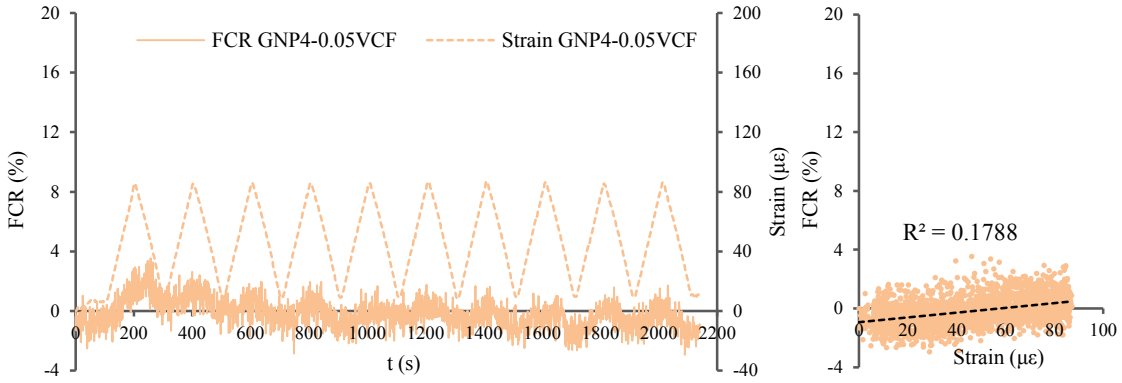

Figure C.12. *GNP4-0.05VCF*

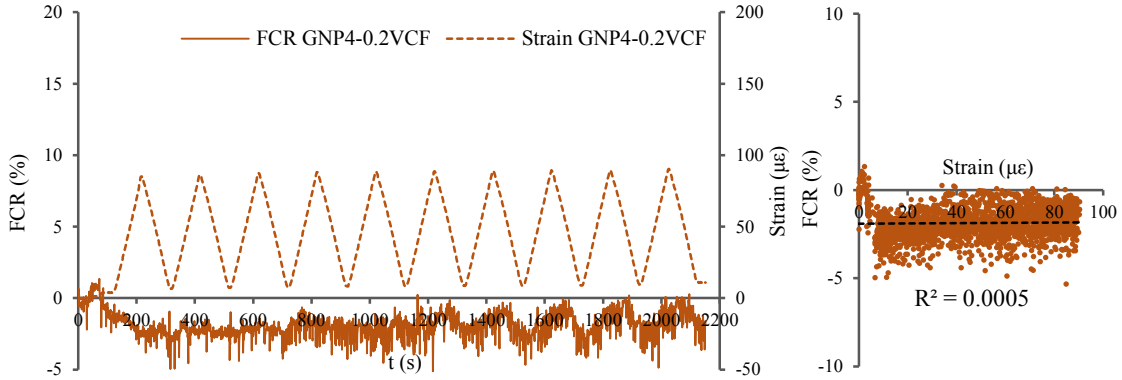

Figure C.13. *GNP4 – 0.2VCF*

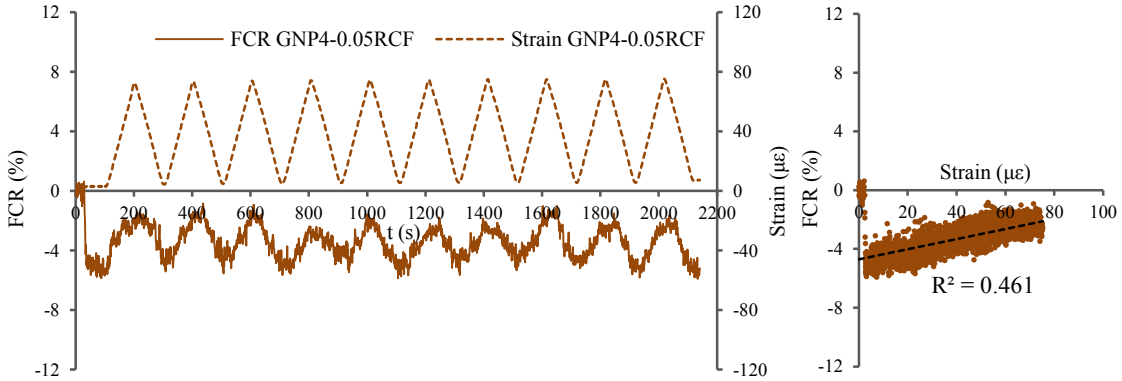

Figure C.14. *GNP4 – 0.05RCF*

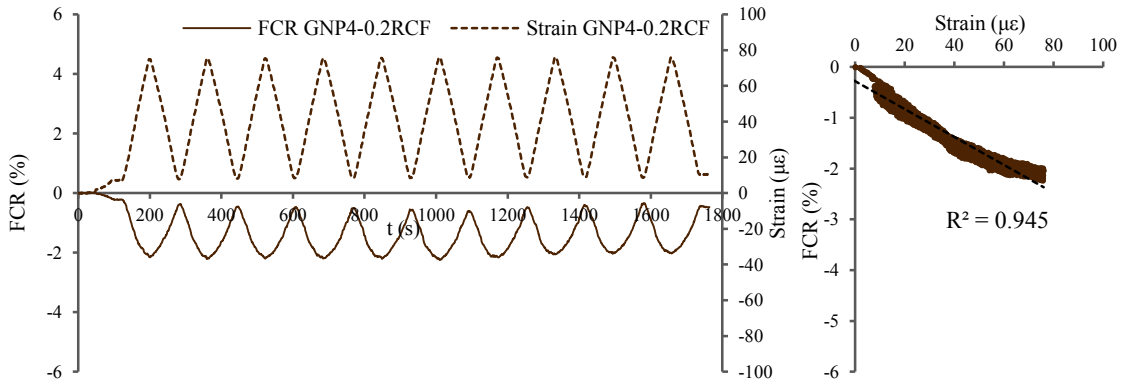

Figure C.15. *GNP4 – 0.2RCF*

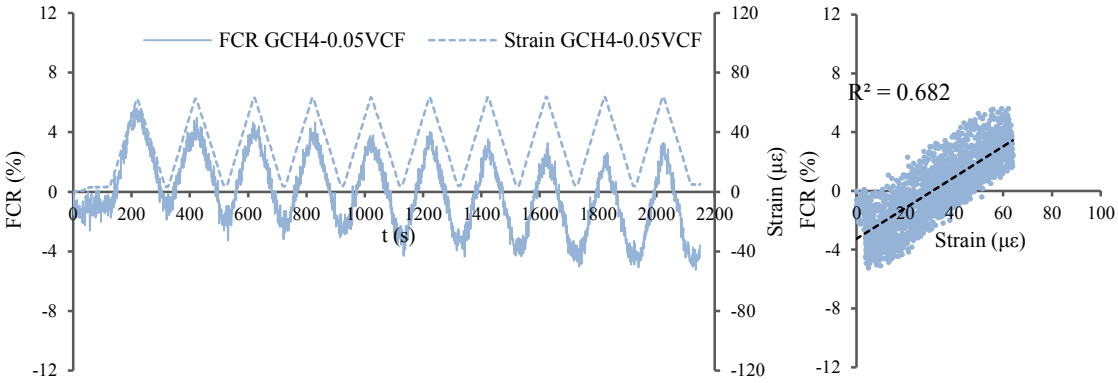

Figure C.16. *GCH4 – 0.05VCF*

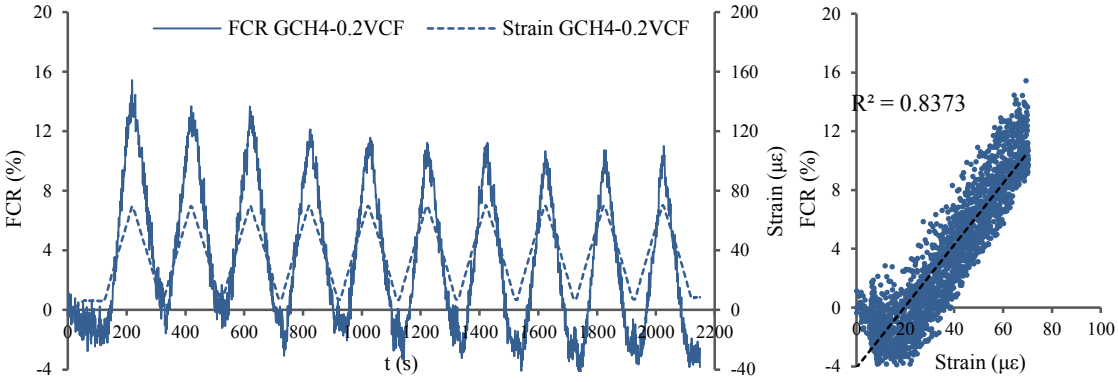

Figure C.17. *GCH4 – 0.2VCF*

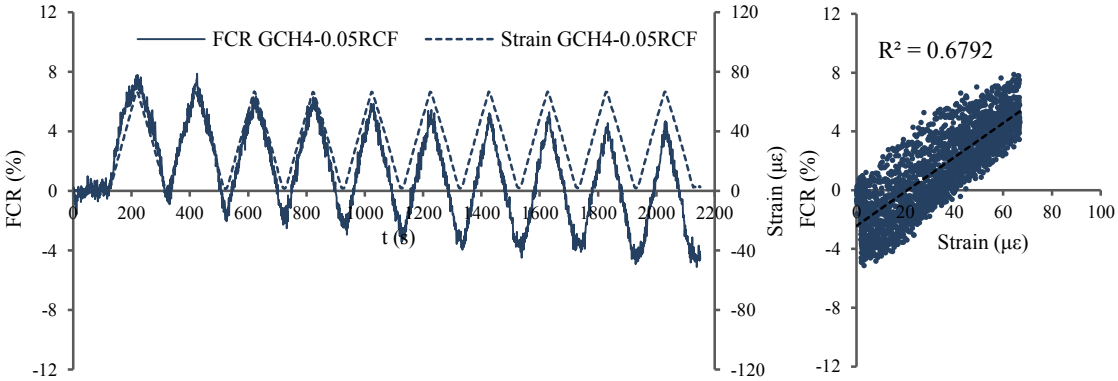

Figure C.18. *GCH4 – 0.05RCF*

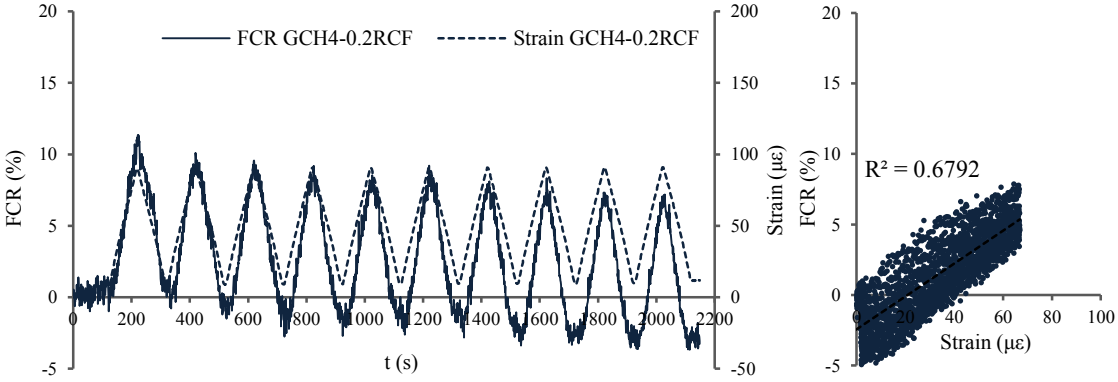

Figure C.19. *GCH4 – 0.2RCF*

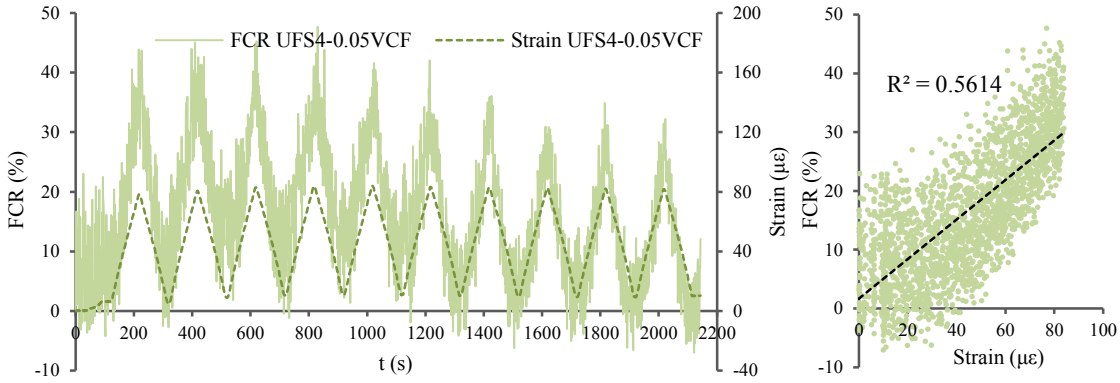

Figure C.20. *UFS4 – 0.05VCF*

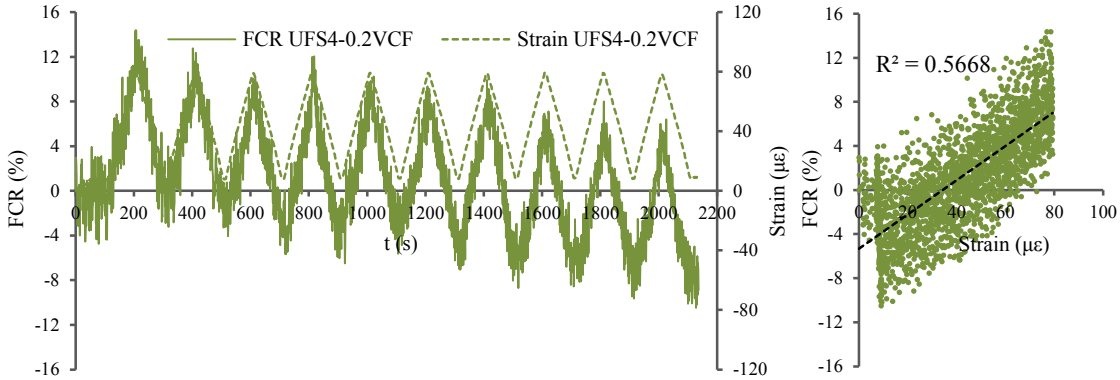

Figure C.20. *UFS4 – 0.2VCF*

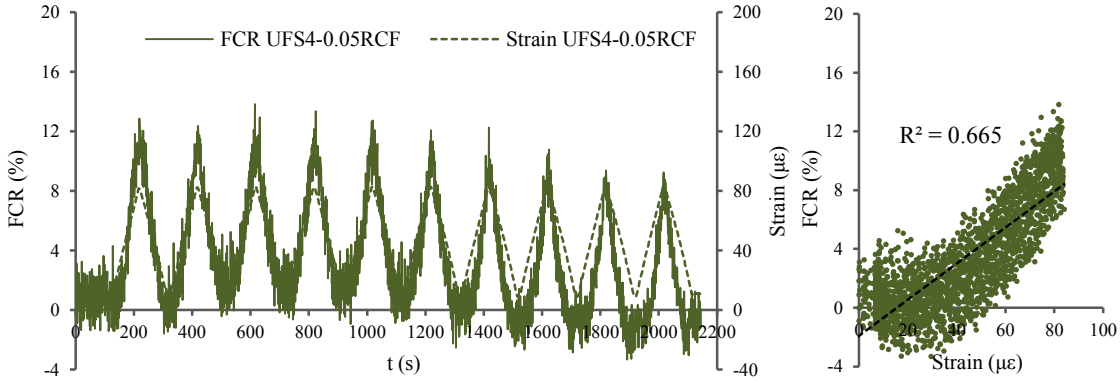

Figure C.20. *UFS4 – 0.05RCF*

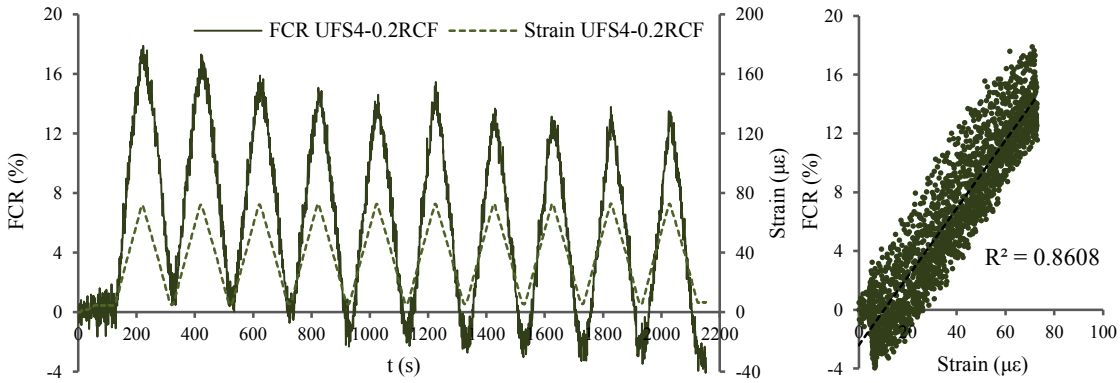

Figure C.23. *UFS4 – 0.2RCF*

a Giuliana, a Carlo, e a Silvia

Grazie…